9th edition

Copernicus Publications
The Innovative Open Access Publisher

STATE OF THE PLANET

COPERNICUS

OCEAN STATE REPORT

9th edition of the Copernicus Ocean State Report | 2025

PROGRAMME OF THE EUROPEAN UNION

Copernicus
Europe's eyes on Earth

Copernicus Marine Service

Implemented by
MERCATOR OCEAN INTERNATIONAL

About the Copernicus Ocean State Report

As part of the Copernicus Marine Service, the annual Copernicus Ocean State Report (OSR) launched in 2015 is the key tool of its ocean reporting framework. The OSR reports on the state, variability, and ongoing changes in the marine environment of the global ocean and the European regional seas over the past decades up to close to real time. Using observation-based (remote sensing, in situ) and ocean reanalysis data, the OSR provides a comprehensive 4-dimensional (latitude, longitude, depth, and time) analysis of the Blue, Green, and White Ocean. The OSR is intended to act as a reference, providing a unique ocean monitoring dashboard for the scientific community and for policy makers and others with decision making responsibilities.

Copernicus Marine Service

PROGRAMME OF THE EUROPEAN UNION

Copernicus Europe's eyes on Earth

Implemented by MERCATOR OCEAN INTERNATIONAL

STATE OF THE PLANET

About State of the Planet

State of the Planet (SP) is a journal dedicated to the publication of scientific synthesis reports and assessments on all subjects of the Earth and environmental sciences. In a rapidly changing world, expert-based assessments of academic findings curated for a wider audience to support decision making, science communication, education, and funder mandates are becoming more and more widespread. Such reports are extensive science community efforts offering timely, state-of-the-art insight into a specific field of the Earth sciences. State of the Planet is open to any reporting and assessment initiative by (inter-) governmental agencies, environmental services, learned societies or associations of researchers that aim to publish on a regular basis.

Copernicus Publications
The Innovative Open Access Publisher

publications@copernicus.org
http://publications.copernicus.org

Cover photo: Welle 1, 2021, Öl auf Leinwand, 40x40 cm by Malte von Schuckmann. Used with permission. https://www.malte-von-schuckmann.de/

von Schuckmann, K., Moreira, L., de Pascual Collar, A., Grégoire, M., Brasseur, P., Garric, G., Karstensen, J., Lionello, P., Marcos, M., Poulain, P.-M., and Staneva, J. (Eds.): 9th edition of the Copernicus Ocean State Report (OSR9), Copernicus Publications, State Planet, 6-osr9, https://doi.org/10.5194/sp-6-osr9, 2025.

State Planet, 6-osr9, 2, 2025
https://doi.org/10.5194/sp-6-osr9-2-2025

Global ocean change in the era of the triple planetary crisis

Karina von Schuckmann[1], Flora Gues[2,1], Lorena Moreira[3], Aurélien Liné[1], and Álvaro de Pascual Collar[3]

[1]Mercator Ocean international, Toulouse, France
[2]CELAD, Mercator Ocean international, Toulouse, France
[3]Nologin Oceanic Weather Systems, Madrid, Spain

Correspondence: Karina von Schuckmann (karina.von.schuckmann@mercator-ocean.fr)

Published: 30 September 2025

Abstract. This ocean narrative is grounded in global ocean indicators and framed around climate, biodiversity, and sustainable development. In 2024, global ocean heat content (OHC) reached record levels, with continued heat uptake of $0.35 \pm 0.1\,W\,m^{-2}$ and steady acceleration of $0.14 \pm 0.1\,W\,m^{-2}$ per decade since the 1960s. Sea surface temperatures (SSTs) exceeded 21 °C globally in both 2023 and 2024, while global mean sea level rise reached its highest recorded rate of $4.1 \pm 0.1\,mm\,yr^{-1}$ (2016–2024). No part of the ocean is untouched by the so-called triple planetary crisis as proclaimed by the United Nations, where pollution, biodiversity loss, and climate change are putting pressure on marine systems worldwide. Over 8 % (10 %) of marine biodiversity hotspots, 8 % (11 %) of large marine ecosystems (LMEs), and 14 % (32 %) of Areas Beyond National Jurisdiction (ABNJ) are exposed to warming (acidification) beyond global rates. The triple planetary crisis converges across all ocean basins, with 16 % (30 %) of endangered (critically endangered) corals exposed to rapid ocean warming or acidification (rapid pH loss), and 75 % of countries emitting > 10 000 t plastic waste are near critically endangered and endangered corals. These overlapping pressures threaten key species, ecosystems, and the ocean's role in climate stability. These findings underscore the need for enhanced and sustained ocean observing systems, improved information on uncertainties in indicator design, and robust science-based information to guide policy, planning, and action for protecting the ocean. The ocean is our sentinel, reflecting the health of the planet and the trajectory of future environmental changes. Protecting the ocean through concerted global cooperation informed by integrated evidence-based and strategic ocean knowledge is essential to ensure the ocean can continue to play its crucial role in sustaining life and regulating Earth's climate.

1 Introduction

The ocean, often viewed as a vast remote frontier, is increasingly recognized as central in maintaining the planet's environmental balance (Bindoff et al., 2019). The ocean regulates global temperatures (von Schuckmann et al., 2023), absorbs anthropogenic carbon dioxide (Friedlingstein et al., 2025), and sustains biodiversity in ways that are vital for life on Earth (IPBES, 2019; Ward et al., 2022). The ocean's ability to act as a natural buffer against climate change – from absorbing heat to moderating weather patterns – makes it vital for global environmental health. The protection of the ocean is hence essential, not only for preserving the health of marine life, but as an active integral force driving environmental resilience for the stability of the planet's climate, ecosystems, and long-term sustainability (Horton and Horton, 2019; Roberts et al., 2024; Yadav and Gjerde, 2020). The essential role of the ocean in sustaining life is receiving heightened recognition – not just as a source of economic opportunity (Jouffray et al., 2020), but as a fundamental pillar for achieving environmental and societal goals (Hoegh-Guldberg et al., 2019).

Providing regular reporting on global and regional ocean indicators offers the opportunity for a broader perspective of ocean change, which allows us to monitor larger systemic

Published by Copernicus Publications.

shifts or changes in the ocean state and climate and allows informed decision-making, international cooperation, and the development of strategies to address both local and global challenges. Some of the ocean changes are inherently global in nature, such as the ocean carbon and heat sink, revealing insight into overall trends that transcend regional boundaries (Friedlingstein et al., 2025; von Schuckmann et al., 2023; Xing et al., 2024). Also, a global perspective allows us to identify changes in interconnected systems, such as the water, carbon, or energy cycle of the Earth, and their ultimate influence worldwide (Barnard et al., 2021; Cheng et al., 2022; Talukder et al., 2022).

Global-scale ocean indicators are effective in informing multilateral and international policy developments and international cooperation, which is essential today, as the ocean is faced with transboundary pressures, such as climate change, pollution, overexploitation, and biodiversity loss (Evans et al., 2025; Polejack, 2021; Ryabinin et al., 2019; von Schuckmann et al., 2020). They can highlight how environmental issues are disproportionately affecting different regions, helping to strengthen the voice of vulnerable communities not overlooked in environmental policies. This can foster more equitable solutions in areas where regional data might mask global patterns of inequality in environmental impacts. Also, global-scale indicators can serve as benchmarks to track progress towards common goals, such as in the context of the 2030 Agenda for Sustainable Development or under the UN Decade of Ocean Science for Sustainable Development. By monitoring ocean and climate change globally, it is possible to identify emerging risks and understand the global capacity for resilience (Abraham et al., 2022; Bouwer et al., 2022; Izaguirre et al., 2021; Rockström et al., 2021).

Here, we provide an ocean narrative to tell a compelling story that communicates the ongoing change in the global ocean in relation to people and the planet, while also drawing on implications from the triple planetary crisis of biodiversity loss, climate change, and pollution (UNEP, 2021). Besides global mean indicators, the concept of large marine ecosystems (LMEs) (Sherman, 2005) – which encompass coastal areas, from river basins and estuaries to the seaward boundaries of continental shelves, along with enclosed and semi-enclosed seas and the outer margins of major current systems – is also addressed. LMEs are of significant socioeconomic importance, as they account for the majority of global fisheries biomass (Guiet et al., 2025; Sherman et al., 2009). Additionally, areas beyond national jurisdiction are included, enabling a comparison between changes occurring in the open ocean and those observed within large marine ecosystems. This narrative aims to further connect scientific understanding with social, economic, and cultural dimensions, helping audiences grasp why there are changes in ocean matter. It aims not only to raise awareness but also to shape how we perceive risks, responsibilities, and opportunities – ultimately encouraging informed decision-making and collective action for a sustainable and healthy ocean future.

2 Method

This study employs a structured multi-indicator approach to describe and assess the state of and change in the ocean. The analysis is grounded in a core set of ocean indicators, which include surface and subsurface ocean warming, surface ocean acidification, sea level rise, and marine heatwaves. These indicators are derived using scientifically validated methods and form part of the Copernicus Ocean Indicator Framework (see Product Table, Supplement).

Primary data sources include products from the Copernicus Marine Service, which are supplemented, where available, by additional publicly accessible datasets to enhance spatial and temporal coverage. A multi-product methodology is applied wherever feasible, combining data from different ocean products. This approach enables an assessment of internal consistency and uncertainty by comparing the spread across product ensembles. Uncertainty ranges are obtained using standard deviation at the 95 % confidence level. A regional trend is considered amplified relative to the global trend when its 95 % confidence interval lies entirely above the global trend. All datasets utilized are documented and referenced in the product table, including links to associated metadata and scientific publications. Each ocean indicator has been updated with the most recent data available at the time of analysis, subject to product-specific update frequencies and data availability constraints.

To integrate the physical changes in the marine environment with broader sustainable development perspectives, additional datasets from the economic and social domains were included. This integrative approach reflects the three pillars of sustainability: environmental, economic, and social. Only data that are publicly available and accompanied by appropriate metadata were used. Metadata documentation and source references are provided in the product table. The three domains – environment, economy, and society – were then brought together to develop an ocean narrative, aimed at contextualizing observed and reported changes. This narrative is not intended as a new quantitative scientific analysis, but rather as a synthesis of available information to support decision-making and communication. Scientific rigour is maintained by basing this synthesis on peer-reviewed literature and established datasets, ensuring an evidence-based assessment framework underpins the development of the narrative.

3 Tracking ocean change: ocean warming, ocean acidification, sea level rise, and Earth's energy imbalance

The global ocean is undergoing widespread and accelerating change. Global ocean warming reached record levels in 2024, continuing a long-term trend in ocean heat uptake at a rate of $0.35 \pm 0.1\,\mathrm{W\,m^{-2}}$ ($0.61 \pm 0.2\,\mathrm{W\,m^{-2}}$ with ocean surface), with a steady acceleration of $0.14 \pm 0.1\,\mathrm{W\,m^{-2}}$ per

decade since the 1960s (Fig. 1). The rate of ocean heat content (OHC) has increased since the 1960s, shifting from a near-equilibrium state in Earth's energy balance to a positive Earth energy imbalance of approximately $0.71 \pm 0.1\,\mathrm{W\,m^{-2}}$ (rel. to the top of the atmosphere) over the 2015–2024 average (Fig. 1a, updated from Minière et al., 2023). Ocean warming undergoes large decadal variations over the period 1960–2024, influenced by massive volcanic eruptions (Fig. 1a) (Trenberth et al., 2014). The acceleration of ocean warming remains consistent across different time periods, with no significant increase observed over the past 2 decades (Fig. 1b).

Global ocean surface temperatures in 2023 and 2024 reached exceptional highs, temporarily exceeding 21 °C on average, reflecting the combined effect of long-term climate-driven warming and natural variability. The global mean sea surface temperature (SST) has increased from decade to decade since satellite records began in 1982 (Fig. 1c). The global mean sea surface temperature exceeded 21 °C during the boreal spring of 2024 – an unprecedented high on record – and, while slightly lower in 2025, remains well above the long-term reference baseline (Fig. 1c). In both 2023 and 2024, intense, persistent, and widespread marine heatwaves were reported in several areas of the global ocean, exceeding previous ocean surface temperature records (e.g. 2015/2016) by 0.25 °C (Terhaar et al., 2025). The record ocean surface temperatures observed are the result of natural variability intensified by long-term global warming – an event that would have been highly unlikely in the absence of the ongoing climate trend (Guinaldo et al., 2025; Terhaar et al., 2025).

Global mean sea level is rising at an accelerating pace, reaching record-high values in 2024. The highest decadal average rate of increase – $4.1 \pm 0.1\,\mathrm{mm\,yr^{-1}}$ – was observed over the period 2016 to 2024. This value is slightly lower than the estimated $4.5\,\mathrm{mm\,yr^{-1}}$ estimated over the period 2017–2024 by Hamlington et al. (2024). Rates of global mean sea level rise increased from 31.4 ± 1.1 mm per decade in 1999–2006 to 39.3 ± 0.8 mm per decade in 2007–2015 to 40.8 ± 1.1 mm per decade in 2016–2024 (Fig. 1d). This amounts to a 25 % increase from the 1990s (1999–2006) to the 2000s (2007–2015), then +4 % for 2007–2015 to the 2010s (2016–2024), resulting in +30 % from the late 1990s to the 2010s (Fig. 1d). Over the period 1901–2024, global mean sea level rise amounts to 228 mm (Forster et al., 2025). Causes of sea level rise are attributed to increasing ice loss from the Greenland and Antarctic ice sheets, ongoing glacier mass loss, and thermal expansion due to ocean warming (WMO, 2025; IPCC, 2021).

4 Ocean warming and acidification: marine biodiversity, ocean protection, and the high seas

Regionally, the ocean is undergoing rapid change, with both warming and acidification occurring at rates above the global average largely affecting the tropics, the northern subtropics, and the southern subpolar ocean areas. Ocean warming from the ocean surface to depth (0–2000 m) at rates exceeding the global mean rates covers 15 % of the ocean area in the tropics (15° S–15° N), 41 % of the northern subtropics (20–40° N), and 16 % in the southern subpolar ocean areas (40–60° S) (Fig. 1e). A total of 13 % of the ocean areas in the tropics, 55 % of the northern subtropics, and 60 % of the southern subpolar ocean areas are exposed to rapid ocean acidification above global mean rates (Fig. 1e). Ocean areas which are concurrently experiencing both rapid ocean acidification and ocean warming are centred around 42° S and 36° N (31 % and 42 % of the ocean area, respectively). In contrast, ocean areas not experiencing rapid ocean acidification or warming are limited to 24 % in the northern subtropics and 34 % in the southern subpolar oceans.

Marine biodiversity is exposed to changes in the physics and biogeochemistry of the ocean. A total of 8 % of marine biodiversity hotspots are experiencing rapid ocean warming above global rates, and 10 % are experiencing surface acidification at rates exceeding the global average. Ocean warming and ocean acidification are known to induce a decline in species richness and harm habitats (Alter et al., 2024; Chaudhary et al., 2021; ter Hofstede et al., 2010; Wernberg et al., 2011). The species richness of many groups in marine biodiversity has been shown to decline from the Equator to the poles, but exceptions such as baleen whales and seafloor species near nutrient-rich margins reveal complex patterns (IPBES, 2019, Chap. 2). Ocean biodiversity hotspots are challenging to define due to widespread species dispersal, but unique habitats, such as the warm-water shallow coral reefs of the western Pacific, are characterized for their rich marine life (IPBES, 2019, Chap. 2; Fig. 2) (Tittensor et al., 2010).

Areas Beyond National Jurisdiction (ABNJ) have been warming at an average rate of $0.58 \pm 0.1\,\mathrm{W\,m^{-2}}$ since the 1960s, and their pH has been decreasing at a rate of -0.0173 ± 0.001 since the early 1980s, with 14 % of ABNJ facing rapid ocean warming exceeding the global rate and 32 % facing rapid surface ocean acidification (Fig. 2). These changes highlight the urgent need to accelerate progress toward the 30 × 30 target, protecting 30 % of coastal and marine waters by 2030 (UNGA, 2023). Although ABNJ – encompassing the high seas (UNCLOS, art. 86) and seabed (UNCLOS, art. 1) – cover 60 % of the global ocean and support complex ecosystems vital to life and essential services, they remain largely unprotected, and increasing pressures from human activities threaten their health (Gjerde et al., 2016). Fishing in high seas poses the greatest threat to marine biodiversity in ABNJ, disrupting entire ecosystems, while shipping and deep-sea mining are also growing concerns (Caldeira et al., 2023). The share of protected marine territorial waters is unevenly spread across the globe (Fig. 2). Advances are underway as global criteria for Marine Protected Areas are increasingly unified, recognizing their role

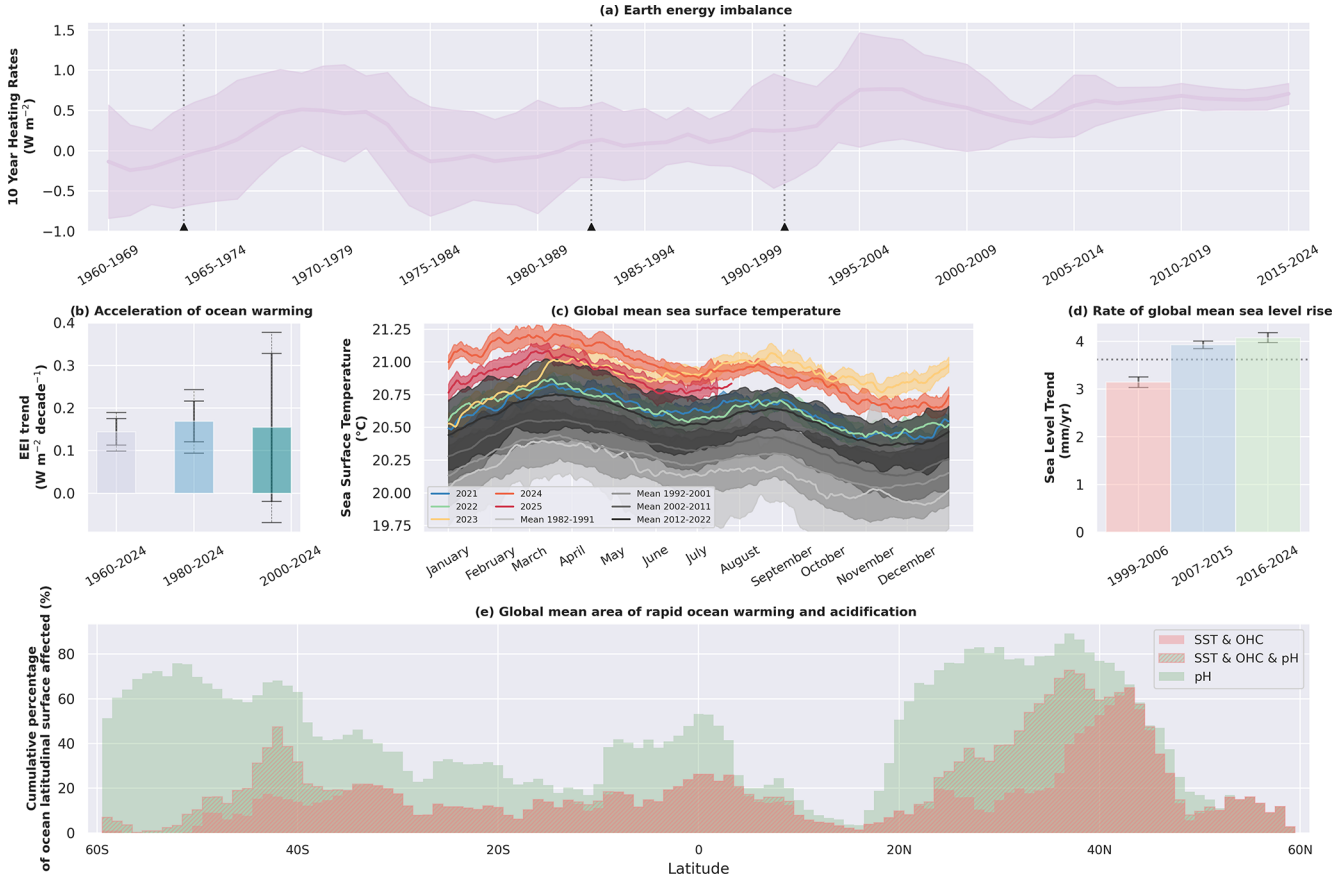

Figure 1. Ocean change acceleration. **(a)** Earth's energy imbalance for the period 1960–2024, with the 95 % uncertainty range shown by shading, based on product ref. no. 1 (Minière et al., 2023). Vertical dashed lines show massive volcanic eruptions from product ref. no. 1. **(b)** Acceleration of the ocean warming for past periods of 64, 44, and 24 years, with the 95 % uncertainty range shown by solid whiskers, based on product ref. no. 1 (Minière et al., 2023). Dashed whiskers indicate the 95 % uncertainty range based on product ref. no. 1 (Minière et al., 2023). **(c)** Global mean surface temperature. Gradients of grey show decadal means (bold lines) and 95 % uncertainty ensemble ranges (shadings) for the period 1982–2022, based on product ref. no. 2. Similarly, the years 2021 to 2025 are shown in colours, based on product ref. no. 3, with the 95 % uncertainty range based on product ref. nos. 3–7 and 21. **(d)** Rate of global sea level rise for the periods 1999–2006, 2007–2015, and 2016–2024, with the 95 % uncertainty range shown by whiskers, based on product ref. no. 8. The horizontal dashed line indicates the trend for the period 1999–2024. **(e)** Cumulative percentage of ocean latitudinal surface (%) experiencing rapid warming (pink), rapid acidification (green), and both rapid changes (pink and green hatches) for the periods 1982–2024 for SST (based on product ref. nos. 2, 4–7, and 21), 1982–2024 for OHC (based on product ref. nos. 9–11), and 1985–2022 for pH (based on product ref. no. 12).

in climate mitigation and embracing broader goals such as sustainability, resilience, and ecosystem health (Maestro et al., 2019).

At the regional level, a total of 8 % of LME areas show rapid ocean warming exceeding the global average rate, 9 % of tropical LME areas show rapid ocean warming, and 7 % show rapid ocean acidification (Fig. 2). For the subpolar LME, the share of impacted areas amounts to 9 % for ocean warming and 6 % for ocean acidification (Fig. 2). Estimates for polar LMEs are challenging due to data limitations resulting from measurement gaps in these areas.

5 The ocean under the triple planetary crisis

No part of the ocean is untouched by the triple planetary crisis, as pollution, biodiversity loss, and climate change are putting pressure on the ocean worldwide (Fig. 3). In 2022, the United Nations General Assembly endorsed the declaration "our ocean, our future, our responsibility", recognizing the ocean's vital role in sustaining life and affirming the urgency of its conservation and sustainable use (UNGA, 2022). However, the reality remains deeply concerning. Despite regional differences, plastic waste from land is polluting all ocean basins (Fig. 3). Rapid ocean warming, acidification, and sea level rise exceeding global mean trends are impacting all ocean basins (Fig. 3), threatening both marine ecosys-

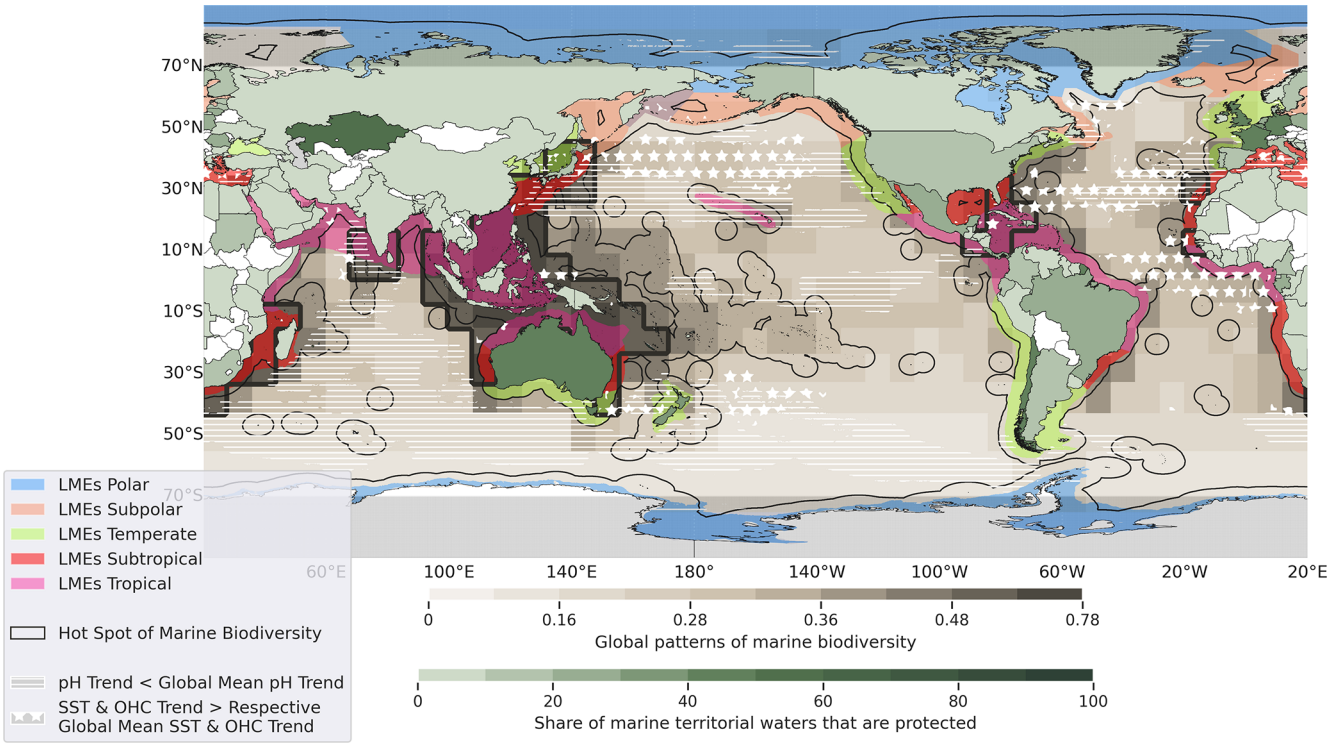

Figure 2. Biodiversity of the ocean under rapid changes. Global patterns of marine biodiversity shown in the ocean (brown gradient, product ref. no. 13), with hotspots surrounded by bold dark-brown polygons (product ref. no. 13). Share of marine territorial waters that are protected in 2022 shown on land (green gradient, product ref. no. 14). Large marine ecosystems (LMEs; product ref. no. 15) are shown in colours along the coasts. The boundaries of Areas Beyond National Jurisdiction (ABNJ) are materialized by black lines off the coasts (product ref. no. 16). Stars represent where 95 % of the local sea surface temperature (SST) and ocean heat content (OHC) trend ranges surpass the global average for the period 1982–2024, based on product ref. nos. 2, 4–6, 9–11, and 21. Horizontal hatching is the same but for the pH trend for the period 1985–2022, based on product ref. no. 12. The Caspian Sea is shaded in grey, as data were not available, except for the share of marine territorial waters of the surrounding countries.

tems and human communities (Bindoff et al., 2019; IPCC, 2022). Biodiversity loss and the degradation of marine habitats are also threatening the foundation of ocean life across all ocean basins (Fig. 3; IPBES, 2019). Although the global data products suffer from limitations in the polar areas due to measurement gaps (Fig. 3, grey mask), region-specific studies show high consensus that these ocean areas are also faced with pollution, biodiversity loss, and climate change (Bindoff et al., 2019; Cai et al., 2023; De-la-Torre et al., 2024; Gutt et al., 2021; IPBES, 2019; Linse et al., 2021; Nissen et al., 2024; Qi et al., 2022; Thomas et al., 2022; Townhill et al., 2022).

The triple planetary crisis converges across all ocean basins. About 16 % (30 %) of endangered (critically endangered) corals are exposed to rapid ocean warming or acidification, putting already at-risk species under even greater pressure (Fig. 3). Nearly 75 % of countries with high plastic waste emissions (> 10 000 t) are adjacent to critically endangered and endangered corals, and 83 % are adjacent to vulnerable corals (Fig. 3). These pressures are deeply interconnected: plastic pollution contributes to climate change and accelerates biodiversity loss (Ford et al., 2022; IPBES, 2019; Jeong et al., 2024), while climate change itself is a major driver of species decline (Bindoff et al., 2019; IPBES, 2019; IPCC, 2022). These reinforcing interactions intensify the overall crisis, making it more urgent to address them together. Plastic pollution poses a well-documented threat to coral reefs (Akhtar et al., 2022), with most large plastic items accumulating along shorelines (Lebreton et al., 2019). Tuna fisheries play a crucial role in global food systems – especially in Oceania – and carry important cultural, social, and public health value (Bell et al., 2015, 2021; Fache and Pauwels, 2016), and they are faced with key stressors from ocean warming and acidification (Fig. 3) known to threaten their survival (Monllor-Hurtado et al., 2017; Erauskin-Extramiana et al., 2019; Nicol et al., 2022). Tuna is classified as endangered or vulnerable in all ocean areas south of 40° N, and large parts of these areas are affected by rapid ocean warming and/or ocean acidification (Fig. 3).

Ocean warming can increase the degradation of plastics into microplastics (Ford et al., 2022), and about 33 % of high-emitting countries for plastics (> 10 000 t) are adjacent to

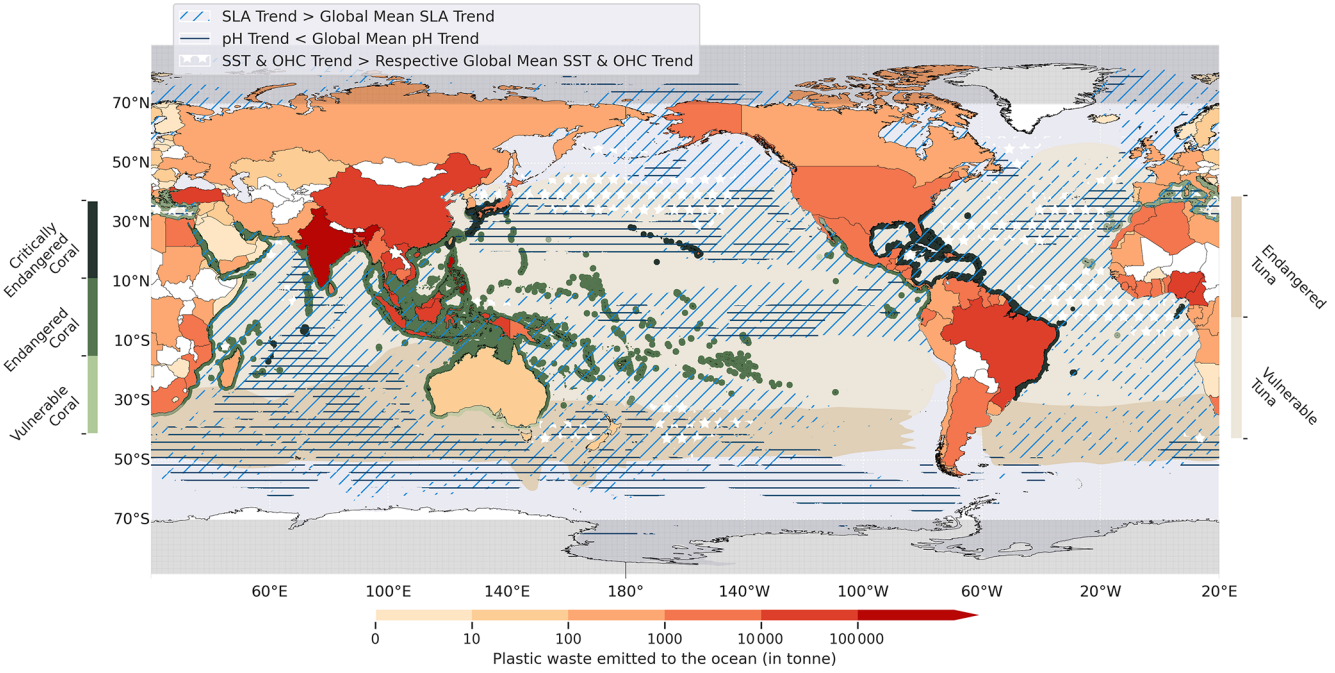

Figure 3. Illustration of the triple planetary crisis. Plastic waste emitted into the ocean by each country is shown on land (red gradient, product ref. no. 17). Vulnerable and endangered tuna is shown in oceans (sand–grey gradient, product ref. no. 18). Vulnerable, endangered, and critically endangered coral is shown with a green gradient (product ref. no. 19). Stars represent where the local sea surface temperature (SST) and ocean heat content (OHC) trends surpass the global average for the period 1982–2024, based on product ref. nos. 2, 4–6, 9–11, and 21. Horizontal hatching is the same, but for the pH trend, for the period 1985–2022, based on product ref. no. 12. Oblique hatching shows where the local sea level rise (SLR) trend surpasses the global trend for the period 1999–2024, based on product ref. no. 20.

areas of rapid ocean warming (Fig. 3). Once in the ocean, plastics break down into microplastics, which also originate directly from sources such as cosmetics, plastic pellets, synthetic textiles, and the wear of tyres and road markings (Woodall et al., 2014). Microplastics can harm marine life, carry toxic chemicals through the food web, and alter water and sediment properties, disrupting ecosystems and biodiversity (Jeong et al., 2024; Li et al., 2024; Lorenz et al., 2019). At the land–ocean interface, sea level rise and plastic pollution intersect, amplifying environmental risks. The majority (92 %) of countries emitting more than 10 000 t of plastic waste also face sea level rise in adjacent ocean areas that exceeds global rates (Fig. 3). Rising seas exacerbate coastal erosion and flooding, increasing the transport of microplastics from land-based sources – such as landfills, waste facilities, and sewage systems – into the ocean (Tang, 2023).

6 Conclusion

Together, these findings provide clear evidence that the ocean is not only a key regulator of the Earth's climate system but also one of the most sensitive global climate indicators of ongoing and accelerating global change. The simultaneous rises in ocean heat content, acidification, and sea level are not isolated; they are interconnected, compounding, and increasingly persistent. They affect the ocean physics and biogeochemistry, the functioning of marine ecosystems, and the wellbeing of coastal societies that depend on them. As scientific analysis and reporting continue to reach more and more robust consensus, the message becomes more urgent: sustained and coordinated measuring, modelling, and monitoring of the ocean are essential to understanding the pace of planetary change and informing decisions that affect climate resilience, biodiversity, and long-term sustainability. The ocean is our sentinel for all our futures to come.

Changes from ocean warming, ocean acidification, and sea level rise are further exacerbated by the adverse impacts of plastic pollution and biodiversity loss. Notably, the changes in ocean warming and sea level rise are not merely linear trends but rather exhibit acceleration over time, indicating that we are facing increasingly rapid change and underscoring the critical need for a unified global response and integrated evidence-based approaches. As ocean health is intricately linked to climate stability, the urgency of addressing these interconnected and rapid environmental pressures cannot be overstated. Only through collective efforts can we ensure the resilience of marine ecosystems and secure the future of our planet's ocean-based resources.

The rapid and interconnected changes occurring in the ocean also demand coordinated and global responses to sus-

tain and strengthen our capacities for monitoring and understanding these changes. Sustained and enhanced ocean observation systems are critical for filling data gaps, particularly in polar and under-monitored regions, and for providing more accurate, real-time information on, for example, ocean warming, acidification, and sea level rise. Expanding these systems, alongside advancements in improved data integration, dissemination, and modelling, will empower decision-makers with the evidence-based and digital knowledge necessary to support sustainable ocean stewardship and to safeguard and protect the ocean. With more comprehensive, timely, and accessible ocean data, we can better address the triple planetary crisis and strengthen the resilience of marine life, ensuring that the ocean can continue to fulfil its vital role in sustaining life on Earth.

As we face increasing and compound impacts of ocean change, the need for high-resolution, evidence-based information becomes even more urgent. While global indicators provide essential insights into overarching trends, uncertainties highlight the importance of strengthening regional and local monitoring systems, forecasts, early warning systems, and downscaled projections. The scientific community must take a more proactive role in ensuring that data products derived from observations and models, along with the indicators based on them, are accompanied by robust uncertainty frameworks. These frameworks should be grounded in scientific principles and methodologies to accurately quantify and communicate the uncertainties inherent in these indicators. This is crucial for enhancing the reliability of the data and indicators, making them more actionable for decision-makers. By incorporating well-informed uncertainty analyses into data products, we can provide policymakers with clearer, more reliable guidance, enabling more effective planning and adaptive management strategies in response to ocean change.

Code availability. All codes are available upon request.

Data availability. All data used are available, and their sources are listed in the Supplement.

Supplement. The supplement related to this article is available online at https://doi.org/10.5194/sp-6-osr9-2-2025-supplement.

Author contributions. KvS: conceptualization, designing, methodology, writing (original draft), investigation, supervision, and formal analysis. FG: conceptualization and analysis. All authors: writing (review and editing).

Competing interests. At least one of the (co-)authors is a member of the editorial board of *State of the Planet*. The peer-review process was guided by an independent editor, and the authors also have no other competing interests to declare.

Disclaimer. Please note that this article has undergone editorial review only.

Publisher's note: Copernicus Publications remains neutral with regard to jurisdictional claims made in the text, published maps, institutional affiliations, or any other geographical representation in this paper. While Copernicus Publications makes every effort to include appropriate place names, the final responsibility lies with the authors. Views expressed in the text are those of the authors and do not necessarily reflect the views of the publisher.

Financial support. This research was carried out as part of the Copernicus Marine service implemented by MOi under a contributing agreement with the European Commission, and "Ocean observations and indicators for climate and assessments" (ObsSea4Clim) is funded by the European Union Horizon Europe Funding Programme for Research and Innovation under grant no. 101136548. This is ObsSea4Clim contribution no. 18.

References

Abraham, J., Cheng, L., Mann, M. E., Trenberth, K., and von Schuckmann, K.: The ocean response to climate change guides both adaptation and mitigation efforts, Atmospheric and Oceanic Science Letters, 15, 100221, https://doi.org/10.1016/j.aosl.2022.100221, 2022.

Akhtar, R., Sirwal, Mohd. Y., Hussain, K., Dar, M. A., Shahnawaz, M., and Daochen, Z.: Impact of Plastic Waste on the Coral Reefs: An Overview, in: Impact of Plastic Waste on the Marine Biota, Springer Nature Singapore, Singapore, 239–256, https://doi.org/10.1007/978-981-16-5403-9_13, 2022.

Alter, K., Jacquemont, J., Claudet, J., Lattuca, M. E., Barrantes, M. E., Marras, S., Manríquez, P. H., González, C. P., Fernández, D. A., Peck, M. A., Cattano, C., Milazzo, M., Mark, F. C., and Domenici, P.: Hidden impacts of ocean warming and acidification on biological responses of marine animals revealed through meta-analysis, Nat. Commun., 15, 2885, https://doi.org/10.1038/s41467-024-47064-3, 2024.

Barnard, P. L., Dugan, J. E., Page, H. M., Wood, N. J., Hart, J. A. F., Cayan, D. R., Erikson, L. H., Hubbard, D. M., Myers, M. R., Melack, J. M., and Iacobellis, S. F.: Multiple climate change-driven tipping points for coastal systems, Sci. Rep., 11, 15560, https://doi.org/10.1038/s41598-021-94942-7, 2021.

Bell, J. D., Allain, V., Allison, E. H., Andréfouët, S., Andrew, N. L., Batty, M. J., Blanc, M., Dambacher, J. M., Hampton, J., Hanich, Q., Harley, S., Lorrain, A., McCoy, M., McTurk, N., Nicol, S., Pilling, G., Point, D., Sharp, M. K., Vivili, P., and Williams, P.: Diversifying the use of tuna to improve food security and public health in Pacific Island countries and territories, Mar. Policy, 51, 584–591, https://doi.org/10.1016/j.marpol.2014.10.005, 2015.

Bell, J. D., Senina, I., Adams, T., Aumont, O., Calmettes, B., Clark, S., Dessert, M., Gehlen, M., Gorgues, T., Hampton, J., Hanich, Q., Harden-Davies, H., Hare, S. R., Holmes, G.,

Lehodey, P., Lengaigne, M., Mansfield, W., Menkes, C., Nicol, S., Ota, Y., Pasisi, C., Pilling, G., Reid, C., Ronneberg, E., Gupta, A. Sen, Seto, K. L., Smith, N., Taei, S., Tsamenyi, M., and Williams, P.: Pathways to sustaining tuna-dependent Pacific Island economies during climate change, Nat. Sustain., 4, 900–910, https://doi.org/10.1038/s41893-021-00745-z, 2021.

Bindoff, N. L., Cheung, W. W. L., Kairo, J. G., Aristegui, J., Guinder, V. A., Hallberg, R., Hilmi, N., Jiao, N., Karim, M. S., Levin, L., O'Donoghue, S., Purca Cuicapusa, S. R., Rinkevich, B., Suga, T., Tagliabue, A., and Williamson, P.: Changing Ocean, Marine Ecosystems, and Dependent Communities, in: IPCC Special Report on the Ocean and Cryosphere in a Changing Climate, edited by: Pörtner, H.-O., Roberts, D. C., Masson-Delmotte, V., Zhai, P., Tignor, M., Poloczanska, E., Mintenbeck, K., Alegria, A., Nicolai, M., Okem, A., Petzold, J., Rama, B., and Weyer, N. M., Cambridge University Press, Cambridge, UK and New York, NY, USA, 447–587, https://doi.org/10.1017/9781009157964.007, 2019.

Bouwer, L. M., Cheong, S.-M., Jacot Des Combes, H., Frölicher, T. L., McInnes, K. L., Ratter, B. M. W., and Rivera-Arriaga, E.: Risk Management and Adaptation for Extremes and Abrupt Changes in Climate and Oceans: Current Knowledge Gaps, Front. Clim., 3, 785641, https://doi.org/10.3389/fclim.2021.785641, 2022.

Cai, W., Gao, L., Luo, Y., Li, X., Zheng, X., Zhang, X., Cheng, X., Jia, F., Purich, A., Santoso, A., Du, Y., Holland, D. M., Shi, J.-R., Xiang, B., and Xie, S.-P.: Southern Ocean warming and its climatic impacts, Sci. Bull., 68, 946–960, https://doi.org/10.1016/j.scib.2023.03.049, 2023.

Caldeira, M., Teixeira, H., and Hilário, A.: Negotiations to implement area-based management tools beyond national jurisdiction: the scientific community's view, Front. Mar. Sci., 10, 1173682, https://doi.org/10.3389/fmars.2023.1173682, 2023.

Chaudhary, C., Richardson, A. J., Schoeman, D. S., and Costello, M. J.: Global warming is causing a more pronounced dip in marine species richness around the equator, P. Natl. Acad. Sci. USA, 118, e2015094118, https://doi.org/10.1073/pnas.2015094118, 2021.

Cheng, L., von Schuckmann, K., Abraham, J. P., Trenberth, K. E., Mann, M. E., Zanna, L., England, M. H., Zika, J. D., Fasullo, J. T., Yu, Y., Pan, Y., Zhu, J., Newsom, E. R., Bronselaer, B., and Lin, X.: Past and future ocean warming, Nat. Rev. Earth Environ., 3, 776–794, https://doi.org/10.1038/s43017-022-00345-1, 2022.

De-la-Torre, G. E., Santillán, L., Dioses-Salinas, D. C., Yenney, E., Toapanta, T., Okoffo, E. D., Kannan, G., Madadi, R., and Dobaradaran, S.: Assessing the current state of plastic pollution research in Antarctica: Knowledge gaps and recommendations, Chemosphere, 355, 141870, https://doi.org/10.1016/j.chemosphere.2024.141870, 2024.

Erauskin-Extramiana, M., Arrizabalaga, H., Hobday, A. J., Cabré, A., Ibaibarriaga, L., Arregui, I., Murua, H., and Chust, G.: Large-scale distribution of tuna species in a warming ocean, Glob. Chang. Biol., 25, 2043–2060, https://doi.org/10.1111/gcb.14630, 2019.

Evans, K., Schmidt, J. O., Addo, K. A., Bebianno, M. J., Campbell, D., Fan, J., Gonzalez-Quiros, R., Mohammed, E. Y., Shojaei, M. G., Smolyanitsky, V., and Zhang, C.-I.: Delivering scientific evidence for global policy and management to ensure ocean sustainability, Sustain. Sci., 20, 299–306, https://doi.org/10.1007/s11625-024-01579-2, 2025.

Fache, E. and Pauwels, S.: Fisheries in the Pacific: The Challenges of Governance and Sustainability, Pacific-Credo Publications, https://doi.org/10.4000/books.pacific.395, 2016.

Ford, H. V., Jones, N. H., Davies, A. J., Godley, B. J., Jambeck, J. R., Napper, I. E., Suckling, C. C., Williams, G. J., Woodall, L. C., and Koldewey, H. J.: The fundamental links between climate change and marine plastic pollution, Sci. Total Environ., 806, 150392, https://doi.org/10.1016/j.scitotenv.2021.150392, 2022.

Forster, P. M., Smith, C., Walsh, T., Lamb, W. F., Lamboll, R., Cassou, C., Hauser, M., Hausfather, Z., Lee, J.-Y., Palmer, M. D., von Schuckmann, K., Slangen, A. B. A., Szopa, S., Trewin, B., Yun, J., Gillett, N. P., Jenkins, S., Matthews, H. D., Raghavan, K., Ribes, A., Rogelj, J., Rosen, D., Zhang, X., Allen, M., Aleluia Reis, L., Andrew, R. M., Betts, R. A., Borger, A., Broersma, J. A., Burgess, S. N., Cheng, L., Friedlingstein, P., Domingues, C. M., Gambarini, M., Gasser, T., Gütschow, J., Ishii, M., Kadow, C., Kennedy, J., Killick, R. E., Krummel, P. B., Liné, A., Monselesan, D. P., Morice, C., Mühle, J., Naik, V., Peters, G. P., Pirani, A., Pongratz, J., Minx, J. C., Rigby, M., Rohde, R., Savita, A., Seneviratne, S. I., Thorne, P., Wells, C., Western, L. M., van der Werf, G. R., Wijffels, S. E., Masson-Delmotte, V., and Zhai, P.: Indicators of Global Climate Change 2024: annual update of key indicators of the state of the climate system and human influence, Earth Syst. Sci. Data, 17, 2641–2680, https://doi.org/10.5194/essd-17-2641-2025, 2025.

Friedlingstein, P., O'Sullivan, M., Jones, M. W., Andrew, R. M., Hauck, J., Landschützer, P., Le Quéré, C., Li, H., Luijkx, I. T., Olsen, A., Peters, G. P., Peters, W., Pongratz, J., Schwingshackl, C., Sitch, S., Canadell, J. G., Ciais, P., Jackson, R. B., Alin, S. R., Arneth, A., Arora, V., Bates, N. R., Becker, M., Bellouin, N., Berghoff, C. F., Bittig, H. C., Bopp, L., Cadule, P., Campbell, K., Chamberlain, M. A., Chandra, N., Chevallier, F., Chini, L. P., Colligan, T., Decayeux, J., Djeutchouang, L. M., Dou, X., Duran Rojas, C., Enyo, K., Evans, W., Fay, A. R., Feely, R. A., Ford, D. J., Foster, A., Gasser, T., Gehlen, M., Gkritzalis, T., Grassi, G., Gregor, L., Gruber, N., Gürses, Ö., Harris, I., Hefner, M., Heinke, J., Hurtt, G. C., Iida, Y., Ilyina, T., Jacobson, A. R., Jain, A. K., Jarníková, T., Jersild, A., Jiang, F., Jin, Z., Kato, E., Keeling, R. F., Klein Goldewijk, K., Knauer, J., Korsbakken, J. I., Lan, X., Lauvset, S. K., Lefèvre, N., Liu, Z., Liu, J., Ma, L., Maksyutov, S., Marland, G., Mayot, N., McGuire, P. C., Metzl, N., Monacci, N. M., Morgan, E. J., Nakaoka, S.-I., Neill, C., Niwa, Y., Nützel, T., Olivier, L., Ono, T., Palmer, P. I., Pierrot, D., Qin, Z., Resplandy, L., Roobaert, A., Rosan, T. M., Rödenbeck, C., Schwinger, J., Smallman, T. L., Smith, S. M., Sospedra-Alfonso, R., Steinhoff, T., Sun, Q., Sutton, A. J., Séférian, R., Takao, S., Tatebe, H., Tian, H., Tilbrook, B., Torres, O., Tourigny, E., Tsujino, H., Tubiello, F., van der Werf, G., Wanninkhof, R., Wang, X., Yang, D., Yang, X., Yu, Z., Yuan, W., Yue, X., Zaehle, S., Zeng, N., and Zeng, J.: Global Carbon Budget 2024, Earth Syst. Sci. Data, 17, 965–1039, https://doi.org/10.5194/essd-17-965-2025, 2025.

Gjerde, K. M., Reeve, L. L. N., Harden-Davies, H., Ardron, J., Dolan, R., Durussel, C., Earle, S., Jimenez, J. A., Kalas, P., Laffoley, D., Oral, N., Page, R., Ribeiro, M. C., Rochette, J., Spadone, A., Thiele, T., Thomas, H. L., Wagner, D., Warner, R., Wilhelm, À., and Wright, G.: Protecting Earth's last conservation frontier: scientific, management and legal priorities for

MPAs beyond national boundaries, Aquat. Conserv., 26, 45–60, https://doi.org/10.1002/aqc.2646, 2016.

Guiet, J., Bianchi, D., Scherrer, K. J. N., Heneghan, R. F., and Galbraith, E. D.: Small Commercial Fish Biomass Limits the Catch Potential in the High Seas, Earths Future, 13, e2024EF004571, https://doi.org/10.1029/2024EF004571, 2025.

Guinaldo, T., Cassou, C., Sallée, J. B., and Liné, A.: Internal variability effect doped by climate change drove the 2023 marine heat extreme in the North Atlantic, Commun. Earth Environ., 6, 1–11, https://doi.org/10.1038/s43247-025-02197-1, 2025.

Gutt, J., Isla, E., Xavier, J. C., Adams, B. J., Ahn, I., Cheng, C. -H. C., Colesie, C., Cummings, V. J., di Prisco, G., Griffiths, H., Hawes, I., Hogg, I., McIntyre, T., Meiners, K. M., Pearce, D. A., Peck, L., Piepenburg, D., Reisinger, R. R., Saba, G. K., Schloss, I. R., Signori, C. N., Smith, C. R., Vacchi, M., Verde, C., and Wall, D. H.: Antarctic ecosystems in transition – life between stresses and opportunities, Biol. Rev., 96, 798–821, https://doi.org/10.1111/brv.12679, 2021.

Hamlington, B., Bellas-Manley, A., Willis, J., Fournier, S., Vinogradova, N., Nerem, R., Piecuch, C., Thompson, P., and Kopp, R.: The rate of global sea level rise doubled during the past three decades, Commun. Earth Environ., 5, 1–4, https://doi.org/10.1038/s43247-025-02197-1, 2024

Hoegh-Guldberg, O., Northrop, E., and Lubchenco, J.: The ocean is key to achieving climate and societal goals, Science, 365, 1372–1374, https://doi.org/10.1126/science.aaz4390, 2019.

Horton, P. and Horton, B. P.: Re-defining Sustainability: Living in Harmony with Life on Earth, One Earth, 1, 86–94, https://doi.org/10.1016/j.oneear.2019.08.019, 2019.

IPBES: Global assessment report on biodiversity and ecosystem services of the Intergovernmental Science-Policy Platform on Biodiversity and Ecosystem Services, Zenodo, https://doi.org/10.5281/zenodo.6417333, 2019.

IPCC: Climate Change: The Physical Science Basis. Contribution of Working Group I to the Sixth Assessment Report of the Intergovernmental Panel on Climate Change, Cambridge University Press, Cambridge, United Kingdom and New York, NY, USA, https://doi.org/10.1017/9781009157896, 2021.

IPCC: Summary for Policymakers: The Ocean and Cryosphere in a Changing Climate, edited by: Pörtner, H.-O., Roberts, D. C., Masson-Delmotte, V., Zhai, P., Tignor, M., Poloczanska, E., Mintenbeck, K., Alegría, A., Nicolai, M., Okem, A., Petzold, J., Rama, B., and Weyer, N. M., Cambridge University Press, 755 pp., https://doi.org/10.1017/9781009157964.001, 2022.

Izaguirre, C., Losada, I. J., Camus, P., Vigh, J. L., and Stenek, V.: Climate change risk to global port operations, Nat. Clim. Chang., 11, 14–20, https://doi.org/10.1038/s41558-020-00937-z, 2021.

Jeong, E., Lee, J.-Y., and Redwan, M.: Animal exposure to microplastics and health effects: A review, Emerg. Contam., 10, 100369, https://doi.org/10.1016/j.emcon.2024.100369, 2024.

Jouffray, J.-B., Blasiak, R., Norström, A. V., Österblom, H., and Nyström, M.: The Blue Acceleration: The Trajectory of Human Expansion into the Ocean, One Earth, 2, 43–54, https://doi.org/10.1016/j.oneear.2019.12.016, 2020.

Lebreton, L., Egger, M., and Slat, B.: A global mass budget for positively buoyant macroplastic debris in the ocean, Sci. Rep., 9, 12922, https://doi.org/10.1038/s41598-019-49413-5, 2019.

Li, Y., Liu, C., Yang, H., He, W., Li, B., Zhu, X., Liu, S., Jia, S., Li, R., and Tang, K. H. D.: Leaching of chemicals from microplastics: A review of chemical types, leaching mechanisms and influencing factors, Sci. Total Environ., 906, 167666, https://doi.org/10.1016/j.scitotenv.2023.167666, 2024.

Linse, K., Peeken, I., and Tandberg, A. H. S.: Editorial: Effects of Ice Loss on Marine Biodiversity, Front. Mar. Sci., 8, 793020, https://doi.org/10.3389/fmars.2021.793020, 2021.

Lorenz, C., Roscher, L., Meyer, M. S., Hildebrandt, L., Prume, J., Löder, M. G. J., Primpke, S., and Gerdts, G.: Spatial distribution of microplastics in sediments and surface waters of the southern North Sea, Environ. Pollut., 252, 1719–1729, https://doi.org/10.1016/j.envpol.2019.06.093, 2019.

Maestro, M., Pérez-Cayeiro, M. L., Chica-Ruiz, J. A., and Reyes, H.: Marine protected areas in the 21st century: Current situation and trends, Ocean Coast. Manage., 171, 28–36, https://doi.org/10.1016/j.ocecoaman.2019.01.008, 2019.

Minière, A., Von Schuckmann, K., Sallée, J.-B., and Vogt, L.: Robust acceleration of Earth system heating observed over the past six decades, Sci. Rep., 13, 22975, https://doi.org/10.1038/s41598-023-49353-1, 2023.

Monllor-Hurtado, A., Pennino, M. G., and Sanchez-Lizaso, J. L.: Shift in tuna catches due to ocean warming, PLoS One, 12, e0178196, https://doi.org/10.1371/journal.pone.0178196, 2017.

Nicol, S., Lehodey, P., Senina, I., Bromhead, D., Frommel, A. Y., Hampton, J., Havenhand, J., Margulies, D., Munday, P. L., Scholey, V., Williamson, J. E., and Smith, N.: Ocean Futures for the World's Largest Yellowfin Tuna Population Under the Combined Effects of Ocean Warming and Acidification, Front. Mar. Sci., 9, 816772, https://doi.org/10.3389/fmars.2022.816772, 2022.

Nissen, C., Lovenduski, N. S., Brooks, C. M., Hoppema, M., Timmermann, R., and Hauck, J.: Severe 21st-century ocean acidification in Antarctic Marine Protected Areas, Nat. Commun., 15, 259, https://doi.org/10.1038/s41467-023-44438-x, 2024.

Polejack, A.: The Importance of Ocean Science Diplomacy for Ocean Affairs, Global Sustainability, and the UN Decade of Ocean Science, Front. Mar. Sci., 8, 664066, https://doi.org/10.3389/fmars.2021.664066, 2021.

Qi, D., Ouyang, Z., Chen, L., Wu, Y., Lei, R., Chen, B., Feely, R. A., Anderson, L. G., Zhong, W., Lin, H., Polukhin, A., Zhang, Y., Zhang, Y., Bi, H., Lin, X., Luo, Y., Zhuang, Y., He, J., Chen, J., and Cai, W.-J.: Climate change drives rapid decadal acidification in the Arctic Ocean from 1994 to 2020, Science, 377, 1544–1550, https://doi.org/10.1126/science.abo0383, 2022.

Roberts, C., Béné, C., Bennett, N., Boon, J. S., Cheung, W. W. L., Cury, P., Defeo, O., De Jong Cleyndert, G., Froese, R., Gascuel, D., Golden, C. D., Hawkins, J., Hobday, A. J., Jacquet, J., Kemp, P., Lam, M. E., Le Manach, F., Meeuwig, J. J., Micheli, F., Morato, T., Norris, C., Nouvian, C., Pauly, D., Pikitch, E., Amargos, F. P., Saenz-Arroyo, A., Sumaila, U. R., Teh, L., Watling, L., and O'Leary, B. C.: Rethinking sustainability of marine fisheries for a fast-changing planet, npj Ocean Sustain., 3, 41, https://doi.org/10.1038/s44183-024-00078-2, 2024.

Rockström, J., Beringer, T., Hole, D., Griscom, B., Mascia, M. B., Folke, C., and Creutzig, F.: We need biosphere stewardship that protects carbon sinks and builds resilience, P. Natl. Acad. Sci. USA, 118, e2115218118, https://doi.org/10.1073/pnas.2115218118, 2021.

Ryabinin, V., Barbière, J., Haugan, P., Kullenberg, G., Smith, N., McLean, C., Troisi, A., Fischer, A., Aricò, S., Aarup, T., Pissierssens, P., Visbeck, M., Enevoldsen, H.

O., and Rigaud, J.: The UN Decade of Ocean Science for Sustainable Development, Front. Mar. Sci., 6, 00470, https://doi.org/10.3389/fmars.2019.00470, 2019.

Sherman, K.: The Large Marine Ecosystem Approach for Assessment and Management of Ocean Coastal Waters, in: Large Marine Ecosystems, Elsevier, vol. 13, 3–16, https://doi.org/10.1016/S1570-0461(05)80025-4, 2005.

Sherman, K., Belkin, I. M., Friedland, K. D., O'Reilly, J., and Hyde, K.: Accelerated Warming and Emergent Trends in Fisheries Biomass Yields of the World's Large Marine Ecosystems, AMBIO, 38, 215–224, https://doi.org/10.1579/0044-7447-38.4.215, 2009.

Talukder, B., Ganguli, N., Matthew, R., vanLoon, G. W., Hipel, K. W., and Orbinski, J.: Climate change-accelerated ocean biodiversity loss & associated planetary health impacts, Journal of Climate Change and Health, 6, 100114, https://doi.org/10.1016/j.joclim.2022.100114, 2022.

Tang, K. H. D.: Climate Change and Plastic Pollution: A Review of Their Connections, Tropical Environment, Biology, and Technology, 1, 110–120, https://doi.org/10.53623/tebt.v1i2.341, 2023.

Terhaar, J., Burger, F. A., Vogt, L., Frölicher, T. L., and Stocker, T. F.: Record sea surface temperature jump in 2023–2024 unlikely but not unexpected, Nature, 639, 942–946, https://doi.org/10.1038/s41586-025-08674-z, 2025.

ter Hofstede, R., Hiddink, J., and Rijnsdorp, A.: Regional warming changes fish species richness in the eastern North Atlantic Ocean, Mar. Ecol. Prog. Ser., 414, 1–9, https://doi.org/10.3354/meps08753, 2010.

Thomas, D. N., Arévalo-Martínez, D. L., Crocket, K. C., Große, F., Grosse, J., Schulz, K., Sühring, R., and Tessin, A.: A changing Arctic Ocean, Ambio, 51, 293–297, https://doi.org/10.1007/s13280-021-01677-w, 2022.

Tittensor, D. P., Mora, C., Jetz, W., Lotze, H. K., Ricard, D., Berghe, E. Vanden, and Worm, B.: Global patterns and predictors of marine biodiversity across taxa, Nature, 466, 1098–1101, https://doi.org/10.1038/nature09329, 2010.

Townhill, B. L., Reppas-Chrysovitsinos, E., Sühring, R., Halsall, C. J., Mengo, E., Sanders, T., Dähnke, K., Crabeck, O., Kaiser, J., and Birchenough, S. N. R.: Pollution in the Arctic Ocean: An overview of multiple pressures and implications for ecosystem services, Ambio, 51, 471–483, https://doi.org/10.1007/s13280-021-01657-0, 2022.

Trenberth, K. E., Fasullo, J. T., and Balmaseda, M. A.: Earth's Energy Imbalance, J. Climate, 27, 3129–3144, https://doi.org/10.1175/JCLI-D-13-00294.1, 2014.

UNGA: Our Ocean, Our Future, Our Responsibility: resolution/adopted by the General Assembly, UN Doc. A/RES/76/296, http://digitallibrary.un.org/record/3982618 (last access: 1 September 2025), 2022.

UNGA: Agreement under the United Nations Convention on the Law of the Sea on the conservation and sustainable use of marine biological diversity of areas beyond national jurisdiction, UN Doc. A/CONF.232/2023/4, https://docs.un.org/en/a/conf.232/2023/4 (last access: 1 September 2025), 2023.

UNEP: Making Peace with Nature: A scientific blueprint to tackle the climate, biodiversity and pollution emergencies, UNEP, https://www.unep.org/resources/making-peace-nature (last access: 1 September 2025), 2021.

von Schuckmann, K., Holland, E., Haugan, P., and Thomson, P.: Ocean science, data, and services for the UN 2030 Sustainable Development Goals, Mar. Policy, 121, 104154, https://doi.org/10.1016/j.marpol.2020.104154, 2020.

von Schuckmann, K., Minière, A., Gues, F., Cuesta-Valero, F. J., Kirchengast, G., Adusumilli, S., Straneo, F., Ablain, M., Allan, R. P., Barker, P. M., Beltrami, H., Blazquez, A., Boyer, T., Cheng, L., Church, J., Desbruyeres, D., Dolman, H., Domingues, C. M., García-García, A., Giglio, D., Gilson, J. E., Gorfer, M., Haimberger, L., Hakuba, M. Z., Hendricks, S., Hosoda, S., Johnson, G. C., Killick, R., King, B., Kolodziejczyk, N., Korosov, A., Krinner, G., Kuusela, M., Landerer, F. W., Langer, M., Lavergne, T., Lawrence, I., Li, Y., Lyman, J., Marti, F., Marzeion, B., Mayer, M., MacDougall, A. H., McDougall, T., Monselesan, D. P., Nitzbon, J., Otosaka, I., Peng, J., Purkey, S., Roemmich, D., Sato, K., Sato, K., Savita, A., Schweiger, A., Shepherd, A., Seneviratne, S. I., Simons, L., Slater, D. A., Slater, T., Steiner, A. K., Suga, T., Szekely, T., Thiery, W., Timmermans, M.-L., Vanderkelen, I., Wjiffels, S. E., Wu, T., and Zemp, M.: Heat stored in the Earth system 1960–2020: where does the energy go?, Earth Syst. Sci. Data, 15, 1675–1709, https://doi.org/10.5194/essd-15-1675-2023, 2023.

Ward, D., Melbourne-Thomas, J., Pecl, G. T., Evans, K., Green, M., McCormack, P. C., Novaglio, C., Trebilco, R., Bax, N., Brasier, M. J., Cavan, E. L., Edgar, G., Hunt, H. L., Jansen, J., Jones, R., Lea, M.-A., Makomere, R., Mull, C., Semmens, J. M., Shaw, J., Tinch, D., van Steveninck, T. J., and Layton, C.: Safeguarding marine life: conservation of biodiversity and ecosystems, Rev. Fish. Biol. Fish., 32, 65–100, https://doi.org/10.1007/s11160-022-09700-3, 2022.

Wernberg, T., Russell, B. D., Moore, P. J., Ling, S. D., Smale, D. A., Campbell, A., Coleman, M. A., Steinberg, P. D., Kendrick, G. A., and Connell, S. D.: Impacts of climate change in a global hotspot for temperate marine biodiversity and ocean warming, J. Exp. Mar. Biol. Ecol., 400, 7–16, https://doi.org/10.1016/j.jembe.2011.02.021, 2011.

WMO Regions: Regions, https://wmo.int/about-wmo/regions (last access: 13 May 2025), 2025.

Woodall, L. C., Sanchez-Vidal, A., Canals, M., Paterson, G. L. J., Coppock, R., Sleight, V., Calafat, A., Rogers, A. D., Narayanaswamy, B. E., and Thompson, R. C.: The deep sea is a major sink for microplastic debris, R Soc. Open Sci., 1, 140317, https://doi.org/10.1098/rsos.140317, 2014.

Xing, Q., Yu, H., and Wang, H.: Global mapping and evolution of persistent fronts in Large Marine Ecosystems over the past 40 years, Nat. Commun., 15, 4090, https://doi.org/10.1038/s41467-024-48566-w, 2024.

Yadav, S. S. and Gjerde, K. M.: The ocean, climate change and resilience: Making ocean areas beyond national jurisdiction more resilient to climate change and other anthropogenic activities, Mar. Policy, 122, 104184, https://doi.org/10.1016/j.marpol.2020.104184, 2020.

State Planet, 6-osr9, 3, 2025
https://doi.org/10.5194/sp-6-osr9-3-2025

Ocean change in the northeastern Atlantic and adjacent seas: a multi-dimensional challenge for the environment, society, and economy

Karina von Schuckmann[1], Flora Gues[2,1], Lorena Moreira[3], Aurélien Liné[1], and Álvaro de Pascual Collar[3]

[1]Mercator Ocean international, Toulouse, France
[2]CELAD, Mercator Ocean international, Toulouse, France
[3]Nologin Oceanic Weather Systems, Madrid, Spain

Correspondence: Karina von Schuckmann (karina.von.schuckmann@mercator-ocean.fr)

Published: 30 September 2025

Abstract. An ocean narrative is a powerful tool for making complex ocean changes better accessible while informing decision-making and inspiring collective action. This ocean narrative reports on ocean change in the northeastern Atlantic and adjacent seas and discusses its broader implications for Europe's environment, economy, and society. The region is experiencing warming and acidification at rates exceeding the global average, with rising sea levels and record severe marine heatwaves (MHWs). These changes threaten marine ecosystems, biodiversity, cultural heritage, and key economic sectors, such as aquaculture and coastal tourism, which rely heavily on the balance and the health of the ocean. This ocean narrative emphasizes the importance of regional ocean indicators for the northeastern Atlantic and adjacent seas and underscores the importance of localized responses, as ocean changes affect regions differently, particularly in semi-enclosed seas such as the Baltic Sea, the Black Sea, and the Mediterranean Sea. The findings stress the urgency of timely action and the need to strengthen evidence-based and strategic ocean knowledge transfer at the science and policy interface for informed decision-making that balances environmental sustainability, economic resilience, and social inclusivity to address the growing challenges of ocean change in the northeastern Atlantic and its adjacent seas.

1 Introduction

The ocean plays a central role in Europe's climate, environment, and society. It acts as a climate regulator by absorbing heat and carbon dioxide (IPCC, 2021), helps drive weather and climate patterns, and supports diverse marine ecosystems that are essential to biodiversity and food security (IOC-UNESCO, 2024; IPBES, 2019; IPCC, 2022). Coastal regions and economies across Europe and abroad rely on the ocean for e.g. fisheries, tourism, transport, and renewable energy (Cramer et al., 2020; Martínez-Vázquez et al., 2021; Mejjad et al., 2022). In addition to its ecological and economic importance, the ocean is deeply connected to European culture and heritage (Delaney and Frangoudes, 2024). As a dynamic and interconnected system, the health and environmental balance of Europe's seas is critical – not only for marine life but also for the wellbeing and resilience of communities across the continent. The ocean in the northeastern Atlantic and its surrounding seas is undergoing rapid and profound change (von Schuckmann et al., 2024). As outlined in the previous Copernicus Ocean State Report, issue 8, temperatures are rising at more than twice the global average, especially in the Baltic, Black, and Mediterranean seas, where warming has become a persistent trend. Sea levels are steadily increasing, ocean waters are growing more acidic, and marine heatwaves (MHWs) are becoming more frequent, intense, and widespread.

Focusing on regional ocean indicators, rather than solely global ones, is essential because ocean conditions can vary significantly across different areas due to factors such as climate variability patterns, currents, and other region-specific ocean and atmospheric dynamics. Regional indicators pro-

Published by Copernicus Publications.

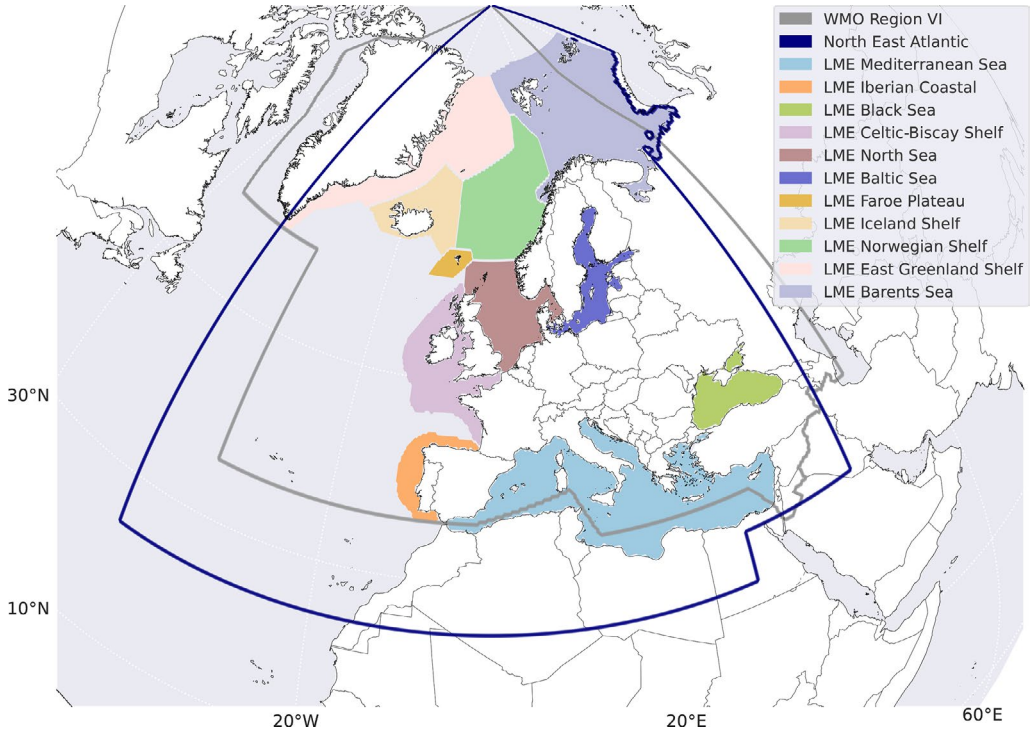

Figure 1. Illustration of the definition of the northeastern Atlantic and adjacent seas (inside the blue polygon, as in the OSR8), the WMO's delineation of Europe (inside the grey polygon), and large marine ecosystems (LMEs; Sherman, 2005; product ref. no. 1, in colours).

vide a more detailed picture of how the ocean is changing in a specific area, which is crucial for e.g. efficient regional to national management and adaptation strategies (Winther et al., 2020). The regionalization approach can vary (Fig. 1), ranging from multilateral frameworks, such as the World Meteorological Organization (WMO; WMO Regions, 2025) or the Copernicus Ocean State Report (von Schuckmann et al., 2024), to more specific models, such as large marine ecosystems (LMEs) (Sherman, 2005). LMEs encompass coastal areas, from river basins and estuaries to the seaward boundaries of continental shelves, and enclosed and semi-enclosed seas and the outer margins of major current systems. They are of significant socioeconomic importance, as they account for the majority of global fisheries biomass (Guiet et al., 2025; Sherman et al., 2009). However, these ecosystems also face challenges, including ocean pollution, overexploitation, and the alteration of coastal habitats, all of which occur within their boundaries (Sherman, 2005).

Here, we provide an ocean narrative to tell a compelling story that communicates the ongoing change in the northeastern Atlantic and adjacent seas in relation to people and the planet. It connects scientific understanding with social, economic, and cultural dimensions, helping audiences grasp why changes in the ocean matter. By connecting these dimensions, the ocean narrative helps make complex changes in the marine environment more relatable and relevant. It aims not only to raise awareness but also to shape how we perceive risks, responsibilities, and opportunities – ultimately encouraging informed decisions and collective action for a sustainable ocean future.

2 Method

This study employs a structured multi-indicator approach to describe and assess the state of the ocean in the northeastern Atlantic and adjacent seas. The analysis is grounded in a core set of ocean indicators, which include surface and subsurface ocean warming, surface ocean acidification, sea level rise, and marine heatwaves. These indicators are derived using scientifically validated methods and form part of the Copernicus Ocean Indicator Framework (see Product Table, Supplement).

Primary data sources include products from the Copernicus Marine Service, which are supplemented, where available, by additional publicly accessible datasets to enhance spatial and temporal coverage. A multi-product methodology is applied wherever feasible, combining data from different ocean products. This approach enables an assessment of internal consistency and uncertainty by comparing the spread across product ensembles. Uncertainty ranges are obtained using standard deviation at the 95 % confidence level. A regional trend amplified compared to the global trend implies that the 95 % range of the local trend exceeds the global trend. All datasets utilized are documented and referenced

in the product table, including links to associated metadata and scientific publications (see Supplement). Each ocean indicator has been updated with the most recent data available at the time of analysis, subject to product-specific update frequencies and data availability constraints.

To integrate the physical changes in the marine environment with broader sustainable development perspectives, additional datasets from the economic and social domains were included. This integrative approach reflects the three pillars of sustainability: environmental, economic, and social. Only data that are publicly available and accompanied by appropriate metadata were used. Metadata documentation and source references are provided in the product table. The three domains – environment, economy, and society – were then brought together to develop an ocean narrative, supported by peer-reviewed scientific knowledge with analysis interlinking ocean and biodiversity change to socioeconomic evidence, aimed at contextualizing observed and reported changes. This narrative is not intended as a new quantitative scientific analysis, but rather as a synthesis of available evidence-based and scientific information to support decision-making and communication. Scientific rigour is maintained by basing this synthesis on peer-reviewed literature and established datasets, ensuring an evidence-based narrative framework.

3 An ocean narrative for the northeastern Atlantic and adjacent seas

Ocean change in the northeastern Atlantic and adjacent seas is widespread from the surface to the ocean abyss. Regional mean sea surface and subsurface ocean warming are higher than the global trends, with rates of $+0.27 \pm 0.04\,^{\circ}\mathrm{C}$ per decade between 1982–2024 and $+0.41 \pm 0.03\,\mathrm{W\,m^{-2}}$ per decade between 1960–2024 (Fig. 2a, b). Ocean acidification in the northeastern Atlantic and adjacent seas continues at a rate comparable to the global trend, with a pH decline of -0.017 ± 0.001 units per decade between 1985 and 2023 (Fig. 2c). The warming and acidification trends are consistent across various large-scale regional definitions, whether based on the WMO's delineation of Europe or the aggregation of Europe's LMEs (Fig. 2c). Sea level is rising in this area at an average trend of $+3.7 \pm 0.8\,\mathrm{mm\,yr^{-1}}$ between 1999–2024 (EU Copernicus Marine Service Information, 2024), affecting the entire area. Since 1982, marine heatwaves in the northeastern Atlantic and adjacent seas have become more frequent, intense, and widespread (von Schuckmann et al., 2024). Marine heatwaves of categories extreme and severe over that period (see Hobday et al., 2016, for definitions) lasting at least 5 d have barely increased in mean duration (+11 %), from an average of 8 d per event in the 1990s (1993–2002) to 9 d per event over the past decade (2015–2024) (Fig. 2e).

Ocean change is not uniform. Semi-enclosed basins, such as the Baltic, Black, and Mediterranean seas, are experiencing the most rapid warming due to limited exchange with the open ocean (Fig. 2a). The Faroe Plateau, Iberian coast, and Celtic-Biscay Shelf show lower warming rates compared to other European seas, though they still exceed the global average (Fig. 2a). These regions lie close to the open Atlantic, where long-term warming interacts with pronounced natural variability (Årthun et al., 2021; Jackson et al., 2022). Also, ocean acidification patterns vary locally, with the Mediterranean Sea and the subtropical Atlantic showing a more rapid decline in pH, indicating intensified acidification in these areas (Fig. 3).

Ocean warming and acidification are well-documented stressors that exceed tolerance thresholds for many marine species, driving habitat loss, population declines, and disruptions to ecosystem functioning and services (Bindoff et al., 2019; Cooley et al., 2022). All United Nations Educational, Scientific and Cultural Organization (UNESCO) World Heritage marine sites in the northeastern Atlantic and adjacent seas are experiencing rapid ocean surface warming at rates exceeding the global average (Fig. 3), which are recognized for their unique marine biodiversity, exceptional ecosystems, remarkable geological processes, or unparalleled beauty, with the aim of ensuring their conservation for future generations (UNESCO, 1972). They represent some of the most iconic and fragile marine environments on Earth, and their status provides the potential for a comprehensive policy framework that allows their identification, management, governance, and protection (Abdulla et al., 2014). However, their conservation status remains relatively unknown (Kuempel et al., 2022), although ocean changes from global warming are putting pressure in these unique environments (Fig. 3).

The years 2023 and 2024 stand out in the historical record (Guinaldo et al., 2025; Terhaar et al., 2025), marking the longest average duration of marine heatwaves observed across the northeastern Atlantic and adjacent seas (Fig. 4). In 2023 alone, around one-third of these waters experienced severe to extreme marine heatwaves, with prolonged events lasting up to 4 months (von Schuckmann et al., 2024). In 2024, the eastern Mediterranean and Black seas, the Bay of Biscay, and the subtropical Atlantic were hit by severe to extreme marine heatwave events (Fig. 4). The northern Mediterranean Sea, Black Sea, and Baltic Sea have experienced recurring (three times or more since 1982) persistent ($>$ 38 d duration and mean sea surface temperature (SST) anomaly exceeding 2.3 °C; Mignot et al., 2022) MHWs that can harm marine life by causing mass die-offs, pushing species to new areas, and disrupting the balance of ocean ecosystems when temperatures get too high (Garrabou et al., 2022; Scannell et al., 2024).

About 17 % of the cold-water corals and 50 % of seagrass in the northeastern Atlantic and adjacent seas experienced extreme and long-lasting MHWs in 2024 (Fig. 4). Marine

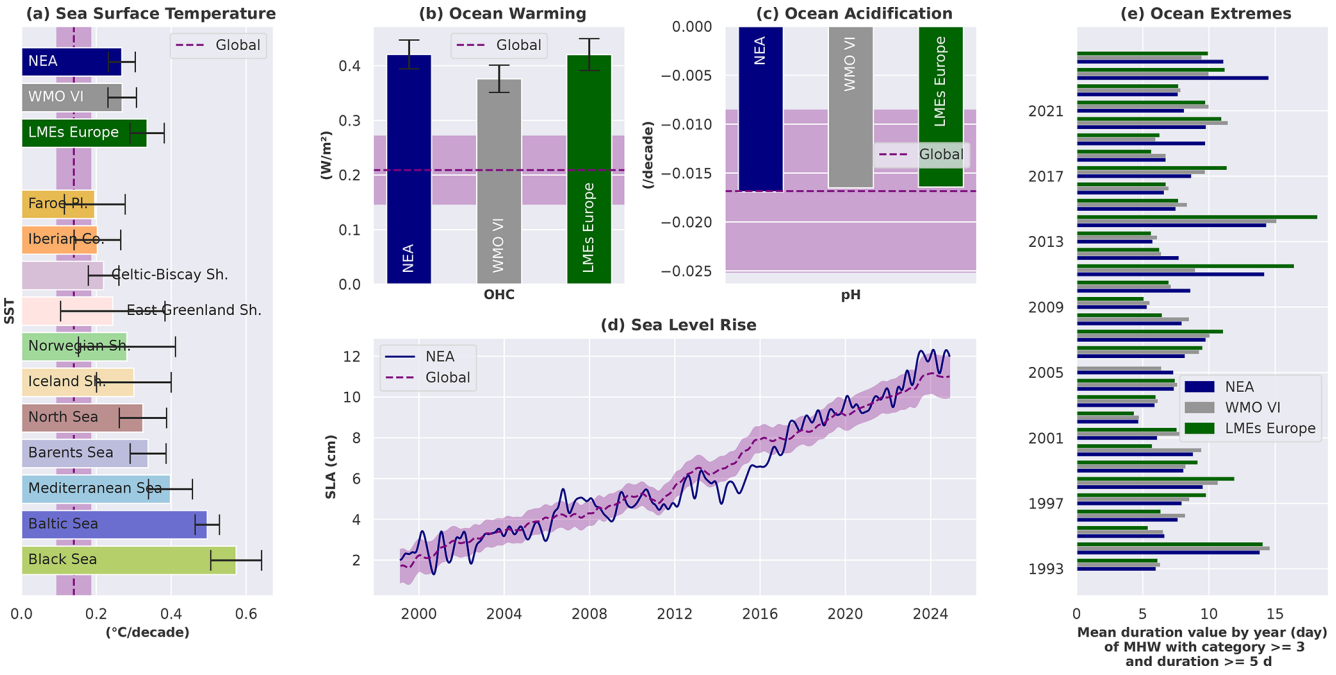

Figure 2. Current state of the northeastern Atlantic and adjacent seas based on a core set of ocean indicators. **(a)** Decadal trends in sea surface temperature (SST; product ref. nos. 2 and 3) anomalies (relative to 1991–2020) for the northeastern Atlantic and adjacent seas (blue), the WMO's delineation of Europe (grey), all large marine ecosystems (LMEs; product ref. no. 1) taken together (green), and each LME taken alone (other colours) for the period 1982–2024. Whiskers indicate the 95 % uncertainty range obtained by considering product ref. nos. 2–5, 28, and 29. The dashed purple line and shadow indicate the global average and its uncertainty envelope. **(b)** Same as panel **(a)** for the trends in ocean heat content (OHC; product ref. nos. 6 and 7) anomalies (relative to 1991–2020) integrated over the upper 300 m depth for the period 1960–2024. Whiskers indicate the 95 % obtained by considering product ref. nos. 6–10. The dashed purple line and shadow indicate the global average and its uncertainty envelope. **(c)** Same as panel **(a)** for the trends in pH for the period 1985–2022 for the global, and 1985–2023 for all regions, based on product ref. nos. 11 and 12. The dashed purple line and shadow indicate the global average and its uncertainty envelope. **(d)** Sea level rise (SLR; product ref. nos. 13 and 14) in the northeastern Atlantic and adjacent seas (blue) and at the global scale (purple and its uncertainty envelope shaded) for the period 1999–2024. **(e)** Annual mean duration of marine heat waves (MHWs) of category 3 and above, lasting at least 5 d, in the northeastern Atlantic and adjacent seas (blue), the WMO's delineation of Europe (grey), and all large marine ecosystems (LMEs) taken together (green) for the period 1993–2024 (climatology 1993–2022) based on product ref. nos. 15 and 16.

heatwaves, particularly the most persistent ones, induce loss of seagrass canopy and severe coral bleaching (Chapron et al., 2021; Corinaldesi et al., 2022; Frölicher et al., 2018; Gómez et al., 2022; Marzonie et al., 2023; Orenes-Salazar et al., 2023; Serrano et al., 2021; Strydom et al., 2020). Cold-water corals – which live in many areas of the northeastern Atlantic and adjacent seas – create habitat structure, host endemic species, sequester carbon, and provide many other ecosystem services (Cordes et al., 2023). Seagrass is a natural attribute of World Heritage properties (UNESCO, 2008), and seagrass habitats are one of the largest natural carbon sinks on the planet (Losciale et al., 2024). Since the start of the century, approximately 19 % of global seagrass coverage has been lost due to the cumulative impacts of direct anthropogenic and climate stressors (Dunic et al., 2021; Dunic and Côté, 2023).

All ocean regions adjacent to countries producing over 5000 t of aquaculture annually are undergoing rates of surface ocean warming and acidification faster than the global average (Fig. 3). Countries bordering the Mediterranean, southern Baltic, and southern North seas and the Bay of Biscay – where aquaculture production of fish, crustaceans, molluscs, and other aquatic organisms is high – are experiencing simultaneous rapid ocean warming and acidification, putting this economically important sector at increasing risk from climate change (Stewart-Sinclair et al., 2020). Altogether, 17 % of shellfish farms along European coasts are located in seas that experienced severe to extreme marine heatwaves in 2024 (Fig. 4). In particular, areas around shellfish farms in the eastern Mediterranean Sea, in the Bay of Biscay, and along the coast of Norway experienced extreme conditions. Marine heatwaves induce stress in species, leading to weight loss, impaired nutrient absorption, and disrupted physiological functions, which adversely affect shellfish welfare and reduce the productivity of the affected aquaculture industry (Kajtar et al., 2024; De Marco et al., 2023; Masanja et al.,

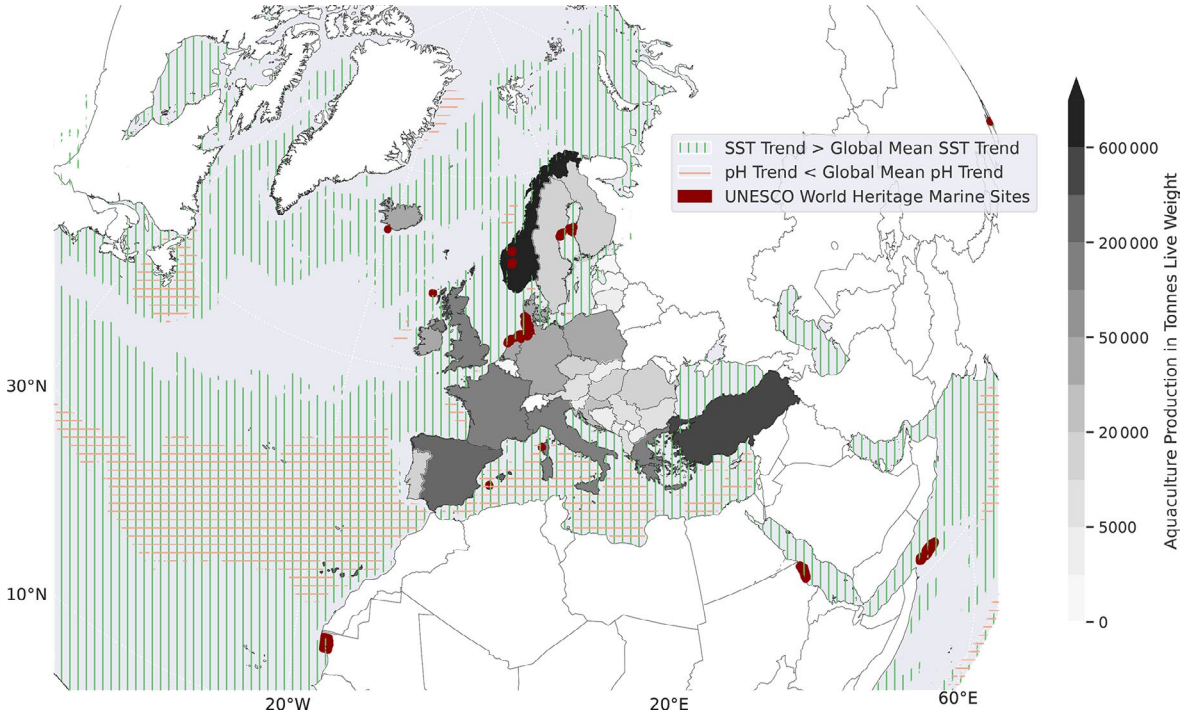

Figure 3. Aquaculture production and UNESCO World Heritage marine sites in a warmed and acidified ocean. Total production of fish, crustaceans, molluscs, and other aquatic organisms from aquaculture, excluding hatcheries and nurseries, in European countries (shown on land) in 2023 (or latest available data; see product ref. no. 17 for more information) (grey gradient). Vertical hatching represents where 95 % of the local sea surface temperature (SST) trend range surpasses the global average trend for the period 1982–2024 based on the product ref. nos. 2–5, 28, and 29. Horizontal hatching is the same but for the pH trend for the period 1985–2022 based on product ref. no. 18. Brown dots and polygons represent marine UNESCO sites (product ref. no. 19).

2023). Monitoring and forecasting marine heatwaves helps aquaculture adapt by allowing early action to reduce losses and protect vulnerable food systems and coastal communities (Masanja et al., 2024).

In the northeastern Atlantic and adjacent seas in 2024, major marine heatwave events of extreme to severe category were located adjacent to countries where 40 %–80 % of blue economy employment relies on coastal tourism (Fig. 4). Marine industries, such as fisheries, aquaculture, and tourism, face increasing risk from extreme climate events such as marine heatwaves, as they disrupt ecosystem functions and services and human–ocean interactions and lead to economic losses (Schaeffer et al., 2023; Smith et al., 2021). For example, loss of marine habitats (Garrabou et al., 2022) or invasive species as observed during marine heatwave events is one of the most profound implications on coastal and marine tourism, as it reduces the destination's attractiveness and degradation of landscapes, particularly where the natural attributes are of high value (Arabadzhyan et al., 2020; Cuttler et al., 2018; Marshall et al., 2013; Scott et al., 2012a, b; Wong et al., 2024; Zeppel and Beaumont, 2012). This in turn induces changes in tourism flows, leading to substantial geospatial shifts in economic costs and benefits associated with tourism revenue and coastal infrastructure protection, repair, and restoration (Arabadzhyan et al., 2020; Bayraktarov et al., 2016; Weatherdon et al., 2016). Regular monitoring and seasonal forecasts of marine heatwaves provide a powerful tool to reduce risks, enabling economy actors to act early and build resilience (Hartog et al., 2023; McAdam et al., 2023).

Fast-rising sea levels increase flood and erosion risks, and hence the loss of property and livelihoods, in areas where about 200 million people live on European coasts (Eurostat, 2025). All European countries with high near-coastal population densities (> 200 persons km^{-2}) border ocean areas where THE sea level is rising faster than the global average, particularly affecting some of the continent's most densely populated and vulnerable regions, such as the Netherlands (Fig. 5). Ocean change is also affecting cultural heritage. Numerous cultural UNESCO World Heritage sites are in low-lying coastal regions, and many of these sites will be partially or totally flooded in the coming centuries/millennia (Cazenave, 2014; Marzeion and Levermann, 2014). Several UNESCO-listed ancient coastal heritage sites in the Mediterranean Sea face sea level rise rates above the global average (Fig. 5) and are projected to be increasingly at risk from coastal hazards (flooding, erosion) due to sea level rise (Reimann et al., 2018).

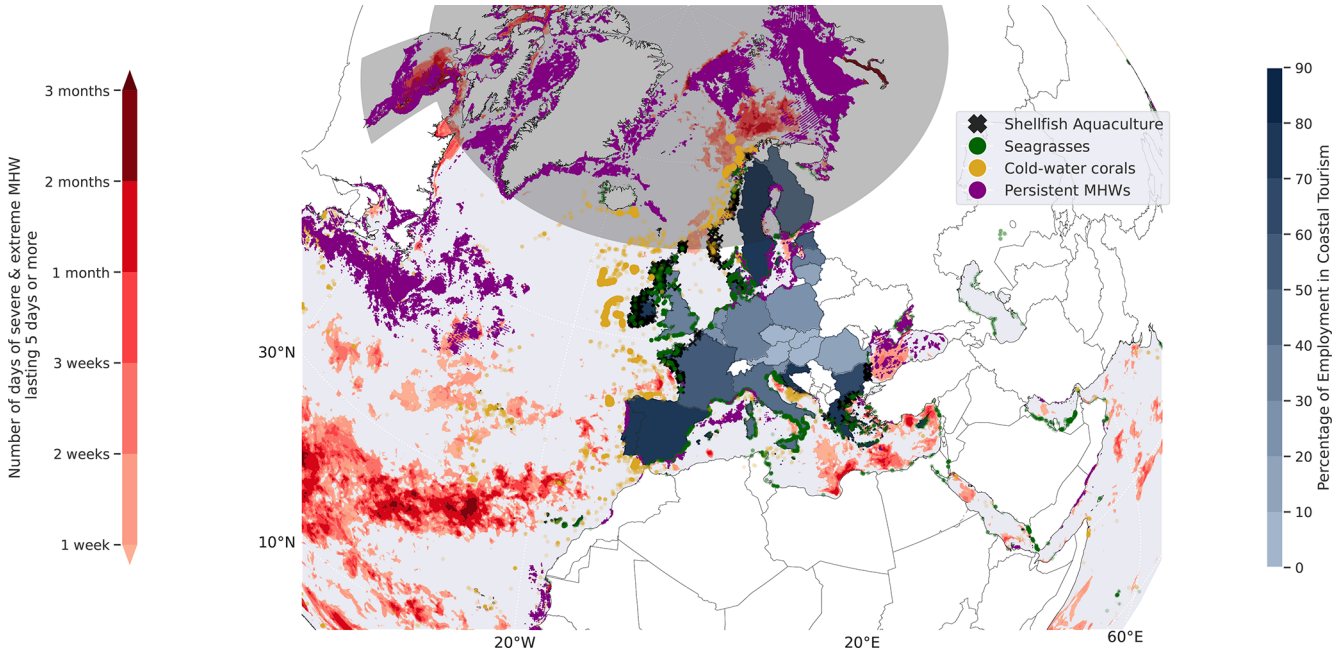

Figure 4. Biodiversity and coastal employment exposition to marine heat waves. Cumulative number of marine heatwave (MHW) days (method following Hobday et al., 2016), considering categories 3 and above, lasting 5 d or more in 2024 based on the product ref. nos. 15 and 16 (red graduation). Purple shading represents satellite sea surface temperature (SST) grid points that have experienced at least three persistent marine heat waves (PMHWs) from 1993 to 2024 based on product ref. nos. 15 and 16. Grey shading represents the area above 60° N and the Hudson Bay, where the surface is partially and temporally covered by ice, implying potentially less accurate MHW detection. Percentage of employment in coastal tourism in European countries (shown on land) in 2017 based on product ref. no. 21. Black crosses show shellfish aquaculture (product ref. no. 22). Green dots show seagrasses (product ref. no. 23). Yellow dots show cold-water corals (product ref. no. 24). A cut-off criterion of 10 km (due to the data grid; product ref. nos. 15 and 16) has been used to obtain % estimates linking seagrass, cold-water corals, and shellfish aquaculture to extreme and long-lasting MHWs in 2024 (see text for more detail).

Lastly, this ocean narrative provides a valuable framework for connecting different regional indicators. For example, in the Aegean Sea, multiple facets of ocean change are intensifying, with increasing sea surface temperatures (SST), ocean acidification (pH), and sea level rise (SLR) and prolonged marine heatwave (MHW) durations. This region, rich in culture (home to coastal and marine UNESCO sites), environment (seagrass meadows), and economy (aquaculture, coastal tourism), faces an increasing imperative to adapt to these local changes. Similarly, the Cantabrian Sea illustrates how regional indicators can collectively signal alarming trends, threatening coral reefs, coastal UNESCO sites, and the livelihoods of the local population. The urgency to address these changes is amplified in areas where the environment, culture, and economy are intricately linked.

4 Conclusion

The northeastern Atlantic and adjacent seas are undergoing rapid and widespread ocean changes driven by warming, acidification, sea level rise, and intensifying marine heatwaves. These transformations present a critical barometer for Europe's ability to align environmental protection, economic resilience, and societal wellbeing within a forward-looking ocean strategy. Regional disparities, particularly in semi-enclosed basins such as the Baltic, Black, and Mediterranean seas, show that local conditions can significantly amplify global and large-scale ocean trends, highlighting the need for locally tailored responses within broader European ocean and climate strategies.

The impacts extend across all dimensions of sustainable development. Marine ecosystems are increasingly vulnerable, with important habitats, such as cold-water corals and seagrass beds, exposed to extreme and prolonged thermal stress. This not only undermines biodiversity and ecosystem services but also affects carbon sequestration and the ecological integrity of protected areas, including UNESCO World Heritage marine sites. Similarly, the risk to cultural heritage is rising, especially in low-lying coastal zones of the Mediterranean, where several UNESCO-listed sites face long-term threats from coastal hazards driven by sea level rise.

The economic implications are equally significant. Aquaculture and tourism – both cornerstones of the coastal blue economy – are already experiencing the consequences of ocean extremes. Without strengthened early warning systems and climate-smart adaptation, these sectors face growing un-

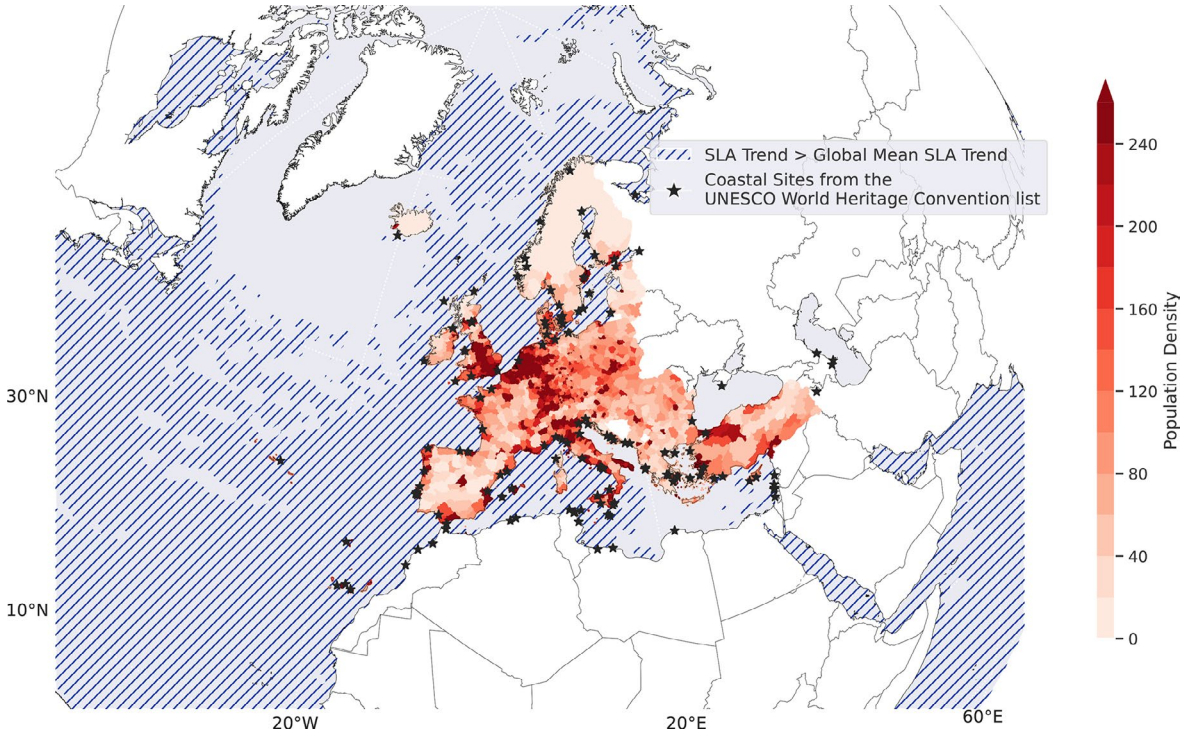

Figure 5. Sea level rise and impacted coasts. Population density (unit of measurement: persons per square kilometre (persons km^{-2})) in European countries in 2023 (or latest available data; see product ref. no. 25 for more details) (red gradient). Oblique hatching shows where the local sea level rise (SLR; product ref. no. 26) trend surpasses the global trend for the period 1999–2024. Black stars represent coastal UNESCO sites (product ref. no. 27).

certainty that could endanger jobs, food security, and coastal livelihoods.

Taken together, these findings highlight the critical need for coordinated, timely action. Climate resilience should be a core component of conservation, economic planning, and marine governance. Safeguarding biodiversity, supporting vulnerable communities, and protecting cultural and natural heritage must serve as key priorities in Europe's strategy for addressing the growing challenges of ocean change. The northeastern Atlantic stands not only as a prominent climate hotspot but also as an essential region for shaping comprehensive ocean policies that balance environmental sustainability, economic resilience, and social inclusivity.

Code availability. All codes are available upon request.

Data availability. All data used are available, and their sources are listed in the Supplement.

Supplement. The supplement related to this article is available online at https://doi.org/10.5194/sp-6-osr9-3-2025-supplement.

Author contributions. KvS: conceptualization, designing, methodology, writing (original draft), investigation, supervision, and formal analysis. FG: conceptualization and analysis. All authors: writing (review and editing).

Competing interests. At least one of the (co-)authors is a member of the editorial board of *State of the Planet*. The peer-review process was guided by an independent editor, and the authors also have no other competing interests to declare.

Disclaimer. Please note that this article has undergone editorial review only.

Publisher's note: Copernicus Publications remains neutral with regard to jurisdictional claims made in the text, published maps, institutional affiliations, or any other geographical representation in this paper. While Copernicus Publications makes every effort to include appropriate place names, the final responsibility lies with the authors. Views expressed in the text are those of the authors and do not necessarily reflect the views of the publisher.

Financial support. This research was carried out as part of the Copernicus Marine Service implemented by MOi under a contributing agreement with the European Commission, and "Ocean obser-

vations and indicators for climate and assessments" (ObsSea4Clim) is funded by the European Union Horizon Europe Funding Programme for Research and Innovation under grant no. 101136548. This is ObsSea4Clim contribution no. 19.

References

Abdulla, A., Obura, D., Bertzky, B., and Shi, Y.: Marine World Heritage: creating a globally more balanced and representative list, Aquat. Conserv., 24, 59–74, https://doi.org/10.1002/aqc.2527, 2014.

Arabadzhyan, A., Figini, P., García, C., González, M. M., Lam-González, Y. E., and León, C. J.: Climate change, coastal tourism, and impact chains – a literature review, Curr. Issues Tour., 24, 2233–2268, https://doi.org/10.1080/13683500.2020.1825351, 2020.

Årthun, M., Wills, R. C. J., Johnson, H. L., Chafik, L., and Langehaug, H. R.: Mechanisms of Decadal North Atlantic Climate Variability and Implications for the Recent Cold Anomaly, J. Climate, 34, 3421–3439, https://doi.org/10.1175/JCLI-D-20-0464.1, 2021.

Bayraktarov, E., Saunders, M. I., Abdullah, S., Mills, M., Beher, J., Possingham, H. P., Mumby, P. J., and Lovelock, C. E.: The cost and feasibility of marine coastal restoration, Ecol. Appl., 26, 1055–1074, https://doi.org/10.1890/15-1077, 2016.

Bindoff, N. L., Cheung, W. W. L., Kairo, J. G., Aristegui, J., Guinder, V. A., Hallberg, R., Hilmi, N., Jiao, N., Karim, M. S., Levin, L., O'Donoghue, S., Purca Cuicapusa, S. R., Rinkevich, B., Suga, T., Tagliabue, A., and Williamson, P.: Changing Ocean, Marine Ecosystems, and Dependent Communities, in: IPCC Special Report on the Ocean and Cryosphere in a Changing Climate, edited by: Pörtner, H.-O., Roberts, D. C., Masson-Delmotte, V., Zhai, P., Tignor, M., Poloczanska, E., Mintenbeck, K., Alegria, A., Nicolai, M., Okem, A., Petzold, J., Rama, B., and Weyer, N. M., Cambridge University Press, Cambridge, UK and New York, NY, USA, 447–587, https://doi.org/10.1017/9781009157964.007, 2019.

Cazenave, A.: Anthropogenic global warming threatens world cultural heritage, Environ. Res. Lett., 9, 051001, https://doi.org/10.1088/1748-9326/9/5/051001, 2014.

Chapron, L., Galand, P. E., Pruski, A. M., Peru, E., Vétion, G., Robin, S., and Lartaud, F.: Resilience of cold-water coral holobionts to thermal stress, P. Roy. Soc. B-Biol. Sci., 288, 20212117, https://doi.org/10.1098/rspb.2021.2117, 2021.

Cooley, S., Schoeman, D., Bopp, L., Boyd, P., Donner, S., Ghebrehiwet D. Y., Ilto, S.-I., Kiessling, W., Martinetto, P., Ojea, E., Racault, M.-F., Rost, B., and Skern-Mauritzen, M.: Ocean and Coastal Ecosystems and their Service, in: Climate Change 2022: Impacts, Adaptation and Vulnerability. Contribution of Working Group II to the Sixth Assessment Report of the Intergovernmental Panel on Climate Change, edited by: Pörtner, H. O., Roberts, D. C., Tignor, M., Poloczanska, E. S., Mintenbeck, K., Alegría, A., Craig, M., Langsdorf, S., Löschke, S., Möller, V., Okem, A., and Rama, B., Cambridge University Press, Cambridge, UK and New York, USA, 379–550, https://doi.org/10.1017/9781009325844.005, 2022.

Cordes, E. E., Mienis, F., Gasbarro, R., Davies, A., Baco, A. R., Bernardino, A. F., Clark, M. R., Freiwald, A., Hennige, S. J., Huvenne, V. A. I., Buhl-Mortensen, P., Orejas, C., Quattrini, A. M., Tracey, D. M., Wheeler, A. J., and Wienberg, C.: A Global View of the Cold-Water Coral Reefs of the World, Springer, Cham, 19, 1–30, https://doi.org/10.1007/978-3-031-40897-7_1, 2023.

Corinaldesi, C., Varrella, S., Tangherlini, M., Dell'Anno, A., Canensi, S., Cerrano, C., and Danovaro, R.: Changes in coral forest microbiomes predict the impact of marine heatwaves on habitat-forming species down to mesophotic depths, Sci. Total Environ., 823, 153701, https://doi.org/10.1016/j.scitotenv.2022.153701, 2022.

Cramer, W., Guiot, J., Marini, K., Azzopardi, B., Balzan, M. V, Cherif, S., Doblas-Miranda, E., dos Santos, M., Drobinski, P., Fader, M., Hassoun, A. E. R., Giupponi, C., Koubi, V., Lange, M. A., Lionello, P., Llassat, M. C., Moncada, S., Mrabet, R., Paz, S., Savé, R., Snoussi, M., Toreti, A., Vafeidis, A. T., and Xoplaki, E.: MedECC 2020 Summary for Policymakers, MedECC Reports, MedECC Secretariat, Marseille, France, https://doi.org/10.5281/zenodo.5513887, 2020.

Cuttler, M. V. W., Hansen, J. E., Lowe, R. J., and Drost, E. J. F.: Response of a fringing reef coastline to the direct impact of a tropical cyclone, Limnol. Oceanogr. Lett., 3, 31–38, https://doi.org/10.1002/LOL2.10067, 2018.

Delaney, A. E. and Frangoudes, K.: Coastal and maritime cultural heritage: from the European Union to East Asia and Latin America, Maritime Studies, 23, 26, https://doi.org/10.1007/s40152-024-00369-x, 2024.

De Marco, A., Baldassarro, V. A., Calzà, L., Giardino, L., Dondi, F., Ferrari, M. G., Bignami, G., Parma, L., and Bonaldo, A.: Prolonged heat waves reduce the condition index and alter the molecular parameters in the pacific oyster Crassostrea gigas, Fish Shellfish Immunol., 133, 108518, https://doi.org/10.1016/J.FSI.2023.108518, 2023.

Dunic, J. C. and Côté, I. M.: Management thresholds shift under the influence of multiple stressors: Eelgrass meadows as a case study, Conserv. Lett., 16, e12938, https://doi.org/10.1111/conl.12938, 2023.

Dunic, J. C., Brown, C. J., Connolly, R. M., Turschwell, M. P., and Côté, I. M.: Long-term declines and recovery of meadow area across the world's seagrass bioregions, Glob. Chang. Biol., 27, 4096–4109, https://doi.org/10.1111/gcb.15684, 2021.

EU Copernicus Marine Service Information: European Seas Mean Sea Level time series and trend from Observations Reprocessing, Mercator Ocean International, https://doi.org/10.48670/mds-00335, 2024.

Eurostat: Portrait of EU coastal regions – Issue number 38/2010 – Products Statistics in Focus, Eurostat, https://ec.europa.eu/eurostat/web/products-statistics-in-focus/-/ks-sf-10-038, last access: 13 May 2025.

Frölicher, T. L., Fischer, E. M., and Gruber, N.: Marine heatwaves under global warming, Nature, 560, 360–364, https://doi.org/10.1038/s41586-018-0383-9, 2018.

Garrabou, J., Gómez-Gras, D., Medrano, A., Cerrano, C., Ponti, M., Schlegel, R., Bensoussan, N., Turicchia, E., Sini, M., Gerovasileiou, V., Teixido, N., Mirasole, A., Tamburello, L., Cebrian, E., Rilov, G., Ledoux, J., Souissi, J. Ben, Khamassi, F., Ghanem, R., Benabdi, M., Grimes, S., Ocaña, O., Bazairi, H., Hereu, B., Linares, C., Kersting, D. K., la Rovira, G., Ortega, J., Casals, D., Pagès-Escolà, M., Margarit, N., Capdevila, P., Verdura, J., Ramos, A., Izquierdo, A., Barbera, C., Rubio-Portillo, E., Anton, I., López-Sendino, P., Díaz, D., Vázquez-Luis, M.,

Duarte, C., Marbà, N., Aspillaga, E., Espinosa, F., Grech, D., Guala, I., Azzurro, E., Farina, S., Cristina Gambi, M., Chimienti, G., Montefalcone, M., Azzola, A., Mantas, T. P., Fraschetti, S., Ceccherelli, G., Kipson, S., Bakran-Petricioli, T., Petricioli, D., Jimenez, C., Katsanevakis, S., Kizilkaya, I. T., Kizilkaya, Z., Sartoretto, S., Elodie, R., Ruitton, S., Comeau, S., Gattuso, J., and Harmelin, J.: Marine heatwaves drive recurrent mass mortalities in the Mediterranean Sea, Glob. Chang. Biol., 28, 5708–5725, https://doi.org/10.1111/gcb.16301, 2022.

Gómez, C. E., Gori, A., Weinnig, A. M., Hallaj, A., Chung, H. J., and Cordes, E. E.: Natural variability in seawater temperature compromises the metabolic performance of a reef-forming cold-water coral with implications for vulnerability to ongoing global change, Coral Reefs, 41, 1225–1237, https://doi.org/10.1007/s00338-022-02267-2, 2022.

Guiet, J., Bianchi, D., Scherrer, K. J. N., Heneghan, R. F., and Galbraith, E. D.: Small Commercial Fish Biomass Limits the Catch Potential in the High Seas, Earths Future, 13, e2024EF004571, https://doi.org/10.1029/2024EF004571, 2025.

Guinaldo, T., Cassou, C., Sallée, J. B., and Liné, A.: Internal variability effect doped by climate change drove the 2023 marine heat extreme in the North Atlantic, Commun. Earth Environ., 6, 1–11, https://doi.org/10.1038/s43247-025-02197-1, 2025.

Hartog, J. R., Spillman, C. M., Smith, G., and Hobday, A. J.: Forecasts of marine heatwaves for marine industries: Reducing risk, building resilience and enhancing management responses, Deep-Sea Res. Pt. II, 209, 105276, https://doi.org/10.1016/J.DSR2.2023.105276, 2023.

Hobday, A., Alexander, L., Perkins, S., Smale, D., Straub, S., Oliver, E., Benthuysen, J., Burrows, M., Donat, M., Feng, M., Holbrook, N., Moore, P., Scannell, H., Sen Gupta, A., and Wernberg, T.: A hierarchical approach to defining marine heatwaves, Prog. Oceanogr., 141, 227–238, https://doi.org/10.1016/j.pocean.2015.12.014, 2016

IOC-UNESCO: State of the Ocean Report, Paris, IOC-UNESCO, IOC Technical Series, 190, https://doi.org/10.25607/4wbg-d349, 2024.

IPBES: Global assessment report on biodiversity and ecosystem services of the Intergovernmental Science-Policy Platform on Biodiversity and Ecosystem Services, Zenodo, https://doi.org/10.5281/zenodo.6417333, 2019.

IPCC: Climate Change 2021: The Physical Science Basis. Contribution of Working Group I to the Sixth Assessment Report of the Intergovernmental Panel on Climate Change, Cambridge University Press, Cambridge, United Kingdom and New York, NY, USA, https://doi.org/10.1017/9781009157896, 2021.

IPCC: Summary for Policymakers: The Ocean and Cryosphere in a Changing Climate, edited by: Pörtner, H.-O., Roberts, D. C., Masson-Delmotte, V., Zhai, P., Tignor, M., Poloczanska, E., Mintenbeck, K., Alegría, A., Nicolai, M., Okem, A., Petzold, J., Rama, B., and Weyer, N. M., Cambridge University Press, 755 pp., https://doi.org/10.1017/9781009157964.001, 2022.

Jackson, L. C., Biastoch, A., Buckley, M. W., Desbruyères, D. G., Frajka-Williams, E., Moat, B., and Robson, J.: The evolution of the North Atlantic Meridional Overturning Circulation since 1980, Nat. Rev. Earth Environ., 3, 241–254, https://doi.org/10.1038/s43017-022-00263-2, 2022.

Kajtar, J. B., Holbrook, N. J., Lyth, A., Hobday, A. J., Mundy, C. N., and Ugalde, S. C.: A stakeholder-guided marine heatwave hazard index for fisheries and aquaculture, Clim. Change, 177, 1–22, https://doi.org/10.1007/S10584-024-03684-8, 2024.

Kuempel, C. D., Simmons, B. A., and Davey, M.: Assessing the status of existing and tentative marine World Heritage areas reveals opportunities to better achieve World Heritage Convention goals, J. Environ. Manage., 304, 114276, https://doi.org/10.1016/j.jenvman.2021.114276, 2022.

Losciale, R., Day, J. C., Rasheed, M. A., and Heron, S. F.: The vulnerability of World Heritage seagrass habitats to climate change, Glob. Chang. Biol., 30, e17113, https://doi.org/10.1111/gcb.17113, 2024.

Marshall, N. A., Tobin, R. C., Marshall, P. A., Gooch, M., and Hobday, A. J.: Social Vulnerability of Marine Resource Users to Extreme Weather Events, Ecosystems, 16, 797–809, https://doi.org/10.1007/S10021-013-9651-6, 2013.

Martínez-Vázquez, R. M., Milán-García, J., and De Pablo Valenciano, J.: Challenges of the Blue Economy: evidence and research trends, Environ. Sci. Eur., 33, 61, https://doi.org/10.1186/s12302-021-00502-1, 2021.

Marzeion, B. and Levermann, A.: Loss of cultural world heritage and currently inhabited places to sea-level rise, Environ. Res. Lett., 9, 034001, https://doi.org/10.1088/1748-9326/9/3/034001, 2014.

Marzonie, M. R., Bay, L. K., Bourne, D. G., Hoey, A. S., Matthews, S., Nielsen, J. J. V., and Harrison, H. B.: The effects of marine heatwaves on acute heat tolerance in corals, Glob. Chang. Biol., 29, 404–416, https://doi.org/10.1111/gcb.16473, 2023.

Masanja, F., Yang, K., Xu, Y., He, G., Liu, X., Xu, X., Xiaoyan, J., Xin, L., Mkuye, R., Deng, Y., and Zhao, L.: Impacts of marine heat extremes on bivalves, Front. Mar. Sci., 10, 1159261, https://doi.org/10.3389/FMARS.2023.1159261/XML/NLM, 2023.

Masanja, F., Luo, X., Jiang, X., Xu, Y., Mkuye, R., and Zhao, L.: Environmental and social framework to protect marine bivalves under extreme weather events, Sci. Total Environ., 946, 174471, https://doi.org/10.1016/J.SCITOTENV.2024.174471, 2024.

McAdam, R., Masina, S., and Gualdi, S.: Seasonal forecasting of subsurface marine heatwaves, Commun. Earth Environ., 4, 225, https://doi.org/10.1038/s43247-023-00892-5, 2023.

Mejjad, N., Rossi, A., and Pavel, A. B.: The coastal tourism industry in the Mediterranean: A critical review of the socio-economic and environmental pressures & impacts, Tour. Manag. Perspect., 44, 101007, https://doi.org/10.1016/j.tmp.2022.101007, 2022.

Mignot, A., von Schuckmann, K., Landschützer, P., Gasparin, F., van Gennip, S., Perruche, C., Lamouroux, J., and Amm, T.: Decrease in air-sea CO_2 fluxes caused by persistent marine heatwaves, Nat. Commun., 13, 4300, https://doi.org/10.1038/s41467-022-31983-0, 2022.

Orenes-Salazar, V., Navarro-Martínez, P. C., Ruíz, J. M., and García-Charton, J. A.: Recurrent marine heatwaves threaten the resilience and viability of a key Mediterranean octocoral species, Aquat. Conserv., 33, 1161–1174, https://doi.org/10.1002/aqc.3997, 2023.

Reimann, L., Vafeidis, A. T., Brown, S., Hinkel, J., and Tol, R. S. J.: Mediterranean UNESCO World Heritage at risk from coastal flooding and erosion due to sea-level rise, Nat. Commun., 9, 4161, https://doi.org/10.1038/s41467-018-06645-9, 2018.

Scannell, H. A., Cai, C., Thompson, L., Whitt, D. B., Gagne, D. J., and Abernathey, R. P.: Spatiotemporal Evolution of Marine

Heatwaves Globally, J. Atmos. Ocean. Tech., 41, 1247–1263, https://doi.org/10.1175/JTECH-D-23-0126.1, 2024.

Schaeffer, A., Sen Gupta, A., and Roughan, M.: Seasonal stratification and complex local dynamics control the subsurface structure of marine heatwaves in Eastern Australian coastal waters, Commun. Earth Environ., 4, 1–12, https://doi.org/10.1038/s43247-023-00966-4, 2023.

Scott, D., Gössling, S., and Hall, C. M.: International tourism and climate change, WIRES Clim. Change, 3, 213–232, https://doi.org/10.1002/WCC.165, 2012a.

Scott, D., Hall, C. M., and Gössling, S.: Tourism and Climate Change: Impacts, adaptation and mitigation, Routledge, Tourism and Climate Change: Impacts, Adaptation and Mitigation, 1–440, https://doi.org/10.4324/9780203127490, 2012b.

Serrano, O., Arias-Ortiz, A., Duarte, C. M., Kendrick, G. A., and Lavery, P. S.: Impact of Marine Heatwaves on Seagrass Ecosystems, Springer, Cham, 241, 345–364, https://doi.org/10.1007/978-3-030-71330-0_13, 2021.

Sherman, K.: The Large Marine Ecosystem Approach for Assessment and Management of Ocean Coastal Waters, in: Large Marine Ecosystems, Elsevier, vol. 13, 3–16, https://doi.org/10.1016/S1570-0461(05)80025-4, 2005.

Sherman, K., Belkin, I. M., Friedland, K. D., O'Reilly, J., and Hyde, K.: Accelerated Warming and Emergent Trends in Fisheries Biomass Yields of the World's Large Marine Ecosystems, AMBIO, 38, 215–224, https://doi.org/10.1579/0044-7447-38.4.215, 2009.

Smith, K. E., Burrows, M. T., Hobday, A. J., Sen Gupta, A., Moore, P. J., Thomsen, M., Wernberg, T., and Smale, D. A.: Socioeconomic impacts of marine heatwaves: Global issues and opportunities, Science, 374, eabj3593, https://doi.org/10.1126/science.abj3593, 2021.

Stewart-Sinclair, P. J., Last, K. S., Payne, B. L., and Wilding, T. A.: A global assessment of the vulnerability of shellfish aquaculture to climate change and ocean acidification, Ecol. Evol., 10, 3518–3534, https://doi.org/10.1002/ece3.6149, 2020.

Strydom, S., Murray, K., Wilson, S., Huntley, B., Rule, M., Heithaus, M., Bessey, C., Kendrick, G. A., Burkholder, D., Fraser, M. W., and Zdunic, K.: Too hot to handle: Unprecedented seagrass death driven by marine heatwave in a World Heritage Area, Glob. Chang. Biol., 26, 3525–3538, https://doi.org/10.1111/gcb.15065, 2020.

Terhaar, J., Burger, F. A., Vogt, L., Frölicher, T. L., and Stocker, T. F.: Record sea surface temperature jump in 2023–2024 unlikely but not unexpected, Nature, 639, 942–946, https://doi.org/10.1038/s41586-025-08674-z, 2025.

UNESCO: Convention concerning the protection of the World cultural and natural heritage, UNESCO, https://whc.unesco.org/archive/convention-en.pdf (last access: 1 September 2025), 1972.

UNESCO: Operational guidelines for the implementation of the world heritage convention, UNESCO, http://whc.unesco.org/archive/opguide08-en.pdf (last access: 1 September 2025), 2008.

von Schuckmann, K., Moreira, L., Cancet, M., Gues, F., Autret, E., Aydogdu, A., Castrillo, L., Ciani, D., Cipollone, A., Clementi, E., Cossarini, G., de Pascual-Collar, A., De Toma, V., Gehlen, M., Giesen, R., Drevillon, M., Fanelli, C., Hodges, K., Jandt-Scheelke, S., Jansen, E., Juza, M., Karagali, I., Lagemaa, P., Lien, V., Lima, L., Lyubartsev, V., Maljutenko, I., Masina, S., McAdam, R., Miraglio, P., Morrison, H., Panteleit, T. R., Pisano, A., Pujol, M.-I., Raudsepp, U., Raj, R., Stoffelen, A., Van Gennip, S., Veillard, P., and Yang, C.: The state of the ocean in the northeastern Atlantic and adjacent seas, in: 8th edition of the Copernicus Ocean State Report (OSR8), edited by: von Schuckmann, K., Moreira, L., Grégoire, M., Marcos, M., Staneva, J., Brasseur, P., Garric, G., Lionello, P., Karstensen, J., and Neukermans, G., Copernicus Publications, State Planet, 4-osr8, 2, https://doi.org/10.5194/sp-4-osr8-2-2024, 2024.

Weatherdon, L. V., Magnan, A. K., Rogers, A. D., Sumaila, U. R., and Cheung, W. W. L.: Observed and projected impacts of climate change on marine fisheries, aquaculture, coastal tourism, and human health: An update, Front. Mar. Sci., 3, 179990, https://doi.org/10.3389/FMARS.2016.00048/XML/NLM, 2016.

Winther, J.-G., Dai, M., Rist, T., Hoel, A. H., Li, Y., Trice, A., Morrissey, K., Juinio-Meñez, M. A., Fernandes, L., Unger, S., Scarano, F. R., Halpin, P., and Whitehouse, S.: Integrated ocean management for a sustainable ocean economy, Nat. Ecol. Evol., 4, 1451–1458, https://doi.org/10.1038/s41559-020-1259-6, 2020.

WMO Regions: https://wmo.int/about-wmo/regions, last access: 13 May 2025.

Wong, J., Münnich, M., and Gruber, N.: Column-Compound Extremes in the Global Ocean, AGU Advances, 5, e2023AV001059, https://doi.org/10.1029/2023AV001059, 2024.

Zeppel, H. and Beaumont, N.: Climate change and tourism futures: Responses by Australian tourism agencies, Tourism and Hospitality Research, 12, 73–88, https://doi.org/10.1177/1467358412444807, 2012.

State Planet, 6-osr9, 1, 2025
https://doi.org/10.5194/sp-6-osr9-1-2025

The 2025 Starfish Barometer

Marina Lévy[1], Karina von Schuckmann[2], Patrick Vincent[2], Bruno Blanke[3], Joachim Claudet[4], Patrice Guillotreau[5], Audrey Hasson[2], Claire Jolly[6], Yunne Shin[5], Olivier Thébaud[7], Adrien Vincent[8], and Pierre Bahurel[2]

[1]Sorbonne Université, LOCEAN-IPSL, CNRS/IRD/MNHN, Paris, France
[2]Mercator Ocean International, Toulouse, France
[3]LOPS-IUEM, UBO/CNRS/Ifremer/IRD, Brest, France
[4]CNRS, PSL-EPHE-UPVD, CRIOBE, Paris, France
[5]MARBEC, IRD/Ifremer/CNRS/Université Montpellier, Montpellier, France
[6]OECD, Paris, France
[7]AMURE, Ifremer/UBO/CNRS/IRD, IUEM, Plouzané, Brest, France
[8]IPOS, Paris, France

Correspondence: Marina Lévy (marina.levy@locean.ipsl.fr)

Received: 29 April 2025 – Discussion started: 30 April 2025
Revised: 8 May 2025 – Accepted: 13 May 2025 – Published: 8 June 2025

Abstract. The Ocean is essential to life on Earth, regulates the climate, supports rich biodiversity, sustains livelihoods, and inspires cultures and societies. However, unregulated human impacts are putting the Ocean and its ability to contribute to humanity at risk. The Starfish Barometer is a new initiative launched on World Ocean Day (8 June 2025) to provide a concise, science-based annual overview of the multiple dimensions of the Ocean through the lens of its interdependence with humanity. Each year, the Starfish Barometer will present a carefully curated selection of Ocean-related developments, chosen for their global significance and grounded in the most up-to-date scientific evidence, intended for a broad non-specialist audience. Rather than offering an exhaustive review, it will spotlight key aspects, robust, evidence-based, and reflective of major developments of the year. The Starfish Barometer emphasizes the two-way relationship between humanity and the Ocean: we impact its future, and it shapes ours. Its distinctive format, a five-armed starfish with the current state of the Ocean on the top arm, visually represents the balance conveyed by the four remaining arms: human-induced pressures that are undermining Ocean health, the resulting harms to society, the Ocean protection efforts underway, and the opportunities that the Ocean continues to offer to humanity. Key figures from the 2025 edition illustrate the alarming state of the Ocean. Sea level has risen by 23 cm since 1901; in 2023 alone, the losses from tropical storms and flooding totalled USD 102 billion. The 2024 Ocean temperatures broke the 64-year record, with sea-surface temperature and marine heatwaves showing a marked increase globally. Marine animal food production reached a record 115×10^6 t in 2022, yet 37.7 % of fish stocks remain overexploited, highlighting the urgent need for sustainable practices. Declared protection policies currently cover 8.34 % of the Ocean's surface, while marine biodiversity is under threat, with now 1677 marine species recorded as being at risk of extinction.

Published by Copernicus Publications.

1 Introduction

The Ocean[1] is essential to life on Earth – it regulates the climate, supports rich biodiversity, sustains livelihoods, and shapes cultures. Yet, information about its current state remains fragmented across disciplines, reports, and institutions, often inaccessible to the general public. The Starfish Barometer responds to a pressing need: to bring together, once a year and in one place, the most recent, reliable, and evidence-based scientific knowledge about the Ocean for the general public. Published each year on World Ocean Day (8 June), the Starfish Barometer serves as a yearly civic rendezvous by translating the year's most significant Ocean-related developments into accessible science-based insights.

What makes the Starfish Barometer unique is not the novelty of the data it presents – on the contrary, all the information it includes has already been published and validated in the scientific literature and institutional or international reports. Its strength lies in how it brings together this dispersed knowledge, synthesizing it into a comprehensive and integrated overview of the Ocean, aligned with the United Nations Sustainable Development Goal related to the Ocean, SDG 14 (UN, 2015). The Barometer is designed to serve a broad non-specialist audience, including policy makers, educators, civil society actors, and the general public, while remaining grounded in peer-reviewed science to ensure credibility and relevance for the scientific community as well. The Starfish Barometer takes stock of the latest available information on historical changes and current status and trends, rather than focusing on projected futures. In this sense, it acts as a snapshot of the year, drawing attention to key developments and current trends or highlighting important knowledge gaps. Each year, the Starfish Barometer selects and curates Ocean-related developments – such as new or updated scientific findings, international policy decisions, or governance milestones – chosen for their global relevance and based on the most recent knowledge available at the time of publication. This selection is not exhaustive but reflects key signals from the year, robust, factual, and representative of major trends.

The Starfish Barometer adopts a distinctive perspective, looking at the Ocean through the lens of its interdependence with humanity. Humans do both good and harm to the Ocean – and the Ocean, in turn, does both good and harm to humans. By presenting this dual relationship in a holistic and balanced way, the Starfish Barometer highlights the complex web of interactions that shapes the Ocean–humanity relationship. It puts into perspective human pressures and protection efforts, societal harms, and opportunities for humanity, offering a clear and accessible overview of these dynamics to empower informed decisions and commitments for Ocean protection. This approach emphasizes that the Ocean is a vital environment from which we derive many benefits – provided we take good care of it.

To visualize the balance in the relationships between humanity and the Ocean, the Starfish Barometer takes the shape of a five-armed starfish (Fig. 1). The top arm offers a global view of the Ocean's state. The two arms on the left side of the starfish represent negative developments: human-induced pressures and resulting harms to society. The two arms on the right side reflect positive dynamics: efforts to protect the Ocean and opportunities the Ocean provides to humanity. The upper arms show humanity's negative and positive impacts, while the lower arms show how the Ocean harms and creates opportunities for humanity. Thus the Starfish can be read horizontally, from left to right (negative to positive), or vertically, from top to bottom (human action to societal consequence). Selected key information is featured as concise, evidence-based news items, arranged along each branch of the Starfish Barometer and highlighted through short, clear, and accessible headlines. This format ensures scientific objectivity while making information accessible to a broad audience. The present article establishes the peer-reviewed scientific foundation of the Starfish Barometer (http://www.starfishbarometer.org, last access: 8 June 2025).

2 Methodology

The content of the Starfish Barometer was curated by a multidisciplinary group of experts, who identified and selected significant recent developments to be featured in the five thematic branches. The process began with each expert proposing candidate news items, based on a set of common criteria: global relevance, robustness of the underlying data, significance of the development, and relevance to the Ocean–human relationship. Sources included scientific assessments (e.g. IPCC, FAO, OECD), new or updated datasets (e.g. Global Carbon Budget), recent peer-reviewed scientific publications, international policy developments, data gaps, and emerging alerts. The proposed items were then collectively reviewed and discussed by the expert group to determine their relevance and final selection. This process is qualitative and adaptive by design, guided by transparent criteria and expert judgement to ensure that each Barometer edition remains accessible to the general public and focused on widely relevant issues.

The allocation of news items to specific branches is guided by thematic relevance but is not exclusive, as many Ocean-related developments intersect multiple dimensions. For example, certain topics, such as illegal, unreported, and unregulated (IUU) fishing, could be considered both a human pressure and a threat to societal equity. In such cases, items were assigned to the branch most closely aligned with the primary focus of the issue, following a consistent editorial framework

[1] Throughout the paper, we have used "Ocean" capitalized, just as one does for Earth, to underscore the scientific recognition of a single, interconnected global Ocean. This usage aligns with the convention adopted by IPCC (2019).

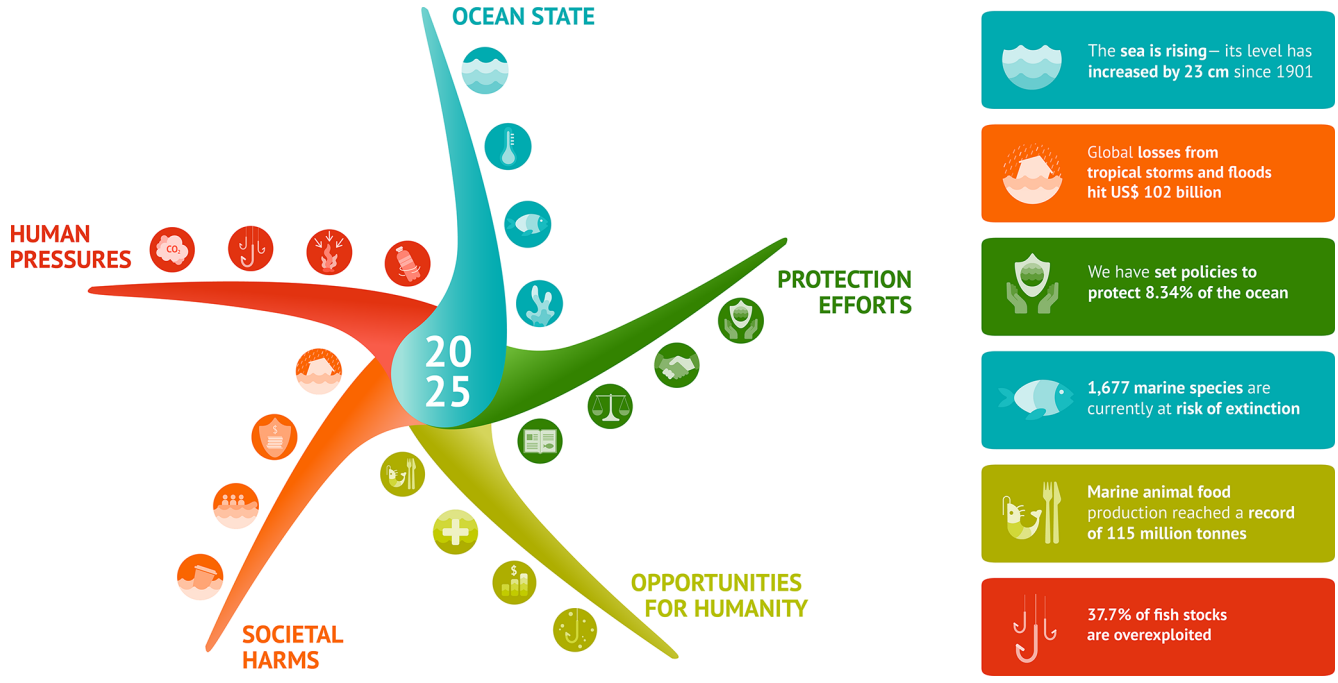

Figure 1. Schematic of the five branches of the Starfish Barometer and key figures for 2025. At the top, the blue branch represents the current state of the Ocean. The four other branches can be read horizontally, from red tones on the left to green tones on the right (negative to positive), or vertically, from darker tones at the top to lighter tones at the bottom (human actions to societal consequences). The figures represent the most recent estimates available on 8 June 2025.

rather than rigid topic boundaries. Each branch was limited to one page and to four key messages, anchored in recent developments and supported, in most cases, by figures and trend analyses.

We intentionally chose not to establish explicit logical connections between the news items within or across branches. While the branches together form a coherent picture of the Ocean–human relationship, forcing a linear or causal narrative might create an illusion of completeness or determinism that does not reflect the complexity of Ocean issues. Instead, each message stands on its own as a robust signal from the past year, contributing to a broader mosaic of understanding.

All figures presented in the Starfish Barometer are drawn directly from authoritative sources and are reported as published, in order to ensure transparency and traceability. Readers interested in the methodological details or associated uncertainties are encouraged to consult the original sources.

Each annual edition of the Starfish Barometer will follow the same symbolic and structural framework, with its five same thematic arms: Ocean state, human pressures, societal harms, protection efforts, and opportunities for humanity. However, the content within each arm will evolve yearly to reflect the most recent and relevant developments. When new data become available – such as for carbon emissions or sea level – they will be updated accordingly. Yet not all information is refreshed annually, and the Barometer's non-exhaustive approach provides the necessary flexibility to highlight either new figures or important issues that may vary from one year to the next. In this sense, the Barometer differs from initiatives like the Global Carbon Project (Friedlingstein et al., 2025) or the Ocean Health Index (Halpern et al., 2012): rather than systematically updating a fixed dataset, it offers a curated, narrative-based selection that captures the most meaningful signals of the year.

3 2025 Starfish five arms

3.1 Ocean state

The sea is rising – its level has increased globally by 23 cm since 1901. This is a direct consequence of accelerated Ocean warming and increasing ice loss from ice sheets and glaciers. In 2024, global sea levels reached the highest level ever recorded since monitoring began, rising 23 cm since 1901 (WMO, 2025; Forster et al., 2025). Over the past decade (2015–2024), the rate of sea-level rise has been twice as fast as in the early years of satellite records (1993–2002), due to increasing ice loss from the Greenland and Antarctic ice sheets, ongoing glacier mass loss, and thermal expansion due to Ocean warming (WMO, 2025).

The Ocean reached its highest recorded temperatures, with oxygen loss and rapid acidification threatening marine life. The year 2024 marks a year of intense, persistent, and

widespread heatwaves in the Ocean, and Ocean heat content reached its highest level in the 64 years for which we have reliable recorded global observations (since 1960), surpassing the previous record high set in 2023 (WMO, 2025; Cheng et al., 2025; Pan et al., 2025) and the 2015/16 record by 0.25 °C at the Ocean surface (Terhaar et al., 2025). The record Ocean surface temperature values reflect natural variability amplified by long-term global warming – an event unlikely to occur without the underlying climate trend (Terhaar et al., 2025; Guinaldo et al., 2025).

Ocean warming has doubled over the past 2 decades and has been accelerating for the past 70 years (IPCC, 2019; von Schuckmann et al., 2023; Minière et al., 2023; Storto and Yang, 2024; Forster et al., 2024). Ocean surface acidity (in $[H^+]$ concentration) has risen by 30 % over the past 39 years (IPCC, 2021; von Schuckmann et al., 2024; WMO, 2025), and open-Ocean waters have experienced an oxygen reduction of 0.8 % to 2.4 % over the past half-century to century (Breitburg et al., 2018; Oschlies, 2021; IPCC, 2021).

1677 marine species are threatened with extinction, with a third of sharks and over a quarter of cetaceans critically endangered, mainly due to overfishing and climate change. As of the most recent update (May 2025), 1677 marine species are listed as being at risk of extinction on the IUCN Red List, including 291 classified as critically endangered, 647 as endangered, and 739 as vulnerable (IUCN, 2025). Among these, 1211 species are experiencing declining populations, 28 are increasing, and the remainder either are stable or have unknown trends. This represents an increase of 204 species at risk since the last reported estimate (IOC-UNESCO, 2024). One-third of sharks, rays, and chimaeras are classified as threatened, with 67 % at risk of extinction due to fisheries (Jabado et al., 2024). A total of 26 % of 92 cetacean species (whales, dolphins, and porpoises) are threatened with extinction, and 11 % are near-threatened. The percentage of threatened cetaceans has increased over time, from 15 % in 1991 to 26 % in 2021 (Braulik et al., 2023). The Ocean Census initiative has discovered 866 new marine species in its first year, highlighting the unknown depths of Ocean life. This pace of discovery highlights a critical risk: countless marine species may go extinct before they are even identified – threatened by multiple stressors such as climate change, deep sea mining, and bottom trawling (IPOS, 2025), making conservation efforts all the more urgent (Ocean Census, 2025).

The fourth major coral bleaching event recorded hit the Ocean, with almost half of all coral species threatened with extinction and a worrying acceleration in reef degradation. Following extreme conditions in 2023 driven by historically high heat stress, the 2024 coral bleaching event is the fourth global event on record since 1985 and the second in the past decade (Hoegh-Guldberg et al., 2023; NOAA, 2024). Live coral cover on reefs has nearly halved over the past 150 years, with the decline dramatically accelerating over the past 2 or 3 decades (IPBES, 2019). A total of 44 % of reef coral species are threatened with extinction (IUCN, 2025). The rapid decline in coral reefs – the Ocean's most biodiverse habitat – is weakening natural storm protection, threatening biodiversity, and endangering livelihoods (IPBES, 2019).

3.2 Human pressures

Fossil fuel CO_2 emissions are rising, including a 2.7 % increase from shipping. The 2024 Global Carbon Budget projects global fossil carbon dioxide (CO_2) emissions of 37.4 Gt (10^9 t), up 0.8 % from 2023 (Friedlingstein et al., 2025). Emissions from international shipping are also on the rise, with a projected 0.6 Gt of CO_2 in 2024 (representing 1.6 % of total global emissions), up 2.7 % from 2023 (Andrew et al., 2024); these figures rely on countries' self-reported data regarding fuel sales for international shipping. Fossil fuel CO_2 emissions are the main contributor to recent climate change (IPCC, 2021). They also lead to Ocean acidification as approximately one-third of these emissions are absorbed by the Ocean (Friedlingstein et al., 2025).

Unsustainable fishing hits 37.7 %, while 75 % of large vessels go untracked. The percentage of marine stocks fished at unsustainable levels (i.e. beyond maximum sustainable yield) has increased since the mid-1970s, from 10 % in 1974 to 37.7 % in 2021 (FAO, 2024). Marine fisheries' activities involved approximately 4.9 million registered motorized and non-motorized fishing vessels in 2022 (FAO, 2024). This estimate represents only part of the sustainability challenge, as it does not account for broader ecological and social impacts of fisheries (Asche et al., 2025), nor for IUU fishing. An estimated 75 % of large (> 15 m) fishing vessels operate without proper tracking (2017–2021), challenging growing efforts to combat IUU fishing and to regulate marine protected areas (MPAs) (Paolo et al., 2024).

Rising human and climate pressures threaten marine habitats globally. A combination of growing pressures is involved, including unsustainable fishing practices, pollution, Ocean warming, acidification, and oxygen loss pushing marine ecosystems and species beyond their tolerance limits. Climate change is driving the loss of suitable habitats globally, with the most pronounced shifts in species richness occurring in tropical ecosystems (Chaudhary et al., 2021). Coastal ecosystems are also showing increasing signs of degradation. Since 1950, coastal hypoxia has increased 10-fold, reducing the extent and quality of coastal habitats critical to marine biodiversity (Breitburg et al., 2018). Climate change and pollution-driven eutrophication have caused a rise in the reporting of nearshore macroalgal blooms (green tides) worldwide over the past 2 decades (Ren et al., 2024), although comprehensive global estimates are lacking. Also, 50 % of mangrove ecosystems are at risk of collapse (IUCN, 2024), and over half of World Heritage seagrass habitats have high vulnerability to climate change (Losciale et al., 2024), while 33 % of the world's sandy coastline is currently hardened by human-made structures (Nawarat et al., 2024). The

multiple uses of coastal areas – like coastal infrastructures, tourism, fish farming, and offshore structures – are putting more pressure on Ocean habitats, through pollution; habitat destruction; and increased risks of marine pathogens, parasites, and invasive species, especially as coastal populations grow: in 2018, about 2.2 billion people, or 30 % of the world's population, lived within 50 km of the coast (Cosby et al., 2024).

Plastic pollution is rising but still no global system to monitor and assess it. Global plastic production surged from 2 Mt (10^6 t) in 1950 to 413.8 Mt in 2023, of which only 8.7 % is from recycled origin (Plastics Europe, 2024). Plastic waste accounts for over 80 % of identified aquatic debris (Harris et al., 2023). In 2021, plastic accumulation in rivers and the Ocean was estimated at 75–199 Mt (UNEP, 2021). Marine plastic pollution has been reported since the 1970s, but the absence of a unified global monitoring system still hampers effective assessment and response (Galgani et al., 2024).

3.3 Societal harms

Global losses from tropical storms and floods hit USD 102 billion. In 2023, the loss of economic assets caused by tropical cyclones and floods was worth USD 102 billion (inflation-adjusted, Munich RE, 2025a, b). Since 1980, losses have grown exponentially and now regularly exceed USD 100 billion per year, costing 25 % more to human populations every decade in inflation-adjusted terms (Nordhaus, 2006). Tropical storms often trigger heavy rainfall resulting in floods, casualties, and destruction of assets worth billions of dollars (Kron et al., 2019). Approximately 560 million people are exposed yearly, and this number has increased across all cyclone intensities over the past 2 decades (Jing et al., 2024).

Insurance premium costs incurred by maritime activities grew by 5.9 % with the expansion of global trade and increasing threats. Global marine insurance premiums totalled USD 38.9 billion in 2023, a 5.9 % increase from 2022 (IUMI, 2024). Steady growth has occurred over the past 5 years. Geopolitical tensions on global trade routes have significantly impacted insurance premiums and increased voyage costs by rerouting vessels, causing longer transit times. The growth also reveals the rise in insurance costs against hurricanes, war conflicts, and piracy. The main insurance premiums reported by the International Union of Maritime Insurance (IUMI) and P&I (Protection and Indemnity) clubs insure around 95 % of all risks, but public insurance figures only provide a partial view of total risk exposure (Knapp and Heij, 2017). In particular, damage to marine ecosystems in the case of oil spills varies widely, and some cannot be valued in monetary terms (El Moussaoui and Idelhakkar, 2023).

9002 migrants lost their lives at sea – the highest casualty loss recorded in the past decade. More than 73 000 migrants have died or disappeared at sea during the past decade, with the highest toll in 2024 with 9002 fatalities or disappearances (IOM, 2025). This represents a 3 % increase from 2023 but a 25 % increase from 2022. Poverty, unemployment, starvation, and insecurity are the main drivers of migration (Ndaliman and Abubakar, 2024). Changing environmental conditions, e.g. from sea-level rise, depletion of marine resources due to overfishing, and climate variability, are also important drivers of forced displacement (McLeman et al., 2025). However, the link between oceanic changes and migrant fatalities remains unclear and requires further investigation.

USD 250 billion health costs and 1200 species affected by marine plastic pollution. In 2015, health costs related to plastic exposure through seafood exceeded USD 250 billion globally (Landrigan et al., 2023). Chemicals carried by microplastics have been found in human blood, fat, and urine and are linked to cancer, infertility, obesity, heart disease, and developmental issues in babies – even before birth (European Environment Agency et al., 2021). Over 1200 marine species were reported to be harmed by plastic pollution through entanglement, ingestion, and chemical contamination (Santos et al., 2021).

3.4 Protection efforts

Global protected areas hits 8.34 %, but efforts are still needed to effectively reach the 30 % target. Over the past decade, the global coverage of MPAs has increased significantly, from 3.72 % of the global Ocean in 2015 (Lubchenco and Grorud-Colvert, 2015) to 8.34 % in 2024 (corresponding to 30.238×10^6 km^2), but is still far from the 30 × 30 target (protecting 30 % of the coastal and marine waters by 2030) (Protected Planet, 2025; UNEP-WCMC and IUCN, 2024). While 19 % of national waters (39 % of the Ocean) are protected, just 1.45 % of areas beyond national jurisdiction (61 % of the global Ocean) have protection (Protected Planet, 2025). Between 2023 and 2024, the surface covered by MPAs only increased by 0.007 % (Protected Planet, 2024). Globally, one in four MPAs exist only on paper (i.e. are not effectively implemented), and an additional third fails to truly support conservation goals (Pike et al., 2024). Only a third of the global coverage of MPAs is fully or highly protected (Pike et al., 2024). Ensuring that the global network of MPAs delivers its expected benefits for climate, biodiversity, and food security requires not only achieving the 30 % coverage target, but also increasing the level of protection within MPAs (Arneth et al., 2023).

Multilateral Ocean governance advances, highlighted by 21 ratifications of the High Seas Treaty. In 2024, the UN High Seas Treaty entered a critical phase with national ratifications and implementation planning. As of April 2025, 21 countries had ratified the treaty (High Seas Alliance, 2025). This treaty aims to promote the conservation and sustainable use of marine Biodiversity Beyond National Jurisdiction (BBNJ) – covering nearly two-thirds of the Ocean

(Blasiak and Claudet, 2024) – including via capacity building, transfer of marine technology and equitable sharing of the benefits of marine genetic resources. In 2024, new global guidelines were adopted to strengthen sustainable fisheries management by improving transparency, combating IUU fishing, restricting catch limits, and expanding AI-powered satellite monitoring (FAO, 2024; European Commission, 2024; Global Fishing Watch, 2024). The year 2024 also saw major advancements in blue carbon initiatives and marine renewable energy (Global Mangrove Alliance, 2024). In March 2022, a resolution was adopted by the UN to end plastic pollution through a legally binding agreement (UNEA-5). In July 2023, the International Maritime Organization adopted a new climate strategy targeting a 40 % cut in carbon intensity from international shipping by 2030, alongside a push for at least 5 % of the sector's energy to come from zero or near-zero emission fuels and technologies (IMO, 2023). In 2024, the International Tribunal for the Law of the Sea issued a landmark opinion (ITLOS, 2024), addressing states' obligations to protect the Ocean from climate change impacts within the framework of the United Nations Convention on the Law of the Sea (UNCLOS).

Equity rises as a driving force in global Ocean conservation, climate and sustainable development. Equity is increasingly recognized as an enabler of environmental sustainability, economic development, and global stability (Österblom et al., 2023; Claudet et al., 2024). The Convention on Biological Diversity (CBD) explicitly introduces equity in the Aichi Target 11 (CBD, 2010) and in the Kunming-Montreal Global Biodiversity Framework (CBD, 2022). Equity is a core principle of the 2030 Sustainable Development Agenda (UN, 2015). Since 2021, the UN Decade of Ocean Science for Sustainable Development has supported equitable access to Ocean knowledge and capacity building (Claudet et al., 2020). Equity is now central in sustainable planning efforts (Strand et al., 2024). Grassroots resistance efforts led by coastal communities have successfully stopped unfair exposure to environmental harms and preserved their livelihoods (Blythe et al., 2023).

Ocean literacy is gaining global momentum, with unprecedented growth in educational activities. Ocean Literacy is becoming a key pillar of Ocean and coastal management and policy (Shellock et al., 2024). Since 2021, 418 Ocean literacy activities and 27 projects have been endorsed under the UN Decade of Ocean Science. In 2024, the release of the Venice declaration offers a global framework for Ocean literacy (IOC-UNESCO, 2024; Ocean Literacy World Conference, 2024).

3.5 Opportunities for humanity

Marine animal food production reached a record 115 million tonnes, meeting a global demand with environmental costs. Marine aquaculture has almost quadrupled since the 1990s, reaching 35.3 Mt in 2022 (FAO, 2024), and now corresponds to 31 % of the total production of marine animal foods (FAO, 2024). In comparison, global marine capture fisheries' production has remained relatively stable since the 1990s, reaching 79.7 Mt in 2022. While sustainable aquaculture production is possible, the sector's diversity means some systems still cause significant environmental harm (Garlock et al., 2024). Overall, the global apparent consumption of aquatic animal food increased by 3 % per year between 1961 and 2021 – outpacing both the growth of the world's population (1.6 % per year) and the consumption of terrestrial meats (FAO, 2024). Over the same period, the internationally traded value of aquatic animal products grew by an average of 4.0 % annually, highlighting their increasing importance as one of the most extensively traded food commodities worldwide (FAO, 2024). These trends underscore that strengthening the sustainability of aquatic food production is essential to reduce environmental impacts and harness emerging economic opportunities.

The marine-derived health market is growing amid high inequity, with +7.5 % for marine-derived pharmaceutical sales. In 2024, a landmark global database containing 308.6 million gene clusters of marine origin was published (Laiolo et al., 2024), marking the largest collection of its kind to date and highlighting the acceleration in bioprospecting for new marine genetic resources (Krusberg et al., 2024). Future potential is vast given that 70 %–90 % of marine species are still undescribed (Sigwart et al., 2021). The global market for marine-derived pharmaceuticals was valued at USD 4.1 billion in 2023 (Fact.MR, 2023), while the marine oligosaccharides market – including pharmaceuticals but also cosmetics and other uses – reached USD 3.56 billion in 2024 (Precedence Research, 2025). Both markets are growing rapidly, with marine-derived pharmaceuticals sales increasing by 7.5 % between 2018 and 2022 (Fact.MR, 2023). However, access to marine genetic resources remains highly inequitable, with nearly half of all patents owned by a single company (Blasiak et al., 2018). Moreover, a critical point is the harvest of sufficient amounts of compounds without harming the marine environment (Lindequist, 2016).

USD 2.6 trillion Ocean economy powers 134 million jobs – but at an environmental cost. Between 1995 and 2020, the Ocean economy contributed between 3 % and 4 % of total global gross value added, doubling from USD 1.3 trillion to USD 2.6 trillion (OECD, 2025). Its share of global employment also rose, from 3.5 % to 4.7 %, with 134 million full-time equivalent (FTE) jobs in 2019 before the COVID-19 pandemic. In 2022, 43.9 million people were engaged in marine fisheries, aquaculture, or unspecified subsectors (FAO, 2024). The expansion has been largely driven by two sectors with high environmental impacts: offshore oil and gas (USD 988 billion in 2020) and coastal and marine tourism (USD 789 billion in 2019), the latter employing 80 million FTEs. Offshore wind and marine renewable energies, however, experienced the fastest growth, with gross value added rising from USD 38.2 million in 2000 to

USD 4.6 billion in 2020 (OECD, 2025; Jouffray et al., 2020). Reducing the environmental costs of Ocean-based industries – through expanding alternative energy sources and improving sustainability – presents major opportunities for sustainable economic growth.

Small-scale fisheries support 88 % of marine harvest jobs and USD 51.8 billion. Marine small-scale fisheries account for a significant fraction of the total annual marine landings with an estimated 25.1 Mt (31.2 % of global landings) (FAO et al., 2023; Gutierrez et al., 2023), representing an average (2013–2017) USD 51.8 billion annual landed economic value, higher than the revenues of cruise tourism, port activities, or offshore wind (Virdin et al., 2023). Although data remain incomplete and vary across regions, available estimates suggest that small-scale fisheries generate around 40 % of global fisheries catches (Basurto et al., 2025). They employ approximately 12.9 million people in the harvesting segment, which represents 88.1 % of total employment in marine fisheries value chains, and they contribute directly to sustainable development by providing livelihoods, cultural value, and critical nutrition – especially to vulnerable societal groups (Basurto et al., 2025). Strengthening the sustainability and resilience of small-scale fisheries – including addressing pressures from other Ocean sectors – is key to safeguarding their vital role in eradicating poverty, hunger, and malnutrition.

4 Conclusion

With the growing demand for evidence-based information, there is an urgent need to improve regular access to coherent, cross-disciplinary Ocean knowledge in order to foster well-informed awareness. The Starfish Barometer addresses this need by acting as a recurring synthesis and access point for such knowledge, drawing on multilateral scientific assessments – such as those from the IPCC, IPBES, and the World Ocean Assessment – as well as recent international reports and peer-reviewed academic research. Several global initiatives already contribute to monitoring various aspects of Ocean health, such as the Ocean Health Index (Halpern et al., 2012, 2017) or the Ocean State Report (von Schuckmann et al., 2024). The Starfish Barometer complements these efforts by adopting a distinct narrative format and focusing each year on a carefully selected set of developments. Its symbolic structure and non-exhaustive nature allow it to highlight new evidence, figures, or issues as they emerge, helping connect scientific knowledge to a broader civic and policy-oriented conversation.

Each year, the Starfish Barometer will spotlight a curated set of Ocean-related developments that have stood out over the past 12 months. For its first edition, the Starfish Barometer has brought together a curated selection of Ocean-related developments, chosen for their global relevance and scientific robustness, drawing on the most recent information available – even when published prior to the past year.

The view of this first Starfish Barometer reveals that the Ocean is undergoing rapid and alarming changes, marked by record heat, rising seas, widespread species decline, and threatened major ecosystems. Increasing pressures from rising greenhouse gas emissions and overexploitation are degrading the health of the Ocean, and pollution and habitat loss, particularly in coastal areas, are intensifying these challenges, while gaps in the global monitoring system hamper effective responses. The escalating costs of tropical storms and floods, coupled with rising migration fatalities, underscore the disproportionate burden for vulnerable populations and ecosystems. Likewise, the persistent threat of marine plastic pollution exposes the environmental injustice faced by both marine life and at-risk human communities, exacerbating existing vulnerabilities. At the same time, global Ocean protection is advancing, with marine protected areas now covering 8.34 % of the Ocean, but urgent action is still needed to reach common targets. Milestones such as the UN High Seas Treaty, progress on plastic pollution agreements, and a growing focus on equity and Ocean literacy are driving significant momentum towards stronger and more sustainable Ocean governance. Also, the Ocean economy is experiencing significant growth, driven by sectors such as marine aquaculture, offshore wind, and tourism. However, this expansion also brings environmental challenges, with the continued pressure on marine ecosystems from high-demand industries. Small-scale fisheries continue to play a critical role in both global food production and coastal livelihoods but are increasingly vulnerable to climate change and pressures from other Ocean activities.

With the third United Nations Ocean Conference taking place in June, and the ratification of the High-Seas Treaty on the horizon, 2025 stands as a critical juncture for Ocean governance – where multilateral cooperation and concrete actions are more urgent than ever. The 2025 Ocean Starfish Barometer highlights several strategic leverage points to accelerate progress on SDG 14 (UN, 2015), including reducing marine pollution (14.1), protecting ecosystems (14.2), tackling overfishing and destructive practices (14.4), conserving marine areas (14.5), strengthening Ocean science (14.A), supporting small-scale fishers (14.B), and upholding international law (14.C). It also highlights major gaps, such as the lack of an operational global monitoring system for plastic pollution in the Ocean.

These alignments demonstrate the Starfish Barometer's potential to serve not only as a communication tool but also as a monitoring instrument that can contribute to tracking progress toward global Ocean commitments. Beyond its global scope, the Starfish Barometer offers a flexible and adaptable framework – one that can be tailored for use at national or regional levels, integrated into educational programmes or used by institutions and NGOs to support reporting and awareness raising. Its accessible design allows

it to serve multiple purposes, from fostering civic engagement to informing policy dialogue. By connecting people to the Ocean through clear, meaningful insights, the Starfish Barometer seeks to spark reflection, responsibility, and action. It is a reminder that while the Ocean sustains life on Earth, its future – and ours – depends on the decisions we make today.

Data availability. No data sets were used in this article.

Author contributions. The concept of the Starfish Barometer was developed by ML and PB, with the support of PV. ML provided overall leadership for this work and led the writing of the manuscript with assistance from KvS. All coauthors contributed to content curation and manuscript preparation.

Competing interests. The contact author has declared that none of the authors has any competing interests.

Disclaimer. Publisher's note: Copernicus Publications remains neutral with regard to jurisdictional claims made in the text, published maps, institutional affiliations, or any other geographical representation in this paper. While Copernicus Publications makes every effort to include appropriate place names, the final responsibility lies with the authors.

Acknowledgements. The authors wish to warmly thank the international scientific committee of the One Ocean Science Congress (OOSC, Nice 3–6 June 2025), namely Janine Adams, Diva Amon, Tamatoa Bambridge, Sanae Chiba, Jorge Cortés-Núñez, Carlos Duarte, Stefan Gelcich, Jessica Gephart, Kristina Gjerde, Deborah Greaves, Peter Haugan, François Houllier, Jean-Pierre Gattuso, Daoji Li, Mere Takoko, and Arthur Tuda, for agreeing to oversee the draft of this paper on very short notice. The authors also wish to express their special thanks to Thomas Froelicher and William Cheung, both members of the OOSC scientific committee, who kindly acted as reviewers outside the oversight group to ensure the neutrality and integrity of the review process. Their promptness, availability, and thoughtful comments were particularly appreciated. This paper would not have come to life without the dedication of editor-in-chief Marilaure Grégoire and the entire editorial staff, whose efficiency and commitment made it possible to complete the editorial process. The Starfish Barometer was developed with the support of Olivier Poivre d'Arvor, French Ambassador for the Ocean and the Poles, and the French President's Special Envoy for the United Nations Ocean Conference (UNOC3). Special thanks go to the International Platform for Ocean Sustainability (IPOS), for sowing the first seeds of the concept, and to CNRS, IFREMER, and IRD for their scientific support. Several colleagues contributed to gathering the most up-to-date data, including Pierre Friedlingstein and Robbie Andrew from the Global Carbon Project; Pierre Cariou and Laurent Fedi from Bordeaux Kedge Business School; Kira Coley from the Ocean Census; Kensuke Obara from the Nippon Foundation; Charles Loiseau from CRIOBE; and Florian Kirchner, Virginie Tsilibaris, and Haizea Jimenez from IUCN. We also thank Laurence Collet for her contribution to the Starfish diagram and Clément Haëck for formatting the article and bibliography.

Review statement. This paper was edited by Marilaure Grégoire and reviewed by Thomas Froelicher and William Cheung.

References

Andrew, R. M. and Peters, G. P.: The Global Carbon Project's fossil CO2 emissions dataset (2024v18), CICERO Center for International Climate Research Oslo, Norway, Zenodo [data set], https://doi.org/10.5281/ZENODO.14106218, 2024.

Arneth, A., Leadley, P., Claudet, J., Coll, M., Rondinini, C., Rounsevell, M. D. A., Shin, Y., Alexander, P., and Fuchs, R.: Making protected areas effective for biodiversity, climate and food, Glob. Chang. Biol., 29, 3883–3894, https://doi.org/10.1111/gcb.16664, 2023.

Asche, F., Garlock, T. M., Anderson, J. L., Pincinato, R. B., Anderson, C. M., Camp, E. V., Chu, J., Cojocaru, A. L., Eggert, H., Lorenzen, K., Love, D. C., and Tveteras, R.: A Review of Global Fisheries Performance, Fish Fish., 26, 444–453, https://doi.org/10.1111/faf.12890, 2025.

Basurto, X., Gutierrez, N. L., Franz, N., Mancha-Cisneros, M. D. M., Gorelli, G., Aguión, A., Funge-Smith, S., Harper, S., Mills, D. J., Nico, G., Tilley, A., Vannuccini, S., Virdin, J., Westlund, L., Allison, E. H., Anderson, C. M., Baio, A., Cinner, J., Fabinyi, M., Hicks, C. C., Kolding, J., Melnychuk, M. C., Ovando, D., Parma, A. M., Robinson, J. P. W., and Thilsted, S. H.: Illuminating the multidimensional contributions of small-scale fisheries, Nature, 637, 875–884, https://doi.org/10.1038/s41586-024-08448-z, 2025.

Blasiak, R. and Claudet, J.: Governance of the High Seas, Annu. Rev. Env. Resour., 49, 549–572, https://doi.org/10.1146/annurev-environ-011023-022521, 2024.

Blasiak, R., Jouffray, J.-B., Wabnitz, C. C. C., Sundström, E., and Österblom, H.: Corporate control and global governance of marine genetic resources, Sci. Adv., 4, eaar5237, https://doi.org/10.1126/sciadv.aar5237, 2018.

Blythe, J. L., Gill, D. A., Claudet, J., Bennett, N. J., Gurney, G. G., Baggio, J. A., Ban, N. C., Bernard, M. L., Brun, V., Darling, E. S., Di Franco, A., Epstein, G., Franks, P., Horan, R., Jupiter, S. D., Lau, J., Lazzari, N., Mahajan, S. L., Mangubhai, S., Naggea, J., Turner, R. A., and Zafra-Calvo, N.: Blue justice: A review of emerging scholarship and resistance movements, Camb. Prisms Coast. Futures, 1, e15, https://doi.org/10.1017/cft.2023.4, 2023.

Braulik, G. T., Taylor, B. L., Minton, G., Notarbartolo Di Sciara, G., Collins, T., Rojas-Bracho, L., Crespo, E. A., Ponnampalam, L. S., Double, M. C., and Reeves, R. R.: Red-list status and extinction risk of the world's whales, dolphins, and porpoises, Conserv. Biol., 37, e14090, https://doi.org/10.1111/cobi.14090, 2023.

Breitburg, D., Levin, L. A., Oschlies, A., Grégoire, M., Chavez, F. P., Conley, D. J., Garçon, V., Gilbert, D., Gutiérrez, D., Isensee, K., Jacinto, G. S., Limburg, K. E., Montes, I., Naqvi, S. W. A., Pitcher, G. C., Rabalais, N. N., Roman, M. R., Rose, K. A.,

Seibel, B. A., Telszewski, M., Yasuhara, M., and Zhang, J.: Declining oxygen in the global ocean and coastal waters, Science, 359, eaam7240, https://doi.org/10.1126/science.aam7240, 2018.

CBD: Aichi Biodiversity Targets, CBD, https://www.cbd.int/sp/targets (last access: 18 April 2025), 2010.

CBD: Kunming-Montreal Global Biodiversity Framework, CBD, https://www.cbd.int/gbf (last access: 18 April 2025), 2022.

Chaudhary, C., Richardson, A. J., Schoeman, D. S., and Costello, M. J.: Global warming is causing a more pronounced dip in marine species richness around the equator, P. Natl. Acad. Sci. USA, 118, e2015094118, https://doi.org/10.1073/pnas.2015094118, 2021.

Cheng, L., Abraham, J., Trenberth, K. E., Reagan, J., Zhang, H.-M., Storto, A., Von Schuckmann, K., Pan, Y., Zhu, Y., Mann, M. E., Zhu, J., Wang, F., Yu, F., Locarnini, R., Fasullo, J., Huang, B., Graham, G., Yin, X., Gouretski, V., Zheng, F., Li, Y., Zhang, B., Wan, L., Chen, X., Wang, D., Feng, L., Song, X., Liu, Y., Reseghetti, F., Simoncelli, S., Chen, G., Zhang, R., Mishonov, A., Tan, Z., Wei, W., Yuan, H., Li, G., Ren, Q., Cao, L., Lu, Y., Du, J., Lyu, K., Sulaiman, A., Mayer, M., Wang, H., Ma, Z., Bao, S., Yan, H., Liu, Z., Yang, C., Liu, X., Hausfather, Z., Szekely, T., and Gues, F.: Record High Temperatures in the Ocean in 2024, Adv. Atmos. Sci., 42, 1092–1109, https://doi.org/10.1007/s00376-025-4541-3, 2025.

Claudet, J., Bopp, L., Cheung, W. W. L., Devillers, R., Escobar-Briones, E., Haugan, P., Heymans, J. J., Masson-Delmotte, V., Matz-Lück, N., Miloslavich, P., Mullineaux, L., Visbeck, M., Watson, R., Zivian, A. M., Ansorge, I., Araujo, M., Aricò, S., Bailly, D., Barbière, J., Barnerias, C., Bowler, C., Brun, V., Cazenave, A., Diver, C., Euzen, A., Gaye, A. T., Hilmi, N., Ménard, F., Moulin, C., Muñoz, N. P., Parmentier, R., Pebayle, A., Pörtner, H.-O., Osvaldina, S., Ricard, P., Santos, R. S., Sicre, M.-A., Thiébault, S., Thiele, T., Troublé, R., Turra, A., Uku, J., and Gaill, F.: A Roadmap for Using the UN Decade of Ocean Science for Sustainable Development in Support of Science, Policy, and Action, One Earth, 2, 34–42, https://doi.org/10.1016/j.oneear.2019.10.012, 2020.

Claudet, J., Blythe, J., Gill, D. A., Bennett, N. J., Gurney, G. G., Evans, L., Mahajan, S. L., Turner, R. A., Ahmadia, G. N., Ban, N. C., Epstein, G., Jupiter, S. D., Lau, J., Mangubhai, S., Zafra-Calvo, N., Lazzari, N., Baggio, J. A., Bernard, M. L., Brun, V., D'Agata, S., Di Franco, A., Horan, R., and Naggea, J.: Advancing ocean equity at the nexus of development, climate and conservation policy, Nat. Ecol. Evol., 8, 1205–1208, https://doi.org/10.1038/s41559-024-02417-5, 2024.

Cosby, A. G., Lebakula, V., Smith, C. N., Wanik, D. W., Bergene, K., Rose, A. N., Swanson, D., and Bloom, D. E.: Accelerating growth of human coastal populations at the global and continent levels: 2000–2018, Sci. Rep., 14, 22489, https://doi.org/10.1038/s41598-024-73287-x, 2024.

El Moussaoui, N. and Idelhakkar, B.: The Impact of Oil Spills on the Economy and the Environment, European Journal of Economic and Financial Research, 7, https://doi.org/10.46827/ejefr.v7i4.1570, 2023.

European Commission: The Commission welcomes the agreement on sustainable fisheries reached at Indian Ocean Tuna Commission, European Commission, https://ec.europa.eu/commission/presscorner/detail/en/ip_24_2683 (last access: 17 April 2025), 2024.

European Environment Agency, Reichel, A., Trier, X., Fernandez, R., Bakas, I., and Zeiger, B.: Plastics, the circular economy and Europe's environment: a priority for action, Publications Office of the European Union, https://doi.org/10.2800/5847, 2021.

Fact.MR: Marine-derived Pharmaceuticals Market Outlook (2023 to 2033), Fact.MR, https://www.factmr.com/report/marine-derived-pharmaceuticals-market (last access: 17 April 2025), 2023.

FAO: The State of World Fisheries and Aquaculture 2024, FAO, Rome, 264 pp., https://doi.org/10.4060/cd0683en, ISBN 978-92-5-138763-4, 2024.

FAO, Duke University, and WorldFish: Illuminating Hidden Harvests: The contributions of small-scale fisheries to sustainable development, FAO, Duke University, WorldFish, Rome, 376 pp., https://doi.org/10.4060/cc4576en, ISBN 978-92-5-137682-9, 2023.

Forster, P. M., Smith, C., Walsh, T., Lamb, W. F., Lamboll, R., Hall, B., Hauser, M., Ribes, A., Rosen, D., Gillett, N. P., Palmer, M. D., Rogelj, J., von Schuckmann, K., Trewin, B., Allen, M., Andrew, R., Betts, R. A., Borger, A., Boyer, T., Broersma, J. A., Buontempo, C., Burgess, S., Cagnazzo, C., Cheng, L., Friedlingstein, P., Gettelman, A., Gütschow, J., Ishii, M., Jenkins, S., Lan, X., Morice, C., Mühle, J., Kadow, C., Kennedy, J., Killick, R. E., Krummel, P. B., Minx, J. C., Myhre, G., Naik, V., Peters, G. P., Pirani, A., Pongratz, J., Schleussner, C.-F., Seneviratne, S. I., Szopa, S., Thorne, P., Kovilakam, M. V. M., Majamäki, E., Jalkanen, J.-P., van Marle, M., Hoesly, R. M., Rohde, R., Schumacher, D., van der Werf, G., Vose, R., Zickfeld, K., Zhang, X., Masson-Delmotte, V., and Zhai, P.: Indicators of Global Climate Change 2023: annual update of key indicators of the state of the climate system and human influence, Earth Syst. Sci. Data, 16, 2625–2658, https://doi.org/10.5194/essd-16-2625-2024, 2024.

Forster, P. M., Smith, C., Walsh, T., Lamb, W. F., Lamboll, R., Cassou, C., Hauser, M., Hausfather, Z., Lee, J.-Y., Palmer, M. D., von Schuckmann, K., Slangen, A. B. A., Szopa, S., Trewin, B., Yun, J., Gillett, N. P., Jenkins, S., Matthews, H. D., Raghavan, K., Ribes, A., Rogelj, J., Rosen, D., Zhang, X., Allen, M., Aleluia Reis, L., Andrew, R. M., Betts, R. A., Borger, A., Broersma, J. A., Burgess, S. N., Cheng, L., Friedlingstein, P., Domingues, C. M., Gambarini, M., Gasser, T., Gütschow, J., Ishii, M., Kadow, C., Kennedy, J., Killick, R. E., Krummel, P. B., Liné, A., Monselesan, D. P., Morice, C., Mühle, J., Naik, V., Peters, G. P., Pirani, A., Pongratz, J., Minx, J. C., Rigby, M., Rohde, R., Savita, A., Seneviratne, S. I., Thorne, P., Wells, C., Western, L. M., van der Werf, G. R., Wijffels, S. E., Masson-Delmotte, V., and Zhai, P.: Indicators of Global Climate Change 2024: annual update of key indicators of the state of the climate system and human influence, Earth Syst. Sci. Data Discuss. [preprint], https://doi.org/10.5194/essd-2025-250, in review, 2025.

Friedlingstein, P., O'Sullivan, M., Jones, M. W., Andrew, R. M., Hauck, J., Landschützer, P., Le Quéré, C., Li, H., Luijkx, I. T., Olsen, A., Peters, G. P., Peters, W., Pongratz, J., Schwingshackl, C., Sitch, S., Canadell, J. G., Ciais, P., Jackson, R. B., Alin, S. R., Arneth, A., Arora, V., Bates, N. R., Becker, M., Bellouin, N., Berghoff, C. F., Bittig, H. C., Bopp, L., Cadule, P., Campbell, K., Chamberlain, M. A., Chandra, N., Chevallier, F., Chini, L. P., Colligan, T., Decayeux, J., Djeutchouang, L. M., Dou, X., Duran Rojas, C., Enyo, K., Evans, W., Fay, A. R., Feely, R. A., Ford, D. J., Foster, A., Gasser, T., Gehlen, M., Gkritzalis, T., Grassi, G.,

Gregor, L., Gruber, N., Gürses, Ö., Harris, I., Hefner, M., Heinke, J., Hurtt, G. C., Iida, Y., Ilyina, T., Jacobson, A. R., Jain, A. K., Jarníková, T., Jersild, A., Jiang, F., Jin, Z., Kato, E., Keeling, R. F., Klein Goldewijk, K., Knauer, J., Korsbakken, J. I., Lan, X., Lauvset, S. K., Lefèvre, N., Liu, Z., Liu, J., Ma, L., Maksyutov, S., Marland, G., Mayot, N., McGuire, P. C., Metzl, N., Monacci, N. M., Morgan, E. J., Nakaoka, S.-I., Neill, C., Niwa, Y., Nützel, T., Olivier, L., Ono, T., Palmer, P. I., Pierrot, D., Qin, Z., Resplandy, L., Roobaert, A., Rosan, T. M., Rödenbeck, C., Schwinger, J., Smallman, T. L., Smith, S. M., Sospedra-Alfonso, R., Steinhoff, T., Sun, Q., Sutton, A. J., Séférian, R., Takao, S., Tatebe, H., Tian, H., Tilbrook, B., Torres, O., Tourigny, E., Tsujino, H., Tubiello, F., van der Werf, G., Wanninkhof, R., Wang, X., Yang, D., Yang, X., Yu, Z., Yuan, W., Yue, X., Zaehle, S., Zeng, N., and Zeng, J.: Global Carbon Budget 2024, Earth Syst. Sci. Data, 17, 965–1039, https://doi.org/10.5194/essd-17-965-2025, 2025.

Galgani, F., Lusher, A. L., Strand, J., Haarr, M. L., Vinci, M., Molina Jack, E., Kagi, R., Aliani, S., Herzke, D., Nikiforov, V., Primpke, S., Schmidt, N., Fabres, J., De Witte, B., Solbakken, V. S., and van Bavel, B.: Revisiting the strategy for marine litter monitoring within the european marine strategy framework directive (MSFD), Ocean Coast. Manage., 255, 107254, https://doi.org/10.1016/j.ocecoaman.2024.107254, 2024.

Garlock, T. M., Asche, F., Anderson, J. L., Eggert, H., Anderson, T. M., Che, B., Chávez, C. A., Chu, J., Chukwuone, N., Dey, M. M., Fitzsimmons, K., Flores, J., Guillen, J., Kumar, G., Liu, L., Llorente, I., Nguyen, L., Nielsen, R., Pincinato, R. B. M., Sudhakaran, P. O., Tibesigwa, B., and Tveteras, R.: Environmental, economic, and social sustainability in aquaculture: the aquaculture performance indicators, Nat. Commun., 15, 5274, https://doi.org/10.1038/s41467-024-49556-8, 2024.

Global Fishing Watch: New research harnesses AI and satellite imagery to reveal the expanding footprint of human activity at sea, Global Fishing Watch, https://globalfishingwatch.org/press-release/new-research-harnesses-ai-and-satellite-imagery-to-reveal-the-expanding-footprint-of-human-activity-at-sea/ (last access: 17 April 2025), 2024.

Global Mangrove Alliance: The State of the World's Mangroves 2024, Global Mangrove Alliance, https://doi.org/10.5479/10088/119867, 2024.

Guinaldo, T., Cassou, C., Sallée, J.-B., and Liné, A.: Internal variability effect doped by climate change drove the 2023 marine heat extreme in the North Atlantic, Commun. Earth Environ., 6, 291, https://doi.org/10.1038/s43247-025-02197-1, 2025.

Gutierrez, N. L., Funge-Smith, S., Gorelli, G., Mancha-Cisneros, M. M., Defeo, O., Johnson, A. F., and Melnychuk, M. C.: Production and environmental interactions of small-scale fisheries, in: Illuminating Hidden Harvests: The contributions of small-scale fisheries to sustainable development, FAO, Duke University, WorldFish, Rome, https://doi.org/10.4060/cc4576en, ISBN 978-92-5-137682-9, 2023.

Halpern, B. S., Longo, C., Hardy, D., McLeod, K. L., Samhouri, J. F., Katona, S. K., Kleisner, K., Lester, S. E., O'Leary, J., Ranelletti, M., Rosenberg, A. A., Scarborough, C., Selig, E. R., Best, B. D., Brumbaugh, D. R., Chapin, F. S., Crowder, L. B., Daly, K. L., Doney, S. C., Elfes, C., Fogarty, M. J., Gaines, S. D., Jacobsen, K. I., Karrer, L. B., Leslie, H. M., Neeley, E., Pauly, D., Polasky, S., Ris, B., Martin, K. S., Stone, G. S., Sumaila, U. R., and Zeller, D.: An index to assess the health and benefits of the global ocean, Nature, 488, 615–620, https://doi.org/10.1038/nature11397, 2012.

Halpern, B. S., Frazier, M., Afflerbach, J., O'Hara, C., Katona, S., Lowndes, J. S. S., Jiang, N., Pacheco, E., Scarborough, C., and Polsenberg, J.: Drivers and implications of change in global ocean health over the past five years, PLoS ONE, 12, e0178267, https://doi.org/10.1371/journal.pone.0178267, 2017.

Harris, P. T., Maes, T., Raubenheimer, K., and Walsh, J. P.: A marine plastic cloud – Global mass balance assessment of oceanic plastic pollution, Cont. Shelf Res., 255, 104947, https://doi.org/10.1016/j.csr.2023.104947, 2023.

High Seas Alliance: High Seas Treaty Ratification Tracker, High Seas Alliance, https://highseasalliance.org/treaty-ratification/ (last access: 17 April 2025), 2025.

Hoegh-Guldberg, O., Skirving, W., Dove, S., Spady, B., Norrie, A., Geiger, E., Liu, G., De La Cour, J., and Manzello, D.: Coral reefs in peril in a record-breaking year, Science, 382, 1238–1240, https://doi.org/10.1126/science.adk4532, 2023.

IMO: 2023 IMO Strategy on Reduction of GHG Emissions from Ships – Annex 15, RESOLUTION MEPC.377(80), IMO, https://wwwcdn.imo.org/localresources/en/OurWork/Environment/Documents/annex/MEPC%2080/Annex%2015.pdf (last access: 18 April 2025), 2023.

IOC-UNESCO: State of the Ocean Report, Paris, UNESCO-IOC, IOC Technical Series, 190, https://doi.org/10.25607/4WBG-D349, 2024.

IOM: Missing Migrants Project: Data, IOM, https://missingmigrants.iom.int/data (last access: 17 April 2025), 2025.

IPBES: Summary for policymakers of the global assessment report on biodiversity and ecosystem services of the Intergovernmental Science-Policy Platform on Biodiversity and Ecosystem Services, edited by: Díaz, S., Settele, J., Brondízio, E. S., Ngo, H. T., Guèze, M., Agard, J., Arneth, A., Balvanera, P., Brauman, K. A., Butchart, S. H. M., Chan, K. M. A., Garibaldi, L. A., Ichii, K., Liu, J., Subramanian, S. M., Midgley, G. F., Miloslavich, P., Molnár, Z., Obura, D., Pfaff, A., Polasky, S., Purvis, A., Razzaque, J., Reyers, B., Roy Chowdhury, R., Shin, Y. J., Visseren-Hamakers, I. J., Willis, K. J., and Zayas, C. N., IPBES secretariat, Bonn, Germany, Zenodo, https://doi.org/10.5281/ZENODO.3553579, 56 pp., ISBN 978-3-947851-13-3, 2019.

IPCC: IPCC Special Report on the Ocean and Cryosphere in a Changing Climate, edited by: Pörtner, H.-O., Roberts, D. C., Masson-Delmotte, V., Zhai, P., Tignor, M., Poloczanska, E., Mintenbeck, K., Alegría, A., Nicolai, M., Okem, A., Petzold, J., Rama, B., and Weyer, N. M., Cambridge University Press, Cambridge, UK and New York, NY, USA, 755 pp., https://doi.org/10.1017/9781009157964, ISBN 978-1-00-915796-4, 2019.

IPCC: Summary for Policymakers, in: Climate Change 2021: The Physical Science Basis. Working Group I Contribution to the Sixth Assessment Report of the Intergovernmental Panel on Climate Change, Cambridge University Press, Cambridge, 3–32, https://doi.org/10.1017/9781009157896.001, 2021.

IPOS: The global deep sea consultation, IPOS, https://ipos.earth/global-deep-sea-consultation-pilot-project (last access: 8 May 2025), 2025.

ITLOS: International Tribunal for the Law of the Sea: Request for an advisory opinion submitted by the commission of small island

states on climate change and international law, Advisory opinion, ITLOS, https://www.itlos.org/fileadmin/itlos/documents/cases/31/Advisory_Opinion/C31_Adv_Op_21.05.2024_orig.pdf (last access: 8 May 2025), 2024.

IUCN: Red List of Mangrove Ecosystems, IUCN, https://iucn.org/resources/conservation-tool/iucn-red-list-ecosystems/red-list-mangrove-ecosystems (last access: 8 May 2025), 2024.

IUCN: The IUCN Red List of Threatened Species, IUCN, https://www.iucnredlist.org/en (last access: 17 April 2025), 2025.

IUMI: IUMI Stats Report 2024, International Union of Marine Insurance, Germany, 40 pp., https://iumi.com/statistics/iumi-stats-report-2024/ (last access: 17 April 2025), 2024.

Jabado, R., Morata, A., Bennett, R., Finucci, B., Ellis, J., Fowler, S., Grant, M., Barbosa Martins, A., and Sinclair, S. (Eds.): The Global Status of Sharks, Rays, and Chimaeras, IUCN, Gland, Switzerland, https://doi.org/10.59216/ssg.gsrsrc.2024, 2024.

Jing, R., Heft-Neal, S., Chavas, D. R., Griswold, M., Wang, Z., Clark-Ginsberg, A., Guha-Sapir, D., Bendavid, E., and Wagner, Z.: Global population profile of tropical cyclone exposure from 2002 to 2019, Nature, 626, 549–554, https://doi.org/10.1038/s41586-023-06963-z, 2024.

Jouffray, J.-B., Blasiak, R., Norström, A. V., Österblom, H., and Nyström, M.: The Blue Acceleration: The Trajectory of Human Expansion into the Ocean, One Earth, 2, 43–54, https://doi.org/10.1016/j.oneear.2019.12.016, 2020.

Knapp, S. and Heij, C.: Evaluation of total risk exposure and insurance premiums in the maritime industry, Transport. Res. D-Tr. E., 54, 321–334, https://doi.org/10.1016/j.trd.2017.06.001, 2017.

Kron, W., Eichner, J., and Kundzewicz, Z. W.: Reduction of flood risk in Europe – Reflections from a reinsurance perspective, J. Hydrol., 576, 197–209, https://doi.org/10.1016/j.jhydrol.2019.06.050, 2019.

Krusberg, T., Schildt, L., Jouffray, J.-B., Zhivkoplias, E., and Blasiak, R.: A review of marine genetic resource valuations, npj Ocean Sustain., 3, 46, https://doi.org/10.1038/s44183-024-00081-7, 2024.

Laiolo, E., Alam, I., Uludag, M., Jamil, T., Agusti, S., Gojobori, T., Acinas, S. G., Gasol, J. M., and Duarte, C. M.: Metagenomic probing toward an atlas of the taxonomic and metabolic foundations of the global ocean genome, Front. Sci., 1, 1038696, https://doi.org/10.3389/fsci.2023.1038696, 2024.

Landrigan, P. J., Raps, H., Cropper, M., Bald, C., Brunner, M., Canonizado, E. M., Charles, D., Chiles, T. C., Donohue, M. J., Enck, J., Fenichel, P., Fleming, L. E., Ferrier-Pages, C., Fordham, R., Gozt, A., Griffin, C., Hahn, M. E., Haryanto, B., Hixson, R., Ianelli, H., James, B. D., Kumar, P., Laborde, A., Law, K. L., Martin, K., Mu, J., Mulders, Y., Mustapha, A., Niu, J., Pahl, S., Park, Y., Pedrotti, M.-L., Pitt, J. A., Ruchirawat, M., Seewoo, B. J., Spring, M., Stegeman, J. J., Suk, W., Symeonides, C., Takada, H., Thompson, R. C., Vicini, A., Wang, Z., Whitman, E., Wirth, D., Wolff, M., Yousuf, A. K., and Dunlop, S.: The Minderoo-Monaco Commission on Plastics and Human Health, Ann. Glob. Health, 89, 23, https://doi.org/10.5334/aogh.4056, 2023.

Lindequist, U.: Marine-Derived Pharmaceuticals – Challenges and Opportunities, Biomol. Ther., 24, 561–571, https://doi.org/10.4062/biomolther.2016.181, 2016.

Losciale, R., Day, J. C., Rasheed, M. A., and Heron, S. F.: The vulnerability of World Heritage seagrass habitats to climate change, Glob. Change Biol., 30, e17113, https://doi.org/10.1111/gcb.17113, 2024.

Lubchenco, J. and Grorud-Colvert, K.: Making waves: The science and politics of ocean protection, Science, 350, 382–383, https://doi.org/10.1126/science.aad5443, 2015.

McLeman, R., Hevesi, C., and Cadham, E.: Evolution of climate-related migration and displacement in IPCC reporting, Working paper, Department of Geography & Environmental Studies, Wilfrid Laurier University, Environmental Science Research Network, https://doi.org/10.2139/ssrn.5166785, 5 March 2025.

Minière, A., Von Schuckmann, K., Sallée, J.-B., and Vogt, L.: Robust acceleration of Earth system heating observed over the past six decades, Sci. Rep., 13, 22975, https://doi.org/10.1038/s41598-023-49353-1, 2023.

Munich RE: Flood risks on the rise: Greater loss prevention is needed, Munich RE, https://www.munichre.com/en/risks/natural-disasters/floods.html (last access: 17 April 2025), 2025a.

Munich RE: Hurricanes, typhoons, cyclones: Tropical storms – The natural hazard with the highest losses, Munich RE, https://www.munichre.com/en/risks/natural-disasters/hurricanes.html (last access: 17 April 2025), 2025b.

Nawarat, K., Reyns, J., Vousdoukas, M. I., Duong, T. M., Kras, E., and Ranasinghe, R.: Coastal hardening and what it means for the world's sandy beaches, Nat. Commun., 15, 10626, https://doi.org/10.1038/s41467-024-54952-1, 2024.

Ndaliman, H. A. and Yukaka, Abubakar.: The Drivers of African Migrants to Europe and the Mediterranean Sea Death Trap, International Journal of Intellectual Discourse, 7, 291–299, 2024.

NOAA: NOAA confirms 4th global coral bleaching event, NOAA, https://www.noaa.gov/news-release/noaa-confirms-4th-global-coral-bleaching-event (last access: 17 April 2025), 2024.

Nordhaus, W.: The Economics of Hurricanes in the United States, National Bureau of Economic Research, Cambridge, MA, https://doi.org/10.3386/w12813, 2006.

Ocean Census: The Ocean Census Discovers Over 800 New Marine Species, Ocean Census, https://oceancensus.org/publications/press-release-the-ocean-census-discovers-over-800-new-marine-species/ (last access: 17 April 2025), 2025.

Ocean Literacy World Conference: Venice Declaration for Ocean Literacy in Action, Ocean Literacy World Conference, 7–8 June 2024, Venice, Italy, https://www.marine-ed.org/news/venice-declaration-for-ocean-literacy-in-action (last access: 17 April 2025), 2024.

OECD: The Ocean Economy to 2050, OECD Publishing, Paris, https://doi.org/10.1787/a9096fb1-en, 2025.

Oschlies, A.: A committed fourfold increase in ocean oxygen loss, Nat. Commun., 12, 2307, https://doi.org/10.1038/s41467-021-22584-4, 2021.

Österblom, H., Wabnitz, C. C. C., Tladi, D., Allison, E. H., Arnaud-Haond, S., Bebbington, J., Bennett, N., Blasiak, R., Boonstra, W., Choudhury, A., Cisneros-Montemayor, A., Daw, T., Fabinyi, M., Franz, N., Harden-Davies, H., Kleiber, D., Lopes, P., McDougall, C., Resosudarmo, B. P., and Selim, S. A.: Towards Ocean Equity, in: The Blue Compendium: From Knowledge to Action for a Sustainable Ocean Economy, edited by: Lubchenco, J. and Haugan, P. M., Springer International Publishing, Cham, 485–521, https://doi.org/10.1007/978-3-031-16277-0_13, 2023.

Pan, Y., Minière, A., von Schuckmann, K., Li, Z., Li, Y., Cheng, L., and Zhu, J.: Ocean heat content in 2024, Nat. Rev. Earth Environ., 6, 249–251, https://doi.org/10.1038/s43017-025-00655-0, 2025.

Paolo, F. S., Kroodsma, D., Raynor, J., Hochberg, T., Davis, P., Cleary, J., Marsaglia, L., Orofino, S., Thomas, C., and Halpin, P.: Satellite mapping reveals extensive industrial activity at sea, Nature, 625, 85–91, https://doi.org/10.1038/s41586-023-06825-8, 2024.

Pike, E. P., MacCarthy, J. M. C., Hameed, S. O., Harasta, N., Grorud-Colvert, K., Sullivan-Stack, J., Claudet, J., Horta E Costa, B., Gonçalves, E. J., Villagomez, A., and Morgan, L.: Ocean protection quality is lagging behind quantity: Applying a scientific framework to assess real marine protected area progress against the 30 by 30 target, Conserv. Lett., 17, e13020, https://doi.org/10.1111/conl.13020, 2024.

Plastics Europe: Plastics – the fast Facts 2024, Plastics Europe, https://plasticseurope.org/knowledge-hub/plastics-the-fast-facts-2024/ (last access: 17 April 2025), 2024.

Precedence Research: Marine Oligosaccharides Market Size, Share and Trends 2025 to 2034, Precedence Research, https://www.precedenceresearch.com/marine-oligosaccharides-market (last access: 17 April 2025), 2025.

Protected Planet: Protected Planet Report, Protected Planet, https://pp-digital-report-files.s3.us-east-1.amazonaws.com/Protected+Planet+Report+2024.pdf (last access: 20 May 2025), 2024.

Protected Planet: Marine Protected Areas, Protected Planet, https://www.protectedplanet.net/en/thematic-areas/marine-protected-areas (last access: 17 April 2025), 2025.

Ren, C.-G., Zhong, Z.-H., Liu, Z.-Y., Lin, S., Luo, Y.-K., and Qin, S.: The ever-lasting green tides: What can we do?, Heliyon, 10, e25220, https://doi.org/10.1016/j.heliyon.2024.e25220, 2024.

Santos, R. G., Machovsky-Capuska, G. E., and Andrades, R.: Plastic ingestion as an evolutionary trap: Toward a holistic understanding, Science, 373, 56–60, https://doi.org/10.1126/science.abh0945, 2021.

Shellock, R. J., Fullbrook, L., McKinley, E., Cvitanovic, C., Kelly, R., and Martin, V.: The nature and use of Ocean Literacy in achieving sustainable ocean futures: A Systematic Map, Ocean Coast. Manage., 257, 107325, https://doi.org/10.1016/j.ocecoaman.2024.107325, 2024.

Sigwart, J. D., Blasiak, R., Jaspars, M., Jouffray, J.-B., and Tasdemir, D.: Unlocking the potential of marine biodiscovery, Nat. Prod. Rep., 38, 1235–1242, https://doi.org/10.1039/D0NP00067A, 2021.

Storto, A. and Yang, C.: Acceleration of the ocean warming from 1961 to 2022 unveiled by large-ensemble reanalyses, Nat. Commun., 15, 545, https://doi.org/10.1038/s41467-024-44749-7, 2024.

Strand, M., Retter, G.-B., Khan, M., Frid, A., Hudson, M., Leonard, K., Paul, K., Baron-Aguilar, C., Boswell, R., Cisneros-Montemayor, A., Copenhaver, A. E., Costa, Y., Hiwasaki, L., Jingwas Russ Jones, N., Kelly, B. P., Kosgei, J., Metcalf, V. K., Moshani, A., Yaa Oduro, G., Scott, C. P., and Rakotondrazafy, V.: Co-producing Sustainable Ocean Plans with Indigenous and traditional knowledge holders, World Resources Institute, Washington DC, https://doi.org/10.69902/8f1075e8, 2024.

Terhaar, J., Burger, F. A., Vogt, L., Frölicher, T. L., and Stocker, T. F.: Record sea surface temperature jump in 2023–2024 unlikely but not unexpected, Nature, 639, 942–946, https://doi.org/10.1038/s41586-025-08674-z, 2025.

UN: 2030 Agenda for Sustainable Development, UN, https://sdgs.un.org/2030agenda (last access: 18 April 2025), 2015.

UNEP: From Pollution to Solution: A global assessment of marine litter and plastic pollution, United Nations Environment Programme, Nairobi, https://www.unep.org/resources/pollution-solution-global-assessment-marine-litter-and-plastic-pollution (last access: 17 April 2025), 2021.

UNEP-WCMC and IUCN: Protected Planet Report 2024, UNEP-WCMC and IUCN, Cambridge, United Kingdom, Gland, Switzerland, https://digitalreport.protectedplanet.net/ (last access: 17 April 2025), 2024.

Virdin, J., Nico, G., Franz, N., Vannuccini, S., Anderson, C., Mancha-Cisneros, M. M., Baio, A., Bennet, A., Fontenele, E., Gozzer Wuest, R., Grillo, J., Harper, S., Muhonda, P., Rice, E., and Sueiro, J. C.: Small-Scale Fisheries Contributions to Economic Value and Livelihoods, in: Illuminating Hidden Harvests: The contributions of small-scale fisheries to sustainable development, FAO, Duke University, WorldFish, Rome, https://doi.org/10.4060/cc4576en, ISBN 978-92-5-137682-9, 2023.

von Schuckmann, K., Minière, A., Gues, F., Cuesta-Valero, F. J., Kirchengast, G., Adusumilli, S., Straneo, F., Ablain, M., Allan, R. P., Barker, P. M., Beltrami, H., Blazquez, A., Boyer, T., Cheng, L., Church, J., Desbruyeres, D., Dolman, H., Domingues, C. M., García-García, A., Giglio, D., Gilson, J. E., Gorfer, M., Haimberger, L., Hakuba, M. Z., Hendricks, S., Hosoda, S., Johnson, G. C., Killick, R., King, B., Kolodziejczyk, N., Korosov, A., Krinner, G., Kuusela, M., Landerer, F. W., Langer, M., Lavergne, T., Lawrence, I., Li, Y., Lyman, J., Marti, F., Marzeion, B., Mayer, M., MacDougall, A. H., McDougall, T., Monselesan, D. P., Nitzbon, J., Otosaka, I., Peng, J., Purkey, S., Roemmich, D., Sato, K., Sato, K., Savita, A., Schweiger, A., Shepherd, A., Seneviratne, S. I., Simons, L., Slater, D. A., Slater, T., Steiner, A. K., Suga, T., Szekely, T., Thiery, W., Timmermans, M.-L., Vanderkelen, I., Wjiffels, S. E., Wu, T., and Zemp, M.: Heat stored in the Earth system 1960–2020: where does the energy go?, Earth Syst. Sci. Data, 15, 1675–1709, https://doi.org/10.5194/essd-15-1675-2023, 2023.

von Schuckmann, K., Moreira, L., Cancet, M., Gues, F., Autret, E., Baker, J., Bricaud, C., Bourdalle-Badie, R., Castrillo, L., Cheng, L., Chevallier, F., Ciani, D., de Pascual-Collar, A., De Toma, V., Drevillon, M., Fanelli, C., Garric, G., Gehlen, M., Giesen, R., Hodges, K., Iovino, D., Jandt-Scheelke, S., Jansen, E., Juza, M., Karagali, I., Lavergne, T., Masina, S., McAdam, R., Minière, A., Morrison, H., Panteleit, T. R., Pisano, A., Pujol, M.-I., Stoffelen, A., Thual, S., Van Gennip, S., Veillard, P., Yang, C., and Zuo, H.: The state of the global ocean, in: 8th edition of the Copernicus Ocean State Report (OSR8), edited by: von Schuckmann, K., Moreira, L., Grégoire, M., Marcos, M., Staneva, J., Brasseur, P., Garric, G., Lionello, P., Karstensen, J., and Neukermans, G., Copernicus Publications, State Planet, 4-osr8, 1, https://doi.org/10.5194/sp-4-osr8-1-2024, 2024.

WMO: State of the Global Climate 2024, WMO-No. 1368, 42 pp., ISBN 978-92-63-11368-5, https://library.wmo.int/idurl/4/69455 (last access: 18 April 2025), 2025.

State Planet, 6-osr9, 4, 2025
https://doi.org/10.5194/sp-6-osr9-4-2025

Micronekton indicators evolution based on biophysically defined provinces

Sarah Albernhe[1,2], Thomas Gorgues[2], Olivier Titaud[1], Patrick Lehodey[3,4], Christophe Menkes[5], and Anna Conchon[1]

[1]Collecte Localisation Satellites, 8–10 rue Hermès, 31520, Ramonville-Saint-Agne, France
[2]Univ Brest, CNRS, Ifremer, IRD, Laboratoire d'Océanographie Physique et Spatiale (LOPS), IUEM, 29280, Plouzané, France
[3]Mercator Ocean International, 2 Av. de l'Aérodrome de Montaudran, 31400, Toulouse, France
[4]Pacific Community, Oceanic Fisheries Programme, Nouméa, New Caledonia
[5]ENTROPIE, IRD, Univ. de La Réunion, CNRS, Ifremer, Univ. de la Nouvelle-Calédonie, BP A5, 98848 Nouméa, New Caledonia

Correspondence: Sarah Albernhe (salbernhe@mercator-ocean.fr)

Received: 20 September 2024 – Discussion started: 1 October 2024
Revised: 5 March 2025 – Accepted: 14 April 2025 – Published: 30 September 2025

Abstract. Micronekton are mid-trophic marine organisms characterized by a size range of 2 to 20 cm, gathering a wide diversity of taxa (crustaceans, fish, molluscs). They are responsible for an important active carbon export to the deep ocean because of their diel vertical migrations and constitute the main prey for pelagic predators. A new method has been proposed in the literature to define provinces that identify micronekton functioning patterns based on environmental variables. Following this methodology, we define homogeneous provinces using environmental variables computed from Copernicus Marine Service products. These provinces represent a relevant way to define regions of interest, offering a regional scope of study for micronekton indicators and their evolution in time. In this study, we observe the evolution of the provinces in time from 1998 to 2023 to account for the decadal to climatic variability. We focus on the variations in surface area and average latitude of each province. We observe a global shrinking of productive provinces and polar provinces in favour of equatorial and tropical provinces' expansion. Additionally, tracking the geographical changes in the provinces over time shows that most are shifting toward the poles.

1 Introduction

The intermediate level of the oceanic food web is constituted by a group of marine organisms called micronekton, understudied but garnering increasing attention. This key component of marine ecosystems characterized by organisms in a size range from 2 to 20 cm contains a wide diversity of taxa such as crustaceans, fish, molluscs and gelatinous species (Brodeur et al., 2004; Escobar-Flores et al., 2019). Micronekton mostly feed on zooplankton and are the main prey of large marine predators, some of which are of crucial economic importance (e.g. tunas; Bell et al., 2015; Terawasi and Reid, 2017; McCluney et al., 2019). In addition to their role as prey for commercially exploited top predators (Young et al., 2015), mesopelagic micronekton itself could become a valuable resource for fisheries due to the increasing demand for fishmeal for aquaculture (St. John et al., 2016; Gatto et al., 2023). Another aspect of micronekton worthy of interest lies in its migratory behaviour, which impacts global carbon export (Pinti et al., 2021; Buesseler et al., 2022) by actively transporting and sequestrating carbon beneath the mixed layer (Bianchi et al., 2013; Boyd et al., 2019; Gorgues et al., 2019).

Therefore, estimating micronekton biomass is a major concern for fisheries management and climate regulation. Direct observations of micronekton primarily rely (i) on ship-borne acoustic measurements, which does not yet provide a

Published by Copernicus Publications.

Table 1. Product table.

Product ref. no.	Product ID and type	Data access	Documentation
01	GLOBAL_MULTIYEAR_BGC_001_033; numerical models	EU Copernicus Marine Service Information (2024a)	Quality information document (QUID): Titaud et al. (2024a) Product user manual (PUM): Titaud et al. (2024b)
02	GLOBAL_MULTIYEAR_BGC_001_029; numerical models	EU Copernicus Marine Service Information (2024b)	Quality information document (QUID): Perruche et al. (2024) Product user manual (PUM): Le Galloudec et al. (2024)
03	MULTIOBS_GLO_PHY_TSUV_3D_MYNRT_015_012; in situ observations, satellite observations	EU Copernicus Marine Service Information (2024c)	Quality information document (QUID): Greiner (2023) Product user manual (PUM): Verbrugge et al. (2023)

reliable representation of the micronekton biomass (McGehee et al., 1998; Kloser et al., 2002), and (ii) on trawl sampling, which is susceptible to biases due for example to species avoidance (Kaartvedt et al., 2012) and has a coarse sampling. Numerical models, such as the Spatial Ecosystem and Population Dynamics Model – Lower and Mid-Trophic Levels (SEAPODYM-LMTL; Lehodey et al., 2010, 2015; Conchon, 2016) are complementary tools for studying micronekton biomass. Indeed, by simulating micronekton dynamics based on key biological and physical processes (such as growth, recruitment, mortality and environmental influences), these models provide a continuous representation of micronekton biomass across space and time. This helps fill observational gaps, enabling the analysis of large-scale patterns, the simulation of future scenarios and ultimately a better understanding of the mesopelagic ecosystem.

One approach to quantify and characterize the mid-trophic level populations is the definition of homogeneous provinces. Longhurst (1995, 2007) was the pioneer and defined a static vision of biogeographical provinces based on chlorophyll fields. Various combinations of features have been used to create accurate definitions of provinces for each field: environmental features such as the distribution of species (Costello et al., 2017) and phytoplankton species assemblages (Elizondo et al., 2021), biogeographic insights from multi-expertise discussions (Sutton et al., 2017), and fisheries-related data such as catch per unit of effort of commercial fisheries (Reygondeau et al., 2012). Acoustic-based regionalization is also explored, using environmental drivers' classifications to model backscattering characteristics (Proud et al., 2017) or recently partitioned acoustic data according to the vertical structure of sound-scattering mid-trophic biomass (Ariza et al., 2022).

Complementing these approaches, Albernhe et al. (2024a) proposed a new methodology for regionalizing the global ocean into biophysical provinces based on environmental variables. Since the present study builds upon Albernhe et al. (2024a), we detail the main and key findings of the prior study in the following sentences. The ambition of the prior study (Albernhe et al., 2024a) was to identify micronekton homogeneous functioning patterns using a parsimonious set of biophysical variables that are known to have an impact on micronekton biomass (epipelagic layer temperature, stratification of the mesopelagic ocean temperature and net primary production (NPP)). Clustering these variables results in a global classification of six distinct biomes (tropical, subtropical, eastern boundary coastal upwelling systems, oceanic mesotrophic systems, subpolar and polar biomes). The authors also defined a monthly time series of biomes for the 1998–2019 time period. From these large biomes, provinces are derived as biomes' subdivisions at the scale of ocean basin and hemisphere. A characterization of these provinces with simulated micronekton from SEAPODYM-LMTL model outputs identifies biome-specific relations between micronekton biomasses and the environmental variables used in the clustering. Additionally, biome-specific vertical structures are indicated by ratios of modelled micronekton functional groups (i.e. groups of micronekton with specific migratory behaviour and specific depth habitat). Boundaries between provinces have also been validated using acoustic data. With demonstrated accuracy in homogeneous micronekton characteristics, these provinces enable the gathering and extrapolation of the few available observation data of micronekton over large homogeneous areas. This could benefit the exploration of the micronekton spatio-temporal variability within global or regional datasets.

In the present study, we focus on provinces' features, such as surface area and positional changes, which serve as valuable indicators providing insights into the evolution of ecosystem structure over time, both globally and regionally. Following Albernhe et al.'s (2024a) methodology, we define in the present study an annual time series of biophysical provinces from 1998 to 2023. We observe the evolution of

two geographical indicators: the surface area and the average latitude of each province.

2 Material and methods

2.1 Environmental variables and biophysical clustering

We define a time series of biophysical provinces from 1998 to 2023 following Albernhe et al.'s (2024a) approach. The publication offers a methodology for global ocean regionalization based on environmental variables, with no gaps and no overlaps, displaying homogeneous biophysical characteristics. While the overall methodology is detailed in Albernhe et al. (2024a), we outline the different steps of the method below to ensure this study is comprehensive and self-contained.

We consider three environmental variables that are known to have an impact on micronekton: the mean temperature in the epipelagic layer, the temperature gradient between the epi- and the meso-pelagic layers as an index of the stratification (hereafter referred to as "stratification"), and the integrated NPP. The pelagic layers mentioned are defined as in SEAPODYM-LMTL. These variables are computed from the biological and physical Copernicus Marine Service datasets of the product *Global Ocean low and mid trophic levels biomass content hindcast*, GLOBAL_MULTIYEAR_BGC_001_033 ($1/12°$ horizontal resolution, product ref01, Table 1). In the product, the weekly 3D temperature fields come from the GLORYS12V1 simulation. NPP and the associated euphotic depth are computed using the Vertically Generalized Production Model (VGPM) of Behrenfeld and Falkowski (1997) which is based on the Satellite Observations reprocessed Global Ocean Chlorophyll product. The spatial domain of our study is restricted to the area where the depth of the water column supports the existence of all three pelagic layers as defined in SEAPODYM-LMTL (i.e. roughly 1000 m deep; see "Material and Method" section of Albernhe et al., 2024a). Consequently, shallow coastal areas are excluded from this analysis. Annual time series of these three variables (i.e. epipelagic layer temperature, stratification and NPP), spatially averaged on a global scale, are provided in the Supplement (Fig. S1). This illustrates how the global mean values of temperature, stratification and NPP fluctuate over time, reflecting interannual variability and decadal trends at the global scale.

As described in Albernhe et al. (2024a), a principal component analysis (PCA) (Hotelling, 1933) is performed on the three environmental variables mentioned above (i.e. epipelagic layer temperature, stratification and NPP), producing empirical orthogonal functions that strongly mirror those identified in Albernhe et al. (2024a). We selected the two principal components that explain the most variance, accounting for 98.1 % of the variance (68.2 % and 29.9 % for the first and second PCA respectively).

Then, a clustering is performed on the two principal components, hereafter referred to as "biophysical clustering". Our goal is to define homogeneous biophysical biomes by detecting intrinsic patterns or structures within the data, without relying on any predefined clustering assumptions. Thus, the biophysical clustering is performed using the unsupervised k-means machine learning algorithm (Lloyd, 1982; Pedregosa et al., 2011), which partitions the observations into k homogeneous clusters (see "Material and Method" section of Albernhe et al., 2024a). In Albernhe et al. (2024a), we identified six clusters ($k = 6$) to classify global-scale environmental data, effectively distinguishing biophysical biomes. In this study, the different metrics used to determine the optimal number of clusters do not exhibit a strongly pronounced pattern. One suggests that $k = 5$ could be a suitable choice, albeit not with strong certainty. To ensure consistency with Albernhe et al. (2024a), we maintain $k = 6$, allowing us to build upon our previous findings on micronekton biomass and vertical structure. The clusters derived from the clustering define six homogeneous biomes on a global scale, hereafter referred to as "biophysical biomes".

First, the training phase of the k-means algorithm is applied to time-averaged $1/12°$ datasets from 1998 to 2023. This process defines static reference biophysical biomes, representing the average state of the ocean over the entire period. After the training phase, the clustering model parameters are estimated, and we can use this model to make predictions on other data. Then, the prediction phase of the k-means algorithm is applied on monthly data over the same time period (1998–2023) (see "Material and Method" section of Albernhe et al., 2024a). This produces a monthly time series of biophysical biomes.

The six biophysical biomes obtained from the clustering of environmental data characterize homogeneous environmental regimes on a global scale. Since similar oceanographic regimes occur in multiple locations, biophysical biomes extend across various ocean basins. In this study, we also delineate "provinces" as subdivisions of biomes at the scale of ocean basins and hemispheres that have been shown to be characterized by stable biophysical drivers and potential taxonomic identity (Spalding et al., 2012; Sutton et al., 2017; Albernhe et al., 2024a). This subdivision of each of the six biophysical biomes results in the definition of 27 provinces, establishing regional frameworks for studying micronekton.

2.2 Trends identification

The aim of this study is to analyse the evolution of the provinces in time from 1998 to 2023. The biophysical data described in the previous section are available at a monthly resolution and monthly provinces are derived through clustering, in order to follow Albernhe et al.'s (2024a) methodology. While provinces are resolved monthly, our analysis focuses on decadal to climatic trends aiming to identify long-term patterns in their evolution. To study the temporal variability and identify potential trends over the 26 years, we consider the annual time series. We calculate indicators based

on the monthly definition of provinces and then compute the annual averages of these indicators. We document the evolution of two geographical indicators for each province: the surface area and the average latitude. The average latitude diagnostic has been designed to assess a potential poleward displacement of certain provinces (see Hastings et al., 2020; Pinsky et al., 2020, and references therein).

To evaluate the evolution of surface area over time, our approach is based on a simple linear regression model applied to the annual surface area (in km^2) of each province from 1998 to 2023. We analyse the slope of the regression (in $km^2\ yr^{-1}$) to account for the direction and first-order magnitude of variability. Rather than directly comparing the years 1998 and 2023 to quantify the variation between these dates (which would assume that surface areas for these 2 years perfectly align with a statistically significant linear trend), we project the equivalent evolution over 26 years based on the slope of the regression (i.e. 26 × slope). From this projected variation, we compute the percentage change in surface area over 26 years (in %) relative to the surface area at the start of the time series (year 1998).

Similarly, to track the poleward drift of provinces over time, our approach is based on a simple linear regression model applied to the average latitude of each province from 1998 to 2023. We analyse the slope of the regression (in degrees poleward per year) to account for the direction and first-order magnitude of variability. The "degree poleward" unit that we use for this diagnostic is associated with degree N for provinces in the Northern Hemisphere and degree S for provinces in the Southern Hemisphere. Thus, provinces belonging to the equatorial Biome 1 (provinces 101, 102 and 103) are not considered in this diagnostic because of their equatorial position. Rather than directly comparing the years 1998 and 2023 to quantify the variation between these dates, we project the equivalent evolution over 26 years based on the slope of the regression (in degree poleward), following the same approach as described for the surface area metric.

To track the poleward drift of provinces over time, we analyse the slope (in degrees poleward per year) of a linear regression model based on the average latitude of each province throughout the annual time series from 1998 to 2023. The "degree poleward" unit that we use for this diagnostic is associated with degree N for provinces in the Northern Hemisphere and degree S for provinces in the Southern Hemisphere. Thus, provinces belonging to the equatorial Biome 1 (provinces 101, 102 and 103) are not considered in this diagnostic because of their equatorial position. Derived from the linear regressions, we estimate the poleward variation trend over the 26 years for each province (in degree poleward), based on the difference between the first and last point of the regression (respectively matching 1998 and 2023).

Recapitulative tables for each of these two metrics are provided in the Supplement (Table S1 for surface area and Table S2 for mean latitude). These tables present, for each province, the trend from the linear regression model, the total variation over the 26 years and the coefficient of determination (R^2) for each regression. R^2 is a statistical measure that evaluates the degree of fit between the observed values and the linear regression model, allowing the statement of statistically significant linear trends. A 26-year period is too short to detect statistically significant trends in such biophysical features. Due to interannual variability, R^2 values are not expected to be close to 1, which would indicate statistical significance of the linear trends. The purpose of the linear regressions is to identify the direction and relative magnitude of the trends rather than to confirm their statistical significance. Caution must be taken while considering such trends. Thus, scatter plots of the annual time series for surface area (Fig. S2) and mean latitude (Fig. S4), with the corresponding linear regression, are provided in the Supplement for each province. These plots allow for the direct observation of the time series.

3 Results

3.1 Biophysical provinces' definition

To define the homogeneous biophysical biomes, we perform a clustering on the two principal components generated by the PCA performed on the three environmental variables (i.e. epipelagic layer temperature, stratification and NPP). From the learning phase of the clustering algorithm, six static reference biophysical biomes (Fig. 1) are defined on a global scale, representing the average state of the ocean over the entire period.

The six reference biophysical biomes are characterized as tropical, subtropical, eastern boundary coastal upwelling systems, oceanic mesotrophic systems, subpolar and polar (respectively numbered from 1 to 6). The subdivision of these biomes according to ocean basin and hemisphere leads to the definition of 27 biophysical provinces (identified by different shades of the biomes' colours in Fig. 1).

The monthly time series of these provinces is available as an animation in the "Video supplement" showing the provinces' geographical evolution in time from 1998 to 2023 (https://doi.org/10.5446/68853, Albernhe et al., 2024b). Together with the variations in ocean environmental conditions, the geographical extent of provinces evolves in time.

The different biomes and associated provinces are characterized by specific environmental regimes (Fig. 2). Focusing on the biophysical conditions for each province, we consider the data distribution for averaged epipelagic layer temperature, stratification and NPP. Figure 2 shows monthly values of these three variables from 1998 to 2023, spatially averaged for each biome.

Biome 1 (the tropical biome) is characterized by the warmest and most stratified waters, associated with relatively low biological production. A similar but less pronounced pattern is observed for Biome 2 (the subtropical biome).

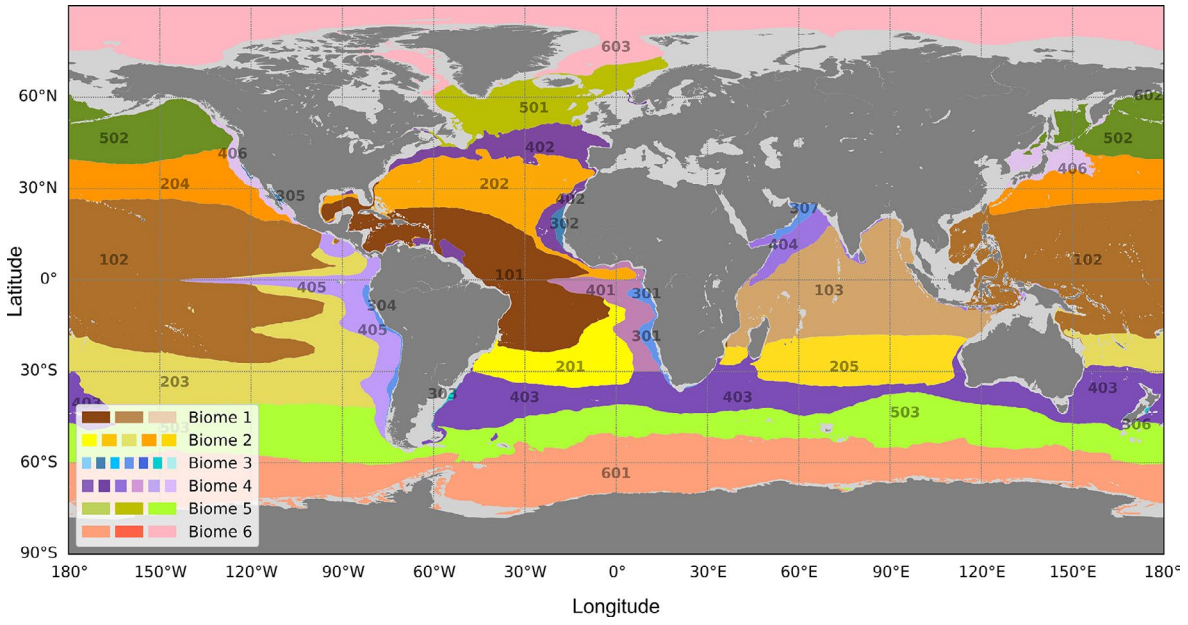

Figure 1. Map of reference biophysical biomes obtained by PCA principal component clustering from averaged epipelagic layer temperature, stratification and NPP over the 1998–2023 time period. Geographical separation between different areas of the same biome defines 27 associated provinces. Provinces are identified by different shades of biomes' colours, defined in the legend. One label is attributed to each province with the hundreds' digits corresponding to the biome in which they belong. Grey areas delimitate the domain where the depth of the water column is not sufficient to ensure the existence of the three pelagic layers of SEAPODYM-LMTL (product ref 01, Table 1).

Biome 3 (the eastern boundary coastal upwelling systems) is by far the most productive biome. Biome 4 (the oceanic mesotrophic systems) also exhibits high NPP values, though weaker than Biome 3. Biome 5 (the subpolar biome) is weakly stratified, is characterized by cold waters, and shares a similar NPP range with Biomes 1 and 2. Biome 6 (the polar biome) features the weakest stratification and the lowest epipelagic layer temperatures among all biomes.

3.2 Provinces' surface area evolution

We aim to observe the geographical evolution of the provinces in time from 1998 to 2023. We provide in the Supplement, for each province, a scatter plot for the annual surface area for the period 1998–2023, with the associated linear regression (Fig. S2). The slopes of the linear regression models computed from the annual time series of surface area for each province are computed (see Supplement Table S1, third column). These trends (in $km^2\ yr^{-1}$) are also expressed as the equivalent percentage of evolution between 1998 and 2023 (in %; Table S1, fourth column). The latter is displayed in Fig. 3 as a map of the reference biophysical provinces showing their surface evolution in time from 1998 to 2023.

From 1998 to 2023, there was a decline in the surface area of productive provinces (i.e. characterized by high NPP) in eastern boundary coastal upwelling systems and oceanic mesotrophic systems (provinces belonging to Biomes 3 and 4, i.e. labelled 300s and 400s), as indicated by the provinces coloured with shades of blue in Fig. 3. Most of the polar and subpolar provinces such as the North Atlantic and North Pacific subpolar areas (respectively provinces 501 and 502) and the circumpolar province of the Southern Ocean (601) also display decreasing trends in their extent. On the other hand, provinces with increasing surface trends are mostly tropical or subtropical areas (Indian Ocean, South Atlantic tropical band or South Pacific tropical band, respectively provinces 103, 201 and 203).

On a global scale, productive provinces and polar provinces seem to shrink in favour of tropical provinces' expansion. However, some biomes exhibit significant discrepancies among the provinces they encompass. For instance, the surface of the Southern Ocean province 503 (belonging to the subpolar Biome 5) shows an increasing trend, in opposition to provinces 501 and 502 belonging to the same biome, showing decreasing trends in the Northern Hemisphere.

3.3 Provinces' average latitude evolution

Together with the evolution of provinces' surface area, provinces' average latitude is a valuable metric to track the geographical evolution of the provinces in time from 1998 to 2023. We provide in the Supplement, for each province, a scatter plot for the annual province's average latitude for the period 1998–2023, with the associated linear regression (Fig. S4). The slopes of the linear regression models computed from the annual time series of average latitude for each

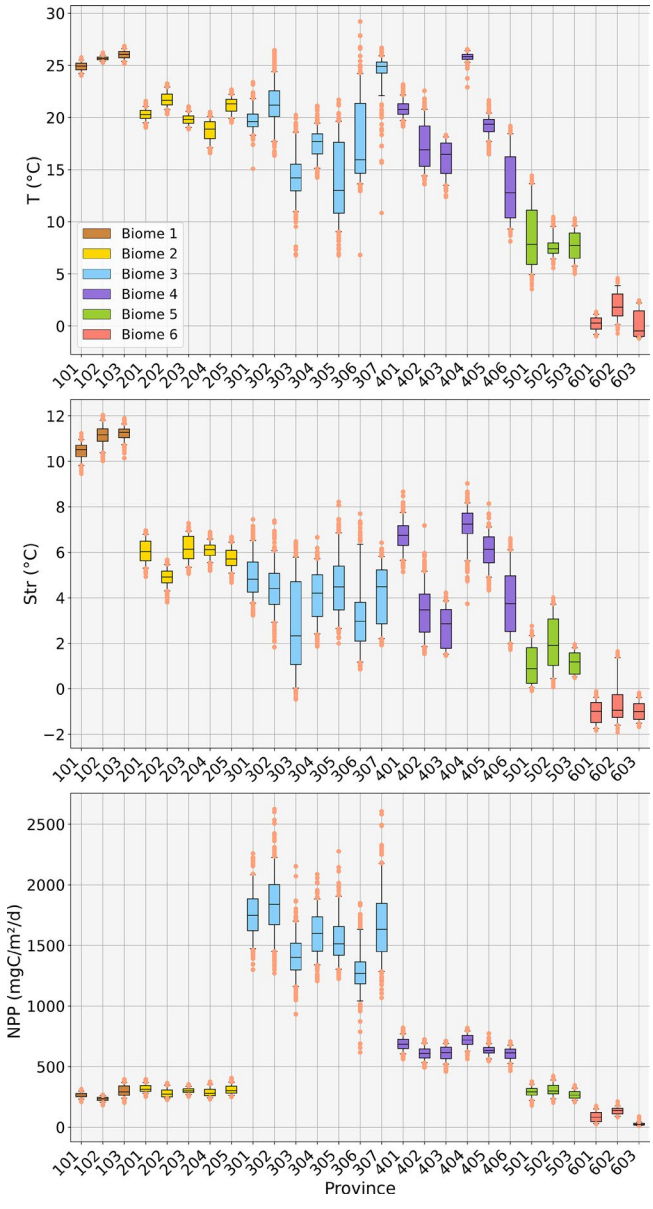

Figure 2. Characterization of biophysical biomes using monthly environmental forcings: temperature of the epipelagic layer (T, °C), stratification (Str, °C) and NPP (mg C m^{-2} d^{-1}) from 1998 to 2023. The analysis uses monthly values of T, Str and NPP, spatially averaged across each biome (i.e. one value per month for each environmental variable per biome). The boxplots depict the data distribution, with the median shown at the centre of each rectangle, the first and third quartiles represented by the top and bottom edges of the rectangles, the whiskers extending to the 5th and 95th percentiles, and orange dots indicating outliers.

province are computed (see Supplement Table S2). The poleward displacement of each province between 1998 and 2023 is displayed in Fig. 4 (in degree poleward).

Most of the provinces experience poleward drifting (provinces coloured with shades of red in Fig. 4). The tropical provinces displaying increasing surface trends (see provinces 201, 202, 203; Fig. 3) experience equatorward drifting, as indicated by provinces coloured with shades of blue in Fig. 4. Provinces with average latitude evolution trends between +0.5 and −0.5° poleward over the time period are considered stable in time in terms of latitude (provinces coloured in yellow in Fig. 4). This range encompasses 20 % of the provinces exhibiting the least latitudinal drift over time, distinguished from the ones undergoing more pronounced and meaningful drifts.

3.4 Sensitivity analysis

The robustness of the biophysical clustering obtained with the reference dataset, i.e. GLORYS12V1 for the physical variables and VGPM for the biological variable (see Sect. 2.1 and Table 1, product ref01), is tested by computing other biophysical clusterings derived from alternative environmental datasets. These alternative datasets include physical data from ARMOR3D (Guinehut et al., 2012; Mulet et al., 2012) and biological data from the biogeochemical model PISCES (Aumont et al., 2015).

The *Multi Observation Global Ocean 3D Temperature Salinity Height Geostrophic Current and MLD* product of Copernicus Marine Service (MULTIOBS_GLO_PHY_TSUV_3D_MYNRT_015_012, product ref03, Table 1) provides 3D temperature from the ARMOR3D dataset, derived from an optimal analysis of 3D observations. This product is used to compute the epipelagic layer temperature and the stratification instead of GLORYS12V1 (used in reference biophysical clustering, product ref01, Table 1). A first alternative clustering, employing the same methodology as the reference biophysical clustering (see Sect. 2.1, "Environmental variables and biophysical clustering"), is performed using this product to compute the physical variables (the epipelagic layer temperature and the stratification) and still using VGPM (product ref01, Table 1) to compute the NPP.

Then, the *Biogeochemical hindcast for global ocean* product of Copernicus Marine Service (GLOBAL_MULTIYEAR_BGC_001_029, product ref02, Table 1) is used to compute the NPP variable for the clustering instead of VGPM (product ref01, Table 1). It provides 3D biogeochemical fields using PISCES biogeochemical model outputs. A second alternative clustering, employing the same methodology as the reference biophysical clustering, is performed using this product to compute the NPP and still using GLORYS12V1 (product ref01, Table 1) to compute the physical variables (as in the reference biophysical clustering).

The two alternative products mentioned above are available at 1/4° from 1998 to 2022 at a monthly resolution. Each of them is used to compute an alternative clustering (respectively using VGPM-ARMOR3D and PISCES-GLORYS12V1). We compare our reference biophysical

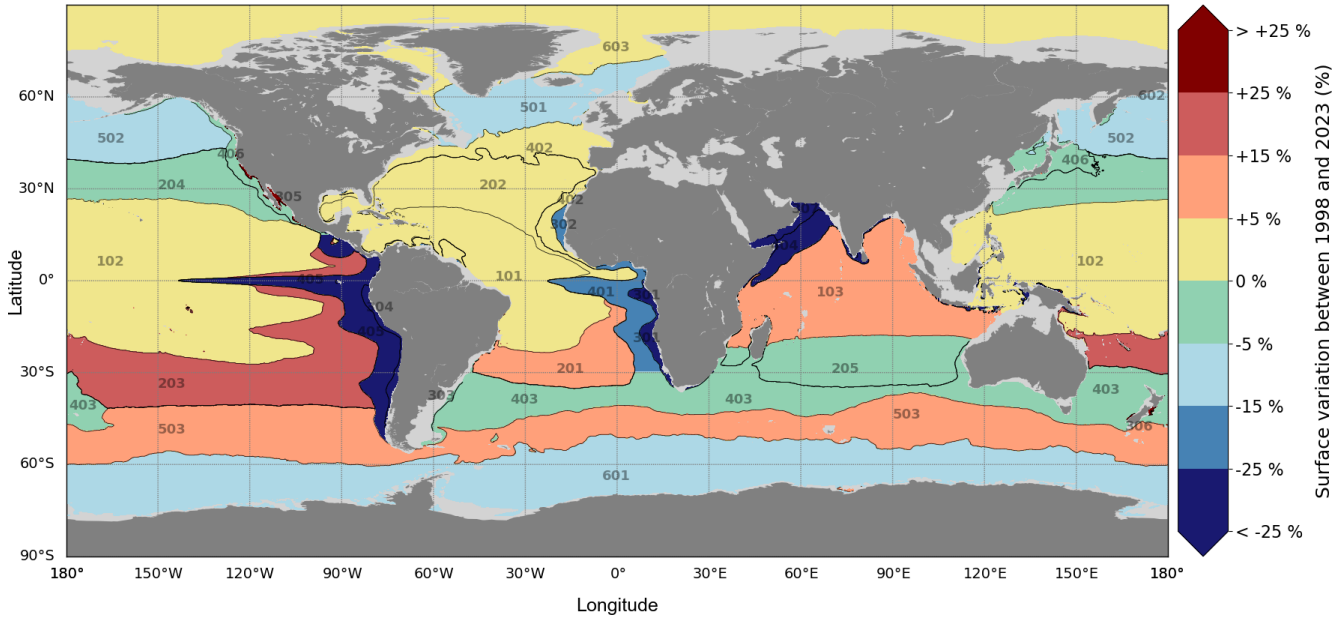

Figure 3. Map of the provinces' surface area evolution in time from 1998 to 2023. Black lines delineate the definition of the 27 reference biophysical provinces (see Fig. 1). Colours represent the trend in surface variation for each province (in % from 1998 to 2023): shades of red indicate increasing surface area, while shades of blue indicate decreasing surface area.

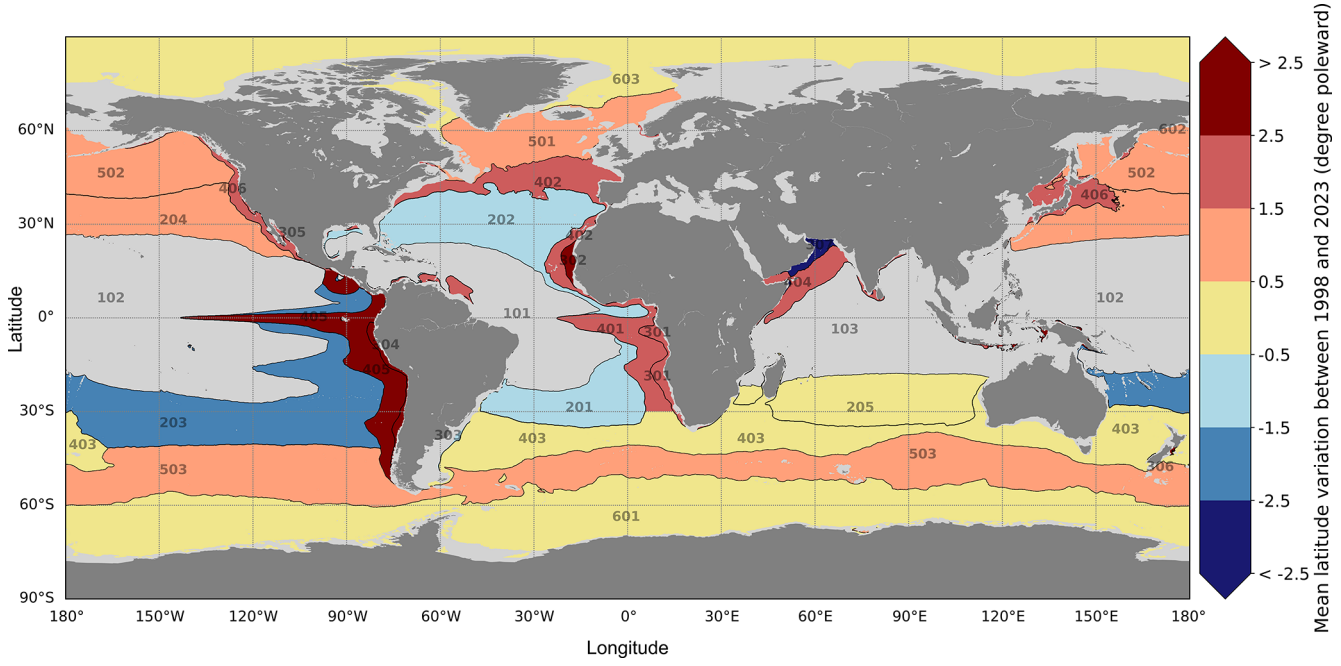

Figure 4. Map of the provinces' average latitude evolution in time from 1998 to 2023. Black lines display the definition of the 27 reference biophysical provinces (see Fig. 1). Colours represent the trend in average latitude variation for each province (in degree poleward from 1998 to 2023): darker shades of red indicate poleward drifting, while darker shades of blue indicate equatorward drifting. Provinces of the equatorial biome coloured in grey (101, 102 and 103) are not considered in this diagnostic because of their equatorial position.

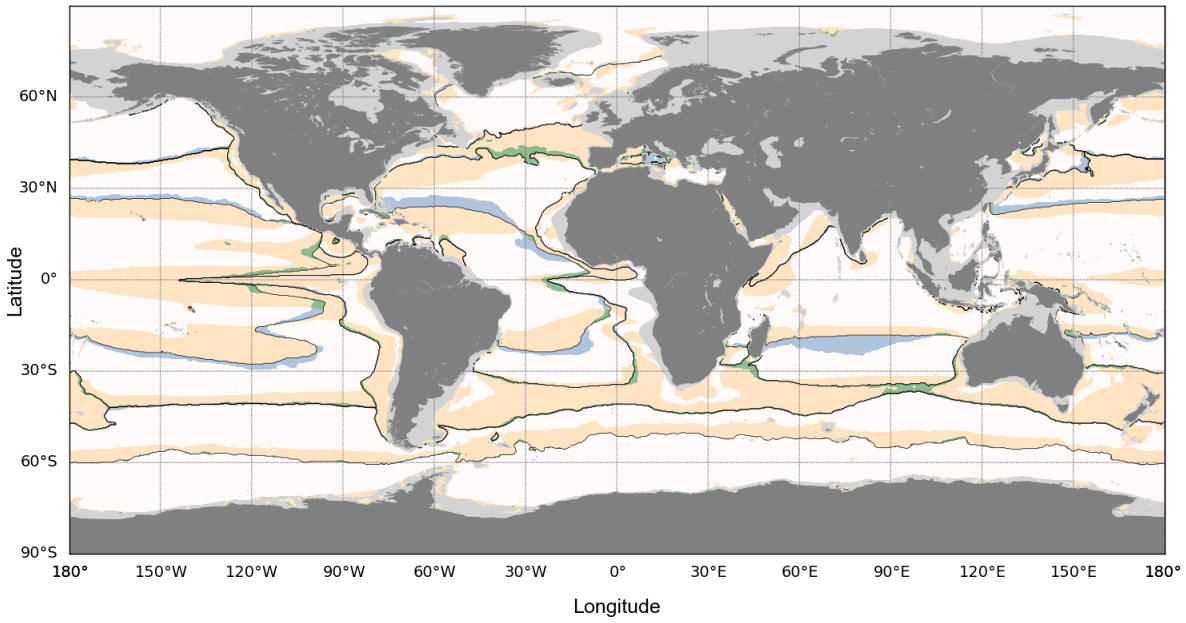

Figure 5. Clustering sensitivity analysis. Map of reference biophysical biomes computed from GLORYS12V1 (product ref01, Table 1) and VGPM (product ref01, Table 1) in black lines (see Fig. 1). The white areas indicate where both alternative clusterings assign the same cluster as the reference biophysical clustering. The blue areas indicate where the clustering using ARMOR3D (product ref03, Table 1) instead of GLORYS12V1 (product ref01, Table 1) assigns a different cluster from the reference biophysical clustering. The yellow areas indicate where the clustering using PISCES (product ref02, Table 1) instead of VGPM (product ref01, Table 1) assigns a different cluster from the reference biophysical clustering. The green areas indicate where both alternative clusterings assign a different cluster from the reference biophysical clustering.

clustering (VGPM-GLORYS12V1; see Sect. 2.1), downscaled from 1/12° to 1/4° resolution, with two alternative clusterings (Fig. 5), all averaged over the period 1998–2022.

Figure 5 shows that the clustering is very stable when changing the physical variable source from GLORYS12V1 (product ref01, Table 1) to ARMOR3D (product ref03, Table 1), as blue areas highlight minor boundary differences. However, when changing the biogeochemical variable source from VGPM (product ref01, Table 1) to PISCES (product ref02, Table 1), the productive Biome 4 is highly impacted. However, NPP estimations from PISCES (product ref02, Table 1) and VGPM (product ref01, Table 1) differ significatively. We notice that the clustering remains relatively stable with respect to the source of forcings, although variations can arise when forcing fields differ widely. The time series and results presented in the study are thus valid using VGPM and GLORYS12V1 (both product ref01, Table 1), but caution should be taken in extrapolating those results to clusters issued from other biogeochemical sources (e.g. models' outputs).

4 Discussion and conclusion

In this study, we defined 27 biophysical provinces linked to micronekton based on a methodology introduced in Albernhe et al. (2024a). Our definition of the reference biophysical provinces (Fig. 1) has been compared to other studies (e.g. Proud et al., 2017; Sutton et al., 2017; Ariza et al., 2022) employing comparable methodologies using environmental variables to derive biogeographic regions. Sutton et al. (2017) classified regions based on environmental drivers and expert knowledge, Proud et al. (2017) used clustering on environmental variables to model deep scattering layer characteristics, and Ariza et al. (2022) derived provinces by clustering acoustic data reconstructed from biophysical variables. Despite methodological differences among these three studies, the resulting biogeographical regions closely align with ours. Notably, beyond the evident latitudinal banding (in the austral ocean for instance), more complex regional structures emerge in the North Atlantic, midlatitude frontal zones (except in the South Pacific) and upwelling regions (see Fig. 4 in Sutton et al., 2017; Fig. 3A in Proud et al., 2017; Fig. 2a in Ariza et al., 2022; and our Fig. 1). This similarity likely arises because all approaches rely on biophysical variables that capture key information on temperature, biological productivity and water column mixing.

The annual time series of biophysical provinces from 1998 to 2023 allows for tracking their temporal evolution capturing decadal to climatic variability, focusing on the variations in surface area and average latitude of each province. The resulting changes observed include a shrinking of productive

and polar provinces, an expansion of equatorial and tropical provinces, and a poleward drift affecting most provinces.

Despite the complexity of the multifactorial causes behind the spatial variation in the provinces, we can attempt to infer the main environmental variables driving the provinces' spatial evolution and how changes in these variables contribute to their size variation and latitude drifting. Based on Fig. 2, boxplots with median values particularly different from the others (e.g. either the highest or lowest) and narrower ranges (indicating low data variance) highlight the environmental variable most likely to characterize a province's specificity. Equatorial provinces (Biome 1) are characterized by very high temperature and stratification values, with narrow boxplots indicating weak data variance. Thus, temperature and stratification seem to be the most explanatory variables for these provinces. A similar but less pronounced pattern is observed in subtropical provinces (Biome 2). Productive provinces (Biomes 3 and 4) are highly distinguishable by their significantly elevated NPP values compared to others, suggesting that NPP is the most explanatory variable for these regions. Subpolar and polar provinces (Biomes 5 and 6, respectively) are marked by low stratification and cold waters, with polar provinces showing the weakest values among all biomes. Therefore, temperature and stratification appear to be the key explanatory variables for subpolar and polar provinces.

The spatial variation in provinces is a multifactorial outcome of expected environmental change in time. This variation arises from complex interactions and feedback mechanisms among biophysical variables, driven by a range of intricate physico-biogeochemical processes. Under global warming, the ocean is warming (Abraham et al., 2013; Kwiatkowski et al., 2020; Masson-Delmotte et al., 2023), which is consistent with the increasing trend observed in the time series of global mean epipelagic layer temperature (Fig. S1). The ocean density structure and vertical dynamics also change (Srokosz and Bryden, 2015), which aligns with the increasing trend observed in the time series of global mean stratification of the mesopelagic ocean (Fig. S1). Both primary production and vertical displacements of phytoplankton are impacted by these physical changes (Denman and Gargett, 1983; Laufkötter et al., 2013), including stratification leading to nutrient limitation. Phytoplankton growth is deeply influenced by temperature (Grimaud et al., 2017), but many other features such as nutrient supply or light induce variability in NPP patterns (Behrenfeld et al., 2006). A global decrease in NPP has been observed in the early 21st century (Behrenfeld et al., 2006; Laufkötter et al., 2013; Kwiatkowski et al., 2020), which is consistent with the decreasing trend observed in the time series of global mean NPP (Fig. S1). However, an analysis of remotely sensed surface chlorophyll *a* concentration (upon which NPP calculations are based) reveals highly contrasted trends between available merged products (Pauthenet et al., 2024), questioning the accuracy of these results. Moreover, future climate model projections of global NPP over the 21st century display a poor level of confidence.

In the present study, we observe a global shrinking of productive provinces and polar provinces in favour of an expansion of equatorial and tropical provinces (Fig. 3). A regional decline in primary production could cause the reduction in the size of productive provinces, with NPP identified as the most probable explanatory variable for provinces within Biomes 3 and 4. The previous reference to Pauthenet et al.'s (2024) work advises caution in interpreting this. Concurrently, the global increase in ocean temperature over the past decades explains both the expansion of equatorial and tropical provinces and the contraction of polar provinces, with temperature identified as the key driving factor for these provinces. Trends in ocean temperature, supported by converging estimations, are much more robust and pronounced than those of NPP (Bopp et al., 2013).

The latitudinal patterns of our provinces' definition are directly impacted by temperature changes. These latitudinal patterns identify the equatorial, subtropical, subpolar and polar biomes (Biomes 1, 2, 5 and 6) which were previously suggested to be primarily influenced by temperature and stratification variables. The increase in ocean temperatures drives the expansion of equatorial provinces, causing their climatic boundaries to shift poleward while they remain centred around the Equator. A similar poleward drift is observed in subtropical provinces. Likewise, polar provinces are affected by warming, as the reduction in cold water areas confines them to higher latitudes and pushes their climatic boundaries poleward. Tracking the geographical evolution of these provinces over time, as illustrated in Fig. 4, demonstrates that most provinces exhibit this poleward drift, apparently likely driven by temperature.

In addition to the provinces' definition methodology, the previous publication upon which the present study is based (Albernhe et al., 2024a) demonstrates that each province features a specific characterization in terms of micronekton biomass and vertical structure. Following the hypothesis that these characteristics are preserved over time, which needs to be further investigated, the evolution of provinces' surface area can account for global micronekton trends and estimations. For instance, the shrinking of provinces featuring the highest density of micronekton biomass would lead to a global decrease in micronekton biomass. Productive provinces and subpolar provinces are characterized by high densities of micronekton biomass (Albernhe et al., 2024a), whereas equatorial and tropical ones display lower densities of micronekton biomass. If provinces' characteristics are preserved over time, the shrinking of productive and polar provinces together with the expansion of the equatorial and tropical provinces would imply a global decline in micronekton biomass. This reasoning is based on a basic deduction from the consequences of ecological niche surface variation. However, the underlying mechanisms that could explain a global decline in micronekton biomass may be partly at-

tributed to the previously mentioned decreasing trend in NPP at the global scale. Since NPP is at the base of the trophic chain, this decline has cascading effects up to micronekton, limiting their energy sources and thus reducing population development. Additionally, the potential global decline in micronekton biomass may also be partly induced by the increasing trend in global ocean temperature, which affects micronekton development times (Gillooly et al., 2002), including growth and mortality.

This potential trend for micronekton biomass evolution on the historical period would be in the same range as studies on micronekton biomass climate projections (Bryndum-Buchholz et al., 2019; Kwiatkowski et al., 2019; Lotze et al., 2019; Tittensor et al., 2021; Ariza et al., 2022). In Ariza et al. (2022), the authors derive acoustic provinces from a clustering using acoustic data as a proxy for micronektonic biomasses, which they reconstructed from biophysical data (satellite-derived chlorophyll concentration, sea surface temperature and subsurface dissolved oxygen). In Albernhe et al. (2024a), our biophysical provinces were compared to these acoustic provinces, revealing a strong overall agreement, particularly in terms of latitudinal patterns, dynamic regions and upwelling areas. However, our clustering method did not capture oxygen-driven patterns. Ariza et al. (2022) also explored the spatio-temporal variability in provinces in future projections extending to 2100. They predict a contraction of upwelling and subpolar provinces alongside an expansion of subtropical and temperate provinces, leading to a global decline in pelagic fauna. Despite the differing time frames of the two studies (1998–2023 in our case vs. projections for 2000–2020 and 2080–2100 in Ariza et al. (2022)), their conclusions align with ours regarding the trends observed in these biogeographical provinces and the consequences for mid-trophic biomass. To end up regarding the poleward drifting of provinces, this valuable observation in the same range as the literature (Hastings et al., 2020; Pinsky et al., 2020) suggests a potential poleward migration of micronektonic populations induced by temperature changes.

The authors would, however, like to draw the reader's attention to the caution required when interpreting the trends. First, the trends presented in this study (whether regarding the surface area of provinces or their mean latitude) are quantified based on linear regressions. However, these regressions exhibit low R^2 values, indicating that the linear relationships are not statistically significant. A 26-year period is insufficient to establish statistically robust linear trends in the characteristics of the provinces under investigation. Moreover, observed trends can vary depending on the temporal scale of the study: short-term trends under 26 years do not necessarily reflect long-term, sustainable changes. Additionally, the data employed in this analysis are subject to various biases and uncertainties (e.g. discrepancies between products estimating chlorophyll *a* concentration used to derive NPP, as noted in Pauthenet et al., 2024). Finally, a detailed analysis of the consistency of each province's micronektonic characteristics over time (regarding biomass and the vertical structure of micronekton) should be conducted. This would provide a more solid basis for confirming the link between changes in province surface areas and the evolution of total micronekton biomass. Misinterpreting these findings could lead to premature conclusions or ineffective communication to the public, thereby increasing the risk of misinformation about critical issues such as climate change.

Despite these uncertainties, the indicators defined in this study show sensitivity to changes in environmental parameters and are valuable metrics that should be monitored over the long term. Examining these parameters over longer timescales may allow us to identify climate trends, with the significance of these trends increasing as the time series extends.

Data availability. All data products used in this paper are listed in Table 1, along with their corresponding documentation and online availability.

Video supplement. This video presents a monthly time series of biophysical provinces linked to micronekton, from 1998 to 2023: https://doi.org/10.5446/68853 (Albernhe et al., 2024b)

Supplement. The supplement related to this article is available online at https://doi.org/10.5194/sp-6-osr9-4-2025-supplement.

Author contributions. SA produced the clustering, the provinces' time series and the associated diagnostic for their evolution in time. SA wrote and edited the report.

TG was involved in the investigation process as an advisor and reviewed the report.

OT was involved in the investigation process as an advisor and produced the lower and mid-trophic level biomass density (*Global Ocean low and mid trophic levels biomass content hindcast*, GLOBAL_MULTIYEAR_BGC_001_033) 1998–2023 time series.

The other authors are supervising the PhD of SA and were involved in the investigation process to define the methodology used for the clustering (Albernhe et al., 2024a).

Competing interests. The contact author has declared that none of the authors has any competing interests.

Disclaimer. The Copernicus Marine Service offering is regularly updated to ensure it remains at the forefront of user requirements. In this process, some products may undergo replacement or renaming, leading to the removal of certain product IDs from the catalogue. If readers have any questions or require assistance regarding these modifications, please feel free to reach out to the Copernicus Marine Service user support team for further guidance. They will be able to provide the necessary information to address

concerns and find suitable alternatives.

The views, opinions and practices used to produce this study are those of the author(s) only and do not necessarily reflect those of the European Union or European Research Executive Agency. Neither the European Union nor the granting authority can be held responsible for them.

Publisher's note: Copernicus Publications remains neutral with regard to jurisdictional claims made in the text, published maps, institutional affiliations, or any other geographical representation in this paper. While Copernicus Publications makes every effort to include appropriate place names, the final responsibility lies with the authors.

Financial support. This work was funded by the NECCTON project, which has received funding from Horizon Europe RIA under grant agreement no. 101081273. This work was partly funded by the GLO-RAN component of the Copernicus Marine Environment Monitoring Service (21003L04-COP-GLO RAN-4300). Patrick Lehodey's contribution was funded by the European Union under grant agreement no. 101083922 (OceanICU).

Review statement. This paper was edited by Marilaure Grégoire and reviewed by Urmas Raudsepp and one anonymous referee.

References

Abraham, J. P., Baringer, M., Bindoff, N. L., Boyer, T., Cheng, L. J., Church, J. A., Conroy, J. L., Domingues, C. M., Fasullo, J. T., Gilson, J., Goni, G., Good, S. A., Gorman, J. M., Gouretski, V., Ishii, M., Johnson, G. C., Kizu, S., Lyman, J. M., Macdonald, A. M., Minkowycz, W. J., Moffitt, S. E., Palmer, M. D., Piola, A. R., Reseghetti, F., Schuckmann, K., Trenberth, K. E., Velicogna, I., and Willis, J. K.: A review of global ocean temperature observations: Implications for ocean heat content estimates and climate change, Rev. Geophys., 51, 450–483, https://doi.org/10.1002/rog.20022, 2013.

Albernhe, S., Gorgues, T., Lehodey, P., Menkes, C., Titaud, O., De La Giclais, S. M., and Conchon, A.: Global characterization of modelled micronekton in biophysically defined provinces, Prog. Oceanogr., 229, 103370, https://doi.org/10.1016/j.pocean.2024.103370, 2024a.

Albernhe, S., Gorgues, T., Titaud, O., Lehodey, P., Menkes, C., and Conchon, A.: Biophysical provinces, monthly times series 1998–2023, TIB AV-Portal [video], https://doi.org/10.5446/68853, 2024b.

Ariza, A., Lengaigne, M., Menkes, C., Lebourges-Dhaussy, A., Receveur, A., Gorgues, T., Habasque, J., Gutiérrez, M., Maury, O., and Bertrand, A.: Global decline of pelagic fauna in a warmer ocean, Nat. Clim. Change, 12, 928–934, https://doi.org/10.1038/s41558-022-01479-2, 2022.

Aumont, O., Ethé, C., Tagliabue, A., Bopp, L., and Gehlen, M.: PISCES-v2: an ocean biogeochemical model for carbon and ecosystem studies, Geosci. Model Dev., 8, 2465–2513, https://doi.org/10.5194/gmd-8-2465-2015, 2015.

Behrenfeld, M. J. and Falkowski, P. G.: A consumer's guide to phytoplankton primary productivity models, Limnol. Oceanogr., 42, 1479–1491, https://doi.org/10.4319/lo.1997.42.7.1479, 1997.

Behrenfeld, M. J., O'Malley, R. T., Siegel, D. A., McClain, C. R., Sarmiento, J. L., Feldman, G. C., Milligan, A. J., Falkowski, P. G., Letelier, R. M., and Boss, E. S.: Climate-driven trends in contemporary ocean productivity, Nature, 444, 752–755, https://doi.org/10.1038/nature05317, 2006.

Bell, J. D., Allain, V., Allison, E. H., Andréfouët, S., Andrew, N. L., Batty, M. J., Blanc, M., Dambacher, J. M., Hampton, J., Hanich, Q., Harley, S., Lorrain, A., McCoy, M., McTurk, N., Nicol, S., Pilling, G., Point, D., Sharp, M. K., Vivili, P., and Williams, P.: Diversifying the use of tuna to improve food security and public health in Pacific Island countries and territories, Mar. Policy, 51, 584–591, https://doi.org/10.1016/j.marpol.2014.10.005, 2015.

Bianchi, D., Stock, C., Galbraith, E. D., and Sarmiento, J. L.: Diel vertical migration: Ecological controls and impacts on the biological pump in a one-dimensional ocean model, Global Biogeochem. Cy., 27, 478–491, https://doi.org/10.1002/gbc.20031, 2013.

Bopp, L., Resplandy, L., Orr, J. C., Doney, S. C., Dunne, J. P., Gehlen, M., Halloran, P., Heinze, C., Ilyina, T., Séférian, R., Tjiputra, J., and Vichi, M.: Multiple stressors of ocean ecosystems in the 21st century: projections with CMIP5 models, Biogeosciences, 10, 6225–6245, https://doi.org/10.5194/bg-10-6225-2013, 2013.

Boyd, P. W., Claustre, H., Levy, M., Siegel, D. A., and Weber, T.: Multi-faceted particle pumps drive carbon sequestration in the ocean, Nature, 568, 327–335, https://doi.org/10.1038/s41586-019-1098-2, 2019.

Brodeur, R. D., Seki, M. P., Pakhomov, E. A., and Suntsov, A. V.: Micronekton – What are they and why are they important?, PICES Press, 13, 7–11, 2004.

Bryndum-Buchholz, A., Tittensor, D. P., Blanchard, J. L., Cheung, W. W. L., Coll, M., Galbraith, E. D., Jennings, S., Maury, O., and Lotze, H. K.: Twenty-first-century climate change impacts on marine animal biomass and ecosystem structure across ocean basins, Glob. Change Biol., 25, 459–472, https://doi.org/10.1111/gcb.14512, 2019.

Buesseler, K. O., Jin, D., Kourantidou, M., Levin, D. S., Ramakrishna, K., and Renaud, P.: The ocean twilight zone's role in climate change, Woods Hole Oceanographic Institution, https://doi.org/10.1575/1912/28074, 2022.

Conchon, A.: Modélisation du zooplancton et du micronecton marins, Doctoral dissertation, Université de La Rochelle, https://theses.hal.science/tel-01661554 (last access: 1 September 2024), 2016.

Costello, M. J., Tsai, P., Wong, P. S., Cheung, A. K. L., Basher, Z., and Chaudhary, C.: Marine biogeographic realms and species endemicity, Nat. Commun., 8, 1057, https://doi.org/10.1038/s41467-017-01121-2, 2017.

Denman, K. L. and Gargett, A. E.: Time and space scales of vertical mixing and advection of phytoplankton in the upper ocean, Limnol. Oceanogr., 28, 801–815, https://doi.org/10.4319/lo.1983.28.5.0801, 1983.

Elizondo, U. H., Righetti, D., Benedetti, F., and Vogt, M.: Biome partitioning of the global ocean based on phytoplankton biogeography, Prog. Oceanogr., 194, 102530, https://doi.org/10.1016/j.pocean.2021.102530, 2021.

Escobar-Flores, P. C., Ladroit, Y., and O'Driscoll, R. L.: Acoustic assessment of the micronekton community on the Chatham Rise, New Zealand, using a semi-automated approach, Front. Mar. Sci., 6, 507, https://doi.org/10.3389/fmars.2019.00507, 2019.

EU Copernicus Marine Service Information (CMEMS): Global ocean low and mid trophic levels biomass content hindcast, Marine Data Store (MDS) [data set], https://doi.org/10.48670/moi-00020, 2024a.

EU Copernicus Marine Service Information (CMEMS): Global Ocean Biogeochemistry Hindcast, Marine Data Store (MDS) [data set], https://doi.org/10.48670/moi-00019, 2024b.

EU Copernicus Marine Service Information (CMEMS): Multi Observation Global Ocean 3D Temperature Salinity Height Geostrophic Current and MLD, Marine Data Store (MDS) [data set], https://doi.org/10.48670/moi-00052, 2024c.

Gatto, A., Sadik-Zada, E. R., Özbek, S., Kieu, H., and Huynh, N. T. N.: Deep-sea fisheries as resilient bioeconomic systems for food and nutrition security and sustainable development, Resour. Conserv. Recycl., 197, 106907, https://doi.org/10.1016/j.resconrec.2023.106907, 2023.

Gillooly, J. F., Charnov, E. L., West, G. B., Savage, V. M., and Brown, J. H.: Effects of size and temperature on developmental time, Nature, 417, 70–73, https://doi.org/10.1038/417070a, 2002.

Gorgues, T., Aumont, O., and Memery, L.: Simulated changes in the particulate carbon export efficiency due to diel vertical migration of zooplankton in the North Atlantic, Geophys. Res. Lett., 46, 5387–5395, https://doi.org/10.1029/2018GL081748, 2019.

Greiner, E., Verbrugge, N., Mulet, S., and Guinehut, S.: Copernicus Marine Service Information (CMEMS) Quality Information Document (QUID): CMEMS-MOB-QUID-015-012 – QUID for MULTIOBS product MULTIOBS_GLO_PHY_TSUV_3D_MYNRT_015_012, Copernicus Mar. Serv., 65 pp., https://documentation.marine.copernicus.eu/QUID/CMEMS-MOB-QUID-015-012.pdf (last access: 1 September 2024), 2023.

Grimaud, G. M., Mairet, F., Sciandra, A., and Bernard, O.: Modeling the temperature effect on the specific growth rate of phytoplankton: a review, Rev. Environ. Sci. Biotechnol., 16, 625–645, https://doi.org/10.1007/s11157-017-9443-0, 2017.

Guinehut, S., Dhomps, A.-L., Larnicol, G., and Le Traon, P.-Y.: High resolution 3-D temperature and salinity fields derived from in situ and satellite observations, Ocean Sci., 8, 845–857, https://doi.org/10.5194/os-8-845-2012, 2012.

Hastings, R. A., Rutterford, L. A., Freer, J. J., Collins, R. A., Simpson, S. D., and Genner, M. J.: Climate change drives poleward increases and equatorward declines in marine species, Curr. Biol., 30, 1572–1577, https://doi.org/10.1016/j.cub.2020.02.043, 2020.

Hotelling, H.: Analysis of a complex of statistical variables into principal components, J. Educ. Psychol., 24, 417–441, https://doi.org/10.1037/h0071325, 1933.

Kaartvedt, S., Staby, A., and Aksnes, D. L.: Efficient trawl avoidance by mesopelagic fishes causes large underestimation of their biomass, Mar. Ecol. Prog. Ser., 456, 1–6, https://doi.org/10.3354/meps09785, 2012.

Kloser, R. J., Ryan, T., Sakov, P., Williams, A., and Koslow, J. A.: Species identification in deep water using multiple acoustic frequencies, Can. J. Fish. Aquat. Sci., 59, 1065–1077, https://doi.org/10.1139/f02-076, 2002.

Kwiatkowski, L., Aumont, O., and Bopp, L.: Consistent trophic amplification of marine biomass declines under climate change, Glob. Change Biol., 25, 218–229, https://doi.org/10.1111/gcb.14468, 2019.

Kwiatkowski, L., Torres, O., Bopp, L., Aumont, O., Chamberlain, M., Christian, J. R., Dunne, J. P., Gehlen, M., Ilyina, T., John, J. G., Lenton, A., Li, H., Lovenduski, N. S., Orr, J. C., Palmieri, J., Santana-Falcón, Y., Schwinger, J., Séférian, R., Stock, C. A., Tagliabue, A., Takano, Y., Tjiputra, J., Toyama, K., Tsujino, H., Watanabe, M., Yamamoto, A., Yool, A., and Ziehn, T.: Twenty-first century ocean warming, acidification, deoxygenation, and upper-ocean nutrient and primary production decline from CMIP6 model projections, Biogeosciences, 17, 3439–3470, https://doi.org/10.5194/bg-17-3439-2020, 2020.

Le Galloudec, O., Perruche, C., Derval, C., Tressol, M., and Dussurget, R.: Copernicus Marine Service Information (CMEMS) Product User Manual (PUM): CMEMS-GLO-PUM-001-029 – PUM for Global MFC Products GLOBAL_MULTIYEAR_BGC_001_029, Copernicus Mar. Serv., 17 pp., https://documentation.marine.copernicus.eu/PUM/CMEMS-GLO-PUM-001-029.pdf (last access: 1 September 2024), 2024.

Laufkötter, C., Vogt, M., and Gruber, N.: Long-term trends in ocean plankton production and particle export between 1960–2006, Biogeosciences, 10, 7373–7393, https://doi.org/10.5194/bg-10-7373-2013, 2013.

Lehodey, P., Murtugudde, R., and Senina, I.: Bridging the gap from ocean models to population dynamics of large marine predators: a model of mid-trophic functional groups, Prog. Oceanogr., 84, 69–84, https://doi.org/10.1016/j.pocean.2009.09.008, 2010.

Lehodey, P., Conchon, A., Senina, I., Domokos, R., Calmettes, B., Jouanno, J., Hernandez, O., and Kloser, R.: Optimization of a micronekton model with acoustic data, ICES J. Mar. Sci., 72, 1399–1412, https://doi.org/10.1093/icesjms/fsu233, 2015.

Lloyd, S. P.: Least squares quantization in PCM, IEEE Trans. Inf. Theory, 28, 129–137, https://doi.org/10.1109/TIT.1982.1056489, 1982.

Longhurst, A. R.: Seasonal cycles of pelagic production and consumption, Prog. Oceanogr., 36, 77–167, https://doi.org/10.1016/0079-6611(95)00015-1, 1995.

Longhurst, A. R.: Toward an ecological geography of the sea, in: Ecological Geography of the Sea, 2nd edn., edited by: Longhurst, A. R., Academic Press, Burlington, 1–17, https://doi.org/10.1016/B978-012455521-1/50002-4, 2007.

Lotze, H. K., Tittensor, D. P., Bryndum-Buchholz, A., Eddy, T. D., Cheung, W. W. L., Galbraith, E. D., Barange, M., Barrier, N., Bianchi, D., Blanchard, J. L., Bopp, L., Büchner, M., Bulman, C. M., Carozza, D. A., Christensen, V., Coll, M., Dunne, J. P., Fulton, E. A., Jennings, S., Jones, M. C., Mackinson, S., Maury, O., Niiranen, S., Oliveros-Ramos, R., Roy, T., Fernandes, J. A., Schewe, J., Shin, Y.-J., Silva, T. A. M., Steenbeek, J., Stock, C. A., Verley, P., Volkholz, J., Walker, N. D., and Worm, B.: Global ensemble projections reveal trophic amplification of ocean biomass declines with climate change, P. Natl. Acad. Sci. USA, 116, 12907–12912, https://doi.org/10.1073/pnas.1900194116, 2019.

Masson-Delmotte, V., Zhai, P., Pirani, A., Connors, S. L., Péan, C., Berger, S., Caud, N., Chen, Y., Goldfarb, L., Gomis, M. I., Huang, M., Leitzell, K., Lonnoy, E., Matthews, J. B. R., May-

cock, T. K., Waterfield, T., Yelekçi, O., Yu, R., and Zhou, B. (Eds.): Climate Change 2021: The Physical Science Basis. Contribution of Working Group I to the Sixth Assessment Report of the Intergovernmental Panel on Climate Change, Cambridge University Press, Cambridge, United Kingdom and New York, NY, USA, https://doi.org/10.1017/9781009157896, 2023.

McCluney, J. K., Anderson, C. M., and Anderson, J. L.: The fishery performance indicators for global tuna fisheries, Nat. Commun., 10, 1641, https://doi.org/10.1038/s41467-019-09466-6, 2019.

McGehee, D. E., O'Driscoll, R. L., and Traykovski, L. M.: Effects of orientation on acoustic scattering from Antarctic krill at 120 kHz, Deep-Sea Res. Pt. II, 45, 1273–1294, https://doi.org/10.1016/S0967-0645(98)00036-8, 1998.

Mulet, S., Rio, M. H., Mignot, A., Guinehut, S., and Morrow, R.: A new estimate of the global 3D geostrophic ocean circulation based on satellite data and in situ measurements, Deep-Sea Res. Pt. II, 77–80, 70–81, https://doi.org/10.1016/j.dsr2.2012.04.012, 2012.

Pauthenet, E., Martinez, E., Gorgues, T., Roussillon, J., Drumetz, L., Fablet, R., and Roux, M.: Contrasted trends in chlorophyll-*a* satellite products, Geophys. Res. Lett., 51, e2024GL108916, https://doi.org/10.1029/2024GL108916, 2024.

Pedregosa, F., Varoquaux, G., Gramfort, A., Michel, V., Thirion, B., Grisel, O., Blondel, M., Prettenhofer, P., Weiss, R., Dubourg, V., Vanderplas, J., Passos, A., Cournapeau, D., Brucher, M., Perrot, M., and Duchesnay, É.: Scikit-learn: Machine learning in Python, J. Mach. Learn. Res., 12, 2825–2830, 2011.

Perruche, C., Szczypta, C., Paul, J., and Drévillon, M.: Copernicus Marine Service Information (CMEMS) Quality Information Document (QUID): CMEMS-GLO-QUID-001-029 – QUID for Global MFC Products GLOBAL_MULTIYEAR_BGC_001_029, Copernicus Mar. Serv., 40 pp., https://documentation.marine.copernicus.eu/QUID/CMEMS-GLO-QUID-001-029.pdf (last access: 1 September 2024), 2024.

Pinsky, M. L., Selden, R. L., and Kitchel, Z. J.: Climate-driven shifts in marine species ranges: Scaling from organisms to communities, Annu. Rev. Mar. Sci., 12, 153–179, https://doi.org/10.1146/annurev-marine-010419-010916, 2020.

Pinti, J., DeVries, T., Norin, T., Serra-Pompei, C., Proud, R., Siegel, D. A., and Visser, A. W.: Metazoans, migrations, and the ocean's biological carbon pump, bioRxiv, https://doi.org/10.1101/2021.03.22.436489, 2021.

Proud, R., Cox, M. J., and Brierley, A. S.: Biogeography of the global ocean's mesopelagic zone, Curr. Biol., 27, 113–119, https://doi.org/10.1016/j.cub.2016.11.003, 2017.

Reygondeau, G., Maury, O., Beaugrand, G., Fromentin, J. M., Fonteneau, A., and Cury, P.: Biogeography of tuna and billfish communities, J. Biogeogr., 39, 114–129, https://doi.org/10.1111/j.1365-2699.2011.02582.x, 2012.

Spalding, M. D., Agostini, V. N., Rice, J., and Grant, S. M.: Pelagic provinces of the world: A biogeographic classification of the world's surface pelagic waters, Ocean Coast. Manag., 60, 19–30, https://doi.org/10.1016/j.ocecoaman.2011.12.016, 2012.

Srokosz, M. A. and Bryden, H. L.: Observing the Atlantic Meridional Overturning Circulation yields a decade of inevitable surprises, Science, 348, 1255575, https://doi.org/10.1126/science.1255575, 2015.

St. John, M. A., Borja, A., Chust, G., Heath, M., Grigorov, I., Mariani, P., Martin, A. P., and Santos, R. S.: A dark hole in our understanding of marine ecosystems and their services: Perspectives from the mesopelagic community, Front. Mar. Sci., 3, 31, https://doi.org/10.3389/fmars.2016.00031, 2016.

Sutton, T. T., Clark, M. R., Dunn, D. C., Halpin, P. N., Rogers, A. D., Guinotte, J., Bograd, S. J., Angel, M. V., Alvarez Perez, J. A., Wishner, K. F., Haedrich, R. L., Lindsay, D. J., Drazen, J. C., Vereshchaka, A., Piatkowski, U., Morato, T., Błachowiak-Samołyk, K., Robison, B. H., Gjerde, K. M., Pierrot-Bults, A., Bernal, P., Reygondeau, G., and Heino, M.: A global biogeographic classification of the mesopelagic zone, Deep-Sea Res. Pt. I, 126, 85–102, https://doi.org/10.1016/j.dsr.2017.05.006, 2017.

Terawasi, P. and Reid, C.: Economic and development indicators and statistics: Tuna fisheries of the western and central Pacific Ocean, Forum Fisheries Agency (FFA), Honiara, https://www.ffa.int/wp-content/uploads/_pda/2022/05/Economic-and-Development-Indicators-and-Statistics-2017.pdf (last access: 1 September 2024), 2017.

Titaud, O., Conchon, A., Mérillet, L., and Goeman, N.: Copernicus Marine Service Information (CMEMS) Quality Information Document (QUID): CMEMS-GLO-QUID-001-033 – QUID for Global MFC Products GLOBAL_MULTIYEAR_BGC_001_033, Copernicus Mar. Serv., 31 pp., https://documentation.marine.copernicus.eu/QUID/CMEMS-GLO-QUID-001-033.pdf (last access: 1 September 2024), 2024a.

Titaud, O., Conchon, A., and Mérillet, L.: Copernicus Marine Service Information (CMEMS) Product User Manual (PUM): CMEMS-GLO-PUM-001-033 – PUM for Global MFC Products GLOBAL_MULTIYEAR_BGC_001_033, Copernicus Mar. Serv., 21 pp., https://documentation.marine.copernicus.eu/PUM/CMEMS-GLO-PUM-001-033.pdf (last access: 1 September 2024), 2024b.

Tittensor, D. P., Novaglio, C., Harrison, C. S., Heneghan, R. F., Barrier, N., Bianchi, D., Blanchard, J. L., Bopp, L., Bryndum-Buchholz, A., Cheung, W. W. L., Galbraith, E. D., Gehlen, M., Lotze, H. K., Maury, O., McCormack, S. A., McInnes, K. L., Mignot, J., Oliveros-Ramos, R., Roy, T., Stock, C. A., Tagliabue, A., and Vichi, M.: Next-generation ensemble projections reveal higher climate risks for marine ecosystems, Nat. Clim. Change, 11, 973–981, https://doi.org/10.1038/s41558-021-01173-9, 2021.

Verbrugge, N., Greiner, E., Mulet, S., and Guinehut, S.: Copernicus Marine Service Information (CMEMS) Product User Manual (PUM): CMEMS-MOB-PUM-015-012 – PUM for MULTIOBS product MULTIOBS_GLO_PHY_TSUV_3D_MYNRT_015_012, Copernicus Mar. Serv., 17 pp., https://documentation.marine.copernicus.eu/PUM/CMEMS-MOB-PUM-015-012.pdf (last access: 1 September 2024), 2023.

Young, J. W., Hunt, B. P. V., Cook, T. R., Llopiz, J. K., Hazen, E. L., Pethybridge, H. R., Ceccarelli, D., Lorrain, A., Olson, R. J., Allain, V., Menkes, C., Patterson, T., Nicol, S., Lehodey, P., Kloser, R. J., Arrizabalaga, H., and Choy, C. A.: The trophodynamics of marine top predators: Current knowledge, recent advances and challenges, Deep-Sea Res. Py. II, 113, 170–187, https://doi.org/10.1016/j.dsr2.2014.05.015, 2015.

State Planet, 6-osr9, 5, 2025
https://doi.org/10.5194/sp-6-osr9-5-2025

Variations in marine heatwaves and cold spells in the Northwest Atlantic during 1993–2023

Li Zhai[1], Youyu Lu[1], Haiyan Wang[2], Gilles Garric[3], and Simon Van Gennip[3]

[1]Fisheries and Oceans Canada, Bedford Institute of Oceanography, 1 Challenger Dr., Dartmouth, NS, B2Y 4A2, Canada
[2]Key Laboratory of Marine Hazards Forecasting, National Marine Environmental Forecasting Center, Ministry of Natural Resources, Beijing, China
[3]Mercator-Ocean International, 2 Av. de l'Aérodrome de Montaudran, 31400 Toulouse, France

Correspondence: Li Zhai (li.zhai@dfo-mpo.gc.ca)

Received: 2 September 2024 – Discussion started: 23 September 2024
Revised: 17 March 2025 – Accepted: 10 June 2025 – Published: 30 September 2025

Abstract. Characteristics of marine heatwaves (MHWs) and cold spells (MCSs) in the Northwest Atlantic during 1993–2023 are derived from a global ocean reanalysis product of the European Union Copernicus Marine Service. For surface parameters, the quantification using the reanalysis data is more advantageous than using the satellite remote sensing data in regions with the presence of seasonal sea ice and strong eddies. At the sea bottom, the reanalysis data reproduces well the observed rising trend and sharp increase in bottom temperature around 2012 on the Scotian Shelf and associated changes in MHW/MCS parameters. The 31 years of reanalysis data enable the quantification of spatial variations, interannual variations, and long-term trends in MHW/MCS parameters in the water column in our study region.

The corresponding parameters of surface MHWs and MCSs are overall similar due to the nearly symmetrical probability distribution of sea surface temperature (SST) anomalies around the mean. On the Scotian Shelf, the MHW parameters present layered structures in the water column, influenced by the heat flux in the upper layer and the different water mass compositions in the deeper layer. During 1993–2023, the surface MHW (MCS) total days show increasing (decreasing) trends corresponding to the gradually increasing SST, and the MHW total days reached a peak value of 215 d in 2012 corresponding to the highest annual SST. The bottom temperature shows a stronger increasing trend than the SST and a regime shift around 2012, resulting in the increasing (decreasing) trend and regime shift in bottom MHW (MCS) total days. In 2012, the bottom MHW total days experienced a sharp increase and the entire water column was warmer than the climatology. Opposite conditions presented in 1998, with the longest bottom MCS total days of $\sim$300 near the coast. The quantification of the extreme conditions in 2012 and 1998 supports the results of previous studies on the impacts of these conditions on several marine life species.

1 Introduction

Marine heatwaves (MHWs) and marine cold spells (MCSs) are extreme warm and cold events of the ocean water, respectively. MHWs have been observed in all ocean basins (Collins et al., 2019) and have been extensively studied. Globally, MHWs, defined relative to a fixed climatological period, have become more frequent, long-lasting, and intense since the 1980s under global warming (Frölicher et al., 2018; Oliver et al., 2018; Fox-Kemper et al., 2021). Regionally, local processes, large-scale climate modes, and teleconnections also play important roles in MHW occurrences (Holbrook et al., 2019; Sen Gupta et al., 2020; Capotondi et al., 2024). For example, in the Northwest Pacific, interannual variations in surface MHWs are correlated with various large-scale atmosphere–ocean indices, including the El Niño

Published by Copernicus Publications.

Table 1. Product reference table.

Product ref. no. and abbreviation	Product ID and type	Data access	Documentation
1: GLORYS12v1	GLOBAL_MULTIYEAR_PHY_001_030, numerical models	EU Copernicus Marine Service Product (2023)	Product User Manual (PUM): Drévillon et al. (2023a) Quality Information Document (QUID): Drévillon et al. (2023b)
2: CMCSST	GHRSST Level 4 CMC 0.2 deg global sea surface temperature analysis, 1993–2016	https://doi.org/10.5067/GHCMC-4FM02 (Canada Meteorological Center, 2012)	Journal article: Brasnett (2008)
3: CMCSST	GHRSST Level 4 CMC 0.1 deg global sea surface temperature analysis, 2017–2023	https://doi.org/10.5067/GHCMC-4FM03 (Canada Meteorological Center, 2016)	Journal article: Meissner et al. (2016)
4: Mooring data	Mooring bottom temperature at ∼ 160 m from the AZMP	https://www.dfo-mpo.gc.ca/science/data-donnees/azmp-pmza/index-eng.html (last access: 25 January 2024)	Hebert et al. (2023)

index (Wang et al., 2024). On the shelf seas of the Northwest Atlantic, nearly half of the surface MHWs are initiated by the positive heat flux anomaly into the ocean, and advection and mixing are the primary drivers for the decay of most MHWs (Schlegel et al., 2021b). On the Newfoundland and Labrador Shelf, the summer and fall MHWs in 2023 were impacted by stratification, winds, and advection (Soontiens et al., 2025, this report). Identifying the physical drivers that trigger and maintain the MHWs (MCSs) is important for understanding and predicting the variations in these events and their impacts on marine ecosystems.

Previous studies have revealed the negative impacts of MHWs and MCSs on marine ecosystems. For example, MHWs can cause coral bleaching, destroy kelp forests, and alter the migration patterns of marine species (Santora et al., 2020; Beaudin and Bracco, 2022). MHWs have also affected commercial fisheries in Canadian waters. In the Northeast Pacific, intense and long-lasting heat events, such as "the Blob", led to the collapse of fisheries (Free et al., 2023). In Atlantic Canada, extreme heat events affect the physiological behaviour of aquaculture Atlantic salmon, i.e., the increases in heart rate and decreases in motion (Korus et al., 2024). The declining North Atlantic right whale population was related to the significant warming in the Gulf of Maine and the western Scotian Shelf over the recent decades (Meyer-Gutbrod et al., 2021). The impacts of the extreme cold (warm) event in 1998 (2012) on fishery species have also been studied. In 1998, shortly after the cold Labrador Slope Water replaced the Warm Slope Water, the catches of porbeagle shark and silver hake in the Emerald Basin dramatically declined (Drinkwater et al., 2003). The widespread 2012 warm event in the Northwest Atlantic, with large anomalies throughout the water column and at the sea bottom, had opposite effects on different commercial fisheries. It adversely impacted the snow crab juvenile stages, resulting in a temporary decrease in snow crab abundance on the western Scotian Shelf (Zisserson and Cook, 2017). In the Gulf of Maine, this warm event caused earlier inshore movement of lobsters in the spring, leading to enhanced lobster growth, an extended fishing season, and record landings (Mills et al., 2013).

Compared with MHWs, there have been fewer studies on MCSs. Globally and regionally, the frequency and intensity of surface MCSs show decreasing trends during 1982–2020 associated with the sea surface temperature (SST) increase (Mohamed et al., 2023; Peal et al., 2023; Schlegel et al., 2021b; Wang et al., 2022). Changes in atmospheric forcing, ocean circulation, and coastal upwelling can drive local cold events at the sea surface (Schlegel et al., 2017) and throughout the water column in shallow coastal bays (Casey et al., 2024).

Studies on surface extreme temperature events commonly use sea surface temperatures (SSTs) based on satellite remote sensing (e.g., Wang et al., 2022; Peal et al., 2023). Such studies are limited to the upper ocean and ice-free areas, and the analysis results are impacted by the observational noise and by cloud correction and interpolation schemes used to generate various levels of satellite SST products. Subsurface extreme events have been less well studied due to the scarcity of temperature observations below the surface, leading to limited knowledge about whether and how extreme events at depth have changed over the past decades (Collins et al., 2019). Results from high-resolution numerical ocean models, particularly those reanalysis products achieved through data assimilation, have been alternatively used to study the extreme temperature events, both at surface and at bottom (e.g., Amaya et al., 2023a; Wang et al., 2024). The study of Amaya et al. (2023a) revealed stronger and longer MHWs at bottom than at surface in the shelf seas of North America, but it did not quantify the interannual and long-term variations in MHW characteristics.

Motivated by the results of previous studies, in this study we quantify the space–time variations in MHWs and MCSs

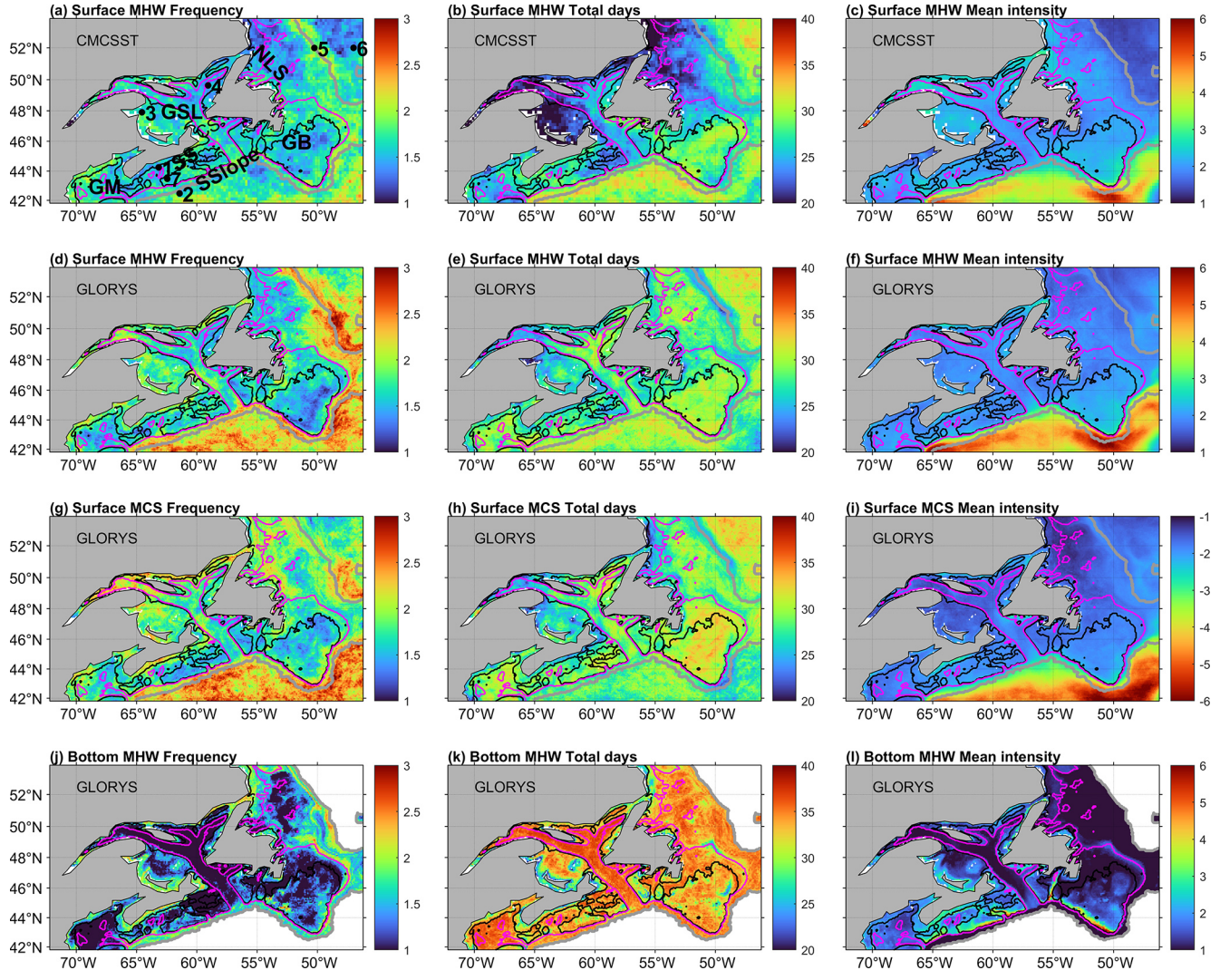

Figure 1. Mean of surface MHW **(a–f)** and MCS **(g–i)** characteristics during 1993–2022 derived from **(a–c)** CMCSST and **(d–i)** GLORYS12V1. **(j–l)** Mean of bottom MHW characteristics during 1993–2022 derived from GLORYS12V1. From left to right: frequency (number of events per year), total days (days per year), and mean intensity (°C). The 100, 200, and 2000 m isobaths are represented by black, magenta, and grey lines, respectively. **(a)** Stations 1–7 indicated by the solid circles for examining the time series of MHW/MCS characteristics, located at latitudes/longitudes of 44.25° N/63.16° W, 42.48° N/61.43° W, 47.91 ° N/64.56° W, 49.64° N/59.06° W, 51.99° N/50.25° W, 52.00° N/47.00° W, and 43.48° N/62.45° W. The Halifax line is the line between stations 1 and 2. Abbreviations: GB, Grand Banks; GM, Gulf of Maine; GSL, Gulf of St. Lawrence; NLS, Newfoundland and Labrador Shelf; SS, Scotian Shelf; SSlope, Scotian Slope; CB, Cabot Strait.

in the Northwest Atlantic, from surface to water column to bottom, with the ultimate goal to better support fisheries in this region. Our study region (Fig. 1a) can be sub-divided into (1) the Newfoundland and Labrador Shelf (NLS) to the north of Grand Banks; (2) Grand Banks; (3) the Gulf of St. Lawrence (GSL), a semi-enclosed sea connecting to the NLS and Scotian Shelf (SS); (4) the Scotian Shelf, an open and rugged shelf, adjoining the Gulf of Maine in the southwest and the Scotian Slope off the shelf; (5) the Gulf of Maine and Bay of Fundy, a tidally energetic semi-enclosed sea; and (6) the Scotian Slope. The physical oceanography in the region is quite complex, due to the influences of the strong multi-scale variability in atmospheric forcing, river runoff, tides, and sea ice; the strong ocean circulation of the Gulf Stream, North Atlantic Current, and Labrador Current; and the meso-scale eddies (e.g., Loder et al., 1998; Brickman et al., 2018; Ma et al., 2022). The water masses of NLS and Grand Banks are strongly affected by the southward Labrador Current that transports cold and fresher water and sea ice. The Scotian Slope water is influenced by the mixture of warm eddies shed from the eastward Gulf Stream/North Atlantic Current and the occasional westward intrusion of the

Labrador Current near the tail of Grand Banks. The GSL is influenced by the significant freshwater discharge of rivers, including the St. Lawrence River; sea ice formed locally and transported in from NLS; and inflows from NLS, Grand Banks, and the Scotian Slope. The SS is influenced by the outflow from the GSL and the intrusion of Scotian Slope water. The Gulf of Maine and Bay of Fundy are influenced by the SS and the Scotian Slope water. Our analysis results will mainly be based on the daily data from an ocean reanalysis product, in comparison with analyses of satellite SST and mooring observations. Main results include (1) characteristics of the spatial distributions of MHW and MCS parameters, (2) the linkages between surface and water column extreme events, and (3) interannual variations and long-term trends and their relationship with temperature variations and the forcing mechanisms.

2 Datasets and analysis methods

2.1 Datasets

Table 1 lists the datasets analyzed in this study. Product ref. no. 1 is the daily temperature during 1993–2023 from the global ocean eddy-resolving reanalysis with a 1/12° horizontal resolution, referred to as GLORYS12V1 (Lellouche et al., 2021). The GLORYS12V1 temperature data remain continuous in ice-covered regions, which helps to compensate for the limitations of spatial and temporal coverage of satellite observations in those areas.

Product ref. no. 2 during 1993–2016 and no. 3 during 2017–2023 are global ocean SST analyses produced daily on an operational basis at the Canadian Meteorological Centre (CMC). The analysis incorporates in situ observations and retrievals from one microwave and three infrared sensors (Brasnett, 2008), referred to as CMCSST. According to the assessment by Fiedler et al. (2019), the CMCSST data show low standard deviations and mean differences to the independent Argo observations in comparison with other long-term SST analyses, including the European Space Agency Sea Surface Temperature Climate Change Initiative (ESA SST CCI) and MyOcean Operational Sea Surface Temperature and Ice Analysis (OSTIA) available from the Copernicus marine catalogues. Product ref. no. 3 at 0.1° resolution during 2017–2023 is linearly interpolated onto the 0.2° grids of product ref. no. 2, thus creating a dataset on unified grids covering 1993–2023. CMCSST has no values at locations and time when sea ice is present.

Product ref. no. 4 is the observed daily bottom temperature since 2008 from a bottom-mounted mooring at a location on the inner Scotian Shelf with a water depth of 160 m (Fig. 1, location 1), from the Atlantic Zone Monitoring Program (AZMP) of Fisheries and Oceans Canada. The mooring is situated on the path of the coastal Nova Scotia Current (Hebert et al., 2023). The mooring is redeployed annually in the fall AZMP survey, and the data are only available until September 2023 for this study.

2.2 Definition and quantification of marine heatwaves and cold spells

Following Hobday et al. (2016), the MHWs are defined as periods of extremely warm water that last continuously for 5 or more days. The MCS are defined similarly as anomalously cold water events following Schlegel et al. (2017). We use the SST data to compute the surface MHW and MCS parameters and the temperature at the ocean floor to compute the bottom MHW and MCS parameters. A seasonally varying climatological percentile threshold method is used to detect MHWs (MCSs). No detrending is applied to the temperature data prior to the MHW/MCS analysis because we want to maintain the consistency and be able to compare with the results of other studies in the Northwest Atlantic (Galbraith et al., 2024; Soontiens et al., 2025) and to emphasize the effects of ocean warming on the changing characteristics of MHWs/MCSs. The climatological mean and thresholds (90th and 10th percentiles of data values) are calculated for each day of the year with all data from multiple years within an 11 d window centred on that day. The climatology and thresholds are defined over 30 years from 1993 to 2022 for GLORYS12V1 and CMCSST and from 2010 to 2022 for the mooring data. A 30 d "moving window" is applied to smooth the daily climatology. The MHWs and MCSs are defined for temperatures above the 90th and below the 10th percentile values, respectively. Events that occur less than 2 d apart are regarded as one continuous event. The statistics for each MHW (MCS) event are calculated using a MATLAB-based tool (Zhao and Marin, 2019). This study will focus on the annual statistics of frequency, total days, and mean intensity. Frequency refers to the total count of MHW (or MCS) events in each year, while total days are the total number of MHW (or MCS) days in each year. The duration of each MHW (MCS) event is defined as the period over which the temperature is greater (lower) than the seasonally varying threshold value. The intensity of each event is the mean SST anomaly during that event. The mean intensity is the average of the intensities of events during that year.

3 Results

3.1 Spatial distribution of annual surface MHW and MCS parameters

For surface MHWs, GLORYS12V1 and CMCSST data (Fig. 1c–f) obtain overall similar magnitudes and spatial patterns of mean intensity but different magnitudes of frequency in deep waters and total days in the seasonally ice-covered areas. For frequency (Fig. 1a and d), both data obtain values of 1–2 events yr^{-1} on the shelf, and, in deep regions (near and beyond the 2000 m isobath), GLORYS12V1 and CMCSST

obtain higher and lower than 2.5 events yr^{-1}, respectively. For the total days (Fig. 1b and e), GLORYS12V1 and CMCSST obtain similar values greater than 30 d yr^{-1} beyond the shelf break on the Scotian Slope and to the east of the Labrador Shelf and over the Grand Banks. Over the Newfoundland and Labrador Shelf and in the southern and western Gulf of St. Lawrence where the seasonal sea ice coverage exists, GLORYS12V1 obtains 25–30 d, higher than about 20 d from CMCSST. In the Gulf of Maine, eastern Scotian Shelf, and eastern Gulf of St. Lawrence, GLORYS12V1 obtains 25–30 d, while CMCSST obtains 20–25 d. For the mean intensity (Fig. 1c and f), both GLORYS12V1 and CMCSST obtain consistently higher values of 3–6 °C in the deep water of the Scotian Slope and to the east of the southern Grand Banks and lower values of less than 2.5 °C on the shelf and in the deep water to the east of the Labrador Shelf. The MHW parameters derived from GLORYS12V1 are consistent with those based on the thermograph network daily mean temperatures in the Gulf of St. Lawrence using the 1991–2020 reference period (Galbraith et al., 2024).

The causes of the differences in the MHW parameters derived from GLORYS12V1, CMCSST, and mooring data and the spatial distributions derived from GLORYS12V1 are explored through examining the time series of sea temperatures and the detection of MHWs at selected locations (denoted in Fig. 1a) in selected years and the variance-preserving spectra during 1993–2022 shown in Fig. 2. The selection of years is based on annual time series of the MHW parameters at these locations (not shown), ensuring that the differences in the MHW parameters between the left and middle columns are consistent with the 1993–2022-averaged statistics shown in Fig. 1. Firstly, on the Scotian Slope, the higher surface MHW frequency from GLORYS12V1 than from CMCSST can be explained by their differences in the variance-preserving spectra of the SST time series during 1993–2022 at location 2 (Fig. 2c). Compared with CMCSST, GLORYS12V1 achieves higher spectral power at timescales shorter than 50 d. In the selected year 2023, GLORYS12V1 shows the more frequent and stronger SST variations and detects three shorter MHW events, whereas CMCSST detected one longer MHW event. Note that the high-frequency SST variations in CMCSST are impacted by the cloud correction and interpolation schemes applied to the original satellite data in generating the CMCSST product.

In the southern and western Gulf of St. Lawrence, the St. Lawrence Estuary, and on the Labrador and Newfoundland Shelf, CMCSST has shorter total days than GLORYS12V1 (Fig. 1b and e). In the selected year 2011, Fig. A3 presents the SST time series at a location (52.8° N, 55.2° W) on the Labrador Shelf. The original CMCSST data have a significant number of missing values from January to April during the presence of seasonal sea ice (Fig. A3a), leading to the 90th threshold above that derived from GLORYS12V1 (Fig. A3a and b). If the missing values of the original CMCSST are filled with a freezing temperature of −1.8 °C, the resulting 90th threshold (Fig. A3c) and the total days of the detected MHWs are closer to those derived from GLORYS12V1 (Fig. A3b). Thus, the shorter MHW total days from CMCSST in regions with the presence of seasonal sea ice are due the biased 90th threshold caused by the missing SST data values.

The spatial patterns of surface MHW parameters from GLORYS12V1 (Fig. 1d–f) are explained next. The differences between the shelf and the Scotian Slope are demonstrated by comparing the SST time series in 2016 and spectra at locations 1 and 2 (Fig. 2d–f). At all the timescales, location 2 shows much stronger SST variability because it is located in the Scotian Slope where the water mass is affected by a succession of warm and cold oscillations and eddies. In the selected year 2016, GLORYS12V1 detects six strong MHW events at location 2 but only one weak event at location 1. In the Gulf of St. Lawrence, the average annual frequency (Fig. 1d) is lower in the northeastern regions (location 4) and higher in the southwestern (location 3) regions, while the total days (Fig. 1e) show the opposite pattern. This is consistent with the SST time series in the selected year 2012 (Fig. 2g–h) and the variance-preserving spectra (Fig. 2i). That is, the spectral energy at location 3 is higher at timescales shorter than 100 d, hence leading to higher MHW frequency, and is higher at location 4 at timescales longer than 100 d, hence leading to longer durations. The higher total days at station 4 in 2012 are due to the long durations of warming above climatology in fall and winter. Off the Labrador Shelf, over a narrow zone near the 2000 m isobath (location 5), the surface MHW frequency is higher, while the total days are shorter, compared to shelf water to the west and the deep water to the east (location 6). This can again be explained by the stronger SST variability at timescales shorter than 100 d at location 5 and longer than 100 d at location 6, respectively (Fig. 2j–l). Location 5 is along the path of the offshore Labrador Current, where the SST anomalies and seasonal cycle are both strong, which can be attributed to the variations in the temperature front in this area (e.g., Lu et al., 2006).

For the surface MCSs derived from GLORYS12V1, their frequency, total days, and mean intensity (Fig. 1g–i) show similar magnitudes and spatial distribution to those of surface MHWs (Fig. 1d–f). The MCS parameters derived from CMCSST (not shown) are also similar to the surface MHW parameters derived from GLORYS12V1 (Fig. 1a–c). Differences between the MCS and MHW parameters derived from GLORYS12V1 are evident in some areas; e.g., on the Scotian Slope (near location 2), the MHWs have higher mean intensity than the MCSs. These similarities and differences can be explained by the probability distribution of SST anomalies at representative sites shown in Fig. A1. The normalized histograms are nearly symmetrical around the mean, with equal median and mean values. At location 2, the median value is less than the mean, suggesting a positive skewness of SST anomalies on the Scotian Slope due to the dominance

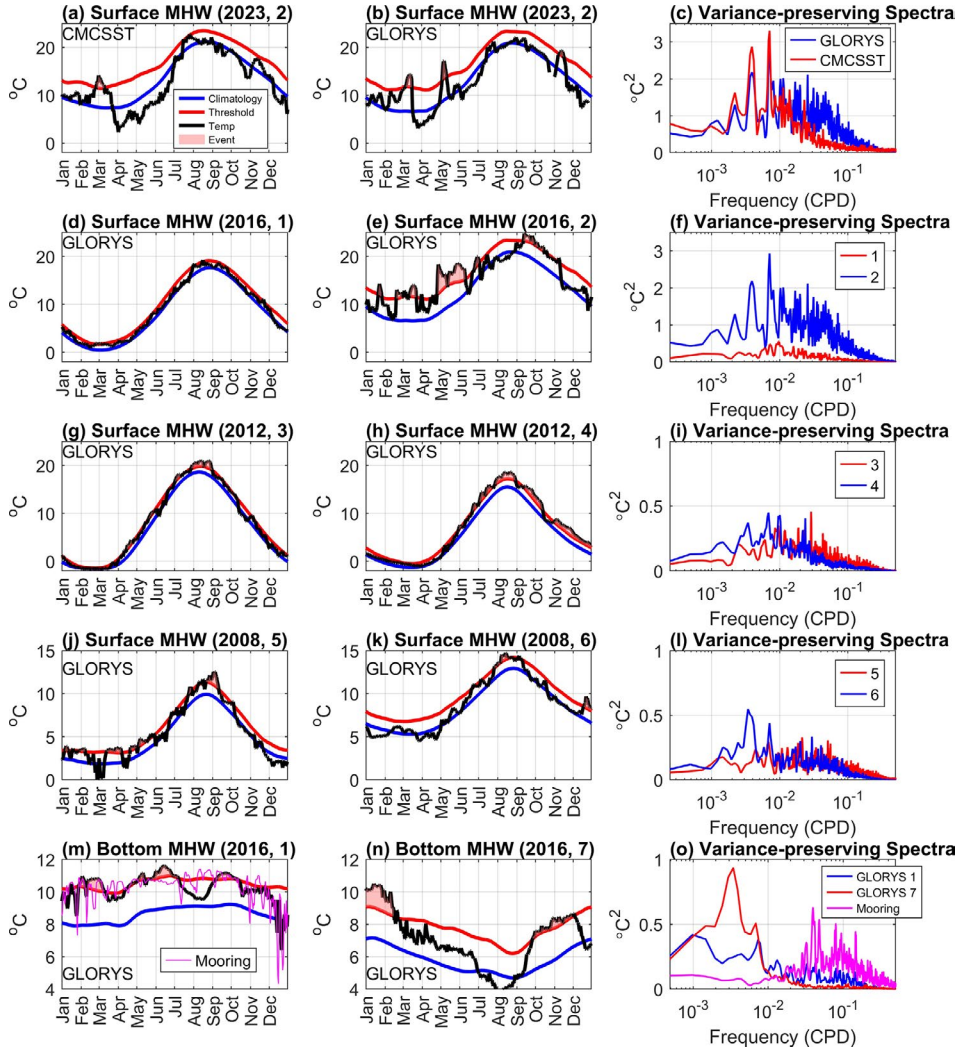

Figure 2. Left and middle columns: time series of sea temperature and detection of MHW in selected years at the surface **(a–b, d–e, g–h, j–k)** and at the seabed **(m–n)** at seven locations marked in Fig. 1a. The numbers in parentheses indicate the year and location. Right column: variance-preserving spectra of **(c, f, i, l)** surface temperature during 1993–2022 and **(o)** bottom temperature during 2010–2022.

of warm-core eddies at the poleward side of the Gulf Stream (e.g., Thompson and Demirov, 2006). Such asymmetric distribution of SST anomalies corresponds to stronger MHWs than MCSs (Schlegel et al., 2021a; Wang et al., 2022).

3.2 Distribution of MHW parameters over the sea floor and in the water column

The frequency, total days, and mean intensity of bottom MHWs on the shelf derived from GLORYS12V1 (Fig. 1j–l) show different magnitudes and spatial distributions compared to surface MHWs. Our findings are consistent with those of Amaya et al. (2023a), who showed that bottom MHW intensity and duration vary strongly with bottom depth. The bottom MHW frequency (Fig. 1j) shows fewer events ($< 1\,\mathrm{yr}^{-1}$) in deep basins and channels and more events ($2–3\,\mathrm{yr}^{-1}$) along the coast and shelf break. The bottom MHW total days (Fig. 1k) exhibit weak spatial variations across the entire region, with values of $30–35\,\mathrm{d\,yr}^{-1}$, and larger values in deeper basins and channels than in shallow waters. This implies that the bottom MHW durations (roughly total days divided by frequency) are longer in deep basins and channels than in shallow water. The bottom MHW intensity (Fig. 1l) ranges from 1 °C in deeper parts of the continental shelves to 6 °C along the edges of the Scotian Shelf and southern Grand Banks, where water intrusions from the shelf break occur.

We selected two locations on the Scotian Shelf (locations 1 and 7) to illustrate the difference in MCS characteristics at the sea floor (Fig. 2m–o). Location 1 is the mooring site near the coast where the water depth is 160 m, and location 7 is on the Emerald Bank in the middle of the Scotian Shelf where the water depth is 66 m. At location 1, both GLORYS12V1

and mooring data (Fig. 2m) show that bottom temperatures in 2016 were generally above the mean climatology, and extreme heat events are detected throughout the year. However, mooring data show some intense cold spikes that are not captured by GLORYS12V1 (Fig. 2m). Correspondingly, compared with the mooring data, the spectral energy of GLORYS12V1 is lower at timescales shorter than 100 d and higher at timescales longer than 100 d (Fig. 2o). At location 7, GLORYS12V1 detects two MHW events with longer durations in 2016 (Fig. 2n). The power spectra (Fig. 2o) show that location 1 has more energy at timescales shorter than 100 d, corresponding to higher MHW frequency and mean intensity, while location 7 shows stronger variability at timescales longer than 100 d, corresponding to longer MHW duration and lower intensity. The strong variations in bottom temperature at shorter than 100 d at location 1 are likely related to the strong fluctuations in the coastal Nova Scotia Current driven by local winds at synoptic scales (Dever et al., 2016).

To examine the linkages between surface and water column extreme events, we show the distributions of MHW parameters in the water column along the section extending off the coast from Halifax between stations 1 and 2 (Fig. 3a–c). This cross-section, referred to as the Halifax line, has regularly been occupied by the AZMP over multiple decades, thus providing extensive observed hydrographic data to assess the quality of model-based data such as GLORYS12V1. The MHW mean intensity (Fig. 3c) shows a clear three-layer structure, with values of about 2 °C in the upper layer from the surface to a mid-depth interface (decreasing from about 70 m near the coast to about 30 m on the Emerald Bank), high values of 3–3.5 °C in the middle layer from the mid-depth interface to about 130 m, and low values of 1.5–2 °C below 130 m depth in the Emerald Basin. The annual MHW frequency (Fig. 3a) is relatively uniform in the water column with values of 1.5–2 yr^{-1}, except low values ($< 1\ yr^{-1}$) below 130 m depth in the Emerald Basin and below 30 m depth over the Emerald Bank, where the annual MHW duration is high.

The distribution of MHW parameters in the water column can be explained by the layered structure of temperature along this section in summer (Fig. 3d–f) and the seasonal evolution of the vertical profiles of temperature at a location in the middle of Emerald Basin (Fig. 3g–i) for the mean climatology over 1993–2022 and in the cold and warm years of 1998 and 2012, respectively (Hebert et al., 2023). The upper layer (from the surface to 50 m) shows strong seasonal variations. This layer is well mixed in fall/winter and has strong stratification developed from spring to summer. Seasonal and interannual variations in this upper layer are mainly due to variations in the surface heat flux and are also influenced near the coast by the outflowing waters from the Gulf of St. Lawrence with strong seasonal and interannual variations in temperature and salinity (Umoh and Thompson, 1994; Dever et al., 2016). The overall major influence of surface heat flux results in a nearly uniform distribution of the MHW parameters in the upper layer. The middle layer (from 50 m to about 130 m depth) presents moderate seasonal variations which can be related to the downward penetration of the surface anomalies driven by surface winds and mixing. On the other hand, this layer is also influenced by the lateral advection of water masses carried by the horizontal currents, mainly from the Cabot Strait subsurface water (30–50 m) and the warm Scotian Slope water and with a smaller portion from the Cabot Strait cold-intermediate layer (50–120 m) and the inshore Labrador Current (Dever et al., 2016). The contributions of the lateral advection vary from the coast to offshore, resulting in the depth range of the mid-depth layer getting smaller from near the coast to the Emerald Bank. The influences of surface forcing and horizontal advection cause high MHW intensity across the whole mid-depth layer and low MHW frequency over the Emerald Bank. The deep layer below 130 m depth in the Emerald Basin (Fig. 3g) presents weak seasonal variations, with a near-constant temperature of 10 °C. However, this layer became colder in 1998 and warmer in 2012 than the climatology (Fig. 3h–i), suggesting strong interannual variations in temperatures in this layer. The temperature variations in this deep layer are mainly caused by the intrusion of the offshore water (Dever et al., 2016), leading to low MHW intensity and frequency and long durations.

3.3 Interannual variations in MHW/MCS parameters

Interannual variations in the MHW/MCS parameters at location 1 in the inner Scotian Shelf are presented in Fig. 4, and some of their statistical quantifications are summarized in Table 2. For the surface parameters (Fig. 4, left column), variations in their values derived from GLORYS12V1 have high correlations with those derived from CMCSST except for the MCS mean intensity. The surface MHW (MCS) total days (Fig. 4a and e) show strong interannual variations which have significantly positive (negative) correlations with the annual SST anomalies from GLORYS12V1 (Table 2). The MHW/MCS mean intensities show weaker interannual variations and have no significant correlations with the SST anomalies.

For the bottom parameters (Fig. 4, right column), significant correlation values derived from GLORYS12V1 and available mooring data are found for the MHW frequency, total days, and mean intensity but not for the MCS parameters (Table 2). This can be attributed to GLORYS12V1 not being able to reproduce the intense cold spikes in the mooring data (Fig. 2m). For both the bottom MHWs and MCSs, interannual variations in their frequency, total days, and mean intensity all have significant correlations with the annual bottom temperature anomalies from GLORYS12V1. The bottom MHW total days and mean intensity derived from the mooring data are significantly lower than those derived from GLORYS12V1. This is due to the differences in the bottom

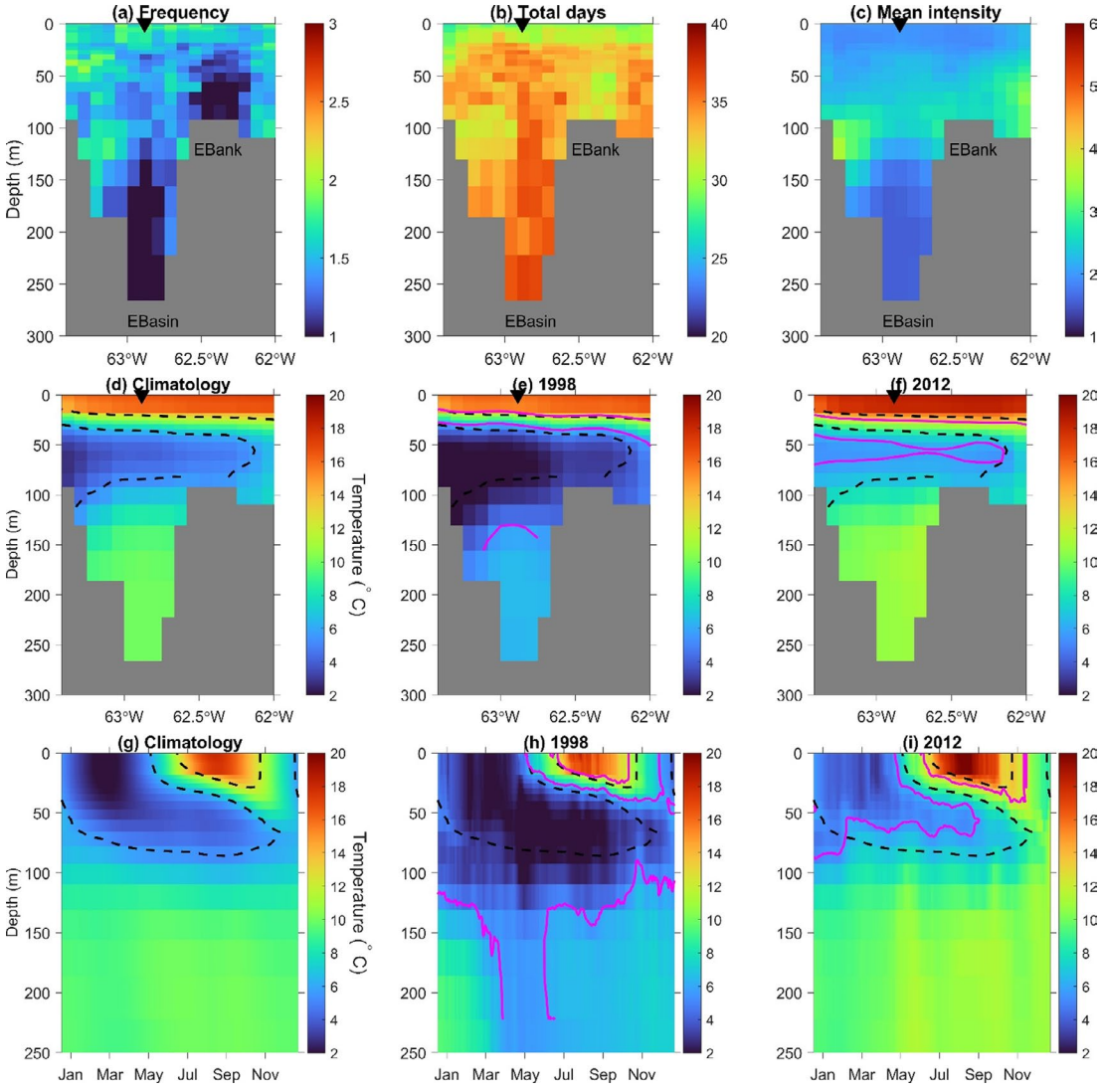

Figure 3. Along the Halifax line (a line between stations 1 and 2 shown in Fig. 1a): MHW **(a)** mean annual frequency (number of events per year), **(b)** mean of annual total days (days per year), and **(c)** mean intensity (°C); summer (July–September) temperature climatology **(d)** over 1993–2022, **(e)** in 1998, and **(f)** in 2022. At a station along the Halifax line (marked as the solid black triangle in panels **(a)**–**(f)**): seasonal evolution of temperature climatology **(g)** over 1993–2022, **(h)** in 1998, and **(i)** in 2012. Contour lines denote the isotherms of 6 and 12 °C: **(d–i)** dashed black contours for averages over 1993–2022 and solid magenta contours in **(e, h)** 1998 and **(f, i)** 2012. Abbreviations: EBasin, Emerald Basin; EBank, Emerald Bank.

temperature climatology of the two datasets defined for the calculation of the MHW/MCS parameters. While the two datasets show similar values and increasing trends in the bottom temperatures, the climatology of mooring data during the 16 years of 2008–2023 has a higher averaged temperature than that of GLORYS12V1 during the 30 years of 1993–2022 (Fig. 4j). As a result, the mooring data obtain shorter and weaker bottom MHW events than GLORYS12V1. If the same reference period of 2008–2023 is used, the difference in MHW parameters between mooring data and GLORYS12V1 is largely reduced. This suggests that the calculation of MHW/MCS parameters is strongly impacted by the duration chosen for computing the climatology and whether detrending is applied, as discussed in Capotondi et al. (2024) and Smith et al. (2025).

At location 1 during 1993–2023, both at surface and bottom, interannual variations in the MHW and MCS total days are negatively correlated; the intensity and total days of MHWs show positive trends, while those for MCSs show negative trends (Table 2). These correspond to warming trends in both the SST and bottom temperature (Fig. 4i–j). The MHW and MCS mean intensities show no significant trends at surface but positive trends at bottom (Table 2). For the bottom MHW/MCS total days, the trends are mostly

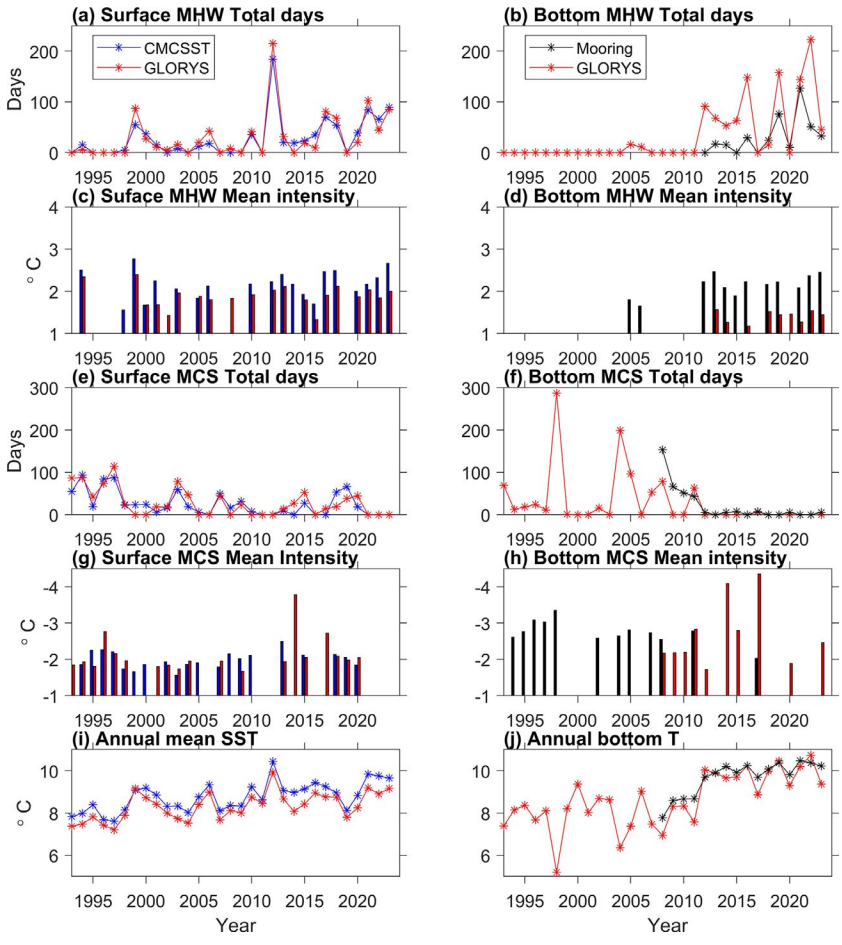

Figure 4. Time series of MHW and MCS characteristics at location 1 (marked in Fig. 1) for surface **(a, c, e, g, i)** and for bottom **(b, d, f, h, j)**. **(a, b)** MHW total days, **(c, d)** MHW mean intensity, **(e, f)** MCS total days, **(g, h)** MCS intensity, **(i, j)** comparison of annual mean time series of GLORYS12V1 with CMCSST and mooring data.

due to their sharp increases (or regime shift) around 2012 (Fig. 4b and f). Out of the 19 years before 2012, bottom MCS events are detected in 11 years, while MHW events are detected only in 2 years. By comparison, out of the 12 years since 2012, bottom MHW events are detected in 10 years, while MCS events are detected only in 1 year. These correspond to the sharp increase in bottom temperature that also occurred around 2012 (Fig. 4j). By comparison, the SST at location 1 shows a more gradual increasing trend (Fig. 4i). After 2012, the annual bottom temperature became higher than the annual SST. As a result, the bottom MHW total days frequently exceed 150, higher than 50–100 for large values of the surface MHW total days (Fig. 4a and b). The long-term trends and regime shifts of bottom MHW/MCS total days are widespread on the Scotian Shelf, as evidenced by the similar time series of location 1 at a location in the Emerald Basin and location 7 on the Emerald Shelf (Fig. A2). This raises the question of how to define MHWs/MCSs in the presence of long-term trends or regime changes in ocean temperature, a point to be discussed in Sect. 4.

The time series plots identify years when severe MHW or MCS events occurred. At location 1, the surface MHW total days show the highest values in 2012, reaching 215 d according to GLORYS (Fig. 4a). Both GLORYS12V1 and CMCSST detect seven MHW events with a duration ranging from 7 to 61 d. These prolonged surface MHW events correspond to the highest peak of annual SST (Fig. 4i) and the well-known warming conditions across the Scotian Shelf (Hebert et al., 2013), in the Gulf of Maine, and on the east coast of the USA in 2012 (Chen et al., 2015). In December 2011, the SST in the region was close to the 90th percentile and likely played a role in preconditioning the MHW in January 2012. Chen et al. (2015) further attributed the widespread MHW events to persistent atmospheric high-pressure systems featured by anomalously weak wind speeds, increased insulation, and reduced ocean heat losses. At location 1, the termination of a long-lasting and strong surface MHW event in the summer of 2012 (Fig. 3i) can be attributed to wind-induced coastal upwelling, resulting in a sudden drop in SST at the end of August (Shan and Sheng, 2022).

Table 2. Statistics of annual values of MHW/MCS parameters during 1993–2023 at location 1 on the inner Scotian Shelf. Column 2: linear trends of MHW/MCS frequency in events per year, total days in days per year, and mean intensity in °C per year derived from GLORYS12V1. Column 3: correlation coefficient of MHW/MCS parameters derived from GLORYS12V1 and from CMCSST at the surface and mooring temperature at the sea floor. Column 4: correlation coefficient between MHW/MCS parameters and annual GLORYS12V1 temperature. Significant trends and correlations with p values less than 0.1 are shown.

	Trend	Correlation between MHW/MCS from GLORYS12V1 and observations	Correlation between MHW/MCS parameters and T
Surface			
MHW frequency	0.07 events yr^{-1}	0.83	0.85
MHW total days	1.9 d yr^{-1}	0.96	0.81
MHW intensity	–	0.77	–
MCS frequency	−0.1 events yr^{-1}	0.69	−0.80
MCS total days	−1.8 d yr^{-1}	0.84	−0.81
MCS intensity	–	–	–
Bottom			
MHW frequency	0.2 events yr^{-1}	0.70	0.72
MHW total days	4.1 d yr^{-1}	0.69	0.70
MHW intensity	0.03 °C yr^{-1}	0.64	0.59
MCS frequency	−0.1 events yr^{-1}	–	−0.75
MCS total days	−2.3 d yr^{-1}	0.78	−0.78
MCS intensity	0.03 °C yr^{-1}	–	0.59

In 2012, at location 1, the bottom MHW total days experienced a sharp increase relative to previous years, reaching ∼ 100 d according to GLORYS12V1 (Fig.4b). In the summer of 2012, the entire water column along the Halifax line was warmer than the climatology (Fig. 3d and f). In the Emerald Basin (Fig. 3g and i), the abnormally warm conditions presented from the surface to about 100 m depth at the beginning of the year (winter), which can be attributed to the smaller heat loss to the atmosphere at the sea surface. Below the 100 m depth, warming started in spring. Below the upper layer directly influenced by surface forcing, the warming in 2012 can be attributed to advection over the Scotian Shelf between 30–50 m, the advection of anomalously warm slope water combined with the reduced contribution of the cold water from the Gulf of St. Lawrence or the inner Labrador Shelf between 50–100 m, and the anomalously warm slope water being advected onto the shelf between 100–200 m (Dever et al., 2016). The warm Scotian Slope water was influenced by the interaction between the Gulf Stream and the Labrador Current at the tail of the Grand Banks (Brickman et al., 2018; Gonçalves Neto et al., 2023).

The conditions in 1998 are opposite to those in 2012; i.e., (1) location 1 experienced the longest bottom MCS total days (nearly 300 d) associated with the lowest annual bottom temperature value (Fig. 4f and j), (2) in summer the entire water column along the Halifax line was colder than the climatology (Fig. 3d and e), and (3) in the Emerald Basin (Fig. 3g and h) the entire water column was anomalously cold throughout the year except for close-to-normal conditions in the upper layer in summer. Below 150 m depth in the Emerald Basin, the lowest temperature occurred during March–June. This can be related to the intrusion of the cold Labrador Slope water. According to Drinkwater et al. (2003), this cold water mass was advected along the shelf break in 1997–1998 and flooded the lower layers of the central and southwestern regions of the Scotian Shelf.

In 2023, at location 1, according to GLORYS12V1, the surface MHW total days amount to 85 (Fig. 4a), which is well above the average value of 31 d. The mean intensity is 2 °C (Fig. 4c), similar to the multi-year-averaged intensity. The longest surface MHW event of that year began on 19 December 2022 and continued until 8 February 2023, coinciding with the warmest January on record in Halifax. The termination of this MHW event is likely related to an extremely cold Arctic air outbreak that set many local meteorological records in early February in Atlantic Canada and caused rapid drops in water temperature in some shallow coastal bays (Casey et al., 2024).

4 Conclusions and discussion

Firstly, in this study, the annual mean MHW/MCS parameters derived from GLORYS12V1 and observational data are compared. At the surface, GLORYS12v1 and CMCSST obtain similar magnitudes and spatial distribution, along with interannual variations in MHW/MCS frequency, total days,

and mean intensity. Differences in the values of the parameters can be attributed to issues in the CMCSST data: (1) shorter MHW total days in the Gulf of St. Lawrence and Labrador and Newfoundland Shelf due to the higher threshold values caused by the missing SST data in the presence of ice and (2) less frequent MHWs on the deep Scotian Slope associated with weaker SST variations caused by the interpolations and cloud correction applied to the satellite remote sensing data for generating the CMCSST. Thus, we suggest that high-resolution data assimilative ocean reanalysis products present more advantages in quantifying surface MHWs and MCSs than SST products based on satellite remote sensing. For the bottom MHWs and MCSs, the analysis results from GLORYS12V1 are compared with those from 16 years of bottom mooring observations at location 1 near the coast of Nova Scotia. GLORYS12V1 captures all parameters of observed bottom MHWs and the total days of bottom MCSs at this location. However, GLORYS12V1 does not reproduce the intense cold spikes of observed bottom temperature and hence detects fewer and less intense bottom MCSs at this location. This can be attributed to the spatial resolution of GLORYS12V1 being insufficient to resolve the sharp spatial gradients of the Nova Scotia Current. Therefore, near the coast of Nova Scotia, GLORYS12V1 underestimates the frequency and intensity of the bottom MCSs, although it provides estimates of the total days in agreement with the mooring data.

Secondly, the horizontal/depth distributions of the annual MHW/MCS parameters are explained by the characteristics of temperature variations and the related ocean dynamics. The corresponding parameters of surface MHWs and MCSs are overall similar due to the nearly symmetrical probability distribution of SST anomalies around the mean, except on the Scotian Slope, where the MHWs have lower frequency and higher mean intensity than the MCSs due to the dominance of warm-core eddies. The surface MHWs have the highest frequency (2–3 events yr^{-1}) and mean intensity (3–6 °C) on the Scotian Slope and to the east of southern Grand Banks, due to the strong SST variability associated with the eddy activities and variations in the Gulf Stream and North Atlantic Current. The shelf waters show nearly uniform values of the surface MHW parameters: 1–2 events yr^{-1} for frequency, 20–30 d yr^{-1} for total days, and ∼2.0 °C for the mean intensity. The bottom MHW frequency, duration (approximately total days divided by frequency), and mean intensity vary strongly with bottom depth, which can be explained by the layered structure of MHW parameters and temperature along a cross-shelf section off Halifax (Fig. 3). In the upper layer from the surface to a mid-depth interface, the nearly uniform MHW mean intensity of ∼2 °C can mainly be attributed to variations in the surface heat flux. From the mid-depth interface to about 130 m depth, the MHW mean intensity has high values of 3–3.5 °C, which can be related to the combined effects of downward penetration of the upper layer (through wind forcing and mixing) and the lateral advection of water masses from the Cabot Strait subsurface and cold-intermediate layers, the Scotian Slope water, and the inshore Labrador Current. In the deep Emerald Basin below 130 m depth, the MHW intensity has the lowest values of 1.5–2 °C due to intrusions of offshore water. The MHW frequency has relatively uniform values of 1.5–2 events yr^{-1} in the water column, except low values of less than 1 event yr^{-1} (corresponding to longer MHW durations) below 130 m depth in the Emerald Basin and below 30 m depth over the Emerald Bank. This can be attributed to the different characteristics of temperature variations caused by different forcings: stronger variations at shorter (longer) timescales by surfacing forcing (lateral intrusion).

Thirdly, analysis of the GLORYS12V1 data reveals interannual variations, long-term trends, and regime shifts in MHW/MCS parameters during 1993–2023. For the surface MHW (MCS) total days, (1) their annual values have significantly positive (negative) correlations with the annual SST anomalies; (2) their increasing (decreasing) trends correspond to the gradual increasing SST; and (3) the peak value (215 d) of MHW total days in 2012 corresponds to the highest annual SST representing the well-known warming conditions across the Scotian Shelf, the Gulf of Maine, and the east coast of the USA. The bottom temperature shows a stronger increasing trend than the SST and a sharp increase (regime shift) around 2012. This causes the increasing (decreasing) trend and regime shift in MHW (MCS) total days. After 2012 at location 1, the annual bottom temperature became higher than the annual SST, and the bottom MHW total days frequently exceeded 200, higher than 50–70 for large values of the surface MHW total days. At location 1 near the coast of Nova Scotia, GLORYS12V1 reproduces well the rising trend and sharp increase in bottom temperature around 2012 in the mooring data. In 2012, the bottom MHW total days at location 1 experienced a sharp increase to ∼100 d. Consistent with the AZMP observations, GLORYS12V1 shows that, in 2012, the entire water column along the Halifax line was warmer than the climatology, which can be attributed to the smaller heat loss to the atmosphere at the sea surface, the advection of abnormally warm Scotian Slope water, and the reduced contribution of the cold water from the Gulf of St. Lawrence or the inner Labrador Shelf. Opposite conditions occurred in 1998 with the longest bottom MCS total days of ∼300 d at location 1, and the entire water column along the Halifax line was colder than the climatology. Further studies are needed to link variations in ocean temperature and MHW/MCS parameters in the Northwest Atlantic, at interannual and longer timescales, to large-scale ocean–atmosphere processes. For example, using long time series of synthetic data, Gregory et al. (2024) recently examined connections between the El Niño–Southern Oscillation and variations in MHWs globally and identified a linkage between La Niña events in the equatorial Pacific and warm conditions in the Northwest Atlantic. Further studies along this line are im-

portant for developing predictions of MHWs and MCSs in the future.

We note that the detection of MHWs and MCSs and the quantification of their parameters depend on the reference climatology of ocean temperature, particularly in our study region, with evident warming trends over the past several decades. Defining the climatology over 30 years (1993–2022) with the GLORYS data obtains longer total days and stronger intensity for bottom MHWs, compared with using the recent 16 years (2008–2023) of bottom temperature from mooring observations. There are ongoing debates in the literature about whether the long-term trends in ocean temperature should be included or excluded in MHW research (Oliver et al., 2021; Zhang et al., 2024). Recent studies (Amaya et al., 2023b; Capotondi et al., 2024; Smith et al., 2025) suggest that both approaches could be useful depending on the applications of interest. The long-term warming trends and short-duration extreme events likely cause different physiological and behavioural responses of marine species. In the present study, the long-term warming trend is retained in defining the water temperature climatology and the detection of MHWs and MCSs, while, in the future, we may explore other definitions when investigating the impacts of MHWs and MCSs on marine ecosystems and fisheries.

Appendix A

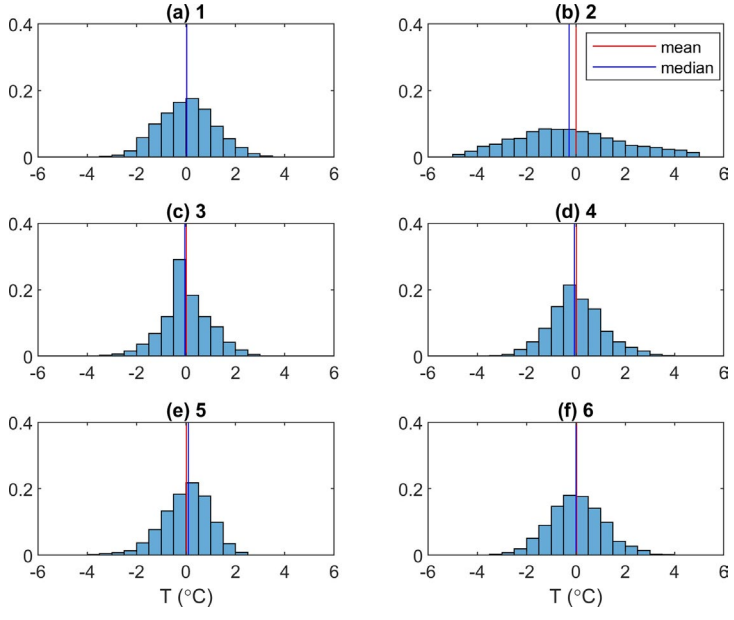

Figure A1. Histogram of sea surface temperature anomalies from GLORYS12V1 at six locations marked in Fig. 1. The height of each bar is the number of data values in each bin divided by the total number of data values.

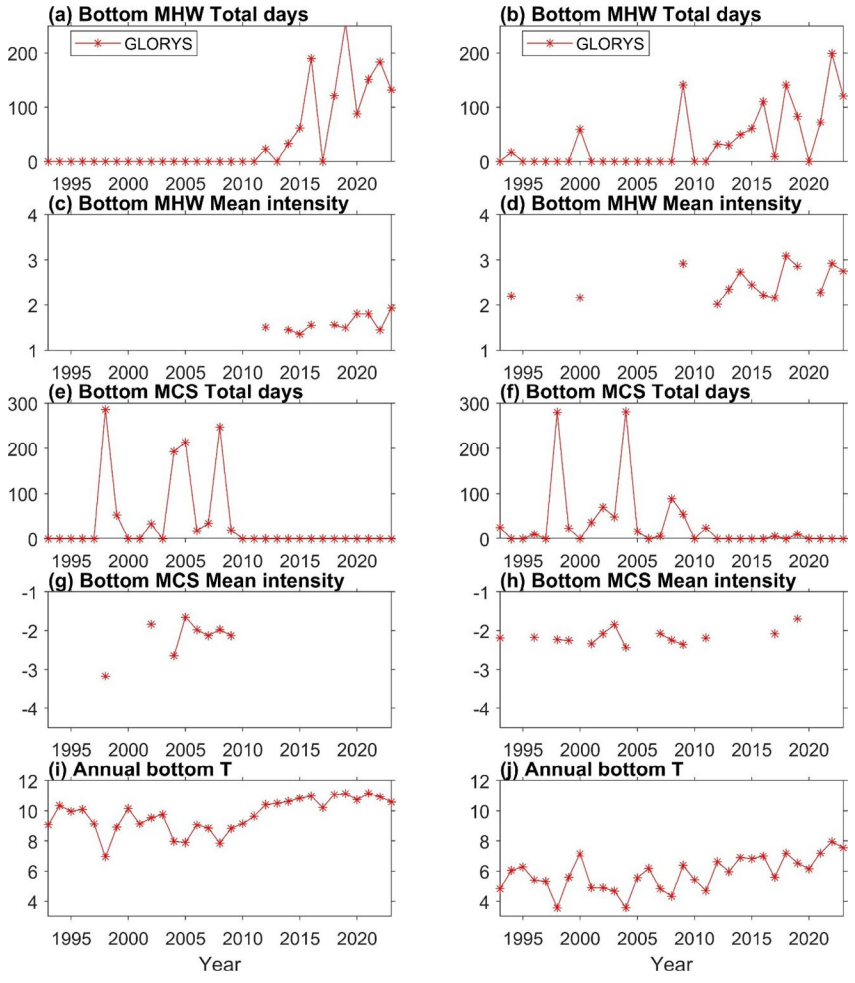

Figure A2. Time series of bottom MHW/MCS parameters and bottom temperature derived from GLORYS12V1 at (left column) a location in the Emerald Basin (marked as a triangle in Fig. 3a) and (right column) location 7 on Emerald Bank (marked in Fig. 1a).

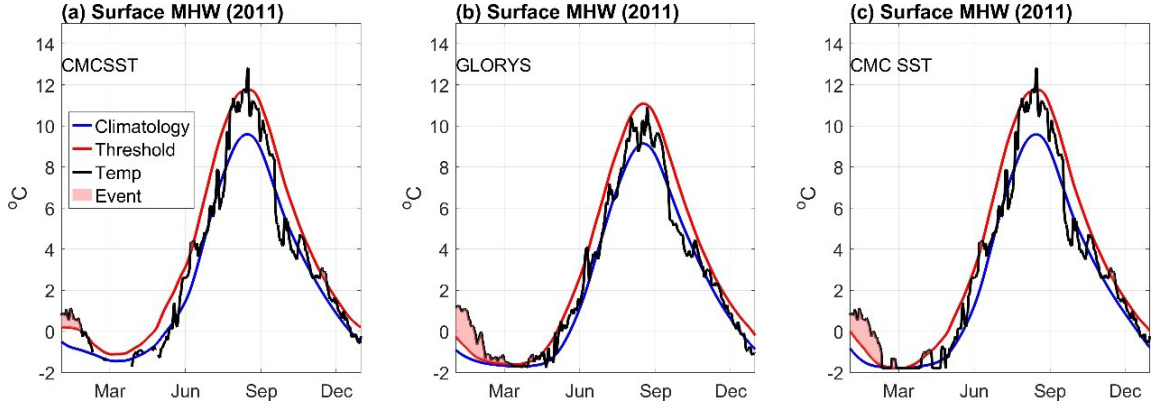

Figure A3. Evolution of surface MHWs in 2011 at a location (52.8° N, 55.2° W) on the Labrador Shelf derived from **(a, c)** CMCSST and **(b)** GLORYS12V1. In panel **(c)**, the missing values of CMCSST are filled with the freezing temperature of −1.8 °C.

Code and data availability. The data used in this study are available as described in Table 1. The code used in this study can be accessed via a GitLab repository upon request via email to the corresponding author.

Author contributions. LZ and YL led the conceptualization of the study, the analysis, and the writing of the article. HW refined the scripts of data analysis. GG and SVG contributed to the conceptualization of the study and to editing and reviewing the article.

Competing interests. At least one of the (co-)authors is a member of the editorial board of *State of the Planet*. The peer-review process was guided by an independent editor, and the authors also have no other competing interests to declare.

Disclaimer. The Copernicus Marine Service offering is regularly updated to ensure it remains at the forefront of user requirements. In this process, some products may undergo replacement or renaming, leading to the removal of certain product IDs from our catalogue. If you have any questions or require assistance regarding these modifications, please feel free to reach out to our user support team for further guidance. They will be able to provide you with the necessary information to address your concerns and find suitable alternatives, maintaining our commitment to delivering top-quality services.

Publisher's note: Copernicus Publications remains neutral with regard to jurisdictional claims made in the text, published maps, institutional affiliations, or any other geographical representation in this paper. While Copernicus Publications makes every effort to include appropriate place names, the final responsibility lies with the authors.

Acknowledgements. We appreciate DFO and Mercator Ocean International for supporting the scientific exchanges and collaboration between the staff of both organizations in recent years under a collaborative agreement; David Brickman for commenting on an early version of the article; Karina Von Schuckmann for insightful comments and advice in developing this article; Xianmin Hu, Justine Mcmillan, and Nancy Soontiens for internal reviews; and Peter Galbraith and two anonymous reviewers for detailed, insightful, and constructive comments that helped to improve the original article.

Review statement. This paper was edited by Joanna Staneva and reviewed by Peter Galbraith and two anonymous referees.

References

Amaya, D. J., Jacox, M. G., Alexander, M. A., Scott, J. D., Deser, C., Capotondi, A., and Phillips, A. S.: Bottom marine heatwaves along the continental shelves of North America, Nat. Commun., 14, 1038, https://doi.org/10.1038/s41467-023-36567-0, 2023a.

Amaya, D. J., Jacox, M. G., Fewings, M. R., Saba, V. S., Stuecker, M. F., Rykaczewski, R. R., Ross, A. C., Stock, C. A., Capotondi, A., Petrik, C. M., Bograd, S. J., Alexander, M. A., Cheng, W., Hermann, A. J., Kearney, K. A., and Powell, B. S.: Marine heatwaves need clear definitions so coastal communities can adapt, Nature, 616, 29–32, https://doi.org/10.1038/d41586-023-00924-2, 2023b.

Beaudin, É. and Bracco, A.: How Marine Heatwaves Impact Life in the Ocean, Front. Young Minds, 10, 712528, https://doi.org/10.3389/frym.2022.712528, 2022.

Brasnett, B.: The impact of satellite retrievals in a global sea–surface–temperature analysis, Q. J. Roy. Meteor. Soc., 134, 1745–1760, https://doi.org/10.1002/qj.319, 2008.

Brickman, D., Hebert, D., and Wang, Z.: Mechanism for the recent ocean warming events on the Scotian Shelf of eastern Canada, Cont. Shelf Res., 156, 11–22, https://doi.org/10.1016/j.csr.2018.01.001, 2018.

Canada Meteorological Center: CMC 0.2 deg global sea surface temperature analysis, Ver. 2.0, PO.DAAC, CA, USA [data set], https://doi.org/10.5067/GHCMC-4FM02, 2012.

Canada Meteorological Center: GHRSST Level 4 CMC 0.1 deg global sea surface temperature analysis, Ver. 3.0, PO.DAAC, CA, USA [data set], https://doi.org/10.5067/GHCMC-4FM03, 2016.

Capotondi, A., Rodrigues, R. R., Sen Gupta, A., Benthuysen, J. A., Deser, C., Frölicher, T. L., Lovenduski, N. S., Amaya, D. J., Le Grix, N., Xu, T., Hermes, J., Holbrook, N. J., Martinez-Villalobos, C., Masina, S., Roxy, M. K., Schaeffer, A., Schlegel, R. W., Smith, K. E., and Wang, C.: A global overview of marine heatwaves in a changing climate, Commun. Earth Environ., 5, 1–17, https://doi.org/10.1038/s43247-024-01806-9, 2024.

Casey, M. P., Petrie, B., Lu, Y., MacDermid, S., and Paquin, J. P.: Rapid drops of ocean temperatures in several shallow bays in Nova Scotia during a recent cold air outbreak, Proceedings of the Nova Scotian Institute of Science, 53, 219–248, 2024.

Chen, K., Gawarkiewicz, G., Kwon, Y., and Zhang, W. G.: The role of atmospheric forcing versus ocean advection during the extreme warming of the Northeast U.S. continental shelf in 2012, J. Geophys Res.-Oceans, 120, 4324–4339, https://doi.org/10.1002/2014JC010547, 2015.

Collins, M., Sutherland, M., Bouwer, L., Cheong, S.-M., Frölicher, T., Jacot Des Combes, H., Koll Roxy, M., Losada, I. McInnes, K., Ratter, B., Rivera-Arriaga, E., Susanto, R. D., Swingedouw, D., and Tibig, L.: Extremes, Abrupt Changes and Managing Risk, in: IPCC Special Report on the Ocean and Cryosphere in a Changing Climate, edited by: Pörtner, H.-O., Roberts, D. C., Masson-Delmotte, V., Zhai, P., Tignor, M., Poloczanska, E., Mintenbeck, K., Alegría, A., Nicolai, M., Okem, A., Petzold, J., Rama, B., and Weyer, N. M., Cambridge University Press, Cambridge, UK and New York, NY, USA, 589–655, https://doi.org/10.1017/9781009157964.003, 2019.

Dever, M., Hebert, D., Greenan, B. J. W., Sheng, J., and Smith, P. C.: Hydrography and Coastal Circulation along the Halifax Line and the Connections with the Gulf of St. Lawrence, Atmos.-Ocean, 54, 199–217, https://doi.org/10.1080/07055900.2016.1189397, 2016.

Drévillon, M., Fernandez, E., and Lellouche, J. M.: EU Copernicus Marine Service Product User Manual for the Global Ocean Physics Reanalysis, GLOBAL_MULTIYEAR_PHY_001_030, Issue 1.5, Mer-

cator Ocean International, https://catalogue.marine.copernicus.eu/documents/PUM/CMEMS-GLO-PUM-001-030.pdf (last access: 19 March 2024), 2023a.

Drévillon, M., Lellouche, J. M., Régnier, C., Garric, G., Bricaud, C., Hernandez, O., and Bourdallé-Badie, R.: EU Copernicus Marine Service Quality Information Document for the Global Ocean Physics Reanalysis, GLOBAL_MULTIYEAR_PHY_001_030, Issue 1.6, Mercator Ocean International, https://catalogue.marine.copernicus.eu/documents/QUID/CMEMS-GLO-QUID-001-030.pdf (last access: 19 March 2024), 2023b.

Drinkwater, K. F., Petrie, B., and Smith, P. C.: Climate variability on the Scotian Shelf during the 1990s, ICES MSS Vol. 219 – Hydrobiological variability in the ICES Area, 1990–1999, https://doi.org/10.17895/ices.pub.19271735.v1, 2003.

EU Copernicus Marine Service Product: Global Ocean Physics Reanalysis, Mercator Ocean International [data set], https://doi.org/10.48670/moi-00021, 2023.

Fiedler, E. K., McLaren, A., Banzon, V., Brasnett, B., Ishizaki, S., Kennedy, J., Rayner, N., Roberts-Jones, J., Corlett, G., Merchant, C. J., and Donlon, C.: Intercomparison of long-term sea surface temperature analyses using the GHRSST Multi-Product Ensemble (GMPE) system, Remote Sens. Environ., 222, 18–33, https://doi.org/10.1016/j.rse.2018.12.015, 2019.

Fox-Kemper, B., Hewitt, H. T., Xiao, C., Aðalgeirsdóttir, G., Drijfhout, S. S., Edwards, T. L., Golledge, N. R., Hemer, M., Kopp, R. E., Krinner, G., Mix, A., Notz, D., Nowicki, S., Nurhati, I. S., Ruiz, L., Sallée, J.-B., Slangen, A. B. A., and Yu, Y.: Ocean, Cryosphere and Sea Level Change, Climate Change 2021: The Physical Science Basis. Contribution of Working Group I to the Sixth Assessment Report of the Intergovernmental Panel on Climate Change, edited by: Masson-Delmotte, V., Zhai, P., Pirani, A., Connors, S. L., Péan, C., Berger, S., Caud, N., Chen, Y., Goldfarb, L., Gomis, M. I., Huang, M., Leitzell, K., Lonnoy, E., Matthews, J. B. R., Maycock, T. K., Waterfield, T., Yelekçi, O., Yu, R., and Zhou, B., Cambridge University Press, 1211–1362, https://doi.org/10.1017/9781009157896.011, 2021.

Free, C. M., Anderson, S. C., Hellmers, E. A., Muhling, B. A., Navarro, M. O., Richerson, K., Rogers, L. A., Satterthwaite, W. H., Thompson, A. R., Burt, J. M., Gaines, S. D., Marshall, K. N., White, J. W., and Bellquist, L. F.: Impact of the 2014–2016 marine heatwave on US and Canada West Coast fisheries: Surprises and lessons from key case studies, Fish Fish., 24, 652–674, https://doi.org/10.1111/faf.12753, 2023.

Frölicher, T. L., Fischer, E. M., and Gruber, N.: Marine heatwaves under global warming, Nature, 560, 360–364, https://doi.org/10.1038/s41586-018-0383-9, 2018.

Galbraith, P. S., Chassé, J., Shaw, J.-L., Dumas, J., and Bourassa, M.-N.: Physical Oceanographic Conditions in the Gulf of St. Lawrence during 2023, Can. Tech. Rep. Hydrogr. Ocean Sci., 378, v + 91 pp., https://waves-vagues.dfo-mpo.gc.ca/library-bibliotheque/41242816.pdf (last access: 28 August 2025), 2024.

Gonçalves Neto, A., Palter, J.B., Xu, X., and Fratantoni, P.: Temporal Variability of the Labrador Current Pathways Around the Tail of the Grand Banks at Intermediate Depths in a High-Resolution Ocean Circulation Model, J. Geophys. Res.-Oceans 128, e2022JC018756, https://doi.org/10.1029/2022JC018756, 2023.

Gregory, C. H., Artana, C., Lama, S., León-FonFay, D., Sala, J., Xiao, F., Xu, T., Capotondi, A., Martinez-Villalobos, C., and Holbrook, N. J.: Global Marine Heatwaves Under Different Flavors of ENSO, Geophys. Res. Lett., 51, e2024GL110399, https://doi.org/10.1029/2024GL110399, 2024.

Hebert, D., Pettipas, R., Brickman, D., and Dever, M.: Meteorological, Sea Ice and Physical Oceanographic Conditions on the Scotian Shelf and in the Gulf of Maine during 2012, DFO Can. Sci. Advis. Sec. Res. Doc. 2013/058, v + 46 pp., https://publications.gc.ca/collections/collection_2013/mpo-dfo/Fs70-5-2013-058-eng.pdf (last access: 28 August 2025), 2013.

Hebert, D., Layton, C., Brickman, D., and Galbraith, P. S.: Physical Oceanographic Conditions on the Scotian Shelf and in the Gulf of Maine during 2022, Can. Tech. Rep. Hydrogr. Ocean Sci. 359, vi + 81 pp., https://waves-vagues.dfo-mpo.gc.ca/library-bibliotheque/41191742.pdf (last access: 28 August 2025), 2023.

Hobday, A. J., Alexander, L. V., Perkins, S. E., Smale, D. A., Straub, S. C., Oliver, E. C. J., Benthuysen, J. A., Burrows, M. T., Donat, M. G., Feng, M., Holbrook, N. J., Moore, P. J., Scannell, H. A., Sen Gupta, A., and Wernberg, T.: A hierarchical approach to defining marine heatwaves, Prog. Oceanogr., 141, 227–238, https://doi.org/10.1016/j.pocean.2015.12.014, 2016.

Holbrook, N. J., Scannell, H. A., Sen Gupta, A., Benthuysen, J. A., Feng, M., Oliver, E. C. J., Alexander, L. V., Burrows, M. T., Donat, M. G., Hobday, A. J., Moore, P. J., Perkins-Kirkpatrick, S. E., Smale, D. A., Straub, S. C., and Wernberg, T.: A global assessment of marine heatwaves and their drivers, Nat. Commun., 10, 2624, https://doi.org/10.1038/s41467-019-10206-z, 2019.

Korus, J., Filgueira, R., and Grant, J.: Influence of temperature on the behaviour and physiology of Atlantic salmon (*Salmo Salar*) on a commercial farm, Aquaculture, 589, 740978, https://doi.org/10.1016/j.aquaculture.2024.740978, 2024.

Lellouche, J.-M., Greiner, E., Bourdallé-Badie, R., Garric, G., Melet, A., Drévillon, M., Bricaud, C., Hamon, M., Le Galloudec, O., Regnier, C., Candela, T., Testut, C.-E., Gasparin, F., Ruggiero, G., Benkiran, M., Drillet, Y., and Le Traon, P.-Y.: The Copernicus Global 1/12° Oceanic and Sea Ice GLORYS12 Reanalysis, Front. Earth Sci., 9, 698876, https://doi.org/10.3389/feart.2021.698876, 2021.

Loder, J. W., Petrie, B., and Gawarkiewicz, G.: The coastal ocean off northeastern North America: a large-scale view, Chap. 5, in: The Global Coastal Ocean: Regional Studies and Synthesis, The Sea, edited by: Robinson, A. R. and Brink, K. H., John Wiley & Sons, Inc., vol. 11, 105–133, ISBN 10: 0674017412, 1998.

Lu, Y., Wright, D. G., and Clarke, R. A.: Modelling deep seasonal temperature changes in the Labrador Sea, Geophys. Res. Lett., 33, L23601, https://doi.org/10.1029/2006GL027692, 2006.

Ma, Y., Lu, Y., Hu, X., Gilbert, D., Socolofsky, S. A., and Boufadel, M.: Model simulated freshwater transport along the Labrador current east of the Grand Banks of Newfoundland, Front. Mar. Sci., 9, 908306, https://doi.org/10.3389/fmars.2022.908306, 2022.

Meissner, T., Wentz, F. J., Scott, J., and Vazquez-Cuervo, J.: Sensitivity of Ocean Surface Salinity Measurements From Spaceborne L-Band Radiometers to Ancillary Sea Surface Temperature, IEEE T. Geosci. Remote, 54, 7105–7111, https://doi.org/10.1109/TGRS.2016.2596100, 2016.

Meyer-Gutbrod, E. L., Greene, C. H., Davies, K. T. A., and Johns, D. G.: Ocean Regime Shift is Driving Collapse of the North Atlantic Right Whale Population, Oceanography, 34, 22–31, https://doi.org/10.5670/oceanog.2021.308, 2021.

Mills, K., Pershing, A., Brown, C., Chen, Y., Chiang, F.-S., Holland, D., Lehuta, S., Nye, J., Sun, J., Thomas, A., and Wahle, R.: Fisheries Management in a Changing Climate: Lessons From the 2012 Ocean Heat Wave in the Northwest Atlantic, Oceanog., 26, 191–195, https://doi.org/10.5670/oceanog.2013.27, 2013.

Mohamed, B., Barth, A., and Alvera-Azcárate, A.: Extreme marine heatwaves and cold-spells events in the Southern North Sea: classifications, patterns, and trends, Front. Mar. Sci., 10, 1258117, https://doi.org/10.3389/fmars.2023.1258117, 2023.

Oliver, E. C. J., Donat, M. G., Burrows, M. T., Moore, P. J., Smale, D. A., Alexander, L. V., Benthuysen, J. A., Feng, M., Sen Gupta, A., Hobday, A. J., Holbrook, N. J., Perkins-Kirkpatrick, S. E., Scannell, H. A., Straub, S. C., and Wernberg, T.: Longer and more frequent marine heatwaves over the past century, Nat. Commun., 9, 1324, https://doi.org/10.1038/s41467-018-03732-9, 2018.

Oliver, E. C. J., Benthuysen, J. A., Darmaraki, S., Donat, M. G., Hobday, A. J., Holbrook, N. J., Schlegel, R. W., and Sen Gupta, A.: Marine Heatwaves, Annu. Rev. Mar. Sci., 13, 313–342, https://doi.org/10.1146/annurev-marine-032720-095144, 2021.

Peal, R., Worsfold, M., and Good, S.: Comparing global trends in marine cold spells and marine heatwaves using reprocessed satellite data, in: 7th edition of the Copernicus Ocean State Report (OSR7), edited by: von Schuckmann, K., Moreira, L., Le Traon, P.-Y., Grégoire, M., Marcos, M., Staneva, J., Brasseur, P., Garric, G., Lionello, P., Karstensen, J., and Neukermans, G., Copernicus Publications, State Planet, 1-osr7, 3, https://doi.org/10.5194/sp-1-osr7-3-2023, 2023.

Santora, J. A., Mantua, N. J., Schroeder, I. D., Field, J. C., Hazen, E. L., Bograd, S. J., Sydeman, W. J., Wells, B. K., Calambokidis, J., Saez, L., Lawson, D., and Forney, K. A.: Habitat compression and ecosystem shifts as potential links between marine heatwave and record whale entanglements, Nat. Commun., 11, 536, https://doi.org/10.1038/s41467-019-14215-w, 2020.

Schlegel, R. W., Oliver, E. C. J., Wernberg, T., and Smit, A. J.: Nearshore and offshore co-occurrence of marine heatwaves and cold-spells, Prog. Oceanogr., 151, 189–205, https://doi.org/10.1016/j.pocean.2017.01.004, 2017.

Schlegel, R. W., Oliver, E. C. J., and Chen, K.: Drivers of Marine Heatwaves in the Northwest Atlantic: The Role of Air–Sea Interaction During Onset and Decline, Front. Mar. Sci., 8, 627970, https://doi.org/10.3389/fmars.2021.627970, 2021a.

Schlegel, R. W., Darmaraki, S., Benthuysen, J. A., Filbee-Dexter, K., and Oliver, E. C. J.: Marine cold-spells, Prog. Oceanogr., 198, 102684, https://doi.org/10.1016/j.pocean.2021.102684, 2021b.

Sen Gupta, A., Thomsen, M., Benthuysen, J. A., Hobday, A. J., Oliver, E., Alexander, L. V., Burrows, M. T., Donat, M. G., Feng, M., Holbrook, N. J., Perkins-Kirkpatrick, S., Moore, P. J., Rodrigues, R. R., Scannell, H. A., Taschetto, A. S., Ummenhofer, C. C., Wernberg, T., and Smale, D. A.: Drivers and impacts of the most extreme marine heatwave events, Sci. Rep., 10, 19359, https://doi.org/10.1038/s41598-020-75445-3, 2020.

Shan, S. and Sheng, J.: Numerical Study of Topographic Effects on Wind-Driven Coastal Upwelling on the Scotian Shelf, J. Mar. Sci. Eng., 10, 497, https://doi.org/10.3390/jmse10040497, 2022.

Smith, K. E., Sen Gupta, A., Amaya, D., Benthuysen, J. A., Burrows, M. T., Capotondi, A., Filbee-Dexter, K., Frölicher, T. L., Hobday, A. J., Holbrook, N. J., Malan, N., Moore, P. J., Oliver, E. C. J., Richaud, B., Salcedo-Castro, J., Smale, D. A., Thomsen, M., and Wernberg, T.: Baseline matters: Challenges and implications of different marine heatwave baselines, Prog. Oceanogr., 231, 103404, https://doi.org/10.1016/j.pocean.2024.103404, 2025.

Soontiens, N., Andres, H. J., Coyne, J., Cyr, F., Galbraith, P. S., and Penney, J.: An analysis of the 2023 summer and fall marine heat waves on the Newfoundland and Labrador Shelf, in: 9th edition of the Copernicus Ocean State Report (OSR9), edited by: Grégoire, M., Marcos, M., Staneva, J., Brasseur, P., Garric, G., Lionello, P., Karstensen, J., and Poulain, P.-M., Copernicus Publications, State Planet, 6-osr9, 12, https://doi.org/10.5194/sp-6-osr9-12-2025, 2025.

Thompson, K. R. and Demirov, E.: Skewness of sea level variability of the world's oceans, J. Geophys. Res.-Oceans, 111, C05005, https://doi.org/10.1029/2004JC002839, 2006.

Umoh, J. U. and Thompson, K. R.: Surface heat flux, horizontal advection, and the seasonal evolution of water temperature on the Scotian Shelf, J. Geophys. Res.-Oceans, 99, 20403–20416, https://doi.org/10.1029/94JC01620, 1994.

Wang, H., Lu, Y., Zhai, L., Chen, X., and Liu, S.: Variations of surface marine heatwaves in the Northwest Pacific during 1993–2019, Front. Mar. Sci., 11, 1323702, https://doi.org/10.3389/fmars.2024.1323702, 2024.

Wang, Y., Kajtar, J. B., Alexander, L. V., Pilo, G. S., and Holbrook, N. J.: Understanding the Changing Nature of Marine Cold-Spells, Geophys. Res. Lett., 49, e2021GL097002, https://doi.org/10.1029/2021GL097002, 2022.

Zhang, M., Cheng, Y., Wang, G., Shu, Q., Zhao, C., Zhang, Y., and Qiao, F.: Long-term ocean temperature trend and marine heatwaves, J. Ocean. Limnol., 42, 1037–1047, https://doi.org/10.1007/s00343-023-3160-z, 2024.

Zhao, Z. and Marin, M.: A MATLAB toolbox to detect and analyze marine heatwaves, Journal of Open Source Software, 4, 1124, https://doi.org/10.21105/joss.01124, 2019.

Zisserson, B. and Cook, A.: Impact of bottom water temperature change on the southernmost snow crab fishery in the Atlantic Ocean, Fish. Res., 195, 12–18, https://doi.org/10.1016/j.fishres.2017.06.009, 2017.

State Planet, 6-osr9, 6, 2025
https://doi.org/10.5194/sp-6-osr9-6-2025

A new conceptual framework for assessing the physical state of the Baltic Sea

Urmas Raudsepp[1], **Ilja Maljutenko**[1], **Priidik Lagemaa**[1], **and Karina von Schuckmann**[2]

[1]Department of Marine Systems, Tallinn University of Technology, Tallinn, 12618, Estonia
[2]Mercator Ocean International, 2 Av. de l'Aérodrome de Montaudran, 31400 Toulouse, France

Correspondence: Ilja Maljutenko (ilja.maljutenko@taltech.ee)

Received: 4 September 2024 – Discussion started: 20 September 2024
Revised: 31 July 2025 – Accepted: 7 August 2025 – Published: 30 September 2025

Abstract. Climate change is placing growing pressure on all parts of the ocean, increasing the need for regular information to support regional assessments and inform policy and decision-making. Understanding not only what is changing and where but also why is essential for effective response and meaningful action. To answer this need a new conceptual framework for the assessment of the physical state of the general natural water basin was introduced and then tested for the Baltic Sea. The approach is based on major process characteristics of the Baltic Sea and includes the analysis of mutual variability of well-established climate indicators such as ocean heat content (OHC), freshwater content (FWC), subsurface temperature, and salinity, combined with atmospheric forcing functions along with salt transport across the open boundaries as well as river runoff. A random forest model is used as the main analysis tool to enable statistical dependencies between state variables and potential forcing factors. Results reveal a clear 30-year warming trend in the Baltic Sea, closely linked on an interannual scale to 2 m air temperature, evaporation, and wind stress magnitude. The study highlights that interannual variations in temperature and salinity within the vertically extended halocline are key drivers of changes in OHC and FWC in the Baltic Sea. Interannual changes of FWC are explained by large-volume saline water inflows, net precipitation, and zonal wind stress. This framework also offers a new perspective of the potential impact of a shallowing mixed layer depth, resulting from sustained sensible heat flux changes at the air–sea interface, on salt export and the overall reduction of FWC in the Baltic Sea. This new framework could be applied to other geographical regions or future datasets, providing consistent information for a basin-wide monitoring tool that tracks the state and variability of the sea. Such a tool could be integrated into regional climate and environmental assessments.

1 Introduction

Human-induced greenhouse gas emissions are warming Earth's climate, causing ocean temperatures to rise and ice to melt globally (IPCC, 2021). The increase in ocean water temperatures has induced a rise in ocean heat content (OHC), and ice melt on land has introduced significant amounts of fresh water into the ocean, contributing to the rise in global sea levels. In 2023, global average sea surface temperature reached a record high relative to the 1973–2024 baseline period (McGrath et al., 2024), and global ocean heat content climbed to record levels (Cheng et al., 2024). In the Baltic Sea, the temperature trends for the period 1850–2008 show fast warming at the surface (~ 0.06 K per decade) and bottom (> 0.04 K per decade) and slow warming in the intermediate layers (< 0.04 K per decade) (Dutheil et al., 2023). Surface warming has progressively increased over time, primarily due to the sensible heat flux and latent heat flux (Kniebusch et al., 2019a). Trends in freshwater content (FWC) are not as consistent globally as those of OHC (Boyer et al., 2007), although the rise in global sea level is widely acknowledged (Frederikse et al., 2020). Salinity patterns differ across various ocean regions of the world (Skliris et al., 2014), with the North Atlantic–North Pacific salinity contrast increasing by $5.9\,\% \pm 0.6\,\%$ since 1965 (Lu et al., 2024). At a regional scale in the Baltic Sea, FWC has shown a significant down-

Published by Copernicus Publications.

Table 1. Product table.

Product ref. no.	Product ID and type	Data access	Documentation
1	BALTICSEA_MULTIYEAR_PHY_003_011; numerical models	EU Copernicus Marine Service Product (2023)	Quality Information Document (QUID): Panteleit et al. (2023) Product User Manual (PUM): Ringgaard et al. (2024)
2	ERA5; numerical models	Copernicus Climate Change Service (2023)	Product reference: Hersbach et al. (2023) Journal article: Hersbach et al. (2020)
3	E-HYPE; numerical models	SMHI	Donnelly et al. (2016)

ward trend over the last 30 years (Raudsepp et al., 2023). Winsor et al. (2001) highlighted the cumulative impact of riverine input on the Baltic's freshwater budget, while Rodhe and Winsor (2002) underscored the importance of episodic saltwater inflows in renewing deep water. An increase in freshwater supply to the Baltic Sea will intensify the regional water cycling, resulting in lower salinity, and vice versa.

The analysis of the physical state of natural water basins typically focuses on the evolution and spatial distribution of temperature and salinity and corresponding uncertainty estimations, which are essential ocean variables (EOVs; Global Ocean Observing System, 2024; Lindstrom et al., 2012). These variables are four-dimensional and therefore provide a spatially and temporarily resolved description of the state of the water body. Meanwhile, OHC and FWC are vital integral characteristics of the ocean, indicative of a water body's energy and mass, respectively. OHC offers a comprehensive view of oceanic heat storage, which is crucial for evaluating climate change impacts, energy budgets, and long-term trends (Forster et al., 2024). FWC represents the mass of the fresh water relative to the total mass of a water parcel with a given salinity (see Raudsepp et al., 2023). The increase in net precipitation over land and sea areas, the decrease in the ice cover, and the increase in river runoff are the main components of the global hydrological cycle that increase FWC in the ocean (Boyer et al., 2007; Cheng et al., 2020; Yu et al., 2020). While OHC is a well-established indicator in ocean and climate research, its counterpart, ocean FWC, has received less attention.

We propose a new conceptual framework for assessing the physical state of the Baltic Sea by integrating multiple physical and statistical approaches (Fig. 1). OHC and FWC serve as integrative indicators of the Baltic Sea's physical state, analogous to essential climate indicators (IPCC, 2021; Forster et al., 2025). The OHC and FWC are well-established measures (IPCC, 2021; Forster et al., 2025) which we integrate into a unified assessment framework with additional analysis layers – vertical distribution and statistical inference – to assess the Baltic Sea's state, and they are central to understanding its energy and mass balance. OHC reflects the vertically integrated heat stored in the water column and is

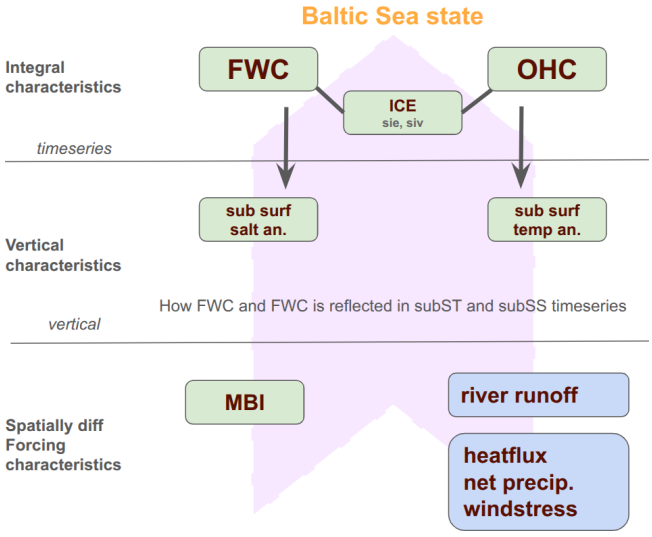

Figure 1. Conceptual scheme of the Baltic Sea state parameters illustrating the interplay among key indicators: ocean heat content (OHC), freshwater content (FWC), sea ice extent (SIE), sea ice volume (SIV), subsurface temperature (subST), subsurface salinity (subSS), and major Baltic inflows (MBIs). Changes in OHC and FWC drive variations in sea ice cover and subsurface conditions, while episodic MBI events inject saline water into deep layers, altering subsurface salinity and temperature. Together, these processes shape the overall state of the Baltic Sea.

primarily influenced by surface heat fluxes, vertical mixing, and subsurface temperature changes (Forster et al., 2025). FWC quantifies the deviation of the water column's salinity from a reference value and serves as a measure of accumulated fresh water (Durack, 2015; Raudsepp et al., 2023). It is affected by net precipitation, river runoff, evaporation, and saltwater intrusions from the North Sea. In this study, these indicators are integrated into a unified assessment framework that includes both their vertical structure and statistical inference layers. The study identifies the importance of these major variables affecting the OHC and FWC, including subsurface temperature, salinity, atmospheric forcing factors, and salt transport.

The framework follows a three-stage process: time series analysis, depth-based variability analysis, and statistical relationships using machine learning. The initial phase consists of calculating the time series of OHC and FWC for the entire Baltic Sea. This provides insights into long-term trends and interannual variability. In basins covered partially by sea ice, the annual mean ice extent (MIE) is considered an important integral characteristic. The next step examines the horizontally averaged vertical distribution of temperature (for OHC) and salinity (for FWC) to determine which depth ranges contribute the most to their variations. While this does not directly attribute causal links, the vertical profiles of temperature and salinity provide strong indications of which forcing factors might be responsible for changes in OHC and FWC. The final stage integrates forcing functions and ocean state characteristics to identify statistical dependencies between them, using a random forest (RF) model to probe potential drivers of variability. A RF model is employed to highlight statistical dependencies between oceanic state variables and external forcing mechanisms. This machine-learning approach enables the identification of general patterns in the temporal evolution of the Baltic Sea's physical state. The main reason we introduced the RF models is to determine, in a data-driven way, the relative importance of different depth layers and forcing factors on the variability of OHC and FWC. The RF approach offers a flexible means to handle nonlinear relationships and multiple predictors simultaneously.

Our proposed framework integrates the analysis of OHC and FWC by considering both their bulk integral values and their vertical distributions, allowing for the identification of key depth ranges contributing to their variability – which goes beyond other similar frameworks. Unlike the GOOS EOV framework (https://goosocean.org/, last access: 22 August 2025), which focuses on structured global ocean monitoring without machine-learning-based statistical analysis, our approach explicitly incorporates machine learning to identify potential drivers of variability. Compared to the IPCC Climate and Ocean Monitoring Framework (IPCC AR6, 2021, Ocean Observations Chapter, https://www.ipcc.ch/report/ar6/wg1/, last access: 22 August 2025), which relies on dynamical climate models for global-scale processes, our framework is designed for regional-scale Baltic Sea analysis, offering a more localized and detailed assessment. Finally, while the NASA Salinity and Heat Budget Analysis (NASA Salinity Budget Project, https://podaac.jpl.nasa.gov, last access: 22 August 2025) is largely empirical and focused on global salinity and heat transport, our approach provides a structured three-stage methodology, incorporating not only empirical analysis but also a cause-and-effect exploration using machine learning. This makes our framework uniquely suited for regional climate monitoring and actionable insights into the physical state of the Baltic Sea.

The Baltic Sea is recognized for its spatially pronounced heterogeneous structure. Its various subregions may exhibit distinct temporal variations in key state variables and overall dynamics, making it a complex environment for testing the conceptual framework. The Baltic Sea, a shallow marginal sea in northeastern Europe, is characterized by its hydrographic fields and sea ice conditions (Leppäranta and Myrberg, 2009). Salinity levels are affected by saline water inflows from the North Sea through the Danish straits, riverine freshwater inputs, and net precipitation (Lehmann et al., 2022). Major Baltic inflows, which introduce saline and oxygen-rich water, are sporadic and unpredictable (Mohrholz, 2018). Temperature fields are influenced by the heat exchange with the atmosphere. The residence time of the Baltic Sea's water is several decades long (Meier et al., 2022). The vertical salinity stratification is defined by the halocline's depth, featuring a well-mixed surface layer and a slightly stratified layer beneath. Water temperature plays a crucial role in forming secondary stratification related to the temperature of the upper mixed layer. Seasonal temperature cycles lead to partial freezing of the Baltic Sea in winter. Changes in sea ice extent over time are a vital indicator of climate change for the area. A reduction in maximum ice extent impacts the sea's vertical stratification and the seasonal trends in ocean heat and freshwater content (Raudsepp et al., 2022, 2023). Despite global warming, there has not been a significant increase in the Baltic Sea's relative sea level (Ranasinghe et al., 2021), which instead shows a strong seasonal cycle.

This conceptual framework is designed as an indicator-based approach relevant to policymakers. OHC and FWC distill complex, high-dimensional data (many temperature and salinity profiles) into two easy-to-interpret indices of the Baltic Sea's thermal and haline state. This kind of simplification is valuable for decision-makers who require clear, high-level indicators. However, interpretation is also necessary – and this becomes particularly challenging at the regional scale, where a variety of interacting processes, including long-term changes, are at play. The framework not only delivers time series and regular statistical assessments, but also provides a structured path toward meaningful interpretation by focusing directly on the main drivers of change. Understanding not just what is changing and where, but also why it is happening, is essential for taking informed action and gaining a comprehensive view of the system. The framework enables the monitoring of climate change impacts on the Baltic Sea while maintaining a balance between scientific rigor and practical accessibility. It is not meant to serve as a comprehensive dynamical model but rather as a tool for assessing the state of the Baltic Sea and guiding regional management decisions. The framework is grounded in well-established physical quantities and validated by statistical analysis, which ensures that its findings are consistent and credible.

The study aims to present a framework for assessing the physical state of the Baltic Sea by integrating annual mean values of OHC, FWC, subsurface temperature and salin-

ity, atmospheric forcing functions, salt transport, and river runoff. The objective is to use a data-driven RF approach as the primary analysis tool to parse out nonlinear relationships and feature importances from a broad dataset. This study introduces an integrative, basin-wide approach, defining the entire Baltic Sea as a single water body for analysis. It computes a time series of total OHC and FWC for the whole sea. Unlike previous approaches that focus mainly on local variations, this methodology prioritizes integrated indices that capture the sea's overall state. This holistic perspective represents a fundamental shift away from fragmented, localized analyses toward a comprehensive understanding of ocean dynamics, making the framework uniquely suited to inform large-scale assessments and decision-making.

2 Data and methods

2.1 Oceanographic and atmospheric data

The Baltic Sea physics reanalysis multi-year product (BAL-MYP; Table 1, product ref. no. 1) is derived from the ocean model NEMO v4.0 (Madec et al., 2019). It assimilates satellite observations of sea surface temperature (SST) (EU Copernicus Marine Service Product, 2022) and in situ temperature and salinity profiles from the ICES database (ICES, 2022). The model data are provided on a grid with a horizontal resolution of 1 nmi (nautical mile), including 56 vertical layers, covering the entire Baltic Sea and the transition zone to the North Sea. The dataset covers the period from 1993 to 2023, with the model setup detailed in the Product User Manual (PUM; Ringgaard et al., 2024).

The BAL-MYP has been extensively validated, as documented in the Quality Information Document (QUID; Panteleit et al., 2023), focusing on the period from 1 January 1993 to 31 December 2018. Additionally, the BAL-MYP data were evaluated using a clustering method with the K-means algorithm (Raudsepp and Maljutenko, 2022), which provided insights into the reanalysis accuracy by categorizing errors (Lindenthal et al., 2024). Fifty-seven percent of the data are clustered with a bias of $\mathrm{d}S = -0.40\,\mathrm{g\,kg^{-1}}$ and $\mathrm{d}T = -0.02\,^{\circ}\mathrm{C}$, encompassing 57 % of all data points with RMSE $S = 0.92\,\mathrm{g\,kg^{-1}}$ and $T = 0.54\,^{\circ}\mathrm{C}$. These points are distributed throughout the Baltic Sea. Clusters with high positive and negative temperature biases account for 11 % and 8 % of total points, respectively, with marginal salinity biases and relatively even spatial distributions across the Baltic Sea. Twenty-six percent of the points have low temperature but high salinity errors, both negative and positive, predominantly located in the southwestern Baltic Sea, indicating occasional underestimation or overestimation of the inflow/outflow salinity.

Given its spatial coverage and validated accuracy, the BAL-MYP reanalysis (Table 1, product ref. no. 1) provides a reliable basis for calculating integrated environmental indicators such as OHC and FWC, which are essential for large-scale climate assessments. OHC directly reflects Earth's energy imbalance, making it a key metric for tracking global warming, unlike basin-averaged temperature, which lacks a direct connection to energy budgets (von Schuckmann et al., 2016, 2023). Consequently, OHC is prioritized in climate models and international assessments (Bindoff et al., 2019) due to its direct relationship with anthropogenic forcing and its predictive value for future climate scenarios. The daily OHC has been computed for each model grid cell from reanalysis (product ref. no. 1), following the methodology of Meyssignac et al. (2019):

$$\mathrm{OHC} = \rho \times c_p \times (T + 273.15), \tag{1}$$

where ρ is the density of seawater calculated following the TEOS10 (IOC et al., 2010), c_p is specific heat capacity calculated as a third-order polynomial function of salinity and temperature according to Millero et al. (1973), and T is daily temperature.

Ocean FWC is deemed more significant than mean salinity for understanding climate dynamics and ocean processes. FWC provides a holistic measure of freshwater storage and its effects on ocean circulation, climate, and sea-level rise (Solomon et al., 2021; Fukumori et al., 2021). It directly measures freshwater inputs (e.g., ice melt, river runoff, rainfall) or losses (e.g., evaporation), whereas mean salinity only indicates the average salt concentration, ignoring volume (Hoffman et al., 2023). A minor salinity change over a large water volume could signify a substantial freshwater flux, which mean salinity alone would not reveal (Schauer and Losch, 2019). The FWC was calculated at each grid point and day as in Boyer et al. (2007):

$$\mathrm{FWC} = \rho(S_{\mathrm{ref}}, T_{\mathrm{ref}}, p)/\rho(0, T_{\mathrm{ref}}, p) \times (S_{\mathrm{ref}} - S)/S. \tag{2}$$

The three-dimensional temperature (T_{ref}) and salinity (S_{ref}) fields are temporal averages over the period of 1993–2023. A detailed description of the calculation procedure is available in Raudsepp et al. (2023). The OHC and FWC were calculated by spatially integrating the gridded OHC (1) and FWC (2) over the Baltic Sea, and then the annual mean OHC and FWC values were calculated from these daily values.

The mixed layer depth (MLD), also referred to as the upper mixed layer (UML), was included in the analysis using data from a multi-year reanalysis product (product ref. no. 1). The MLD was calculated based on density stratification following the method of de Boyer Montégut et al. (2004), which defines MLD as the depth at which seawater density deviates from the reference density at 10 m depth by a specified threshold. For the Baltic Sea, this threshold was adjusted to $0.03\,\mathrm{kg\,m^{-3}}$ to better represent the characteristics of the regional upper mixed layer (Panteleit et al., 2023).

Atmospheric data for the RF input (Atm8) were obtained from the ERA5 reanalysis (product ref. no. 2) for the period 1993–2023. The parameters (eight in total) included 2 m air temperature, total precipitation, evaporation, wind stress

magnitude, and the x and y components of wind stress, along with total cloud cover and surface net solar radiation. The time series for the annual mean values of these atmospheric parameters were computed as horizontal averages across the Baltic Sea region (8–33° E and 52–68° N).

Additionally, total river runoff to the Baltic Sea (RNF) (product ref. no. 3) and a proxy for saltwater inflows – represented by bottom salinity in the Bornholm Basin (SOB) (product ref. no. 1) – were included as external forcing factors. These variables capture key hydrological and oceanographic influences not fully accounted for by atmospheric drivers alone and contribute to a more comprehensive assessment of interannual variability in FWC.

Horizontally average temperature and salinity profiles calculated from the BAL-MYP (product ref. no. 1) at 42 different depth layers (shown on Fig. 3) and Baltic Sea domain (13–31° E and 53–66° N; excluding the Skagerrak strait) were used as predictors in two of the RF models. The rationale for using the full vertical profiles is to allow the model to identify which depth layers most strongly influence the total OHC or FWC. Instead of assuming a priori which depths matter, the RF can learn this from data: if variations at a particular depth are consistently associated with changes in total OHC/FWC, the model's feature importance for that depth will be high.

2.2 Random forest

Random forest (RF) is an ensemble learning method predominantly used for classification and regression tasks (Breiman, 2001). It functions by building multiple decision trees during the training phase and outputs the class that is the mode of the classes (classification) or the mean prediction (regression) of the individual trees. This method enhances accuracy and helps prevent overfitting, thus making it resilient to noise in the dataset. RF proves to be highly effective in analyzing complex interactions between variables, such as the relationships between marine state variables and atmospheric parameters. Its effectiveness is due to its capability to manage high-dimensional data and its resistance to outliers and noise, which are prevalent in environmental datasets. Additionally, RF is adept at detecting nonlinear relationships between predictor variables (atmospheric parameters) and response variables (marine state variables), which linear models often overlook.

In the context of a RF model, feature importance is a technique that identifies the most influential input features (variables) in predicting the output variable. The importance of each feature is determined by the decrease in model accuracy when the data for that feature are permuted, while all other features remain unchanged. If permuting a feature's values significantly increases the model's error, that feature is deemed crucial for the model's predictions. This approach aids in discerning the contribution of each feature to the model's decision-making process and in identifying key atmospheric parameters that significantly impact marine state variables. A positive value for a feature implies that permuting that predictor variable's values raises the model's prediction error, indicating the variable's importance for the model's predictive accuracy. A higher positive value suggests greater reliance on that variable by the model.

In this study we have trained the four different RF models to fit the OHC and FWC annual average time series from annual average predictor variables with the hyperparameter configurations shown in Table 2. Two models are trained to predict the OHC and FWC values from the set of the atmospheric variables (VAR arguments). The OHC model uses only atmospheric input variables, whereas the FWC model includes, in addition to atmospheric variables, two external predictors: total river runoff to the Baltic Sea and bottom salinity in the Bornholm Basin. In addition, two more models are trained to predict OHC and FWC using horizontally averaged temperature and salinity profiles (Z arguments). To study variability independent of long-term trends, all input variables and target time series used in the VAR models were linearly detrended prior to training. This ensures the models capture interannual to decadal fluctuations rather than long-term changes.

To optimize the performance of the RF models while ensuring robustness and generalizability, a set of hyperparameters was selected based on best practices outlined by Probst et al. (2019), along with and based on sensitivity analysis conducted for the number of trees (Fig. A2). The minimum leaf size (MinLS) was set to 1, allowing the trees to fully grow and capture complex data patterns. The number of predictors to sample at each split (Pred2Samp) was dynamically determined as one-third of the total number of predictors, tackling a balance between feature randomness and predictive strength. This approach promotes diversity among trees while preventing excessive correlation. The number of trees (NumTrees) in each RF model was set to 100, providing sufficient ensemble stability while maintaining computational efficiency (Appendix A2). Since this study employs RF models to investigate nonlinear relationships between predictors and state variables, we use the entire dataset (all available data) as the training set to maximize the models' ability to learn patterns. We conducted 5-fold cross-validation, which yielded similar conclusions regarding which predictors are most influential, suggesting that the RF importance measures are qualitatively robust. To further enhance predictive reliability, assess uncertainty, and evaluate the stability of both predictions and feature importances, an ensemble of 150 independently trained RF models was constructed.

We employed MATLAB's TreeBagger function to assess the feature importance of atmospheric predictors on marine state variables. The OOBPermutedPredictorDeltaError method, a robust metric from MATLAB's TreeBagger, quantifies each predictor's importance via the out-of-bag (OOB) prediction error. This involves permuting each variable's values across OOB observations for each tree. The resulting

Table 2. Hyperparameter configurations and validation for different random forest models. All models use the same random forest configuration: number of trees set to 100 and forest ensemble size to 150. The variable number of predictors to sample at each split (Pred2Samp) is set to 2/3 of the number of input parameters. The minimum leaf size is fixed at 1. Asterisks (*) indicate RF models applied to variability using detrended variables. Models performance is shown by means of Pearson's correlation coefficient (CC) and root mean square difference (RMSD).

Model	Predictors	Pred2Samp	CC	RMSD
RF_OHC(Z)	Tprof_42[1]	14	0.986	0.0016
RF_FWC(Z)	Sprof_42[1]	14	0.973	0.004
RF_OHC(VAR)*	ATM_8[2]	3	0.9012	0.3432
RF_FWC(VAR)*	ATM_8[2] + RNF[3] + SOB[4]	4	0.8994	0.3624

[1] Tprof_42, Sprof_42: horizontally averaged annual mean temperature and salinity profiles at 42 depth levels (Fig. 3). [2] ATM_8: horizontally averaged annual mean values of eight atmospheric variables. [3] RNF: total annual river runoff into the Baltic Sea. [4] SOB: annual mean bottom salinity in the Bornholm Basin.

change in prediction error from these permutations is calculated for each tree. These measures are averaged across all trees and normalized by the standard deviation of the changes, providing a standardized score that highlights the variables with the most significant impact on predictive accuracy. Averaging the feature importance scores across all models in ensembles minimizes the noise and variability from any single model's training, offering a more consistent and dependable indication of each atmospheric parameter's contribution to predicting marine state variables. A larger importance value means that permuting (randomizing) that predictor greatly degrades model accuracy, indicating the predictor was influential. Conversely, near-zero or negative importance means that randomizing the predictor had little effect or even slightly improved the model's error, suggesting the predictor is not informative (or that its influence is redundant or noisy).

3 Results

Both OHC and FWC display a statistically significant linear trend, as shown in Fig. 2. Using a z-score time series allows for the comparison of trends per year (trend*) and data distributions without the influence of their units. OHC shows an increasing trend* of 0.089 ± 0.025, while FWC exhibits a decreasing trend* of -0.092 ± 0.023, both comparable in magnitude (Table 3). The corresponding absolute values are $0.34 \pm 0.095\,\mathrm{W\,m^{-2}}$ for OHC and $-36.99 \pm 9.20\,\mathrm{km^3\,yr^{-1}}$ for FWC (Table 3). Between 1993 and 2003, OHC and FWC varied similarly, both rising and falling concurrently (blue dots in Fig. 2). After this period, their patterns diverged (yellow and red dots in Fig. 2). Interannual variations of the annual mean sea ice extent and OHC are strongly correlated but in opposite phases (not shown). Among the forcing functions, the 2 m air temperature shows a distinct positive trend (Fig. 2), albeit weaker than the trends of OHC and FWC (Table 3). The air temperature over the Baltic Sea area has risen with a trend* of 0.074 ± 0.031 (Table 3). Surface net solar radiation has a weaker but still significant positive trend* of 0.058 ± 0.035, and the evaporation time series shows a negative trend* of -0.041 ± 0.039 (Fig. 2, Table 3). Other atmospheric variables did not exhibit statistically significant trends (Fig. 2). Correlation coefficients among various atmospheric datasets were generally low (Table 4). The two highest correlation coefficients, 0.76 and 0.73, are between wind stress magnitude and its zonal component, indicating a predominance of westerly airflow over the Baltic Sea and between 2 m air temperature and surface net solar radiation, respectively. The low correlations suggest a weak statistical relationship between the annual mean atmospheric parameters, supporting the inclusion of all forcing functions in the RF model.

In analyzing OHC variations, we use a RF_OHC(Z) model (Table 2). This model employs horizontally averaged annual temperature values at each depth level, derived from the depth levels of a multi-year product (product ref. no. 1), as input features. The RF model finely replicates the annual OHC time series (Fig. 3a), with a high correlation coefficient (0.986) and a RMSD of the standardized time series at 0.0016. However, it did not capture the extreme OHC event in 2020 or the low OHC extreme in 1996 (Fig. 3). Feature importance is significant within a depth range of 10–80 m (Fig. 3b), with two peaks at depths of 18 and 60 m, aligning with the average depths of the seasonal thermocline and the permanent halocline, respectively. This suggests that interannual OHC variations are mainly influenced by temperature changes within these layers. Subsurface temperatures from 1993 to 2023 indicate warming trends of approximately $0.06\,^{\circ}\mathrm{C\,yr^{-1}}$ across all depths (CMS, 2024a). From 1993 to 1997, deep water temperatures remained relatively low (below 6 °C). Since 1998, deeper waters have warmed, with temperatures above 7 °C occupying the layer below 100 m since 2019. The water temperature below the halocline has risen by about 2 °C since 1993, and the cold intermediate layer's temperature also increased during the 1993–2023 period.

A similar method is employed to elucidate the interannual fluctuations of FWC using RF_FWC(Z) (Table 2), utilizing horizontally averaged salinity at each depth level. The model's precision is slightly lower (correlation: 0.973;

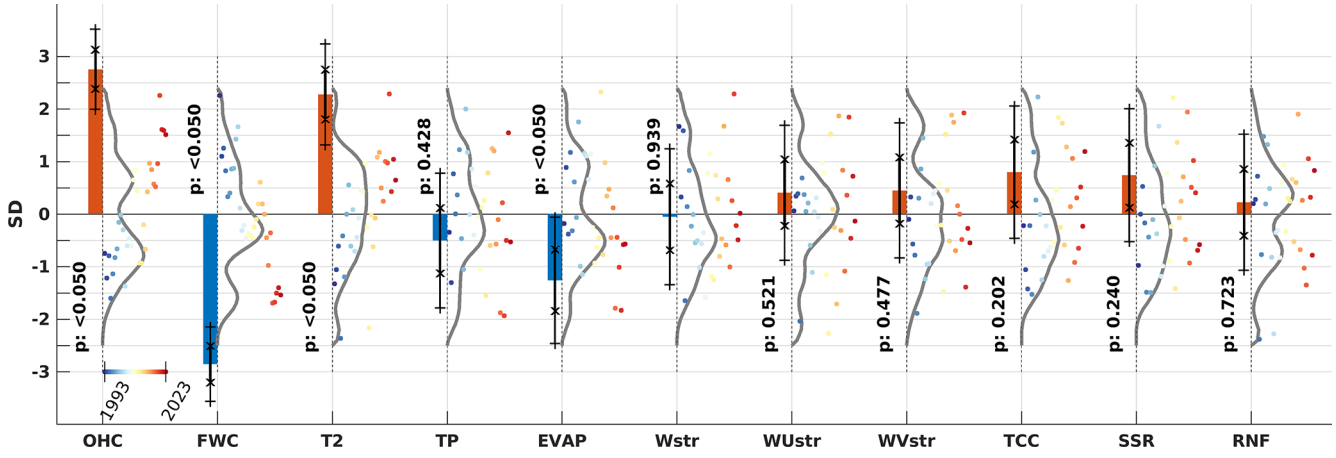

Figure 2. Trend analysis and probability distribution functions (PDFs) of the annual time series of standardized (*z scores) Baltic Sea state and meteorological parameters. To the left of the dashed line, the period-normalized annual trend values (multiplied by the period length in years, i.e., 30) are displayed as red (positive) and blue (negative) bars with corresponding p values (95 % confidence level), along with whiskers representing ±1 standard error (x ticks) and the 95 % uncertainty range (+ ticks). On the right side of the dashed line, probability density functions (PDFs) are shown as the solid lines for the standardized time series, which are represented by colored dots. The color of the dots represents the year on a common color scale shown at the OHC variable. OHC: ocean heat content; FWC: freshwater content; T2: 2 m temperature; TP: total precipitation; EVAP: evaporation; Wstr: wind stress; WUstr and WVstr: wind stress u and v component; TCC: total cloud cover; SSR: surface net solar radiation; RNF: river runoff.

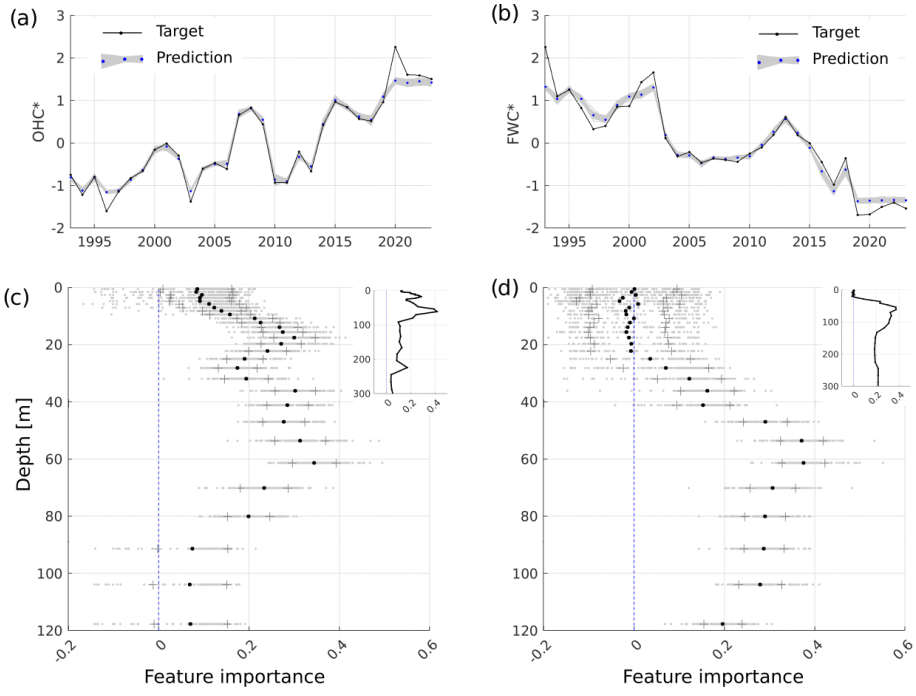

Figure 3. OHC* and FWC* ensemble predictions (ensemble mean as blue dots) using the horizontal average salinity and temperature profiles **(a, b)**. The prediction feature importance, with ensemble spread (1 SD shown with "+" marker), for each depth in the upper 120 m layer shown on panels **(c)** and **(d)** and for the full depth range in the upper-right inset panels. All variables are z-scored.

RMSD of standardized time series: 0.004) compared to that for OHC. The model consistently underperforms in predicting the FWC peaks, encompassing both the lows and highs (Fig. 3c). The most notable features cover the depth range of 40–120 m (Fig. 3d), coinciding with a halocline layer and its vertical extensions to both shallower and deeper depth. The salinity levels at the bottom layer are of secondary importance to the inter-annual variations of FWC in the Baltic Sea. The salinity in the top 25 m stratum exerts a minimal influence on FWC changes. The interannual variability of salinity in the upper stratum is minor relative to the deeper stratum. The salinity gradient ascends steadily from zero at a depth of 25 m to 0.04 g kg^{-1} annually at 70 m (CMS, 2024b). The most marked trend, 0.045 g kg^{-1} yr^{-1}, occurs within the expanded halocline layer extending from 70 to 150 m. Notably, there is a slight dip in the salinity trend to 0.04 g kg^{-1} yr^{-1} between the depths of 150 and 220 m. While this reduction is slight, it indicates that salt influx into the expanded halocline layer is more significant than into the deeper strata. A salinity trend of 0.05 g kg^{-1} annually is detected in the deepest stratum of the Baltic Sea.

Building a RF model targeting OHC and FWC time series with atmospheric forcing functions reveals the 2 m air temperature as the most significant contributor (Appendix A1). This correlation is physically plausible for OHC but less so for FWC. The 2 m air temperature affects the air–sea heat exchange via the sensible heat flux component. To further explore the declining FWC trend, we examined interannual changes in the annual average upper mixed layer depth (MLD). In the Baltic Sea, MLD varies widely across different areas and seasons. A shallowing of MLD is observed in the Baltic Proper and to some extent in the Bothnian Sea, while a MLD deepening is noted in the Bothnian Bay, the Gulf of Finland, and the Gulf of Riga. Typically, the Baltic Sea's stratification is influenced by salinity, although a seasonal thermocline forms across the sea. In the northern and eastern basins, the dispersal of river water during spring and summer leads to the development of the seasonal pycnocline. Conversely, in the southern Baltic Sea, the spread of river water is mostly restricted to the coastal areas, so the mixed layer is less affected by the seasonal halocline.

We performed test experiments with the RF model, incorporating the upper mixed layer (UML) as an additional feature. We determined the annual mean UML depth across the Baltic Sea and specifically for the Eastern Gotland Basin. The decline in the UML depth was more significant in the Eastern Gotland Basin compared to the entire Baltic Sea. The UML depth in the Eastern Gotland Basin decreased from 30 m in 1993 to 22 m in 2023. The MLD feature became more significant than the 2 m temperature in explaining the FWC when we considered the UML depth in the Eastern Gotland Basin. However, the results were contentious when we applied the average UML depth for the entire Baltic Sea. An increase in the 2 m temperature may cause a shallower

Table 3. Linear annual trend values of z-scored time series (trend*), standard deviation (SD), linear trend of physical value (unit per year, except for OHC), and mean value (mean) of original time series. OHC: ocean heat content; FWC: freshwater content; T2: 2 m temperature; TP: total precipitation; EVAP: evaporation; Wstr: wind stress; WUstr: wind stress u component; WVstr: wind stress v component; TCC: total cloud cover; SSR: surface net solar radiation; RNF: river runoff.

Variable	OHC	FWC	T2	TP	EVAP	Wstr	WUstr	WVstr	TCC	SSR	RNF
Unit	MJ m^{-2}	km^3	°C	m yr^{-1}	m yr^{-1}	N m^{-2}	N m^{-2}	N m^{-2}	1	W m^{-2}	m^3 s^{-1}
Trend*	0.089 ± 0.025	-0.092 ± 0.023	0.074 ± 0.031	0.032 ± 0.04	-0.041 ± 0.039	-0.0016 ± 0.0418	0.013 ± 0.041	0.015 ± 0.041	-0.0077 ± 0.0417	0.058 ± 0.035	0.0073 ± 0.0417
SD	122.02	402.00	0.73	0.071	0.041	0.0056	0.0100	0.0072	0.0226	3.16	1687.92
Trend	0.344 (W m^{-2})	−36.987	0.054	0.0023	−0.0016	-8.85×10^{-6}	1.32×10^{-4}	1.05×10^{-4}	-1.75×10^{-4}	0.18	12.31
Mean	60.20	−63.73	7.65	0.73	−0.55	0.0999	0.0244	0.0138	0.6493	113.92	17 807.77

Table 4. Correlation coefficients (lower triangle) and standard errors (Gnambs, 2023) (upper triangle) of atmospheric parameters. Correlation coefficients which pass a two-tailed t test at 95 % confidence are in bold. OHC: ocean heat content; FWC: freshwater content; T2: 2 m temperature; TP: total precipitation; EVAP: evaporation; Wstr: wind stress magnitude; WUstr: wind stress u component; WVstr: wind stress v component; TCC: total cloud cover; SSR: surface net solar radiation.

	T2	TP	EVAP	Wstr	WUstr	WVstr	TCC	SSR
T2		0.19	0.17	0.17	0.15	0.14	0.15	0.09
TP	0.12		0.18	0.17	0.18	0.18	0.13	0.17
EVAP	−0.28	−0.18		0.19	0.18	0.16	0.19	0.15
Wstr	0.31	0.35	−0.10		0.08	0.15	0.18	0.19
WUstr	**0.47**	0.25	0.16	**0.76**		0.15	0.16	0.18
WVstr	**0.48**	0.16	0.37	**0.43**	**0.43**		0.19	0.19
TCC	−0.43	**0.58**	−0.04	−0.20	−0.42	−0.13		0.09
SSR	**0.73**	−0.31	−0.43	0.07	0.18	0.11	−0.73	

mixed layer, potentially reducing the mixing between the surface freshwater layer and the denser saline layer beneath.

By eliminating trends, we utilized RF models to identify the primary characteristics of the interannual fluctuations of OHC and FWC. The ensemble mean forecast of RF_OHC(VAR)* (Table 2) effectively captures these interannual changes (Fig. 4a), evidenced by a correlation coefficient of 0.9012 and a RMSD of 0.3432. Factors such as 2 m temperature, wind stress, and evaporation significantly influence the interannual variability of OHC (Fig. 4c). Additionally, total cloud cover and solar radiation have a minor impact on the shape of OHC.

In the RF_FWC(VAR)* model, we incorporated bottom salinity from the Bornholm Basin as a supplementary feature. The direct calculation of salt transport from model data across a section at the Baltic Sea entrance is error-prone. Utilizing daily average cross-section velocities and salinities overlooks high-frequency fluctuations with considerable residual salt flux. The model's precision in predicting accurate salinity levels at the Baltic Sea's entrance is quite low (Lindenthal et al., 2024). Time series of bottom salinity changes in the Arkona and Bornholm basins facilitate the tracking of the intermittent nature of water inflow and outflow events. The Arkona Basin, being relatively shallow, is known for its dynamic nature regarding volume and salt transport. Here, bottom salinity reflects the salinity shifts caused by inflow and outflow variations at the Baltic Sea entrance. These variations mask the large volume inflows chiefly responsible for the Baltic Sea's salt influx, thus not significantly affecting the Arkona Basin's bottom salinity over time. Conversely, the Bornholm Basin's greater depth means its bottom salinity is less affected by the upper layer's varying salinity water movements. Hence, the Bornholm Basin's bottom salinity serves as a more accurate indicator of the Baltic Sea's salt inflow. We also factored in the annual average river runoff (product ref. no. 3) into the Baltic Sea in our RF model.

The ensemble mean predictions of the RF_FWC(VAR)* are marginally less precise, with a correlation coefficient of 0.8994 and a root mean square difference of 0.3624. The bottom salinity in the Bornholm Basin – used here as an indicator of salt flux into the Baltic Sea – and total precipitation and the zonal wind component emerge as the primary drivers of interannual variations in freshwater content (FWC) (Fig. 4d). In contrast, riverine freshwater discharge shows no significant impact on FWC variability at the interannual scale. Raudsepp et al. (2023) showed that there are multi-year periods when river runoff is in phase or out of phase with the FWC as calculated for the whole Baltic Sea.

Notable FWC peaks occurred in 1993, 2002, and 2013, each followed by a rapid decline in subsequent years (Fig. 4b). The elevated FWC in 1993 reflects the end of a preceding stagnation period characterized by low salinity, which was interrupted by the major Baltic inflow (MBI) of 1993 occurring at the end of that year. The gradual increases in FWC observed from 1997 to 2002 and from 2004 to 2013 represent periods during which the influence of earlier MBIs – specifically those of 1993 and 2002 – on the basin's total salinity diminished over time.

Reductions in FWC are associated with increases in water salinity, driven primarily by the advection of saline water through the Danish straits. The highest bottom salinity values correspond to the MBIs that occurred at the end of 1993, 2002, and 2014. These inflows had a limited effect on annual FWC during the years of the inflows themselves (1993 and 2002), with their primary impact becoming evident in the following years – 1994 and 2003, respectively. Although the 2014 MBI took place at the end of that year, an increase in deepwater salinity was already underway prior to the event, leading to a decrease in FWC during 2014.

Finally, profiles of salinity, temperature, and dissolved oxygen concentration in the Gotland Basin from 1993 to 2023 – sourced from the Copernicus Marine Service Baltic Sea in situ multi-year and near-real-time observations (INSITU_BAL_PHYBGCWAV_DISCRETE_MYNRT_013_032) (CMS, 2024c) – complement our analyses of OHC and FWC by providing additional context on the evolution of the Baltic Sea's physical and biogeochemical conditions.

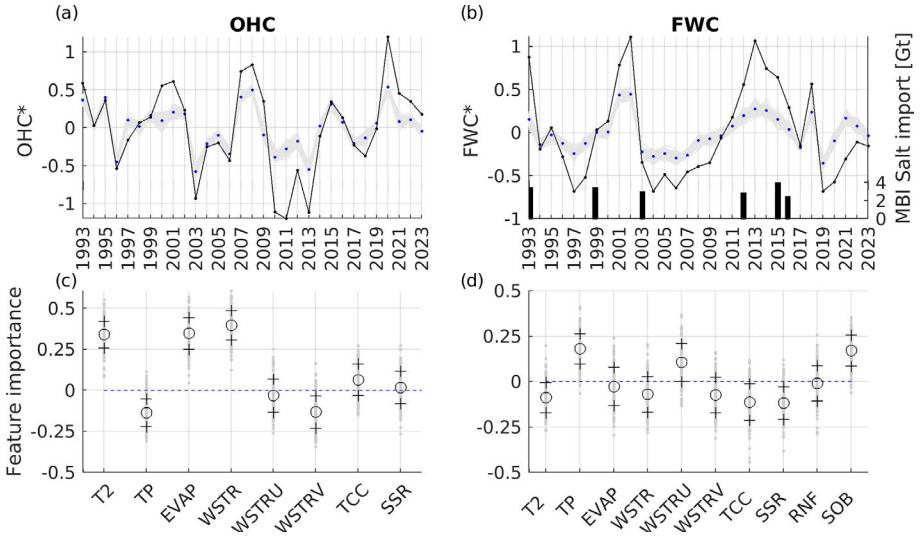

Figure 4. Time series of detrended OHC* **(a)** and FWC* **(b)** ensemble predictions (ensemble mean as blue dots) using RF ensembles. Ensembles of corresponding models feature importances, with ensemble spread ("+" markers corresponding to 1 SD) shown on panels **(c)** and **(d)** for OHC and FC, respectively. All variables are z-scored. OHC: ocean heat content; FWC: freshwater content; T2: 2 m temperature; TP: total precipitation; EVAP: evaporation; WSTR: wind stress; WSTRU and WSTRV: wind stress u and v component; TCC: total cloud cover; SSR: surface net solar radiation; RNF: river runoff; SOB: bottom salinity in the deepest location of the Bornholm Basin. Importance values are scaled by the permutation effect's standard deviation; positive values indicate reduced model performance when a predictor is permuted, while negative values reflect spurious performance improvements from permutation.

4 Discussion and conclusions

The growing complexity of climate-driven changes in marine environments necessitates a comprehensive framework that transcends traditional localized assessments. By integrating key indicators into holistic indices representing the overall state of the sea, this approach advances beyond fragmented analyses to provide a coherent basis for regional evaluation. Such an integrative methodology is essential for delivering actionable insights that can effectively inform policy and support sustainable management of ocean resources.

OHC and FWC are established large-scale metrics widely used to track global ocean changes. Here we adapt these metrics to the regional Baltic Sea and integrate them with additional analysis layers. This framework distinguishes itself by linking these integral metrics with depth-resolved information and machine-learning-based attribution, which to our knowledge has not been previously applied in the Baltic Sea context. OHC and FWC are proposed as key descriptors of the Baltic Sea's physical state because they encapsulate the overall thermal and haline content of the entire basin. While temperature and salinity at specific locations or layers provide detailed information, OHC and FWC offer a high-level integration of those details. OHC and FWC reflect temperature and salinity changes across the entire basin. OHC variations primarily follow surface layer temperature changes. The negative trend and interannual variability in FWC are mainly driven by subsurface salinity changes, as surface salinity remains relatively stable (Fig. 3c, d). High feature importance values indicate the depths where temperature and salinity changes most closely align with OHC and FWC variations, respectively.

We employed the RF model (Breiman, 2001) to link the atmospheric and hydrologic variables with the variability of OHC and FWC. Given the limited sample size of 31 annual observations, overfitting represents a potential concern in our modeling approach. To mitigate this, we employed an ensemble of 150 independently trained RF models, each with controlled tree complexity (e.g., limited depth, minimum leaf size). This ensemble strategy helps stabilize feature importance estimates and reduces prediction variance arising from random sampling effects, thereby enhancing the robustness of the results. Nonetheless, caution is warranted, as some predictor importances may reflect spurious correlations. Because our RF models were trained on the full time series (1993–2023) with no independent test period, the reported errors (based on OOB) could underestimate true predictive error. The results should thus be interpreted as patterns learned from the given dataset rather than as fully generalizable predictions. Future analyses could leverage extended reanalysis or model datasets (e.g., BMIP; Gröger et al., 2022) to independently validate the machine-learning results, thereby strengthening confidence in the predictive skill of the proposed framework.

OHC and FWC are particularly useful for monitoring long-term trends and basin-wide changes, which is why we argue that they effectively define the large-scale physical state. Indeed, our framework's indicators, total OHC and

FWC of the Baltic Sea, are integrative and require comprehensive observation or modeling efforts to compute in real time. In situ monitoring of the entire water column at sufficient spatial coverage is needed to directly measure OHC/FWC, which is more demanding than, say, monitoring a few atmospheric indices. However, these integrated indices provide a succinct summary of the state that individual predictors cannot fully capture. Advancements in remote sensing can help estimate these indices indirectly (e.g., Kondeti and Palanisamy, 2025).

Our results confirm a long-term warming and salinization trend in the Baltic Sea, as evidenced by increasing OHC and a slight decreasing trend in FWC (Table 3). At the same time, by removing these trends for the RF analysis, we isolated the interannual variability and identified its drivers.

Our analysis across the entire Baltic Sea reveals the direct impact of atmospheric forcing on ocean warming. Moreover, this framework provides new insights into the role of salt import/export in FWC's interannual variability and draws on the basin-wide decline of FWC, elevating the potential role of a flatting MLD from long-term sensible flux change at the air–sea interface. Particularly, results reveal that the Baltic Sea has undergone substantial change over the past decade as evidenced by the increase in OHC over the last 30 years.

Simultaneously, there has been a reduction in FWC, suggesting an increase in seawater salinity. The analysis of average subsurface temperature and salinity indicates that interannual variations in OHC and FWC are mainly influenced by temperature shifts in both the seasonal thermocline and permanent halocline and changes in salinity within the permanent halocline. This highlights the critical need for a comprehensive framework while reporting on the state of the Baltic Sea, allowing for the evaluation of basin-wide conditions, including its trends, interannual variations, and extremes, as well as the factors driving these changes. Using this approach could prove to be a valuable asset for the science–policy interface, aiding in regional evaluations of the sea state.

Previous studies have reported a positive trend in OHC and a negative trend in FWC (Raudsepp et al., 2022, 2023), along with an inverse relationship between OHC and the maximum ice extent in the Baltic Sea (Raudsepp et al., 2022). The increase in OHC has been attributed to the rising air temperature over the Baltic Sea, yet the decline in FWC remains largely unexplained. Raudsepp et al. (2023) noted that neither salt transport to the Baltic Sea, net precipitation, nor total river runoff accounted for the FWC's downward trend. Despite this, deepwater salinity in the central Baltic Sea has been increasing at a rate of 0.2–0.25 g kg^{-1} per decade (Lehmann et al., 2022). A basin-wide analysis linking FWC changes to atmospheric forces revealed a relation with air temperature, a connection that is physically tenuous, prompting further investigation into other factors. This led to the hypothesis that the decreasing trend in the upper mixed layer thickness in the Baltic Sea might be influencing FWC changes. Over the last 3 decades, there has been a noticeable reduction in the upper mixed layer depth. While it is plausible to suggest a dynamic relationship between the shrinking mixed layer depth and the decrease in FWC, verifying this hypothesis requires more research than what is covered in the present study.

Interannual variations of OHC are influenced by air temperature, evaporation, and wind stress magnitude over the Baltic Sea (Fig. 4). When considering the lesser impact of total cloud cover and surface net solar radiation, it becomes clear that air–sea heat exchange primarily drives OHC changes in the Baltic Sea. Notably, the annual mean OHC parallels the long-term trend of winter OHC in the Baltic Sea's upper 50 m layer and yearly maximum sea ice extent of the Baltic Sea (Raudsepp et al., 2022), highlighting the coherence of seasonal ice cover and OHC fluctuations. In seas with seasonal ice cover, the characteristics of sea ice are crucial for determining the sea's physical state. Typically, the maximum sea ice extent in the Baltic Sea indicates the severity of the winters (Uotila et al., 2015). Sea ice is vital for temporarily storing ocean heat and fresh water and then releasing it back into the sea (Raudsepp et al., 2022).

The interannual variations of FWC were associated with major Baltic inflows, overall precipitation, and zonal wind stress (Fig. 4 d). The signals of the MBIs are evident in the bottom salinity of the Bornholm Basin. Figure 4d illustrates that interannual variations in FWC are linked to the bottom salinity in the Bornholm Basin, which serves as a proxy for MBIs, as well as zonal wind stress and net precipitation. Therefore, Fig. 4d highlights the drivers of FWC, while Fig. 3d emphasizes the significance of halocline salinity's response to FWC. Consequently, we can infer that inflows from the North Sea and net precipitation are responsible for changes in halocline salinity. Because MBIs are short-lived, our use of annual mean wind is a coarse indicator. A high annual mean westerly wind might reflect a generally stormy winter with possible inflows, but it will likely miss isolated inflow events that occur even in otherwise average years. Therefore, we interpret the RF finding of zonal wind importance (Fig. 4d) cautiously – it may be serving as a proxy for the cumulative effect of many small inflows or sustained minor exchange rather than any single MBI. Meier and Kauker (2003) demonstrated that increasing westerly winds could hinder the outflow of fresh water from the Baltic Sea, leading to decreased salt transport into the sea. However, we were unable to directly associate moderate and small inflows from the North Sea with changes in halocline salinity. This aspect requires further investigation and precise simulation of salt transport between the North Sea and the Baltic Sea, which is beyond the scope of the current study. While several studies have underscored a correlation of the Baltic Sea's salinity with river runoff (Kniebusch et al., 2019b; Radtke et al., 2020; Lehmann et al., 2022), our research did not find this connection.

The OHC displays quasi-periodic fluctuations with a period of approximately 5–7 years, with 2020 and 2011 stand-

ing out as relative high and low points, respectively (Fig. 4). The elevated wintertime OHC in 2020 coincided with an unusually warm January–March period over the Northern Hemisphere (Schubert et al., 2022) and was accompanied by an exceptionally high marine heatwave index and a large number of marine heatwave days in the Baltic Sea (Bashiri et al., 2024; Lindenthal et al., 2024). In contrast, 2011 featured the most extensive sea ice cover and volume recorded in the past 3 decades (Raudsepp et al., 2022). Similarly, certain peaks in FWC, such as those observed in 2002 and 2013, align temporally with the years preceding major Baltic inflows, while declines in FWC, as seen in 1997 and 2019, occurred following such events. While these specific years are highlighted as examples, they are not the basis for broader conclusions but serve to illustrate patterns consistent with previous studies.

Global warming, with its increased frequency and intensity of extreme events, has had widespread negative impacts on nature and significant socioeconomic repercussions (IPCC, 2021). Our methodology has highlighted the extremes of interannual variability in OHC and FWC. In our study, we utilized the RF model to investigate the relationships between changes in OHC and FWC and their potential drivers. Although the model pinpointed the primary factors, it failed to capture the extremes (Gnecco et al., 2024), as illustrated in Fig. 4a and b. RF models tend to underperform when extreme values are not well represented in the training data – a common issue in ecological modeling and other practical applications (Fox et al., 2017). This can result in a bias where the model does not recognize or accurately predict rare but impactful events, such as extreme weather conditions, uncommon species occurrences, or anomalies in financial markets (Fox et al., 2017). Acknowledging this, we hypothesize that while primary forces set the stage for extreme events, these events themselves fall outside the scope of standard interannual variability and stem from a distinct combination of forces. Consequently, it is advantageous to analyze extreme events independently from typical interannual variations (Nontapa et al., 2020; Chen et al., 2021). To account for the variations in OHC and FWC, models other than RF, such as deep machine-learning models, could be employed, especially if the temporal resolution is monthly (e.g., Barzandeh et al., 2024) or finer, ensuring a representative dataset is available. It should be noted that the random forest analysis reveals statistical connections rather than definitive physical causation. We interpret these connections in light of known mechanisms to ensure they are plausible. Advancing this methodology will further our comprehension of the causes behind extreme events, thereby improving our predictive abilities.

A sustained decline in the Baltic Sea's FWC, indicating increasing salinity, could alert policymakers to intensified saltwater intrusion or reduced freshwater input, prompting investigation into inflow events or drought conditions. Conversely, an ongoing rise in OHC is a clear signal of warming that can inform climate adaptation strategies. The concept of indicators – such as used in this study for OHC and FC – plays an important role in facilitating knowledge transfer at the science and policy interface (von Schuckmann et al., 2020; Evans et al., 2025). Integrated indices, OHC and FWC, could be incorporated into regional climate and environmental assessments (HELCOM, 2023) as part of UNEP regional seas conventions (UNEP, 2024), aiding communication of changes to stakeholders. Our framework based on an indicator-based approach yields quantitative indicators (annual OHC, FWC, etc.) that can be tracked over time, much like other environmental indicators, to gauge the Baltic Sea's response to climate variability and change.

This framework could be generalized or applied to other regions or to future data. After defining the region of interest and preprocessing relevant data, the three-stage approach combining (i) analysis of OHC and FWC time series, (ii) examination of their vertical distribution, and (iii) RF analysis of their drivers could be applied.

Appendix A

A1

We also examined the fit of the trend-included time series and their correspondence with meteorological variables for OHC and FWC (Fig. A1). The correlation coefficient and RMSD for the OHC model are 0.9537 and 0.4310, respectively; for FWC model, they are 0.8897 and 0.5994.

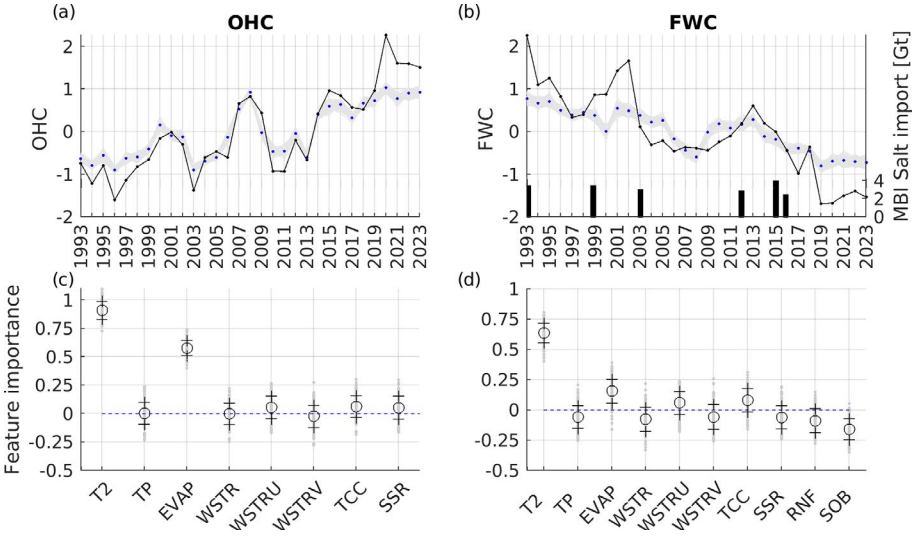

Figure A1. Same as in Fig. 4 but the RF models are fit for the original FWC and OHC including trends.

A2

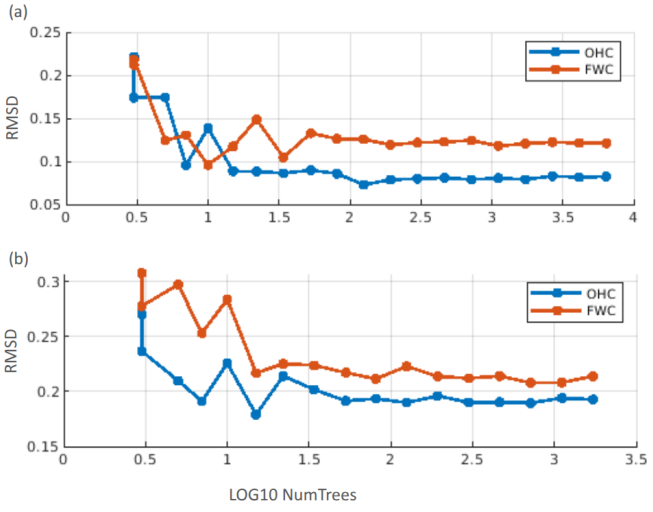

Figure A2. Random forest models for ZAX **(a)** and VAR **(b)** sensitivity to $\log_{10}$ of the number of trees (NumTrees).

Data availability. This study is based on public databases, and the references are listed in Table 1.

Author contributions. UR designed the conceptual framework for this study, interpreted the results, and wrote the initial manuscript. IM performed the calculations of OHC and FWC, trained the RF models, and prepared the figures; IM also contributed to the manuscript development. PL and KvS contributed to the design of the framework and the presentation of the results. All authors contributed to writing and revising the manuscript.

Competing interests. At least one of the (co-)authors is a member of the editorial board of *State of the Planet*. The peer-review process was guided by an independent editor, and the authors also have no other competing interests to declare.

Disclaimer. The Copernicus Marine Service offering is regularly updated to ensure it remains at the forefront of user requirements. In this process, some products may undergo replacement or renaming, leading to the removal of certain product IDs from our catalogue.

If you have any questions or require assistance regarding these modifications, please feel free to reach out to our user support

team for further guidance. They will be able to provide you with the necessary information to address your concerns and find suitable alternatives, maintaining our commitment to delivering top-quality services.

Publisher's note: Copernicus Publications remains neutral with regard to jurisdictional claims made in the text, published maps, institutional affiliations, or any other geographical representation in this paper. While Copernicus Publications makes every effort to include appropriate place names, the final responsibility lies with the authors. Views expressed in the text are those of the authors and do not necessarily reflect the views of the publisher.

Acknowledgements. OpenAI's GPT-4o model was used to assist with drafting and editing sections of the manuscript. All content was reviewed, verified, and approved by the authors.

Financial support. This research has been supported by the European Climate, Infrastructure and Environment Executive Agency (CINEA), LIFE program, through the AdapEST project "Implementation of national climate change adaptation activities in Estonia" (grant no. VEU23019).

Review statement. This paper was edited by Johannes Karstensen and reviewed by two anonymous referees.

References

Barzandeh, A., Maljutenko, I., Rikka, S., Lagemaa, Männik, A., P., Uiboupin, R., and Raudsepp, U.: Sea surface circulation in the Baltic Sea: decomposed components and pattern recognition, Sci. Rep., 14, 18649, https://doi.org/10.1038/s41598-024-69463-8, 2024.

Bashiri, B., Barzandeh, A., Männik, A., and Raudsepp, U.: Variability of marine heatwaves´ characteristics and assessment of their potential drivers in the Baltic Sea over the last 42 years, Sci. Rep., 14, 22419, https://doi.org/10.1038/s41598-024-74173-2, 2024.

Bindoff, N. L., Cheung, W. W. L., Kairo, J. G., Arístegui, J., Guinder, V. A., Hallberg, R., Hilmi, N., Jiao, N., Karim, M. S., Levin, L., O'Donoghue, S., Purca Cuicapusa, S. R., Rinkevich, B., Suga, T., Tagliabue, A., and Williamson, P.: Changing Ocean, Marine Ecosystems, and Dependent Communities, in: IPCC Special Report on the Ocean and Cryosphere in a Changing Climate, edited by: Pörtner, H.-O., Roberts, D. C., Masson-Delmotte, V., Zhai, P., Tignor, M., Poloczanska, E., Mintenbeck, K., Alegría, A., Nicolai, M., Okem, A., Petzold, J., Rama, B., and Weyer, N. M., Cambridge University Press, Cambridge, United Kingdom and New York, NY, USA, 447–587, https://doi.org/10.1017/9781009157964.007, 2019.

Boyer, T., Levitus, S., Antonov, J., Locarnini, R., Mishonov, A., Garcia, H., and Josey, S. A.: Changes in freshwater content in the North Atlantic Ocean 1955–2006. Geophys. Res. Lett., 34, L16603, https://doi.org/10.1029/2007GL030126, 2007.

Breiman, L.: Random forests, Mach. Learn., 45, 5–32, https://doi.org/10.1023/A:1010933404324, 2001.

Chen, S., Ren, M., and Sun, W.: Combining two-stage decomposition based machine learning methods for annual runoff forecasting, J. Hydrol., 603B, 126945, https://doi.org/10.1016/j.jhydrol.2021.126945, 2021.

Cheng, L., Trenberth, K. E., Gruber, N., Abraham, J. P., Fasullo, J. T., Li, G., Mann, M. E., Zhao, X., and Zhu, J.: Improved estimates of changes in upper ocean salinity and the hydrological cycle, J. Climate, 33, 10357–10381, https://doi.org/10.1175/JCLI-D-20-0366.1, 2020.

Cheng, L., von Schuckmann, K., Minière, A., Schmidt, G. A., and Pan, Y.: Ocean heat content in 2023, Nat. Rev. Earth Environ., 5, 232–234, https://doi.org/10.1038/s43017-024-00539-9, 2024.

CMS: Baltic Sea subsurface temperature trend from reanalysis, E.U. Copernicus Marine Service Information (CMEMS) Marine Data Store (MDS), https://doi.org/10.48670/moi-00208, 2024a.

CMS: Baltic Sea subsurface salinity trend from reanalysis, E.U. Copernicus Marine Service Information (CMEMS) Marine Data Store (MDS), https://doi.org/10.48670/moi-00207, 2024b.

CMS: EU Copernicus Marine Service Product: Baltic Sea Major Baltic Inflow: time/depth evolution S, T, O2 from Observations Reprocessing, E.U. Copernicus Marine Service Information (CMEMS) Marine Data Store (MDS), https://doi.org/10.48670/moi-00210, 2024c.

Copernicus Climate Change Service, Climate Data Store: ERA5 hourly data on single levels from 1940 to present, Copernicus Climate Change Service (C3S) Climate Data Store (CDS), https://doi.org/10.24381/cds.adbb2d47, 2023.

de Boyer Montégut, C., Madec, G., Sok Fischer, A., Lazar, A., and Iudicone, D.: Mixed layer depth over the global ocean: An examination of profile data and a profile-based climatology, J. Geophys. Res., 109, C12003, https://doi.org/10.1029/2004JC002378, 2004.

Donnelly, C., Andersson, J. C., and Arheimer, B.: Using flow signatures and catchment similarities to evaluate the E-HYPE multi-basin model across Europe, Hydrol. Sci. J., 61, 255–273, https://doi.org/10.1080/02626667.2015.1027710, 2016.

Durack, P. J.: Ocean salinity and the global water cycle, Oceanography, 28, 20–31, https://doi.org/10.5670/oceanog.2015.03, 2015.

Dutheil, C., Meier, H. E. M., Gröger, M., and Börgel, F.: Warming of Baltic Sea water masses since 1850, Clim. Dynam., 61, 1311–1331, https://doi.org/10.1007/s00382-022-06628-z, 2023.

EU Copernicus Marine Service Product: Baltic Sea – L3S Sea Surface Temperature Reprocessed, Mercator Ocean Int. [data set], https://doi.org/10.48670/moi-00312, 2022.

EU Copernicus Marine Service Product: Baltic Sea physics reanalysis, Mercator Ocean Int. [data set], https://doi.org/10.48670/moi-00013, 2023.

Evans, K., Schmidt, J. O., Addo, K. A., Bebianno, M. J., Campbell, D., Fan, J., Gonzalez-Quiros, R., Mohammed, E. Y., Shojaei, M. G., Smolyanitsky, V., and Zhang, C.-I.: Delivering scientific evidence for global policy and management to ensure ocean sustainability, Sustain. Sci., 20, 299–306, https://doi.org/10.1007/s11625-024-01579-2, 2025.

Forster, P. M., Smith, C., Walsh, T., Lamb, W. F., Lamboll, R., Hall, B., Hauser, M., Ribes, A., Rosen, D., Gillett, N. P., Palmer, M. D., Rogelj, J., von Schuckmann, K., Trewin, B., Allen, M., Andrew, R., Betts, R. A., Borger, A., Boyer, T., Broersma, J. A., Buontempo, C., Burgess, S., Cagnazzo, C., Cheng, L., Friedlingstein, P., Gettelman, A., Gütschow, J., Ishii, M., Jenkins, S., Lan,

X., Morice, C., Mühle, J., Kadow, C., Kennedy, J., Killick, R. E., Krummel, P. B., Minx, J. C., Myhre, G., Naik, V., Peters, G. P., Pirani, A., Pongratz, J., Schleussner, C.-F., Seneviratne, S. I., Szopa, S., Thorne, P., Kovilakam, M. V. M., Majamäki, E., Jalkanen, J.-P., van Marle, M., Hoesly, R. M., Rohde, R., Schumacher, D., van der Werf, G., Vose, R., Zickfeld, K., Zhang, X., Masson-Delmotte, V., and Zhai, P.: Indicators of Global Climate Change 2023: annual update of key indicators of the state of the climate system and human influence, Earth Syst. Sci. Data, 16, 2625–2658, https://doi.org/10.5194/essd-16-2625-2024, 2024.

Forster, P. M., Smith, C., Walsh, T., Lamb, W. F., Lamboll, R., Cassou, C., Hauser, M., Hausfather, Z., Lee, J.-Y., Palmer, M. D., von Schuckmann, K., Slangen, A. B. A., Szopa, S., Trewin, B., Yun, J., Gillett, N. P., Jenkins, S., Matthews, H. D., Raghavan, K., Ribes, A., Rogelj, J., Rosen, D., Zhang, X., Allen, M., Aleluia Reis, L., Andrew, R. M., Betts, R. A., Borger, A., Broersma, J. A., Burgess, S. N., Cheng, L., Friedlingstein, P., Domingues, C. M., Gambarini, M., Gasser, T., Gütschow, J., Ishii, M., Kadow, C., Kennedy, J., Killick, R. E., Krummel, P. B., Liné, A., Monselesan, D. P., Morice, C., Mühle, J., Naik, V., Peters, G. P., Pirani, A., Pongratz, J., Minx, J. C., Rigby, M., Rohde, R., Savita, A., Seneviratne, S. I., Thorne, P., Wells, C., Western, L. M., van der Werf, G. R., Wijffels, S. E., Masson-Delmotte, V., and Zhai, P.: Indicators of Global Climate Change 2024: annual update of key indicators of the state of the climate system and human influence, Earth Syst. Sci. Data, 17, 2641–2680, https://doi.org/10.5194/essd-17-2641-2025, 2025.

Fox, E. W., Hill, R. A., Leibowitz, S. G., Olsen, A. R., Thornbrugh, D. J., and Weber, M. H.: Assessing the accuracy and stability of variable selection methods for random forest modeling in ecology, Environ. Monit. Assess., 189, 316, https://doi.org/10.1007/s10661-017-6025-0, 2017.

Frederikse, T., Landerer, F., Caron, L., Adhikari, S., Parkes, D., Humphrey, V.W., Dangendorf, S., and Wu, Y.-H.: The causes of sea-level rise since 1900, Nature, 584, 393–397, https://doi.org/10.1038/s41586-020-2591-3, 2020.

Fukumori, I., Wang, O., and Fenty, I.: Causal Mechanisms of Sea Level and Freshwater Content Change in the Beaufort Sea, J. Phys. Oceanogr., 51, 3217–3234, https://doi.org/10.1175/JPO-D-21-0069.1, 2021.

Global Ocean Observing System: Essential ocean variables, EOV, Global Ocean Observing System, https://goosocean.org/what-we-do/framework/essential-ocean-variables/, last access: 4 September 2024.

Gnambs, T.: A brief note on the standard error of the Pearson correlation, Collabra Psychol., 9, 1–7, https://doi.org/10.1525/collabra.87615, 2023.

Gnecco, N., Terefe, E. M., and Engelke, S.: Extremal random forests, J. Am. Stat. Assoc., 119, 3059–3072, https://doi.org/10.1080/01621459.2023.2300522, 2024.

Gröger, M., Placke, M., Meier, H. E. M., Börgel, F., Brunnabend, S.-E., Dutheil, C., Gräwe, U., Hieronymus, M., Neumann, T., Radtke, H., Schimanke, S., Su, J., and Väli, G.: The Baltic Sea Model Intercomparison Project (BMIP) – a platform for model development, evaluation, and uncertainty assessment, Geosci. Model Dev., 15, 8613–8638, https://doi.org/10.5194/gmd-15-8613-2022, 2022.

HELCOM: State of the Baltic Sea, Third HELCOM holistic assessment 2016–2021, Baltic Sea Environment Proceedings No. 194, HELCOM, https://helcom.fi/post_type_publ/holas3_sobs (last access: 22 August 2025), 2023.

Hersbach, H., Bell, B., Berrisford, P., Hirahara, S., Horányi, A., Muñoz-Sabater, J., Nicolas, J., Peubey, C., Radu, R., Schepers, D., Simmons, A., Soci, C., Abdalla, S., Abellan, X., Balsamo, G., Bechtold, P., Biavati, G., Bidlot, J., Bonavita, M., De Chiara, G., Dahlgren, P., Dee, D., Diamantakis, M., Dragani, R., Flemming, J., Forbes, R., Fuentes, M., Geer, A., Haimberger, L., Healy, S., Hogan, R. J., Hólm, E., Janisková, M., Keeley, S., Laloyaux, P., Lopez, P., Lupu, C., Radnoti, G., de Rosnay, P., Rozum, I., Vamborg, F., Villaume S., and Thépaut, J.-N.: The ERA5 global reanalysis, Q. J. Roy. Meteor. Soc., 146, 1999–2049, https://doi.org/10.1002/qj.3803, 2020.

Hersbach, H., Bell, B., Berrisford, P., Hirahara, S., Horányi, A., Muñoz-Sabater, J., Nicolas, J., Peubey, C., Radu, R., Schepers, D., Simmons, A., Soci, C., Abdalla, S., Abellan, X., Balsamo, G., Bechtold, P., Biavati, G., Bidlot, J., Bonavita, M., De Chiara, G., Dahlgren, P., Dee, D., Diamantakis, M., Dragani, R., Flemming, J., Forbes, R., Fuentes, M., Geer, A., Haimberger, L., Healy, S., Hogan, R.J., Hólm, E., Janisková, M., Keeley, S., Laloyaux, P., Lopez, P., Lupu, C., Radnoti, G., de Rosnay, P., Rozum, I., Vamborg, F., Villaume, S., and Thépaut, J.-N.: Complete ERA5 from 1950: Fifth generation of ECMWF atmospheric reanalyses of the global climate, Copernicus Climate Change Service (C3S) Data Store (CDS) [data set], https://doi.org/10.24381/cds.adbb2d47, 2023.

Hoffman, E. L., Subrahmanyam, B., Trott, C. B., and Hall, S. B.: Comparison of Freshwater Content and Variability in the Arctic Ocean Using Observations and Model Simulations, Remote Sens., 15, 3715, https://doi.org/10.3390/rs15153715, 2023.

ICES: ICES Bottle and low-resolution CTD dataset, Extractions 22 DEC 2013 (for years 1990–2012), 25 FEB 2015 (for year 2013), 13 OCT 2016 (for year 2015), 15 JAN 2019 (for years 2016–2017), 22 SEP 2020 (for year 2018), 10 MAR 2021 (for years 2019–202), 28 FEB 2022 (for year 2021), ICES [data set], https://data.ices.dk (last access: 30 April 2024), 2022.

IOC, SCOR, and IAPSO: The international thermodynamic equation of seawater – 2010: calculation and use of thermodynamic properties., Intergovernmental Oceanographic Commission, Manuals and Guides No. 56, UNESCO, 196 pp., http://www.teos-10.org (last access: 11 October 2021), 2010.

IPCC: Climate Change 2021: The Physical Science Basis. Working Group I Contribution to the IPCC Sixth Assessment Report, edited by: Masson-Delmotte, V., Zhai, P., Pirani, A., Connors, S. L., Péan, C., Berger, S., Caud, N., Chen, Y., Goldfarb, L., Gomis, M. I., Huang, M., Leitzell, K., Lonnoy, E., Matthews, J. B. R., Maycock, T. K., Waterfield, T., Yelekçi, O., Yu, R., and Zhou, B., Cambridge University Press, Cambridge, United Kingdom and New York, NY, USA, https://doi.org/10.1017/9781009157896, 2021.

Kniebusch, M., Meier, H. M., Neumann, T., and Börgel, F.: Temperature variability of the Baltic Sea since 1850 and attribution to atmospheric forcing variables, J. Geophys. Res.-Oceans, 124, 4168–4187, https://doi.org/10.1029/2018JC013948, 2019a.

Kniebusch, M., Meier, H. E. M., and Radtke, H.: Changing salinity gradients in the Baltic Sea as a consequence of altered freshwater budgets, Geophys. Res. Lett., 46, 9739–9747, https://doi.org/10.1029/2019GL083902, 2019b.

Kondeti, V. P. and Palanisamy, S.: Estimating ocean heat content from the ocean thermal expansion parameters using satellite data, Earth Syst. Dynam., 16, 91–114, https://doi.org/10.5194/esd-16-91-2025, 2025.

Lehmann, A., Myrberg, K., Post, P., Chubarenko, I., Dailidiene, I., Hinrichsen, H.-H., Hüssy, K., Liblik, T., Meier, H. E. M., Lips, U., and Bukanova, T.: Salinity dynamics of the Baltic Sea, Earth Syst. Dynam., 13, 373–392, https://doi.org/10.5194/esd-13-373-2022, 2022.

Leppäranta, M. and Myrberg, K.: Physical Oceanography of the Baltic Sea, Springer-Verlag, 378 pp., ISBN 978-3-540-79702-9, 2009.

Lindenthal, A., Hinrichs, C., Jandt-Scheelke, S., Kruschke, T., Lagemaa, P., van der Lee, E. M., Maljutenko, I., Morrison, H. E., Panteleit, T. R., and Raudsepp, U.: Baltic Sea surface temperature analysis 2022: a study of marine heatwaves and overall high seasonal temperatures, in: 8th edition of the Copernicus Ocean State Report (OSR8), edited by: von Schuckmann, K., Moreira, L., Grégoire, M., Marcos, M., Staneva, J., Brasseur, P., Garric, G., Lionello, P., Karstensen, J., and Neukermans, G., Copernicus Publications, State Planet, 4-osr8, 16, https://doi.org/10.5194/sp-4-osr8-16-2024, 2024.

Lindstrom, E., Gunn, J., Fischer, A., McCurdy, A., and Glover, L. K.: A Framework for Ocean Observing, By the Task Team for an Integrated Framework for Sustained Ocean Observing, IOC/INF-1284 rev.2, UNESCO, https://unesdoc.unesco.org/ark:/48223/pf0000211260 (last acess: 6 Septmeber 2025), 2012.

Lu, Y., Li, Y., Lin, P., Duan, J., and Wang, F.: North Atlantic–Pacific salinity contrast enhanced by wind and ocean warming, Nat. Clim. Chang., 14, 723–731, https://doi.org/10.1038/s41558-024-02033-y, 2024.

Madec, G., Bourdallé-Badie, R., Chanut, J., Clementi, E., Coward, A., Ethé, C., Iovino, D., Lea, D., Lévy, C., Lovato, T., Martin, N., Masson, S., Mocavero, S., Rousset, C., Storkey, D., Vancoppenolle, M., Müeller, S., Nurser, G., Bell, M., and Samson, G.: NEMO ocean engine, Notes du Pôle de modélisation de l'Institut Pierre-Simon Laplace (IPSL), v4.0, Number 27, Zenodo, https://doi.org/10.5281/zenodo.3878122, 2019.

McGrath, M., Poynting, M., and Rowlatt, J.: Climate change: World's oceans suffer from record-breaking year of heat, BBC News Climate & Science, https://www.bbc.com/news/science-environment-68921215 (last access: 22 August 2025), 2024.

Meier, H. E. M. and Kauker, F.: Modeling decadal variability of the Baltic Sea: 2. Role of freshwater inflow and large-scale atmospheric circulation for salinity, J. Geophys. Res., 108, 3368, https://doi.org/10.1029/2003JC001799, 2003.

Meier, H. E. M., Dieterich, C., Gröger, M., Dutheil, C., Börgel, F., Safonova, K., Christensen, O. B., and Kjellström, E.: Oceanographic regional climate projections for the Baltic Sea until 2100, Earth Syst. Dynam., 13, 159–199, https://doi.org/10.5194/esd-13-159-2022, 2022.

Meyssignac, B., Boyer, T., Zhao, Z., Hakuba, M. Z., Landerer, F. W., Stammer, D., Köhl, A., Kato, S., L'ecuyer, T., Ablain, M., and Abraham, J. P.: Measuring global ocean heat content to estimate the Earth energy imbalance, Front. Mar. Sci., 6, 432, https://doi.org/10.3389/fmars.2019.00432, 2019.

Millero, F. J., Perron, G., and Desnoyers, J. E.: Heat capacity of seawater solutions from 5° to 35 °C and 0.5 to 22‰ chlorinity, J. Geophys. Res., 78, 4499–4507, https://doi.org/10.1029/JC078i021p04499, 1973.

Mohrholz, V.: Major Baltic inflow statistics – revised, Front. Mar. Sci., 5, 384, https://doi.org/10.3389/fmars.2018.00384, 2018.

Nontapa, C., Kesamoon, C., Kaewhawong, N., and Intrapaiboon, P.: A New Time Series Forecasting Using Decomposition Method with SARIMAX Model, in: Neural Information Processing, edited by: Yang, H., Pasupa, K., Leung, A. C. S., Kwok, J. T., Chan, J. H., and King, I., Commun. Comput. Inf. Sci., Springer, Cham, vol. 1333, https://doi.org/10.1007/978-3-030-63823-8_84, 2020.

Panteleit, T., Verjovkina, S., Jandt-Scheelke, S., Spruch, L., and Huess, V.: EU Copernicus Marine Service Quality Information Document for the Baltic Sea Physics Reanalysis Product, Mercator Ocean International, https://catalogue.marine.copernicus.eu/documents/QUID/CMEMS-BAL-QUID-003-011.pdf, last access: 12 April 2023.

Probst, P., Wright, M. N., and Boulesteix, A. L.: Hyperparameters and tuning strategies for random forest, WIRES Data Min. Knowl., 9, e1301, https://doi.org/10.1002/widm.1301, 2019.

Radtke, H., Brunnabend, S.-E., Gräwe, U., and Meier, H. E. M.: Investigating interdecadal salinity changes in the Baltic Sea in a 1850–2008 hindcast simulation, Clim. Past, 16, 1617–1642, https://doi.org/10.5194/cp-16-1617-2020, 2020.

Ranasinghe, R., Ruane, A. C., Vautard, R., Arnell, N., Coppola, E., Cruz, F. A., Dessai, S., Islam, A. S., Rahimi, M., Ruiz Carrascal, D., Sillmann, J., Sylla, M. B., Tebaldi, C., Wang, W., and Zaaboul, R.: Climate Change Information for Regional Impact and for Risk Assessment, in: Climate Change 2021: The Physical Science Basis., Contribution of Working Group I to the Sixth Assessment Report of the Intergovernmental Panel on Climate Change, edited by: Masson-Delmotte, V., Zhai, P., Pirani, A., Connors, S. L., Péan, C., Berger, S., Caud, N., Chen, Y., Goldfarb, L., Gomis, M. I., Huang, M., Leitzell, K., Lonnoy, E., Matthews, J. B. R., Maycock, T. K., Waterfield, T., Yelekçi, O., Yu, R., and Zhou, B., Cambridge University Press, Cambridge, United Kingdom and New York, NY, USA, 1767–1926, https://doi.org/10.1017/9781009157896.014, 2021.

Raudsepp, U. and Maljutenko, I.: A method for assessment of the general circulation model quality using the K-means clustering algorithm: a case study with GETM v2.5, Geosci. Model Dev., 15, 535–551, https://doi.org/10.5194/gmd-15-535-2022, 2022.

Raudsepp, U., Maljutenko, I., Haapala, J., Männik, A., Verjovkina, S., Uiboupin, R., von Schuckmann, K., and Mayer, M.: Record high heat content and low ice extent in the Baltic Sea during winter 2019/20, in: Copernicus Ocean State Report, Issue 6, J. Oper. Oceanogr., 15, s175–s185, https://doi.org/10.1080/1755876X.2022.2095169, 2022.

Raudsepp, U., Maljutenko, I., Barzandeh, A., Uiboupin, R., and Lagemaa, P.: Baltic Sea freshwater content, in: 7th edition of the Copernicus Ocean State Report (OSR7), edited by: von Schuckmann, K., Moreira, L., Le Traon, P.-Y., Grégoire, M., Marcos, M., Staneva, J., Brasseur, P., Garric, G., Lionello, P., Karstensen, J., and Neukermans, G., Copernicus Publications, State Planet, 1-osr7, 7, https://doi.org/10.5194/sp-1-osr7-7-2023, 2023.

Ringgaard, I., Korabel, V., Spruch, L., Lindenthal, A., and Huess, V.: EU Copernicus Marine Service Product User Manual for the Baltic Sea Physics Reanalysis Product, Mercator Ocean In-

ternational, https://documentation.marine.copernicus.eu/PUM/CMEMS-BAL-PUM-003-011-012.pdf, last access: 1 July 2024.

Rodhe, J. and Winsor, P.: On the influence of the freshwater supply on the Baltic Sea mean salinity, Tellus A, 54, 175–186, https://doi.org/10.3402/tellusa.v54i2.12134, 2002.

Schauer, U. and Losch, M.: Freshwater in the ocean is not a useful parameter in climate research, J. Phys. Oceanogr., 49, 2309–2321, https://doi.org/10.1175/JPO-D-19-0102.1, 2019.

Schubert, S. D., Chang, Y., DeAngelis, A. M., Koster, R. D., Lim, Y.-K., and Wang, H.: Exceptional Warmth in the Northern Hemisphere during January–March of 2020: The Roles of Unforced and Forced Modes of Atmospheric Variability, J. Climate, 35, 2565–2584, https://doi.org/10.1175/JCLI-D-21-0291.1, 2022.

Skliris, N., Marsh, R., Josey, S. A., Good, S. A., Liu, C., and Allan, R. P.: Salinity changes in the World Ocean since 1950 in relation to changing surface freshwater fluxes,. Clim. Dynam., 43, 709–736, https://doi.org/10.1007/s00382-014-2131-7, 2014.

Solomon, A., Heuzé, C., Rabe, B., Bacon, S., Bertino, L., Heimbach, P., Inoue, J., Iovino, D., Mottram, R., Zhang, X., Aksenov, Y., McAdam, R., Nguyen, A., Raj, R. P., and Tang, H.: Freshwater in the Arctic Ocean 2010–2019, Ocean Sci., 17, 1081–1102, https://doi.org/10.5194/os-17-1081-2021, 2021.

UNEP: Regional Seas Programmes and Conventions, United Nations Environment Programme, https://www.unep.org/explore-topics/oceans-seas/what-we-do/working-regional-seas/regional-seas-programmes/regional-seas, last access: 4 September 2024.

Uotila, P., Vihma, T., and Haapala, J.: Atmospheric and oceanic conditions and the extremely low Bothnian Bay sea ice extent in 2014/2015, Geophys. Res. Lett., 42, 7740–7749, https://doi.org/10.1002/2015GL064901, 2015.

von Schuckmann, K., Palmer, M. D., Trenberth, K. E., Cazenave, A. Chambers, D., Champollion, N., Hansen, J., Josey, S. A., Loeb, N., Mathieu, P.-P., Meyssignac, B., and Wild, M.: An imperative to monitor Earth's energy imbalance, Nat. Clim. Change, 6, 138–144, https://doi.org/10.1038/nclimate2876, 2016.

von Schuckmann, K., Holland, E., Haugan, P., and Thomson, P.: Ocean science, data, and services for the UN 2030 Sustainable Development Goals, Mar. Policy, 121, 104154–104154, https://doi.org/10.1016/j.marpol.2020.104154, 2020.

von Schuckmann, K., Minière, A., Gues, F., Cuesta-Valero, F. J., Kirchengast, G., Adusumilli, S., Straneo, F., Ablain, M., Allan, R. P., Barker, P. M., Beltrami, H., Blazquez, A., Boyer, T., Cheng, L., Church, J., Desbruyeres, D., Dolman, H., Domingues, C. M., García-García, A., Giglio, D., Gilson, J. E., Gorfer, M., Haimberger, L., Hakuba, M. Z., Hendricks, S., Hosoda, S., Johnson, G. C., Killick, R., King, B., Kolodziejczyk, N., Korosov, A., Krinner, G., Kuusela, M., Landerer, F. W., Langer, M., Lavergne, T., Lawrence, I., Li, Y., Lyman, J., Marti, F., Marzeion, B., Mayer, M., MacDougall, A. H., McDougall, T., Monselesan, D. P., Nitzbon, J., Otosaka, I., Peng, J., Purkey, S., Roemmich, D., Sato, K., Sato, K., Savita, A., Schweiger, A., Shepherd, A., Seneviratne, S. I., Simons, L., Slater, D. A., Slater, T., Steiner, A. K., Suga, T., Szekely, T., Thiery, W., Timmermans, M.-L., Vanderkelen, I., Wjiffels, S. E., Wu, T., and Zemp, M.: Heat stored in the Earth system 1960–2020: where does the energy go?, Earth Syst. Sci. Data, 15, 1675–1709, https://doi.org/10.5194/essd-15-1675-2023, 2023.

Winsor, P., Rodhe, J., and Omstedt, A.: Baltic Sea ocean climate: an analysis of 100 yr of hydrographic data with focus on the freshwater budget, Clim. Res., 18, 5–15, http://www.jstor.org/stable/24861552 (last access: 22 August 2025), 2001.

Yu, L., Josey, S. A., Bingham, F. M., and Lee, T.: Intensification of the global water cycle and evidence from ocean salinity: A synthesis review, Ann. N. Y. Acad. Sci., 1472, 76–94, https://doi.org/10.1111/nyas.14354, 2020.

State Planet, 6-osr9, 7, 2025
https://doi.org/10.5194/sp-6-osr9-7-2025

Consistent long-term observations of surface phytoplankton functional types from space

Hongyan Xi[1], Marine Bretagnon[2], Ehsan Mehdipour[1,3], Julien Demaria[2], Antoine Mangin[2], and Astrid Bracher[1,4]

[1]Alfred Wegener Institute, Helmholtz-Centre for Polar and Marine Research, 27570 Bremerhaven, Germany
[2]ACRI-ST, Sophia Antipolis CEDEX, France
[3]School of Business, Social & Decision Sciences, Constructor University, Bremen, Germany
[4]Institute of Environmental Physics, University of Bremen, 28359 Bremen, Germany

Correspondence: Hongyan Xi (hongyan.xi@awi.de)

Received: 29 August 2024 – Discussion started: 20 September 2024
Revised: 18 May 2025 – Accepted: 14 June 2025 – Published: 30 September 2025

Abstract. Global products of phytoplankton functional types (PFTs) derived from multi-sensor ocean color (OC) data provide important long-term biogeochemical quantifications indexed by chlorophyll *a* concentration (Chl *a*) of PFTs, including diatoms, haptophytes, prokaryotic phytoplankton, dinoflagellates, and green algae. Due to the distinctive lifespans and radiometric characteristics of ocean color sensors, the consistency of the PFT products derived from different sensors needs to be assured to establish a complete and systematic frame for long-term monitoring of multiple PFTs on a global scale. This study introduces a machine-learning-based (ML-based) correction scheme to eliminate the discrepancies between different sensors' PFT products. The correction scheme is applied to the Sentinel 3A/B Ocean and Land Colour Instrument (OLCI)-derived PFT data to match them with the PFT data derived from GlobColour-merged ocean color products using the overlapped period. This correction has generated consistent PFT data across the sensors, enabling the analyses of multi-year PFT observations by describing their variability and 2-decade trends. Analysis of PFT time series has revealed an increasing trend in diatoms and dinoflagellates and a decreasing trend in haptophytes and prokaryotic phytoplankton on a global scale. The overall trend in green algae remains relatively stable, although with some spatial variations. These PFT trends are more significant in high latitudes and coastal regions (and also in the equatorial region for prokaryotic phytoplankton). The anomaly of PFTs in 2023 shows significant increases in Chl *a* of diatoms and dinoflagellates (+24 % and +9.4 %, respectively) but only weak changes in Chl *a* for prokaryotic phytoplankton (−2.1 %) and haptophytes (∼ 1.6 %). These consistent time series data will act as an important ocean indicator to infer possible changes in the marine environment.

1 Introduction

Climate-induced changes stress the ocean's contemporary biogeochemical cycles and ecosystems, impacting the base of the marine food web: phytoplankton communities (Gruber et al., 2021). In the past decades, various observations of ocean color (OC) information, especially the chlorophyll *a* concentration (Chl *a*) as a proxy of phytoplankton biomass, have been able to revolutionize our understanding of the marine biogeochemical processes and provide insights on the changes in phytoplankton (e.g., Antoine et al., 2005; Gregg and Rousseaux, 2014; Behrenfeld et al., 2016). However, phytoplankton biomass cannot comprehensively describe the complex nature of the phytoplankton community, concerning their composition and function. Phytoplankton community composition varies in ocean biomes, and phytoplankton groups drive the marine ecosystem and biogeochemical processes differently (Bracher et al., 2017). Therefore, continuous long-term monitoring of phytoplankton functional types (PFTs) with interannual variation and trend analysis will help

Published by Copernicus Publications.

Table 1. Products used.

Product ref. no	Product ID and type	Data access	Documentation
1	OCEANCOLOUR_GLO_BGC_L3_MY_009_103; satellite observations	EU Copernicus Marine Service Product (2024)	Quality Information Document (QUID): Garnesson et al. (2024); Product User Manual: Colella et al. (2024)
2	Self-processed PFT data based on merged OC products for the period of May 2016–April 2017 overlapped with the OLCI-based PFT data available on the Copernicus Marine Service; satellite observations	Our own archive	Xi et al. (2021, 2023a)
3	In situ PFT data; in situ observations	Our own archive	PANGAEA (Xi et al., 2025)

us better understand the biogeochemical processes and benefit the assessment of ocean health (Xi et al., 2023a).

Previously, we developed and further improved an approach, referred to as EOF-PFT, consisting of a set of empirical-orthogonal-function-based algorithms for the retrieval of PFTs on a global scale (Xi et al., 2020, 2021). Two algorithms within the EOF-PFT approach were built for two sets of OC satellite products, namely the GlobColour-merged products with sensors of SeaWiFS, MODIS-Aqua, MERIS, and VIIRS-SNPP included and the products from the Ocean and Land Color Instrument (OLCI) sensors on board Sentinel 3A and 3B. Using multi-spectral remote sensing reflectance data (Rrs) from these OC products and sea surface temperature (SST) data, the EOF-PFT approach enables satellite retrievals of Chl *a* for five PFTs with pixel-by-pixel uncertainty, which include diatoms, dinoflagellates, haptophytes, green algae, and prokaryotic phytoplankton (prokaryotes hereafter for brevity). These PFT Chl *a* products, covering the period from 2002 until today, are available on the Copernicus Marine Service and updated regularly upon reprocessing with refined algorithms.

The PFT products enable the analysis of multi-year PFT observations by describing their variability and trends. However, prior to the time series analysis, the consistency of the PFT datasets derived from the GlobColour-merged OC products and from OLCI data needs to be assured. In the frame of the Copernicus Marine Evolution Project GLOPHYTS, we aim to merge the aforementioned two PFT datasets into one long-term consistent satellite PFT product. A first attempt was carried out by Xi et al. (2023a) with a correction scheme based on linear regressions with PFT uncertainty considered, which was applied to PFT data from Sentinel 3A/B OLCI sensors to generate PFT time series in the Atlantic Ocean. Though such a straightforward correction scheme provides an overall consistent time series, the spatial variation cannot be adequately corrected, and large biases between sensors can still exist at regional scales. Therefore, we intend to enhance the correction procedure by incorporating spatial variability. In this study, we propose a new correction scheme based on a random forest machine learning method for delivering 2-decade quality-assured global PFT datasets, which are cross-validated within model training and further validated with in situ data. The harmonized PFT time series with high spatiotemporal consistency are analyzed on both global and regional scales to investigate the trend and anomaly for different PFTs. Considering that ocean color missions are planned to be continued into the next decade and beyond, such PFT time series will further act as an important ocean indicator to help sustain the ocean health by providing interannual variation and trend analyses of the surface phytoplankton community composition, especially for the key regions that have been defined as vital marine environments by the Copernicus Marine Service.

2 Data and methodology

2.1 PFT products from the Copernicus Marine Service

The PFT datasets with per-pixel uncertainty (product ref. no. 1 in Table 1) are produced with a modified version of the EOF-PFT approach proposed by Xi et al. (2021). The modified algorithms within EOF-PFT were developed using the latest global in situ pigment matchup dataset and trained separately for the merged OC products (including SeaWiFS, MODIS, MERIS, and VIIRS) from 2002 with 8 bands and for Sentinel 3A/B OLCI data (from May 2016) with 10 bands from the GlobColour archive. The official PFT data (product ref. no. 1 in Table 1) are generated from the merged OC products for the period of July 2002–April 2016 and from OLCI products from May 2016 onwards (hereafter referred to as merged-sensor-derived PFTs and OLCI-derived PFTs, respectively). However, we extended the merged-sensor-derived PFT products to April 2017 in this study (product ref. no. 2 in Table 1), in order to have the 1-year overlapping period with the OLCI-derived PFT data for consistency analysis. The merged-sensor-derived PFT products were processed only until 2017 because VIIRS-SNPP data from the NASA release R2018 reprocessed ver-

sion were identified with significant trends (possibly due to degradation) after 2017 that are not identified in other sensors (NASA Ocean Color, 2025).

Updated EOF-PFT algorithms were also assessed with an independent validation dataset with satisfactory performance (details in the corresponding QUID). The corresponding prototypes were prepared and implemented into the Copernicus Marine Service to generate reprocessed PFT products with per-pixel uncertainty through EiS (Enter into Service) by November 2024. With these updates, we obtained PFT retrievals from the aforementioned two sensor sets; however, consistency between the PFT data across the two sets must be assured to generate long-term time series data and prepare for the next-generation reprocessing.

2.2 Machine-learning-based ensemble (MLBE) for inter-sensor correction of PFT data

The merged-sensor-derived PFT products have a longer time span ($\sim$ 15 years) than the OLCI (Sentinel-3A/B)-derived PFTs ($\sim$ 7 years) and are generated based on the algorithms trained with a larger global matchup dataset ($\sim$ 1500 data points compared to $\sim$ 300 for OLCI due to its shorter running time and limited in situ data from 2016). The merged-sensor-derived products also carry relatively lower uncertainty compared to the OLCI-derived PFT data (Xi et al., 2021, 2023a). Therefore, we set up the modification scheme for the OLCI-derived PFTs to match the merged-sensor-derived PFTs. A similar inter-sensor correction has been done for the OC-CCI-merged OC data (Mélin and Franz, 2014; Sathyendranath et al., 2019). We tested a few machine learning methods (random forest, 1D convolutional neural network, self-organizing map) to upgrade the consistency of OLCI-derived products with the merged-sensor-derived products on a pixel basis. At last, we used the random-forest-based ensemble "TreeBagger" with regression decision trees embedded in MATLAB (R2023b), which selects a subset of predictors for each decision split by the random forest algorithm to establish the correction model (Breiman, 2001). The ensemble is powerful in extracting spatial features from the predictors and establishing connections with the response variables through an optimal number of regression trees. Figure 1a shows a simplified flowchart of this machine learning ensemble, which is referred to as the machine-learning-based ensemble (MLBE) hereafter. A brief description of the ensemble establishment is as follows:

1. Input data are the monthly PFT products with 25 km resolution derived from both merged-sensor and OLCI data (May 2016 to April 2017, product ref. no. 2 in Table 1), from which the latitude, longitude, and OLCI-derived PFT products during the 12 months are the predictor variables and the merged-sensor-derived PFTs are response data. Only pixels with available data from both products were taken into account. The input dataset was randomly divided into a training dataset (70 %, $\sim$ 3 million pixels) and a testing dataset (30 %, $\sim$ 1.26 million pixels). Before the training was performed, the PFT datasets were log-transformed due to their nature of log-normal distribution (Xi et al., 2021). The geographic information (latitude and longitude) was simply normalized to the range $[-1, 1]$ by scaling the original ranges of $[-89.875, 89.875]$ and $[-179.875, 179.875]$ (with 0.25° pixel size).

2. The MLBE was trained separately for each PFT. After testing different numbers of regression trees for the training, we chose 30 regression trees to obtain the optimal training performance with relatively low computation cost (Fig. 1b). Trained models applied to the test datasets have shown equivalent performance with the training sets, indicating that the ensembles are robust.

3. The ensembles trained for the five PFTs (diatoms, haptophytes, dinoflagellates, prokaryotes, and green algae) were applied to all monthly PFT products derived from OLCI from May 2016 to December 2023 to generate the corrected OLCI PFT data.

Following the same steps above, a similar MLBE model based on the PFT products with 4 km spatial resolution was also established to enable the validation with in situ data, as described below in Sect. 2.3, as the corrected OLCI PFT generated from the 25 km MLBE model is too coarse for a valid comparison with the field measurements. PFT time series analysis is, however, still based on the monthly 25 km product to alleviate the computation.

2.3 Validation data

We compiled two in situ PFT datasets to validate the MLBE-corrected OLCI-derived PFT products (product ref. no. 3 in Table 1). The in situ data were derived from quality-controlled in situ HPLC pigment concentrations using the diagnostic pigment analysis (DPA) with updated pigment-specific weighting coefficients following Xi et al. (2023a, b), consistent with the calculation of the in situ PFT data used for the updated EOF-PFT algorithms described in Sect. 2.1. Dataset 1 is the test dataset (99 matchups) extracted from the global in situ PFT matchup data, which takes up 30 % of the whole matchup dataset, while the other 70 % was used for the retuning of the PFT algorithm for OLCI sensors. Dataset 1 spans 2016 to 2021 and spreads widely in the global ocean. Dataset 2 containing 134 matchups is a newly compiled dataset that composites in situ PFT data collected from four recent mostly polar expeditions with the research vessel *Polarstern* (Alfred-Wegener-Institut Helmholtz-Zentrum für Polar- und Meeresforschung, 2017): PS126 (May–June 2021), PS131/1 (June–August 2022), and PS136 (May–June 2023) in the North Atlantic Ocean to the Arctic Ocean; PS133 (October–November 2022) in the

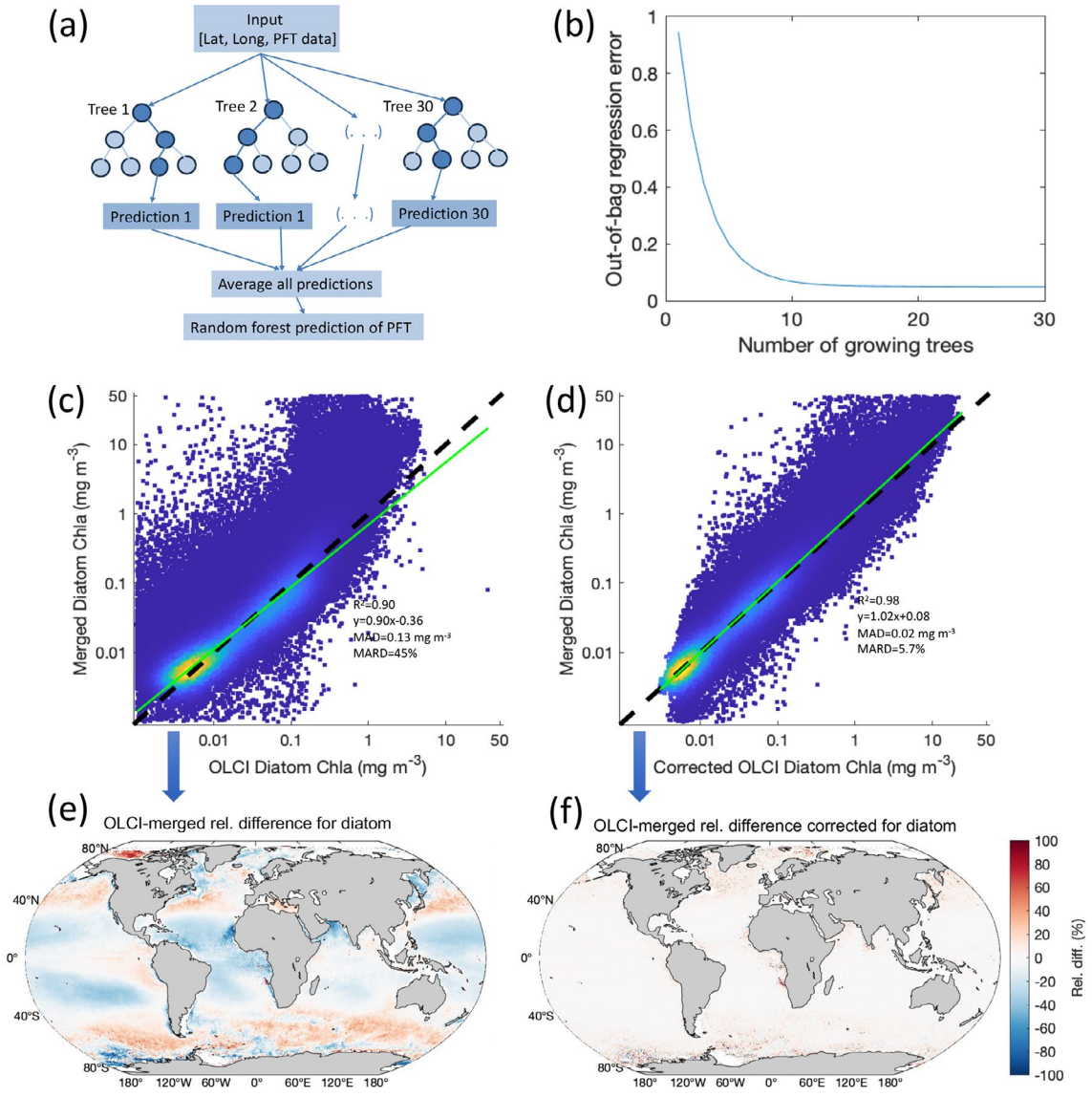

Figure 1. **(a)** Flowchart of the MLBE. **(b)** Ensemble error with number of growing trees. Scatterplots of **(c)** diatom Chl *a* from OLCI non-corrected against that from merged-sensor products and **(d)** MLBE-corrected OLCI diatom Chl *a* against that from merged-sensor products. **(e)** RD between OLCI-based and merged-sensor-derived diatom Chl *a* and **(f)** RD between MLBE-corrected OLCI-based and merged-sensor-derived diatom Chl *a*.

Southern Ocean. Geographical distribution maps of the two datasets are included in Fig. 3 together with the validation plots. These matchup data are made available on PANGAEA: https://doi.org/10.1594/PANGAEA.982433 (Xi et al., 2025).

2.4 Trend and anomaly analysis

We focus on explorations of the consistent PFT products to reveal and understand the trends and variations in the global PFTs in the last 2 decades. We prepared time series on a global scale and on four regional scales, including the North Atlantic Ocean, the Mediterranean Sea, the Arctic Ocean, and the Southern Ocean. The other two regions of interest to the Copernicus Marine Service, the Baltic Sea and the Black Sea, were not included, as the PFT algorithms were developed for open-ocean waters (bathymetry > 200 m) and the quality of the PFT data generated in these regions could not be assured (Xi et al., 2021). PFT time series of different spatial scales were calculated by applying the weighted average (taking cosine of the latitude as weights) to the monthly PFT data over the defined regions, to take into account the proportional contribution of each pixel to the global surface ocean due to area distortion in the gridded dataset. The latitude-weighted averaging was applied to the logarithmically transformed PFT Chl *a* to obtain the log-based mean,

which was then converted to natural values. A deseasonalization, referring to the process of removing the signal caused by seasonality from the time series, was first applied to the PFT time series. The deseasonalized time series were then prepared by decomposing the monthly data of each variable into a trend: seasonal and residual components with Seasonal-Trend decomposition using LOESS (STL; Cleveland et al., 1990). A non-parametric Mann–Kendall test was used to identify statistically significant trends over time with a p value < 0.05 (Mann, 1945; Kendall, 1975; Gilbert, 1987), and then the slope of the linear trend was estimated with the non-parametric Sen's slope (Sen, 1968). The standard deviation of the trend slope has been also calculated by considering PFT uncertainty assessed by the EOF-PFT retrieval algorithms. Time series analysis has been done both per pixel and for the whole global ocean and selected regions. We detected trends reflected by the satellite observations and derived anomalies to observe the interannual changes. Anomalies of 2023 (the last year of the considered period) were also obtained following Xi et al. (2023a) by comparing the PFT situation of 2023 to the mean of the last 2 decades.

2.5 Statistical metrics

To evaluate the correction ensemble performance, relative difference (RD), median absolute difference (MAD), and median absolute relative difference (MARD) were calculated based on the Chl a data of each PFT, which are defined as below.

$$\mathrm{RD}_i = \left(\mathrm{Chl}\ a_i^{\mathrm{OLCI}} - \mathrm{Chl}\ a_i^{\mathrm{Merged}}\right) / \mathrm{Chl}\ a_i^{\mathrm{Merged}},$$

where i is the ith PFT.

$$\mathrm{RD}_{\mathrm{PFT}} = \frac{\left(\mathrm{Chl}\ a_{\mathrm{PFT}_{\mathrm{OLCI}}} - \mathrm{Chl}\ a_{\mathrm{PFT}_{\mathrm{merged}}}\right)}{\mathrm{Chl}\ a_{\mathrm{PFT}_{\mathrm{merged}}}} \times 100\,\% \quad (1)$$

$$\mathrm{MAD}_{\mathrm{PFT}} = \text{median of } \left|\mathrm{Chl}\ a_{\mathrm{PFT}_{\mathrm{OLCI}}} - \mathrm{Chl}\ a_{\mathrm{PFT}_{\mathrm{merged}}}\right| \quad (2)$$

$$\mathrm{MARD}_{\mathrm{PFT}} = \text{median of } \frac{\left|\mathrm{Chl}\ a_{\mathrm{PFT}_{\mathrm{OLCI}}} - \mathrm{Chl}\ a_{\mathrm{PFT}_{\mathrm{merged}}}\right|}{\mathrm{Chl}\ a_{\mathrm{PFT}_{\mathrm{merged}}}} \times 100\,\% \quad (3)$$

To validate the corrected PFT Chl a data with in situ data, statistical metrics, including regression slope and intercept, determination coefficient (R^2), root-mean-square difference (RMSD; mg m^{-3}), and median percent difference (MDPD; %), were used. For the definition equations of these terms, please refer to Xi et al. (2020). Note that only the slope and R^2 are calculated on the base 10 logarithmic scale.

3 Results

3.1 Correction of the OLCI-derived PFT data using the MLBE scheme

To reduce cross-sensor data shift and generate consistent PFTs, we firstly applied a correction method while using the type II regression relationships with uncertainties included between the merged-sensor-derived PFTs and OLCI-derived PFTs in the overlapped period, to correct the latter to the former. The methodology was described in Xi et al. (2023a). However, even though the final PFT time series over the global ocean shows good consistency, the difference between the two PFT products is still prominent in different regions. Taking the diatom product as a showcase, we calculated the relative difference (RD in %) between the OLCI-derived and merged-sensor-derived diatom Chl a using Eq. (1). The median absolute relative difference (MARD in %) over the globe, calculated using Eq. (3), was reduced significantly after the linear correction (from 45 % to 26 %); nevertheless, the RD can still reach as high as 80 %–100 % in different regions (figure not shown). High RD variations have also been found for other PFTs with the previously proposed correction scheme based on type II linear regression.

The scatterplot and statistics in Fig. 1d with the MLBE-corrected OLCI diatom Chl a show significant improvement in consistency with the merged-sensor-derived diatom retrievals compared to the non-corrected OLCI-derived diatom data (Fig. 1c). Figure 1f highlights the reduced RD variation over the global ocean compared to the RD between the non-corrected OLCI- and merged-sensor-derived PFTs shown in Fig. 1e. The slope of the regression when using the corrected dataset is close to 1, the median absolute difference (MAD; defined in Eq. 2) reduced from 0.13 to 0.02 mg m^{-3}, and the MARD reduced from 45 % to 5.7 %. The trained ensembles applied to the other four PFT products (haptophytes, dinoflagellates, prokaryotes, and green algae; see Fig. 2 for the global distribution of the RD for each) have also shown significant improvements in MAD of 0.002, 0.002, 0.003, and 0.006 mg m^{-3} and improvements in MARD of 5.2 %, 4.2 %, 4.8 %, and 7.2 %, respectively. The median of RD over the globe for all five PFTs is within ±1.5 % and shows no significant over-/underestimation.

The low RD observed for the overlapping year suggests that the MLBE correction scheme effectively aligns the OLCI-derived PFT data with the merged-sensor-derived PFTs, ensuring a strong spatial correspondence between the two datasets.

3.2 Validation of the MLBE-corrected OLCI-derived PFT data

Validation of the corrected OLCI-derived PFTs was carried out by applying the 4 km MLBE to the OLCI-derived PFT data that are collocated with the two independent in situ

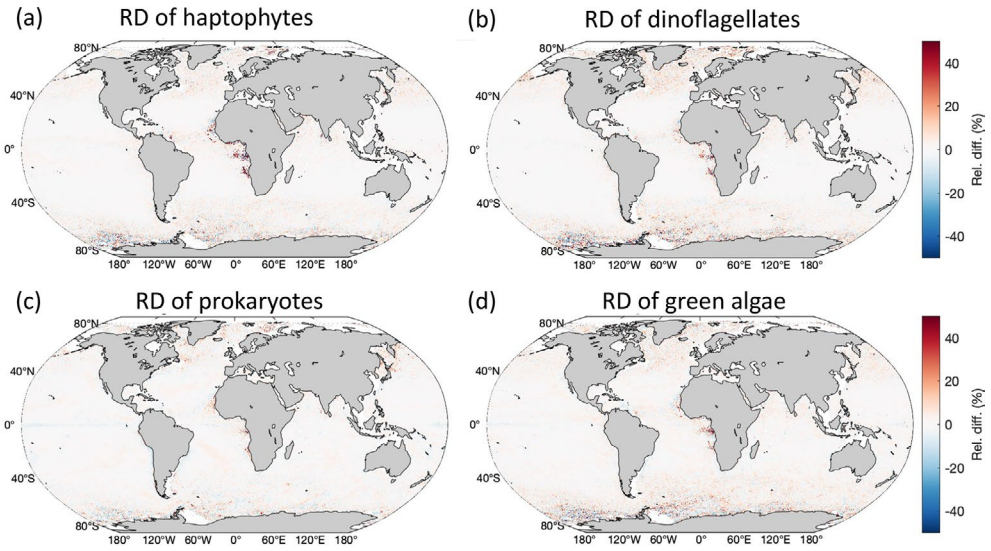

Figure 2. Global distribution of the RD between MLBE-corrected OLCI- and merged-sensor-derived PFT Chl *a* over the 1-year overlapped period (May 2016–April 2017).

datasets, as described in Sect. 2.3. Scatterplots and statistics of the validation using dataset 1 displayed in Fig. 3a show good agreements between the corrected OLCI PFT data and the in situ data, $R^2 > 0.51$ and MDPD $< 56\,\%$, with diatoms showing the best slope (0.78) and correlation coefficient (0.80) and with prokaryotes showing the lowest MDPD (33.5 %). We also provided a similar validation analysis for the OLCI data before the correction (Fig. S1 in the Supplement) to have a direct comparison. The overall validation shows that the MLBE correction on the OLCI-derived PFT data preserves the distribution features from the original OLCI-derived PFT dataset; however, overall, slightly downgraded statistics have been observed for nearly all PFTs, except for the MLBE-corrected haptophytes and prokaryotes, which showed slightly better MDPD against the in situ data compared to the validation of the original OLCI-derived data. The validation using dataset 1 indicates that the MLBE correction does not significantly change the PFT variability, showing its feasibility to generate consistent time series data. On the other hand, validation using dataset 2, which contains recently obtained in situ data at high latitudes only, exhibited larger discrepancies than that from dataset 1 (Fig. 3b). All PFTs showed low correlation between the MLBE-corrected and in situ data, with the highest R^2 only 0.21 for diatoms and the lowest R^2 for green algae. Though the MDPD values are all below 60 %, the low R^2 indicates weak agreements between the corrected and in situ data. Prokaryotes show underestimations in the corrected OLCI data compared to the in situ data, mostly for the Arctic data. A similar validation for the original OLCI-derived PFTs using dataset 2 has also been provided in Fig. S2 in the Supplement, showing overall almost equivalent statistics with the validation of the corrected data, with a slightly higher R^2 of 0.24 for diatoms and the lowest R^2 for green algae (0.09). This confirms that PFT data at high latitudes bear large uncertainties, which is in line with the per-pixel uncertainty estimated by considering errors induced by the input satellite data and the EOF-PFT algorithm parameters (Xi et al., 2021). The satellite PFTs were not improved even with the MLBE correction, suggesting that the inherent high uncertainties in high latitudes are mostly attributed to the retrieval models that are not efficient enough in these regions. Therefore, PFT observations in the high latitudes need more attention in terms of improved estimation methods and higher data quality.

3.3 PFT time series analysis

We applied the MLBE correction scheme on a global scale to the OLCI monthly products and generated time series for the five PFTs from July 2002 to December 2023. With the corrections applied to OLCI data, all five PFTs show very consistent time series (Fig. 4a). The MLBE-corrected OLCI-derived PFT data and the merged-sensor-derived PFT data showed almost identical values during the overlapped period (May 2016–April 2017). Only for green algae is the correction slightly less satisfactory than the others, which should be due to the weaker correlation ($R^2 < 0.7$; figure not shown) between the original OLCI- and merged-sensor-derived PFT data, whereas the other four PFTs all show R^2 above 0.9. This weaker correlation for green algae has subsequently led to reduced performance in the MLBE correction. The PFT time series have been analyzed at the global scale and at four regional scales, including the North Atlantic Ocean, the Mediterranean Sea, the Arctic Ocean, and the Southern Ocean. Figure 4b shows the time series with slopes indicating the PFT trends per decade and the corresponding slope

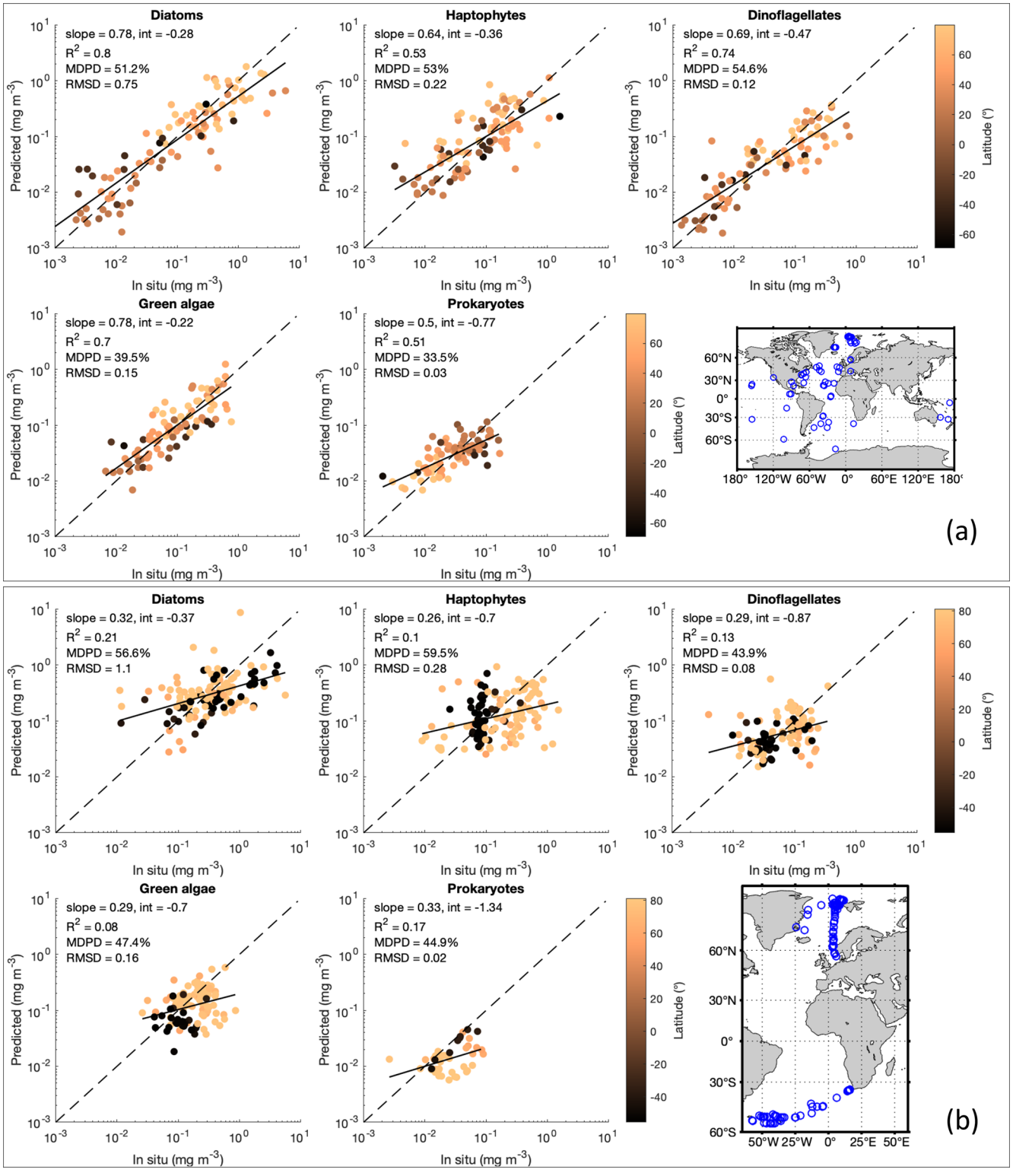

Figure 3. **(a)** MLBE-corrected PFT Chl *a* from OLCI sensors in comparison with in situ PFT dataset 1. **(b)** Same as the validation in panel **(a)** but using in situ PFT dataset 2. A map of the data distribution for datasets 1 and 2 (product ref. no. 3 in Table 1) is shown in each panel, respectively.

errors for all the PFTs at different scales. Figure 5 shows the significant PFT trends (p value < 0.05) on a pixel basis over the globe for a better understanding of the spatial distribution of the trends.

Diatoms show a significant increasing trend for the global ocean and selected regions, especially in the Atlantic section of the polar regions (Fig. 5a). Furthermore, a distinct increase was found in more recent years since autumn 2017 and is still prominent in 2023. The global trend in diatom Chl a is increasing by $0.0011 \pm 0.0001\,\mathrm{mg\,m^{-3}}$ per decade and with a dramatic increase in the polar regions (0.03 and $0.034\,\mathrm{mg\,m^{-3}}$ per decade for the Southern Ocean and the Arctic Ocean, respectively). This overall increasing trend is mainly driven by the significant elevation in diatom biomass observed since 2018, especially due to the higher minimum diatom Chl a in spring and late autumn, which are the beginning and ending times of the available OC satellite observations in the polar areas. This might suggest a longer growth period for diatoms in latest years.

Haptophyte Chl a exhibits a very slight decrease in general on the global scale ($-0.0002 \pm 0.0001\,\mathrm{mg\,m^{-3}}$ per decade) and in all other selected regional zones, but the decrease is not significant in the North Atlantic Ocean. There is a slight oscillation pattern in the global time series, which shows the haptophyte biomass was the highest in late summer 2011 and remained at a stably lower biomass in the following years until 2018/2019, when it started to elevate again. This feature is not clearly reflected in the four selected regions; therefore it should be attributed to other regions that are not included here. The global per-pixel trend (Fig. 5b) shows a more significant decrease in coastal areas and in the sub-Arctic and Arctic regions, along with high variability in the Southern Ocean with an overall decrease.

Dinoflagellates show a similar pattern with diatoms, i.e., an increasing trend ($0.0002 \pm 0.0000\,\mathrm{mg\,m^{-3}}$ per decade) in the last 2 decades mainly driven by the increase in dinoflagellate Chl a since mid-2017, but their biomass is still low compared to other PFTs, as they are usually undominant in the phytoplankton community composition. No significant trends have been found for dinoflagellate biomass in the Mediterranean Sea and Arctic Ocean.

Green algae show no significant trend on the global scale. The time series show a less obvious seasonal pattern than the other PFTs, possibly due to the fact that they are barely the dominant group in the global ocean and mostly co-exist with the other PFTs which show clear dominance in certain regions at specific times, depending on their ecological functions. The biomass reached its peak in October 2011, followed by a few years of decrease, but started to increase in 2018. On the regional scale, a decrease in the Mediterranean Sea and Arctic Ocean and a slight increase in the Southern Ocean have been observed, which are also clearly shown in the per-pixel trend (Fig. 5d). The decreasing trend is seen in coastal regions, such as the northern European coastlines, the west coasts of America and Africa, and the north coast of the Arabian Sea.

Prokaryote Chl a displays an overall significant decreasing trend on the global scale ($-0.0012 \pm 0.0001\,\mathrm{mg\,m^{-3}}$ per decade) and in the selected regional zones, except for the Southern Ocean. The global per-pixel trend (Fig. 5e) shows the Northern Hemisphere with significant decrease near the Equator within 15° S–25° N (Indian Ocean, western Africa, low latitudes in the Pacific Ocean), but a slight increase is shown in the belt of 15–35° S. Very mild changes have been found at high latitudes, where the prokaryotic phytoplankton abundance is in general very low ($\ll 0.01\,\mathrm{mg\,m^{-3}}$ on area average).

3.4 PFT anomaly of 2023

Figure 6 shows the relative anomalies (%) of the five PFTs in 2023 compared to the average PFT state over the 20 years. The diatom anomaly presents higher Chl a for most of the global ocean, with a dramatic increase in latitudes $> 40°$. This can already be expected from the time series in Fig. 4a, where diatoms show elevated Chl a from autumn 2017 and keep a similarly high biomass in 2023. The global mean of the diatom in 2023 is about 24 % higher than the 2-decade average, and the anomaly varies from −30 % to 110 %, with extremely high values in the Arctic Ocean and the coastal regions in the southern part of South America. Dinoflagellates show a similar anomaly, with diatoms in a much milder pattern, which has a global mean of about 9.4 %. The haptophyte anomaly presents changes without a clear pattern, showing slight increases in Chl a in the Pacific gyres, the eastern Indian Ocean, and the Southern Ocean but slight decreases in the temperate latitudes. The overall global mean anomaly of haptophyte Chl a is only very slightly higher compared to the 2-decade average (1.6 %). Green algae show a similar distribution in biomass change to haptophytes but a slightly more prominent increase in most of the global oceans (global mean of 6.5 %). Prokaryotes generally show decreased Chl a in 2023 (global mean of −2.1 %), with only slight increases observed in the South Pacific Ocean and part of the Southern Ocean.

4 Discussion, conclusions and outlook

4.1 The need for harmonization

Generating long-term consistent PFT data from a single sensor/set of sensors is challenging due to discontinuous satellite missions and different sensor specifications. PFT data derived using models established based on different sensor sets bear different levels of uncertainty. OLCI, being the newest sensor, has more spectral bands, which should be beneficial for PFT retrievals; however, due to limited in situ pigment datasets available for the model training, it does not show superior performance to the merged OC products. Har-

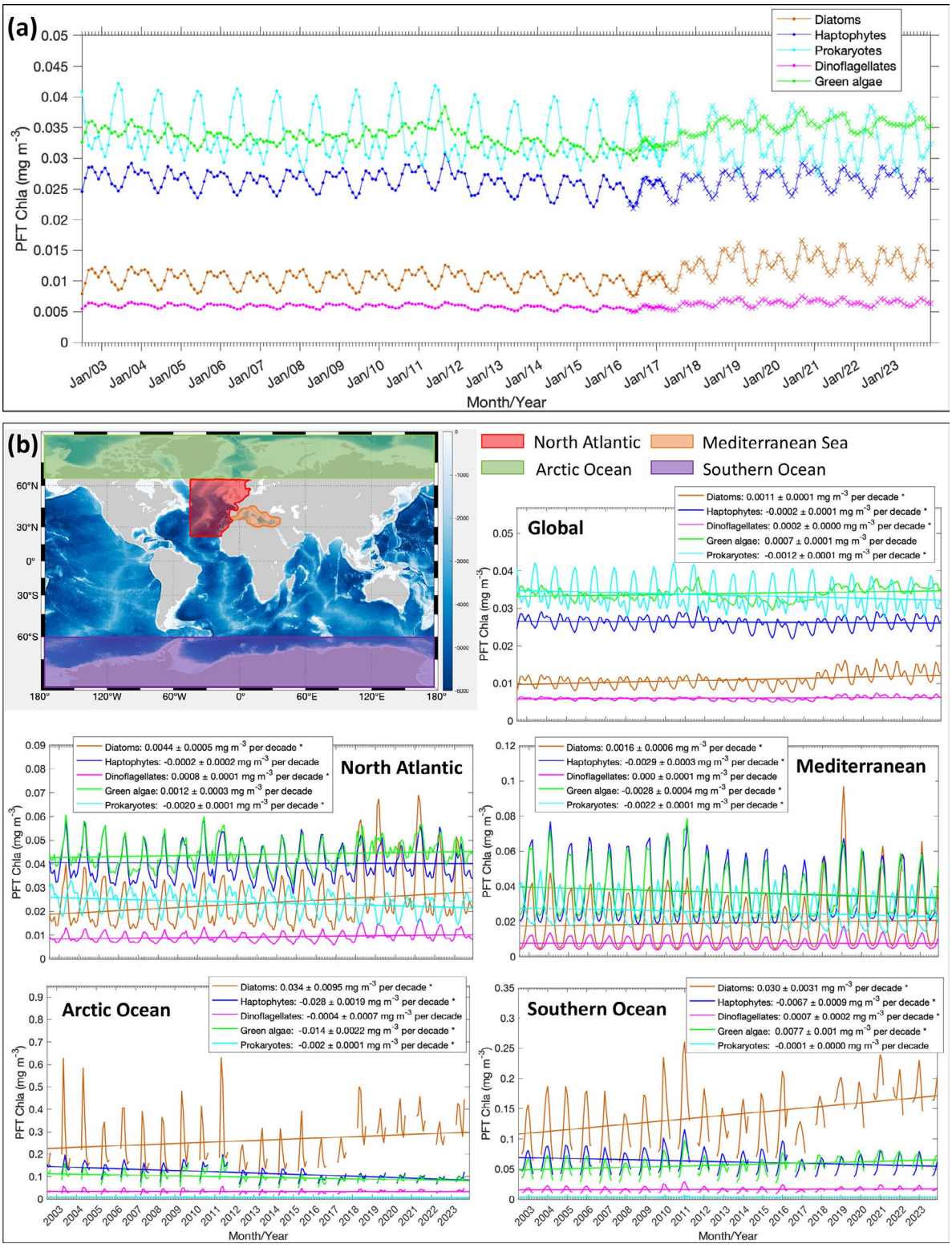

Figure 4. **(a)** Updated (corrected) time series of the five PFT Chl *a* based on the global mean from 2002 to 2023. Merged-sensor-derived PFT products cover the period of July 2002–April 2017 (indicated with dots), and OLCI-derived PFT products are for May 2016–December 2023 (indicated with crosses). Note that the OLCI-derived products are corrected to merged products based on MLBE. **(b)** Trends in the Chl *a* of diatoms, haptophytes, dinoflagellates, green algae, and prokaryotes on the global scale and on four regional scales (the North Atlantic Ocean, the Mediterranean Sea, the Arctic Ocean, and the Southern Ocean). Trend slopes per decade with uncertainties are indicated, with significant trends marked with an asterisk (*).

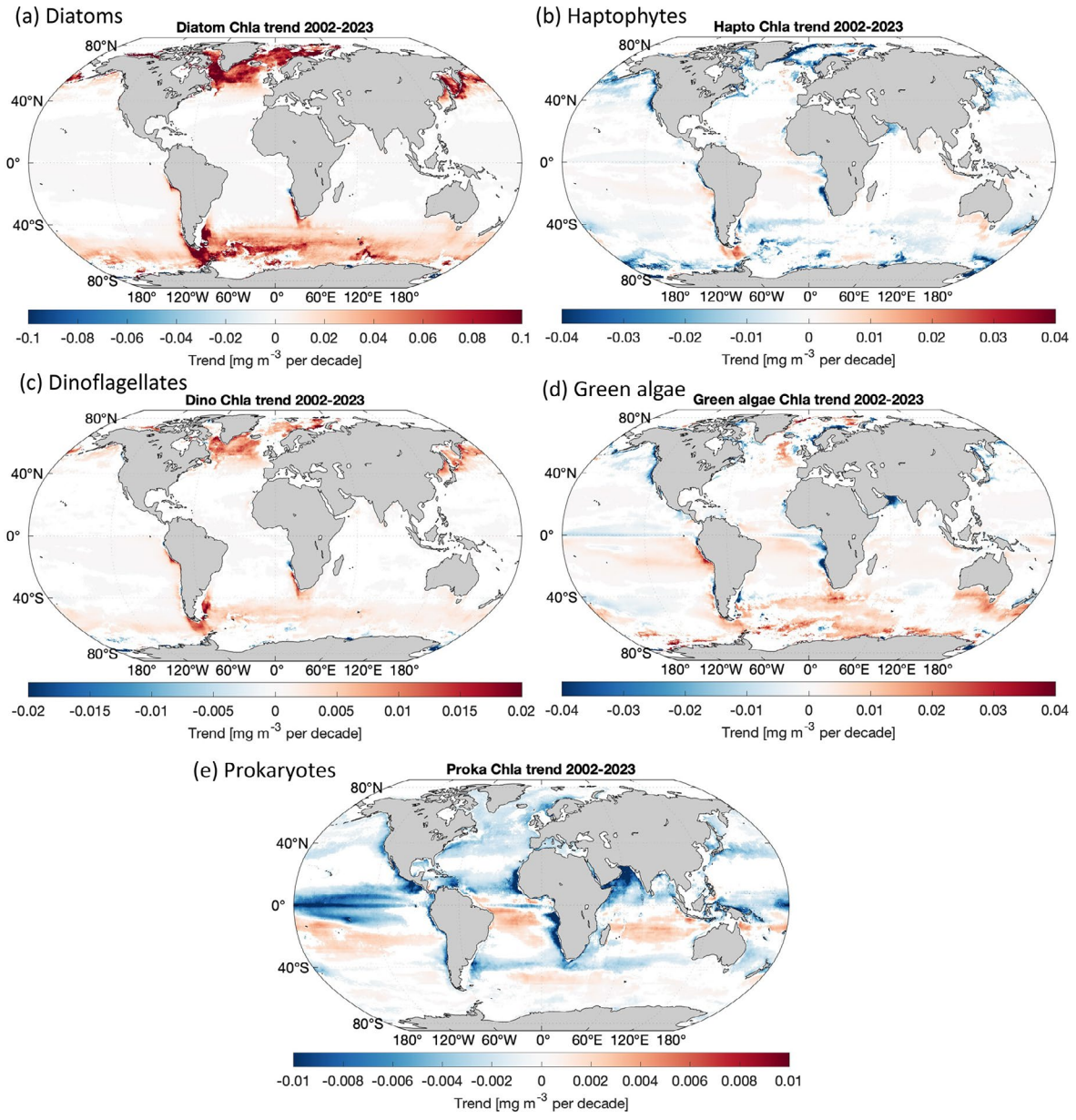

Figure 5. Per-pixel trends for Chl *a* of **(a)** diatoms, **(b)** haptophytes, **(c)** dinoflagellates, **(d)** green algae, and **(e)** prokaryotes (only where $p < 0.05$ is shown; slope unit: mg m^{-3} per decade).

monization is so far necessary for the current derived PFT products of the Copernicus Marine Service, as it is not yet possible to produce consistent long-term PFT products using harmonized radiometric data from historic and current sensors using the proposed approach, which requires more bands. Attempts have been carried out for consistent PFT products derived from large data-driven deep learning ensembles by incorporating Rrs at only 5–6 merged bands, together with other ocean color and physical/biogeochemical variables (e.g., Zhang et al., 2024), and this shows potential for upgrading the operational datasets; however, the applicability of the implementation of such an approach for operational products has yet to be proven.

4.2 MLBE correction scheme

This study aims to demonstrate consistent PFT time series data on the global scale and for the polar regions and European seas, which were developed based on a robust machine learning correction scheme. The proposed MLBE correction scheme outperforms the previously proposed method that was based on type II linear regression with considerations of PFT uncertainties (Xi et al., 2023a). For the overlapping

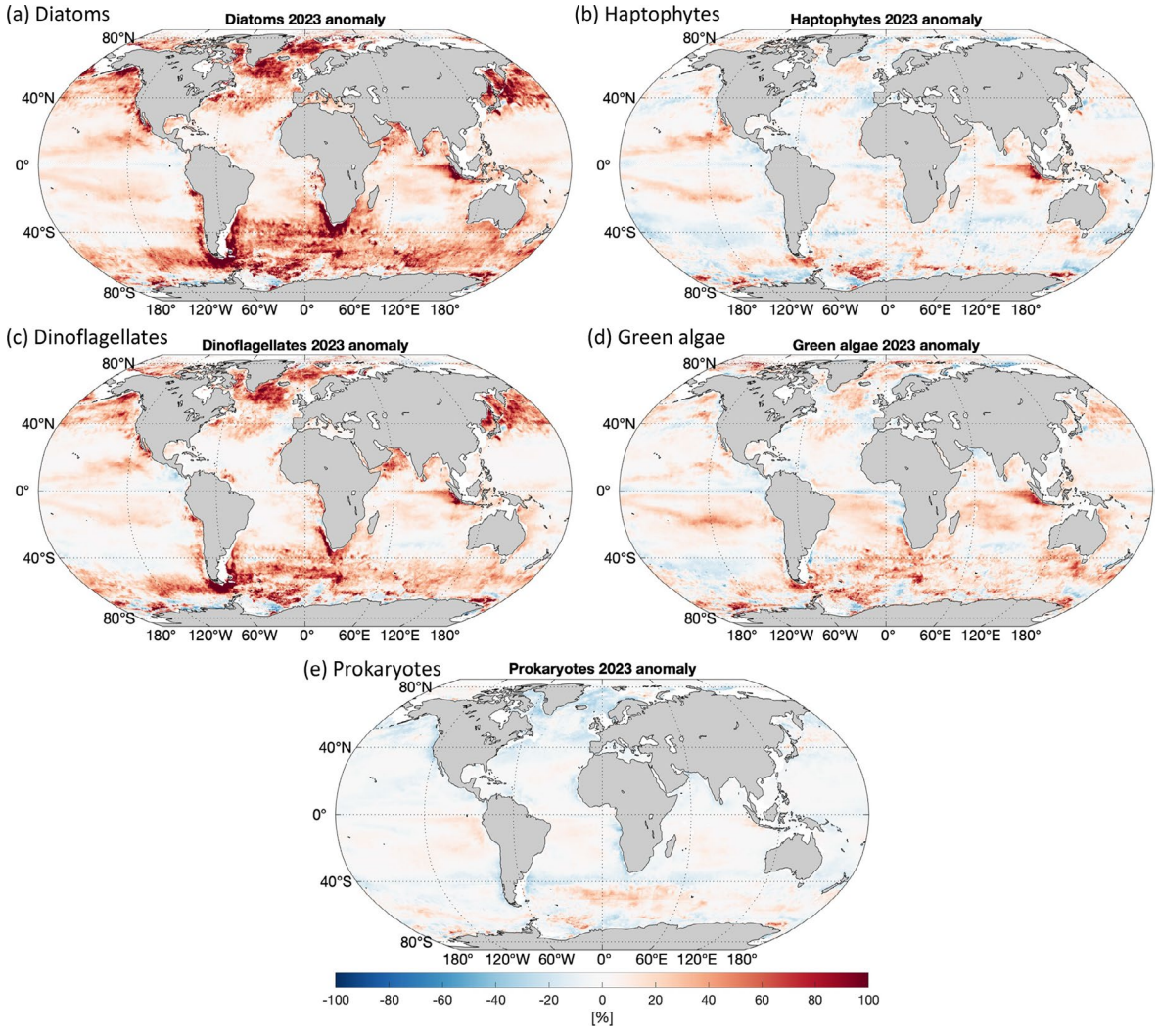

Figure 6. Relative anomaly of 2023 for Chl *a* of **(a)** diatoms, **(b)** haptophytes, **(c)** dinoflagellates, **(d)** green algae, and **(e)** prokaryotes.

period, the MLBE scheme demonstrates high consistency between the corrected OLCI-derived PFTs and the merged-sensor-derived PFTs, both in space and time, increasing our confidence in employing the data for further time series studies.

However, the MLBE model training was based on 12-month satellite data spanning only 1 year (the overlapping period of the two sensor sets), in an attempt to identify the spatial variation of the PFT data from the two sensor sets, so that it could fit one pattern to the other on the whole global scale. It has been reported that random splitting between training and test sets may produce data leakages (Meyer et al., 2018; Stock et al., 2023), potentially leading to overoptimistic test performance that does not generalize well in actual application to other datasets. To avoid data leakage, temporal partitioning was suggested to ensure that the training and test datasets are independent. However, a random split was applied in the study, as temporal partitioning was impractical due to the limited duration of the dataset in our case. The MLBE model is basically a correction scheme trained based on all pixel data (over 50 million available data points) from 12 monthly PFT products. The purpose was to cover as completely as possible the global region to ensure that the training learns the pattern globally. By applying the suggested temporal partitioning, we would lose data, e.g., at high latitudes, if we excluded a certain month in the training. This can cause biases in the learning process, ensuring that the trained model would very likely not be applicable to either the test set or the other datasets that contain the missing periods. The straightforward random splitting in our study ensured the homogeneous splitting between the training and test datasets over space and time, thanks to the large number of data points, so that the trained model learned the most knowledge from the available data within the limited time period. Though such random partitioning has widely been used (e.g., Li et al., 2023; Zoffoli et al., 2025), one

should keep in mind that having data for only a single year is challenging because the year may present conditions that are specific to that year only, which may cause unrealistic predictions for other years. It is therefore noteworthy that target-oriented data splitting and cross-validation, such as considering spatial and temporal blocks, should be applied in machine-learning-based studies when the dataset allows it (e.g., Zhang et al., 2024).

For the next cycle of the implementation to the Copernicus Marine Service, updates will be necessary for the PFT retrievals and the MLBE scheme. It is expected that the VIIRS-SNPP drifting after 2017 is better calibrated with the new reprocessing, so our data used for the training in the correction scheme can be extended to more recent years to achieve an even better consistency between the merged-sensor-derived and OLCI-derived PFT products.

4.3 Consistent PFT time series and validation

The time series generated based on the consistent PFT data on the global scale from 2002 to 2023 has shown a clear increasing trend for diatoms and dinoflagellates and a slight decreasing trend for haptophytes and prokaryotes, while the green algae exhibit no significant trend but with higher interannual variability. To date, the longest time series for ocean color products still covers less than 3 decades (starting in 1997 with the launch of SeaWiFS). Though this may still not be long enough for a robust trend analysis due to a decadal variability that is too strong (Henson et al., 2010, 2016), these time series can help to catch distinct changes on different scales by comparing them to the climatological state. Indeed, the findings, such as the significant increase in diatoms, particularly after 2017, are of interest to in-depth investigations linking climate drivers to such prominent changes. For instance, potential responses of phytoplankton biomass to increasingly frequent marine heat waves in the past years can be a suitable starting point.

Changes in phytoplankton biomass have been described by the Chl *a* derived from ocean color satellites covering the last decades. Trends in the Chl *a* at different scales can be generated using current operational chlorophyll products, such as OC-CCI and GlobColour. For instance, Chl *a* as an Ocean Monitoring Indicator (OMI) has been included by the Copernicus Marine Service where the climate trends in various OMIs are provided to indicate the state of the ocean health. The current published time series of Chl *a* shows a general increase during 1997–2022 on the global scale and also for the North Atlantic and Arctic regions. The published per-pixel Chl *a* trend map shows a more prominent increasing trend at high latitudes but a slight decrease at mid- to low latitudes (e.g., EU Copernicus Marine Service Information, 2022). These trends are in good agreement with our PFT time series, which shows an overall increasing trend in the total biomass mainly due to the increased diatom biomass. Similar findings on both global and regional scales were reported by van Oostende et al. (2023), where the OC-CCI dataset was used but with careful consideration of the spatiotemporal coverage of the different sensor datasets by applying a temporal gap detection method. Other techniques, such as gap filling and statistical temporal decomposition, are also in demand for more robust PFT data analysis to increase the accuracy in separating the long-term signal from the seasonal component of the time series. Nevertheless, studies have shown that the OC-satellite-derived surface Chl *a* presents contrasted trends between available products that are generated based on different retrieval algorithms and merging methods, e.g., the OC-CCI and GlobColour products (Yu et al., 2023), suggesting the need for careful interpretation of the trends for multi-OC-sensor-derived products. Inconsistencies between missions remain a significant challenge to overcome in order to provide climate-quality time series, which requires efforts from both spatial agencies and scientific communities to correct the inconsistencies in radiometric data with long-term time series and apply proper harmonization to the merged products (Pauthenet et al., 2024).

So far, there are limited studies investigating or reporting the PFT interannual variability covering recent years. There are also quite limited long-term in situ PFT data available over large scales. However, our recent investigation at a smaller scale in the Fram Strait (Xi et al., 2024) indicated that the surface diatom from the in situ data collected in the LTER Hausgarten area (75 to 80° N, 5° W to 10° E) from 2009 onwards has shown a unanimous pattern with the satellite PFT time series; i.e., diatoms have shown an overall increase in this region in more recent years (satellite from 2018 but in situ from 2019 due to lack of data in 2018). The other PFTs show rather an oscillational feature but not as dramatic as seen in diatoms. It should also be noted that the in situ data were collected mostly in the spring to summer months (which vary from May to September) and cannot fully represent the phytoplankton development during the whole season or the interannual variabilities. However, these Fram Strait in situ data support our satellite time series with the diatom increase in the years 2018 to 2023 in the Arctic region. More field observations on phytoplankton community composition are constantly collected for further evaluations and hypothesis verifications.

Validation has been performed at different levels, from the model development stage (details not shown in this study) to the corrected OLCI-derived PFT data, in order to understand the reliability of the datasets well. Using validation data covering different times and regions, we observed that the satellite PFT data have larger discrepancies compared to the in situ data at high latitudes, especially in the Arctic Ocean, which was also reflected in the per-pixel uncertainty assessment for the EOF-PFT algorithm (Xi et al., 2021). Compared to the original OLCI-derived PFT data, the MLBE-corrected data showed comparable but unimproved validation statistics against the in situ datasets, and this can be explained by the following aspects: (1) limited temporal coverage of

the training data used in the MLBE might transfer further errors to the corrected data. (2) Dataset 1 served as the test set randomly extracted from the global in situ dataset from which the other 70 % was used to train EOF-PFT model for the OLCI sensors; therefore dataset 1 possessed similar features to the training set and exhibited the best agreements with the OLCI-derived PFTs before correction, very possibly due to the aforementioned data leakage effect. (3) The MLBE scheme bears lower correction efficiency at high latitudes due to larger inherent uncertainties in the satellite-derived PFT products. However, our validation for diatoms and dinoflagellates in the Arctic Ocean using dataset 2, collected during 2021–2023, shows no overestimation of the satellite retrievals compared to the in situ data despite the weak correlation and higher discrepancies (Fig. 3b), indicating that our satellite retrievals correctly presented the increased biomass for the two PFTs. Since the ecosystem in the Arctic Ocean undergoes fast changes as a consequence of the arctic warming and sea ice retreat, there are still a lot of unknowns on how the phytoplankton community adapts and responds to these changes (Oziel et al., 2020; Meredith et al., 2019). It is potentially essential for the Copernicus Marine Service to provide not only for the white ocean (sea ice) but also for the green ocean (biogeochemical parameters), a wide range of biological/biogeochemical variables to better understand the state and possible tendencies of the ecosystems in the Arctic Ocean.

4.4 Conclusion and outlook

The correction scheme proposed in this study is specifically designed to address inter-sensor data inconsistencies in the current Copernicus Marine Service PFT products. The present trained model can only be used to correct the OLCI-derived PFT product to match the merged-sensor-derived product. However, the underlying technical framework is adaptable to other common ocean color products, such as optical properties derived from multiple sensors, thereby enhancing the overall continuity and consistency of ocean color data. As a rapidly emerging and powerful technique, machine learning can be further leveraged in ocean color data services, supporting agencies and data platforms in delivering high-quality, consistent operational products. This work is at the cutting edge of research attempting to demonstrate the most up-to-date long-term phytoplankton community in several functional groups derived from ocean color products. Providing interannual variation and trend analyses of the surface phytoplankton community structure, the PFT products will complement the chlorophyll products of the Copernicus Marine Service as an essential ocean variable and help in the assessment of the ocean health in the biogeochemical aspect.

Data availability. Data and products used in this study and their availabilities and supporting documentation are listed in Table 1, from which the in situ HPLC pigment concentrations and the corresponding derived in situ PFT Chl *a* data used for validation are published on PANGAEA (https://doi.org/10.1594/PANGAEA.982433; Xi et al., 2025).

Supplement. The supplement related to this article is available online at https://doi.org/10.5194/sp-6-osr9-7-2025-supplement.

Author contributions. HX, AB, MB, and AM conceptualized the study. HX designed and carried out the experiments. MB and JD provided support with satellite products and matchup data extraction. EM contributed to the machine learning algorithms. HX drafted and revised the article with contributions from all coauthors.

Competing interests. The contact author has declared that none of the authors has any competing interests.

Disclaimer. Publisher's note: Copernicus Publications remains neutral with regard to jurisdictional claims made in the text, published maps, institutional affiliations, or any other geographical representation in this paper. While Copernicus Publications makes every effort to include appropriate place names, the final responsibility lies with the authors.

Acknowledgements. We acknowledge the two Copernicus Marine – Innovation Service Evolution R&D Projects, GLOPHYTS (2022-2024) and ML-PhyTAO (2024-2026), for funding. Copernicus Marine Service is implemented by Mercator Ocean International in the framework of a delegation agreement with the European Union. This work was also partly supported by the German Research Foundation (DFG) "Transregional Collaborative Research Center ArctiC Amplification: Climate Relevant Atmospheric and SurfaCe Processes and Feedback Mechanisms (AC)3" (Project C03) and by the ESA project 4DMED-Sea (4000141547/23/I-DT). Ehsan Mehdipour's work was supported by the project "4D-Phyto" funded by AWI-INSPIRES and HGF-MarDATA. We thank ESA, EUMETSAT, and NASA for distributing ocean color satellite data and especially thank the ACRI-ST GlobColour team for providing OLCI and merged ocean color L3 products. In situ data from four *Polarstern* expeditions were funded under grant nos. AWI_PS126_02, AWI_PS131_5, AWI_PS133/1_11, and AWI_PS136_04. The captain, crew, and expedition scientists are also acknowledged for their support at sea. We also acknowledge Alexandre Castagna and the other reviewer for their constructive comments in improving this study.

Financial support. This research has been supported by the Deutsche Forschungsgemeinschaft (grant no. (AC)3 Project C03), the European Space Agency (project 4DMED-Sea (grant no. 4000141547/23/IDT)), the Helmholtz-Gemeinschaft Deutscher Forschungszentren (Program MarData for project "4D-Phyto"),

the Alfred-Wegener-Institut, Helmholtz-Zentrum für Polar- und Meeresforschung (Program INSPIRES for project "4D-Phyto", Expedition Programs with grants AWI_PS126_02, AWI_PS131_5, AWI_PS133/1_11 and AWI_PS136_04), and the Mercater Ocean International (project GLOPHYTS (2022–2024), 21036L05B-COP-INNO SCI-9000, and project ML-PhyTAO (2024-2026), 23138L03D-COP-INNO SCI-9000).

Review statement. This paper was edited by Pierre-Marie Poulain and reviewed by Alexandre Castagna and one anonymous referee.

References

Alfred-Wegener-Institut Helmholtz-Zentrum für Polar- und Meeresforschung: Polar Research and Supply Vessel *POLARSTERN* Operated by the Alfred-Wegener-Institute, Journal Of Large-Scale Research Facilities, 3, A119, https://doi.org/10.17815/jlsrf-3-163, 2017.

Antoine, D., Morel, A., Gordon, H. R., Banzon, V. F., and Evans, R. H.: Bridging ocean color observations of the 1980s and 2000s in search of long-term trends, J. Geophys. Res.-Oceans, 110, C06009, https://doi.org/10.1029/2004JC002620, 2005.

Behrenfeld, M. J., O'Malley R. T., Boss, E. S., Westberry, T. K., Graff, J. R., Halsey, K. H., Milligan, A. J., Siegel, D. A., and Brown, M. B.: Revaluating ocean warming impacts on global phytoplankton, Nat. Clim. Change, 6, 3223–3330, https://doi.org/10.1038/nclimate2838, 2016.

Bracher, A., Bouman, H. A., Brewin, R. J. W., Bricaud, A., Brotas, V., Ciotti, A. M., Clementson, L., Devred, E., Di Cicco, A., Dutkiewicz, S., Hardman-Mountford, N. J., Hickman, A. E., Hieronymi, M., Hirata, T., Losa, S. N., Mouw, C. B., Organelli, E., Raitsos, D. E., Uitz, J., Vogt, M., and Wolanin, A.: Obtaining phytoplankton diversity from ocean color: a scientific roadmap for future development, Front. Mar. Sci., 4, 1–15, https://doi.org/10.3389/fmars.2017.00055, 2017.

Breiman, L: Random Forests, Mach. Learn., 45, 5–32, https://doi.org/10.1023/A:1010933404324, 2001.

Cleveland, R. B., Cleveland, W. S., McRae, J. E., and Terpenning, I.: STL: A seasonal-trend decomposition procedure based on Loess, J. Off. Stat., 6, 3–73, https://doi.org/10.1007/978-1-4613-4499-5_24, 1990.

Colella, S., Böhm, E., Cesarini, C., Jutards, Q., and Brando, V. E.: EU Copernicus Marine Service Product User Manual for the Global Ocean Colour (Copernicus-GlobColour), Bio-Geo-Chemical, L3 (daily) from Satellite, OCEANCOLOUR_GLO_BGC_L3_MY_009_103, Issue 5.0, Mercator Ocean International, https://documentation.marine.copernicus.eu/PUM/CMEMS-OC-PUM.pdf (last access: 18 February 2024), 2024.

EU Copernicus Marine Service Information: Global Ocean Chlorophyll-a trend map from Observations Reprocessing, Mercator Ocean International [data set], https://doi.org/10.48670/moi-00230, 2022.

EU Copernicus Marine Service Product: Global Ocean Colour (Copernicus-GlobColour), Bio-Geo-Chemical, L3 (daily) from Satellite Observations (1997–ongoing), Mercator Ocean International [data set], https://doi.org/10.48670/moi-00280, 2024.

Garnesson, P., Mangin, A., and Bretagnon, M., and Jutard, Q.: EU Copernicus Marine Service Quality Information Document for the Global Ocean Colour (Copernicus-GlobColour), Bio-Geo-Chemical, L3 (daily) from Satellite, OCEANCOLOUR_GLO_BGC_L3_MY_009_103, Issue 5.0, Mercator Ocean International, https://documentation.marine.copernicus.eu/QUID/CMEMS-OC-QUID-009-101to104-111-113-116-118.pdf (last access: 22 August 2024), 2024.

Gilbert, R. O.: Statistical Methods for Environmental Pollution Monitoring, John Wiley and Sons, United States, 336 pp., ISBN 978-0471288787, 1987.

Gregg, W. W. and Rousseaux, C. S.: Decadal trends in global pelagic ocean chlorophyll: A new assessment integrating multiple satellites, in situ data, and models, J. Geophys. Res.-Oceans, 119, 5921–5933, https://doi.org/10.1002/2014JC010158, 2014.

Gruber, N., Boyd, P. W., Frölicher T. L., and Vogt, M.: Biogeochemical extremes and compound events in the ocean, Nature, 600, 395–407, https://doi.org/10.1038/s41586-021-03981-7, 2021.

Henson, S. A., Sarmiento, J. L., Dunne, J. P., Bopp, L., Lima, I., Doney, S. C., John, J., and Beaulieu, C.: Detection of anthropogenic climate change in satellite records of ocean chlorophyll and productivity, Biogeosciences, 7, 621–640, https://doi.org/10.5194/bg-7-621-2010, 2010.

Henson, S. A., Beaulieu, C., and Lampitt, R.: Observing climate change trends in ocean biogeochemistry: when and where, Glob. Chang. Biol., 22, 1561–1571, https://doi.org/10.1111/gcb.13152, 2016.

Kendall, M. G.: Rank Correlation Methods, in: 4th edn., Charles Griffin, London, UK, 202 pp., ISBN 978-0852641996, 1975.

Li, X., Yang, Y., Ishizaka, J., and Li, X.: Global estimation of phytoplankton pigment concentrations from satellite data using a deep-learning-based model., Remote Sens. Environ., 294, 113628, https://doi.org/10.1016/j.rse.2023.113628, 2023.

Mann, H. B.: Nonparametric tests against trend, Econometrica, 13, 245–259, https://doi.org/10.2307/1907187, 1945.

Mélin, F. and Franz, B. A.: Chapter 6.1 – Assessment of satellite ocean colour radiometry and derived geophysical products, Experimental Methods in the Physical Sciences, 47, 609–638, https://doi.org/10.1016/B978-0-12-417011-7.00020-9, 2014.

Meredith, M., Sommerkorn, M., Cassotta, S., Derksen, C., Ekaykin, A., Hollowed, A., Kofinas, G., Mackintosh, A., Melbourne-Thomas, J., Muelbert, M. M. C., Ottersen, G., Pritchard, H., and Schuur, E. A. G.: Polar Regions, In: IPCC Special Report on the Ocean and Cryosphere in a Changing Climate, edited by: Pörtner, H.-O., Roberts, D. C., Masson-Delmotte, V., Zhai, P., Tignor, M., Poloczanska, E., Mintenbeck, K., Alegria, A., Nicolai, M., Okem, A., Petzold, J., Rama, B., and Weyer, N. M., Cambridge University Press, Cambridge, UK and New York, NY, USA, 203–320, https://doi.org/10.1017/9781009157964.005, 2019.

Meyer, H., Reudenbach, C., Hengl, T., Katurji, M., and Nauss, T.: Improving performance of spatio-temporal machine learning models using forward feature selection and target-oriented validation, Environ. Model. Softw., 101, 1–9, https://doi.org/10.1016/j.envsoft.2017.12.001, 2018.

NASA Ocean Color: VIIRSN-vs-VIIRSN (vr2022.0m_vr2018.0m) Global Remote Sensing Reflectance Trends, NASA Ocean

Color, https://oceancolor.gsfc.nasa.gov/data/analysis/global, last access: 7 May 2025.

Oziel, L., Baudena, A., Ardyna, M., Massicotte, P., Randelhoff, A., Sallée, J. -B., Ingvaldsen, R. B., Devred, E., and Babin, M: Faster Atlantic currents drive poleward expansion of temperate phytoplankton in the Arctic Ocean, Nat. Comm., 11, 1705, https://doi.org/10.1038/s41467-020-15485-5, 2020.

Pauthenet, E., Martinez, E., Gorgues, T., Roussillon, J., Drumetz, L., Fablet, R., and Roux, M.,: Contrasted trends in chlorophyll-a satellite products, Geophys. Res. Lett., 51, e2024GL108916, https://doi.org/10.1029/2024GL108916, 2024.

Sathyendranath, S., Brewin, R. J. W., Brockmann, C., Brotas, V., Calton, B., Chuprin, A., Cipollini, P., Couto, A. B., Dingle, J., Doerffer, R., Donlon, C., Dowell, M., Farman, A., Grant, M., Groom, S., Horseman, A., Jackson, T., Krasemann, H., Lavender, S., Martinez-Vicente, V., Mazeran, C., Mélin, F., Moore, T. S., Müller, D., Regner, P., Roy, S., Steele, C., Steinmetz, F., Swinton, J., Taberner, M., Thompson, A., Valente, A., Zühlke, M., Brando, V. E., Feng, H., Feldman, G., Franz, B. A., Frouin, R., Gould, R. W., Hooker, S. B., Kahru, M., Kratzer, S., Mitchell, B. G., Muller-Karger, F. E., Sosik, H. M., Voss, K. J., Werdell, J., and Platt, T.: An ocean-colour time series for use in climate studies: The experience of the Ocean-Colour Climate Change Initiative (OC-CCI), Sensors, 19, 4285, https://doi.org/10.3390/s19194285, 2019.

Sen, P. K.: Estimates of the regression coefficient based on Kendall's tau, J. Am. Stat. Assoc., 63, 1379–1389, https://doi.org/10.1080/01621459.1968.10480934, 1968.

Stock, A., Gregr, E. J., and Chan, K. M. A.: Data leakage jeopardizes ecological applications of machine learning, Nat. Ecol. Evol., 7, 1743–1745, https://doi.org/10.1038/s41559-023-02162-1, 2023.

van Oostende, M., Hieronymi, M., Krasemann, H., and Baschek, B.: Global ocean colour trends in biogeochemical provinces, Front. Mar. Sci., 10, 1052166, https://doi.org/10.3389/fmars.2023.1052166, 2023.

Xi, H., Losa, S. N., Mangin, A., Soppa, M. A., Garnesson, P., Demaria, J., Liu, Y., d'Andon, O. H. F., and Bracher, A.: A global retrieval algorithm of phytoplankton functional types: Towards the applications to CMEMS GlobColour merged products and OLCI data, Remote Sens. Environ., 240, 111704, https://doi.org/10.1016/j.rse.2020.111704, 2020.

Xi, H., Losa, S. N., Mangin, A., Garnesson, P., Bretagnon, M., Demaria, J., Soppa, M. A., d'Andon, O. H. F., and Bracher, A.: Global chlorophyll a concentrations of phytoplankton functional types with detailed uncertainty assessment using multi-sensor ocean color and sea surface temperature satellite products, J. Geophys. Res.-Oceans, 126, e2020JC017127, https://doi.org/10.1029/2020JC017127, 2021.

Xi, H., Bretagnon, M., Losa, S. N., Brotas, V., Gomes, M., Peeken, I., Alvarado, L. M. A., Mangin, A., and Bracher, A.: Satellite monitoring of surface phytoplankton functional types in the Atlantic Ocean over 20 years (2002–2021), in: 7th edition of the Copernicus Ocean State Report (OSR7), edited by: von Schuckmann, K., Moreira, L., Le Traon, P.-Y., Grégoire, M., Marcos, M., Staneva, J., Brasseur, P., Garric, G., Lionello, P., Karstensen, J., and Neukermans, G., Copernicus Publications, State Planet, 1-osr7, 5, https://doi.org/10.5194/sp-1-osr7-5-2023, 2023a.

Xi, H., Peeken, I., Gomes, M., Brotas, V., Tilstone, G., Brewin, R. J. W., Dall'Olmo, G., Tracana, A., Alvarado, L. M. A., Murawski, S., Wiegmann, S., and Bracher, A.: Phytoplankton pigment concentrations and phytoplankton groups measured on water samples collected from various expeditions in the Atlantic Ocean from 71° S to 84° N, PANGAEA [data set], https://doi.org/10.1594/PANGAEA.954738, 2023b.

Xi, H., Peeken, I., Nöthig, E.M., Kraberg, A., Metfies, K., Bretagnon, M., Mehdipour, E., Lampe, V., Mangin, A., and Bracher, A.: How is the surface phytoplankton community composition changing in the Arctic Fram Strait in the last two decades?, Ocean Optics Conference XXVI, 6–11 October 2024, Las Palmas Spain, https://epic.awi.de/id/eprint/59785/ (last access: 18 May 2025), 2024.

Xi, H., Wiegmann, S., Hohe, C., Schmidt, I., and Bracher, A.: A validation data set of phytoplankton pigment concentrations and phytoplankton groups measured on water samples collected from various expeditions, PANGAEA [data set], https://doi.org/10.1594/PANGAEA.982433, 2025.

Yu, S., Bai, Y., He, X., Gong, F., and Li, T.: A new merged dataset of global ocean chlorophyll-a concentration for better trend detection, Front. Mar. Sci., 10, 1051619, https://doi.org/10.3389/fmars.2023.1051619, 2023.

Zhang, Y., Shen, F., Li, R., Li, M., Li, Z., Chen, S., and Sun, X.: AIGD-PFT: the first AI-driven global daily gap-free 4 km phytoplankton functional type data product from 1998 to 2023, Earth Syst. Sci. Data, 16, 4793–4816, https://doi.org/10.5194/essd-16-4793-2024, 2024.

Zoffoli, M. L., Brando, V., Volpe, G., González Vilas, L., Davies, B. F. R., Frouin, R., Pitarch, J., Oiry, S., Tan, J., Colella, S., and Marchese, C.: CIAO: A machine-learning algorithm for mapping Arctic Ocean Chlorophyll-a from space, Science of Remote Sensing, 11, 100212, https://doi.org/10.1016/j.srs.2025.100212, 2025.

State Planet, 6-osr9, 8, 2025
https://doi.org/10.5194/sp-6-osr9-8-2025

Relationship between variations in sea bottom temperature and American lobster catch rate off southwestern Nova Scotia during 2008–2023

Adam M. Cook[1], Youyu Lu[1], Xianmin Hu[1], David Brickman[1], David Hebert[1], Chantelle Layton[1], and Gilles Garric[2]

[1]Fisheries and Oceans Canada, Bedford Institute of Oceanography, 1 Challenger Dr., Dartmouth, NS, B2Y 4A2, Canada
[2]Mercator-Ocean International, 2 Av. de l'Aérodrome de Montaudran, 31400 Toulouse, France

Correspondence: Youyu Lu (youyu.lu@dfo-mpo.gc.ca)

Received: 2 September 2024 – Discussion started: 18 November 2024
Revised: 23 January 2025 – Accepted: 24 January 2025 – Published: 30 September 2025

Abstract. American lobsters (*Homarus americanus*) are an iconic species and are the socioeconomic and cultural mainstay for many communities across Nova Scotia. Describing the changes in population biomass and providing annual stock assessment advice for this species are required for sustainable fisheries. In many areas the best information available for providing this advice comes from commercial fishery data. Often there is an assumed relationship between fishery performance (catch per unit effort; CPUE) and available biomass; however several studies indicate that this relationship can be affected by external factors such as sea bottom temperature. Including bottom temperature when developing a standardized CPUE index will potentially address these concerns; however it has proven difficult in the past due to the lack of readily available (near-real-time) and unbiased bottom temperature data at the spatial and temporal scales required. Here we explore a global ocean reanalysis product of the European Union Copernicus Marine Service with an application to the fishery catch data from Lobster Fishing Area 33 during 2008–2023. A comparison with observational data shows that this reanalysis product provides realistic variations in sea bottom temperatures in this region. Next, a hierarchical generalized linear modelling approach is applied to evaluate the relationship between within-season changes in lobster CPUE and sea bottom temperature. Positive relationships between the rates of change of two model parameters, during the first 60 d of the fishing season (from mid-November to mid-January), are found in the majority of the 10 subregions. A standardized CPUE index with the influence of bottom temperature included, compared to the index without such influence, explains a high percentage of the deviance of CPUE data and hence is more consistent with available stock biomass. The outcomes of the model evaluation and relationship analysis encourage further applications of multi-decadal ocean reanalysis products to understand past changes, as well as the development of ocean forecasts for predicting future changes in marine ecosystems and fisheries, a product with wide-reaching socioeconomic value.

1 Introduction

The Scotian Shelf (SS) is one of the regions of Atlantic Canada possessing highly valuable fishery resources. The fish population and fishery yields vary in both space and time, owing to multiple factors including changes in ocean conditions, which are known to affect fish bioenergetics and behaviour. For example, in the fishing areas of the snow crab (*Chionoecetes opilio*) on the western SS, Zisserson and Cook (2017) identified the adverse impacts of a significant positive anomaly of sea bottom temperature in 2011/2012 on the local population of some life stages of snow crabs, with juvenile stages being the most affected as they are less likely to migrate out of suboptimal conditions. Similar studies have

Published by Copernicus Publications.

Table 1. Data product reference table.

Product ref. no. and abbreviation	Product ID and type	Data access	Documentation
1: Logbooks	Estimates of daily catch per unit effort (CPUE; kilograms per trap haul) for 10 subregions of the Lobster Fishing Area 33 of the east coast of Canada, based on commercial fishing logbooks	Commercial Data Division, Maritimes Region, DFO	Cook et al. (2020)
2: GLORYS12v1	GLOBAL_MULTIYEAR_PHY_001_030, numerical models	EU Copernicus Marine Service Product (2023) https://doi.org/10.48670/moi-00021	Product User Manual (PUM): Drévillon et al. (2023a) Quality Information Document (QUID): Drévillon et al. (2023b) Journal article: Lellouche et al. (2021)
3: AZMP	Bottom temperature from the AZMP July survey	Government of Canada (2024) https://www.dfo-mpo.gc.ca/science/data-donnees/azmp-pmza/index-eng.html	DFO (2023); Hebert et al. (2024).
4: DFO Temp Database	A database of geo- and date-referenced observed bottom temperatures collected both systematically on DFO surveys and opportunistically through collaborations with the fishing industry	Population Ecology Division, Maritimes Region, DFO	

also been carried out for American lobster (*Homarus americanus*), another commercially important crustacean species in the region. The American lobster is an iconic species and is the socioeconomic and cultural mainstay for many communities across Nova Scotia. Describing the changes in American lobster population biomass and providing annual stock assessment advice are required for sustainable fisheries. In many areas the best information available for providing this advice comes from commercial fishery data, in particular fishery performance (catch per unit effort; CPUE; Cook et al., 2020). When relying on CPUE to provide stock advice, there is an assumed relationship with available biomass; however several studies have shown that this relationship can be affected by external factors such as the sea bottom temperature (Wright and Liu, 2024; Crossin et al., 1998) and improvements in vessel technology (bottom mapping, global positioning systems; Wiber and Barnett, 2023). Lobster fishery CPUE is affected by bottom temperature through the interaction of the passive trap-based fishery and lobster behaviour as lobster activity and digestion rates are influenced by temperature (McLeese, 1956; McLeese and Wilder, 1958). In warmer waters, lobsters are more active and digest faster thereby making them more susceptible to baited traps, leading to potentially higher CPUE independent of available biomass. In order to develop informative stock assessment advice incorporating bottom temperature two criteria must be met: (1) the bottom temperature information (from models or observations) should be available at appropriate spatial and temporal scales, unbiased (or able to be bias-corrected), and available in real time (or approximately real time) and (2) the relationship between bottom temperature and CPUE should be evaluated outside the stock assessment model and follow expected trends.

In previous studies on the relationship between the fishery performance and ocean conditions, sea bottom temperatures from both observation and numerical ocean models have been used. Ocean observations and models both possess strengths and weakness in depicting the complicated space–time variations in oceanic conditions of the SS, which are influenced by the strong multi-scale variability in atmospheric forcing at the surface and laterally from the Gulf of St. Lawrence, the Newfoundland Shelf, the Gulf Stream and the Labrador Current (e.g., Loder et al., 1998; Brickman et al., 2018). Observational data provide "ground-truthing" of ocean variations and are very valuable for model evaluation and bias correction but are often limited by sparseness in space and time. For example, the Atlantic Zonal Monitoring Program (AZMP) of Fisheries and Oceans Canada (DFO) conducts SS-wide surveys, but these were mainly in July with some complementary seasonal surveys along specific sections (e.g., DFO, 2023; Hebert et al., 2024). The results of high-resolution ocean models fill gaps in observational data but usually contain biases that need to be quantified and corrected. One systematic approach to reduce the model biases is the assimilation of observational data. This led to the creation of data-assimilative ocean reanalysis products, such as product reference number 2 (product ref. no. 2; Table 1). Due to the open-ocean nature of most observational data used for assimilation, the accuracy of the reanalysis products for shelf and coastal seas needs to be evaluated using available shelf and coastal observational data.

We explore a global ocean reanalysis product of the European Union Copernicus Marine Service to (1) examine the

relationship between lobster CPUE and sea bottom temperature on the SS and (2) develop a temperature-corrected standardized index of CPUE including seasonal and interannual changes in bottom temperature. The analysis focuses on Lobster Fishing Area 33 (LFA33; Fig. 1a) due to the availability of lobster CPUE data from different subregions in this area during 2008–2023. The sea bottom temperature is taken from product ref. no. 2 because of its high resolution and continuous coverage in space and time. This allows for examining the variations in the relationship among different subregions not previously detailed in studies. As discussed above, prior to delving into this analysis, the accuracy of product ref. no. 2 needs to be first evaluated with available observational data. Positive outcomes of the model evaluation and analysis could encourage further applications of multi-decadal ocean reanalysis products to reveal more linkages between variations in ocean conditions and marine ecosystems and fisheries. This could further encourage the development and improvement of ocean forecasts for predicting future changes in marine ecosystems and fisheries, a product with wide-reaching socioeconomic value.

2 Datasets

A number of datasets were used in this study. Commercial fishing logbooks (hereafter "Logbooks") provide the most detailed accounting of the spatial and temporal extent of effort and landings for commercial lobster fishing currently available. These logbooks are completed daily and submitted monthly to dockside monitoring companies for data entry and transmission to the Commercial Data Division of DFO. Logbooks contain fishing information including date fished, vessel registration number, fishing licence number and reporting grid number(s). For each day fished, grid number, effort (number of traps hauled) and estimated landings are provided. Based on the data in logbooks, we derive product ref. no. 1 (Table 1), which is the estimates of daily CPUE (kilograms per trap haul) for 10 different subregions of LFA33 (Fig. 1a).

Daily sea bottom temperature data on the Scotian Shelf from 1 January 1993 to 31 December 2023 are obtained from product ref. no. 2, which is a global ocean reanalysis available on a horizontal grid of $1/12°$ in longitude and latitude and with 50 vertical levels. Major ocean observational datasets are being assimilated to generate this data product (hereafter GLORYS12v1).

The observed bottom temperature is obtained from two products. Product ref. no. 3 is the July AZMP survey. Product ref. no. 4 is a geo- and date-referenced dataset of observed bottom temperatures collected both systematically on DFO surveys and opportunistically through collaborations with the fishing industry (Fig. 1a; solid red circles; hereafter "DFO Temp Database").

3 Analysis methods and results

3.1 Evaluation of modelled bottom temperature with observational data

Figure 2 presents the spatial distribution of bottom temperature anomalies in July from the AZMP survey (product ref. no. 3, with a certain level of horizontal interpolation being applied) and GLORYS12v1 reanalysis (product ref. no. 2), for the 5 selected years of 2008, 2012, 2015, 2022 and 2023. Focusing on the SS (east of 66° W), the spatial patterns and the magnitudes of anomalies during these years agree well. Among the 5 years, 2008 shows cold anomalies from the central deep basin (Emerald Basin) to the offshore bank (Western/Emerald Banks) and near the shelf break, with near-normal conditions along the coast. In 2012, significant warm anomalies occurred along the coast and the western part of the SS (up to 3 °C) and over the offshore bank, as well as near-normal conditions in the central basin. In 2015 and 2022, strong warm anomalies occurred in the eastern and western SS, respectively. In 2023, observations suggest moderate warm anomalies (about 1 °C) over two large areas in the eastern and western SS, while the reanalysis overestimated the magnitudes of temperature anomalies in the eastern SS. On the SS, similar patterns are found for other years during 1993–2023 (figures not shown).

The ocean model used to create the reanalysis does not include tides, so the agreement between the observational and reanalysis data on SS is possibly due to the generally weak tidal mixing in the region. In the Bay of Fundy (west of the SS) tides and tidal mixing are strong and the reanalysis data show larger discrepancy from observations, e.g., in 2022 and 2023. The differences in the impacts of tidal mixing on ocean temperatures, between the SS and Bay of Fundy, have been quantified using model sensitivity experiments by Wang et al. (2020).

Figure 3 presents the monthly time series of bottom temperature during 1993–2023 from the GLORYS12v1 reanalysis and the July values from AZMP observations during 1993–2023 for the 10 subregions for LFA33. Note that in regions 1–3 the observation are very limited and the observed July values are heavily influenced by the spatial interpolation. Based on reanalysis data, the seasonal variations are strong in subregions 1, 2 and 3 – along the coast with a maximum water depth of about 50 m. In these three subregions, depth–time sections of water temperature (figures not shown) demonstrate that (1) for January–March the whole water column is well-mixed and the impacts of surface cooling reach the bottom, resulting in a minimum bottom temperature near 0 °C; (2) in April–August the impacts of surface warming penetrate downward due to vertical diffusion, leading to a steady increase in bottom temperature; and (3) in September–October the ocean's surface heat loss results in strong mixing (convection) of the heat in upper layer through the whole water column, resulting in a maximum bottom temperature

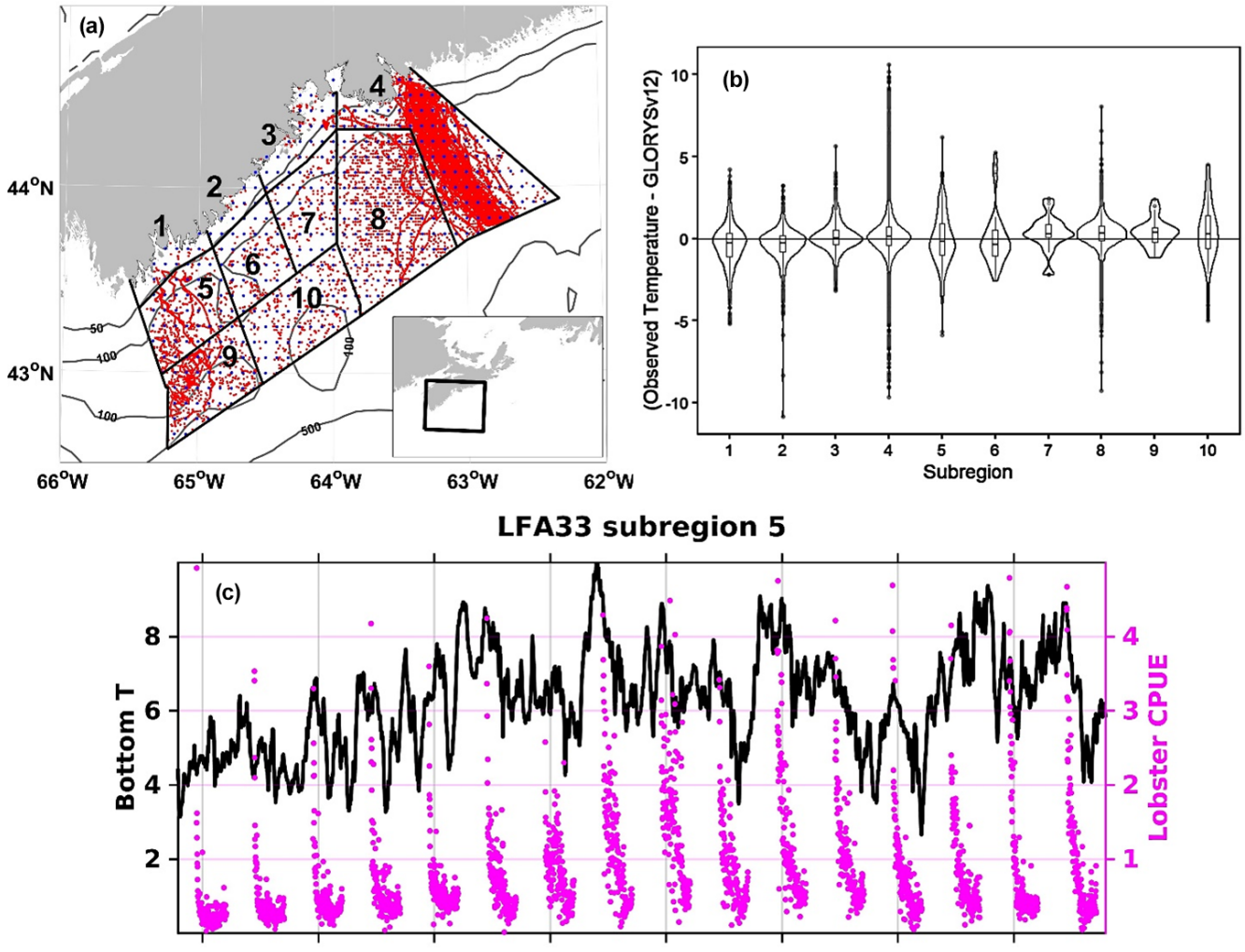

Figure 1. **(a)** The division of 10 subregions of LFA33 off southwestern Nova Scotia; the locations of observed bottom temperatures during the lobster fishing seasons of 2008–2023 (solid red circles); and the bathymetry contours of 50, 100 and 500 m. **(b)** Violin plots of observed bottom temperature during the commercial lobster fishing season (product ref. no 4) minus that extracted from reanalysis (product ref. no. 2) at matching times and grid points nearest to the observations for subregions 1 to 10. **(c)** Daily time series of bottom temperature from product ref. no. 2 (black curve) and the lobster CPUE (product ref. no. 1, solid magenta circles) during the lobster seasons of 2008–2023 in subregion 5.

of about 10 °C. The seasonal variations in bottom temperature are relatively weak in subregions 4–10 with water depths reaching ∼ 200 m. In these regions, depth–time sections of water temperature (figures not shown) show that in winter the impacts of surface cooling do not reach the bottom, and in summer and fall there exists a "cold intermediate layer" at depths of 50–100 m. This results in a weak fluctuation in monthly bottom temperature of around 5 °C throughout the year.

For all the 10 subregions, the reanalysis data show interannual variation in bottom temperature, accompanied by stronger or weaker seasonal variations. The interannual variations in July bottom temperatures, from the GLORYS12v1 reanalysis and AZMP observations, show high correlations (0.68–0.92) in subregions 4–10 with weaker seasonal variations. In subregions 1–3 with stronger seasonal variations, the correlation values (0.53–0.67) are relatively low but are still statistically significant. It is also notable that the reanalysis overestimates the observed July bottom temperature in subregions 1–3, while it slightly underestimates or obtains similar values as the observations in subregions 4–10.

Figure 1b compares the observed bottom temperature during the lobster fishing season (product ref. no. 4) and the corresponding values from the GLORYS12v1 reanalysis in the form of "violin plots". The observations are matched to the GLORYS12v1 data values by date and nearest-neighbour distances across each of the subregions within LFA33 during the lobster fishing season (December–May). The matching

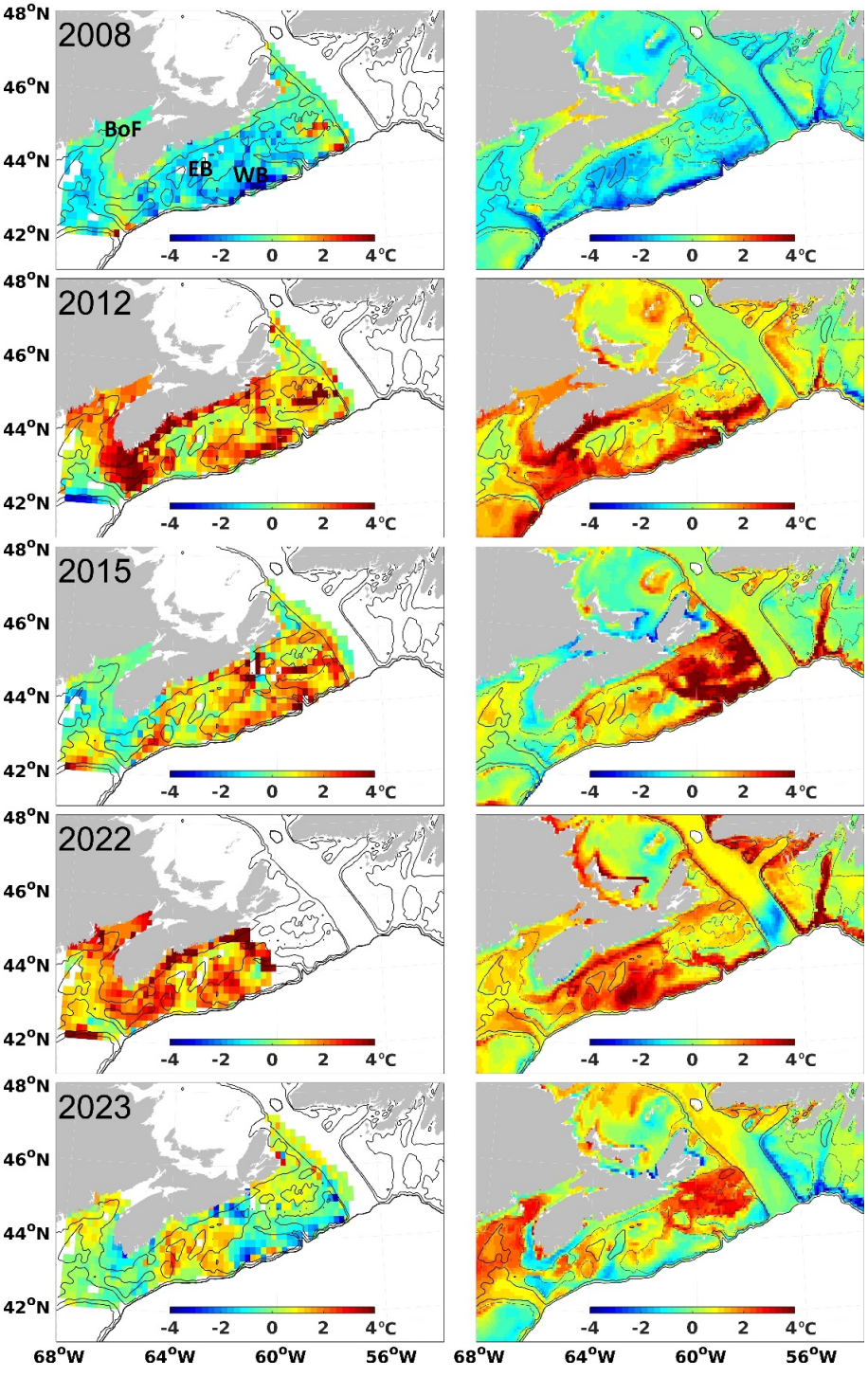

Figure 2. Spatial distributions of bottom temperature anomalies (°C) in July of 2008, 2012, 2015, 2022 and 2023 from (left) AZMP observations (product ref. no. 3) and (right) GLORYS12v1 reanalysis (product ref. no. 2) for regions with water depth less than 500 m. Bathymetry contours of 131 and 500 m are overlaid. "BoF", "EB" and "WB" in the top-left panel denote the locations of the Bay of Fundy, Emerald Basin and the Western/Emerald Banks, respectively. The temperature anomalies are referenced to the July average during 1991–2020 and 1993–2020 for data shown in the left and right columns, respectively.

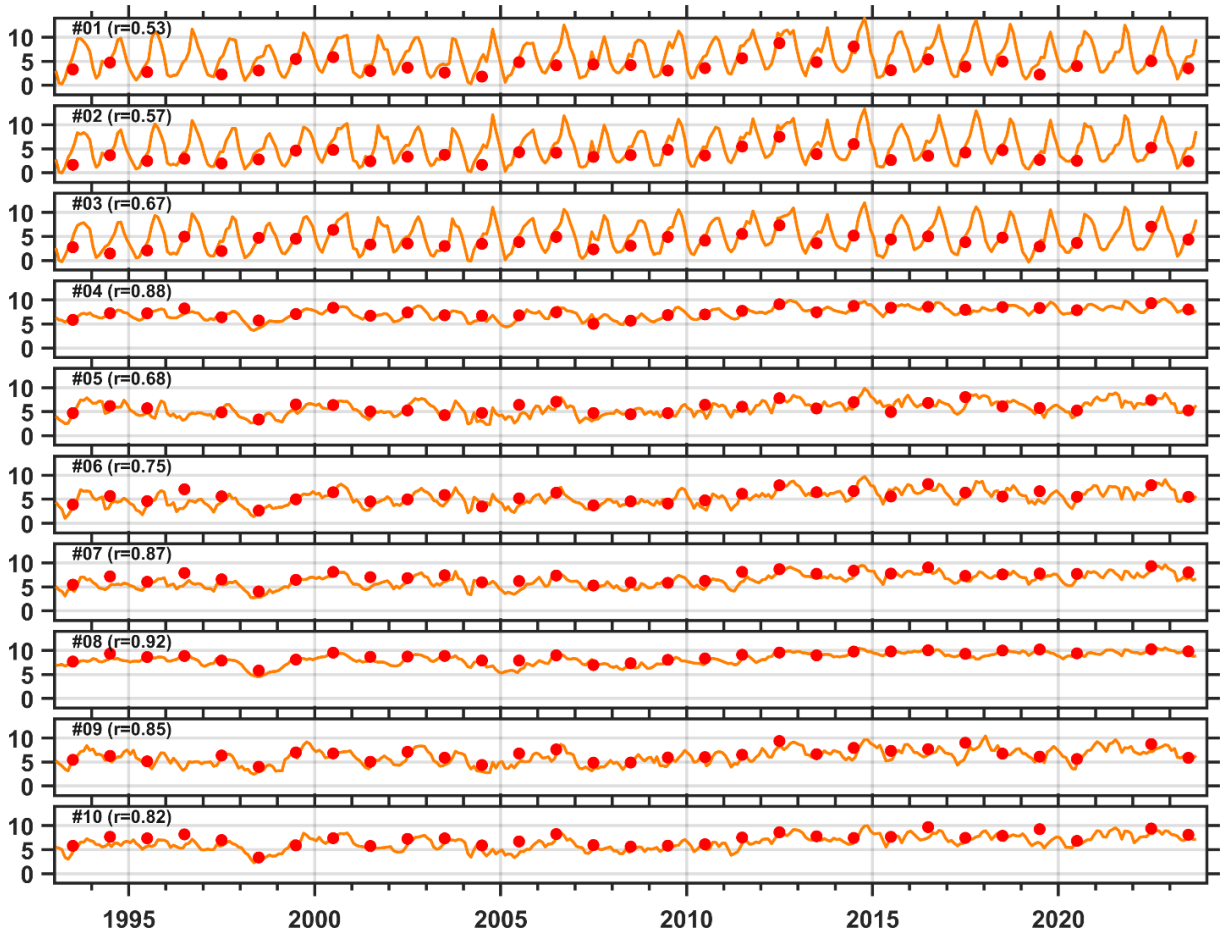

Figure 3. Bottom temperatures averaged for each of the 10 subregions of LFA33: (red curves) monthly time from reanalysis (product ref. no. 2) and (solid red circle) July values from observations (product ref. no. 3). The correlation coefficients between the modelled and observed July values are indicated by the r values in each panel.

requires the distance between an observation location and reanalysis grid to be less than 5 km. The overall median difference between observations ($n = 28\,794$) and the reanalysis is 0.13 °C. Bottom temperatures in the westernmost, inshore and mid-shore subregions (1, 2, 5 and 6) are lower in the observational data than the reanalysis (median difference −0.26 °C), whereas in the offshore and eastern subregions (3, 4, 7, 8, 9 and 10) the observational data are higher (median difference 0.18 °C). Although the median differences are quite low, point differences ranged between ±10 °C.

In summary, evaluations with available observational data suggest that space–time variations in bottom temperatures from GLORYS12v1 on the SS are quite realistic and are hence used to analyze the relationship between variations in bottom temperature and lobster CPUE in LFA33.

3.2 Relationship between variations in bottom temperature and lobster catch rate off southwestern Nova Scotia

Separate analyses are performed to explore (1) the relationship between the temperature changes within the fishing season and lobster CPUE and (2) the development of standardized CPUE indices with and without annual and seasonal bottom temperature corrections on the overall catch rate trends.

The first analysis focuses on the first 60 d of the fishing season (from mid-November to mid-January). As lobsters moult and grow during summer months, the lobster fishery in this area is considered a recruitment fishery (i.e., a large component of the fishery catch are lobsters having reached minimum legal size that year). As an example, Fig. 1c shows the time series of the lobster CPUE and bottom temperature in subregion 5 during 2008–2023. Prior to the fishing season the fishable biomass can be considered an unfished state and sea bottom temperatures remain high (from seasonal increases in spring and summer); hence the CPUE is maxi-

mized at the start of each fishing season. The CPUE rapidly decreases over the course of the first half of the fishing season (till mid-January) due to depletion (cumulative removal of individuals through harvesting) and the cooling of bottom water.

The decreasing rates of both CPUE and bottom temperature have interannual variations. The rate of CPUE change is assumed to be independent of the initial size of the harvestable lobster stock. Its relationship with the bottom temperature, if identified, indicates the impacts the interannual variations in bottom temperature on the fishery performance. Here we adopt a hierarchical generalized linear modelling (HGLM; Lee and Nelder, 1996) approach to explore such a relationship. In our analysis, different quantifications of the bottom temperature, e.g., the mean, median and rates of changes, have been tried. The highest correlation is found between the rates of change in bottom temperature and CPUE, and the HGLM analysis between them is formulated as follows.

$$C_i = \beta_0 + \alpha_{j[i]} + \left(\beta_1 + \gamma_{j[i]}\right) \mathrm{ST}_i + \varepsilon_i$$
$$\alpha_j \sim N(0, \sigma^2_{p,0})$$
$$\gamma_j \sim N(0, \sigma^2_{p,1})$$

For each subregion (j) and each year (i), the rates of changes in CPUE and bottom temperature are denoted as C_i and ST_i, respectively. The HGLM describes their relationship in each subregion and takes account of the random spatial effects on both the intercept β_0 and the slope β_1, denoted as $\alpha_{j[i]}$ and $\gamma_{j[i]}$, which are specified as a normal distribution (N) with mean 0 and variance $\sigma^2_{p,0}$ and $\sigma^2_{p,1}$ respectively.

The daily values of bottom temperature from GLORYS12v1, averaged for each subregion, are obtained, and then the rate of change (ST_i) is estimated through linear regression. For the CPUE, the logbook data can be variable in both the number of observations and the scale of fishing with time and in different subregions. Hence, in each subregion the rate of change in CPUE (C_i) over the first 60 d of each fishing season is estimated using weighted robust linear regression, with the total trap hauls being used as the weighting variable.

Positive relationships between C_i and ST_i are found in the majority of the subregions of LFA33 (Fig. 4). The annual values of C_i and ST_i are within confidence intervals of the HGLM-derived relationship obtained in subregions 1, 2, 3 and 6. This positive relationship is less evident in subregions 4 and 8, where the fishery is likely occurring in smaller areas of the subregions.

In the second analysis, two generalized additive models (GAMs; Wood, 2017) for standardizing lobster CPUE are developed, one as the "base-line" model without incorporating bottom temperature and the other as the "temperature-corrected" model, denoted as CM and CMT respectively. GAMs are chosen as they do not force a functional shape to the relationships (i.e., linear, quadratic) between dependent and independent variables; they rather use penalized splines (denoted as s) to allow flexible relationships. The CM model is

$$\mathrm{CPUE}_{ijk} = \beta_0 + s(D_{ijk}) + \beta_1 Y_{ij} + \varepsilon_{ijk},$$

and the CMT model is

$$\mathrm{CPUE}_{ijk} = \beta_0 + s(D_{ijk}) + s(T_{ijk}) + \beta_1 Y_{ij} + \varepsilon_{ijk},$$

where subscripts i and j represent the year and sub-region, and k represents the day of fishing season. In the above equations, D_{ijk} denotes the date corresponding to the day of the fishing season which varies with i, j and k; Y_{ij} represents the year variable that varies with i and j only; ε_{ijk} represents a random error term; and T_{ijk} is the bottom temperature included in the CMT model. We focus on the conditional predictions from both models for a fixed day 10 of the fishing season (when CPUE is the highest). For CMT, T_{ijk} is replaced by the catch-adjusted mean temperature across all years and all subregions on day 10 of the fishing season, calculated as

$$\mathrm{CA}_{10} = \frac{\sum \left(C_{ij10} \times T_{ijk10}\right)}{\sum C_{ij10}},$$

where C_{ij10} is the CPUE for day 10. The catch-adjusted mean temperature is used to account for the uneven distribution of the fishing effort and catch and thus to ensure that the predictions from CMT with the impacts of bottom temperature included can be meaningfully compared with the predictions of CM.

Figure 5 compares the annual time series of the standardized CPUE indices from CM and CMT on day 10 of the fishing season averaged for all the 10 subregions of LFA33. The deviance of CPUE data explained by CMT is 59.6 %, 5.8 % higher than 53.8 % by CM. Evident differences between the CM and CMT annual CPUE indices result from differences in bottom temperature: CPUE estimates from CM are higher than those from CMT in years when bottom temperatures are higher. Essentially, the temperature standardization accounts for the effects of warmer or cooler waters on the catch rates and thus improves the relationship between CPUE and fishable biomass.

4 Conclusions and discussions

The state-of-the-art ocean reanalysis (product ref. no. 2) is seen to provide the information required to develop better models describing changes in fishable biomass for American lobster stocks which will reduce uncertainty in fishery advice and potentially lead to more sustainable fisheries. This reanalysis product meets the criteria of being unbiased, being available in near-real time, and having sufficient spatial and temporal resolution. Due to complex regional oceanographic

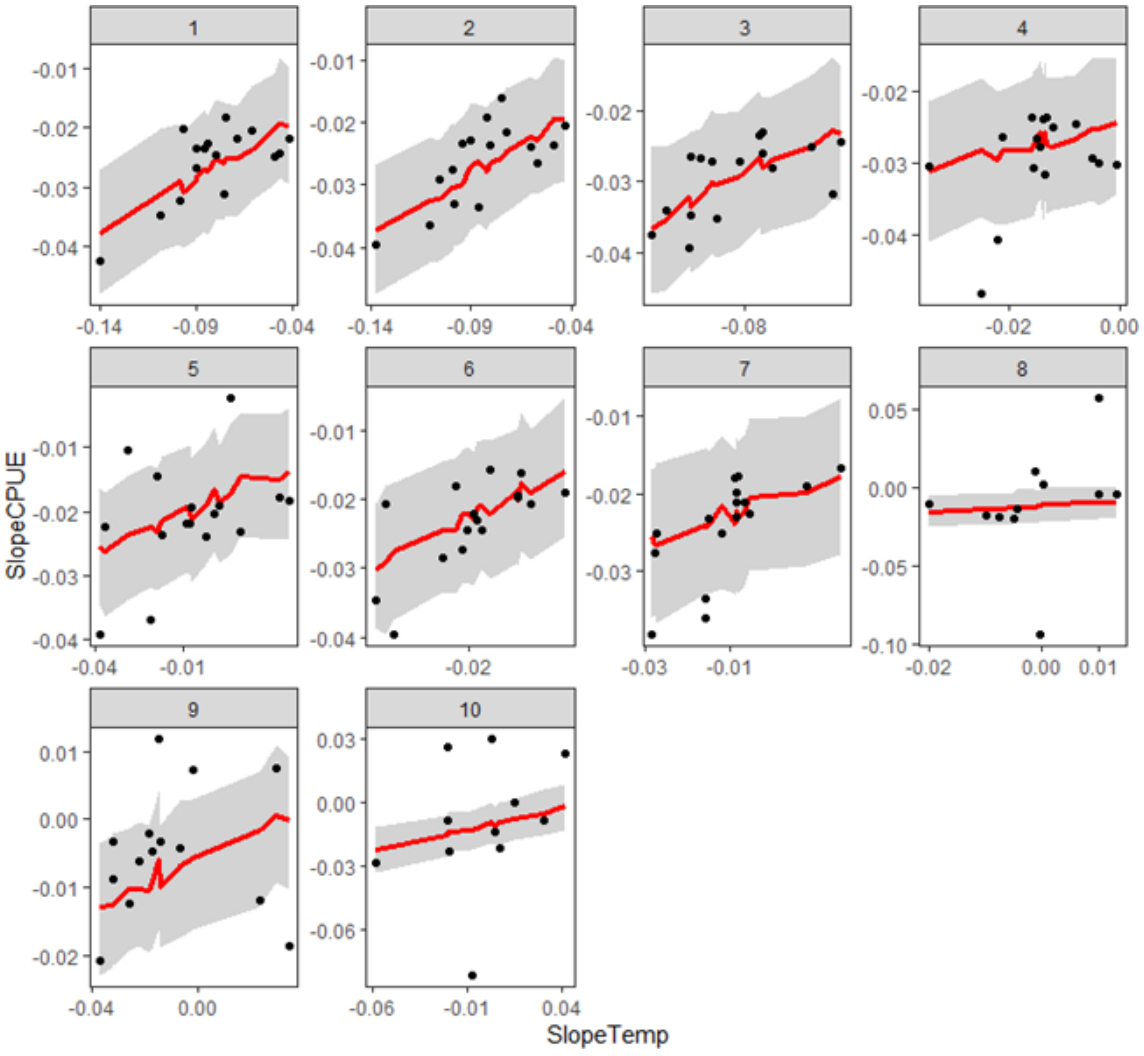

Figure 4. The slope of lobster CPUE (CPUE per day, y axis) versus slope of bottom temperature from GLORYS12v1 (°C d^{-1}, x axis) during the first 60 d of the fishing season in subregions 1–10 of LFA33. Dots represent data from different years, and the red lines are the relationship obtained by applying the HGLM approach, with the shading denoting the confidence intervals.

processes under the influence of various forcing factors, observational data are insufficient to fully quantify the space–time variations in ocean conditions on the Scotian Shelf and are even more sparse during the lobster fishing season from late autumn to early spring. In this study, evaluation shows that this data-assimilative reanalysis is able to reproduce the features of variations derived from available observations during 1993–2023 on the Scotian Shelf, where the influences of tidal mixing are relatively weak. The agreement is less satisfactory in the adjacent Bay of Fundy where tidal mixing is strong, while the ocean model used to generate the reanalysis does not include tidal mixing.

The evaluation results encourage the application of the reanalysis product to explore the relationship between the variations in sea bottom temperature and lobster catch rate within LFA33. Both lobster CPUE and bottom temperatures have strong seasonal variations, and the rapid decrease in CPUE during the first half of the season (mid-November to mid-January) can be partially described by the decreasing bottom temperature. Focusing on the CPUE changes during the initial 60 d of the fishing season (independent of stock size), a hierarchical generalized linear modelling approach (accounting for random spatial effects) is applied to explore the relationship between the rate changes in the CPUE and the rate of changes in the bottom temperature in the 10 subregions. Clear positive relationships between the two rates are found in the majority of the subregions. This relationship is consistent with the previous understanding that cold bottom temperature anomalies reduce the movement of lobsters and hence the catch rate. The relationship is strong in subregions 1, 2, 3 and 6 but is less tight in subregions 4 and 8, which can partially be attributed to the smaller spatial ex-

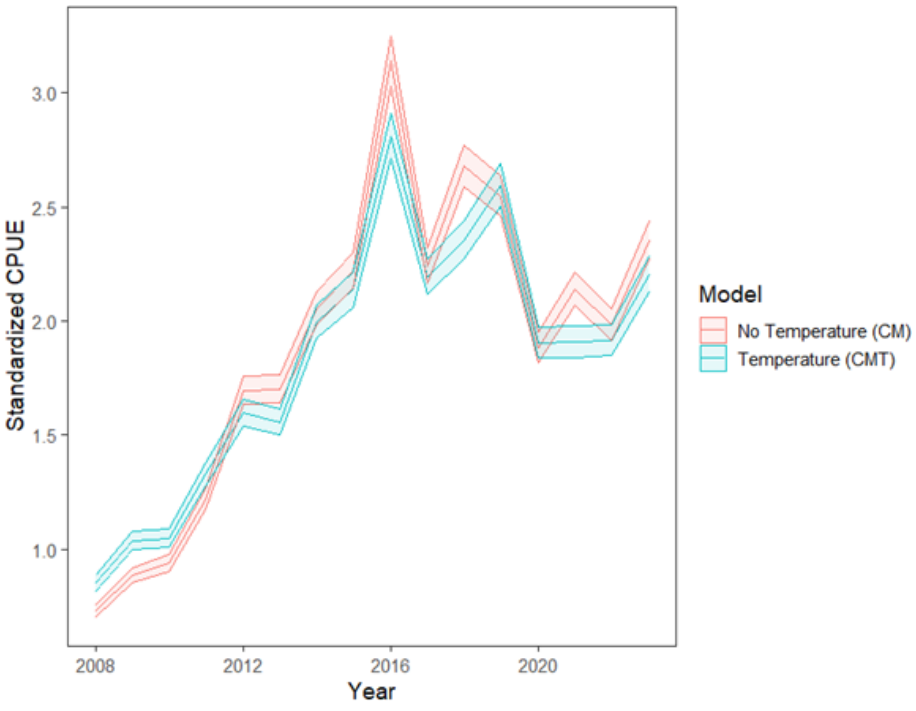

Figure 5. Modelled index of annual lobster CPUE for LFA33 with (blue) and without (red) bottom temperature as a predictor variable. The solid line represents mean effect, whereas shaded polygons represent the 95 % confidence bounds.

tent of fishing within those subregions. This result is congruent with previous reports which indicate that sea temperatures can play a role in fishery performance (e.g., Wright and Liu, 2024). Factors other than bottom temperatures (such as increases in fishing efficiency through advances in technology) also affect the relationship between CPUE and biomass. Though estimated values of CPUE indices will decrease during warm events and increase during cooling events, these other factors are more difficult to quantify and are likely unidirectional as the fishing industry strives to increase CPUE whenever possible. That said, the incorporation of bottom temperature effects on CPUE represents a valuable contribution to the development of stock assessment advice and an improved understanding of the dynamics of lobster populations.

Other quantitative measures of the lobster CPUE data (i.e., in different stages of the lobster fishing season) and their relationship with variations in sea bottom temperature will be further explored in ongoing studies. The outcomes of this model evaluation and relationship analysis encourage further applications of multi-decadal ocean reanalysis products to study changes in the marine ecosystems and fisheries. Furthermore, this also encourages the ongoing development and improvement of ocean forecasts for potentially predicting future changes in marine ecosystems and fisheries, a product with wide-reaching socioeconomic value.

Code and data availability. The data used in this study are available as described in Table 1. The code used in this study can be accessed via a GitLab repository upon request via email to the corresponding author.

Author contributions. AMC and YL led the conceptualization of the study and the writing of the manuscript. AMC contributed to the collection and compiling of lobster data and bottom temperature data during the lobster fishing season, the analysis on relationship between the lobster catch rate and bottom temperature, and the writing of the above aspects. XH carried out the evaluation of GLORYS12v1 with the AZMP survey data. DH and CL provided the AZMP data. All authors contributed to the conceptualization of the study and editing and reviewing the manuscript.

Competing interests. At least one of the (co-)authors is a member of the editorial board of *State of the Planet*. The peer-review process was guided by an independent editor, and the authors also have no other competing interests to declare.

Disclaimer. The Copernicus Marine Service offering is regularly updated to ensure it remains at the forefront of user requirements. In this process, some products may undergo replacement or renaming, leading to the removal of certain product IDs from our catalogue. If you have any questions or require assistance regarding these modifications, please feel free to reach out to our user support team for further guidance. They will be able to provide you with the

necessary information to address your concerns and find suitable alternatives, maintaining our commitment to delivering top-quality services.

Publisher's note: Copernicus Publications remains neutral with regard to jurisdictional claims made in the text, published maps, institutional affiliations, or any other geographical representation in this paper. While Copernicus Publications makes every effort to include appropriate place names, the final responsibility lies with the authors.

Acknowledgements. We appreciate DFO and Mercator Ocean International for supporting the scientific exchanges and collaboration between the staff of both organizations – in recent years under a collaborative agreement. Karina Von Schuckmann provided insightful comments and advice on developing the manuscript, and Nancy Soontiens and Ben Zisserson served as internal reviewers for the manuscript. Comments and suggestions from anonymous reviewers improved the quality and readability of the manuscript.

Review statement. This paper was edited by Pierre-Marie Poulain and reviewed by two anonymous referees.

References

Brickman, D., Hebert, D., and Wang, Z.: Mechanism for the recent ocean warming events on the Scotian Shelf of eastern Canada, Cont. Shelf Res., 156, 11–22, https://doi.org/10.1016/j.csr.2018.01.001, 2018.

Cook, A. M., Hubley, P. B., Denton, C., and Howse, V.: 2018 Framework Assessment of American Lobster (Homarus americanus) in LFA 27–33. DFO Can. Sci. Advis. Sec. Res. Doc. 2020/017, vi + 251 pp., https://waves-vagues.dfo-mpo.gc.ca/library-bibliotheque/40946204.pdf (last access: 21 August 2024), 2020.

Crossin, G. T., Al-Ayoub, S. H. Jury, S. H., Howell, W. H., and Watson, W. H.: Behavioral Thermoregulation in the American Lobster Homarus Americanus, J. Exp. Biol., 201, 365–374, https://doi.org/10.1242/jeb.201.3.365, 1998.

DFO: Oceanographic Conditions in the Atlantic Zone in 2022, DFO Can. Sci. Advis. Sec. Sci. Advis. Rep. 2023/019, https://waves-vagues.dfo-mpo.gc.ca/library-bibliotheque/41188792.pdf (last access: 15 August 2024), 2023.

Drévillon, M., Fernandez, E., and Lellouche, J. M.: EU Copernicus Marine Service Product User Manual for the Global Ocean Physics Reanalysis, GLOBAL_MULTIYEAR_PHY_001_030, Issue 1.5, Mercator Ocean International, https://catalogue.marine.copernicus.eu/documents/PUM/CMEMS-GLO-PUM-001-030.pdf (last access: 19 March 2024), 2023a.

Drévillon, M., Lellouche, J. M., Régnier, C., Garric, G., Bricaud, C., Hernandez, O., and Bourdallé-Badie, R.: EU Copernicus Marine Service Quality Information Document for the Global Ocean Physics Reanalysis, GLOBAL_MULTIYEAR_PHY_001_030, Issue 1.6, Mercator Ocean International, https://catalogue.marine.copernicus.eu/documents/QUID/CMEMS-GLO-QUID-001-030.pdf (last access: 19 March 2024), 2023b.

EU Copernicus Marine Service Product: Global Ocean Physics Reanalysis, Mercator Ocean International [data set], https://doi.org/10.48670/moi-00021, 2023.

Government of Canada: Atlantic Zone Monitoring Program (AZMP), Government of Canada [data set], https://www.dfo-mpo.gc.ca/science/data-donnees/azmp-pmza/index-eng.html, last access: 18 August 2024.

Hebert, D., Layton, C., Brickman, D., and Galbraith, P. S.: Physical Oceanographic Conditions on the Scotian Shelf and in the Gulf of Maine during 2023, Can. Tech. Rep. Hydrogr. Ocean Sci. 380, vi + 71 pp., https://publications.gc.ca/collections/collection_2024/mpo-dfo/Fs97-18-380-eng.pdf (last access: 18 August 2024.

Lee, Y. and Nelder, J. A.: Hierarchical Generalized Linear Models, J. Roy. Stat. Soc. B Met., 58, 619–56, https://doi.org/10.1111/j.2517-6161.1996.tb02105.x, 1996.

Lellouche, J. M., Greiner, E., Bourdallé-Badie, R., Garric, G., Melet. A., Drévillon, M., Bricaud, C., Hamon, M., le Galloudec, O., Regnier, C., Candela, T., Testut, C.-E., Gasparin, F., Ruggiero, G., Benkiran, M., Drillet, Y., and Le Traon, P.-Y.: The Copernicus Global 1/12° Oceanic and Sea Ice GLORYS12 Reanalysis, Front. Earth Sci. 9, 698876, https://doi.org/10.3389/feart.2021.698876, 2021.

Loder, J. W., Petrie, B., and Gawarkiewicz, G.: The coastal ocean off north- eastern North America: A large-scale view, in: The Sea, edited by: Robinson, A. R. and Brink, K. H., 11, Wiley, New York, 105–133, ISBN-13 978-0674017412, 1998.

McLeese, D. W.: Effects of Temperature, Salinity and Oxygen on the Survival of the American Lobster, J. Fish. Res. Board Can., 13, 247–72, https://doi.org/10.1139/f56-016, 1956.

McLeese, D. W. and Wilder, D. G.: The Activity and Catchability of the Lobster (Homarus americanus) in Relation to Temperature, J. Fish. Res. Board Can., 15, 1345–1354, https://doi.org/10.1139/f58-073, 1958.

Wang, Y., Sheng, J., and Lu, Y.: Examining tidal impacts on seasonal circulation and hydrography variability over the eastern Canadian shelf using a coupled circulation-ice regional model, Prog. Oceanogr., 189, 102448, https://doi.org/10.1016/j.pocean.2020.102448, 2020.

Wiber, M. G. and Barnett, A.: (Re)Assembling Marine Space: Lobster Fishing Areas under Conditions of Technological and Legal Change in Atlantic Canada, Sci. Technol. Hum. Val., 48, 500–524, https://doi.org/10.1177/01622439211042416, 2023.

Wood, S. N.: Generalized Additive Models: An Introduction with R, 2nd edn., Chapman & Hall/CRC, https://doi.org/10.1201/9781315370279, 2017.

Wright, D. and Liu, Y.: Assessing the Impact of Environmental Variability on Harvest in a Heterogeneous Fishery: A Case Study of the Canadian Lobster Fishery, Journal of Environmental Economics and Policy, 13, 55–69, https://doi.org/10.1080/21606544.2023.2207535, 2024.

Zisserson, B. and Cook, A.: Impact of bottom water temperature change on the southernmost snow crab fishery in the Atlantic Ocean, Fisheries Res., 195, 12–18, https://doi.org/10.1016/j.fishres.2017.06.009, 2017.

State Planet, 6-osr9, 9, 2025
https://doi.org/10.5194/sp-6-osr9-9-2025

Mediterranean marine heatwave 2023: ecosystem and fisheries impacts in Italian waters

Riccardo Martellucci[1], Francesco Tiralongo[2], Sofia F. Darmaraki[3], Michela D'Alessandro[1], Giorgio Mancinelli[4], Emanuele Mancini[4,5], Roberto Simonini[6], Milena Menna[1], Annunziata Pirro[1], Diego Borme[1], Rocco Auriemma[1], Marco Graziano[1], and Elena Mauri[1]

[1]Oceanography Section, National Institute of Oceanography and Applied Geophysics, Trieste, Italy
[2]Department of Biological, Geological and Environmental Sciences, University of Catania, Catania, Italy
[3]Foundation for Research and Technology Hellas, Heraklion, Greece
[4]Department of Biological and Environmental Sciences and Technologies, University of Salento, Lecce, Italy
[5]National Biodiversity Future Center (NBFC), Palermo, Itay
[6]Department of Life Sciences, University of Modena and Reggio Emilia, Modena, Italy

Correspondence: Riccardo Martellucci (rmartellucci@ogs.it) and Sofia F. Darmaraki (sofia.darmaraki@dal.ca)

Received: 30 August 2024 – Discussion started: 20 September 2024
Revised: 7 March 2025 – Accepted: 13 May 2025 – Published: 30 September 2025

Abstract. In 2023, the Mediterranean Sea experienced the longest recorded marine heatwave (MHW) in four decades, affecting marine biodiversity, fisheries and coastal livelihoods. In this study, we assess the effects of this extreme event on the spread of the invasive species *Callinectes sapidus* (Atlantic blue crab) and *Hermodice carunculata* (bearded fireworm) along the Italian coasts. We focus on the coastal area of the Po River Delta in the northern Adriatic and on the northern and southern coasts of Sicily and investigate to what extent the increased seawater temperatures contribute to the increase in the monthly biomass of these species. Considering that the spread of the Atlantic blue crab is responsible for significant economic losses in the shellfish fishery and that the spread of the bearded fireworm poses a health risk to the artisanal fishing industry, we also assess the socio-economic impact of this MHW by analysing fish market data and online surveys. Finally, we discuss possible strategies to mitigate the spread and ecological impact of these invasive species. We take into account the aggressive feeding behaviour of the fireworm and the thermophilic nature of the fireworm, whose toxic antennae also pose a health risk to humans. Overall, the sustainability of marine ecosystems and coastal communities in the Mediterranean requires robust interdisciplinary collaboration to address the challenges posed by biological invasions and climate change in this region.

1 Introduction

The Mediterranean Sea, one of the most biodiverse marine ecosystems in the world (Coll et al., 2010), is currently facing unprecedented challenges due to extreme temperature events caused by climate change, known as marine heatwaves (MHWs) (Darmaraki et al., 2019). In recent decades, the frequency, intensity and duration of these record-breaking episodes have increased in the region, mainly due to the mean sea surface temperature (SST) warming trend in the Mediterranean Sea, which ranges between 0.035–0.041 °C yr^{-1} (EU Copernicus Marine Service Information, 2022a), almost twice as high as the corresponding global SST trend of 0.015 ± 0.001 °C yr^{-1} (EU Copernicus Marine Service Information, 2022b). This has significant implications for the region's biodiversity and economy, as the warming trend and MHWs may facilitate the proliferation of invasive species (Joyce et al., 2024).

Species that pose a significant threat include the Atlantic blue crab, *Callinectes sapidus*, and the bearded fireworm, *Hermodice carunculata*, which have attracted attention due

Published by Copernicus Publications.

Table 1. Products used in the present work. Complete references for the articles in Prod. 1, Prod. 2, Prod. 3 and Prod. 6 are reported in the References.

Ref. no.	Product name & type	Documentation
Copernicus products		
1	Copernicus Marine SST_MED_SST_L4_REP_OBSERVATIONS_010_021 Mediterranean Sea – High Resolution L4 Sea Surface Temperature Reprocessed	Quality Information Document (QUID): Pisano et al. (2016, 2024a); Product User Manual (PUM): Pisano et al. (2024b)
2	Copernicus Marine MEDSEA_MULTIYEAR_PHY_006_004 Mediterranean Sea Physics reanalysis	Quality Information Document (QUID): Escudier al. (2022); Product User Manual (PUM): Lecci et al. (2022)
Non-Copernicus products		
3	Crab and clam fishery data	CONSORZIO COOPERATIVE PESCATORI DEL POLESINE Organizzazione di Produttori Soc. Coop. A r.l., Via della Sacca, 11 45018 Scardovari (RO) – ITALIA. P.IVA 00224140293
4	Worms Out questionnaire	Link: bit.ly/3L3TWUc https://www.facebook.com/MonitoraggioVermocane (last access: 7 February 2025)
5	Righi et al. (2020) questionnaire	https://doi.org/10.12681/mms.23117
6	iNaturalist	https://www.inaturalist.org/ (last access: 7 February 2025)

to their rapid spread and negative impact on Italian fisheries (e.g. Heilskov et al., 2006; Riera et al., 2014; Simonini et al., 2019; Righi et al., 2020; Bardelli et al., 2023; Tiralongo et al., 2023). In particular, *C. sapidus*, which is native to the Atlantic, has rapidly colonised the Italian coasts (Mancinelli et al., 2021). *C. sapidus* is characterised by its voracious predatory behaviour and opportunistic feeding habits (Mancinelli et al., 2021) and has led to considerable economic losses in shellfish fisheries and enormous challenges for native species (Clavero et al., 2022). Similarly, *H. carunculata*, a thermophilic polychaete, has spread in Italian waters, affecting artisanal fisheries by both ruining the catch and posing health risks to human health (Heilskov et al., 2006; Riera et al., 2014; Simonini et al., 2019; Righi et al., 2020; Tiralongo et al., 2023). In fact, *H. carunculata* with its toxic setae can cause painful stings in humans, leading to burns and redness upon physical contact and posing a health risk for tourists in coastal areas and for the fishing community, especially when cleaning nets (Tiralongo et al., 2023). In addition, *H. carunculata* is an ecological disruptor as well as a direct threat to the well-being of coastal communities. The resilience of both species to environmental stressors and the rapid spread of the population emphasise the urgency of addressing the intensifying risks of climate change and bioinvaders with comprehensive management strategies.

The year 2023 marked a turning point when average global air temperatures reached an unprecedented high (Copernicus, 2024). The European continent experienced its second warmest year on record, with the Mediterranean basin experiencing a series of extreme temperature events (Marullo et al., 2023). Of particular concern was the occurrence of the longest recorded and one of the strongest surface MHWs of the last four decades, which persisted in the northwestern Mediterranean from May 2022 to boreal spring 2023 (Marullo et al., 2023; Pirro et al., 2024). At its peak in July 2022, this MHW covered almost the entire western Mediterranean basin, with maximum daily SST anomalies reaching about 2.6 and 4.3 °C and anomalously warm conditions comparable to the 2003 summer MHW (Guinaldo et al., 2023). The long duration of the event was attributed to a combination of anomalously low wind speeds, high solar radiation and weak vertical mixing in the ocean (Marullo et al., 2023). These warming-related events had far-reaching impacts on marine life and coastal communities (He and Silliman, 2019).

The aim of this study is to investigate the spread and increase in the abundance of *C. sapidus* and *H. carunculata* associated with moderate and extreme warming in two coastal areas of Italy, particularly during the MHWs of 2022/2023. Relevant socio-economic impacts were also assessed by analysing fish market data and responses to questionnaires

handed out to the local fishing community and completed online, which addressed issues related to the bioinvasion of these species. In addition, we discuss possible solutions to mitigate the invasion of these species.

2 Methods

2.1 Study areas

The study was conducted in two different regions within Italian waters: two adjacent lagoons in the northern Adriatic Sea (Canarin and Scardovari) and two coastal areas of Sicily (Fig. 1).

2.1.1 The Po River Delta

The two lagoons studied in the northern Adriatic are transitional and shallow-water environments located in the Po River Delta and connected to the sea and various river branches (Fig. 1b and c). As they are directly influenced by the outflows of the Po River, these regions have highly dynamic hydro-morphological characteristics and are subject to rapid changes due to biotic and abiotic forces (Maicu et al., 2018; Franzoi et al., 2023). Although the lagoons are subject to various forms of anthropogenic pressure that have progressively altered their natural ecological characteristics (Franzoi et al., 2023), the lagoons support several mussel and oyster farms, which represent the main productive activities and vital economic resources at both local and regional level (Turolla, 2008; Bordignon et al., 2020; Chiesa et al., 2025). The Scardovari lagoon covers an area of 32 km^2, has an average depth of 1.5 m (Mistri et al., 2018), and is connected to the sea via two bays in the north-east and south-west of the basin. The Canarin lagoon covers an area of about 6.4 km^2 in the southern part of the study area and has an average depth of 0.9 m. It is connected to the Adriatic Sea by a shallow, approximately 200 m wide estuary with a maximum depth of 2.5 m.

2.1.2 Sicily

The island of Sicily (Fig. 1d) lies at the convergence of the eastern and western basins of the Mediterranean, which are influenced by both the relatively cooler Atlantic waters and the warmer Levantine waters. In particular, the eastern coast of Sicily (Ionian Sea) is significantly affected by quasidecadal reversals of the Northern Ionian Gyre driven by the mechanisms of the bimodal oscillation system in the Ionian Sea (Gačić et al., 2021; Menna et al., 2022). The distribution of water masses is altered by the bringing-in of warm and salty Levantine water during the cyclonic phase (anti-clockwise) and transportation of cooler Atlantic water during the anticyclonic phase (clockwise). This dynamic influences marine ecosystems and favours the occurrence of Levantine species during the cyclonic phase and vice versa (Civitarese et al., 2023). In comparison, the northern coast of Sicily (Tyrrhenian Sea) experiences less saline and relatively cooler Atlantic water flowing in through the Sardinian Channel (Vetrano et al., 2010), while the southern coast of Sicily is characterised by cold water due to semi-permanent upwelling (Raffa et al., 2017).

2.2 Biological characteristics of the two species

2.2.1 *Callinectes sapidus*

The Atlantic blue crab *C. sapidus* Rathbun, 1896 is a species native to the western coasts of the Atlantic Ocean and is naturally distributed from Nova Scotia to northern Argentina (Millikin and Williams, 1984). It was first recorded in Europe in 1901 and in the Mediterranean in 1947 (Mancinelli et al., 2021). The first record in Italian waters dates back to 1949 from the lagoon of Venice, and ballast water is considered the most likely cause (Nehring, 2011). In Mediterranean waters, *C. sapidus* is considered one of the 100 most invasive alien species (Zenetos et al., 2005; Katsanevakis et al., 2018; Tsirintanis et al., 2022) and is present in at least seven of the nine southern European marine ecoregions (Mancinelli et al., 2017a, b). In the last 10 years, it has rapidly expanded its range to new ecosystems throughout the Mediterranean, such as the European Atlantic waters of Portugal, France, Belgium and Germany but also in Italian waters (Tiralongo et al., 2021; Bardelli et al., 2023). This eurythermal and euryhaline species is a voracious predator characterised by aggressive behaviour, high fecundity, excellent swimming abilities and high fertility (Tsirintanis et al., 2022), and it inhabits lagoons, estuaries and other coastal environments. *C. sapidus* has a complex, biphasic life cycle consisting of marine planktonic larvae (zoea) and benthic postlarvae (megalopa), with juveniles and adults living in estuaries, lagoons and other coastal habitats (Lipcius et al., 2007). In marine waters, this species lives mainly on soft substrates at depths between 1 and 90 m. Their life cycle is very complex and includes different habitats depending on sex and ontogenetic stage: adults can reach a relatively large size, with a carapace up to 25 cm wide in males and 18 cm in females (Millikin and Williams, 1984), and reside in lagoons and estuaries where males settle and moult. After mating, the egg-laying females migrate to the sea where they lay their eggs. The young return to the transitional areas and, after rapid growth, reach sexual maturity in their second year of life (Millikin and Williams, 1984; Taylor and Fehon, 2021). *C. sapidus* exhibits opportunistic feeding behaviour and feeds mainly on fish and invertebrates, especially bivalves and polychaetes, and may consume detritus and macrophytes when other food sources are scarce (Mancinelli et al., 2017a; Tiralongo et al., 2024b). Recent studies in the Po River Delta have shown that *C. sapidus* significantly affects the aquaculture of *Ruditapes philippinarum* (Manila clam). Predation by *C. sapidus* resulted in mussel losses of up to 100 % in certain areas, with up to 56 % of

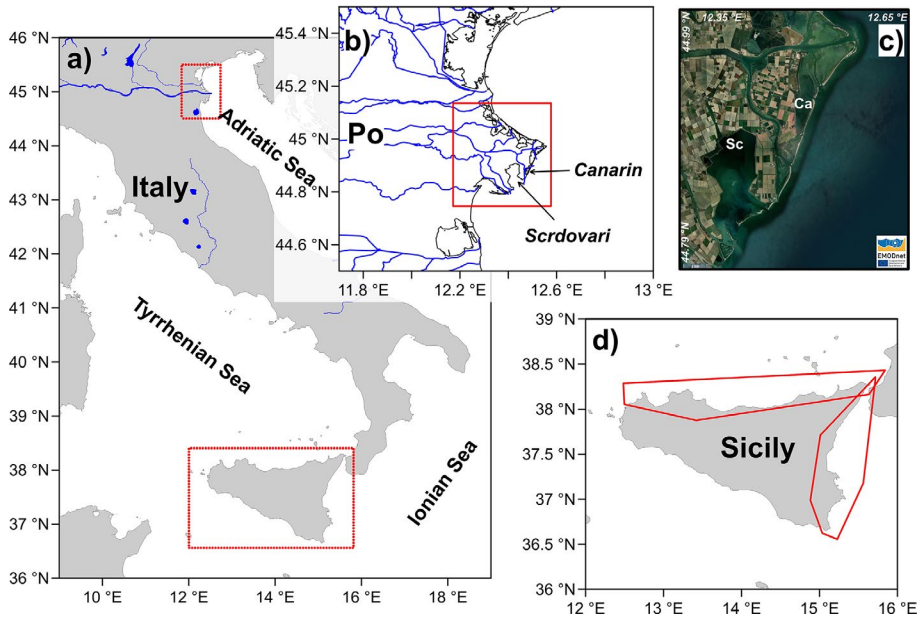

Figure 1. Map of Italy **(a)** with the two study areas highlighted in red boxes. The map shows the main water basins in the region, with the blue line indicating 10 m rivers and lakes (retrieved from https://www.naturalearthdata.com, last access: 7 February 2025). The Po River Delta **(b)** and a detailed enlargement of the Scardovari (Sc) and Canarin (Ca) are highlighted in panel **(c)** (maps were downloaded from the EMODnet Digital Bathymetry available at https://portal.emodnet-bathymetry.eu/, last access: 7 February 2025). The examined study (coastal) areas around Sicily **(d)**. For images of *C. sapidus* and *H. carunculata*, refer to Figs. S4 and S5.

mussel shells showing signs of predation and a complete absence of seeds in natural recruitment zones (Azzurro et al., 2024; Chiesa et al., 2025). Although several studies have been conducted on this species, the impacts and interactions of *C. sapidus* on native species and Mediterranean aquatic ecosystems are still poorly understood and require further investigation (Mancinelli et al., 2017b; Clavero et al., 2022).

2.2.2 *Hermodice carunculata*

The thermophilic amphinomid *H. carunculata* (Pallas, 1766), commonly known as the bearded fireworm, is a large predator/scavenger polychaeta found in warm and temperate areas of the Caribbean, Atlantic, Red Sea (Fishelson, 1971; Ahrens et al., 2013; Ramos and Schizas, 2023) and Mediterranean Sea (Simonini et al., 2018; Toso et al., 2022, 2024). Although it is native to the Mediterranean region, it is also considered a highly invasive species due to its increasing spread. Previous studies indicate that its abundance across the Mediterranean has increased in recent years, likely due to warmer temperatures favouring its northward spread (Righi et al., 2020; Toso et al., 2022). This may have a detrimental effect on the region's ecosystems and associated species, as well as human health, as it is resilient to natural and anthropogenic stressors (Schulze et al., 2017) and may also become a carrier of new pathogens (Sussman et al., 2003; Schulze et al., 2017). Similarly, coastal and anthropogenic activities such as fishing (Fig. S5 in the Supplement) and bathing can also be affected (Celona and Comparetto, 2010; Cosentino and Giacobbe, 2011; Schulze et al., 2017; Simonini et al., 2018; Righi et al., 2020; Toso et al., 2020; Tiralongo et al., 2023). *H. carunculata* can grow to over 70 cm in length and reach a lifespan of 9 years (Simonini and Ferri, 2022). Its metamers are equipped with dorsal calcareous chaetae filled with a venom that is very effective against predators (Kicklighter and Hay, 2006; Schulze et al., 2017; Simonini et al., 2018, 2021; Righi et al., 2021, 2022). The presence of these defence mechanisms makes the polychaete highly resistant to predators, as none of the species identified in the Mediterranean region are able to effectively prey on it (Ladd and Shantz, 2016; Righi et al., 2021; Simonini et al., 2021). In contrast, *H. carunculata* is a voracious predator of sessile and benthic invertebrates (Wolf and Nugues, 2013; Wolf et al., 2014; Jumars et al., 2015; Barroso et al., 2016; Schulze et al., 2017; Simonini et al., 2018; Righi et al., 2020), and its ability to regenerate favours its dispersal (Toso et al., 2024). In addition, this species is characterised by a remarkable dispersal ability, which is attributed to the production of planktotrophic and particularly long-lived larvae (Ahrens et al., 2013; Schulze et al., 2017; Toso et al., 2020). In Italian waters, *H. carunculata* is widespread on rocky substrates between 1 and 20 m (Righi et al., 2020; Simonini et al., 2021), but in some areas of the Mediterranean it reaches greater depths and has also been observed in association with coralligenous and precoralligenous bioformations (Fishelson, 1971; Righi et al., 2020).

2.3 Temperature datasets

To identify surface MHWs on the study areas we obtained daily SST data from the Mediterranean Sea SST Analysis L4 product of the Copernicus Marine Service, covering the period 1982–2023 (Table 1, product ref. 1). This dataset provides gap-free, optimally interpolated, satellite-based estimates of SST with a resolution of $0.05° \times 0.05°$. For the analysis of subsurface temperatures in the areas of interest, daily vertical temperature profiles were obtained from the Mediterranean Sea Physics Reanalysis dataset for the period from 1993 to 2023 (Table 1, product ref. 2) with a spatial resolution of $0.042° \times 0.042°$. MHWs are detected whenever the SST exceeds a daily, 40-year (1982–2023) climatological threshold for at least 5 consecutive days, based on the identification framework proposed by Hobday et al. (2016).

2.4 The crab and clam fishery data

To assess the impact of the spread of *C. sapidus* on the local fishing industry, we use data on the production of mussels (*Ruditapes philippinarum*) provided by the Scardovari and Canarin Cooperative, which has been farming this species in the Po River Delta for years. The dataset contains monthly values for waste and sales of *C. sapidus*, representing the sum of daily harvests by fishers before reaching the market for fish sales (Table 1, ref. 3). Recent studies in the area have shown that *C. sapidus* eats mussels, as evidenced by claw marks on the mussels. Compared to previous years, mussel production in 2023 has decreased by 75 % in the Scardovari lagoon and 100 % in the Canarin lagoon (Azzurro et al., 2024; Chiesa et al., 2025), which is why we use discard data as an indicator of *C. sapidus* biomass and damage to fisheries.

2.5 Questionnaire for *Hermodice carunculata*

In recent decades, citizen participation in the collection of data useful for science has increased thanks to numerous awareness-raising initiatives (Turrini et al., 2018) and has already been recognised as a valuable resource for research, biodiversity monitoring and conservation (Lopez et al., 2019; Toivonen et al., 2019). Although in some cases this information lacks a solid scientific basis and needs to be validated by experts in the field, it offers the advantage that it can be collected over wide geographical areas at low cost (Ballard et al., 2017; Tirelli et al., 2021; Sun et al., 2021). For this reason, citizen science projects are currently on the rise in various areas, particularly as a tool for solving environmental and conservation issues (Kullenberg and Kasperowski, 2016; Turrini et al., 2018). For example, citizen participation is widely used in projects and initiatives for the sighting of non-indigenous, invasive and rare species such as the *AlienFish* project (https://www.facebook.com/alienfish, last access: 10 February 2025), *avvistAPP* (https://www.avvistapp.it/, last access: 10 February 2025), *Monitoraggio Vermocane* (https://www.facebook.com/MonitoraggioVermocane) and *iNaturalist* (https://www.inaturalist.org/). To assess the impact of *H. carunculata* on human activities such as fishing and tourism, a questionnaire was developed and distributed to the fishing community as an online survey. The questionnaire, which builds on the observations of Righi et al. (2020), was distributed to a large number of people in 2023, who provided a total of 151 responses. It was primarily distributed via websites such as "Monitoraggio del Vermocane" and "Fauna Marina Mediterranea" (https://www.facebook.com/groups/230601830399549, last access: 10 February 2025) as well as via social media pages of various authors and also Italian diving centres. The questionnaire included 19 questions, of which 4 single-choice questions focusing on the frequency of sightings, the abundance of specimens and the perception of the species as a potential problem were analysed in this study. Most respondents reported having observed the fireworm while diving (74 %), spearfishing (10 %) and snorkelling (15 %), while no questions were asked about respondents' age or employment status. Due to its distinctive morphology and bright colouration, *H. carunculata* is unlikely to be confused with other species, as there are no comparable organisms in the Mediterranean. This study was carried out as part of the "Worms Out" project funded by the National Institute of Oceanography and Applied Geophysics and the ECCSEL NatLab Italy project (Table 1, ref. 5). In addition to the real-time data collected by marine users, the use of this questionnaire is important to identify and assess the occurrence of this species. This is to address the current lack of scientific reports on this species, which is probably due to the limited number of sampling efforts (e.g. Fraschetti et al., 2002; Giangrande et al., 2003; Corriero et al., 2004; Mastrototaro et al., 2010). To address the scarcity of scientific reports, we integrated observations from various sources such as the *iNaturalist* observations, the results of Righi et al. (2020) and the most recent observations from the 2023 online survey. Integrating this information with the scientific literature and observations is crucial for monitoring biological invasions and studying native invasive species (Azzurro et al., 2019; Giovos et al., 2019; Toivonen et al., 2019).

3 Results

3.1 Northern Adriatic

In the first half of 2023, mussel production in the area was around 400 t per month and peaked in August (800 t) before drastically declining from September to December (Fig. 2a). In contrast, the sale of crabs began in the summer months, with the highest discard observed in August 2023 with a total of 300 t. Towards the end of 2023, crab discards were comparable to sales (Fig. 2b). Throughout 2023, the study area in the northern Adriatic was also characterised by particularly high SSTs with six MHWs observed (Fig. 2c and d). The

first event occurred in March, lasted 5 d and had a moderate intensity, while the remaining events occurred during the summer and autumn seasons. The most intense MHW was observed at the end of August 2023 and was characterised by temperatures that were more than 3 °C above normal and lasted 11 d (Table S1 in the Supplement). The longest event was observed in October and lasted 36 d with a strong intensity (> 2.6 °C). The high temperatures of 2023 also affected the entire water column, with the strongest subsurface temperature anomalies (> 4 °C) observed between 4 m and 15 m depth during the summer season (Fig. 2d). This indicates a significant increase in subsurface temperatures in this area, as typical deviations from the 1993–2016 mean are between 0.8 and 1.2 °C (Fig. S1). Regarding the potential cumulative effects of temperature on the life cycle of *C. sapidus*, although the SST in 2023 was not below the threshold for hibernation (5 °C), it exceeded the temperatures for reproductive activity (10.8 °C) and larval development (19 °C) by 300 and 170 d, respectively (dashed lines in Fig. 2c).

3.2 Sicily

In the two coastal regions of northern and eastern Sicily, the SST remained above the climatological values throughout 2023 (Fig. 3b, c): eastern Sicily experienced three MHWs that lasted about 60 d in total (Table S1). The most intense event occurred in July and lasted 21 d, and the longest was in October with a duration of 30 d. On the north coast of Sicily, there were slightly longer MHWs on average: the first event occurred in March, lasted 5 d and had an intensity of 1.4 °C. The most intense MHW (> 2.5 °C) was observed between July and August with a duration of 25 d, while the longest event (49 d) occurred in autumn with an intensity of 1.6 °C. Compared to the period 1993–2016, temperatures in the entire water column in both regions were around 1.2–4 °C warmer than normal and even warmer on the north coast of Sicily. The upper 80 m of the water column shows the highest temperature anomalies (> 2 °C) throughout the year, especially in the autumn months (> 2.5 °C) in both areas. However, during some days in summer, the subsurface layers between 10 and 50 m depth show negative temperature anomalies (down to −2 °C) (Fig. 3d, e), with temperatures dropping below 14° at greater depths. Typically, subsurface temperatures deviate by about 0.8–2 °C from the 1993–2016 mean, with the highest values observed in the upper 20–80 m depth between June–November (Fig. S1). The progressive temperature increase of around 0.03 °C yr^{-1} observed on the north coast of Sicily seems to be consistent with an increasing trend in the records of *Hermodice carunculata* over the last 20 years, especially in 2007–2008, 2014–2015 and 2023, when the highest number of observations was recorded (Fig. 3a). This increasing trend is also supported by the results of our proposed questionnaire, which shows a significant increase in the frequency of sightings in recent years compared to 2018, particularly during recreational activities. In particular, the results of the questionnaire show that the presence of this species is increasingly recognised as a problem, particularly as *H. carunculata* is observed in areas where it was not previously seen (Fig. 3h and j). The data from the *Hermodice* questionnaire were compared with those from the iNaturalist platform (Table 1, ref. 6), and the two datasets showed similar observations, particularly in relation to the observed trend (Fig. 2a).

4 Discussion

The two Mediterranean regions analysed in the present study experienced multiple, prolonged and strong surface MHWs throughout 2023, with temperature anomalies ranging between 1.6–2.6 °C on the eastern and northern coasts of Sicily and between 2–3 °C on the northern Adriatic coast during the events. These events were associated with a general warming trend that was evident in increased monthly temperature anomalies occurring throughout the year, especially during summer in the northern Adriatic. Additionally, a trend of 0.03 °C per year was particularly evident in the sea surface temperature along the coast of northern Sicily during the period 2000–2023. Compared to the study areas in Sicily, the northern Adriatic showed a slightly stronger warming of the entire water column, which is probably due to its shallower depth. Also, lower-than-normal subsurface temperatures were observed in the upper 40 m of the two study areas in Sicily in summer and autumn. This is likely related to a stronger stratification of the upper ocean during these periods and a shift in the thermocline (see Figs. S2, S3), resulting in cooler temperatures near the surface, similar to what Pirro et al. (2024) observed. Overall, a significant warming was observed in all study areas in 2023, which in turn may have led to an increase in the abundance of the two invasive species in both areas.

In the case of *Callinectes sapidus*, the higher temperatures may have triggered a positive feedback loop in the phenology of the larval and adult stages, ultimately leading to higher survival and reproduction rates and driving the population increase (Costlow, 1967; Gencer, 2024). For marine invertebrates with complex life cycles, the effects of climate warming are particularly pronounced during critical stages (Libralato et al., 2015; Alter et al., 2024) such as larval development, reproductive activity or winter dormancy (dashed line in Fig. 2c). A similar mechanism has been proposed for other invasive crayfish such as *Hemigrapsus takanoi* as well as for other native brachyurans (Valdes et al., 1991; Anger, 2001; van den Brink et al., 2012; Oh and Lee, 2020). In this context, rising temperatures may have increased the invasiveness of the species in regions where established populations remained at low levels, as has been observed in the northern Adriatic Sea, where *C. sapidus* has been detected episodically since 1949 (Manfrin et al., 2016). Considering that in this species winter dormancy, adult reproduction and

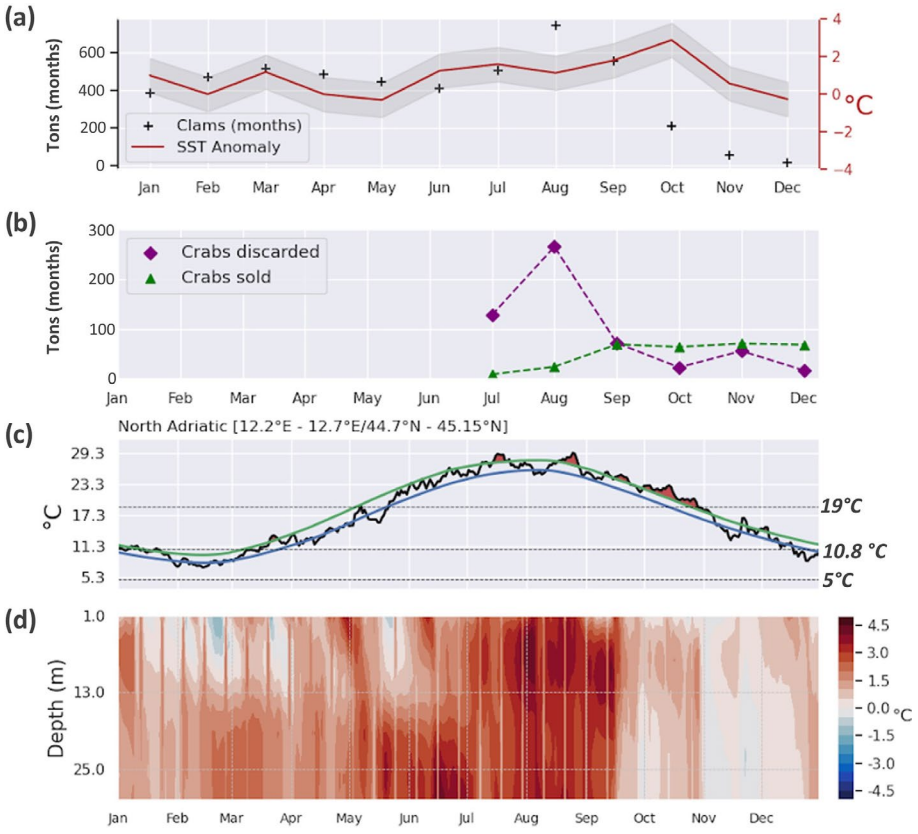

Figure 2. Northern Adriatic study area: **(a)** time series of daily, spatially averaged SST anomalies of 2023 relative to the period 1993–2016 (red line) and monthly evolution of sold clams (black cross). **(b)** Monthly evolution of sold (green triangles) and discharged (purple diamonds) *C. sapidus* during 2023. **(c)** Time series of daily, spatially averaged SST during 2023 (black), smoothed SST climatology (blue) and 90th percentile threshold of SST (green) based on the 1982–2023 period. MHWs are indicated in red and identified using the Hobday et al. (2016) definition. The three dashed lines represent the temperature thresholds for winter dormancy (5 °C), reproductive activity (10.8 °C) and larval development (19 °C) of *C. sapidus*. **(d)** Vertical profile of temperature anomalies during 2023, relative to the period 1993–2016, spatially averaged at each depth. Temperature data were obtained from Copernicus Marine Service (Table 1, product ref. 1, 2). Clams and crab data were obtained from the Consorzio Cooperative Pescatori del Polesine (Table 1, product ref. 3).

early life stages (egg maturation, zoea and megalopa development) are strongly regulated by temperature minima (Brylawsky and Miller 2006; Rogers et al., 2022; Schneider et al., 2024), an increase in water temperatures may have additionally accelerated metamorphosis from zoea to megalopa, reducing predation risk and promoting survival and ultimately population abundance. On the other hand, a further increase in temperature above 26 °C may have an opposite effect by reducing the number of moults per larva and causing a reduction in blue crab growth (Gencer, 2024).

An increase in water temperatures also accelerates development and growth rates in *Hermodice carunculata* (Libralato et al., 2015; Alter et al., 2024), and several studies identify water temperature as a decisive factor in the spread of the species (Righi et al., 2020; Tiralongo et al., 2023; Toso et al., 2024) by influencing the species range shifts and facilitating its establishment and spread (Stachowicz et al., 2002; Samperio-Ramos et al., 2015). Our questionnaires and iNaturalist observations confirm this spread and show a significant increase in sightings over the last 5 years. Our results are thus consistent with the documented increase in the presence of the species and its bathymetric extent over the last two decades, which coincides with a general increase in water temperatures along the coasts of Sicily (Pisano et al., 2020; Righi et al., 2020; Tiralongo et al., 2023; Kubin et al., 2023), which has been particularly evident since 2023 (Fig. 3a). Given the ongoing warming trend in the Mediterranean, it is likely that this thermophilic species will continue to spread along the north-western Mediterranean coast, where it was frequently observed in shallow-water conditions, especially in the summer months (Schulze et al., 2017; Encarnação et al., 2019; Righi et al., 2020). Noticeably, both the remarkable increase in the monthly biomass of *C. sapidus* in the coastal areas of the northern Adriatic and the annual records of *H. carunculata* on the coasts of Sicily share a number of common implications. In particular, we show that the prolif-

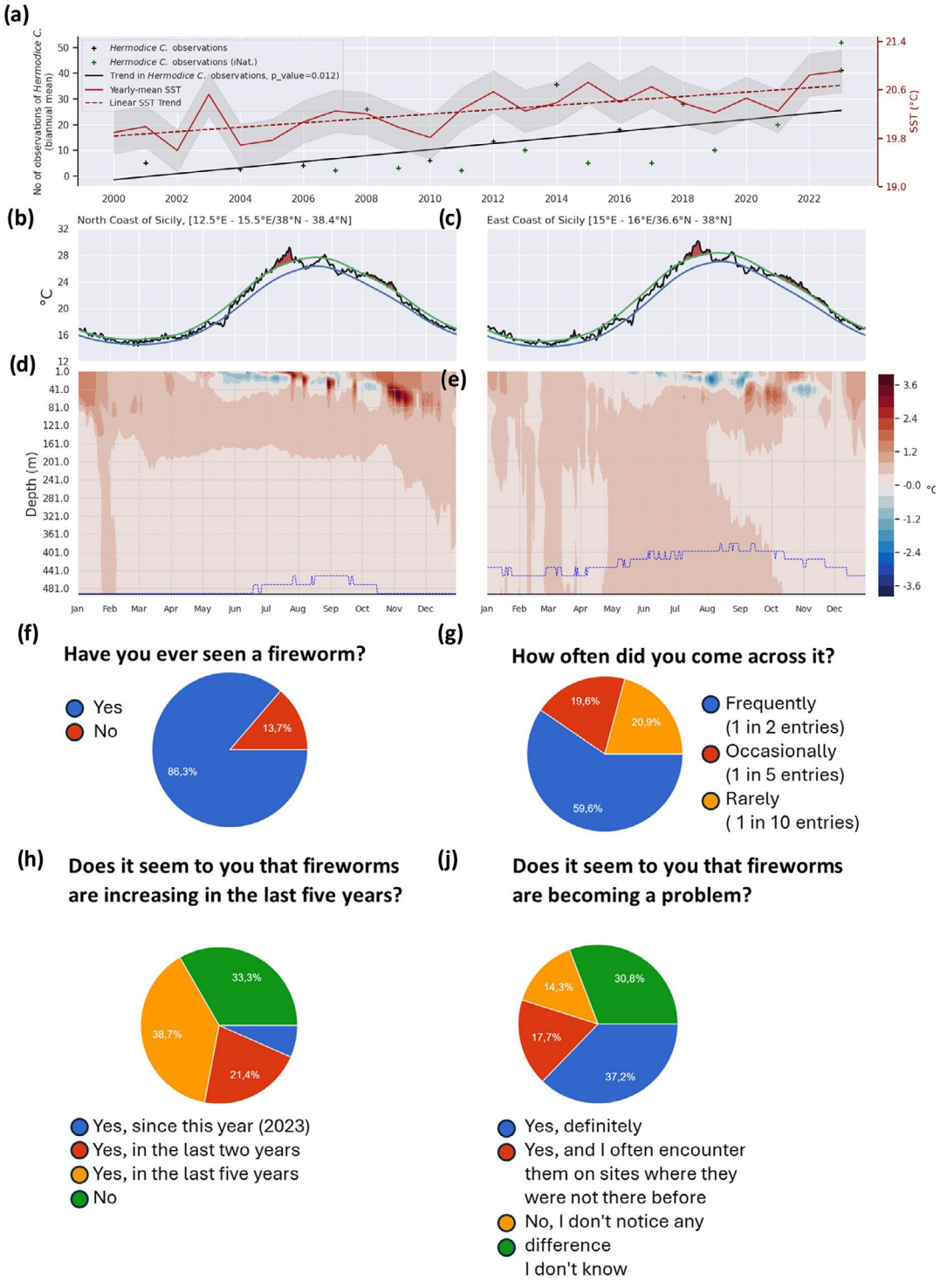

Figure 3. **(a)** Yearly-averaged time series and linear trend of SST (red), spatially averaged over the northern coast of Sicily, and yearly records of *H. carunculata* (black cross) with their linear trend, based on Righi et al. (2020) and our questionnaire for the period 2000–2023 (Table 1, product ref. 4 and 5); the green crosses represent the biannual mean of *H. carunculata* from iNaturalist. Daily and spatially averaged SST time series during 2023 (black), smoothed SST climatology (blue), and 90th percentile threshold of SST (green) based on the 1982–2023 period for the northern **(b)** and eastern **(c)** coasts of Sicily. MHWs are indicated in red and identified using the Hobday et al. (2016) definition. Vertical profile of spatially averaged temperature anomalies during 2023, relative to the climatological period of 1993–2016 for the northern **(d)** and eastern **(e)** coasts of Sicily. The climatological depth of the 14 °C isotherm is displayed by the dashed blue line, whereas the depth of the 14 °C isotherm during 2023 by the solid black line. **(f–j)** Main results of the Worms Out questionnaire (Table 1, product ref. 4). Temperature data were obtained from Copernicus Marine Service (Table 1, product ref. 1, 2).

eration of *C. sapidus* in the Po River Delta significantly disrupted mussel production in 2023 (Fig. S4) and that, under current conditions, no resurgence of mussel populations is expected in 2024 (Chiesa et al., 2025). The dramatic impact on the mussel fishery is exacerbated by the cost of removing the crabs discarded by the fishery (Fig. S4). This expansion is also expected to disrupt benthic habitats, altering community composition and leading to remarkable changes at the level of the entire food web, as observed in the Ebro River Delta (Clavero et al., 2022) and recently in the Po River Delta in the Goro lagoon (Gavioli et al., 2025).

Similarly, *H. carunculata* poses a threat to both marine biodiversity and the economic stability of local fisheries, as has been observed for other annelids (Berke et al., 2010; Pires et al., 2015). Although comprehensive information on the impact of the species has only recently been presented (Tiralongo et al., 2023), the fireworm is known to cause both direct and indirect damage to fisheries. Direct damage includes the severing of secondary lines attached to hooks, either by the worm's teeth or by hiding among the rocks after consuming the bait (Tiralongo et al., 2023). To minimise this impact on the target species, the soaking time of the fishing gear has been reduced, which leads to a decrease in catch rates (Simonini et al., 2021; Tiralongo et al., 2020). The scavenging activities of *H. carunculata* not only affect the efficiency of fisheries, but also impact the fishing industry by damaging fish catches and reducing the market value of fish. The economic impact is estimated at around EUR 7.32 kg^{-1} of damaged fish, resulting in significant annual losses given the total weight of commercially valuable catches (Tiralongo et al., 2023). The continued temperature-induced spread of *H. carunculata*, as observed in our results and documented by Righi et al. (2020) and Tiralongo et al. (2023), emphasises the urgent need for effective mitigation strategies to address the impacts caused by climate change on fisheries, tourism and the coastal economy.

Implication for human life and solutions for stakeholder

The ongoing invasion of *C. sapidus* provides an opportunity to evaluate strategies and measures to contain this spread and mitigate its ecological impact, even in freshwater ecosystems (Scalici et al., 2022; Tiralongo et al., 2024b, a; Bedmar et al., 2024). As the economic value of the species is already internationally recognised, this species can be used for both food and other purposes. Several studies have shown that overharvesting plays an important role in the control of invasive species (Mancinelli et al., 2017b; Giakoumi et al., 2019), as exemplified by the commercial harvest of *C. sapidus*, which supports a significant fishery on the coasts of the USA (Hines, 2007; Kennedy et al., 2007; Bunnell et al., 2010); accordingly, control measures should target similar commercialisation strategies. Despite its introduction to the Italian market, the consumption of *C. sapidus* is not yet widespread, complicating efforts to eradicate it (Azzurro et al., 2024). Effective management strategies should therefore include the cultural integration of this species. For example, the Italian government has promoted *C. sapidus* by showcasing it at the 2024 G7 summit and distributing online promotional content. Expanding outreach efforts through targeted events and educational campaigns could further boost consumption of this species, similar to what has been done successfully with other species. Furthermore, the extraction of chitosan and astaxanthin from crab shells could support the ongoing shellfish market while providing valuable compounds with multiple applications in pharmaceutical, biomedical, cosmetic, agricultural and biotechnological fields (Ambati et al., 2014; see also Demir et al., 2016, and Baron et al., 2017, for recent examples on *C. sapidus*).

Similarly, the increasing frequency of *H. carunculata* sightings emphasises the need for effective management strategies to contain its spread. As an efficient scavenger, predatory generalist and opportunistic consumer that can also feed on carrion, *H. carunculata* has also been found in large numbers under aquaculture net cages and in places with high anthropogenic pressure and organic enrichment, such as artisanal fishing harbours (Heilskov et al., 2006; Riera et al., 2014; Righi et al., 2020). Due to its ability to tolerate captivity, *H. carunculata* offers potential applications for the disposal of waste from the production and processing of marine products. Recent biorefinery research is investigating the use of *H. carunculata* in the processing of molluscan waste, particularly expired mussels from retail outlets, to recover and valorise the shells. Preliminary results show that *H. carunculata* consumes mussel meat at high rates and leaves the shells almost completely clean (Simonini et al., 2024). Given the ability to maintain them at high densities without substrate, the species could prove useful for the valorisation of waste shells, with clean shells serving as a source of "green" calcium carbonate (Seesanong et al., 2023). In addition, experiments could be conducted to determine the effectiveness of this species when used in IMTA (integrated multitrophic aquaculture) systems to determine its performance as a bioremediator organism (Giangrande et al., 2020). The development of practical applications for this invasive species could also support the elimination of areas where *H. carunculata* becomes a pest (Simonini et al., 2024).

Thus, the costs of managing and controlling invaded habitats may ultimately yield gains for the local population while greatly reducing the impact of the invader and even enhancing the ecosystem goods and services provided by coastal habitats. Collaborative efforts are essential to formulate adaptation measures that protect both marine ecosystems and the livelihoods of Mediterranean coastal communities. Through interdisciplinary collaboration and proactive management strategies, it is possible to mitigate the negative impacts of climate change and the spread of invasive species, thus ensuring the long-term sustainability of the Mediterranean marine environment and the well-being of coastal communities.

5 Conclusions

Overall, global warming and biological invasions in marine ecosystems are so far recognised to be closely linked, although the extent of their interactions and the role of climate change as a driving force remain controversial, as they vary along the invasion process and are influenced by species-specific responses to warming (Blackburn et al., 2011; Katsanevakis et al., 2014; Joyce et al., 2024). These responses affect the distribution, demography and life histories of invasive species. Currently, there is an urgent need for additional studies investigating the relationship between climate warming and the phenology of bioinvasive species to elucidate the indirect effects that may occur on both the distribution and abundance of the latter. The present study, focusing on *Callinectes sapidus* and *Hermodice carunculata*, is one of the first attempts to address this important issue in the Mediterranean. However, temperature alone may not be the only determinant of increases in invasive species abundance: for example, for *H. carunculata*, Simonini et al. (2021) suggest that fishing practices may facilitate the spread, establishment and survival of the species, with fish waste and other organic debris resulting from the cleaning of nets potentially providing increased trophic resource availability. In addition, releasing pregnant *C. sapidus* females after capture can significantly increase the number of larvae and increase populations (Hines et al., 2008). In the Po River Delta, this practise has become common among fishing companies given the low value of egg-laying females in local fish markets (Tiralongo, personal observation; see also Fig. S4). These examples illustrate how inadequate management practises can inadvertently favour the spread of invasive species and ultimately highlight the need for integrated control and mitigation strategies that take into account the diverse range of factors that can actually contribute to the success of a bioinvasion.

Code and data availability. The codes and data are available upon request to Annunziata Pirro (rmartellucci@ogs.it). Further information can also be found in Table 1.

Supplement. The supplement related to this article is available online at https://doi.org/10.5194/sp-6-osr9-9-2025-supplement.

Author contributions. RM, FT, SFD, MD'A, GM and EmM contributed to the original draft writing, conceptualisation, investigation, data curation and formal analysis. RM and SFD were also responsible for visualisation, while FT and SFD coordinated project management. MD'A provided additional resources, and GM contributed supervision. RS, MM, AP, DB, RA and MG were involved in review and editing, supporting investigation, data maintenance, resourcing, and validation. ElM also oversaw project administration and acquired funding.

Competing interests. The contact author has declared that none of the authors has any competing interests.

Disclaimer. Publisher's note: Copernicus Publications remains neutral with regard to jurisdictional claims made in the text, published maps, institutional affiliations, or any other geographical representation in this paper. While Copernicus Publications makes every effort to include appropriate place names, the final responsibility lies with the authors.

Acknowledgements. Sofia F. Darmaraki acknowledge the financial support from the Hellenic Foundation for Research and Innovation (HFRI) under the third call of the "Research projects to support Post-Doctoral Researchers" scheme, project number 7077, acronym TexMed. This work was partly funded by the ECCSEL-NatLab Italy project, made by the extraordinary MIUR contribution (FOE) for the participation of Italy in the activities related to the international ECCSEL infrastructure (European Carbon Dioxide Capture and Storage Laboratory Infrastructure), with the aim of developing and maintaining the natural laboratories of Panarea (Aeolian Islands) and Latera (Lazio).

The publication has been funded by EU – Next Generation EU Mission 4, Component 2 – CUP B53C22002150006 – Project IR0000032 – ITINERIS – Italian Integrated Environmental Research Infrastructures System.

Additional financial support was provided to Emanuele Mancini by the National Recovery and Resilience Plan (NRRP), Mission 4 Component 2 Investment 1.4 – Call for tender No. 3138 of 16 December 2021, rectified by Decree no. 3175 of 18 December 2021 of Italian Ministry of University and Research funded by the European Union – Next Generation EU Project code CN_00000033, Concession Decree No. 1034 of 17 June 2022 adopted by the Italian Ministry of University and Research, CUP D33C22000960007, Project title "National Biodiversity Future Center – NBFC".

Financial support. This research has been supported by the EU – Next Generation (grant nos. CUP B53C22002150006 and CUP D33C22000960007), the Hellenic Foundation for Research and Innovation (HFRI, project number 7077, TexMed), and the ECCSEL-NatLab Italy project.

Review statement. This paper was edited by Marta Marcos and reviewed by Rodrigo Riera and one anonymous referee.

References

Ahrens, J. B., Borda, E., Barroso, R., Paiva, P. C., Campbell, A. M., Wolf, A., Nugues, M. M., Rouse, G. W., and Schulze, A.: The curious case of *Hermodice carunculata* (Annelida: Amphinomidae): evidence for genetic homogeneity throughout the Atlantic Ocean and adjacent basins, Mol. Ecol., 22, 2280–2291, https://doi.org/10.1111/mec.12263, 2013.

Alter, K., Jacquemont, J., Claudet, J., Lattuca, M. E., Barrantes, M. E., Royer, C., Cormier, M., Ferrari, R., Cominassi, L., Crochelet,

E., Boudouresque, C. F., and Lejeusne, C.: Hidden impacts of ocean warming and acidification on biological response of marine animals revealed through meta-analysis, Nat. Commun., 15, 2885, https://doi.org/10.1038/s41467-024-47064-3, 2024.

Ambati, R. R., Phang, S. M., Ravi, S., and Aswathanarayana, R. G.: Astaxanthin: sources, extraction, stability, biological activities and its commercial applications – A review, Mar. Drugs, 12, 128–152, https://doi.org/10.3390/md12010128, 2014.

Anger, K.: The biology of decapod crustacean larvae, AA Balkema Publishers, Lisse, Vol. 14, 1–420, ISBN 9026518285, 2001.

Azzurro, E., Sbragaglia, V., Cerri, J., Bariche, M., Bolognini, L., Ben Souissi, J., and Moschella, P.: Climate change, biological invasions, and the shifting distribution of Mediterranean fishes: A large-scale survey based on local ecological knowledge, Glob. Change Biol., 25, 2779–2792, https://doi.org/10.1111/gcb.14724, 2019.

Azzurro, E., Bonanomi, S., Chiappi, M., De Marco, R., Luna, G. M., Cella, M., Guicciardi, S., Tiralongo, F., Bonifazi, A., and Strafella, P.: Uncovering unmet demand and key insights for the invasive blue crab (*Callinectes sapidus*) market before and after the Italian outbreak: Implications for policymakers and industry stakeholders, Mar. Policy, 167, 106295, https://doi.org/10.1016/j.marpol.2024.106295, 2024.

Ballard, H. L., Dixon, C. G., and Harris, E. M.: Youth-focused citizen science: Examining the role of environmental science learning and agency for conservation, Biol. Conserv., 208, 65–75, https://doi.org/10.1016/j.biocon.2017.01.021, 2017.

Bardelli, R., Mancinelli, G., Mazzola, A., and Vizzini, S.: The Atlantic blue crab *Callinectes sapidus* spreading in the Tyrrhenian sea: Evidence of an established population in the Stagnone di Marsala (Sicily, southern Italy), NAŠE MORE: znanstveni časopis za more i pomorstvo, 70, 177–183, https://doi.org/10.17818/NM/2023/SI6, 2023.

Baron, R. D., Pérez, L. L., Salcedo, J. M., Córdoba, L. P., and Sobral, P. J. d. A.: Production and characterization of films based on blends of chitosan from blue crab (*Callinectes sapidus*) waste and pectin from Orange (Citrus sinensis Osbeck) peel, Int. J. Biol. Macromol., 98, 676–683, https://doi.org/10.1016/j.ijbiomac.2017.01.061, 2017.

Barroso, R., Almeida, D., Contins, M., Filgueiras, D., and Dias, R.: *Hermodice carunculata* (Pallas, 1766) (Polychaeta: Amphinomidae) preying on starfishes, Mar. Biodivers., 46, 333–334, https://doi.org/10.1007/s12526-015-0394-9, 2016.

Bedmar, S., Oficialdegui, F. J., and Clavero, M.: Far-reaching blues: Long-distance migration of the invasive Atlantic blue crab, Aquat. Conserv., 34, e4136, https://doi.org/10.1002/aqc.4136, 2024.

Berke, S. K., Mahon, A. R., Lima, F. P., Halanych, K. M., Wethey, D. S., and Woodin, S.A.: Range shifts and species diversity in marine ecosystem engineers: Patterns and predictions for European sedimentary habitats, Global Ecol. Biogeogr., 19, 223–232, https://doi.org/10.1111/j.1466-8238.2009.00509.x, 2010.

Blackburn, T. M., Pyšek, P., Bacher, S., Carlton, J. T., Duncan, R. P., Jarošík, V., and Richardson, D. M.: A proposed unified framework for biological invasions, Trends Ecol. Evol., 26, 333–339, https://doi.org/10.1016/j.tree.2011.03.023, 2011.

Bordignon, F., Zomeño, C., Xiccato, G., Birolo, M., Pascual, A., and Trocino, A.: Effect of emersion time on growth, mortality and quality of Pacific oysters (*Crassostrea gigas*, Thunberg 1973) reared in a suspended system in a lagoon in Northern Italy, Aquaculture, 528, 735481, https://doi.org/10.1016/j.aquaculture.2020.735481, 2020.

Bunnell, D. B., Lipton, D. W., and Miller, T. J.: The bioeconomic impact of different management regulations on the Chesapeake Bay blue crab fishery, N. Am. J. Fish. Manage., 30, 1505–1521, https://doi.org/10.1577/M09-182.1, 2010.

Celona, A. and Comparetto, G.: Prime osservazioni sulla predazione opportunistica del "vermocane" *Hermodice carunculata* (Pallas, 1766), ai danni della piccola pesca artigianale nelle acque di Lampedusa (Is. Pelagie), Annali della Società Italiana di Scienze Naturali e del Museo Civico di Storia Naturale di Milano, 20, 15–20, http://www.dlib.si/details/URN:NBN:SI:DOC-YNXLVSYP (last access: 7 February 2025), 2010.

Chiesa, S., Petochi, T., Brusà, R. B., Raicevich, S., Cacciatore, F., Franceschini, G., Antonini, C., Vallini, C., Bernarello, V., Oselladore, F., Ciani, M., Di Blasio, L., Campolunghi, M. P., Baldessin, F., Boldrin, L., and Marino, G.: Impacts of the blue crab invasion on Manila clam aquaculture in Po Delta coastal lagoons (Northern Adriatic Sea, Italy), Estuar. Coast. Shelf Sc., 312, 109037, https://doi.org/10.1016/j.ecss.2024.109037, 2025.

Civitarese, G., Gačić, M., Batistić, M., Bensi, M., Cardin, V., Dulčić, J., and Menna, M.: The BiOS mechanism: history, theory, implications, Prog. Oceanogr., 216, 103056, https://doi.org/10.1016/j.pocean.2023.103056, 2023.

Clavero, M., Franch, N., Bernardo, R., López, V., Abelló, P., and Mancinelli, G.: Severe, rapid, and widespread impacts of an Atlantic blue crab invasion, Mar. Pollut. Bull., 176, 113479, https://doi.org/10.1016/j.marpolbul.2022.113479, 2022.

Coll, M., Piroddi, C., Steenbeek, J., Kaschner, K., Ben Rais Lasram, F., Aguzzi, J., and Voultsiadou, E.: The biodiversity of the Mediterranean Sea: estimates, patterns, and threats, PLOS ONE, 5, e11842, https://doi.org/10.1371/journal.pone.0011842, 2010.

Copernicus: 2023 is the hottest year on record, with global temperatures close to the 1.5 °C limit, Copernicus, https://climate.copernicus.eu/copernicus-2023-hottest-year-record (last access: 7 February 2025), 2024.

Corriero, G., Gherardi, M., Giangrande, A., Longo, C., Mercurio, M., and others: Inventory and distribution of hard bottom fauna from the marine protected area of Porto Cesareo (Ionian Sea): Porifera and Polychaeta, Ital. J. Zool., 71, 237–245, https://doi.org/10.1080/11250000409356578, 2004.

Cosentino, A. and Giacobbe, S.: The new potential invader *Linopherus canariensis* (Polychaeta: Amphinomidae) in a Mediterranean coastal lake: Colonization dynamics and morphological remarks, Mar. Pollut. Bull., 62, 236–245, https://doi.org/10.1016/j.marpolbul.2010.10.013, 2011.

Costlow, J. D.: The effect of salinity and temperature on survival and metamorphosis of megalops of the blue crab *Callinectes sapidus*, Helgoländ. Wiss. Meer., 15, 84–97, https://doi.org/10.1007/BF01618611, 1967.

Darmaraki, S., Somot, S., Sevault, F., Nabat, P., Cabos Narvaez, W. D., Cavicchia, L., and Sein, D. V.: Future evolution of marine heatwaves in the Mediterranean Sea, Clim. Dynam., 53, 1371–1392, https://doi.org/10.1007/s00382-019-04661-z, 2019.

Demir, D., Öfkeli, F., Ceylan, S., and Bölgen, N.: Extraction and characterization of chitin and chitosan from blue crab and synthesis of chitosan cryogel scaffolds, Journal of the

Turkish Chemical Society Section A: Chemistry, 3, 131–144, https://doi.org/10.28978/nesciences.970546, 2016.

Encarnação, J., Morais, P., Baptista, V., Cruz, J., and Teodósio, M. A.: New evidence of marine fauna tropicalization off the Southwestern Iberian Peninsula, Diversity, 11, 48, https://doi.org/10.3390/d11040048, 2019.

Escudier, R., Clementi, E., Nigam, T., Aydogdu, A., Fini, E., Pistoia, J., Grandi, A., and Miraglio, P.: EU Copernicus Marine Service Quality Information Docu ment for Mediterranean Sea Physics Reanalysis, MED SEA_MULTIYEAR_PHY_006_004, Issue 2.3, Mercator Ocean International, https://catalogue.marine.copernicus.eu/documents/QUID/CMEMS-MED-QUID-006-004.pdf (last access: 10 February 2025), 2022.

EU Copernicus Marine Service Information (CMEMS): Mediterranean Sea Surface Temperature time series and trend from Observations Reprocessing, Mercator Ocean International, Marine Data Store (MDS) [data set], https://doi.org/10.48670/moi-00268, 2022a.

EU Copernicus Marine Service Information (CMEMS): Global Ocean Sea Surface Temperature time series and trend from Observations Reprocessing, Marine Data Store (MDS) [data set], https://doi.org/10.48670/moi-00242, 2022b.

Fishelson, L.: Ecology and distribution of the benthic fauna in the shallow waters of the Red Sea, Mar. Biol., 10, 113–133, https://doi.org/10.1007/BF00354828, 1971.

Franzoi, P., Facca, C., Redolfi Bristol, S., Boschiero, M., Matteo, Z., and Scapin, L.: Application of the Habitat Fish Biological Index (HFBI) for the assessment of the ecological status of Po Delta lagoons (Italy), Italian Journal of Freshwater Ichthyology, 9, 91–106, https://iris.unive.it/handle/10278/5046422 (last access: 7 February 2025), 2023.

Fraschetti, S., Giangrande, A., Terlizzi, A., Miglietta, M. P., Della Tommasa, L., and Boero, F.: Spatio-temporal variation of hydroids and polychaetes associated with *Cystoseira amentacea* (Fucales: Phaeophyceae), Mar. Biol., 140, 949–958, https://doi.org/10.1007/s00227-001-0770-9, 2002.

Gačić, M., Ursella, L., Kovačević, V., Menna, M., Malačič, V., Bensi, M., Negretti, M.-E., Cardin, V., Orlić, M., Sommeria, J., Viana Barreto, R., Viboud, S., Valran, T., Petelin, B., Siena, G., and Rubino, A.: Impact of dense-water flow over a sloping bottom on open-sea circulation: laboratory experiments and an Ionian Sea (Mediterranean) example, Ocean Sci., 17, 975–996, https://doi.org/10.5194/os-17-975-2021, 2021.

Gavioli, A., Mancinelli, G., Turolla, E., Lanzoni, M., Paesanti, V., Soana, E., and Castaldelli, G.: Impacts of the invasive blue crab *Callinectes sapidus* on small-scale fisheries in a Mediterranean lagoon using fishery landing data, Sci. Total Environ., 974, 179236, https://doi.org/10.1016/j.scitotenv.2025.179236, 2025.

Gencer, Ö.: The impact of an abiotic variable, temperature, on larvae of the blue crab, *Callinectes sapidus* Rathbun, 1896 (Brachyura, Portunidae), Crustaceana, 97, 137–150, https://doi.org/10.1163/15685403-bja10239, 2024.

Giakoumi, S., Katsanevakis, S., Albano, P. G., Azzurro, E., Cardoso, A. C., Cebrian, E., and Sghaier, Y. R.: Management priorities for marine invasive species, Sci. Total Environ., 688, 976–982, https://doi.org/10.1016/j.scitotenv.2019.06.282, 2019.

Giangrande, A., Delos, A. L., Fraschetti, S., Musco, L., and Licciano, M.: Polychaete assemblages along a rocky shore on the South Adriatic coast (Mediterranean Sea): patterns of spatial distribution, Mar. Biol., 143, 1109–1116, https://doi.org/10.1007/s00227-003-1162-0, 2003.

Giangrande, A., Pierri, C., Arduini, D., Borghese, J., Licciano, M., Trani, R., Corriero, G., Basile, G., Cecere, E., Petrocelli, A., Stabili, L., and Longo, C.: An innovative IMTA system: Polychaetes, sponges and macroalgae co-cultured in a Southern Italian in-shore mariculture plant (Ionian Sea), Journal of Marine Science and Engineering, 8, 733, https://doi.org/10.3390/jmse8100733, 2020.

Giovos, I., Kleitou, P., Poursanidis, D., Batjakas, I., Bernardi, G., Crocetta, F., Doumpas, N., Kalogirou, S., Kampouris, T. E., Keramidas, I., Langeneck, J., and Azzurro, E.: Citizen-science for monitoring marine invasions and stimulating public engagement: a case project from the eastern Mediterranean, Biol. Invasions, 21, 3707–3721, https://doi.org/10.1007/s10530-019-02083-w, 2019.

Guinaldo, T., Voldoire, A., Waldman, R., Saux Picart, S., and Roquet, H.: Response of the sea surface temperature to heatwaves during the France 2022 meteorological summer, Ocean Sci., 19, 629–647, https://doi.org/10.5194/os-19-629-2023, 2023.

He, Q. and Silliman, B. R.: Climate change, human impacts, and coastal ecosystems in the Anthropocene, Curr. Biol., 29, R1021–R1035, https://doi.org/10.1016/j.cub.2019.08.042, 2019.

Heilskov, A. C., Alperin, M., and Holmer, M.: Benthic fauna bio-irrigation effects on nutrient regeneration in fish farm sediments, J. Exp. Mar. Biol. Ecol., 339, 204–225, https://doi.org/10.1016/j.jembe.2006.08.002, 2006.

Hines, A. H.: Ecology of Juvenile and Adult Blue Crabs, in: The Blue Crab: *Callinectes sapidus*, edited by: Kennedy, V. S. and Cronin, L. E., Maryland Sea Grant College, College Park, MD, 565–654, ISBN 978-0-943676-67-8, 2007.

Hines, A. H., Johnson, E. G., Young, A. C., Aguilar, R., Kramer, M. A., Goodison, M., and Zohar, Y.: Release strategies for estuarine species with complex migratory life cycles: stock enhancement of Chesapeake blue crabs (*Callinectes sapidus*), Rev. Fish. Sci., 16, 175–185, https://doi.org/10.1080/10641260701678090, 2008.

Hobday, A. J., Alexander, L. V., Perkins, S. E., Smale, D. A., Straub, S. C., Oliver, E. C. J., Benthuysen, J. A., Burrows, M. T., Donat, M. G., Feng, M., Holbrook, N. J., Moore, P. J., Scannell, H. A., Sen Gupta, A., and Wernberg, T.: A hierarchical approach to defining marine heatwaves, Prog. Oceanogr., 141, 227–238, https://doi.org/10.1016/j.pocean.2015.12.014, 2016.

Joyce, P. W. S., Tong, C. B., Yip, Y. L., and Falkenberg, L. J.: Marine heatwaves as drivers of biological and ecological change: implication of current research patterns and future opportunities, Mar. Biol., 171, 20, https://doi.org/10.1007/s00227-023-04340-y, 2024.

Jumars, P. A., Dorgan, K. M., and Lindsay, S. M.: Diet of worms emended: an update of polychaete feeding guilds, Annu. Rev. Mar. Sci., 7, 497–520, https://doi.org/10.1146/annurev-marine-010814-020007, 2015.

Katsanevakis, S., Wallentinus, I., Zenetos, A., Leppäkoski, E., Çinar, M. E., Oztürk, B., Grabowski, M., Golani, D., and Cardoso, A. C.: Impacts of invasive alien marine species on ecosystem services and biodiversity: a pan-European review, Aquat. Invasions, 9, 391–423, https://doi.org/10.3391/ai.2014.9.4.01, 2014.

Katsanevakis, S., Rilov, G., and Edelist, D.: Impacts of marine invasive alien species on European fisheries and aquaculture–plague or boon?, CIESM Monograph, 50, 125–132, 2018.

Kennedy, V. S., Oesterling, M., and Van Engel, W. A.: History of Blue Crab Fisheries on the US Atlantic and Gulf Coasts, in: The Blue Crab: Callinectes sapidus, edited by: Kennedy, V. S. and Cronin, L. E., Maryland Sea Grant College, 655–710, ISBN 978-0-943676-67-8, 2007.

Kicklighter, C. E. and Hay, M. E.: Integrating prey defensive traits: contrasts of marine worms from temperate and tropical habitats, Ecol. Monogr., 76, 195–215, https://doi.org/10.1890/0012-9615(2006)076[0195:IPDTCO]2.0.CO;2, 2006.

Kubin, E., Menna, M., Mauri, E., Notarstefano, G., Mieruch, S., and Poulain, P. M.: Heat content and temperature trends in the Mediterranean Sea as derived from Argo float data, Front. Mar. Sci., 10, 1271638, https://doi.org/10.3389/fmars.2023.1271638, 2023.

Kullenberg, C. and Kasperowski, D.: What is citizen science? – A scientometric meta-analysis, PLOS ONE, 11, e0147152, https://doi.org/10.1371/journal.pone.0147152, 2016.

Ladd, M. C. and Shantz, A. A.: Novel enemies–previously unknown predators of the bearded fireworm, Front. Ecol. Environ., 14, 342–343, https://doi.org/10.1002/fee.1310, 2016.

Lecci, R., Drudi, M., Grandi, A., Cretì, S., and Clementi, E.: EU Copernicus Marine Service Product User Manual for For Mediterranean Sea Physics Reanalysis, MED SEA_MULTIYEAR_PHY_006_004, Issue 2.3, Mercator Ocean International, https://catalogue.marine.copernicus.eu/documents/PUM/CMEMS-MED-PUM-006-004.pdf (last access: 10 February 2025), 2022.

Libralato, S., Caccin, A., and Pranovi, F.: Modeling species invasions using thermal and trophic niche dynamics under climate change, Front. Mar. Sci., 2, 29, https://doi.org/10.3389/fmars.2015.00029, 2015.

Lipcius, R. N., Eggleston, D. B., Heck, K. L., Seitz, R. D., and Van Montfrans, J.: The Blue Crab: *Callinectes sapidus*, edited by: Kennedy, V. S. and Cronin, L. E., Maryland Sea Grant College, 535–564, ISBN 978-0-943676-67-8, 2007.

Lopez, B. E., Magliocca, N. R., and Crooks, A. T.: Challenges and Opportunities of Social Media Data for Socio-Environmental Systems Research, Land, 8, 107, https://doi.org/10.3390/land8070107, 2019.

Maicu, F., De Pascalis, F., Ferrarin, C., and Umgiesser, G.: Hydrodynamics of the Po River-Delta-Sea System, J. Geophys. Res.-Oceans, 123, 6349–6372, https://doi.org/10.1029/2017JC013601, 2018.

Mancinelli, G., Alujević, K., Guerra, M. T., Raho, D., Zotti, M., and Vizzini, S.: Spatial and seasonal trophic flexibility of the Atlantic blue crab *Callinectes sapidus* in invaded coastal systems of the Apulia region (SE Italy): a stable isotope analysis, Estuar. Coast. Shelf Sc., 198, 421–431, https://doi.org/10.1016/j.ecss.2017.10.013, 2017a.

Mancinelli, G., Chainho, P., Cilenti, L., Falco, S., Kapiris, K., Katselis, G., and Ribeiro, F.: The Atlantic blue crab *Callinectes sapidus* in southern European coastal waters: Distribution, impact and prospective invasion management strategies, Mar. Pollut. Bull., 119, 5–11, https://doi.org/10.1016/j.marpolbul.2017.03.024, 2017b.

Mancinelli, G., Bardelli, R., and Zenetos, A.: A global occurrence database of the Atlantic blue crab *Callinectes sapidus*, Scientific Data, 8, 111, https://doi.org/10.1038/s41597-021-00879-x, 2021.

Manfrin, C., Comisso, G., Dall'Asta, A., Bettoso, N., and Sook Chung, J.: The return of the Blue Crab, *Callinectes sapidus* Rathbun, 1896, after 70 years from its first appearance in the Gulf of Trieste, northern Adriatic Sea, Italy (Decapoda: Portunidae), Check List, 12, 1–7, https://doi.org/10.15560/12.6.2006, 2016.

Marullo, S., Serva, F., Iacono, R., Napolitano, E., di Sarra, A., Meloni, D., and Santoleri, R.: Record-breaking persistence of the 2022/23 marine heatwave in the Mediterranean Sea, Environ. Res. Lett., 18, 114041, https://doi.org/10.1088/1748-9326/acfdbc, 2023.

Mastrototaro, F., d'Onghia, G., Corriero, G., Matarrese, A., and Maiorano, P.: Biodiversity of the white coral bank off Cape Santa Maria di Leuca (Mediterranean Sea): An update, Deep-Sea Res. Pt. II, 57, 412–430, https://doi.org/10.1016/j.dsr2.2009.10.010, 2010.

Menna, M., Gačić, M., Martellucci, R., Notarstefano, G., Fedele, G., Mauri, E., and Poulain, P. M.: Climatic, Decadal, and Interannual Variability in the Upper Layer of the Mediterranean Sea Using Remotely Sensed and In-Situ Data, Remote Sens., 14, 1322, https://doi.org/10.3390/rs14061322, 2022.

Millikin, M. R. and Williams, A. B.: Synopsis of biological data on blue crab, *Callinectes sapidus* Rathbun, FAO Fisheries Synopsis, 38, https://repository.library.noaa.gov/view/noaa/5574 (last access: 10 February 2025), 1984.

Mistri, M., Borja, A., Aleffi, I. F., Lardicci, C., Tagliapietra, D., and Munari, C.: Assessing the ecological status of Italian lagoons using a biomass-based index, Mar. Pollut. Bull., 126, 600–605, https://doi.org/10.1016/j.marpolbul.2017.09.048, 2018.

Nehring, S.: Invasion History and Success of the American Blue Crab *Callinectes sapidus* in European and Adjacent Waters, in: In the Wrong Place – Alien Marine Crustaceans: Distribution, Biology and Impacts, edited by: Galil, B. S., Clark, P. F., and Carlton, J. T., Invading Nature – Springer Series in Invasion Ecology, Springer Netherlands, 607–624, https://doi.org/10.1007/978-94-007-0591-3, 2011.

Oh, I. K. and Lee, S. W.: Effects of temperature on the survival and larval development of *Deiratonotus japonicus* (Brachyura, Camptandriidae) as a biological indicator, Journal of Marine Science and Engineering, 8, 213, https://doi.org/10.3390/jmse8030213, 2020.

Pallas, P. S.: Miscellanea zoologica: quibus novae imprimis atque obscurae animalium species describuntur et observationibus iconibusque illustrantur, apud Sam et Joan Luchtmans, https://www.biodiversitylibrary.org/bibliography/44341 (last access: 10 February 2025), 1766.

Pires, A., Martins, R., Magalhães, L., Soares, A. M. V. M., Figueira, Quintino, E. V., Rodrigues A. M., and Freitas, R.: Expansion of lugworms towards southern European habitats and their identification using combined ecological, morphological and genetic approaches, Mar. Ecol. Prog. Ser., 533, 177–190, https://doi.org/10.3354/meps11315, 2015.

Pirro, A., Martellucci, R., Gallo, A., Kubin, E., Mauri, E., Juza, M., Notarstefano, G., Pacciaroni, M., Bussani, A., and Menna, M.: Subsurface warming derived from Argo floats during the 2022 Mediterranean marine heat wave, in: 8th edition of the Copernicus Ocean State Report (OSR8), edited by: von Schuck-

mann, K., Moreira, L., Grégoire, M., Marcos, M., Staneva, J., Brasseur, P., Garric, G., Lionello, P., Karstensen, J., and Neukermans, G., Copernicus Publications, State Planet, 4-osr8, 18, https://doi.org/10.5194/sp-4-osr8-18-2024, 2024.

Pisano, A., Nardelli, B. B., Tronconi, C., and Santoleri, R.: The new Mediterranean optimally interpolated pathfinder AVHRR SST Dataset (1982–2012), Remote Sens. Environ., 176, 107–116, https://doi.org/10.1016/j.rse.2016.01.019, 2016.

Pisano, A., Marullo, S., Artale, V., Falcini, F., Yang, C., Leonelli, F. E., and Buongiorno Nardelli, B.: New evidence of Mediterranean climate change and variability from sea surface temperature observations, Remote Sens., 12, 132, https://doi.org/10.3390/rs12010132, 2020.

Pisano, A., Fanelli, C., Massi, A., Tronconi, C., Cesarini, C., La Padula, F., Buongiorno Nardelli, B., and Ciani D.: Sea Surface Temperature Production Centre Mediterranean Sea and Black Sea Sea Surface Temperature Reprocessing, Sea Surface Temperature Production Centre Mediterranean Sea and Black Sea Sea Surface Temperature Reprocessing, Issue 4.0, Mercator Ocean International, https://catalogue.marine.copernicus.eu/documents/QUID/CMEMS-SST-QUID-010-021-022-041-042.pdf (last access: 10 February 2025), 2024a.

Pisano, A., Fanelli, C., Massi, A., Tronconi, C., Cesarini, C., La Padula, F., Buongiorno Nardelli, B., and Ciani D.: EU Copernicus Marine Service Product User Manual for Mediterranean Sea and Black Sea L3S and L4 SST Reprocessed Products, SST_MED_SST_L4_REP_OBSERVATIONS_010_021, Issue 4.0, Mercator Ocean International, https://catalogue.marine.copernicus.eu/documents/PUM/CMEMS-SST-PUM-010-021-022-041-042.pdf (last access: 10 February 2025) 2024b.

Raffa, F., Ludeno, G., Patti, B., Soldovieri, F., Mazzola, S., and Serafino, F.: X-band wave radar for coastal upwelling detection off the southern coast of Sicily, J. Atmos. Sol.-Terr. Phy., 34, 21–31, https://doi.org/10.1175/JTECH-D-16-0049.1, 2017.

Ramos, M. A. C. and Schizas, N. V.: Population structure of the fireworm *Hermodice carunculata* in the wider Caribbean, Atlantic and Mediterranean Sea, J. Mar. Biol. Assoc. UK, 103, e14, https://doi.org/10.1017/S0025315422001114, 2023.

Riera, R., Pérez, O., Rodríguez, M., Ramos, E., and Monterroso, Ó.: Are assemblages of the fireworm *Hermodice carunculata* enhanced in sediments beneath offshore fish cages?, Acta Oceanol. Sin., 33, 108–111, https://doi.org/10.1007/s13131-014-0449-y, 2014.

Righi, S., Prevedelli, D., and Simonini, R.: Ecology, distribution and expansion of a Mediterranean native invader, the fireworm *Hermodice carunculata* (Annelida), Mediterr. Mar. Sci., 21, 558–574, https://doi.org/10.12681/mms.23117, 2020.

Righi, S., Savioli, M., Prevedelli, D., Simonini, R., and Malferrari, D.: Unraveling the ultrastructure and mineralogical composition of fireworm stinging bristles, Zoology, 144, 125851, https://doi.org/10.1016/j.zool.2020.125851, 2021.

Righi, S., Forti, L., Simonini, R., Ferrari, V., Prevedelli, D., and Mucci, A.: Novel Natural Compounds and Their Anatomical Distribution in the Stinging Fireworm *Hermodice carunculata* (Annelida), Mar. Drugs, 20, 585, https://doi.org/10.3390/md20090585, 2022.

Rogers, T. L., Gouhier, T. C., and Kimbro, D. L.: Distinct temperature stressors acting on multiple ontogenetic stages influence the biogeography of Atlantic blue crabs, Mar. Ecol. Prog. Ser., 690, 97–111, https://doi.org/10.3354/meps14039, 2022.

Samperio-Ramos, G., Olsen, Y. S., Tomas, F., and Marbà, N.: Ecophysiological responses of three Mediterranean invasive seaweeds (*Acrothamnion preissii*, *Lophocladia lallemandii* and *Caulerpa cylindracea*) to experimental warming, Mar. Pollut. Bull., 96, 418–423, https://doi.org/10.1016/j.marpolbul.2015.05.024, 2015.

Scalici, M., Chiesa, S., Mancinelli, G., Rontani, P. M., Voccia, A., and Nonnis Marzano, F.: Euryhaline aliens invading Italian inland waters: The case of the Atlantic blue crab *Callinectes sapidus* Rathbun, 1896, Appl. Sci., 12, 4666, https://doi.org/10.3390/app12094666, 2022.

Schneider, A. K., Fabrizio, M. C., and Lipcius, R. N.: Reproductive phenology of the Chesapeake Bay blue crab population in a changing climate, Front. Ecol. Evol., 11, 1304021, https://doi.org/10.3389/fevo.2023.1304021, 2024.

Schulze, A., Grimes, C. J., and Rudek, T. E.: Tough, armed and omnivorous: *Hermodice carunculata* (Annelida: Amphinomidae) is prepared for ecological challenges, J. Mar. Biol. Assoc. UK, 97, 1075–1080, https://doi.org/10.1017/S0025315417000091, 2017.

Seesanong, S., Seangarun, C., Boonchom, B., Laohavisuti, N., Thompho, S., Boonmee, W., and Rungrojchaipon, P.: Bio-green synthesis of calcium acetate from oyster shell waste at low cost and reducing the emission of greenhouse gases, Sustainable Environment Research, 33, 26, https://doi.org/10.1186/s42834-023-00187-6, 2023.

Simonini, R. and Ferri, A.: Prime stime della longevità del verme di fuoco *Hermodice carunculata* (Annelida) dedotte grazie al contributo dei fotografi subacquei alla scienza partecipata, Atti della Società dei Naturalisti e Matematici di Modena, 153, 207–222, 2022.

Simonini, R., Maletti, I., Righi, S., Fai, S., and Prevedelli, D.: Laboratory observations on predator–prey interactions between the bearded fireworm (*Hermodice carunculata*) and Mediterranean benthic invertebrates, Freshwater Behaviour and Physiology, 51, 145–158, https://doi.org/10.1080/10236244.2018.1502031, 2018.

Simonini, R., Prevedelli, D., and Righi, S.: Esemplari mediterranei del verme di fuoco *Hermodice carunculata* (Annelida) catalogati nelle raccolte zoologiche di musei europei, Atti della Società dei Naturalisti e Matematici di Modena, 150, 145–159, https://iris.unimore.it/handle/11380/1184301 (last access: 10 February 2025), 2019.

Simonini, R., Righi, S., Zanetti, F., Fai, S., and Prevedelli, D.: Development and catch efficiency of an attracting device to collect and monitor the invasive fireworm *Hermodice carunculata* in the Mediterranean Sea, Mediterr. Mar. Sci., 22, 706–714, https://doi.org/10.12681/mms.26916, 2021.

Simonini, R., Ferri, A., Righi, S., Cenni, E., Ferrari, V., Sabia, C., and Prevedelli, D.: Potenziali applicazioni biotecnologiche dei policheti *Halla parthenopeia* (Oenonidae) e *Hermodice carunculata* (Amphinomidae), Biologia Marina Mediterranea, 28, 27–30, 2024.

Stachowicz, J. J., Terwin, J. R., Whitlatch, R. B., and Osman, R. W.: Linking climate change and biological invasions: ocean warming facilitates nonindigenous species

invasions, P. Natl. Acad. Sci. USA, 99, 15497–15500, https://doi.org/10.1073/pnas.242437499, 2002.

Sun, C. C., Hurst, J. E., and Fuller, A. K.: Citizen science data collection for integrated wildlife population analyses, Front. Ecol. Evol., 9, 682124, https://doi.org/10.3389/fevo.2021.682124, 2021.

Sussman, M., Loya, Y., Fine, M., and Rosenberg, E.: The marine fireworm *Hermodice carunculata* is a winter reservoir and spring-summer vector for the coral-bleaching pathogen Vibrio shiloi, Environ. Microbiol., 5, 250–255, https://doi.org/10.1046/j.1462-2920.2003.00392.x, 2003.

Taylor, D. L. and Fehon, M. M.: Blue Crab (*Callinectes sapidus*) population structure in Southern New England tidal rivers: Patterns of shallow-water, unvegetated habitat use and quality, Estuar. Coast., 44, 1320–1343, https://doi.org/10.1007/s12237-020-00867-1, 2021.

Tiralongo, F., Crocetta, F., Riginella, E., Lillo, A. O., Tondo, E., Macali, A., and Azzurro, E.: Snapshot of rare, exotic and overlooked fish species in the Italian seas: A citizen science survey, J. Sea Res., 164, 101930, https://doi.org/10.1016/j.seares.2020.101930, 2020.

Tiralongo, F., Villani, G., Arciprete, R., and Mancini, E.: Filling the gap on Italian records of an invasive species: first records of the Blue Crab, *Callinectes sapidus* Rathbun, 1896 (Decapoda: Brachyura: Portunidae), in Latium and Campania (Tyrrhenian Sea), Acta Adriat., 61, 99–104, https://doi.org/10.32582/aa.62.1.8, 2021.

Tiralongo, F., Marino, S., Ignoto, S., Martellucci, R., Lombardo, B. M., Mancini, E., and Scacco, U.: Impact of *Hermodice carunculata* (Pallas, 1766) (Polychaeta: Amphinomidae) on artisanal fishery: A case study from the Mediterranean Sea, Mar. Environ. Res., 192, 106227, https://doi.org/10.1016/j.marenvres.2023.106227, 2023.

Tiralongo, F., Nota, A., Di Pasquale, C., Muccio, E., and Felici, A.: Trophic interactions of *Callinectes sapidus* (Blue Crab) in Vendicari Nature Reserve (Central Mediterranean, Ionian Sea) and first record of Penaeus aztecus (Brown Shrimp), Diversity, 16, 724, https://doi.org/10.3390/d16120724, 2024a.

Tiralongo, F., Marcelli, M., Anselmi, G., Gattelli, R., and Felici, A.: Invasion of freshwater systems by the Atlantic blue crab *Callinectes sapidus* Rathbun, 1896 – new insights from Italian regions, Acta Adriat., 65, 193–204, https://doi.org/10.32582/aa.65.2.7, 2024b.

Tirelli, V., Goruppi, A., Riccamboni, R., and Tempesta, M.: Citizens' Eyes on Mnemiopsis: How to Multiply Sightings with a Click!, Diversity, 13, 224, https://doi.org/10.3390/d13060224, 2021.

Toivonen, T., Heikinheimo, V., Fink, C., Hausmann, A., Hiippala, T., Karhu, M., Orellana, J., and Tenkanen, H.: Social media data for conservation science: A methodological overview, Biol. Conserv., 233, 298–315, https://doi.org/10.1016/j.biocon.2019.02.013, 2019.

Toso, A., Boulamail, S., Lago, N., Pierri, C., Piraino, S., and Giangrande, A.: First description of early developmental stages of the native invasive fireworm *Hermodice carunculata* (Annelida, Amphinomidae): a cue to the warming of the Mediterranean Sea, Mediterr. Mar. Sci., 21, 442–447, https://doi.org/10.12681/mms.22043, 2020.

Toso, A., Furfaro, G., Fai, S., Giangrande, A., and Piraino, S.: A sea of fireworms? New insights on ecology and seasonal density of *Hermodice carunculata* (Pallas, 1766) (Annelida) in the Ionian Sea (SE Italy), European Zoological Journal, 89, 1104–1114, https://doi.org/10.1080/24750263.2022.2113156, 2022.

Toso, A., Mammone, M., Rossi, S., Piraino, S., and Giangrande, A.: Effect of temperature and body size on anterior and posterior regeneration in *Hermodice carunculata* (Polychaeta, Amphinomidae), Mar. Biol., 171, 152, https://doi.org/10.1007/s00227-024-04468-5, 2024.

Tsirintanis, K., Azzurro, E., Crocetta, F., Dimiza, M., Froglia, C., Gerovasileiou, V., Langeneck, J., Mancinelli, G., Rosso, A., Stern, N., Triantaphyllou, M., Tsiamis, K., Turon, X., Verlaque, M., Zenetos, A., and Katsanevakis, S.: Bioinvasion impacts on biodiversity, ecosystem services, and human health in the Mediterranean Sea, Aquat. Invasions, 17, 308–352, https://doi.org/10.3391/ai.2022.17.3.01, 2022.

Turolla, E.: La venericoltura in Italia. Estado actual de cultivo y manejo de moluscos bivalvos y su proyección futura: factores que afectan su sustentabilidad en América Latina, edited by: Lovatelli, A., Farías, A., and Uriarte, I., Taller Técnico Regional de la FAO, 20–24 August 2007, Puerto Montt, Chile, FAO Actas de Pesca y Acuicultura, No. 12. Roma, FAO, 177–188, ISBN 978-92-5-306115-0, 2008.

Turrini, T., Dörler, D., Richter, A., Heigl, F., and Bonn, A.: The threefold potential of environmental citizen science – Generating knowledge, creating learning opportunities and enabling civic participation, Biol. Conserv., 225, 176–186, https://doi.org/10.1016/j.biocon.2018.06.003, 2018.

Valdes, L., Alvarez-Ossorio, M. T., and Gonzalez-Gurriaran, E.: Influence of temperature on embryonic and larval development in *Necora puber* (Brachyura, Portunidae), J. Mar. Biol. Assoc. UK, 71, 787–789, https://doi.org/10.1017/S0025315400053455, 1991.

van den Brink, A. M., McLay, C. L., Hosie, A. M., and Dunnington, M. J.: The effect of temperature on brood duration in three *Halicarcinus anger* species (Crustacea: Brachyura: Hymenosomatidae), J. Mar. Biol. Assoc. UK, 92, 515–520, https://doi.org/10.1017/S0025315411000579, 2012.

Vetrano, A., Napolitano, E., Iacono, R., Schroeder, K., and Gasparini, G. P.: Tyrrhenian Sea circulation and water mass fluxes in spring 2004: Observations and model results, J. Geophys. Res.-Oceans, 115, C06011, https://doi.org/10.1029/2009JC005837, 2010.

Wolf, A. T. and Nugues, M. M.: Predation on coral settlers by the corallivorous fireworm *Hermodice carunculata*, Coral Reefs, 32, 227–231, https://doi.org/10.1007/s00338-012-0969-x, 2013.

Wolf, A. T., Nugues, M. M., and Wild, C.: Distribution, food preference, and trophic position of the corallivorous fireworm *Hermodice carunculata* in a Caribbean coral reef, Coral Reefs, 33, 1153–1163, https://doi.org/10.1007/s00338-014-1184-8, 2014.

Zenetos, A., Çinar, M. E., Pancucci-Papadopoulou, M. A., Harmelin, J. G., Furnari, G., Andaloro, F., Bellou, N., Streftaris, N., and Zibrowius, H.: Annotated list of marine alien species in the Mediterranean with records of the worst invasive species, Mediterr. Mar. Sci., 6, 63–118, https://doi.org/10.12681/mms.186, 2005.

State Planet, 6-osr9, 10, 2025
https://doi.org/10.5194/sp-6-osr9-10-2025

Insights into sea surface temperature variability and the impact of long-term warming on marine heatwaves in the Mediterranean Sea

Dimitra Denaxa[1,2], Gerasimos Korres[1], Sofia Darmaraki[3], and Maria Hatzaki[2]

[1]Hellenic Centre for Marine Research (HCMR), Institute of Oceanography, Anavyssos, Greece
[2]Department of Geology and Geoenvironment, National and Kapodistrian University of Athens, Athens, Greece
[3]Coastal & Marine Research Laboratory (CMRL), Institute of Applied and Computational Mathematics (IACM), Foundation for Research and Technology–Hellas (FORTH), Crete, Greece

Correspondence: Dimitra Denaxa (ddenaxa@hcmr.gr)

Received: 24 July 2024 – Discussion started: 20 September 2024
Revised: 18 March 2025 – Accepted: 13 May 2025 – Published: 30 September 2025

Abstract. In the context of a warming Mediterranean Sea, marine heatwaves (MHWs) have progressively intensified, leading to multiple environmental and socioeconomic damage. This study explores the origin of the observed trends in surface MHWs in the basin using sea surface temperature (SST) observations for the period 1982–2023. Results show a basin-wide increase in SST and extreme SST occurrences over the study period, emphasized in the eastern basin. The Adriatic, Aegean, and northern Levantine seas exhibit the highest trends in both SST and extreme SST percentiles, suggesting that these are the most vulnerable areas in the basin in terms of both accumulated warming and extreme SST occurrences. On top of the underlying mean warming, increased variability in SST is observed in parts of the western and central Mediterranean Sea, while decreased variability in SST is found in most of the eastern basin. Results reveal a basin-wide dominance of mean warming versus interannual variability in causing higher maximum MHW intensities, more extreme MHWs, longer heat exposure, and a greater accumulation of heat stress on an annual basis. Interannual variability becomes the dominant driver of the mean MHW intensity trends in most of the basin and particularly in the western and central Mediterranean areas. Mean MHW intensity is also differentiated from the other examined metrics due to the higher sensitivity of our trend attribution results for this metric to different methodological choices for climatological baselines, thus implying a more complex nature of this metric. To advance our understanding of forcing factors behind MHW trends in the Mediterranean Sea, future work should incorporate climate models that can explicitly represent the anthropogenic nature of trends against natural ocean variability.

1 Introduction

Over the past 4 decades, the Mediterranean Sea has undergone continuous warming of the sea surface temperature (SST) at observed rates ranging from 0.37 to 0.41 °C per decade between 1982–2022 (e.g., Mohamed et al., 2019; Pisano et al., 2020; Pastor et al., 2020; Juza and Tintoré, 2021; E.U. Copernicus Marine Service Information, 2024b; Martínez et al., 2023). Additionally, extreme warm events, named marine heatwaves (MHWs), have garnered significant attention due to their severe environmental and socioeconomic impacts and their notable intensification over recent decades (Darmaraki et al., 2019; Juza et al., 2022; Dayan et al., 2023; Hamdeno and Alvera-Azcaráte, 2023; Pastor and Khodayar, 2023; Denaxa et al., 2024).

Recent studies have addressed the origin of observed MHW trends in the Mediterranean Sea by assessing the relative contributions of long-term changes in mean SST and changes in SST variability. Simon et al. (2023) investigated the role of the long-term SST warming (mean warming from now on) and interannual variability in SST in altering summer MHW activity. They showed that the mean warming is

Published by Copernicus Publications.

Table 1. Copernicus Marine Service dataset used in the study.

Product ref. no	Product ID and type	Data access	Documentation
1	SST_MED_SST_L4_REP_OBSERVATIONS_010_021; Satellite observations Mediterranean Sea High Resolution L4 Sea Surface Temperature Reprocessed	EU Copernicus Marine Service Product (CMEMS, 2024a)	Product User Manual (PUM): Pisano et al. (2024a) https://catalogue.marine.copernicus.eu/documents/PUM/CMEMS-SST-PUM-010-021-022-041-042.pdf QUality Information Document (QUID): Pisano et al. (2024b) https://catalogue.marine.copernicus.eu/documents/QUID/CMEMS-SST-QUID-010-021-022-041-042.pdf

the main driver of the increase in MHW activity across the basin. They also showed that the SST variability contributes to long-term trends in MHW activity in the western and Adriatic regions, while it acts towards reducing these trends in central and eastern Mediterranean regions. Ciappa (2022) and Martínez et al. (2023) also showed that MHW intensification mainly results from the mean warming in the basin. Moreover, Oliver (2019) used a statistical climate model to simulate trends in surface MHWs originating from mean warming or changes in variance of SST in the global ocean. Their results for the Mediterranean Sea show that trends in the annual number of MHW days and the maximum MHW intensity are mainly driven by the mean warming. The latter has been also suggested as the primary driver behind observed trends in properties of surface MHWs at coastal locations globally by Marin et al. (2021). In particular, they quantified the mean warming contribution versus that of interannual variability using a trend attributional ratio (TAR) based on an ensemble approach. Their results reveal that mean warming is mainly responsible for the observed trends in all examined MHW metrics except for mean MHW intensity, whose trends are largely attributed to internal variability.

As a biodiversity hotspot and one of the most sensitive marine regions to climate change, the Mediterranean Sea necessitates a comprehensive, basin-wide investigation of MHWs, accounting for areas that support key ecological processes susceptible to disruptions by MHWs. For instance, pelagic species may be affected by MHWs, with potential repercussions for the fishery industry. A climate risk assessment by Hidalgo et al. (2022) identifies the southeastern basin as the most impacted for both pelagic and demersal fisheries, highlighting geographic differences in drivers and impacts and recommending regionally tailored adaptation strategies. In addition, MHWs pose significant risks to aquaculture, a rapidly expanding industry in the Mediterranean Sea, by increasing fish mortality and facilitating the proliferation of pathogens and disease outbreaks, which can lead to substantial financial losses (Cascarano et al., 2021; Mengual et al., 2021). A comprehensive understanding of MHWs across the basin can further inform conservation measures in Marine Protected Areas (MPAs), which host vulnerable species, such as marine mammals and turtles (Chatzimentor et al., 2023). In fact, a regional-scale approach can provide critical insights for identifying spatial refugia and establishing new MPAs, strengthening the resilience of Mediterranean marine ecosystems to climate change (e.g., Zentner et al., 2023; Bates et al., 2019).

Given the broad ecological and socioeconomic challenges associated with Mediterranean MHWs, this study investigates extreme warming conditions and the effect of mean SST warming versus that of interannual variability in SST on MHW trends across the basin. We firstly provide insights into changes in the Mediterranean SST over the 42-year period using observational SST data. This part provides essential context on long-term changes in extremes and variability throughout the basin, setting the stage for the subsequent MHW analysis while also highlighting areas where extreme warming is particularly pronounced and might be disproportionately impacted. Then, we quantify the relative contributions of mean SST warming and interannual variability in SST to observed trends in the selected MHW properties, applying the methodological approach proposed by Marin et al. (2021) to the entire Mediterranean basin.

2 Data and methods

2.1 SST observations

For the SST analysis and detection of MHWs in this study, we use satellite SST observational data in the Mediterranean Sea for the period Jan 1982–Dec 2023. Gridded SST data at daily frequency and $0.05° \times 0.05°$ horizontal resolution are obtained from the Reprocessed satellite SST dataset of the Copernicus Marine catalog for the study period (product ref. no. 01, Table 1). This reprocessed product provides optimally interpolated estimates of the foundation SST based on satellite observations across the Mediterranean Sea and is extensively validated against drifter buoy measurements as outlined in its Quality Information Document (Pisano et al., 2024b), confirming its suitability for MHW studies. For computational reasons, the SST values are re-gridded to a $0.25° \times 0.25°$ spatial grid.

De-seasonalized daily SST anomaly time series are constructed by subtracting the daily climatological SST for the period 1982–2023 at each grid point, thus removing the effect of seasonal fluctuations. To investigate changes in extreme SST occurrences, the 99th percentile (P99) of the daily

SST anomalies of each year and the corresponding trend over the study period are also computed. In addition, the standard deviation (SD) of the daily SST anomalies is calculated over each year to obtain an annual measure of SST variability. The linear trend in the annual SD time series is computed to gain insights into changes in SST variability over the study period. Trends are computed using linear regression, and their statistical significance is assessed using the Mann–Kendall test at the 95 % confidence level. Confidence intervals for the trend estimates are calculated based on the standard error of the regression coefficients, using the Student's t distribution ($\alpha = 0.05$).

To exclude long-term variations, we subsequently remove the linear trend over the 42-year study period from the SST anomaly time series, creating a detrended daily SST dataset. This additional dataset is used to investigate MHWs independently of the long-term warming in the basin. Notably, we assume that the variability in SST in the detrended dataset may arise from internal ocean variability and from potential indirect effects of the climate change signal, given the ocean inertia and the complex ocean dynamics at multiple temporal and spatial scales. On these grounds, we use the term interannual (rather than internal) variability to address the remaining temperature variations after removing the long-term trend component.

2.2 MHW analysis: detection and origin of trends

MHWs are defined upon the exceedance of a locally determined climatological threshold (90th percentile) of SST for a 5 d period at each grid point, following Hobday et al. (2016), and are identified using the MATLAB toolbox by Zhao and Marin (2019).

To investigate the effect of mean warming and interannual variability on MHW trends, we follow Marin et al. (2021), where the origins of observed trends in MHW metrics are assessed using a trend attributional ratio (TAR). We firstly identify MHWs in the daily SST anomaly time series between 1982–2023, where long-term SST trends are included (named the non-detrended dataset from now on). Subsequently, we detect MHWs that emerge solely due to interannual variability within the study period, by applying the MHW detection algorithm on the detrended dataset. We then use the two MHW detection outputs to compute selected metrics, listed in Sect. 2.3. To isolate the effect of the mean SST warming on a particular MHW metric, we remove the interannual variability (iv) component from the observed (obs) value of that metric as follows:

$$M = M_{\mathrm{obs}} - M_{\mathrm{iv}}, \tag{1}$$

where M_{obs} and M_{iv} are the annual values of the metric obtained from the non-detrended dataset and the detrended dataset, respectively. Linear trends in M and M_{iv} are then computed for the entire Mediterranean Sea and for the western, central, and eastern sub-basins, which are separated by the Strait of Sicily and a fixed-longitude boundary at 22° E (Fig. 1a). Following Marin et al. (2021), the TAR is obtained at each grid point by computing the linear trend in the M and M_{iv} component for each MHW metric according to the following equation:

$$\mathrm{TAR} = \frac{\left(|\mathrm{Trend}_M| - |\mathrm{Trend}_{M_{\mathrm{iv}}}|\right)}{\max\left(|\mathrm{Trend}_M|, |\mathrm{Trend}_{M_{\mathrm{iv}}}|\right)}, \tag{2}$$

where Trend_M and $\mathrm{Trend}_{M_{\mathrm{iv}}}$ are the trends in the M and M_{iv} components representing MHW properties due to long-term SST changes and interannual variability, respectively. Scaling this difference with the maximum absolute value of the aforementioned trends forces TAR to range from −1 to 1. Positive (negative) TAR values indicate a stronger role of the mean warming (interannual variability) in forming the observed trends in a given MHW property.

A daily SST climatology of the detrended SST dataset is constructed following Hobday et al. (2016) based on the en-

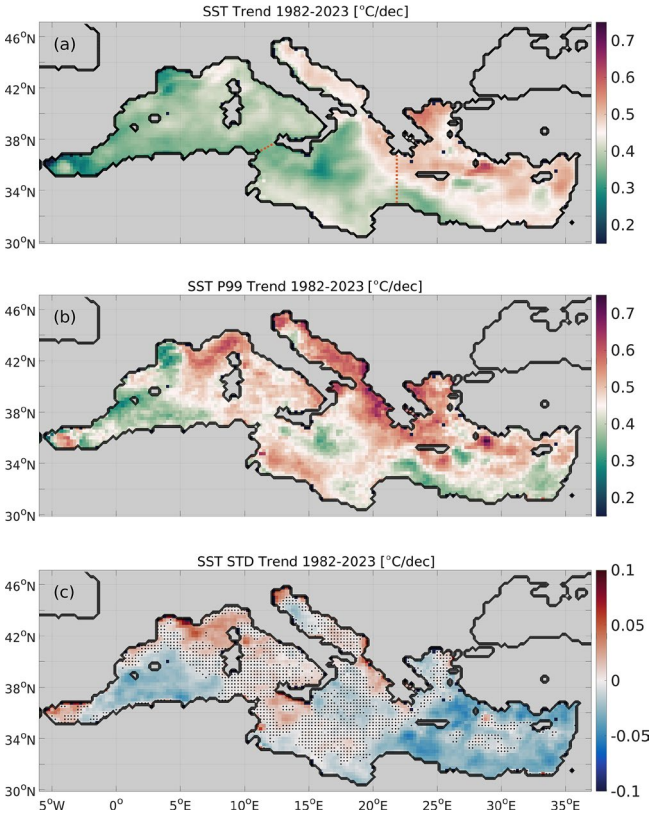

Figure 1. Linear trend in **(a)** SST, **(b)** the 99th percentile (P99) of SST, and **(c)** the standard deviation (SD) of SST, for the period 1982–2023, using de-seasonalized SST anomalies. Black dots superimposed on trend fields denote the locations with statistically insignificant trends (Mann–Kendall test, 95 % confidence level). The western, central, and eastern sub-basins are separated by the Strait of Sicily and a fixed-longitude boundary at 22° E (dashed red lines in panel **(a)**). Product used: Mediterranean Sea High Resolution L4 Sea Surface Temperature Reprocessed (Table 1, product ref. no. 1).

tire period (1982–2023). Similarly to Marin et al. (2021), this climatology is used for the detection of MHWs in both the non-detrended and detrended datasets. MHWs derived from both datasets are therefore relative to the initial state of the study period (1982), offering insights into what would have occurred without the mean warming effect. This approach for the climatological baseline aims to better represent the impact of long-term changes in MHW metrics and facilitates a direct inter-comparison with the findings of Marin et al. (2021) for Mediterranean coastal locations. Nonetheless, to examine the sensitivity of TAR values of the examined metrics to the approach followed for the climatological baseline, two extra experiments are carried out (EXP2 and EXP3) in addition to the initial approach (EXP1). In EXP2, the aforementioned methodology for computing TAR is repeated after detecting MHWs in the non-detrended dataset based on its own climatology (1982–2023), instead of using the climatology obtained from the detrended dataset as in EXP1. EXP3 follows the climatology computation approach of EXP2 but reduces the reference period to its first half (1982–2002) to explore the impact of using a shorter reference period on the attribution of trends.

2.3 Selected MHW metrics

To complement existing knowledge and provide impact-related insights, we examine the yearly cumulative intensity and the normalized maximum event intensity, in addition to the mean MHW intensity (SST anomaly with respect to climatology averaged over the event duration), the maximum MHW intensity (maximum SST anomaly with respect to climatology over the event duration), and the total number of MHW days (total count of days with an MHW activated).

The yearly cumulative intensity (CI_{yearly}) serves as a measure of the long-term thermal stress induced by MHWs, combining the effect of mean intensity (I_{mean}) and duration accumulated on a yearly basis. Considering the total events (N) of the year, it is computed as follows:

$$CI_{yearly} = \sum_{i=1}^{N} I_{mean} \cdot \text{duration}. \quad (3)$$

The normalized maximum event intensity is indicative of the degree to which SST exceeds the local climatology. It is defined as the peak intensity over the event (i.e., $SST_{max} - SST_{clim}$) divided by the deviation of the detection threshold (SST_{P90}) from the corresponding daily climatology (SST_{clim}), as in Sen Gupta et al. (2020):

$$SI = \frac{(SST_{max} - SST_{clim})}{(SST_{P90} - SST_{clim})}. \quad (4)$$

Values ranging from (1–2], (2–3], and (3–4] and above 4 correspond to moderate, strong, severe, and extreme conditions, respectively (Hobday et al., 2018). Here, we choose to focus on the maximum value of this index (SI_{max}) each year. The SI_{max} represents MHW severity by means of capturing the most extreme temperatures with respect to local SST variability, regardless of the event duration, thus informing on the "local worst" extremely warm instances occurring on a yearly basis.

As different marine organisms exhibit different (i) upper thermal limits, (ii) adaptation capacities to local temperature variations, and (iii) abilities to geographically shift in order to avoid excess heat stress, the usefulness of CI_{yearly} and SI_{max} relies on the context of specific impact assessment studies and application. For instance, the cumulative effect of multiple MHWs (represented by CI_{yearly}) may be relevant for several species, such as gorgonian populations, which have been severely impacted by recurrent events in the basin (Orenes-Salazar et al., 2023), or fish species, such as the gilthead sea bream, whose thermal tolerance can be affected by past exposure to thermal stress (Kır, 2020). Such species may also be vulnerable to extreme temperature peaks (represented by SI_{max}). For example, unlike wild marine species that can often escape unfavorable aquatic conditions, farmed species confined to aquaculture environments are more vulnerable to warm extremes (Beever et al., 2017). Such distinctions in behavioral adaptability are important for selecting appropriate metrics to assess MHW impacts on different marine populations and environments.

3 Results

3.1 Mean and extreme SST trends

This section examines the trends and spatial distribution of the observed mean (Fig. 1a) and extreme (Fig. 1b) warming of SST in the Mediterranean Sea for the period 1982–2023. Results reveal a continuous surface warming over the past 42 years in terms of both mean annual and extreme warming conditions, in agreement with previous studies (e.g., Pisano et al., 2020; Pastor et al., 2020). In our study, the average warming trend for the basin for the examined period is 0.41 °C per decade. The warming trend is statistically significant across the basin, with higher values observed over the eastern Mediterranean Sea, reaching up to 0.6 °C per decade in the Aegean and northern Levantine seas. The lowest warming trend is observed in the Alboran Sea (0.25 °C per decade), followed by the Gulf of Lions and the southwestern Ionian Sea (0.3 °C per decade) (Fig. 1a).

Long-term changes in extreme SST occurrences are shown through the trend in the 99th percentile of SST anomalies (P99) depicted in Fig. 1b. The P99 shows statistically significant positive trends across the entire basin, suggesting a basin-wide intensification of extremely warm surface conditions (Fig. 1b). The highest trend values of P99 are observed in the Ligurian, Adriatic, northeastern Ionian, and Aegean seas at about 0.6 °C per decade and locally exceeding 0.7 °C per decade (e.g., to the southeast of Rhodes). Weaker warming trends in the P99 are observed in the western basin, the

western Ionian, and certain areas in the southern Levantine Sea, with minimum values in the Gulf of Lions (lower than 0.3 °C per decade).

While long-term trends in SST anomalies (Fig. 1a) provide insights into the overall warming of the sea surface, they do not capture how temperatures fluctuate around the observed trend over the study period. In this respect, the linear trend in the SD of the daily SST anomalies informs on changes in their variability (Fig. 1c). Specifically, we observe a statistically significant increase in the SD mainly in areas of the western and central Mediterranean Sea. Maximum SD trend values are observed in the northwestern basin (eastern part of Gulf of Lions, Ligurian Sea) and the northern Adriatic Sea, indicating heightened variability in SST. Conversely, the area south of the Balearic Islands and a great portion of the eastern Mediterranean basin exhibit a statistically significant negative SD trend, indicating a weaker variability in SST towards the most recent years in these areas.

Notably, the SD trend is independent of the mean warming trend and reflects changes in the variability in SST around mean annual values. Our findings therefore indicate that, on top of the underlying mean warming, few distinct areas, primarily in the western basin, experience increased variability, while most of the eastern basin and the region south of the Balearic Islands show reduced variability. These results are in agreement with Martínez et al. (2023), who compared the SD of SST anomalies between the periods 1982–2002 and 2002–2022 for different Mediterranean sub-basins, reporting a decreased variability in the Ionian, Aegean, and Levantine seas and increased variability in the western basin and the Adriatic and Tyrrhenian seas during the most recent period.

3.2 Attribution of trends in MHW metrics

This section studies the relative role of the mean SST warming and the SST interannual variability in MHW trends. The temporal evolution and long-term trends in the selected MHW metrics (Sect. 2.3) derived from the non-detrended and detrended datasets are presented in Fig. 2 for the entire Mediterranean Sea and its sub-basins.

Results show an increase in all MHW metrics derived from the non-detrended SST dataset over the study period (Fig. 3a–e, Table 2). The mean intensity of MHWs increases by 0.03° per decade, with higher values in the western compared to the central and eastern sub-basins (Fig. 2a, Table 2). The total number of MHW days shows significant positive trends, increasing from the western to the eastern basin, with approximately 16, 18, and 23 d per decade for the western, central, and eastern sub-basins, respectively (Fig. 2c). The basin-averaged yearly cumulative intensity increases by ~ 33 °C d per decade, with its highest values and linear trends seen in the eastern sub-basin (Fig. 2d, Table 2).

The maximum intensity (I_{max}) shows a higher positive trend in the western (0.38 °C per decade) than in the eastern (0.32 °C per decade) sub-basin (Fig. 2b). In contrast, the maximum severity index (SI_{max}) exhibits a stronger increasing trend in the eastern (0.3 units per decade) than in the western (0.23 units per decade) sub-basin (Table 2). This pattern arises potentially due to SI_{max} quantifying the extremity of MHW intensity relative to a fixed climatological threshold (Eq. 4). Since this threshold remains constant over time, the larger increase in SI_{max} in the eastern sub-basin suggests that maximum intensities in this region are becoming proportionally more extreme compared to historical conditions. The observed differences in trends between I_{max} and SI_{max} across sub-basins highlight that absolute MHW intensities are increasing more rapidly in the western sub-basin, while their relative extremity compared to the historical baseline is increasing more in the eastern sub-basin.

MHW metrics originating from the detrended dataset represent MHW conditions that would have occurred solely due to interannual variability. Most metrics from this dataset show insignificant trends over the study period, with MHW intensity being a noteworthy exception (Fig. 2f–j, Table 2). In particular, both mean and maximum intensity exhibit higher trends in the western basin, similarly to the non-detrended dataset. The statistically significant basin-wide positive trend in mean intensity ranges from 0.12 to 0.08 and 0.05 °C per decade for the western, central, and eastern sub-basins, (Fig. 2f). Interestingly, these trends are higher than those from the non-detrended dataset, suggesting that interannual variability alone would still result in a statistically significant increase in mean MHW intensity (Fig. 2a, f).

I_{max} in the detrended dataset also shows positive trends, though they are not significant for the central and eastern sub-basins (Fig. 2g). Despite this, SI_{max} in the detrended dataset shows non-significant trends (Fig. 2j). In conjunction with the positive SI_{max} trends in the non-detrended dataset, this indicates that the observed increase in SI_{max} is primarily driven by the long-term warming trend, particularly in the eastern sub-basin (Table 2).

Moreover, the annual number of MHW days derived from the detrended dataset shows an insignificant trend of -1.4 d per decade for the entire basin, with a larger decrease for the eastern sub-basin (Fig. 2h, Table 2). Similarly. the yearly cumulative intensity derived from the detrended dataset shows non-significant trends (Fig. 2i), with higher (absolute) values again found in the eastern sub-basin (-2.28 °C d per decade). This aligns with the trends in MHW days, which constitute an annual measure of the total duration of MHW conditions and are therefore closely linked to the yearly cumulative intensity. These results potentially suggest that the decreasing duration of MHW conditions in the detrended dataset (Fig. 2h) counterbalance the rising mean intensity (Fig. 2f), leading to a lower accumulation of heat stress as represented by yearly cumulative intensity (see Eq. 3).

Overall, with the exception of MHW intensity, our results suggest that interannual variability mainly tends to dampen the climate-change-driven increase in MHW characteristics in the Mediterranean Sea, particularly in the eastern sub-

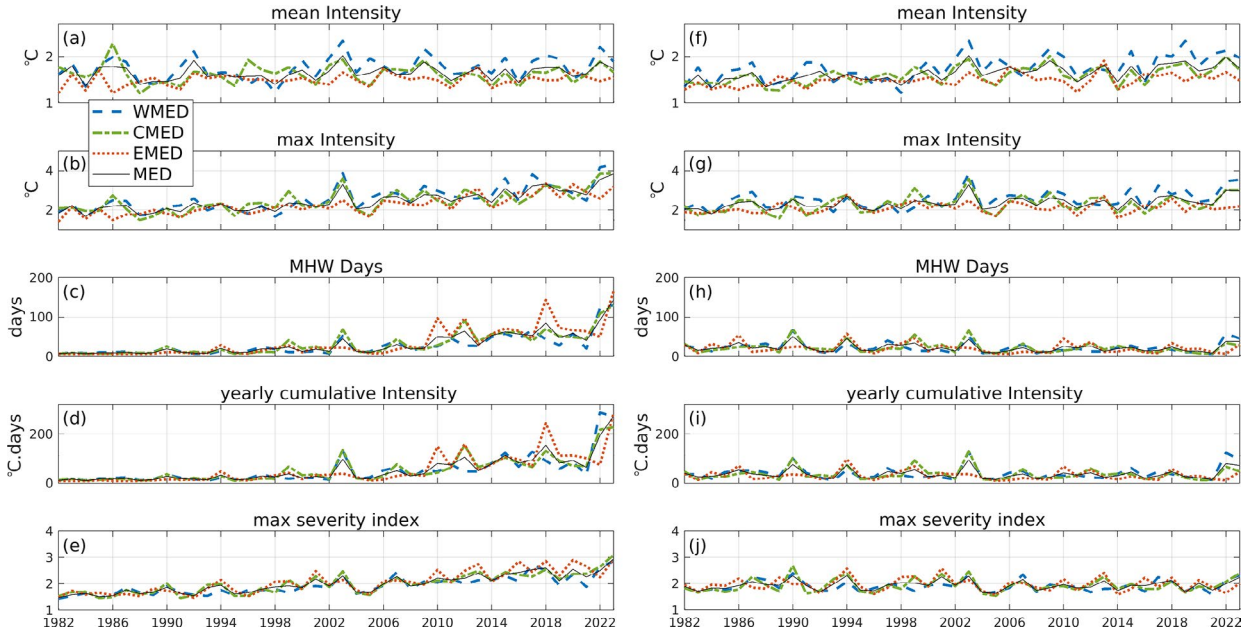

Figure 2. Temporal evolution of MHW characteristics over 1982–2023 using the non-detrended **(a–e)** and the detrended **(f–j)** SST anomaly time series. From top to bottom: mean intensity **(a, f)**, maximum intensity **(g, b)**, number of MHW days **(c, h)**, yearly cumulative intensity **(d, i)**, and maximum severity index **(e, j)**. Blue, green, and red lines and the dashed black line correspond to spatial averages for the western (WMED), central (CMED), and eastern (EMED) Mediterranean sub-basins and the entire Mediterranean basin (MED), respectively. Product used: Mediterranean Sea High Resolution L4 Sea Surface Temperature Reprocessed (Table 1, product ref. no. 1).

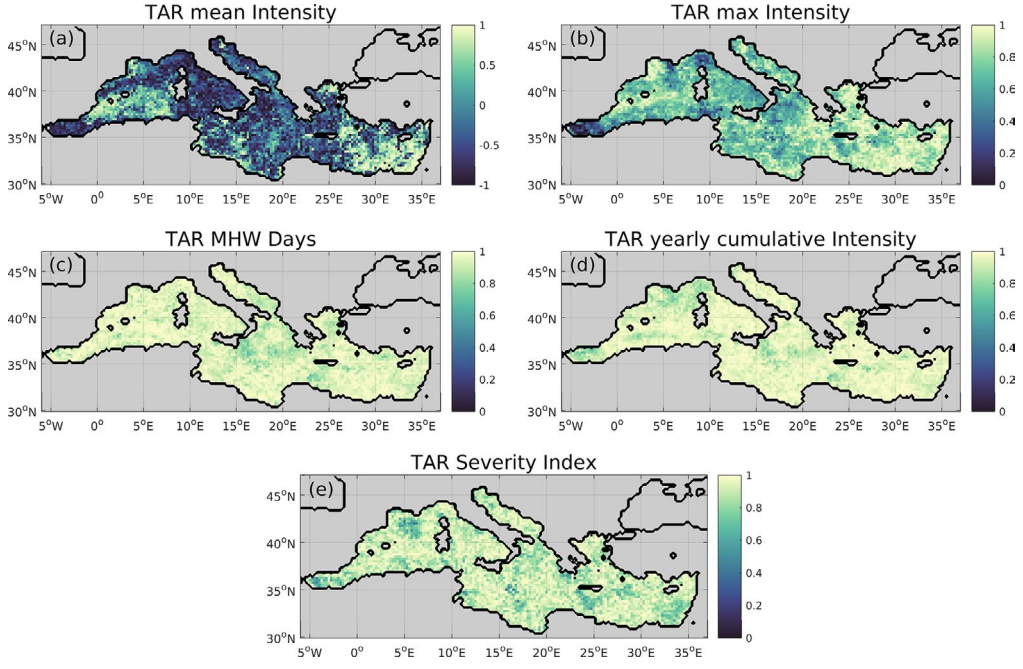

Figure 3. Trend attributional ratio (TAR) for MHW characteristics over 1982–2023: **(a)** mean MHW intensity, **(b)** maximum MHW intensity, **(c)** number of MHW days, **(d)** yearly cumulative MHW intensity, and **(e)** maximum MHW severity index. Positive (negative) TAR values indicate that mean SST warming (interannual variability) is the dominant driver of the trend in an MHW metric. The range of TAR values in colorbar axes varies for mean intensity and the rest of the variables to allow the visualization of spatial variations. Product used: Mediterranean Sea High Resolution L4 Sea Surface Temperature Reprocessed (Table 1, product ref. no. 1).

Table 2. Linear trends and confidence intervals for the spatially averaged MHW metrics of the non-detrended (N-DET) and the detrended (DET) SST datasets over 1982–2023. Metrics used: mean intensity (I_{mean}), maximum intensity (I_{max}), number of MHW days (MHW days), yearly cumulative intensity (CI_{yearly}), and maximum severity index (SI_{max}). Sub-regions considered: western (WMED), central (CMED), and eastern (EMED) Mediterranean and the entire Mediterranean basin (MED). Values in bold correspond to statistically significant trends (Mann–Kendall test, 95 % confidence level). Product used: Mediterranean Sea High Resolution L4 Sea Surface Temperature Reprocessed (Table 1, product ref. no. 1).

		MED		WMED		CMED		EMED	
		Trend	CI (±)	Trend	CI (±)	Trend	CI (±)	Trend	CI (±)
I_{mean} trend (°C per decade)	N-DET	0.03	0.04	0.06	0.06	0.01	0.05	0.03	0.03
	DET	0.09	0.04	0.12	0.06	0.08	0.04	0.05	0.03
I_{max} trend (°C per decade)	N-DET	0.34	0.08	0.38	0.120	0.32	0.11	0.32	0.07
	DET	0.11	0.07	0.17	0.11	0.11	0.11	0.04	0.07
MHW days trend (days per decade)	N-DET	18.41	4.62	15.69	5.21	18.22	5.02	22.71	6.56
	DET	−1.40	2.68	−0.94	3.55	−1.95	3.75	−2.11	3.27
CI_{yearly} trend (°C days per decade)	N-DET	33.20	9.31	32.20	12.07	31.47	9.6	36.75	11.25
	DET	0.13	4.94	1.90	7.12	−1.23	6.60	−2.28	5.01
SI_{max} trend (units per decade)	N-DET	0.26	0.05	0.23	0.06	0.26	0.06	0.30	0.06
	DET	0.01	0.05	0.01	0.06	0.02	0.07	−0.01	0.07

basin, in agreement with Simon et al. (2023). This observation is in line with results presented in Sect. 3.1 showing an increase (decrease) in SST variability mainly in western (eastern) Mediterranean areas throughout the study period. Nevertheless, further investigations are needed to unravel the cause of the differentiation of MHW intensity compared to other MHW properties.

To attribute MHW trends over the study period to the mean warming or the interannual variability in SST, TAR values are computed for the examined MHW properties (Fig. 3). As explained in Sect. 2.2, positive TAR values correspond to a major role of the mean SST warming, while negative values correspond to a major role of interannual variability in driving MHW trends.

Results reveal a basin-wide dominance of the mean warming in driving the observed trends in all MHW characteristics, except for the mean MHW intensity, which is found to be mainly forced by interannual variability over most of the Mediterranean Sea (Fig. 3a). In particular, a great part of the western basin and most of the central basin reaching up to 26° E exhibit large negative TAR values, often reaching −1, indicating that the mean MHW intensity trend is primarily driven by interannual variability. In contrast, the mean SST warming appears to dominate interannual variability over the eastern Levantine Sea and part of the Aegean Sea, as well as in certain areas in the southwestern basin, as indicated by high positive mean-intensity TAR values in these areas (Fig. 3a). These positive TAR locations largely coincide with the ones showing a decreasing SD of SST anomalies over the study period (Figs. 1c and 3a). The dominance of the mean warming signal in explaining the MHW intensity trends in these areas appears associated with the decreasing trend in the variability in SST in the same areas. We note that the positive mean-intensity TAR values in these areas result from significant positive trends in the mean warming component and insignificant trends in the interannual variability component for this metric (not shown).

For the rest of the examined MHW properties' trends, positive TAR values across the entire basin indicate a dominant role of mean SST warming in driving their increase during 1982–2023 (Fig. 3b–e). We note here that, the greater the value of TAR, the stronger the impact of the mean SST warming. Positive TAR values for the maximum MHW intensity shown in Fig. 3b range from 0 to 1 across the basin, revealing areas with a marginally stronger influence of the mean SST warming signal compared to that of the interannual SST variability (Alboran Sea, followed by the Ligurian Sea). However, there seems to be a clear prevalence of the mean SST warming especially over the eastern basin for this metric (Fig. 3b). Spatial distribution of TAR for the maximum severity index exceeds 0.6 in most of the basin, indicating a basin-wide dependence of this metric on the mean SST warming (Fig. 3e). Furthermore, high positive TAR values are seen for the number of MHW days and the yearly cumulative intensity, exceeding 0.8 throughout the basin (Fig. 3c, d).

Overall, from a basin-wide perspective, our findings suggest a dominant role of the mean SST warming in the development of more severe and prolonged MHW conditions. By contrast, interannual variability becomes the dominant driver of the mean MHW intensity trend in most of the basin, playing an important role, and of the maximum MHW intensity trends in certain Mediterranean areas, though to a notably lesser extent.

To examine the sensitivity of TAR values of the examined metrics to the approach followed for climatological baseline, two additional tests are performed as described in Sect. 2.2. These experiments reveal minimal TAR sensitivity for all metrics except for mean intensity (Fig. 4). The bar graphs of Fig. 4 summarize this finding, showing the number of locations (as a percentage of the total number of Mediterranean grid points) exhibiting a positive TAR sign (i.e., a dominant role of the mean warming in MHW trends). In all experiments, the long-term trends in maximum intensity, yearly cumulative intensity, maximum severity index, and annual number of MHW days are mainly attributed to the mean warming across more than 97 % of the Mediterranean Sea. On the other hand, we observe a differentiated sensitivity of the mean-intensity TAR to the examined approaches for climatology. Based on the initial approach (EXP1), 34 % of the Mediterranean Sea shows mean-warming-driven mean-intensity trends, while, for the second and third approach, this percentage is 46 % (EXP2) and 30 % (EXP3) (Fig. 4). We note that the spatial distribution of mean-intensity TAR values is similar in the three experiments (the same applies for the rest of the metrics), with the easternmost and a part of the southwestern basin showing a dominant role of mean warming (not shown), as shown in Fig. 3a. Notably, mean MHW intensity is the metric found to be largely associated with interannual variability, as opposed to the rest of the examined MHW properties. The higher sensitivity of our results for mean intensity to different methodological choices further suggests a less predictable future behavior for this MHW property.

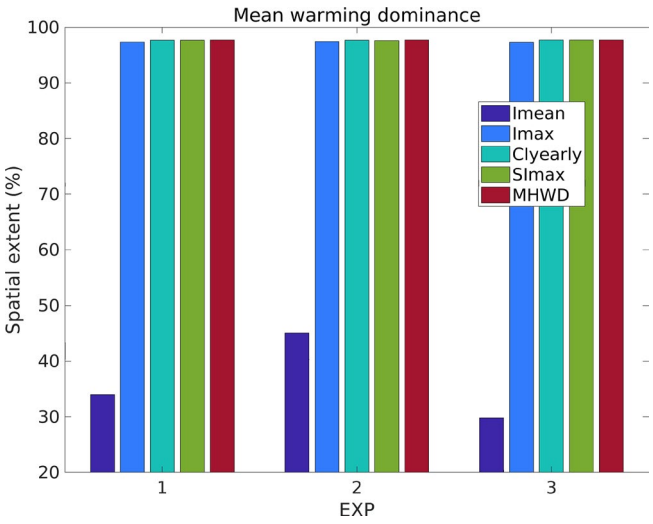

Figure 4. Sensitivity of the trend attributional ratio (TAR) to different approaches for base climatology used in MHW detection in the original (non-detrended) dataset. Vertical axis: percentage of Mediterranean locations with positive TAR (i.e., mean warming dominance in trends in MHW metrics). Horizontal axis: EXP1 – climatology computed based on the detrended dataset with reference period 1982–2023; EXP2 – climatology computed based on the non-detrended dataset with reference period 1982–2023; EXP3 – as EXP2 but with reference period 1982–2002. Metrics used: mean intensity (Imean), maximum intensity (Imax), number of MHW days (MHWD), yearly cumulative intensity (CIyearly), and maximum severity index (SImax). Product used: Mediterranean Sea High Resolution L4 Sea Surface Temperature Reprocessed (Table 1, product ref. no. 1).

4 Summary and conclusions

This study investigates the role of long-term changes in SST in observed trends in MHWs in the Mediterranean Sea, using SST observations for the period 1982–2023. Our results show a basin-wide increase in SST and extreme SST occurrences over the study period, with stronger trends in the eastern basin. The Adriatic, Aegean, and northern Levantine Seas show the highest trends in both SST and its 99th percentile, highlighting these areas as particularly vulnerable in terms of both accumulated warming and extreme SST occurrences. Increased SST variability is observed in parts of the western and central Mediterranean Sea, while decreased variability is found in most of the eastern basin, alongside the underlying basin-wide mean warming. Results potentially suggest a stronger climate change effect in the southern Aegean Sea and most of the Levantine Sea, where the highest warming rates are observed despite the reduced variability in SST over the study period.

Applying the trend attributional ratio (TAR) proposed by Marin et al. (2021) for the Mediterranean Sea, we find a basin-wide dominance of the long-term SST change in causing more extreme events, longer heat exposure, and a greater accumulation of heat stress on an annual basis. Interannual variability mainly tends to mitigate the observed increase in these MHW properties, particularly in the eastern sub-basin. In contrast, interannual variability emerges as the primary driver of mean MHW intensity trends in the western and central Mediterranean areas.

These findings are in agreement with Marin et al. (2021), who demonstrated that trends in mean MHW intensity are predominantly forced by interannual variability at coastal sites globally and in the western and central Mediterranean Sea in particular, based on multiple SST datasets covering a shorter period. In the eastern Mediterranean areas, where the highest warming rates are observed, their findings for mean intensity trends at coastal locations show that mean warming dominates interannual variability, in line with our results. Moreover, they showed that trends in the yearly cumulative intensity and the number of MHW days are primarily attributed to the mean warming, in agreement with our findings for these metrics across the basin. This inter-comparison enhances confidence in the current results derived from applying their methods to an observational SST dataset (Table 1) spanning the satellite period and covering the entire Mediterranean Sea.

The current study is also in line with other recent studies that follow different approaches to investigate origins of MHW trends in the Mediterranean Sea. Our findings for the mean MHW intensity trends are consistent with Simon et al. (2023), although they focus on summer MHW activity, which is an index combining the occurrence, intensity, duration, and spatial extent of MHWs. In particular, they showed that interannual variability explains one-third of the total trend in summer activity in the western basin and in the Adriatic Sea, while our results suggest that interannual variability predominates over the mean warming signal in most of the western and central sub-basins for mean intensity trends based on all events throughout the year.

In addition, Martínez et al. (2023) suggest that the intensification of MHW conditions in the Mediterranean Sea is primarily driven by the mean SST warming in the basin. Their analysis focuses on MHW duration, cumulative intensity, spatial extent, frequency, and maximum intensity, with the latter being the only metric directly comparable to our study. A difference with respect to our results appears in the maximum intensity derived from detrended SST data: while Martínez et al. (2023) report an insignificant positive trend (basin-averaged), we detect a significant positive trend, which is more pronounced in the western basin. Notably, both studies agree on the dominant contribution of mean warming to the long-term trends in maximum intensity (and the rest of the metrics as well), though through different approaches. Martínez et al. (2023) base their conclusion on the insignificant long-term trends in basin-averaged metrics obtained from the detrended dataset, while our study relies on weighting the mean SST warming and interannual SST variability within the TAR framework. Specifically, TAR for maximum intensity confirms the dominant role of the mean SST warming, in line with Martínez et al. (2023), but also highlights non-negligible contributions from interannual SST variability, especially in the Alboran and Ligurian seas.

Overall, this study reveals a dominant role of the mean SST warming in increasing the severity, total heat exposure, and maximum intensity of MHWs in the Mediterranean Sea with a notably smaller effect on mean MHW intensity, which is largely influenced by interannual variability. The sensitivity of the employed attribution metric to different methodological choices for climatological baselines is higher for the mean MHW intensity compared to the rest of the examined metrics. This differentiation further suggests a more complex and likely less predictable behavior of this property. In this respect, Marin et al. (2021) show that mean intensity trends exhibit significant sensitivity to different datasets, in contrast to other metrics. Also consistent with our findings, Oliver (2019) shows that trends in the annual number of MHW days and the maximum intensity are mainly forced by mean warming in the basin, noting a less clear origin of the trends for the latter. Nevertheless, their results cannot be directly inter-compared to ours, as they use a substantially different methodology based on a statistical climate model. Moreover, Schlegel et al. (2019) show that, while linear trends significantly increase MHW duration, their effect on the maximum intensity can be either positive or negative. Their finding aligns with our results on the increased uncertainty associated with mean intensity; however, since it is based on the maximum intensity of averaged MHWs, it cannot be directly comparable to ours. Therefore, further investigation is needed to understand the reasons behind the distinct behavior of mean intensity – whether in terms of trends, trend attribution, or sensitivity to climatological baselines.

Finally, while the approach used to decompose SST signals in this study is commonly employed, there are limitations in interpreting the origin of the different components. To specifically assess the impact of anthropogenic influence, a future study for the Mediterranean Sea could employ an ensemble approach using climate models. This would offer a clearer understanding of the effects of climate change on extreme SST events relative to the role of natural variability while also minimizing the impact of single-product characteristics on MHW metrics.

Data availability. Information on the product used in this paper is included in Table 1.

Author contributions. DD defined the research problem. DD conducted the analysis and wrote the article, with contributions from GK, SD, and MH. All authors contributed to the interpretation of results.

Competing interests. The contact author has declared that none of the authors has any competing interests.

Disclaimer. The Copernicus Marine Service products are subject to updates and revisions as part of the Service's ongoing efforts to meet user needs. As such, product identifiers and documentation for the product Mediterranean Sea High Resolution L4 Sea Surface Temperature Reprocessed used in this paper may change over time. For the most current information or if assistance is needed regarding this product, readers are encouraged to contact the Copernicus Marine Service user support team.

Publisher's note: Copernicus Publications remains neutral with regard to jurisdictional claims made in the text, published maps, institutional affiliations, or any other geographical representation in this paper. While Copernicus Publications makes every effort to include appropriate place names, the final responsibility lies with the authors.

Financial support. This research has been supported by the Copernicus Med-MFC (LOT reference: 21002L5-COP-MFC MED-5500, supporting Dimitra Denaxa) and the Hellenic Foun-

dation for Research and Innovation (HFRI, TexMed, project no. 07077, supporting Sofia Darmaraki).

Review statement. This paper was edited by Marta Marcos and reviewed by two anonymous referees.

References

Bates, A. E., Cooke, R. S. C., Duncan, M. I., Edgar, G. J., Bruno, J. F., Benedetti-Cecchi, L., Côté, I. M., Lefcheck, J. S., Costello, M. J., Barrett, N., Bird, T. J., Fenberg, P. B., and Stuart-Smith, R. D.: Climate resilience in marine protected areas and the "Protection Paradox", Biol. Conserv., 236, 305–314, https://doi.org/10.1016/j.biocon.2019.05.005, 2019.

Beever, E. A., Hall, L. E., Varner, J., Loosen, A. E., Dunham, J. B., Gahl, M. K., Smith, F. A., and Lawler, J. J.: Behavioral flexibility as a mechanism for coping with climate change, Front. Ecol. Environ., 15, 299–308, https://doi.org/10.1002/fee.1502, 2017.

Cascarano, M. C., Stavrakidis-Zachou, O., Mladineo, I., Thompson, K. D., Papandroulakis, N., and Katharios, P.: Mediterranean aquaculture in a changing climate: Temperature effects on pathogens and diseases of three farmed fish species, Pathogens, 10, 1205, https://doi.org/10.3390/pathogens10091205, 2021.

Chatzimentor, A., Doxa, A., Katsanevakis, S., and Mazaris, A. D.: Are Mediterranean marine threatened species at high risk by climate change?, Glob. Chang. Biol., 29, 1809–1821, https://doi.org/10.1111/gcb.16577, 2023.

Ciappa, A. C.: Effects of Marine Heatwaves (MHW) and Cold Spells (MCS) on the surface warming of the Mediterranean Sea from 1989 to 2018, Prog. Oceanogr., 205, 102828, https://doi.org/10.1016/j.pocean.2022.102828, 2022.

Darmaraki, S., Somot, S., Sevault, F., and Nabat, P.: Past Variability of Mediterranean Sea Marine Heatwaves, Geophys. Res. Lett., 46, 9813–9823, https://doi.org/10.1029/2019GL082933, 2019.

Dayan, H., McAdam, R., Juza, M., Masina, S., and Speich, S.: Marine heat waves in the Mediterranean Sea: An assessment from the surface to the subsurface to meet national needs, Front. Mar. Sci., 10, 1–21, https://doi.org/10.3389/fmars.2023.1045138, 2023.

Denaxa, D., Korres, G., Bonino, G., Masina, S., and Hatzaki, M.: The role of air–sea heat flux for marine heatwaves in the Mediterranean Sea, in: 8th edition of the Copernicus Ocean State Report (OSR8), edited by: von Schuckmann, K., Moreira, L., Grégoire, M., Marcos, M., Staneva, J., Brasseur, P., Garric, G., Lionello, P., Karstensen, J., and Neukermans, G., Copernicus Publications, State Planet, 4-osr8, 11, https://doi.org/10.5194/sp-4-osr8-11-2024, 2024.

E.U. Copernicus Marine Service Information (CMEMS): Mediterranean Sea – High Resolution L4 Sea Surface Temperature Reprocessed, Marine Data Store (MDS) [data set], https://doi.org/10.48670/moi-00173, 2024a.

E.U. Copernicus Marine Service Information (CMEMS): Mediterranean Sea Surface Temperature time series and trend from Observations Reprocessing, Marine Data Store (MDS) [data set], https://doi.org/10.48670/moi-00268, 2024b.

Hamdeno, M. and Alvera-Azcaráte, A.: Marine heatwaves characteristics in the Mediterranean Sea: Case study the 2019 heatwave events, Front. Mar. Sci., 10, 1–19, https://doi.org/10.3389/fmars.2023.1093760, 2023.

Hidalgo, M., El-Haweet, A. E., Tsikliras, A. C., Tirasin, E. M., Fortibuoni, T., Ronchi, F., Lauria, V., Ben Abdallah, O., Arneri, E., Ceriola, L., Milone, N., Lelli, S., Hernández, P., Bernal, M., and Vasconcellos, M.: Risks and adaptation options for the Mediterranean fisheries in the face of multiple climate change drivers and impacts, ICES J. Mar. Sci., 79, 2473–2488, https://doi.org/10.1093/icesjms/fsac185, 2022.

Hobday, A. J., Alexander, L. V., Perkins, S. E., Smale, D. A., Straub, S. C., Oliver, E. C. J., Benthuysen, J. A., Burrows, M. T., Donat, M. G., Feng, M., Holbrook, N. J., Moore, P. J., Scannell, H. A., Sen Gupta, A., and Wernberg, T.: A hierarchical approach to defining marine heatwaves, Prog. Oceanogr., 141, 227–238, https://doi.org/10.1016/j.pocean.2015.12.014, 2016.

Hobday, A. J., Oliver, E. C. J., Sen Gupta, A, Benthuysen, J. A., Burrows, M. T., Donat, M. G., Holbrook, N. J., Moore, P. J., Thomsen, M. S., Wernberg, T., and Smale, D. A.: Categorizing and naming marine heatwaves, Oceanography, 31, 162–173, 2018.

Juza, M. and Tintoré, J.: Multivariate Sub-Regional Ocean Indicators in the Mediterranean Sea: From Event Detection to Climate Change Estimations, Front. Mar. Sci., 8, 610589, https://doi.org/10.3389/fmars.2021.610589, 2021.

Juza, M., Fernández-Mora, A., and Tintoré, J.: Sub-Regional Marine Heat Waves in the Mediterranean Sea From Observations: Long-Term Surface Changes, Sub-Surface and Coastal Responses, Front. Mar. Sci., 9, 785771, https://doi.org/10.3389/fmars.2022.785771, 2022.

Kır, M.: Thermal tolerance and standard metabolic rate of juvenile gilthead seabream (Sparus aurata) acclimated to four temperatures, J. Therm. Biol., 93, 102739, https://doi.org/10.1016/j.jtherbio.2020.102739, 2020.

Marin, M., Feng, M., Phillips, H. E., and Bindoff, N. L.: A Global, Multiproduct Analysis of Coastal Marine Heatwaves: Distribution, Characteristics, and Long-Term Trends, J. Geophys. Res.-Oceans, 126, 1–17, https://doi.org/10.1029/2020JC016708, 2021.

Martínez, J., Leonelli, F. E., García-Ladona, E., Garrabou, J., Kersting, D. K., Bensoussan, N., and Pisano, A.: Evolution of marine heatwaves in warming seas: the Mediterranean Sea case study, Front. Mar. Sci., 10, 1193164, https://doi.org/10.3389/fmars.2023.1193164, 2023.

Mengual, I. L., Sanchez-Jerez, P., and Ballester-Berman, J. D.: Offshore aquaculture as climate change adaptation in coastal areas: sea surface temperature trends in the Western Mediterranean Sea, Aquac. Environ. Interact., 13, 515–526, https://doi.org/10.3354/AEI00420, 2021.

Mohamed, B., Abdallah, A. M., Alam El-Din, K., Nagy, H., and Shaltout, M.: Inter-Annual Variability and Trends of Sea Level and Sea Surface Temperature in the Mediterranean Sea over the Last 25 Years, Pure Appl. Geophys., 176, 3787–3810, https://doi.org/10.1007/s00024-019-02156-w, 2019.

Oliver, E. C. J.: Mean warming not variability drives marine heatwave trends, Clim. Dynam., 53, 1653–1659, https://doi.org/10.1007/s00382-019-04707-2, 2019.

Orenes-Salazar, V., Navarro-Martínez, P. C., Ruíz, J. M., and García-Charton, J. A.: Recurrent marine heatwaves threaten the resilience and viability of a key Mediterranean octocoral

species, Aquat. Conserv. Mar. Freshw. Ecosyst., 33, 1161–1174, https://doi.org/10.1002/aqc.3997, 2023.

Pastor, F. and Khodayar, S.: Marine heat waves: Characterizing a major climate impact in the Mediterranean, Sci. Total Environ., 861, 160621, https://doi.org/10.1016/j.scitotenv.2022.160621, 2023.

Pastor, F., Valiente, J. A., and Khodayar, S.: A Warming Mediterranean: 38 Years of Increasing Sea Surface Temperature, Remote Sens., 12, 2687, https://doi.org/10.3390/rs12172687, 2020.

Pisano, A., Marullo, S., Artale, V., Falcini, F., Yang, C., Leonelli, F. E., Santoleri, R., and Buongiorno Nardelli, B.: New evidence of Mediterranean climate change and variability from Sea Surface Temperature observations, Remote Sens., 12, 1–18, https://doi.org/10.3390/RS12010132, 2020.

Pisano, A., Fanelli, C., Cesarini, C., Tronconi, C., La Padula, F., and Buongiorno Nardelli, B.: EU Copernicus Marine Service Product User Manual for the Mediterranean Sea – High Resolution L4 Sea Surface Temperature Reprocessed Product, SST_MED_SST_L4_REP_OBSERVATIONS_010_021, Issue 4.0, Mercator Ocean International, https://catalogue.marine.copernicus.eu/documents/PUM/CMEMS-SST-PUM-010-021-022-041-042.pdf (last access: 14 May 2025), 2024a.

Pisano, A., Fanelli, C., Cesarini, C., Tronconi, C., La Padula, F., and Buongiorno Nardelli, B.: EU Copernicus Marine Service Quality Information Document for the Mediterranean Sea – High Resolution L4 Sea Surface Temperature Reprocessed Product, SST_MED_SST_L4_REP_OBSERVATIONS_010_021, Issue 4.0, Mercator Ocean International, https://catalogue.marine.copernicus.eu/documents/QUID/CMEMS-SST-QUID-010-021-022-041-042.pdf (last access: 14 May 2025), 2024b.

Schlegel, R. W., Oliver, E. C. J., Hobday, A. J., and Smit, A. J.: Detecting Marine Heatwaves With Sub-Optimal Data, Front. Mar. Sci., 6, 1–14, https://doi.org/10.3389/fmars.2019.00737, 2019.

Sen Gupta, A., Thomsen, M., Benthuysen, J. A., Hobday, A. J., Oliver, E., Alexander, L. V, Burrows, M. T., Donat, M. G., Feng, M., Holbrook, N. J., Perkins-Kirkpatrick, S., Moore, P. J., Rodrigues, R. R., Scannell, H. A., Taschetto, A. S., Ummenhofer, C. C., Wernberg, T., and Smale, D. A.: Drivers and impacts of the most extreme marine heatwave events, Sci. Rep., 10, 19359, https://doi.org/10.1038/s41598-020-75445-3, 2020.

Simon, A., Pires, C., Frölicher, T. L., and Russo, A.: Long-term warming and interannual variability contributions' to marine heatwaves in the Mediterranean, Weather Clim. Extrem., 42, 100619, https://doi.org/10.1016/j.wace.2023.100619, 2023.

Zhao, Z. and Marin, M.: A MATLAB toolbox to detect and analyze marine heatwaves, J. Open Source Softw., 4, 1124, https://doi.org/10.21105/joss.01124, 2019.

Zentner, Y., Rovira, G., Margarit, N., Ortega, J., Casals, D., Medrano, A., Pagès-Escolà, M., Aspillaga, E., Capdevila, P., Figuerola-Ferrando, L., Riera, J. L., Hereu, B., Garrabou, J., and Linares, C.: Marine protected areas in a changing ocean: Adaptive management can mitigate the synergistic effects of local and climate change impacts, Biol. Conserv., 282, 110048, https://doi.org/10.1016/j.biocon.2023.110048, 2023.

State Planet, 6-osr9, 11, 2025
https://doi.org/10.5194/sp-6-osr9-11-2025

The 2023 marine heatwave in the North Atlantic tropical ocean

Amélie Loubet, Simon J. van Gennip, Romain Bourdallé-Badie, and Marie Drevillon

Mercator Océan International, 2 Av. de l'Aérodrome de Montaudran, 31400, Toulouse, France

Correspondence: Simon J. van Gennip (svangennip@mercator-ocean.fr)

Received: 17 September 2024 – Discussion started: 2 October 2024
Revised: 1 July 2025 – Accepted: 11 July 2025 – Published: 30 September 2025

Abstract. In the context of climate change, marine heatwaves (MHWs) are becoming more intense and frequent and/or lasting longer. During the year 2023 and based on the Copernicus Marine forecasting system, the Mercator Ocean International MHW bulletin (https://www.mercator-ocean.eu/ocean-intelligence/ocean-bulletins-and-insights/marine-heatwaves-archive/, last access: 14 May 2025) highlighted week after week a MHW event occurring in the North Atlantic (NA) tropical ocean. In this paper, we propose a 4D characterisation of this event using the Copernicus Marine global reanalyses. We demonstrate how this 2023 MHW event in the NA tropical ocean is extraordinary compared to previous years. All indices commonly used for characterising MHWs (intensity, duration, total activity and area) reached values not observed before at the surface but also in the subsurface. The timing of the event and its vertical structure differ across the basin, with the MHW developing first in the north-east, with peaks of intensity in May and progressively moving south-westward across the basin. A characterisation of MHWs at all vertical levels reveals that the vertical structure differs across subregions with different processes at play: in the eastern and subtropical centre of the gyre heat propagates from the surface to the subsurface, spanning beyond the mixed layer depth, whereas in the Caribbean region, abnormally warm waters at depth are transported from remote equatorial regions by eddies traversing the area.

1 Introduction

The year 2023 was the warmest year on record, with annual average global atmospheric temperature reaching 1.43 ± 0.11 °C above pre-industrial levels (Forster et al., 2024). Air temperature records were broken for multiple months and regions (WMO, 2024). Europe and the subtropical North Atlantic (NA) region were particularly affected, with the highest recorded air temperature anomalies (ESOTC, 2024). Abnormally high temperature anomalies have also been detected at the surface of the ocean consistently across products (observation, forecasting system, reanalysis) in the NA, where mean temperature estimates have exceeded those of previous years (Copernicus, 2024). A direct result of this warming ocean is the increase in the occurrence of extreme warm events.

When abnormally high ocean temperatures occur for a sustained period of time, it leads to an extreme event referred to in the literature as marine heatwaves (MHWs). A MHW definition was proposed by Hobday at al. (2016, 2018), which has enabled MHW characteristics such as MHW duration, intensity and extent to be documented in a standardised manner on a global scale. MHW frequency increased between 1925–2016 (Oliver et al., 2018) and will keep on increasing due to anthropogenic forcing (Frölicher et al., 2018; Oliver et al., 2019). MHWs threaten marine ecosystems, causing harm from a species to an ecosystem level, such as coral bleaching, reduction of habitat-forming seaweed, harmful algal blooms, species range shift and mass mortality events (Le Nohaïc et al., 2017; Wernberg et al., 2013, 2016; Smith et al., 2023; Cavole et al., 2016).

The regular monitoring of MHW conditions globally (Mercator Ocean International weekly bulletin: https://www.mercator-ocean.eu/ocean-intelligence/ocean-bulletins-and-insights/marine-heatwaves-archive/) revealed the prolonged presence across the year of an MHW event within the North Atlantic basin (NA). Studies

Published by Copernicus Publications.

Table 1. Product reference table.

Product ref. no.	Product ID & type	Data access	Documentation
1	GLOBAL_MULTIYEAR_PHY_001_030, numerical model	EU Copernicus Marine Service Product (2023)	Product User Manual (PUM): Drévillon et al. (2023) Quality Information Document (QUID): Drévillon et al. (2024)
2	ERA5 hourly data on single levels from 1940 to present, numerical models	Copernicus Climate Change Service, Climate Data Store (2023)	Hersbach et al. (2023)

documenting MHWs in the NA have only been local to regional, with no records of such widespread events occurring (Frölicher and Laufkötter, 2018; Smith et al., 2021; Zhang et al., 2023). Furthermore, MHWs have been well studied for the surface where long satellite records exist, but their subsurface extent should be considered in more details (Schaeffer et al., 2023). Their vertical structure has been studied using in situ data (Elzahaby and Schaeffer, 2019, 2021; Zhang et al., 2023; Juza et al., 2022; Pirro et al., 2024). Alternative approaches consist of the use of numerical models (Darmaraki et al., 2019; Sun et al., 2023), which provide a continuous complete 3-dimensional ocean state. In this study, we decided to use an eddy-resolving ocean reanalysis (ocean models that use data assimilation) at daily resolution, covering a sufficiently long period to build a 30-year-long reliable climatology, as advised by the World Meteorological Organisation (WMO) (WMO, 2018; Hobday et al., 2016, 2018). The regular update of such a product so that it stays close to real time enables the study of recent events and the assessment of their characteristics relative to previous years.

We propose a 4-dimensional description (3D + time) of the ocean temperature extreme event of 2023 in the NA tropical ocean using the temperature field of the Copernicus Marine Service GLORYS12V1 reanalysis product (Lellouche et al., 2021), to which Hobday's MHW algorithm has been applied (Hobday at al., 2016, 2018). After the method description in Sect. 2, we propose, in Sect. 3, a characterisation of the 2023 event in the NA tropical ocean, from the surface to the subsurface. Conclusions and perspectives are given in Sect. 4.

2 Methods

2.1 Datasets

The main product used for this study is the GLOBAL_MULTIYEAR_PHY_001_030 reanalysis distributed by Copernicus Marine Service (product ref. no. 01; Table 1). This reanalysis is developed from the NEMO global ocean model, with a horizontal resolution of 1/12° (9 km at the Equator and 2 km close to the poles) and with 50 vertical levels where observational products are assimilated using a reduced-order Kalman filter. Along-track altimeter data (sea level anomaly), satellite sea surface temperature, sea ice concentration, and in situ temperature and salinity vertical profiles are jointly assimilated. Moreover, a 3D-VAR scheme provides a correction for the slowly evolving large-scale biases in temperature and salinity. This reanalysis covers the period 1993 onward. It was driven by the ERA Interim atmospheric fluxes from 1993 to 2019 and ERA5 thereafter. A more detailed description and study is proposed by Lellouche et al. (2021). The use of ocean reanalysis makes it possible to both study surface MHWs and compare the results with other satellite datasets but also to gain insight in their vertical structure. This reanalysis is particularly well suited to the study of near-surface phenomena due to its refined vertical discretisation in the first 50 m of the ocean (first 18 layers of the reanalysis). In this study we calculated a 30-year 3D daily climatology of temperature using the baseline period 1993–2022 and used the data from the year 2023 to characterise MHWs in the NA tropical ocean.

2.2 Characterisation of marine heatwaves

MHWs are prolonged periods of abnormally high seawater temperature. We identified an MHW event as a period of at least 5 consecutive days where the temperature exceeds the 90th percentile of a 30-year climatology, following the recommendations by Hobday et al. (2016). The 90th percentile and the mean temperature climatology were smoothed using a 31 d moving window to reduce high-frequency noise while detecting MHWs. First, we detected MHWs for the surface layer in 2023 using this definition to characterise the studied event. Then, we detected surface MHWs from 1993 to 2022 in order to compare the MHW characteristics over the climatology period. Additionally, we detected 2023 MHWs from the surface to 2225 m depth (the first 41 depth layers of the reanalysis) to investigate subsurface MHW signatures for this particular year.

The detected MHWs were characterised using common metrics such as duration (number of consecutive days above

the 90th percentile threshold), intensity and intensity-based category (moderate, strong, severe and extreme) (Hobday et al., 2016, 2018). Note that depending on the method, MHW intensity is defined either by the temperature anomaly relative to the mean climatology (Hobday et al., 2016; Oliver et al., 2018) or relative to the threshold (Darmaraki et al., 2019; Juza et al., 2022). Here, to focus on the study of extremes, we define MHW intensity as the temperature anomaly relative to the 90th percentile threshold. We also calculated the annual surface MHW activity (from 1993 to 2023) following the definition by Simon et al. (2022):

$$activity = \sum_{\text{event} \subset \text{year}} \overline{A}_{\text{event}} \times d_{\text{event} \subset \text{year}} \times S_{\text{event}}, \quad (1)$$

where "event" refers to a specific MHW event, "year" refers to a specific year, $\overline{A}_{\text{event}}$ (in °C) is the temperature anomaly during the event averaged over its duration, $d_{\text{event} \subset \text{year}}$ (in days) is the event duration within the specific year and S_{event} (in km^2) is the spatial extent of the event. Here we calculated activity for each grid cell, so S_{event} is the surface of the grid cell. Then we averaged the activity over the studied area to get the annual spatial mean activity (in °C d km^2).

We defined the studied area to focus on regions with long-lasting and intense MHWs, choosing the Atlantic from 10° S to 50° N. We divided the study area into coherent subregions following the definition of the Longhurst biogeochemical provinces (Reygondeau et al., 2013; Longhurst, 2007; shapefile from Flanders Marine Institute, 2009). Based on the highest mean activity regions for 2023 (not shown), we focused on the provinces denoted North Atlantic Subtropical Gyral Province (east) (NASE), North Atlantic Tropical Gyral Province (NATR) and Caribbean Province (CARB) (Fig. 2).

For time series, we spatially averaged the daily MHW intensity and the mixed layer depth (MLD) over each chosen Longhurst province. To generate the mean vertical MHW intensity profiles for a given province, we first temporally averaged the daily MHW intensity (using MHW days only) for each grid cell in the province at each depth; then, we spatially averaged the temporal mean values across all grid cell within the province, at each depth. We thus obtained one spatiotemporally averaged intensity vertical profile in the given province. We computed the standard deviation of the spatial mean, which provides insight into the degree of variability or spatial inhomogeneity across the province at each depth. For each province we estimated the MLD by averaging the MLD data distributed by GLOBAL_MULTIYEAR_PHY_001_030 first temporally (over 2023) and then spatially (over each province).

For horizontal Hovmöller diagrams, daily intensities were spatially selected using a mask with the three provinces of focus and then averaged across latitudes. Thus, when regions overlap in longitude (for instance NASE and NATR), data from both regions are averaged together. This method was used to generate Hovmöller diagrams for different depth. For the depth–time Hovmöller diagram, MHW intensity was selected using a mask of the specific region and then averaged over latitude and longitude.

2.3 Atmospheric variables

Using ERA5 reanalysis air temperature (TAIR) and 10 m wind ($U10$) data, we computed 2023 anomalies based on 30-year climatologies (1993–2022) to match the sea temperature climatology baseline (used to detect MHWs) (product ref. no. 02; Table 1). The air temperature anomaly ($\text{TAIR} - \text{TAIR}_{\text{clim}}$) was then smoothed over a 7 d window. For the wind at 10 m, we calculated the anomaly of the absolute values ($|U10| - |U10_{\text{clim}}|$) to focus on anomalies of intensity and not of direction. Then the anomaly was averaged over 2023.

Daily air temperature anomaly was averaged over latitude and used to generate a Hovmöller diagram (using the same method than for MHW intensity Hovmöller diagrams; see Sect. 2.2).

3 Results

3.1 An event of unprecedented characteristics at the surface

During the year 2023 an MHW event of extraordinary characteristics occurred in the NA tropical ocean, impacting the entire ocean region between 10° S and 50° N (Fig. 1a). The event developed in March, covering ∼20 % of the region predominantly in moderate conditions, to progressively peak from August to mid-October gaining in both extent and intensity occupying over 60 % of the area, with strong and higher categories progressively accounting for nearly 60 % of the MHW surface by mid-October (43.5 % for strong, 14.8 % for severe and 1.1 % for extreme on 15 October). A decrease in extent occurred in October and in December, with a small increase in November in between (Fig. 1b).

Overall, nearly the entire area (> 99 %) has been in MHW conditions at some point across the year, with such conditions going beyond moderate in terms of category (Fig. 2a). Indeed, only 8.3 % of the region was exposed to moderate-only events during the year, and this corresponds to regions in the vicinity of the Gulf Stream and its extension. In total, 40.2 % of the region has been exposed to a maximum level of the category strong, 40.7 % of the category severe, and 10.8 % of the category extreme and beyond. The most intense events span the Iberian Peninsula, the eastern side of the basin and the Caribbean region. It is noteworthy that the regions with most intense MHW events (Fig. 2a) coincide with regions with the highest number of marine heatwave days (long-lasting MHW areas of Fig. 1a); for instance, the region between 15 and 35° N spanning the east of the African coast until 40° W and the one close to Hispaniola island in the Caribbean region.

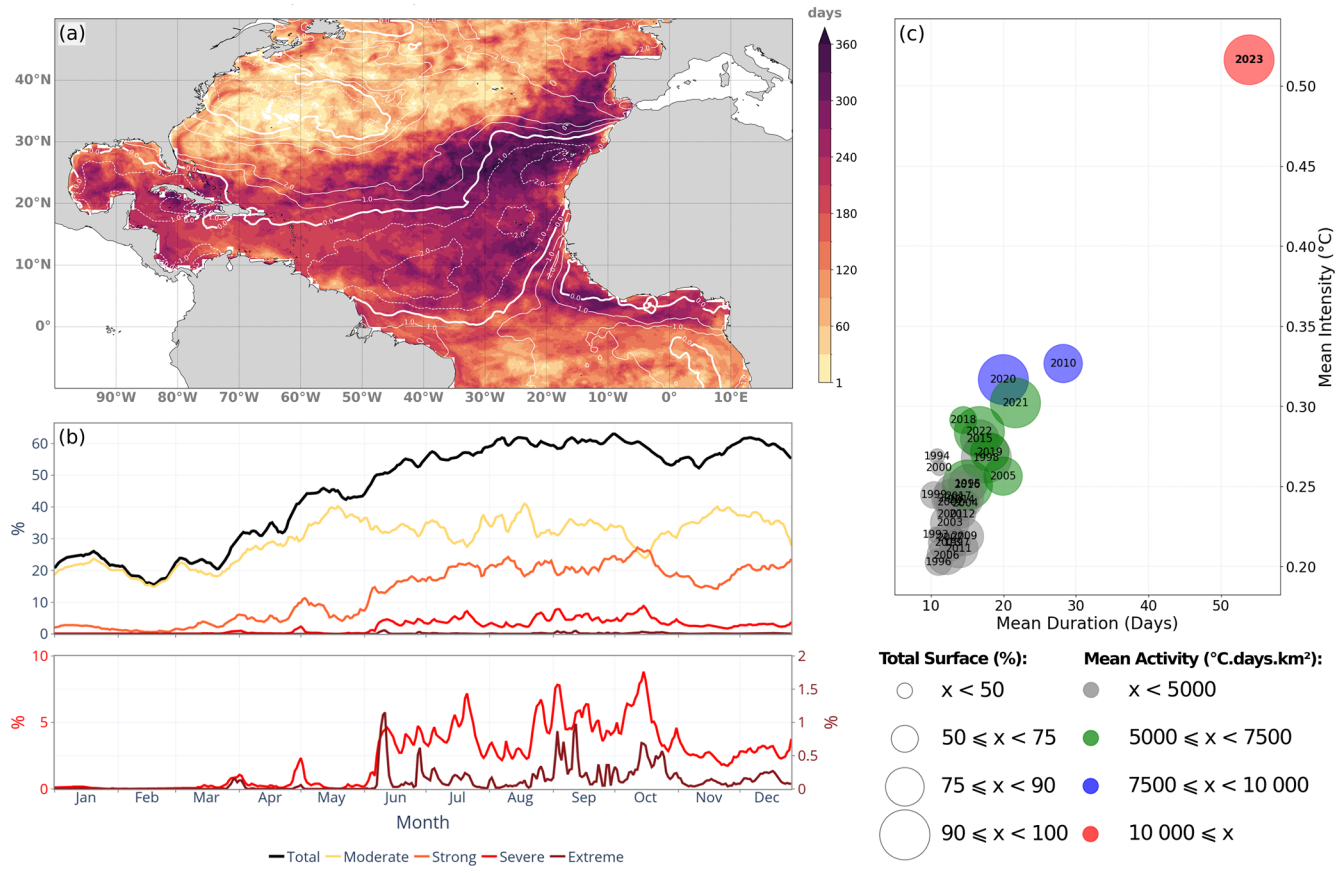

Figure 1. Characteristics of the marine heatwave hitting the North Atlantic across 2023 between 10° S and 50° N: total number of heatwave days **(a)**; evolution of the total area and area by category affected by MHW events **(b)**; and representation of the MHW event for 2023 in terms of mean duration, intensity, maximum coverage (bubble size) and activity (coloured bubble) relative to previous years **(c)**. White contours in panel **(a)** refers to the annual mean of absolute wind anomaly ($m\,s^{-1}$).

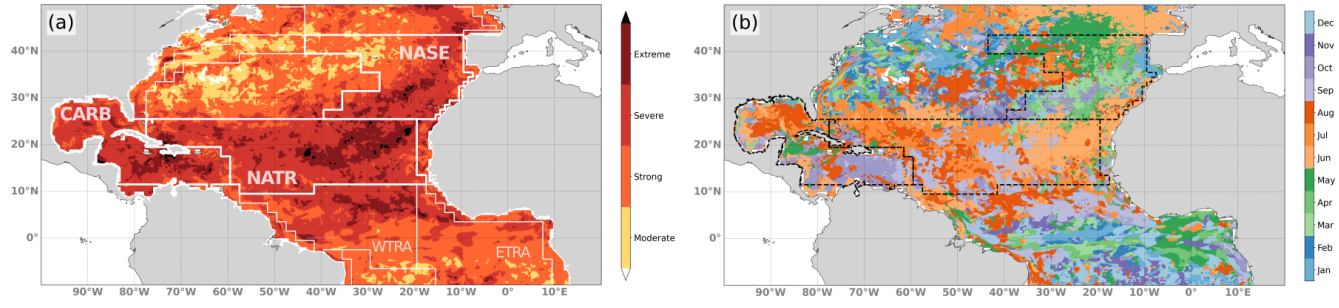

Figure 2. Highest marine heatwave category reached in 2023 **(a)** and month during which the highest category first occurred **(b)**. Zones delimited in white in panel **(a)** and black in panel **(b)** refer to the Longhurst biogeochemical provinces.

In terms of duration, a large proportion (19.9 % of the study region, mostly constrained within the triangle formed by the Iberian Peninsula, western Africa and the Caribbean region) was in MHW conditions for more than 250 d during the year (Fig. 1a). Most notably, the region off the coast of Morocco was exposed to more than 300 MHW days. The Gulf Stream region was more moderately impacted, with around 100 MHW days over the year 2023.

The year 2023 is characterised by an unprecedented MHW event outstanding in all indices commonly used to describe MHWs, with the highest mean daily intensity, mean duration, total surface exposed and mean activity (Fig. 1c). On average over a year, 2023 exceeds all previous years of the reanalysis product (1993–2022), with a mean duration of 54 d over the area, mean daily intensity of 0.52 °C and mean activity of 17 204 °C d km^2 (Simon et al., 2022). No other year

presents similar high values for a single one of these metrics (nor all three combined), underlining the extraordinary nature of the 2023 MHW event. Note that this extent corresponds to a strong negative anomaly in surface wind intensity (Fig. 1a).

The timing corresponding to the peak of the event in terms of MHW category (Fig. 2b) varied geographically, with the highest category first reached during springtime in the eastern part of the basin, then during July/August for the centre of the basin and during autumn for the western part.

3.2 Regional vertical structure of MHW

Beyond the extraordinary surface signature of the 2023 MHW event, we further investigate this event by characterising its vertical structure and evolution over time. For this, we divided the study area into physically coherent subregions as defined by Longhurst (Reygondeau et al., 2013; Longhurst, 2007) (Fig. 2a).

We focused on three subregions where intense and long MHW events occurred (Figs. 1a, 2a): the North Atlantic Subtropical Gyral Province (NASE), to the east of the basin; the North Atlantic Tropical Gyral Province (NATR), in the centre; and Caribbean Province (CARB) to the west. For each subregion, we computed the mean intensity depth profile and estimated the mean mixed layer depth (MLD) (see Methods).

The depth profile of MHW intensity is not identical across the basin, with significant differences across the region, most notably for the depth where the maximum intensity occurred (Fig. 3a). Intensity peaks at much deeper depth in the CARB region (max at 156 m, deeper than the mean MLD of 23.8 m represented by red dotted horizontal line) than for NASE and NATR regions. For NASE and NATR regions, maxima occur at 40 m and close to the surface, respectively, both within the mixed layer (MLD represented by blue and green dotted horizontal lines). The mean intensity profile of MHWs for NASE shows homogeneous levels across the mixed layer with slightly higher values at subsurface (40.3 m depth), at the bottom of the mixed layer. The NATR region shows a different MHW intensity profile than the NASE region, with a maximum in the surface layer. In addition, we notice from the standard deviation of the MHW intensity (shaded area) that spatial inhomogeneity is largest for the CARB region for depths between 150 and 400 m.

3.3 Evolution of MHW intensity and extent across depth

Further insight into MHW characteristics was obtained for each region by evaluating the evolution of intensity and spatial extent of the MHW at depths where maximum intensity occurred in each region (at the surface, 40 m and 156 m) (Fig. 3b, c and d).

At the surface, as observed in the month of highest MHW categories (Fig. 2b), later timing in the peak of MHW for the more westward regions is evidenced in the area-averaged intensity. Maximum intensity is reached earlier in the most eastern region, the NASE region (beginning of May), then in the NATR region (late July) and in the CARB region (October) (Fig. 3b solid blue line, Fig. 3c solid green line and Fig. 3d solid red lines). We also note a peak in March in the CARB region (lasting 10 d and reaching an intensity of 0.9 °C), which seems to be an isolated event and would require further investigation that is not done here.

For the NASE region, the intensity at the surface shows large fluctuations across the year: in total, six maxima of intensity higher than 0.8 °C are observed, followed by low troughs (with differences of 0.3 to 0.8 °C relative to the peaks) (Fig. 3b, solid blue line). The intensity at 40 m depth – where the maximum occurs in the mean intensity depth profile – increases progressively from 0.3 °C in early March to a peak in mid-December at 1.0 °C (Fig. 3b, dashed blue line). In between, some variations exist, with smaller peaks in mid-May and mid-October (occurring shortly after the surface peaks). The MHW signature at the surface develops earlier than at the subsurface. It suggests that the signal propagates from the surface, across the water column to the subsurface and below the MLD (Fig. 3b, orange line). The increase in area occupied by MHWs in March, for both the surface and 40 m depth, coincides with the shoaling of the MLD (Fig. 3b, solid and dashed grey lines, orange line). The horizontal extent is similar for both depths, with values fluctuating around 70 % of the area from April to mid-October. We note that the intensity at the surface and at 40 m depth is equal during the winter period. This is linked to the deepening of the MLD to levels deeper than 40 m, which homogenise temperature (Fig. 3b, orange line). Unlike shallower depths, the intensity at 156 m remains stable around 0.4 °C across the year (Fig. 3b, dotted blue line). Extent is lower at 156 m depth, with values remaining between 20 % and 30 %. Note that, in between 40 and 156 m, surface warming propagates progressively at depth across the year. For instance, at 100 m depth, from February onwards, the intensity levels steadily increase from values of 0.29 to 0.61 °C by mid-November (see Fig. 4e).

The evolution of the mean intensity for NATR, at the surface and at depth, describes a different kind of MHW than for the NASE region (Fig. 3c, green lines). The MHW is characterised by one long temporal event – rather than a series of shorter events – that peaks at the end of July. At the surface, high intensity develops rapidly in early June and remains high until the end of September, with values constantly above 0.5 °C (Fig. 3c, solid green line). Horizontal extent of the MHW increases in two steps: first reaching ∼ 70 % at the end of April–May and then above 90 % from mid-June to November, to finally drop slightly below 80 % (Fig. 3c, solid grey line).

At 40 m depth, a rapid increase in intensity occurs later relative to the surface, starting at the end of May at 0.4 °C to reach a maximum of 0.77 °C by the end of July (Fig. 3c, dashed green line). Spatial extent increases progressively

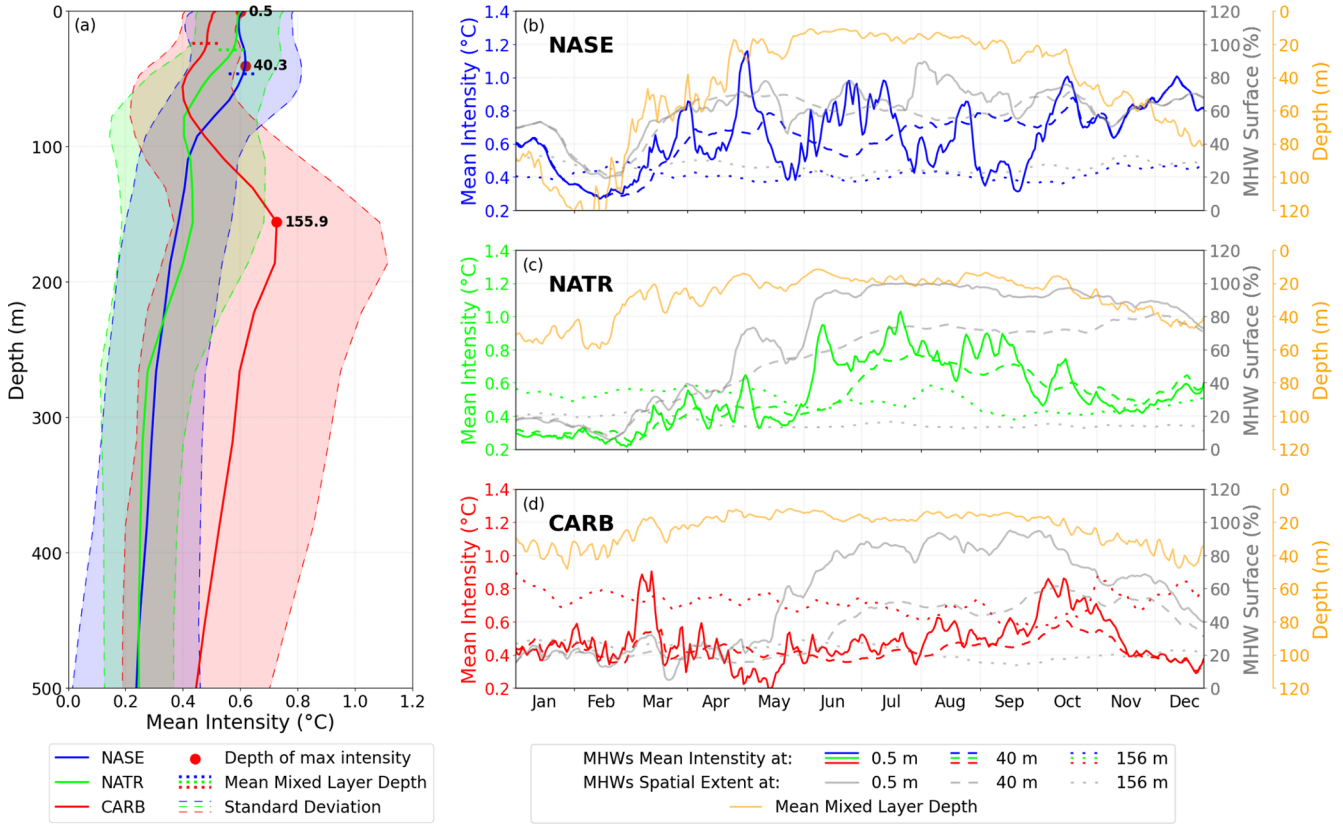

Figure 3. Evolution of the intensity and spatial extent of the 2023 marine heatwave for different regions in the North Atlantic. Mean MHW intensity (in °C) profile **(a)** of NASE (blue), NATR (green) and CARB (red). Shaded areas represent standard deviations of spatial mean. Dotted horizontal lines represent the mean MLD, and red dots represent depth of highest mean intensity for each region. Time series of mean intensity (in °C), surface coverage (in %) and mean mixed layer depth (in m) in NASE **(b)**, NATR **(c)** and CARB **(d)** provinces. Blue, green and red lines (NASE, NATR and CARB, respectively) represent the mean intensity at the surface (solid), at 40 m (dashed) and at 156 m (dotted). Grey lines represent the surface coverage at the surface (solid), at 40 m (dashed) and at 156 m (dotted). Orange lines represent the mean layer depth in the corresponding region.

from ∼ 40 % coverage in April to above 80 % by the end of November (Fig. 3c, dashed grey line). These increases (in intensity and at surface) occur when the MLD is shallowest (about 20 m), meaning that the MHW reaches below the MLD (Fig. 3c, orange line). At 156 m depth, intensity levels vary across the year around 0.4–0.6 °C, and the horizontal extent of MHW remains low and stable (around 15 %–20 %) (Fig. 3c, dotted green and grey lines). This signal is decorrelated with what is observed for surface layers.

Dynamics for the CARB region differ with the NASE and NATR regions, with an MHW signal at both surface and depth (Fig. 3d). At the surface, a late and long-lasting peak of MHW intensity (larger than 0.6 °C for 30 d) occurs in October (peaks at 0.86 °C), after the observed peaks in the other two regions (Fig. 3b, c and d, coloured solid lines). At 40 m depth, intensity levels and fluctuations are similar to the surface, with lower magnitude and reduced high-frequency variations (Fig. 3d, red dashed line). Timing in the peaks in March and October shows a lag relative to the surface. MHW horizontal extent at the surface increases from mid-May (∼ 30 %) to a peak in late September (up to 95 % of the area) to then decrease by the end of the year (∼ 40 %) (solid grey line). A similar pattern can be seen at 40 m depth, with an increase in surface occurring later (mid-June) and peaking mid-October at ∼ 60 % to drop to ∼ 30 % by the end of the year (dashed grey line). Again, these similar features between the surface and 40 m depth happen with a MLD of about 20 m, suggesting that the MHW also propagates below the MLD in this region (Fig. 3d, orange line).

At 156 m depth – corresponding to the maximum intensity in the mean profile – unlike for the other two regions, intensity levels are higher than levels reached for shallower depths (dotted red line). The intensity remains stable throughout the year, ranging between 0.6 and 0.8 °C. It is higher than the intensity at shallower depth, except for May and October when surface MHWs develop. High levels of intensity are however not widespread across the subregion as the surface exposed to MHWs remains around 20 % across the year (dotted grey line). It is noteworthy that sub-monthly variations are present

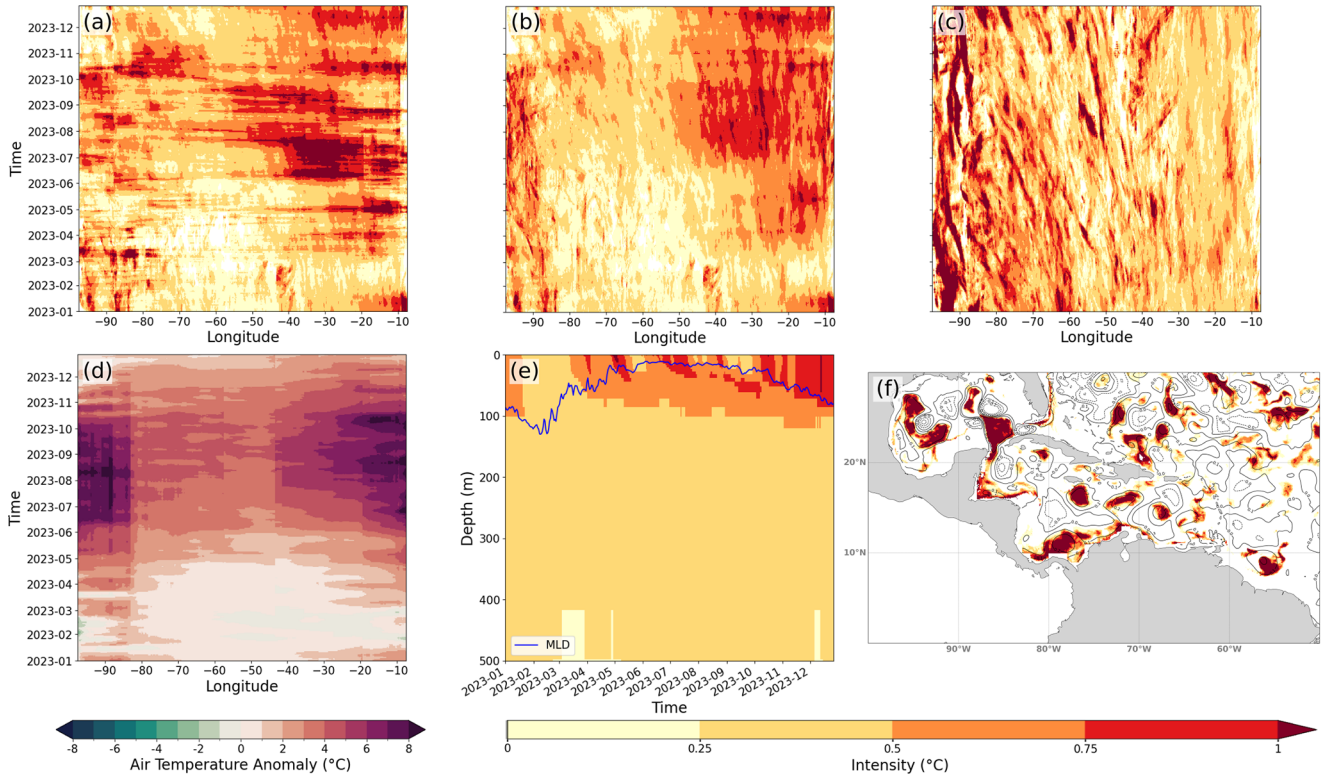

Figure 4. Horizontal MHW and atmospheric characteristics evolution in NASE, NATR and CARB regions. Hovmöller diagrams of MHW intensity at the surface **(a)**, at 40 m **(b)** and at 156 m **(c)** (data averaged over latitude); Hovmöller diagram of daily air temperature anomaly at 2 m smoothed over a 7 d window **(d)**; depth–time Hovmöller diagram of intensity in NASE region (date averaged over latitude and longitude), where the blue line represents the average MLD over the region **(e)**; and map of MHW intensity on 7 July 2023 at 156 m depth with SSH anomaly contours in black **(f)**.

in the MHW intensity time series, suggestive of advective transient features like eddies crossing the domain.

3.4 MHW westward and vertical evolution

Analysis of MHW within the three subregions of the NA suggests that MHW surface signature propagates westward and at depth. To further investigate such dynamics and potential drivers, a 3-dimensional decomposition along longitude, depth and time of the MHW intensity field and its possible drivers is carried out. The evolution of MHW across the year and the studied regions is highlighted using Hovmöller diagrams of latitudinal averaged intensity over the three subregions at the three depths of maximum intensity (surface, 40 and 156 m) (see Methods, Fig. 4a, b and c).

For the surface, the strongest intensity (greater than 0.5 °C) takes place primarily in the eastern half of the region (between 60 and 10° W) and during the months of May to December (Fig. 4a). This surface signature of the MHW can be directly associated with atmospheric features as large positive air temperature anomalies are observed, which coincide in time and space with the MHW intensity patterns (Fig. 4d). This suggests a direct response of the surface ocean to the atmospheric anomaly. The eastern part is characterised by a larger number of peaks from March to December (as seen in the MHW intensity time series for the NASE subregion Fig. 3b), whereas moving westwards to the central part of the region, the period of high intensity is reduced to the July to October period, forming a single large spatiotemporal peak. Furthermore, we note that the pronounced intensity patterns in the eastern part (anomalies larger than 0.75 °C) propagate rapidly westward, most notably between 10 and 70° W at an estimated velocity of $\sim 11\,\mathrm{m\,s^{-1}}$ (first-order estimations based on the slope of the intensity pattern in Fig. 4a), starting in July and occurring nearly every month. To the west (70 to 100° W), fast west propagation from signal in the central part of the basin can be observed in October. Further west than 80° W, a period of strong MHW intensity (July to October) coincides with a period of strong positive air temperature anomalies.

The patterns of intensity at 40 m depth relate strongly with patterns at the surface, namely large intensity in the eastern half of the region spanning April to December (Fig. 4b). Peaks in intensity are smaller than for the surface, and patterns contain less high-frequency signal. Similarly to the sur-

face, multiple peaks in intensity characterise the eastern part and a single long event the central part (30–50° W).

The similarity of the MHW signature at 40 m to the surface suggests that the atmospheric-driven MHW at the surface also reaches deeper layers. This correlation is confirmed by a depth–time Hovmöller diagram of the NASE region (Fig. 4e). Across the period from March to November, the region is exposed to several high peaks in MHW intensity at the surface (as seen in Fig. 3b). These propagate rapidly across the mixed layer and vary from 100 to 20 m in depth between winter and summer seasons.

This vertical propagation also extends below the MLD (Fig. 4e). MHW intensity larger than 0.5 °C can be observed below the MLD from April onwards: at 70 m depth in April and progressively reaching 100 m by November. The propagation across the mixed layer is rapid, with an estimated velocity of $\sim 4\,\mathrm{m\,d^{-1}}$. Below the MLD, the propagation is slower, ranging between 0.7–1.3 $\mathrm{m\,d^{-1}}$. A direct consequence is that the MHW-driven heat accumulation is trapped below the MLD to remain within the ocean interior and to be advected far away from the formation area.

At 156 m depth, patterns in MHW intensity are very different to what is observed at the surface (Fig. 4c). On the eastern side, there is no clear signature with only low MHW intensity levels. To the west, MHW intensity also differs from the surface, but unlike the east some small-spatial-scale patterns emerge: west of 70° W and for the period of September to November, intensity displays diagonal patterns, showing MHW intensity propagating westward with an estimated velocity of $\sim 0.1\,\mathrm{m\,s^{-1}}$. Such westward velocity is characteristic of eddies crossing the Caribbean Basin (Richardson, 2005; Cailleau et al., 2024), suggesting such features are responsible for the intense MHW conditions locally as they trap and carry westward abnormally warm waters. A snapshot of the MHW intensity on 7 July 2023 at 156 m depth overlaid with the sea surface height (SSH) anomaly confirms the intensities are trapped in the anticyclonic eddies at depth in this region (Fig. 4f). Note that blank areas represent areas where no MHWs were detected or that are outside the studied area (e.g. in the Pacific Ocean).

These very strong local intensities (larger than 2 °C above the 90th percentile threshold) are limited in space and explain the low and stable horizontal extent of MHWs in the CARB region at 156 m depth (Fig. 3d, dotted grey line). Some of these anomalies come from the NATR region but predominantly from the Equatorial and North Brazil currents located below the NATR region (e.g. the eddies located at 57° W–10° N on Fig. 4f). A detailed study of this region is necessary to understand the processes leading to eddy-trapped heat crossing the region; this however falls beyond the range of our study area and would also require a longer study period spanning beyond 2023 as MHW signatures are still strongly present in 2024 at the Equator.

4 Discussion and conclusions

Various meteorological and oceanographic estimates showed that the year 2023 was exceptional in terms of heat records and in particular the NA region. We studied the region using the Copernicus Marine global reanalysis product and characterised the MHW signature both at the surface and at depth. Compared to previous years, we show the exceptional nature of the 2023 MHW in the NA tropical ocean, which surpasses the last 30 years in terms of duration, intensity and coverage. A strong link with surface atmospheric conditions is shown (air temperature, negative trade wind anomaly). We also note an evolution of the timing of MHW maxima during the year, with maxima in the east of the basin during the months of May and June, the central part in mid-summer, and the Caribbean Sea in September. A decomposition into different regions of interest for marine biology (Longhurst provinces) and an in-depth study on these regions highlighted the vertical structure and evolution of MHWs in each region. We note a progressive penetration of the MHW below the MLD in the eastern part, together with a progressive intensification of the MHW intensity across the year. This is a remarkable phenomenon, which could potentially be important because it induces transport into the ocean interior of heat anomalies following surface extreme events. In the west, the Caribbean Sea region shows a very strong yet very localised MHW signal in the subsurface, with a maximum around 156 m. These anomalies characteristic of heat trapping eddies originate partly from the NA tropical ocean but mainly from the North Brazil Current. A dedicated study on eddy-trapped heat pathways to the ocean interior should be considered in the future but will have to extend beyond the year 2023 because in the tropical zone (2° S–2° N) MHWs are still ubiquitous in 2024.

Also, a more comprehensive and detailed quantification of the different contributions of ocean and atmospheric processes is needed to thoroughly understand this unprecedented event. In this sense, Guinaldo et al. (2025) describe the ocean preconditioning and mechanism that lead to the occurrence of this unprecedent event. Also, an approach based on the reconstruction of the heat equation could be taken for which the use of the reanalysis would be instrumental to quantify dominant processes (as it would provide gridded 3D fields at a 1 d frequency that reduce errors due to the non-linearity of the equation and the approximation of the estimation of the depth of the mixed layer). In view of the exceptional general characteristics of the MHW of 2023 in the NA, further studies are needed, for example to quantify the impact on marine biogeochemistry (BGC), a study for which a BGC reanalysis of Copernicus Marine can be used (GLOBAL_MULTIYEAR_BGC_001_029), but also on the distribution of *Sargassum* algae – which have a strong societal harmful impact – that develop largely in the Gulf of Guinea and are advected as far as the Caribbean region (Jouanno et al., 2021). In addition, the definition of ex-

tremes could be regionalised and tailored to be representative of harm towards key local species (Capotondi et al., 2024; Oliver et al., 2021).

In this study, the potential of ocean reanalyses to characterise a specific event was shown. Further work on the detection and analysis of extremes would be of interest to assess the MHW impact and importance on the more general climate context. Heat from this NA MHW propagates under the mixed layer to reach different depths depending on the region. Such strong anomalies once away from the surface and trapped within subsurface water masses can potentially be advected over long distances, such as the heat anomalies observed in this study at the Equator, which were consequently advected to the Caribbean region, the Gulf of Mexico and potentially back into the NA through the Gulf Stream. Detection and monitoring of extremes over the 30 years of the reanalysis will enable an initial scheme and an initial quantification of the importance of such extremes for the overall ocean interior heat content to be proposed. This estimate will then have to be compared to datasets with a longer time period in order to validate the hypotheses deduced from the study of the GLORYS12 reanalysis fields.

Code availability. MHW detection was done using the marineHeatWaves Python module (Oliver, 2016).

Data availability. Data access information is listed in Table 1.

Author contributions. SJVG and RBB led the conceptualisation of the study, the analysis and writing of the manuscript. AL performed the simulations, data analysis and the writing of the manuscript. MD contributed to the conceptualisation of the study and review of the manuscript.

Competing interests. The contact author has declared that none of the authors has any competing interests.

Disclaimer. Publisher's note: Copernicus Publications remains neutral with regard to jurisdictional claims made in the text, published maps, institutional affiliations, or any other geographical representation in this paper. While Copernicus Publications makes every effort to include appropriate place names, the final responsibility lies with the authors.

Acknowledgements. We would like to thank the Ocean State Report team for the insightful comments and advice during the development of this paper.

Review statement. This paper was edited by Pierre-Marie Poulain and reviewed by Milena Menna and one anonymous referee.

References

Cailleau, S., Bessières, L., Chiendje, L., Dubost, F., Reffray, G., Lellouche, J.-M., van Gennip, S., Régnier, C., Drevillon, M., Tressol, M., Clavier, M., Temple-Boyer, J., and Berline, L.: CAR36, a regional high-resolution ocean forecasting system for improving drift and beaching of *Sargassum* in the Caribbean archipelago, Geosci. Model Dev., 17, 3157–3173, https://doi.org/10.5194/gmd-17-3157-2024, 2024.

Capotondi, A., Rodrigues, R. R., Sen Gupta, A., Benthuysen, J. A., Deser, C., Frölicher, T. L., Lovenduski, N. S., Amaya, D. J., Le Grix, N., Xu, T., Hermes, J., Holbrook, N. J., Martinez-Villalobos, C., Masina, S., Roxy, M. K., Schaeffer, A., Schlegel, R. W., Smith, K. E., and Wang, C.: A global overview of marine heatwaves in a changing climate, Commun. Earth Environ., 5, 1–17, https://doi.org/10.1038/s43247-024-01806-9, 2024.

Cavole, L., Demko, A., Diner, R., Giddings, A., Koester, I., Pagniello, C., Paulsen, M.-L., Ramirez-Valdez, A., Schwenck, S., Yen, N., Zill, M., and Franks, P.: Biological Impacts of the 2013–2015 Warm-Water Anomaly in the Northeast Pacific: Winners, Losers, and the Future, Oceanography, 29, 273–285, https://doi.org/10.5670/oceanog.2016.32, 2016.

Copernicus: Record high global sea surface temperatures continue in August, Copernicus, https://climate.copernicus.eu/record-high-global-sea-surface-temperatures-continue-august (last access: 14 May 2025), 2023.

Copernicus Climate Change Service, Climate Data Store: ERA5 hourly data on single levels from 1940 to present, Copernicus Climate Change Service (C3S) Climate Data Store (CDS) [dataset], https://doi.org/10.24381/cds.adbb2d47, 2023.

Darmaraki, S., Somot, S., Sevault, F., and Nabat, P.: Past Variability of Mediterranean Sea Marine Heatwaves, Geophysical Research Letters, 46, 9813–9823, https://doi.org/10.1029/2019GL082933, 2019.

Drévillon, M., Lellouche, J.-M., Régnier, C., Garric, G., Bricaud, C., Hernandez, O., and Bourdallé-Badie, R.: EU Copernicus Marine Service Quality Information Document for the Globam Physics Reanalysis, GLOBAL_REANALYSIS_PHY_001_030, issue 1.6, Mercator Ocean International, https://documentation.marine.copernicus.eu/QUID/CMEMS-GLO-QUID-001-030.pdf (last access: 14 May 2025), 2023.

Drévillon, M., Fernandez, E., and Lellouche, J. M.: EU Copernicus Marine Service Product User Manual for the Global Ocean Physics Reanalysis, GLOBAL_MULTIYEAR_PHY_001_030, issue 1.6, Mercator Ocean International, https://documentation.marine.copernicus.eu/PUM/CMEMS-GLO-PUM-001-030.pdf (last access: 14 May 2025), 2024.

Elzahaby, Y. and Schaeffer, A.: Observational Insight Into the Subsurface Anomalies of Marine Heatwaves, Front. Mar. Sci., 6, 745, https://doi.org/10.3389/fmars.2019.00745, 2019.

Elzahaby, Y., Schaeffer, A., Roughan, M., and Delaux, S.: Oceanic Circulation Drives the Deepest and Longest Marine Heatwaves in the East Australian Current Sys-

tem, Geophysical Research Letters, 48, e2021GL094785, https://doi.org/10.1029/2021GL094785, 2021.

ESOTC: European State of the Climate 2023, Copernicus Climate Change Service (C3S), https://doi.org/10.24381/BS9V-8C66, 2024.

EU Copernicus Marine Service Product (CMEMS): Global Ocean Physics Reanalysis, Mercator Ocean International [dataset], https://doi.org/10.48670/moi-00021, 2023.

Flanders Marine Institute: Longhurst Provinces, Marine Regions, Flanders Marine Institute [dataset], https://www.marineregions.org/ (last access: 2 August 2024), 2009.

Forster, P. M., Smith, C., Walsh, T., Lamb, W. F., Lamboll, R., Hall, B., Hauser, M., Ribes, A., Rosen, D., Gillett, N. P., Palmer, M. D., Rogelj, J., von Schuckmann, K., Trewin, B., Allen, M., Andrew, R., Betts, R. A., Borger, A., Boyer, T., Broersma, J. A., Buontempo, C., Burgess, S., Cagnazzo, C., Cheng, L., Friedlingstein, P., Gettelman, A., Gütschow, J., Ishii, M., Jenkins, S., Lan, X., Morice, C., Mühle, J., Kadow, C., Kennedy, J., Killick, R. E., Krummel, P. B., Minx, J. C., Myhre, G., Naik, V., Peters, G. P., Pirani, A., Pongratz, J., Schleussner, C.-F., Seneviratne, S. I., Szopa, S., Thorne, P., Kovilakam, M. V. M., Majamäki, E., Jalkanen, J.-P., van Marle, M., Hoesly, R. M., Rohde, R., Schumacher, D., van der Werf, G., Vose, R., Zickfeld, K., Zhang, X., Masson-Delmotte, V., and Zhai, P.: Indicators of Global Climate Change 2023: annual update of key indicators of the state of the climate system and human influence, Earth Syst. Sci. Data, 16, 2625–2658, https://doi.org/10.5194/essd-16-2625-2024, 2024.

Frölicher, T. L. and Laufkötter, C.: Emerging risks from marine heat waves, Nat. Commun., 9, 650, https://doi.org/10.1038/s41467-018-03163-6, 2018.

Frölicher, T. L., Fischer, E. M., and Gruber, N.: Marine heatwaves under global warming, Nature, 560, 360–364, https://doi.org/10.1038/s41586-018-0383-9, 2018.

Guinaldo, T., Cassou, C., Sallée, J.-B., and Liné, A.: Internal variability effect doped by climate change drove the 2023 marine heat extreme in the North Atlantic, Commun. Earth Environ., 6, 1–11, https://doi.org/10.1038/s43247-025-02197-1, 2025.

Hersbach, H., Bell, B., Berrisford, P., Biavati, G., Horányi, A., Muñoz Sabater, J., Nicolas, J., Peubey, C., Radu, R., Rozum, I., Schepers, D., Simmons, A., Soci, C., Dee, D., and Thépaut, J.-N.: ERA5 hourly data on single levels from 1940 to present, Copernicus Climate Change Service (C3S) Climate Data Store (CDS) [dataset], https://doi.org/10.24381/cds.adbb2d47, 2023.

Hobday, A. J., Alexander, L. V., Perkins, S. E., Smale, D. A., Straub, S. C., Oliver, E. C. J., Benthuysen, J. A., Burrows, M. T., Donat, M. G., Feng, M., Holbrook, N. J., Moore, P. J., Scannell, H. A., Sen Gupta, A., and Wernberg, T.: A hierarchical approach to defining marine heatwaves, Prog. Oceanogr., 141, 227–238, https://doi.org/10.1016/j.pocean.2015.12.014, 2016.

Hobday, A. J., Oliver, E. C. J., Gupta, A. S., Benthuysen, J. A., and Burrows, M. T.: Categorizing and Naming Marine Heatwaves, Oceanography, 31, 162–173, https://doi.org/10.5670/oceanog.2018.205, 2018.

Jouanno, J., Benshila, R., Berline, L., Soulié, A., Radenac, M.-H., Morvan, G., Diaz, F., Sheinbaum, J., Chevalier, C., Thibaut, T., Changeux, T., Menard, F., Berthet, S., Aumont, O., Ethé, C., Nabat, P., and Mallet, M.: A NEMO-based model of *Sargassum* distribution in the tropical Atlantic: description of the model and sensitivity analysis (NEMO-Sarg1.0), Geosci. Model Dev., 14, 4069–4086, https://doi.org/10.5194/gmd-14-4069-2021, 2021.

Juza, M., Fernández-Mora, À., and Tintoré, J.: Sub-Regional Marine Heat Waves in the Mediterranean Sea From Observations: Long-Term Surface Changes, Sub-Surface and Coastal Responses, Front. Mar. Sci., 9, 785771, https://doi.org/10.3389/fmars.2022.785771, 2022.

Lellouche, J.-M., Greiner, E., Bourdallé-Badie, R., Garric, G., Melet, A., Drévillon, M., Bricaud, C., Hamon, M., Le Galloudec, O., Regnier, C., Candela, T., Testut, C.-E., Gasparin, F., Ruggiero, G., Benkiran, M., Drillet, Y., and Le Traon, P.-Y.: The Copernicus Global 1/12° Oceanic and Sea Ice GLORYS12 Reanalysis, Front. Earth Sci., 9, 698876, https://doi.org/10.3389/feart.2021.698876, 2021.

Le Nohaïc, M., Ross, C. L., Cornwall, C. E., Comeau, S., Lowe, R., McCulloch, M. T., and Schoepf, V.: Marine heatwave causes unprecedented regional mass bleaching of thermally resistant corals in northwestern Australia, Sci. Rep., 7, 14999, https://doi.org/10.1038/s41598-017-14794-y, 2017.

Longhurst, A. R.: Ecological Geography of the Sea, Academic Press., Londre, 560 pp., https://doi.org/10.1016/B978-0-12-455521-1.X5000-1, 2007.

Oliver, E. C. J: marineHeatWaves, GitHub [code], https://github.com/ecjoliver/marineHeatWaves (last access: 2 August 2025), 2016.

Oliver, E. C. J., Donat, M. G., Burrows, M. T., Moore, P. J., Smale, D. A., Alexander, L. V., Benthuysen, J. A., Feng, M., Sen Gupta, A., Hobday, A. J., Holbrook, N. J., Perkins-Kirkpatrick, S. E., Scannell, H. A., Straub, S. C., and Wernberg, T.: Longer and more frequent marine heatwaves over the past century, Nat. Commun., 9, 1324, https://doi.org/10.1038/s41467-018-03732-9, 2018.

Oliver, E. C. J., Burrows, M. T., Donat, M. G., Sen Gupta, A., Alexander, L. V., Perkins-Kirkpatrick, S. E., Benthuysen, J. A., Hobday, A. J., Holbrook, N. J., Moore, P. J., Thomsen, M. S., Wernberg, T., and Smale, D. A.: Projected Marine Heatwaves in the 21st Century and the Potential for Ecological Impact, Front. Mar. Sci., 6, 734, https://doi.org/10.3389/fmars.2019.00734, 2019.

Oliver, E. C. J., Benthuysen, J. A., Darmaraki, S., Donat, M. G., Hobday, A. J., Holbrook, N. J., Schlegel, R. W., and Gupta, A. S.: Marine Heatwaves, Annu. Rev. Mar. Sci., 13, 313–342, https://doi.org/10.1146/annurev-marine-032720-095144, 2021.

Pirro, A., Martellucci, R., Gallo, A., Kubin, E., Mauri, E., Juza, M., Notarstefano, G., Pacciaroni, M., Bussani, A., and Menna, M.: Subsurface warming derived from Argo floats during the 2022 Mediterranean marine heat wave, in: 8th edition of the Copernicus Ocean State Report (OSR8), edited by: von Schuckmann, K., Moreira, L., Grégoire, M., Marcos, M., Staneva, J., Brasseur, P., Garric, G., Lionello, P., Karstensen, J., and Neukermans, G., Copernicus Publications, State Planet, 4-osr8, 18, https://doi.org/10.5194/sp-4-osr8-18-2024, 2024.

Reygondeau, G., Longhurst, A., Martinez, E., Beaugrand, G., Antoine, D., and Maury, O.: Dynamic biogeochemical provinces in the global ocean, Global Biogeochem. Cy., 27, 1046–1058, https://doi.org/10.1002/gbc.20089, 2013.

Richardson, P. L.: Caribbean Current and eddies as observed by surface drifters, Deep-Sea Res. Pt. II, 52, 429–463, https://doi.org/10.1016/j.dsr2.2004.11.001, 2005.

Schaeffer, A., Sen Gupta, A., and Roughan, M.: Seasonal stratification and complex local dynamics control the subsurface structure of marine heatwaves in Eastern Australian coastal waters, Commun. Earth Environ., 4, 1–12, https://doi.org/10.1038/s43247-023-00966-4, 2023.

Simon, A., Plecha, S. M., Russo, A., Teles-Machado, A., Donat, M. G., Auger, P.-A., and Trigo, R. M.: Hot and cold marine extreme events in the Mediterranean over the period 1982-2021, Front. Mar. Sci., 9, 892201, https://doi.org/10.3389/fmars.2022.892201, 2022.

Smith, K. E., Burrows, M. T., Hobday, A. J., Sen Gupta, A., Moore, P. J., Thomsen, M., Wernberg, T., and Smale, D. A.: Socioeconomic impacts of marine heatwaves: Global issues and opportunities, Science, 374, eabj3593, https://doi.org/10.1126/science.abj3593, 2021.

Smith, K. E., Burrows, M. T., Hobday, A. J., King, N. G., Moore, P. J., Gupta, A. S., Thomsen, M. S., Wernberg, T., and Smale, D. A.: Biological Impacts of Marine Heatwaves, Annu. Rev. Mar. Sci., 15, 119–145, https://doi.org/10.1146/annurev-marine-032122-121437, 2023.

Sun, D., Li, F., Jing, Z., Hu, S., and Zhang, B.: Frequent marine heatwaves hidden below the surface of the global ocean, Nat. Geosci., 16, 1099–1104, https://doi.org/10.1038/s41561-023-01325-w, 2023.

Wernberg, T., Smale, D. A., Tuya, F., Thomsen, M. S., Langlois, T. J., De Bettignies, T., Bennett, S., and Rousseaux, C. S.: An extreme climatic event alters marine ecosystem structure in a global biodiversity hotspot, Nat. Clim. Change, 3, 78–82, https://doi.org/10.1038/nclimate1627, 2013.

Wernberg, T., Bennett, S., Babcock, R. C., de Bettignies, T., Cure, K., Depczynski, M., Dufois, F., Fromont, J., Fulton, C. J., Hovey, R. K., Harvey, E. S., Holmes, T. H., Kendrick, G. A., Radford, B., Santana-Garcon, J., Saunders, B. J., Smale, D. A., Thomsen, M. S., Tuckett, C. A., Tuya, F., Vanderklift, M. A., and Wilson, S.: Climate-driven regime shift of a temperate marine ecosystem, Science, 353, 169–172, https://doi.org/10.1126/science.aad8745, 2016.

World Meteorological Organization (WMO): Guide to climatological practices, Doc., WMO-No 100, Geneva, 139 pp., ISBN 978-92-63-10100-6, 2018.

World Meteorological Organization (WMO): WMO confirms that 2023 smashes global temperature record, World Meteorological Organization, https://wmo.int/news/media-centre/wmo-confirms-2023-smashes-global-temperature-record (last access: 14 May 2025), 2024.

Zhang, Y., Du, Y., Feng, M., and Hobday, A. J.: Vertical structures of marine heatwaves, Nat. Commun., 14, 6483, https://doi.org/10.1038/s41467-023-42219-0, 2023.

State Planet, 6-osr9, 12, 2025
https://doi.org/10.5194/sp-6-osr9-12-2025

An analysis of the 2023 summer and fall marine heat waves on the Newfoundland and Labrador Shelf

Nancy Soontiens[1], Heather J. Andres[1], Jonathan Coyne[1], Frédéric Cyr[1,a], Peter S. Galbraith[2], and Jared Penney[1]

[1]Northwest Atlantic Fisheries Centre, Fisheries and Oceans Canada, St. John's, NL, A1C 5X1, Canada
[2]Institut Maurice-Lamontagne, Fisheries and Oceans Canada, Mont-Joli, QC, G5H 3Z4, Canada
[a]now at: Center for Fisheries and Ecosystem Research, Fisheries and Marine Institute of Memorial University of Newfoundland, St. John's, NL, Canada

Correspondence: Nancy Soontiens (nancy.soontiens@dfo-mpo.gc.ca)

Received: 29 July 2024 – Discussion started: 25 September 2024
Revised: 30 April 2025 – Accepted: 13 May 2025 – Published: 30 September 2025

Abstract. In this study, we investigated a series of moderate to severe surface marine heat waves (MHWs) impacting the Newfoundland and Labrador (NL) Shelf during the summer and fall of 2023. Using a combination of ocean model reanalysis data, in situ data collected under the Atlantic Zone Monitoring Program (AZMP), and atmospheric reanalysis data, we explored several factors that contributed to the intensity of these MHWs. We concluded that, firstly, due to an unusually cold spring and abnormally fresh conditions advected from upstream, the water column was highly stratified. Secondly, atmospheric conditions were calm and anomalously warm, and wind speeds were unusually low for prolonged periods in the summer. The combination of increased stratification and lower wind speeds caused a reduction in vertical mixing, limiting the exchange of warm surface waters with colder waters below and amplifying the retention of heat near the surface. However, by the late fall, the signature of the surface heat wave had vanished when the cooler subsurface waters were mixed vertically due to increased winds, storms, and surface cooling. During the most intense MHW in July 2023, we found that this event was confined to the surface as demonstrated by temperature anomalies along several standard transects which showed a thin layer of warm anomalies in the upper 10 m and cold anomalies below. Consequently, the vertical extent and distribution of MHWs are important considerations when exploring ecosystem impacts because not all elements of the ecosystem are equally sensitive to surface conditions. Finally, these results suggest that ocean model nowcast and reanalysis products can complement observational methods for studying MHWs in near real-time over large geographic areas and at multiple depths.

1 Introduction

In the summer of 2023, the North Atlantic Ocean experienced a series of significant marine heat waves (MHWs), sparking media attention and public interest in the associated record-setting high ocean temperatures. These MHWs were first detected in the Northeast Atlantic in June and, later, in the Northwest Atlantic in July (Copernicus, 2023). Ocean warming and MHWs can have significant impacts on the marine ecosystem (e.g. Le Grix et al., 2021; Geoffroy et al., 2023, Smith et al., 2023), air–sea exchange (e.g. Edwing et al., 2024), and weather (e.g. Frölicher and Laufkötter, 2018). Globally, MHWs are occurring more frequently and with greater duration (Oliver et al, 2018; IPCC, 2019, 2023). As such, it is critical to develop a more complete understanding of their drivers (Oliver et al., 2021) which will lead to improved real-time monitoring efforts and forecasting capabilities (e.g. McAdam et al., 2023).

Published by Copernicus Publications.

Table 1. Overview of the data products used in this study.

Product ref. no.	Product ID and type	Data access	Documentation
1	GLOBAL_MULTIYEAR_PHY_001_030 (GLORYS12V1), numerical models	E.U. Copernicus Marine Service Information (CMEMS) (2024)	Product User Manual (PUM): Drévillon et al. (2023a)* Quality Information Document (QUID): Drévillon et al. (2023b)* Journal article: Lellouche et al. (2021)
2	CASTS, observed temperature and salinity profiles	Federated Research Data Repository, https://doi.org/10.20383/102.0739	Coyne et al. (2023)
3	ERA5, atmospheric reanalyses	Copernicus Climate Change Service (2023)	Product reference: Hersbach et al. (2023) Journal article: Hersbach et al. (2020)
4	ETOPO 2022, gridded bathymetry	https://doi.org/10.25921/fd45-gt74	Product reference: NOAA National Centers for Environmental Information (2022)

* PUM and QUID were updated during publication (please see Disclaimer section).

Studies of MHWs in the Northwest Atlantic have documented the role of air–sea fluxes and oceanic processes such as advection in the onset and decay of MHWs. Schlegel et al. (2021) applied statistical methods to a combination of remotely sensed sea surface temperature (SST) data and atmospheric and oceanic reanalyses to link latent heat flux and mixed-layer depth as drivers of MHWs over the Northwest Atlantic continental shelf. They show that the onset of many surface MHWs in this area is linked with a positive air–sea heat flux anomaly into the ocean, most often driven by latent heat flux and shortwave radiation, but that the decay is more often associated with oceanic processes such as advection and mixing. Other studies have correlated MHWs with large-scale atmospheric conditions and spatial variability in heat flux anomalies. For example, Perez et al. (2021) link the 2015/16 MHW in the Northwest Atlantic to the position of the jet stream modifying the spatial distribution of heat fluxes, a finding confirmed by Sims et al. (2022), who further correlate sea surface temperature (SST) and sea surface salinity anomalies near the shelf break in a subregion (40–48° N, 48–70° W,) with the North Atlantic Oscillation (NAO). These studies indicate that a combination of oceanic and atmospheric processes drove the 2015/16 MHW. Other studies link abrupt sea ice melt and strong stratification with intensified surface MHWs in the Arctic (see e.g. Barkhordarian et al., 2024; Richaud et al., 2024), and recent work by Sun et al. (2024) identifies a strong relationship between mixed-layer depth shoaling, restratification, and MHW occurrence globally.

In this study, we describe a series of MHWs that occurred on the Newfoundland and Labrador (NL) Shelf during the summer and fall of 2023. The NL Shelf is a region of economic, environmental, and cultural importance, as it supports numerous commercial, recreational, and Indigenous fisheries (Templeman, 2010). The oceanographic conditions are characteristic of Arctic and subarctic environments and are influenced by the Labrador Current, which transports relatively cold and fresh water equatorward along the continental shelf (e.g. Lazier and Wright, 1993; Fratantoni and Pickart, 2007). The region undergoes interannual variability cycling through warm and cold phases associated with changes in air temperature, sea ice conditions, and climate indices such as the NAO (Petrie, 2007; Urrego-Blanco and Sheng, 2012; Han et al., 2019; Cyr and Galbraith, 2021). These warm and cold phases are linked to marine ecosystem characteristics such as the timing of the spring phytoplankton bloom and primary and secondary productivity (Cyr et al., 2024a) and the productivity of higher trophic levels (Cyr et al., 2025). Variability in the offshore transport of the Labrador Current (e.g. Jutras et al., 2023) is also linked with ecosystem characteristics such as marine bivalve growth, as suggested by Poitevin et al. (2019). Seasonal ice cover in the region has important implications for stratification and, in turn, primary productivity (e.g. Wu et al., 2007).

We conduct our analysis over several geographic subregions of the NL Shelf with distinct ecosystem characteristics, as described in Sect. 2.2, and explore the influence of several meteorological and oceanographic phenomena such as winds, air–sea heat fluxes, stratification, and advection on this series of MHWs. Studying the factors driving MHWs on the NL Shelf will support understanding on how these events may impact the local marine ecosystem.

2 Methods

2.1 Datasets

A number of datasets were used in this study. MHWs were characterized using the sea surface temperature (SST) from product ref. no. 1 (Table 1), which is a 1/12° global ocean reanalysis (herein GLORYS12V1) covering 31 December 1992 to 25 December 2023. Daily mean temperature and salinity fields were also used to describe oceanographic conditions such as stratification, depth-averaged temperature, and freshwater density. Sea ice concentration was also analyzed to characterize the monthly maximum sea ice extent, defined as regions where the concentration is greater than 0.15. Sea ice volume, defined as the product between the GLORYS12V1 sea ice concentration, sea ice thickness, and grid cell area, summed over the NL Shelf was also calculated and analyzed. Following recommendations by McDougall et al. (2021), we interpreted the GLORYS12V1 prognostic temperature and salinity variables to be conservative temperature and preformed salinity – a salinity variable not affected by biogeochemistry – scaled by a factor of $u_{\mathrm{ps}} = \frac{35.16504}{35}\,\mathrm{g\,kg^{-1}}$.

The GLORYS12V1 dataset was complemented by temperature and salinity profiles from product ref. no. 2 (CASTS; Table 1), which is composed of historical profiles in Atlantic Canada and the Eastern Arctic dating back to 1912 but is limited here to the period 1993–2023. Many of the CASTS profiles used in this study were collected under the Atlantic Zone Monitoring Program (AZMP; Therriault et al., 1998), which routinely monitors core stations and transects at annual and seasonal frequencies. Two AZMP transects (Seal Island and Flemish Cap) and one high-frequency sampling station (Station 27) were considered in this study (Fig. 1). To facilitate comparison with GLORYS12V1, the CASTS potential temperature and practical salinity variables were converted to conservative temperature and preformed salinity using the Python implementation of the Gibbs-SeaWater (GSW) Oceanographic Toolbox (McDougall and Barker, 2011).

Finally, 10 m wind speeds were taken from product ref. no. 3, which is a global atmospheric reanalysis (ERA5; Table 1). Daily mean wind speeds were smoothed using an 11 d rolling mean in order to isolate synoptic-scale events by removing high-frequency variability. Additionally, the role of air–sea interaction was examined using the following ERA5 variables: net surface shortwave radiation (Q_{swr}), net surface longwave radiation (Q_{lwr}), surface latent heat flux (Q_{lh}), and surface sensible heat flux (Q_{sh}). Following Denaxa et al. (2024), the sum of these four components was used to determine the net surface heat flux (Q), and Q_{swr} was taken as the surface value. All heat flux and radiation variables are positive downwards and represent a daily average. The ERA5 daily averaged 2 m air temperature was also analyzed. Climatologies for all ERA5 variables were calculated in the same way as the MHW climatologies. Bathymetry data for plotting are taken from product ref. no. 4 (ETOPO 2022; Table 1).

2.2 Marine heat wave definitions

Following Hobday et al. (2016), we defined an MHW as a period of 5 d or longer during which the daily averaged SST exceeds the climatological 90th percentile (T_{90}) for the given time of year. The World Meteorological Organization recommends, when possible, to use a 30-year time series (1991–2020) to calculate climatologies (World Meteorological Organization, 2017). In this study, because GLORYS12V1 starts in 1993, the climatology was calculated for each day of the year from 1993 to 2022. See the Supplement for the temperature and freshwater density trends over this period (Fig. S1) and a discussion on the sensitivity of the results to the climatological period. The climatological mean and 90th and 10th percentiles were determined using an 11 d window (see Hobday et al. (2016) for details), and the percentiles and climatological mean were smoothed using a 31 d rolling average.

Spatially, the analysis was performed over (1) every grid cell in GLORYS12V1 from 41 to 62° N and 65 to 39° W and (2) the spatially averaged SST in regions relevant to the NL Shelf ecosystem. Shown in Fig. 1a, these regions are the Labrador Shelf (LS), the Northeast Newfoundland Shelf (NNS), the Grand Banks (GB), and the Flemish Cap (FC). Each represents an area of distinct primary productivity and a well-defined food web system (Open Government, 2014; Pepin et al., 2014). A fifth region covering the entire NL Shelf (Fig. 1c) was also included.

Finally, using Δ as the difference between T_{90} and the climatological mean, we followed Hobday et al. (2018) to define four heat wave categories when temperature T exceeds T_{90} as follows: moderate ($T_{90} \le T < T_{90}+\Delta$), strong ($T_{90}+\Delta \le T < T_{90}+2\Delta$), severe ($T_{90}+2\Delta \le T < T_{90}+3\Delta$), and extreme ($T \ge T_{90}+3\Delta$). Some additional MHW metrics, suggested by Hobday et al. (2016), are reported in Table 2, including the start and end dates (t_{s} and t_{e}); the duration or number of MHW days (D); and the mean, maximum, and cumulative intensities (i_{mean}, i_{max}, and i_{cum}, respectively). The mean intensity is the mean of the temperature anomaly, the maximum intensity is the maximum of the temperature anomaly, and the cumulative intensity is the integrated daily temperature anomaly over the MHW period.

2.3 Stratification, depth-averaged temperature, and freshwater density

The 2023 daily time series and climatologies (1993–2022) of three additional metrics (stratification, depth-averaged temperature, and freshwater density) were calculated. The metric climatologies were determined using the same methodology as applied to the SST climatologies. Firstly, the stratification was assessed by calculating the squared-buoyancy frequency,

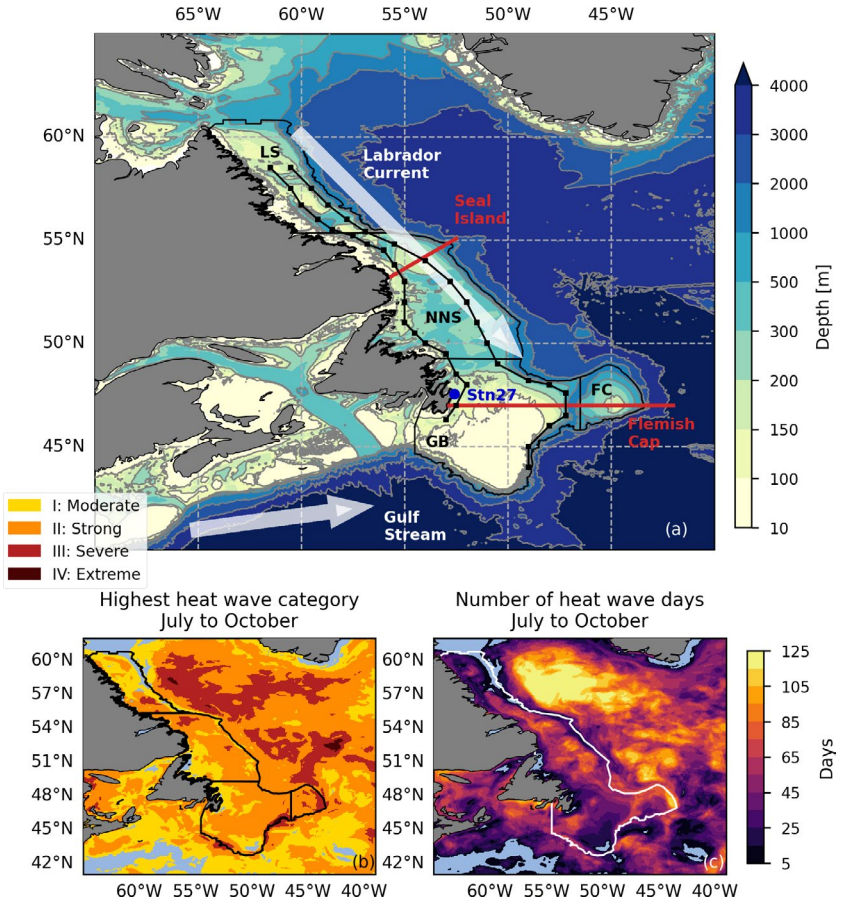

Figure 1. **(a)** Bathymetry from ETOPO 2022 (product ref. no. 4) in the study region. The thin black lines represent the regions over which MHW statistics are calculated: Labrador Shelf (LS), Northeast Newfoundland Shelf (NNS), Grand Banks (GB), and Flemish Cap (FC). Standard AZMP transects Seal Island and Flemish Cap are represented by the red lines. The dark-blue dot is the location of Station 27 (Stn27). Light-coloured arrows represent schematics of the Labrador Current and Gulf Stream. Black line segments with dots represent the Outer and Inner Shelf transects. **(b)** Spatial map of highest heat wave categories in July through October 2023 calculated from GLORYS12V1 (product ref. no. 1). Subregion polygons are shown for reference in black. **(c)** Total number of heat wave days in July through October 2023 (maximum 122 d), also calculated from the GLORYS12V1 product. The white line represents the polygon used to define the entire NL Shelf. The region definitions are derived from Ecosystem Production Units (Pepin et al., 2014) and contain information licensed under the Open Government Canada Licence – Canada. Maps were created with the Cartopy software package (Met Office, 2010–2015) and data from Natural Earth.

$N^2(z)$, over the entire water column using the GSW Oceanographic Toolbox (McDougall and Barker, 2011); then, its vertical maximum, $N^2_{\max}$, was used as a measure of stratification. A large value indicates strong stratification, which can limit the vertical exchange of heat and salt content. This quantity was analyzed as a spatial average over each region and at the grid cell closest to Station 27 where comparisons with observed data were made. In order to compare modelled and observed profiles of $N^2(z)$ at Station 27, the observed temperature and salinity fields were first interpolated to GLORYS12V1 depth levels, then $N^2(z)$ was calculated, and then its vertical maximum was determined. Furthermore, we defined the mixed-layer depth as the depth of the vertical maximum of $N^2(z)$.

Secondly, the depth-averaged temperature and freshwater density were used to examine the daily time evolution of temperature and freshwater content in the uppermost 20 m spatially averaged over the NL Shelf region (see Fig. S5 in the Supplement for additional depth bins). The depth-averaged temperature is defined as

$$T_{z_1-z_2} = \frac{\int_{z_1}^{z_2} T \, \mathrm{d}z}{\int_{z_1}^{z_2} \mathrm{d}z}, \tag{1}$$

where T is the temperature and z_1 and z_2 are the depth levels over which the integral is calculated. The freshwater density is

$$\mathrm{FWD}_{z_1-z_2} = \frac{\int_{z_1}^{z_2} \frac{\rho(T,S,p)}{\rho(T,0,p)} \frac{S_{\mathrm{ref}}-S}{S_{\mathrm{ref}}} \mathrm{d}z}{\int_{z_1}^{z_2} \mathrm{d}z}, \tag{2}$$

Table 2. MHW metrics and stratification for each region and the entire NL Shelf calculated from GLORYS12V1 (product ref. no. 1). For MHW metrics, t_s and t_e are the start and end dates of each heat wave; D is the duration or number of MHW days; and i_{max}, i_{mean}, and i_{cum} are the maximum, mean, and cumulative intensities derived from the spatially averaged sea surface temperature anomaly during each heat wave period. For stratification, $\overline{N^2_{max}}$, $\overline{N^2_{max\,clim}}$, and $\overline{N^2_{max\,90th}}$ are the spatially averaged quantities from 2023, the 1993–2022 climatological mean, and the 1993–2022 90th percentile, respectively. The angled brackets, $\langle\ \rangle$, denote a time average over the MHW period.

Region	t_s Start date (yyyy-mm-dd)	t_e End date (yyyy-mm-dd)	D MHW days	i_{max} (° C)	i_{mean} (° C)	i_{cum} (°C days)	$\overline{\langle N^2_{max}\rangle}$ (10^{-4} s^{-2})	$\overline{\langle N^2_{max\,clim}\rangle}$ (10^{-4} s^{-2})	$\overline{\langle N^2_{max\,90th}\rangle}$ (10^{-4} s^{-2})
Labrador Shelf (LS)	2023-07-16	2023-07-27	11	2.03	1.77	214.50	12.94	10.10	12.70
	2023-10-07	2023-10-23	16	1.01	0.88	224.47	5.50	4.30	6.00
Northeast Newfoundland Shelf (NNS)	2023-07-16	2023-08-10	25	3.23	2.53	1579.88	14.48	8.95	10.70
	2023-08-22	2023-09-01	10	2.32	2.1	209.94	13.54	9.56	11.52
	2023-09-14	2023-09-19	5	1.60	1.51	37.68	10.25	7.34	9.06
	2023-10-09	2023-10-30	21	1.63	1.26	553.66	5.61	4.21	5.84
Grand Banks (GB)	2023-07-15	2023-08-06	22	4.01	2.92	1411.51	12.97	7.46	9.07
	2023-09-07	2023-09-24	17	3.02	2.22	641.43	12.17	9.60	10.94
Flemish Cap (FC)	2023-07-08	2023-08-08	31	5.5	3.71	3566.89	9.83	4.88	6.46
	2023-08-27	2023-09-01	5	2.11	1.89	47.28	9.40	7.42	9.11
	2023-09-05	2023-09-24	19	3.59	2.78	1002.69	10.51	7.80	9.35
Entire NL Shelf	2023-07-14	2023-08-08	25	2.74	2.05	1281.54	11.75	10.11	12.65
	2023-09-06	2023-09-23	17	1.76	1.37	396.52	7.78	6.43	8.93
	2023-10-10	2023-10-24	14	1.24	1.01	198.37	5.35	4.22	5.87

where $\rho(T, S, p)$ is the in situ density calculated with the GSW Oceanographic Toolbox, S is the salinity, p is the pressure, $\rho(T, 0, p)$ is the density of seawater with zero salinity, and S_{ref} is a reference salinity of 35 g kg^{-1}. Quantities that were spatially averaged over a region or across a transect are denoted by an overbar symbol. For example, the spatially averaged sea surface temperature over a region is defined by

$$\overline{SST} = \frac{\int_{area} SST\, dA}{\int_{area} dA}. \quad (3)$$

3 Results

From July through October, MHWs were detected over most of the Northwest Atlantic (Fig. 1). Over the NL Shelf, MHW categories mainly ranged from moderate to severe, with spatial variability in the intensity and duration. No MHWs were present continuously throughout the entire July to October period, but, rather, a series of MHWs transpired in each region (Table 2). Each MHW period was associated with higher-than-typical stratification, in many cases exceeding the 90th percentile. The most intense and longest duration MHW began in July in FC. Each of the other subregions experienced their strongest MHW (in terms of maximum and mean intensity) around the same time, also commencing in July. A large portion of the southern GB received relatively short-duration and low-intensity MHWs, while both LS and NNS contained localized areas of higher-intensity MHWs (e.g. up to severe) that were approximately collocated with areas of greater total MHW days in the July through October period (Fig. 1).

When the MHW metrics were determined by spatially averaging over the entire NL Shelf, the result was three MHW periods (Table 2). These three periods approximately coincide with the MHW periods identified in the regional analysis. However, the late-August MHW in FC and NNS is not captured in the larger spatial average. Nevertheless, we used MHW metrics over the entire NL Shelf region to identify local oceanographic and meteorological conditions that contributed to the evolution of this series of MHWs.

An intriguing feature of this series of MHWs is that it was preconditioned by an unusually cold spring (Fig. 2a–b). In mid-June, spatially averaged SST anomalies over the entire shelf were as low as −0.56 °C. In some areas, such as the southwestern extent of GB and coastal regions of southern NNS, monthly averaged SST anomalies in June were below −1.50 °C (Fig. 2b). In contrast, anomalies in July were positive over nearly the entire NL Shelf, and the highest anomalies occurred in the FC region. High positive anomalies continued over most of the NL Shelf in August, but the highest anomalies were found in the NNS region. In September, high anomalies returned to the FC area and were concentrated in areas with steep bathymetric gradients that are strongly influenced by the Labrador Current, suggesting a possible advective source of warm water from upstream. Finally, October saw a reduction in the strength of the anomalies, but SSTs were still warmer than usual across the entire NL Shelf.

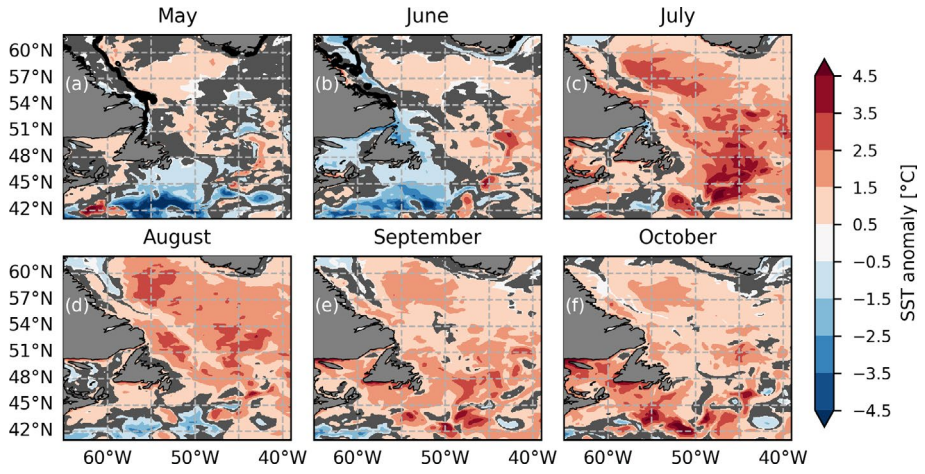

Figure 2. Sea surface temperature anomaly from GLORYS12V1 (product ref. no. 1) averaged over **(a)** May, **(b)** June, **(c)** July, **(d)** August, **(e)** September, and **(f)** October 2023. A reference period of 1993–2022 is used to calculate climatology. The thick black contours in panels **(a)** and **(b)** indicate the monthly maximum sea ice extent from the GLORYS12V1 in 2023. GLORYS12V1 had no sea ice in this area from July through October. The grey shading represents regions where the absolute value of the anomaly is less than 0.5 times the interannual standard deviation of the monthly mean sea surface temperature. Maps were created with the Cartopy software package (Met Office, 2010–2015) and data from Natural Earth.

In addition to unusually cold spring SSTs (Fig. 2a–b), subsurface temperatures from about 10–50 m in July were below normal across the Seal Island and Flemish Cap transects in both the GLORYS12V1 (product ref. no. 1) and AZMP (product ref. no. 2) profiles (Fig. 3a–b). Both transects displayed a very warm surface layer reaching to approximately 10 m in depth. Additionally, the Seal Island transect showed anomalously fresh conditions in the upper 20 m across most of the transect in July (Fig. 3c), particularly over the shelf break. Along the Flemish Cap transect, fresh signals were not as strong as at Seal Island at this time, but salinity anomalies between -0.25 and $-0.75\,\mathrm{g\,kg^{-1}}$ were apparent near the coast.

The anomaly structures of vertical profiles for both temperature and salinity suggest high stratification during the AZMP occupations in July. The squared-buoyancy frequency and mixed-layer depth during those occupations, shown in Fig. 3e and f, indicate stratified conditions in the upper 20 m of the water column. Furthermore, high stratification was apparent at Station 27 in both the GLORYS12V1 and AZMP data throughout nearly the entire summer and early fall (Fig. 4b). High stratification is partially explained by the anomalously cold spring which resulted in a colder-than-typical subsurface layer and, in turn, strong vertical temperature gradients when surface warming commenced as a result of solar heating (see Figs. S6, S7). Furthermore, the 0–20 m freshwater density in Fig. 4d reveals fresher-than-typical near-surface conditions from July through October. This fresh anomaly was concentrated in the upper 20 m (see Fig. S5), further explaining the higher-than-usual stratification. The source of the fresh anomaly is not yet clear, but it is present in both GLORYS12V1 and observations (Fig. 3c and d). Freshwater input due to sea ice melt from both local and remote areas is a possible explanation. Unfortunately, sea ice in GLORYS12V1 may not be helpful to describe this, as its sea ice cover does not appear to match observations very well, with no sea ice present in July 2023 or even in the 90th percentile of the 1993–2022 climatology (Fig. 4e).

Another factor that impacts stratification is the degree of vertical mixing introduced by wind forcing at the ocean surface. The 10 m wind speeds from ERA5 (product ref. no. 3) at Station 27 shown in Fig. 4f demonstrate that periods of below-average wind speeds in the summer and fall (e.g. early July, mid-August to early September, and late September to early October) preceded the three heat wave periods identified in Fig. 4. Furthermore, a return to average wind speeds preceded the end of each heat wave period, with the exception of a wind event in mid-July. This mid-July event corresponded with a reduction in the Station 27 stratification and was followed by a slight dip in the spatially averaged SST as the cold subsurface layer was mixed with the warm surface. Although the periods of average wind speeds were linked with a pause in heat wave conditions, it is likely that these wind events were not strong enough to significantly erode the strongly stratified conditions introduced by a cold spring and fresh early summer. In turn, cold subsurface conditions (from about 20–50 m; not shown), high stratification, and retention of heat near the surface persisted throughout most of the summer and fall.

Additionally, heat transfer between the ocean and atmosphere is an important element to consider (see Figs. 4g and h, and S2). During the July MHW, the 2 m air temperature from ERA5 was extremely high: at times, it was greater than the annual maximum of the climatological 90th percentile

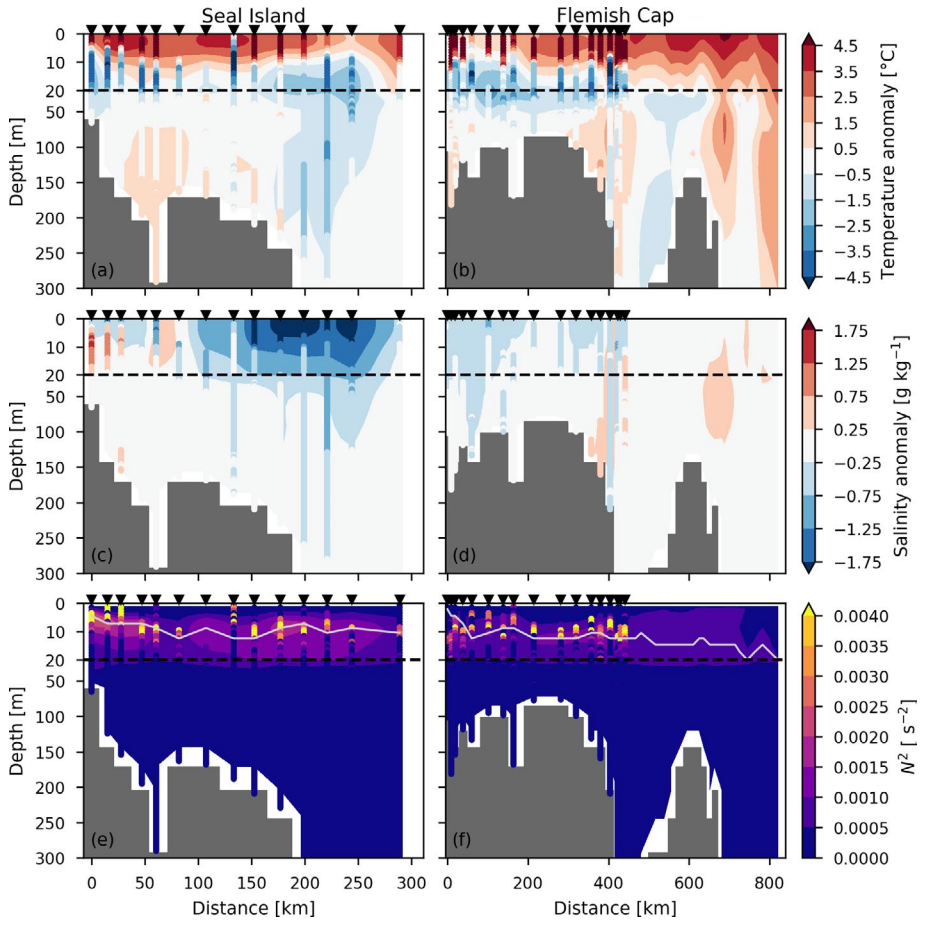

Figure 3. Vertical cross-section of temperature anomalies **(a, b)**, salinity anomalies **(c, d)**, and squared-buoyancy frequency **(e, f)** along the Seal Island **(a, c, e)** and Flemish Cap **(b, d, f)** transects shown for AZMP July 2023 occupation dates. For Seal Island, the AZMP occupation occurred on 25 July. For Flemish Cap, the stations inshore of 200 km were sampled on 20 July and the others were sampled on 30 July. GLORYS12V1 data (product ref. no. 1) matched to the AZMP sampling dates are shown in shaded contours, and AZMP data (product ref. no. 2) are shown in the coloured circles which appear as lines extending from top to bottom. In panels **(e)** and **(f)**, the solid grey line represents the mixed-layer depth defined as the depth of the maximum squared-buoyancy frequency. For Flemish Cap, GLORSY12V1 data at locations offshore of approximately 400 km, which were not sampled by AZMP in July 2023, are taken as the mean of 20 and 30 July. A reference period of 1993–2022 is used to calculate climatologies for both GLORYS12V1 and AZMP. For AZMP, all July and August occupations in the reference period were used to construct the climatology. The black triangles represent the positions of the AZMP stations sampled in July 2023. Note the difference in vertical scale above and below 20 m (dashed black line).

(Fig. 4h). Furthermore, the net surface heat flux was anomalously high during the first few days of the July MHW event but approached anomalously low values as the event reached its end. Similarly, the September and October MHWs exhibited higher-than-average air temperature and surface heat flux, although not every period in 2023 with these conditions resulted in an MHW (e.g. mid- to late January, mid-May, December).

Finally, the role of advection is illustrated by examining the evolution of surface temperature and freshwater density anomalies and the vertical maximum of the squared-buoyancy frequency along the shelf (Fig. 5). Firstly, advection is evident where periods of positive freshwater density anomaly and high stratification that are seen in May through June in the upstream parts of the transects (approximately 0 to 200 km) gradually propagate downstream. These anomalously fresh conditions arrived at Seal Island by the time of the mid-July MHW, increasing the stratification to above typical conditions (see Fig. S4 for climatological stratification). Throughout the shelf, there is typically a link between periods of increased freshwater density and increased stratification (see Figs. S3 and S4), suggesting advected and/or local freshwater input plays an important role in establishing stratification in this region. Advection may also impact sea surface temperatures through the transport of warm water masses. However, during the July MHW, advection of warm anomalies is not apparent in Fig. 5. Rather, this event was nearly simultaneous and widespread across the entire shelf.

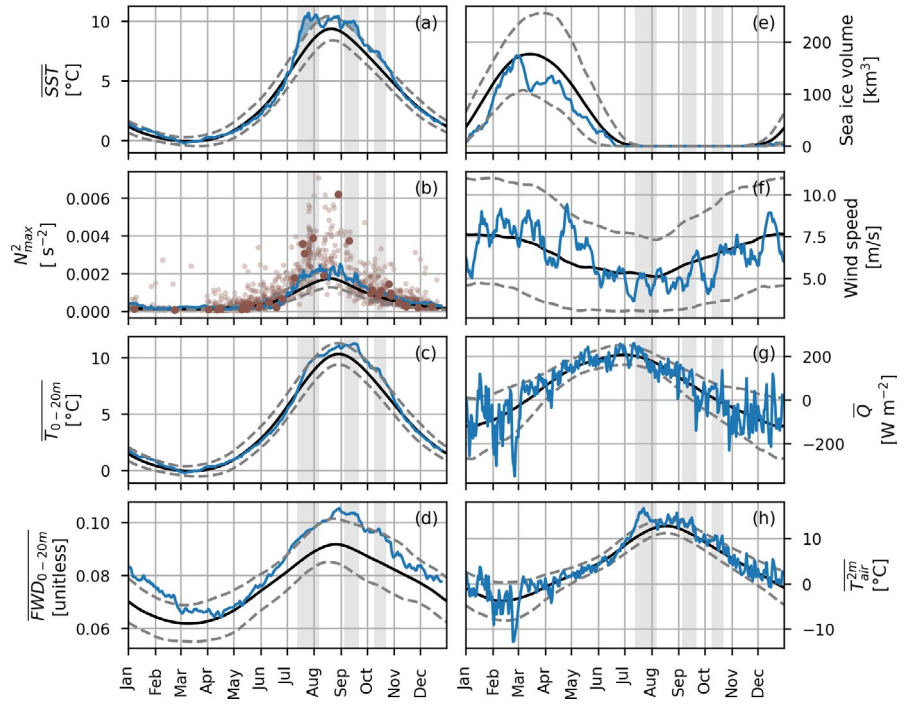

Figure 4. Time series plots for 2023 in blue lines, the 1993–2022 climatology in black lines, and the 1993–2022 10th and 90th percentiles in dashed grey lines. Variables from GLORYS12V1 (product ref. no. 1) are **(a)** sea surface temperature averaged over the NL Shelf, **(b)** maximum squared-buoyancy frequency at Station 27, **(c)** depth-averaged temperature from 0–20 m averaged over the NL Shelf, **(d)** freshwater density from 0–20 m averaged over the NL Shelf, and **(e)** sea ice volume over the NL Shelf. ERA5 (product ref. no. 3) variables include **(f)** 10 m wind speed at Station 27, **(g)** net daily averaged surface heat flux averaged over the NL Shelf (where positive indicates a downward flux), and **(h)** 2 m air temperature averaged over the NL Shelf. Maximum squared-buoyancy frequency data at Station 27 from AZMP (product ref. no. 2) are shown in panel **(b)** for 2023 with large dark-brown dots and for 1993–2022 with small light-brown dots. Heat wave periods are indicated by the grey shading.

Advection of warm water may have been a contributor for the MHW downstream of Seal Island in September through October, although a more detailed analysis is warranted in the future.

4 Discussion and conclusions

A combination of factors illustrated in Fig. 6 resulted in the series of MHWs detected on the NL Shelf in 2023. As an example, stratification increased as the surface layer warmed in July, preconditioned by unusually cold water temperatures in the spring. In addition, conditions were fresher than typical in the upper 20 m (e.g. Figs. 3c, 4d, 5b and e, S5c–d). Although the source of these fresh conditions was not analyzed in this work, other studies suggest that increased Arctic sea ice melt and freshwater release from the Beaufort Gyre are responsible for recent freshening trends in the North Atlantic (Wang et al., 2024; Yashayaev, 2024). In other regions, Barkhordarian et al. (2024) and Richaud et al. (2024) link abrupt sea ice melt and strong stratification with intensified surface MHWs in the Arctic. In 2023, sea ice conditions on the Labrador Shelf were above normal in June, leading to late last occurrence on the southern Labrador Shelf, and decreased very rapidly to zero prior to mid-July (Cyr et al., 2024b; Galbraith et al., 2024). Additionally, periods of low winds during the summer maintained the high stratification by limiting vertical mixing. As a result, heat was retained near the surface resulting in a series of MHWs throughout the summer and fall. This series was interrupted by occasional wind events which excited vertical mixing and reduced SSTs. Recent work by Sun et al. (2024) indicates a strong correlation between changes in the oceanic mixed-layer depth and the occurrence of MHWs globally, highlighting an important connection between mixed-layer restratification and surface MHWs.

The role of air–sea interactions and heat transfer between the atmosphere and the ocean is also important. During the July MHW, the 2 m air temperature was extremely high, exceeding the annual maximum of the 1993–2022 climatological 90th percentile for nearly half of the duration of the event. The 2 m air temperature was also higher than normal during the other MHWs in 2023. Previous work by Schlegel et al. (2021) indicates that latent heat flux is an important driver during the onset of MHWs. Indeed, during the beginning of each MHW on the NL Shelf in 2023, the net surface heat flux

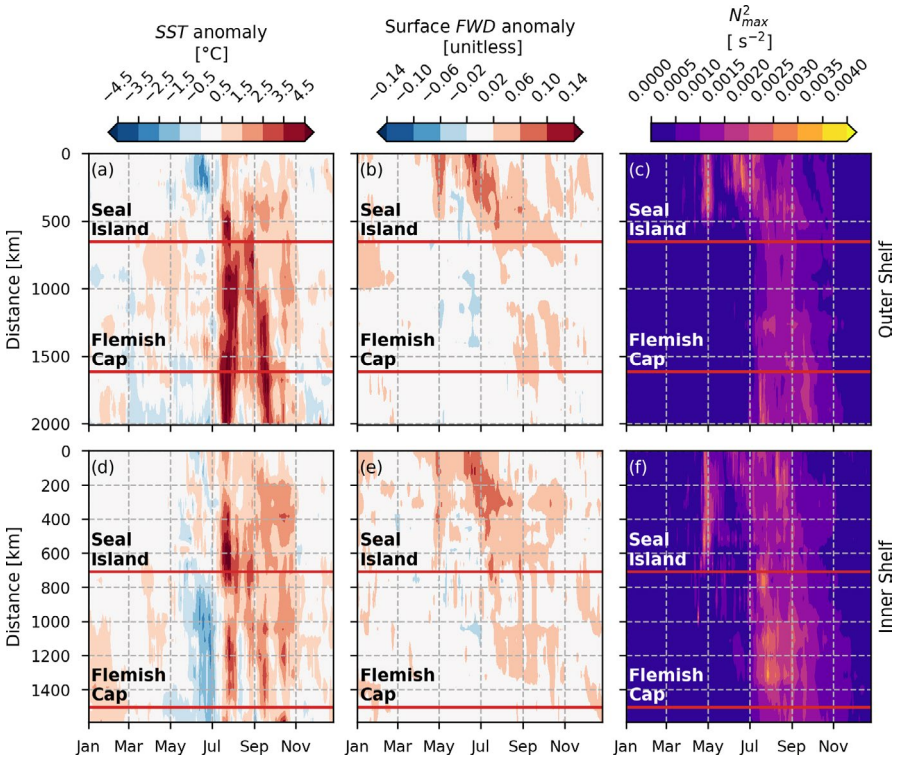

Figure 5. Time series of GLORYS12V1 (product ref. no. 1) sea surface temperature anomaly **(a, d)**, surface freshwater density anomaly **(b, e)**, and vertical maximum of the squared-buoyancy frequency **(c, f)** along the Outer Shelf **(a–c)** and Inner Shelf **(d–f)** transects for the year 2023. See Fig. 1a for Outer Shelf and Inner Shelf transect definitions. Distance is measured along each transect starting from the most upstream station. The red horizontal lines represent the along-shelf locations of the Seal Island **(a–c)** and Flemish Cap **(d–f)** transects. A reference period of 1993–2022 is used to calculate the climatology used to determine the anomalies.

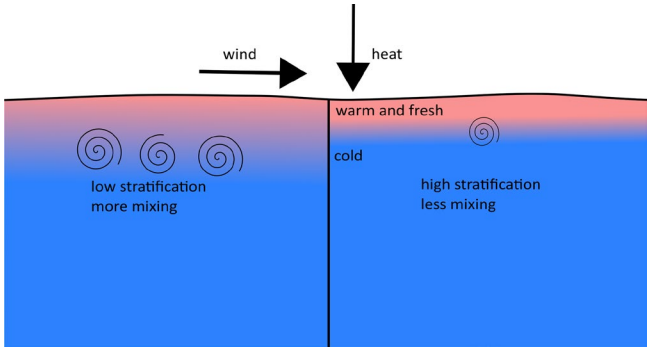

Figure 6. Schematic diagram describing the role of increased stratification on surface MHWs. On the left, lower stratification leads to more mixing. On the right, higher stratification leads to less mixing. Both scenarios receive the same heat flux and wind forcing at the surface. The case with higher stratification results in higher SSTs because the heat is confined to the surface due to less mixing.

was higher than typical (Fig. 4g), driven by positive anomalies in the surface latent heat flux and the surface longwave radiation (Fig. S2). However, not all periods of anomalously positive net surface heat flux resulted in an MHW, suggesting a combination of oceanic and atmospheric processes were at play in these surface MHWs.

The role of advection should also be considered. The Labrador Current is responsible for transporting water properties southward along the NL Shelf. For example, the anomalously fresh conditions detected at Seal Island in July (Fig. 3c) were transported south, carrying with them properties such as high stratification. Indeed, Figs. 2d–f and 5a–b show signs that warm anomalies were potentially associated with transport from NNS in August to the outer (inner) edges of GB (FC) in September. A bifurcation of the Labrador Current exists near the northern boundary of GB, directing some of the conditions associated with warm anomalies along the coast of GB in October. However, the October onset of MHWs in LS and NNS and the abrupt initiation of the July MHW across the entire shelf cannot be explained by transport. These events are more likely linked with local meteorological and oceanographic conditions.

A more thorough investigation quantifying the magnitude of these factors and relationships with large-scale atmospheric conditions is considered for future work in the NL Shelf region. For instance, a heat budget analysis in the mixed layer (see Oliver et al., 2021, as an example) could quantify the role of various elements, such as air–sea inter-

action, transport, and vertical mixing, in establishing MHW conditions. Furthermore, processes such as mesoscale eddies (e.g. Sun et al., 2024) and changes in coastal and shelf-break upwelling (e.g. Reyes-Mendoza et al., 2022) are likely to influence surface temperatures in the NL Shelf region. Higher-resolution modelling experiments could also be used to explore and quantify controls on MHW conditions, particularly when examining shelf-scale processes that are not resolved or well constrained by global reanalysis products.

Finally, the impact of MHWs on the NL Shelf ecosystem is an important area for future work. One area of interest is the vertical distribution of MHWs (e.g. Fig. S5) because not all elements of the marine ecosystem are impacted by high sea surface temperatures. Furthermore, regional differences in MHW intensity, frequency, and duration are important elements when considering ecosystem impacts. Tools such as ocean model reanalyses, analyses, and forecasts can aid in near-real-time monitoring by linking surface MHWs with vertical characteristics such as stratification and by exploring spatial structures in remote areas that are difficult to study directly with observations. These results suggest that ocean model nowcast and reanalysis products can complement observational methods for studying MHWs in near real-time over large geographic areas and at multiple depths.

Code and data availability. The data used in this study are available as described in Table 1. The code used in this study can be accessed via a GitLab repository upon request via email to the corresponding author. This study has been conducted using EU Copernicus Marine Service Information: https://doi.org/10.48670/moi-00021 (E.U. Copernicus Marine Service Information (CMEMS), 2024). The data from Hersbach et al. (2023) were downloaded from https://doi.org/10.24381/cds.adbb2d47 (Copernicus Climate Change Service, 2023). The results for ERA5 contain modified Copernicus Climate Change Service information (1993–2023).

Supplement. The supplement related to this article is available online at https://doi.org/10.5194/sp-6-osr9-12-2025-supplement.

Author contributions. NaS conducted the analysis, produced the visualizations, and prepared the initial draft. NaS, HJA, and JC organized and curated data. All authors contributed to conceptualization of the study, discussions on the methodology and results, and editing and reviewing the article.

Competing interests. The contact author has declared that none of the authors has any competing interests.

Disclaimer. The Copernicus Marine Service offering is routinely updated to ensure it remains at the forefront of user requirements. In this process, some product documents and manuals may undergo replacement or renaming, leading to the removal of certain document versions.

If readers have any questions or require assistance regarding these modifications, please feel free to reach out to the Copernicus Marine Service user support team for further guidance. They will be able to provide the necessary information to address concerns and find suitable alternatives.

Neither the European Commission nor ECMWF is responsible for any use that may be made of the Copernicus information or data it contains.

Publisher's note: Copernicus Publications remains neutral with regard to jurisdictional claims made in the text, published maps, institutional affiliations, or any other geographical representation in this paper. While Copernicus Publications makes every effort to include appropriate place names, the final responsibility lies with the authors.

Acknowledgements. We thank the two anonymous reviewers for constructive comments on the article. We greatly appreciate input from and discussions with David Bélanger regarding 2023 nutrient inventories and primary productivity, along with thoughtful comments from Pierre Pepin. This work is a contribution to the science mission of the Atlantic Zone Monitoring Program.

Review statement. This paper was edited by Gilles Garric and reviewed by two anonymous referees.

References

Barkhordarian, A., Nielsen, D. M., Olonscheck, D., and Baehr, J.: Arctic marine heatwaves forced by greenhouse gases and triggered by abrupt sea-ice melt, Commun. Earth Environ., 5, 57, https://doi.org/10.1038/s43247-024-01215-y, 2024.

Copernicus: https://climate.copernicus.eu/global-sea-surface-temperature-reaches-record-high (last access: 8 May 2024), 2023.

Copernicus Climate Change Service: ERA5 hourly data on single levels from 1940 to present, Copernicus Climate Change Service (C3S) Climate Data Store (CDS) [data set], https://doi.org/10.24381/cds.adbb2d47, 2023.

Coyne, J., Cyr, F., Donnet, S., Galbraith, P., Geoffroy, M., Hebert, D., Layton, C., Ratsimandresey, A., Snook, S., Soontiens, N., and Walkusz, W.: Canadian Atlantic Shelf Temperature-Salinity (CASTS), Federated Research Data Repository [data set], https://doi.org/10.20383/102.0739, 2023.

Cyr, F. and Galbraith, P. S.: A climate index for the Newfoundland and Labrador shelf, Earth Syst. Sci. Data, 13, 1807–1828, https://doi.org/10.5194/essd-13-1807-2021, 2021.

Cyr, F., Lewis, K., Bélanger, D., Regular, P., Clay, S., and Devred, E.: Physical controls and ecological implications of the timing of the spring phytoplankton bloom on the Newfoundland and Labrador shelf, Limnol. Oceanogr. Lett., 9, 191–198, https://doi.org/10.1002/lol2.10347, 2024a.

Cyr, F., Coyne, J., Snook, S., Bishop, C., Galbraith, P. S., Chen, N., and Han, G.: Physical Oceanographic Conditions on the New-

foundland and Labrador Shelf during 2023, Can. Tech. Rep. Hydrogr. Ocean Sci., 382, iv + 54 pp., ISBN 978-0-660-72810-0, 2024b.

Cyr, F., Adamack, A. T., Bélanger, D., Koen-Alonso, M., Mullowney, D., Murphy, H., Regular, P., and Pepin, P.: Environmental control on the productivity of a heavily fished ecosystem, Nat. Commun.,16, 5277, https://doi.org/10.1038/s41467-025-60453-6, 2025.

Denaxa, D., Korres, G., Bonino, G., Masina, S., and Hatzaki, M.: The role of air–sea heat flux for marine heatwaves in the Mediterranean Sea, in: 8th edition of the Copernicus Ocean State Report (OSR8), edited by: von Schuckmann, K., Moreira, L., Grégoire, M., Marcos, M., Staneva, J., Brasseur, P., Garric, G., Lionello, P., Karstensen, J., and Neukermans, G., Copernicus Publications, State Planet, 4-osr8, 11, https://doi.org/10.5194/sp-4-osr8-11-2024, 2024.

Drévillon, M., Fernandez, E., and Lellouche, J. M.: EU Copernicus Marine Service Product User Manual for the Global Ocean Physics Reanalysis, GLOBAL_MULTIYEAR_PHY_001_030, Issue 1.5, Mercator Ocean International, https://catalogue.marine.copernicus.eu/documents/PUM/CMEMS-GLO-PUM-001-030.pdf (last access: 19 March 2024), 2023a.

Drévillon, M., Lellouche, J. M., Régnier, C., Garric, G., Bricaud, C., Hernandez, O., and Bourdallé-Badie, R.: EU Copernicus Marine Service Quality Information Document for the Global Ocean Physics Reanalysis, GLOBAL_MULTIYEAR_PHY_001_030, Issue 1.6, Mercator Ocean International, https://catalogue.marine.copernicus.eu/documents/QUID/CMEMS-GLO-QUID-001-030.pdf (last access: 19 March 2024), 2023b.

Edwing, K., Wu, Z., Lu, W., Li, X., Cai, W.-J., and Yan, X.-H.: Impact of Marine Heatwaves on Air-Sea CO_2 Flux Along the US East Coast, Geophys. Res. Lett., 51, e2023GL105363, https://doi.org/10.1029/2023GL105363, 2024.

E.U. Copernicus Marine Service Information (CMEMS): Global Ocean Physics Reanalysis, Marine Data Store (MDS) [data set], https://doi.org/10.48670/moi-00021, 2024.

Fratantoni, P. S. and Pickart, R. S.: The western North Atlantic shelfbreak current system in summer, J. Phys. Oceanogr., 37, 2509–2533, https://doi.org/10.1175/JPO3123.1, 2007.

Frölicher, T. L. and Laufkötter, C.: Emerging risks from marine heat waves, Nat. Commun., 9, 650, https://doi.org/10.1038/s41467-018-03163-6, 2018.

Galbraith, P. S., Blais, M., Lizotte, M., Cyr, F., Bélanger, D., Casault, B., Clay, S., Layton, C., Starr, M., Chassé, J., Azetsu-Scott, K., Coyne, J., Devred, E., Gabriel, C.-E., Johnson, C. L., Maillet, G., Pepin, P., Plourde, S., Ringuette, M., and Shaw, J.-L.: Oceanographic conditions in the Atlantic zone in 2023, Can. Tech. Rep. Hydro. and Ocean Sci., 379, v + 39 pp., ISBN 978-0-660-72620-5, 2024.

Geoffroy, M., Bouchard, C, Flores, H., Robert, D., Gjøsæter, H., Hoover, C., Hop, H., Hussey, N. E., Nahrgang, J., Steiner, N., Bender, M., Berge, J., Castellani, G., Chernova, N., Copeman, L., David, C. L., Deary, A., Divoky, G., Dolgov, A. V., Duffy-Anderson, J., Dupont, N., Durant, J. M., Elliott, K., Gauthier, S., Goldstein, E. D., Gradinger, R., Hedges, K., Herbig, J., Laurel, B., Loseto, L., Maes, S., Mark, F. C., Mosbech, A., Pedro, S., Pettitt-Wade, H., Prokopchuk, I., Renaud, P. E., Schembri, S., Vestfals, C., and Walkusz, W.: The circumpolar impacts of climate change and anthropogenic stressors on Arctic cod (Boreogadus saida) and its ecosystem, Elem. Sci. Anth., 11, 00097, https://doi.org/10.1525/elementa.2022.00097, 2023.

Han, G., Ma Z., and Chen, N.: Ocean climate variability off Newfoundland and Labrador over 1979–2010: A modelling approach, Ocean Model., 144, 101505, https://doi.org/10.1016/j.ocemod.2019.101505, 2019.

Hersbach, H., Bell, B., Berrisford, P., Hirahara, S., Horányi, A., Muñoz-Sabater, J., Nicolas, J., Peubey, C., Radu, R., Schepers, D., Simmons, A., Soci, C., Abdalla, S., Abellan, X., Balsamo, G., Bechtold, P., Biavati, G., Bidlot, J., Bonavita, M., De Chiara, G., Dahlgren, P., Dee, D., Diamantakis, M., Dragani, R., Flemming, J., Forbes, R., Fuentes, M., Geer, A., Haimberger, L., Healy, S., Hogan, R. J., Hólm, E., Janisková, M., Keeley, S., Laloyaux, P., Lopez, P., Lupu, C., Radnoti, G., de Rosnay, P., Rozum, I., Vamborg, F., Villaume, S., and Thépaut, J.-N.: The ERA5 global reanalysis, Q. J. Roy. Meteor. Soc., 146, 1999–2049, https://doi.org/10.1002/qj.3803, 2020.

Hersbach, H., Bell, B., Berrisford, P., Biavati, G., Horányi, A., Muñoz Sabater, J., Nicolas, J., Peubey, C., Radu, R., Rozum, I., Schepers, D., Simmons, A., Soci, C., Dee, D., and Thépaut, J.-N.: ERA5 hourly data on single levels from 1940 to present, Copernicus Climate Change Service (C3S) Climate Data Store (CDS) [data set], https://doi.org/10.24381/cds.adbb2d47, 2023.

Hobday, A. J., Alexander, L. V., Perkins, S. E., Smale, D. A., Straub, S. C., Oliver, E. C. J., Benthuysen, J. A., Burrows, M. T., Donat, M. G., Feng, M., Holbrook, N. J., Moore, P. J., Scannell, H. A., Sen Gupta, A., and Wernberg, T.: A hierarchical approach to defining marine heatwaves, Prog. Oceanogr., 141, 227–238, https://doi.org/10.1016/j.pocean.2015.12.014, 2016.

Hobday, A. J., Oliver, E. C. J., Sen Gupta, A., Benthuysen, J. A., Burrows, M. T., Donat, M. G., Holbrook, N. J., Moore, P. J., Thomsen, M. S., Wernberg, T., and Smale, D. A.: Categorizing and naming marine heatwaves, Oceanography, 31, 162–173, https://doi.org/10.5670/oceanog.2018.205, 2018.

IPCC: IPCC Special Report on the Ocean and Cryosphere in a Changing Climate, edited by: Pörtner, H.-O., Roberts, D. C., Masson-Delmotte, V., Zhai, P., Tignor, M., Poloczanska, E., Mintenbeck, K., Alegría, A., Nicolai, M., Okem, A., Petzold, J., Rama, B., and Weyer, N. M., Cambridge University Press, Cambridge, UK and New York, NY, USA, 755 pp., https://doi.org/10.1017/9781009157964, 2019.

IPCC: Climate Change 2023: Synthesis Report. Contribution of Working Groups I, II and III to the Sixth Assessment Report of the Intergovernmental Panel on Climate Change, edited by: Core Writing Team, Lee, H., and Romero, J., IPCC, Geneva, Switzerland, 35–115, https://doi.org/10.59327/IPCC/AR6-9789291691647, 2023.

Jutras, M., Dufour, C. O., Mucci, A., and Talbot, L. C.: Large-scale control of the retroflection of the Labrador Current, Nat. Commun., 14, 2623, https://doi.org/10.1038/s41467-023-38321-y, 2023.

Lazier, J. R. N. and Wright, D. G.: Annual velocity variations in the Labrador Current, J. Phys. Oceanogr., 23, 659–678, https://doi.org/10.1175/1520-0485(1993)023<0659:AVVITL>2.0.CO;2, 1993.

Le Grix, N., Zscheischler, J., Laufkötter, C., Rousseaux, C. S., and Frölicher, T. L.: Compound high-temperature and low-

chlorophyll extremes in the ocean over the satellite period, Biogeosciences, 18, 2119–2137, https://doi.org/10.5194/bg-18-2119-2021, 2021.

Lellouche, J.-M., Grenier, E., Bourdallé-Badie, R., Garric, G., Melet, A., Drévillon, M., Bricaud, C., Hamon, M., Le Galloudec, O., Regnier, C., Candela, T., Testut, C.-E., Gasparin, R., Ruggiero, G., Benkiran, M., Drillet, R., and Le Traon, P.-Y.: The Copernicus Global 1/12° Oceanic and Sea Ice GLORYS12 Reanalysis, Front. Earth Sci., 9, 698876, https://doi.org/10.3389/feart.2021.698876, 2021.

McAdam, R., Masina, S., and Gualdi, S.: Seasonal forecasting of subsurface marine heatwaves, Commun. Earth Environ., 4, 225, https://doi.org/10.1038/s43247-023-00892-5, 2023.

McDougall, T. J. and Barker, P. M.: Getting started with TEOS-10 and the Gibbs Seawater (GSW) Oceanographic Toolbox, SCOR/IAPSO WG127, 28 pp., ISBN 978-0-646-55621-5, 2011.

McDougall, T. J., Barker, P. M., Holmes, R. M., Pawlowicz, R., Griffies, S. M., and Durack, P. J.: The interpretation of temperature and salinity variables in numerical ocean model output and the calculation of heat fluxes and heat content, Geosci. Model Dev., 14, 6445–6466, https://doi.org/10.5194/gmd-14-6445-2021, 2021.

Met Office: Cartopy: a cartographic python library with a Matplotlib interface, Exeter, Devon, https://scitools.org.uk/cartopy (last access: January 2025), 2010–2015.

NOAA National Centers for Environmental Information: ETOPO 2022 15 Arc-Second Global Relief Model, NOAA National Centers for Environmental Information, https://doi.org/10.25921/fd45-gt74, 2022.

Oliver, E. C. J., Donat, M. G., Burrows, M.T., Moore, P. J., Smale, D. A., Alexander, L. V., Benthuysen, J. A., Feng, M., Sen Gupta, A., Hobday, A. J., Holbrook, N. J., Perkins-Kirkpatrick, S. E., Scannell, H. A., Straub, S. C., and Wernberg, T.: Longer and more frequent marine heatwaves over the past century, Nat. Commun., 9, 1324, https://doi.org/10.1038/s41467-018-03732-9, 2018.

Oliver, E. C. J., Benthuysen, J. A., Darmaraki, S., Donat, M. G., Hobday, A. J., Holbrook, N. J., Schlegel, R. W., and Sen Gupta, A.: Marine heatwaves, Annu. Rev. Mar. Sci., 13, 313–342, https://doi.org/10.1146/annurev-marine-032720-095144, 2021.

Open Government: Ecosystem Production Units in the Northwest Atlantic, Government of Canada, https://open.canada.ca/data/en/dataset/9a515ef8-0e2a-479e-9b25-55658eae30be (last access: 15 February 2024), 2014.

Pepin, P., Higdon, J., Koen-Alonso, M., Fogarty, M., and Ollerhead, N.: Application of ecoregion analysis to the identification of Ecosystem Production Units (EPUs) in the NAFO Convention Area, NAFO Sci. Counc. Res. Doc, 14/069, no. N6412, https://www.nafo.int/Portals/0/PDFs/sc/2014/scr14-069.pdf (last access: July 2025), 2014.

Perez, E., Ryan, S., Andres, M., Gawarkiewicz, G., Ummenhofer, C. C., Bane, J., and Haines, S.: Understanding physical drivers of the 2015/16 marine heatwaves in the Northwest Atlantic, Sci. Rep., 11, 17623, https://doi.org/10.1038/s41598-021-97012-0, 2021.

Petrie, B.: Does the north Atlantic oscillation affect hydrographic properties on the Canadian Atlantic continental shelf?, Atmos.-Ocean, 45, 141–151, https://doi.org/10.3137/ao.450302, 2007.

Poitevin, P., Thébault, J., Siebert, V., Donnet, S., Archambault, P., Doré, J., Chauvaud, L., and Lazure, P.: Growth Response of Arctica Islandica to North Atlantic Oceanographic Conditions Since 1850, Front. Mar. Sci., 6, 483, https://doi.org/10.3389/fmars.2019.00483, 2019.

Reyes-Mendoza, O., Manta, G., and Carrillo, L.: Marine heatwaves and marine cold-spells on the Yucatan Shelf-break upwelling region, Cont. Shelf Res., 239, 104707, https://doi.org/10.1016/j.csr.2022.104707, 2022.

Richaud, B., Hu, X., Darmaraki, S., Fennel, K., Lu, Y., and Oliver, E. C. J.: Drivers of marine heatwaves in the Arctic Ocean, J. Geophy. Res-Oceans, 129, e2023JC020324, https://doi.org/10.1029/2023JC020324, 2024.

Schlegel, R. W., Oliver, E. C. J., and Chen, K.: Drivers of Marine Heatwaves in the Northwest Atlantic: The Role of Air–Sea Interaction During Onset and Decline, Front. Mar. Sci., 8, 627970, https://doi.org/10.3389/fmars.2021.627970, 2021.

Sims, L. D., Subrahmanyam, B., and Trott, C. B.: Ocean–Atmosphere Variability in the Northwest Atlantic Ocean during Active Marine Heatwave Years, Remote Sens., 14, 2913, https://doi.org/10.3390/rs14122913, 2022.

Smith, K. E., Burrows, M. T., Hobday, A. J., G. King, N. G., Moore, P. J., Sen Gupta, Thomsen, M., S., Wernberg, T., and Smale, D. A.: Biological impacts of marine heatwaves, Annu. Rev. Mar. Sci., 15, 119–145, https://doi.org/10.1146/annurev-marine-032122-121437, 2023.

Sun, W., Wang, Y., Yang, Y., Yang, J., Ji, J., and Dong, C.: Marine heatwaves/cold-spells associated with mixed layer depth variation globally, Geophy. Res. Lett., 51, e2024GL112325, https://doi.org/10.1029/2024GL112325, 2024.

Templeman, N. D.: Ecosystem Status and Trends Report for the Newfoundland and Labrador Shelf. DFO Can. Sci. Advis. Sec. Res. Doc. 2010/026, vi + 72 pp., 2010.

Therriault, J.-C., Petrie, B., Pepin, P., Gagnon, J., Gregory, D., Helbig, J., Herman, A., Lefaivre, D., Mitchel, M., Pelchat, B., Runge, J., and Sameoto, D.: Proposal for a Northwest Atlantic Zonal Monitoring Program, Can. Tech. Rep. Hydro. and Ocean Sci., 194, vii + 57 pp., 1998.

Urrego-Blanco, J. and Sheng, J.: Interannual Variability of the Circulation over the Eastern Canadian Shelf, Atmos.-Ocean, 50, 277–300, https://doi.org/10.1080/07055900.2012.680430, 2012.

Wang, Q., Danilov, S., and Jung, T.: Arctic freshwater anomaly transiting to the North Atlantic delayed within a buffer zone, Nat. Geosci. 17, 1218–1221, https://doi.org/10.1038/s41561-024-01592-1, 2024.

World Meteorological Organization: WMO guidelines on the calculation of climate normals, Tech. rep., Geneva, Switzerland, ISBN 978-92-63-11203-3, 2017.

Wu, Y., Peterson, I. K., Tang, C. C. L., Platt, T., Sathyendranath, S., and Fuentes-Yaco, C.: The impact of sea ice on the initiation of the spring bloom on the Newfoundland and Labrador Shelves, J. Plankton Res., 29, 509–514, https://doi.org/10.1093/plankt/fbm035, 2007.

Yashayaev, I.: Intensification and shutdown of deep convection in the Labrador Sea were caused by changes in atmospheric and freshwater dynamics. Commun. Earth Environ., 5, 156, https://doi.org/10.1038/s43247-024-01296-9, 2024.

Table of contents

Copernicus Ocean State Report | OSR9 | 2025